

MONOCYTES AND
MACROPHAGES
IN CHRONIC INFLAMMATION

**PERIPHERAL MONOCYTES
AND INTESTINAL MACROPHAGES
DURING CHRONIC INFLAMMATION**

By JESSICA ANN BREZNIK, HB.Sc., M.Sc.

A Thesis Submitted to the School of Graduate Studies in Partial Fulfillment
of the Requirements for the Degree Doctor of Philosophy

McMaster University
© Copyright by Jessica Ann Breznik, October 14, 2020

DOCTOR OF PHILOSOPHY 2020 (Medical Sciences, Infection and Immunity)

Department of Pathology & Molecular Medicine

McMaster University, Hamilton, Ontario, Canada

TITLE: Peripheral monocytes and intestinal macrophages during chronic inflammation

AUTHOR: Jessica Ann Breznik, HBSc., MSc.

SUPERVISOR: Dr. Dawn M. E. Bowdish

NUMBER OF PAGES: xxii,341

Lay Abstract

High levels of inflammation in the absence of infection or injury, as occurs in obesity, can increase an individual's susceptibility to developing chronic disease (e.g. diabetes, heart disease). Inflammation changes numbers and functions of immune cells like monocytes and macrophages. Inflammation is influenced by biological sex, and increases naturally in pregnancy and with age. The goal of this thesis was to characterize how inflammation affects monocyte and macrophage numbers and functions within the blood and the gut, which may contribute to risk of chronic disease. We identified that obesity alters monocytes within the blood of young individuals and in pregnancy, but reduction of inflammation in obesity had distinct effects in males and females. We also found that obesity, pregnancy, and aging cause different changes to macrophages in the gut. These findings suggest that monocytes and macrophages have altered numbers and functions under different biological conditions associated with inflammation.

Abstract

Inflammation is a complex biological response required to maintain homeostasis, but chronic inflammation increases risk of morbidity and mortality. Monocytes and macrophages often contribute to pathology in chronic inflammatory disorders. We hypothesized that chronic inflammation alters peripheral monocyte and intestinal macrophage prevalence, phenotype, and functions. We predicted these effects are modulated by different biological conditions, and they can be mediated by TNF and the intestinal microbiota. In Chapter 3, we investigated peripheral blood immune cell quantities (immunophenotype) under conditions of homeostasis. We observed that the female reproductive cycle did not have a significant effect on immunophenotype, though there were sex differences. In Chapter 4, we examined the relationships between adiposity, chronic inflammation, circulating monocytes, hyperglycemia, and hyperinsulinemia, in male mice. We found that increased circulating Ly6C^{high} monocytes correlated with insulin resistance, and that this was mediated by TNF. In Chapter 5, we observed in non-pregnant female mice that there were temporal effects of obesity on peripheral blood immunophenotype, with an increase in Ly6C^{high} monocytes. Pregravid obesity altered immunophenotype at mid-pregnancy. In late pregnancy, removal of TNF did not prevent obesity-associated changes to immunophenotype. Excess gestational weight gain also influenced peripheral immunophenotype in lactation. In Chapter 6, we found that obesity altered ileum and colon CD4⁻TIM4⁻, CD4⁺, and CD4⁺TIM4⁺ macrophage numbers, phenotype, and cytokine production, in a temporal and tissue-specific manner. Neither peripheral nor intestinal effects of obesity in non-pregnant

female mice were mediated by TNF. We identified that there were microbiota-associated and age-associated effects that contributed to changes in colon macrophages between young and old mice. Obesity, excess gestational weight gain, and biological aging had different effects on intestinal macrophage populations. This research provides a better understanding of how peripheral monocytes and intestinal macrophages change in response to inflammation under different biological conditions across the life course.

Acknowledgements

I have been beyond fortunate in my experiences as a PhD student in the Bowdish and Sloboda, or ‘Slobowdish’ labs these past four years. I would like to express my sincere gratitude to Dr. Bowdish and Dr. Sloboda for their unwavering guidance and encouragement, and for always supporting me to pursue opportunities to expand my scientific and professional skills, throughout my experiences as a graduate student. In different, yet completely complementary ways, they both embody the tenets of being remarkable scientists and supervisors.

I have also been fortunate to have Dr. Charu Kaushic and Dr. Jon Schertzer as my committee members. Dr. Kaushic always asked critical questions that made me reconsider my data in new ways and expand my knowledge, gave me the opportunity to collaboratively redesign aspects of 4II3 and supported my interest in pedagogy and teaching. I am especially grateful to Dr. Schertzer for welcoming me into his lab from my first day, helping me prepare my first manuscript, teaching me about immunometabolism, and for his invaluable guidance on experimental design and my research project.

The experiments in this thesis would not have been possible without the support of Dr. Elena Verdú and the Axenic Gnotobiotic Unit at McMaster University, in particular Joe Notarangelo who coordinated exports, and especially Jennifer Jury, who was always willing to take time out of her busy schedule to help facilitate my experiments. I am also thankful for the support of Jun Lu and the Bercik/Collins lab, and the Steinberg lab, for letting me use their space and equipment on occasion. I would like to express my gratitude to the staff at the Central Animal Facility, in particular Wendy, Sally, Darlene, and Janice, as well as Hong Liang, Mary-Jo Smith, Mari Bruni, and Carrie Hasenack from MIRC for their technical support.

Scientific research thrives on collaboration, and I have been very fortunate as both the Bowdish and Sloboda labs are filled with undergraduates, graduate, and post-doc students who are always willing to lend their hands for animal experiments and their minds to discuss science. I would like to acknowledge and thank past and present members of the Bowdish, Sloboda, and Schertzer labs.

I am incredibly grateful to have studied in a supportive and collaborative environment at the McMaster Immunology Research Centre and the Farncombe Research Institute. The advice and feedback that I received from seminars and interacting with other graduate students and faculty helped to guide my project, and I have had the opportunity to learn about so much interesting and innovative science that has inspired my own research.

I would like to thank my parents for their constant, unwavering support. Thank you for always taking an interest in my work, and for helping me to look at situations and my data in new ways. You both inspire me - thank you for believing in me.

for my parents

Table of Contents

Lay Abstract.....	iii
Abstract	iv
Acknowledgements	vi
List of Figures	xi
List of Tables	xv
List of Appendices	xvi
Declaration of Academic Achievement	xvii
List of Abbreviations	xx
Chapter 1. Introduction.....	1
1.1 Inflammation	1
Acute Inflammation	1
Chronic Inflammation.....	3
Inflammation in Obesity	4
Inflammation in Aging	6
Inflammation in Pregnancy.....	8
1.2 Macrophages.....	11
Macrophage Discovery and Functions	11
Macrophage Ontogeny – RES and MPS	13
Macrophage Ontogeny – MPS, Embryonic Origins and Core Programming	14
1.3 Monocytes	17
Monocyte Discovery and Ontogeny	17
Monocyte Identification.....	19
Monocyte Movement.....	20
Monocyte Functions – Steady-State	20
Monocyte Functions - Inflammation	21
Monocytes and Macrophages in Chronic Inflammation	23
1.4 Structure and Functions of the Gastrointestinal Tract	24
1.5 The Microbiome and Immunity.....	26
1.6 Intestinal Macrophages.....	28

Intestinal Macrophages - Ontogeny	29
Intestinal Macrophages – Localization	32
Intestinal Macrophages - Anti-inflammatory Character	36
Intestinal Macrophages - Response to Inflammation	37
1.7 Rationale	39
Chapter 2. Materials & Methods	42
2.1 Animal experiments	42
2.2 <i>In vivo</i> experiments	48
2.2.1 Metabolic and body composition assessments	48
2.2.2 CCL2-elicited monocyte response assay	50
2.2.3 Intestinal permeability	50
2.3 Cytokine ELISA	51
2.4 Adipose tissue histology and immunohistochemistry	52
2.5 Flow cytometry analysis of immune cells	53
2.6 Statistical analysis	59
Chapter 3. Biological sex, not reproductive cycle, influences peripheral blood immune cell prevalence in mice	63
Chapter 4. TNF, but not hyperinsulinemia or hyperglycemia, is a key driver of obesity-induced monocytosis revealing that inflammatory monocytes correlate with insulin in obese male mice	116
Chapter 5. Peripheral immunophenotype and obesity-associated chronic inflammation in female mice	133
5.1 Peripheral immunophenotype and diet-induced obesity in non-pregnant female mice	134
5.1.1 Introduction	134
5.1.2 Results	136
5.1.3 Discussion	154
5.2 Peripheral immunophenotype, diet-induced obesity, and excess gestational weight gain, in female mice during pregnancy and lactation	159
5.2.1 Introduction	159
5.2.2 Maternal peripheral immunophenotype and diet-induced obesity at E14.5	161
5.2.3 Maternal immunophenotype, TNF, and diet-induced obesity at E18.5	166

5.2.4 Maternal excess gestational weight gain and peripheral immunophenotype during lactation	167
5.2.5 Discussion.....	172
Chapter 6. Intestinal macrophages in chronic inflammation	179
6.1 Intestinal macrophages in diet-induced obesity.....	180
6.1.1 Introduction.....	180
6.1.2 Results	183
6.1.3 Discussion.....	202
6.2 The role of TNF in diet-induced obesity	207
6.2.1 Introduction.....	207
6.2.2 Results	208
6.2.3 Discussion.....	216
6.3 Immunological effects of the microbiome.....	218
6.3.1 Introduction.....	218
6.3.2 Results	220
6.3.3 Discussion.....	233
6.4 Intestinal macrophages in aging	236
6.4.1 Introduction.....	236
6.4.2 Results	239
6.4.3 Discussion.....	250
6.5 Intestinal macrophages in lactation with excess weight gain	255
6.5.1 Introduction.....	255
6.5.3 Results	257
6.5.4 Discussion.....	265
Chapter 7. Discussion	276
Review of premise	276
Effects of TNF on cellular inflammation in obesity	278
Immunological implications of pregravid obesity and excess gestational weight gain	280
Intestinal macrophages under conditions of homeostasis and chronic inflammation ...	283
Colon macrophages across the life course.....	287
Concluding remarks.....	291

List of Figures

*Note that figures in Chapters 3 and 4 are not included in this list
as they are part of complete manuscripts*

Chapter 1

Figure 1.1. Myeloid cell differentiation in the steady state	18
Figure 1.2. Monocyte and macrophage populations in the intestines	31
Figure 1.3. CD4 ⁻ TIM4 ⁻ , CD4 ⁺ , and CD4 ⁺ TIM4 ⁺ macrophage prevalence along the intestines	32
Figure 1.4. Summary of intestinal macrophage localization and functions	34
Figure 1.5. Central thesis aims to investigate effects of chronic inflammation	41

Chapter 5

Figure 5.1.1. Model phenotype - female mice fed standard chow or HF diet.....	137
Figure 5.1.2. Peripheral blood immune cell prevalence in mice fed chow or HF diet	140
Figure 5.1.3. Peripheral blood absolute cell counts in mice fed chow or HF diet	141
Figure 5.1.4. Response of peripheral monocyte populations to chemotactic ligand CCL2	144
Figure 5.1.5. Ly6C ^{high} monocyte production of TNF and IL-6 in mice fed chow or HF diet.....	145
Figure 5.1.6. Bone marrow monocytes and precursors in mice fed chow or HF diet.....	146
Figure 5.1.7. Body weight, adiposity, and fasting blood glucose in WT and TNF ^{-/-} mice on HF diet	149
Figure 5.1.8. Effects of HF diet feeding on immunophenotype of WT and TNF ^{-/-} mice	150

Figure 5.1.9. Peripheral blood immune cell prevalence in WT and TNF ^{-/-} mice on HF diet.....	151
Figure 5.1.10. Peripheral blood immune cell absolute cell counts in WT and TNF ^{-/-} mice on HF diet	152
Figure 5.2.1. Maternal, fetal, and placental physiological measurements	163
Figure 5.2.2. Effects of diet-induced obesity on peripheral blood and bone marrow immune cells at E14.5.....	164
Figure 5.2.3. Effects of diet-induced obesity and TNF on peripheral blood immunophenotype at E18.5.....	166
Figure 5.2.4. Effects of excess gestational weight gain on dam and offspring measurements	168
Figure 5.2.5. Effects of excess gestational weight gain on maternal blood leukocytes at P21	169
Figure 5.2.6. Effects of excess gestational weight gain on maternal peripheral blood monocyte surface phenotype at P21	170
Figure 5.2.7. Effects of excess gestational weight gain on bone marrow monocytes at P21.....	171
Figure 5.2.8. Comparison of blood leukocyte populations in non-pregnant and pregnant mice	172

Chapter 6

Figure 6.1.1. Intestinal lengths and permeability in chow and HF-fed mice	184
Figure 6.1.2. Ussing chamber assessments of intestines in chow and HF-fed mice	186
Figure 6.1.3. Intestinal monocyte and macrophage prevalence in chow and HF-fed mice.....	188
Figure 6.1.4. Intestinal monocyte and macrophage cell counts in chow and HF-fed mice.....	190
Figure 6.1.5. Ileum macrophage populations in chow and HF-fed mice	191

Figure 6.1.6. Colon macrophage populations in chow and HF-fed mice.....	192
Figure 6.1.7. Colon and ileum macrophage proliferation in chow and HF-fed mice.....	194
Figure 6.1.8. TNF and IL-10 expression in ileum and colon macrophages of chow and HF-fed mice.....	200
Figure 6.1.9. Colon and ileum eosinophils, neutrophils, and CD4 ⁺ T cells	201
Figure 6.2.1. Intestine lengths and permeability in littermate WT and TNF ^{-/-} mice	209
Figure 6.2.2. Ileum monocytes and macrophages in littermate WT and TNF ^{-/-} mice	211
Figure 6.2.3. Colon monocytes and macrophages in littermate WT and TNF ^{-/-} mice	212
Figure 6.2.4. Ileum macrophage surface phenotype in littermate WT and TNF ^{-/-} mice	214
Figure 6.2.5. Colon macrophage surface phenotype in littermate WT and TNF ^{-/-} mice	215
Figure 6.3.1. Chow and HF microbiota effects on physiological measurements.....	222
Figure 6.3.2. Chow and HF microbiota effects on intestinal permeability and physiology	223
Figure 6.3.3. Chow and HF microbiota effects on prevalence of ileum or colon immune cells.....	225
Figure 6.3.4. Chow and HF microbiota effects on ileum or colon macrophage surface phenotype.....	226
Figure 6.3.5. Peripheral immunophenotype of chow and HF microbiota groups – prevalence.....	228
Figure 6.3.6. Peripheral immunophenotype of chow and HF microbiota groups – absolute cell counts	229
Figure 6.3.7. Peripheral blood Ly6C ^{high} monocyte characteristics in chow and HF microbiota groups.....	230

Figure 6.3.8. Bone marrow myeloid progenitors in chow and HF microbiota groups	232
Figure 6.4.1. Young and old SPF mouse colon physiology and macrophage populations	240
Figure 6.4.2. Young and old SPF mouse colon macrophage intracellular cytokines.....	241
Figure 6.4.3. Young and old germ free mouse intestinal physiology and colon macrophage prevalence	243
Figure 6.4.4. Cohousing young and old mice does not alter colon macrophage dynamics in old mice.....	244
Figure 6.4.5. Effects of young and old microbiota colonization on intestinal physiology and colon immune cell populations	246
Figure 6.4.6. Effects of young and old microbiota colonization on colon macrophages	247
Figure 6.4.7. Comparison of colon macrophage populations by biological sex and age in SPF and GF mice	249
Figure 6.5.1. Maternal intestinal physiological measurements and permeability	258
Figure 6.5.2. Maternal ileum and colon eosinophils, neutrophils, and CD4 ⁺ T cells	259
Figure 6.5.3. Maternal ileum and colon Ly6C ^{high} monocytes and total macrophages.....	260
Figure 6.5.4. Maternal ileum and colon macrophage prevalence and cell counts	262
Figure 6.5.5. Intestinal physiology and macrophage prevalence in non-pregnant GF mice and GF mice at E14.5	264

Chapter 7

Figure 7.1. Review of central thesis premise and areas of investigation	276
---	-----

List of Tables

Chapter 2

Table 2.1. Mouse diet allocation and composition by experiment cohort	42
Table 2.2. TNF genotyping PCR primers.....	43

Chapter 5

Table 5.1.1. Peripheral blood monocyte surface phenotype in WT mice fed HF vs chow diet	143
Table 5.1.2. Bone marrow monocyte surface phenotype in WT mice fed HF vs chow diet	148
Table 5.1.3. Blood monocyte surface phenotype in WT and TNF ^{-/-} mice fed HF diet	154
Table 5.2.1. Summary of effects of HF diet feeding in female mice	173

Chapter 6

Table 6.1.1. Surface marker expression of ileum macrophages from chow and HF-fed mice	196
Table 6.1.2. Surface marker expression of colon macrophages from chow and HF-fed mice	196
Table 6.3.1. Composition and variability of peripheral immunophenotype at export and after colonization of recipient chow and HF microbiota groups	227
Table 6.5.1. Summary of intestinal macrophage surface expression changes between HF-fed and chow-fed dams at P21	263

Chapter 7

Table 7.1 Summary of observations of ileum and colon macrophage populations.....	283
--	-----

List of Appendices

Chapter 2

Appendix I. Flow Cytometry Analysis - Myeloid and Lymphocyte Gating	60
Appendix II. Flow Cytometry Analysis - Bone Marrow Gating	61
Appendix III. Flow Cytometry Analysis - Intestinal Tissue Gating.....	62

Chapter 5

Appendix I. Surface phenotype changes of the Ly6C ^{high} to Ly6C ^{low} monocyte transition in the bone marrow, monocyte migration in blood, and monocyte to macrophage differentiation.....	177
Appendix II. Comparison of peripheral blood immunophenotype in age-matched non-pregnant non-lactating female mice and dams in lactation at P21	178

Chapter 6

Appendix I. Monocyte and macrophage progression of surface marker expression.....	268
Appendix II. Macrophage intracellular staining of TNF and IL-10	272
Appendix III. Comparison of macrophage populations in young naïve germ free mice, colonized mice, and SPF mice	273
Appendix IV. Colon macrophage prevalence in GF mice colonized with young or old microbiota and young and old SPF mice.....	274
Appendix V. Intestine lengths and macrophage populations in chow-fed non-pregnant non-lactating female mice and in dams at P21	275

Declaration of Academic Achievement

In accordance with the Guide for the Preparation of Theses at McMaster University, this thesis document is an accurate summary of the research that I have conducted during my time as a doctoral candidate. This thesis and the manuscripts included within were written entirely by myself with editing input provided by Dr. Dawn Bowdish and Dr. Deborah Sloboda. Some of the work presented herein involved collaborations with other students and scientists at McMaster University. Details of my contributions, and contributions of collaborators, are described below.

Chapter 3: I am the primary author of this manuscript. I performed all flow cytometry experiments for female mouse data and 30 male mice, and Dr. Christian Schulz performed experiments and contributed data for 37 male mice. I collated and analyzed the data, performed all statistical analyses, generated all figures and tables, and wrote the manuscript. The paper was conceptualized by Dr. Bowdish, Dr. Sloboda, and myself. Dr. Bowdish and Dr. Sloboda provided guidance and editorial input at every stage of the writing process. Dr. Ma provided advice, reviewed, and approved the approach for statistical analysis.

Chapter 4: I am a primary author of this manuscript, along with Dr. Kevin Foley and Avee Naidoo. The paper was originally conceptualized by Dr. Schertzer, Avee Naidoo, and Dr. Foley, but was redesigned by Dr. Schertzer, Dr. Bowdish, Dr. Sloboda, Dr. Foley, and myself. I performed the experiments in Figures 1 and 3. I compiled and analyzed all experimental data, performed all statistical calculations, made all graphs, tables, and

figures, and wrote the final version of the manuscript with Dr. Schertzer, Dr. Sloboda, and Dr. Bowdish. Dr. Foley contributed to experimental design and performed experiments that contributed to Figures 3 to 6 with myself or Avee Naidoo. Dr. Christian Schulz and Dr. Trevor Lau performed the experiments in Figure 2. Avee Naidoo contributed to experimental design and experiments in Figures 4 to 6, and she wrote an early version of the manuscript which appeared in her MSc thesis with data from Figures 4 to 6 and human cohort data from a collaboration between Dr. Bowdish and Dr. Mark Loeb (McMaster University), which was not included in the final version of the paper. Dr. Dessi Loukov provided invaluable insight and critical input on experimental methods and analysis.

Chapter 5: I performed all experiments and analyzed and interpreted all data, with the following exceptions. Dr. Kevin Foley (Schertzer lab) assisted with GTT, insulin during GTT, and ITT tests, and the IL-6 ELISA in Section 5.1 (Figure 5.1.1I, K-M). Dr. Brittany Duggan (Schertzer lab) also assisted with the insulin during GTT test. Dhanyasri Maddiboina (thesis student in the Bowdish lab) contributed to Section 5.1 Figure 5.1.1G-H (measurements of adipocyte cross-sectional area and macrophage counts). For Section 5.2 Figure 5.2.8, Christian Bellissimo (Sloboda lab) generated E6.5 pregnancies and I collected blood for flow cytometry analysis. For Section 5.2 Figures 5.2.1 and 5.2.2, as well as Figure 5.2.8 E14.5 data, I performed all animal work and generated the E14.5 pregnancies, and Kate Kennedy, Brendan Patterson, Patrycja Jazwiec, and Christian Bellissimo (Sloboda lab) assisted with maternal and fetal dissections. For Section 5.2 Figures 5.2.3 and 5.2.8, Kate Kennedy generated the E18.5 pregnancies, and I collected

blood for flow cytometry analysis. For Section 5.2 Figures 5.2.4 to 5.2.7, and the lactation data depicted in the accompanying Appendix II, Dr. Tatiane Ribeiro and Brianna Kennelly (Sloboda lab) performed mating and mouse care up to experimental endpoint, and I collected blood for flow cytometry analysis.

Chapter 6: I performed all experiments, analyzed, and performed all statistical assessments and interpreted all data, with the following exceptions. Dr. Kevin Foley (Schertzer Lab), Kate Kennedy, and Jessica Wallace (Sloboda Lab) assisted with the *in vivo* permeability assays in Section 6.1 (Figure 6.1.1). Jennifer Jury (Verdú Lab) performed the *in vitro* permeability Ussing chamber experiments and data analysis presented in Section 6.1 (Figure 6.1.2) and Section 6.3 (Figure 6.3.2). Erica DeJong, Dr. Janine Strehmel, and Braeden Cowbrough (Bowdish lab) and Erica Yeo (Sloboda Lab) assisted with the *in vivo* permeability experiments in Section 6.2 (Figure 6.2.1) and Section 6.3 (Figure 6.3.2). In Section 6.4, Erica DeJong established the aging mouse and germ free mouse colonization cohorts and I collected tissues at endpoint for Figures 6.4.4 to 6.4.6. Netusha Thervarajan conducted the experiments in Figure 6.4.2A-C. For Section 6.5 and the accompanying Appendix V, Dr. Tatiane Ribeiro and Brianna Kennelly (Sloboda lab) performed mating and mouse care up to experimental endpoint, and I collected intestinal tissues for flow cytometry analysis. In Section 6.5, Dr. Tatiane Ribeiro, Kate Kennedy, Patrycja Jazwiec, Brianna Kennelly and myself performed the *in vivo* permeability assay in Figure 6.5.1.

List of Abbreviations

The following abbreviations were used in addition to those commonly accepted
for units of measure and quantities.

Ab	antibody
ANOVA	analysis of variance
ATP	adenosine triphosphate
BMI	body mass index
bp	base pair(s)
BSA	bovine serum albumin
CBC	complete blood count
CCL	chemokine (C-C motif) ligand
CCR	C-C chemokine receptor
CD	cluster of differentiation
C/EBP β	CCAAT/enhancer-binding protein β
cKit	tyrosine-protein kinase Kit (CD117/SCFR)
cMoP	common monocyte progenitor
CMP	common myeloid progenitor
CO ₂	carbon dioxide
CRP	C-Reactive Protein
CSF1	colony-stimulating factor 1
CSF1R	colony-stimulating factor 1 receptor, CD115
CXCL	C-X-C motif ligand
CXCR	C-X-C motif receptor
CX ₃ CL ₁	CX3C chemokine ligand-1 (fractalkine)
CX ₃ CR ₁	CX3C chemokine receptor 1
DAMP	danger-associated molecular pattern
DNA	deoxyribonucleic acid
dNTPs	deoxynucleotides
DSS	dextran sodium sulphate
DTT	dithiothreitol
E__	embryonic gestational day (e.g. E0.5)
EDTA	ethylenediaminetetraacetic acid
ELISA	enzyme-linked immunosorbent assay
FBS	fetal bovine serum
FITC	fluorescein isothiocyanate
GMP	Granulocyte-Monocyte Progenitor
GF	germ free (mice)
H ₂ O ₂	hydrogen peroxide
HEPES	4-(2-hydroxyethyl)-1-piperazineethanesulfonic acid
HF	high fat (diet)
HIV	human immunodeficiency virus (HIV-1)
HLA-G	human leukocyte antigen G

HSC	hematopoietic stem cell
HSP	heat shock protein
IBD	inflammatory bowel disease
ICAM-1	intercellular adhesion molecule 1
IFN	Interferon (e.g. IFN γ)
Ig	Immunoglobulin (e.g. IgA)
IKK	I κ B kinase
IL	interleukin
ILC	innate lymphoid cell
i.p.	intraperitoneal
JNK	c-Jun N-terminal kinase
kcal	kilocalories
KO	knockout
LBP	lipopolysaccharide binding protein
Lin ⁻	lineage negative (cell)
LPS	lipopolysaccharide
Ly	lymphocyte antigen
Ly6C	lymphocyte antigen 6 complex, locus C1
Ly6G	lymphocyte antigen 6 complex, locus G6D
LTA	lipoteichoic acid
MDP	macrophage and dendritic cell progenitor
MyD88	myeloid differentiation primary response gene 88
CSF1	macrophage colony-stimulating factor 1
CSF1R	macrophage colony stimulating factor 1 receptor (CD115)
MerTK	tyrosine kinase Mer
MHC	major histocompatibility complex (e.g. MHCII)
MPS	mononuclear phagocytic system
Nf κ B	nuclear factor kappa-light-chain-enhancer of activated B cells
NK	natural killer (immune cell)
NLR	nucleotide-binding oligomerization domain-like receptor
NLRP3	NOD-like receptor pyrin domain-containing 3
NO	nitric oxide
NOD	nucleotide-binding oligomerization domain
NP	non-pregnant
P _{__}	post-natal day (e.g. P21)
PCA	principal component analysis
PAMP	pathogen-associated molecule pattern
PBMC	peripheral blood mononuclear cell
PBS	phosphate buffered saline
PCR	polymerase chain reaction
PKR	protein kinase R
PRR	pattern recognition receptor
RAGE	receptor for advanced glycation end products
RES	reticuloendothelial system

RLR	retinoic acid-inducible gene-I-like receptor
ROS	reactive oxygen species
Sca1	stem cell antigen 1 (Ly6A/E)
SCFA	short chain fatty acid
scRNAseq	single-cell RNA (ribonucleic acid) sequencing
SDS	sodium dodecyl sulphate
SPF	specific pathogen free
TAE	tris-acetate EDTA (buffer)
TGFβ	transforming growth factor beta
Th	T helper (cell; e.g. Th1, Th2)
TIM4	T-cell immunoglobulin mucin protein 4
TLR	toll-like receptor
TNBS	2,4,6-trinitrobenzene sulfonic acid
TNF	tumour necrosis factor
TNFR	tumour necrosis factor receptor (e.g. TNFR1, TNFR2)
T _{reg}	T regulatory cell
TREM	triggering Receptors Expressed on Myeloid cells (e.g. TREM2)
TRAF	tumor necrosis factor receptor (TNFR)-associated factor (e.g. TRAF6)
TSLP	thymic stromal lymphopoietin
Tris	tris(hydroxymethyl)aminomethane
wk	week
WT	wildtype (mice)

Chapter 1. Introduction

1.1 Inflammation

Inflammation is a biological response by host soluble and cellular mediators that provides defense against pathogens and is necessary for many physiological processes, but in itself has the potential to cause tissue damage and disease¹. Inflammation is instigated in response to perturbations of homeostasis, and involves complex immune-mediated processes that coordinate to restore balance. The magnitude of the response is dependent on biological sex, age, and genetics, as well as an individual's health status, and all of these factors also influence homeostasis in the absence of inflammation^{1,2}. Inflammation is characterized as having an acute or chronic duration.

Acute Inflammation

Acute inflammation is a strong but self-resolving response to injury or infection. Classical clinical symptoms of acute inflammation include redness and swelling, with heat, pain, and loss of function. Acute inflammation elicited by an infectious microorganism activates innate immune cells, such as tissue-resident macrophages, which produce chemokines (to recruit additional immune cells) and cytokines (to activate and instruct immune cells)². Macrophages often phagocytose pathogens to separate them from the environment and cause cell death¹. The acute inflammatory response may also induce host hyperglycemia and peripheral insulin resistance, which support macrophage metabolic and functional reprogramming^{3,4}. Innate immune cell recruitment and antimicrobial activities are usually sufficient to eradicate the infectious agent, and this non-specific acute response also provides time for the generation of a pathogen-specific

response by adaptive immune cells (i.e. T cells, B cells, and antibodies), should the innate immune response be insufficient.

The soluble effector products secreted by immune cells during the inflammatory response do not differentiate between target pathogens, infected cells, or bystander host cells, so uninfected host cells in the proximity can become damaged⁵. Too little inflammation can be ineffective, allowing the pathogen to spread beyond its initial site of infection, and too much inflammation can result in septic shock^{2, 5}. However, as acute inflammation is generally highly controlled and self-limiting, the benefits usually outweigh the consequences of short term repairable damage. Tissue repair mechanisms are therefore a crucial component of the protective acute inflammatory response. Just as macrophages are involved in the initiation of the inflammatory response, they are also involved in its resolution, removing dead cells, secreting anti-inflammatory cytokines, and facilitating tissue remodelling and repair^{6, 7, 8}.

While inflammation is classically considered to be initiated in response to pathogens, innate immune cells respond to the presence of diverse exogenous or endogenous factors including pathogen-associated molecular patterns (PAMPs, e.g. LPS, LTA, peptidoglycan, flagellin) derived from pathogens or commensal bacteria^{9, 10}, non-microbial exogenous factors like allergens and toxins^{1, 11}, or damage/danger-associated molecular patterns (DAMPs, e.g. fibrinogen, ATP, HSPs, DNA, histones, defensins) derived from host cells^{12, 13}. PAMPs and DAMPS bind to pattern recognition receptors (PRRs, e.g. TLRs, NLRs, RLRs, RAGE, and C-type lectin receptors) present on innate immune cells¹⁰. PRR binding activates transcriptional and post-translational changes that lead to the release of chemokines and cytokines that promote leukocyte recruitment and

activation. DAMPs are often nuclear or cytosolic molecules released from host cells in response to trauma, stress, hypoxia, and/or functional dysregulation^{10, 12}. A self-limiting localized DAMP-driven inflammatory response (often referred to as ‘sterile’ or ‘non-infectious’) can be used to recruit immune cells, without eliciting clinical signs of an infection-driven inflammatory response, to facilitate tissue repair and maintenance.

Chronic Inflammation

Chronic inflammation occurs when the inflammatory trigger, whether PAMP, DAMP, or another factor, is not removed. As homeostasis is continually disturbed, there is sustained activation and recruitment of immune cells to the site of inflammation, without resolution. Although this inflammation is generally of lower magnitude than in an acute response, sustained immune activation can result in local pathology from cellular damage and/or restructuring of tissue (i.e. fibrosis, formation of granulomas and/or tertiary lymphoid tissues)^{14, 15, 16}, as well as spread to have a multi-organ and systemic impact, leading to dysregulation of immune and metabolic signalling pathways⁴. Chronic inflammation may potentially alter hematopoiesis¹⁷, epigenetic regulation^{18, 19, 20}, and trigger cellular senescence²¹, which interferes with acute inflammatory responses to pathogens, immune tolerance, and tissue maintenance. Chronic inflammation is therefore a serious complication of infection with pathogens that are not effectively removed by an acute response, including HIV and *Mycobacterium tuberculosis*^{15, 22, 23}. Sterile chronic inflammation, and its alterations to monocyte and macrophage numbers and functions, are associated with a plethora of diseases including obesity^{24, 25}, but are also a component of biological aging^{26, 27}, and sterile inflammation also accompanies normal maternal adaptations in pregnancy^{28, 29}.

Inflammation in Obesity

The World Health Organization reported in 2016 that globally at least 1.9 billion adults were overweight (~39% of the global population) and 650 million were obese (~13% of the global population), and these numbers are only expected to rise³⁰. Adults with a body mass index (BMI) of 18.5-24.9 kg/m² are defined as being a healthy weight, 25-30 kg/m² are overweight, and those with a BMI >30 kg/m² are obese³¹. Obesity can lower health-related quality of life^{32, 33} and its comorbidities pose a serious personal and financial cost to individuals, their families, and the health care system^{34, 35, 36}. Obesity is a risk factor for other chronic inflammatory disorders including type 2 diabetes, cardiovascular disease, and non-alcoholic fatty liver disease^{37, 38}, musculoskeletal disorders (from increased stress on tendons and joints)³⁹, neurological disorders^{40, 41}, certain cancers and their metastasis (i.e. endometrial, ovarian, breast, liver, gallbladder, kidney, colon)^{42, 43}, as well as reduced vaccine efficacy^{44, 45}, all of which contribute to increased risk of morbidity and early mortality^{31, 46}. While there is increasing recognition that improvements in physical and mental health and well-being, not only weight loss (i.e. by changing diet and physical activity), are important in management of obesity as a complex chronic disease^{47, 48}, a better understanding of the biological premise of obesity is of immediate importance to gain insight into causality to design approaches for intervention.

Obesity fundamentally occurs from a long-term imbalance between energy intake and energy expenditure. The etiology of obesity is multifactorial, as genetic, environmental, sociocultural, endocrine, neurological, microbiota-associated, and other modifiable and non-modifiable risk factors, have been identified^{25, 46}. Obesity is

characterized by an expansion of adipose tissue by hypertrophy (adipocyte expansion due to accumulation of triglycerides) and hyperplasia (adipocyte proliferation)⁴⁹. This remodelling of adipose tissue is accompanied by an accumulation of pro-inflammatory macrophages^{50, 51}, which are activated by an unknown inflammatory signal. These macrophages are derived to a small extent from local proliferation and resident hematopoietic stem cells^{50, 51, 52, 53}, but most are recruited from circulating monocyte precursors^{54, 55, 56, 57}. Adipocytes, and to a greater extent pro-inflammatory macrophages, promote a chronic inflammatory response within adipose tissue by secreting pro-inflammatory cytokines including TNF α , IL-6 and IL-1 β , as well as chemokines to recruit additional monocytes and other immune cells into the expanding adipose tissue^{50, 55, 56, 58, 59, 60}. Macrophages can act as antigen-presenting cells and promote T cell proliferation and Th1-type pro-inflammatory cytokine responses⁶¹. Macrophages also facilitate activation of evolutionarily conserved IKK⁶², JNK⁶³, PKR⁶⁴, and Wnt^{65, 66} signalling pathways in adipocytes and immune cells, which initiate transcription of pro-inflammatory genes, and suppress genes that contribute to control of cellular metabolism⁶⁷. Continued pro-inflammatory cytokine production and local immune and metabolic dysfunction eventually lead to systemic low-grade chronic inflammation, insulin resistance, and other features of metabolic syndrome (i.e. hyperglycemia, hyperlipidemia, and hypertension)^{25, 68, 69}.

Most studies of obesity and chronic inflammation focus, understandably, on macrophages and other immune cell populations in adipose tissue, as there is a causal role of adipose tissue inflammation in systemic inflammation and insulin resistance. However, it is clear that there are extensive inter-organ effects of obesity, and that both intra-organ

paracrine signalling and inter-organ endocrine signalling (i.e. by factors such as tissue-secreted cytokines^{70, 71, 72}, miRNA-containing exosomes^{73, 74}, LPS⁷⁵, and free-fatty acids^{72, 76}) are crucial for the development of systemic inflammation and metabolic dysfunction. For example, mouse models of adipocyte-specific gene knockouts can modulate insulin resistance in the liver or muscle^{77, 78, 79, 80, 81}, and bacterial products from the gut can enter circulation and promote inflammation within other metabolic organs^{75, 82, 83, 84}. Accordingly, increased activation of pro-inflammatory signalling pathways and altered tissue macrophage populations in the context of obesity have been detected within other metabolic tissues including the liver⁸⁵, skeletal muscle⁸⁶, pancreatic islets⁸⁷, the central nervous system⁸⁸, and the gastrointestinal tract⁸⁹.

Inflammation in Aging

Life expectancy at birth in Canada was 80 years for males and 84 years for females as of 2017⁹⁰. From 2010 to 2063, the proportion of people over 65 will increase from less than 15% to over 25%⁹¹. Canadians are living longer, but it is important to ensure that individuals also experience healthy aging. In a study examining the global burden of disease across 187 countries, while life expectancy increased between 1990 and 2010, there was also an increase in the number of healthy years lost to disability⁹².

From an immunological perspective, aging, like obesity, is characterized by a state of chronic low-grade inflammation referred to as ‘inflammaging’²⁶. Inflammaging is thought to be the combined effect of lifelong antigenic exposure and normal cellular changes with aging. Age-associated inflammation contributes to and is influenced by damage to cellular functions (i.e. genomic instability, epigenetic alterations, telomere attrition, loss of proteostasis) and antagonistic responses to cellular damage (i.e.

mitochondrial and stem cell dysfunction, detrimental changes to nutrient sensing and intercellular communication, and initiation of cellular senescence)^{93, 94}. These factors contribute to immunosenescence, involving involution of the thymus^{95, 96} and bone marrow^{97, 98, 99}, which decreases naïve T cells and B cells, with concomitant expansion of memory and effector T cells¹⁰⁰. To contrast, there is an enhancement in bone marrow and extramedullary splenic myelopoiesis, leading to a progressive increase of circulating neutrophils and monocytes^{99, 101, 102}.

Age-associated chronic inflammation also influences the ability of the immune system to respond to endogenous and exogenous stimuli. Aging does not necessarily result in a decline in immune function, but rather a gradual dysregulation of immune response efficiency and effectiveness that can result in prolonged inflammation and tissue pathology^{103, 104}. Certain responses remain ‘normal’, others are weakened or lost, and some are amplified. These changes, in association with chronic inflammation, can impair defense against infection^{105, 106, 107}, and efficiency of tissue repair^{104, 108}, and may lead to overproduction of inflammatory mediators¹⁰⁹, loss of tolerance and recognition of ‘self’ leading to autoimmunity¹¹⁰, subclinical persistent infections (e.g. cytomegalovirus)¹¹¹, poor vaccine responses^{105, 106}, and accelerated cellular aging^{93, 112}.

Age-associated inflammation is a major predictor of morbidity and mortality and decreased quality of life^{27, 106, 112}. While even clinically healthy individuals have elevated inflammation with increasing biological age, the onset and course of age-associated disorders are influenced by levels of circulating pro-inflammatory cytokines, including TNF, IL-6, CRP and IL-1 β ^{27, 113, 114, 115, 116}. Ten-year all-cause mortality is positively correlated with serum IL-6 and TNFR1 in older adults¹¹⁷. Consequently, chronic

inflammation is a natural biological component of aging, and studying its effects is of paramount importance to better understand its contributions to unhealthy aging.

Inflammation in Pregnancy

Pregnancy and lactation require extensive and highly coordinated temporal adaptations to maternal physiology to ensure adequate nutrient and oxygen supply for fetal growth, involving changes to morphology, size, and responsiveness of tissues and organs, which alter cardiovascular, pulmonary, musculoskeletal, gastrointestinal, metabolic, and immune functions^{118, 119, 120, 121, 122, 123}. These adaptations start early in pregnancy and continue throughout lactation, and are mediated by placentally-derived hormones, including prolactin and placental lactogen, sex hormones like estradiol and progesterone, and neuropeptides including serotonin, melatonin and oxytocin^{124, 125, 126}. Placental cytokines, soluble HLA-G, and placental extracellular vesicles like exosomes, microvesicles, and microparticles, are also mediators of maternal adaptations^{28, 29, 127}. These antigenically ‘foreign’ fetal/placental-derived factors have the potential to elicit a maternal inflammatory response.

The pioneering transplantation researcher Peter Medawar recognized that pregnancy represents a complex immunological paradox, in which the maternal immune system must continue to provide protection from foreign pathogens yet tolerate the semi-allogeneic fetus for 40 weeks¹²⁸. Maternal immunological adaptations to pregnancy involve extensive local and systemic immunomodulation, not suppression, of immune responses. These adaptations are temporally regulated and integrate signals from the mother, the fetus, and the environment^{120, 129, 130}. Controlled inflammation is therefore a crucial component of normal maternal pregnancy and lactational adaptations. Local

immunomodulation at the maternal-fetal interface in early pregnancy involves an inflammatory response in the uterus^{131, 132, 133}, with recruitment of leukocytes, such as monocytes, to assist in implantation, remodelling, growth, and differentiation of maternal endometrial tissue into the decidua, as well as the development of the placenta^{134, 135}. Subsequently, maintenance of an anti-inflammatory region at the maternal-fetal interface is necessary to ensure maternal tolerance for fetal growth and development^{136, 137}. In the late third trimester, a localized inflammatory response is involved in parturition¹³⁸.

The kinetics of circulating immune cells and systemic inflammation change throughout pregnancy in a chronological manner^{120, 129, 130, 139}. Longitudinal studies of peripheral whole blood have reported that expression of genes and proteins related to the host immune response continuously increase from week 10 through to week 40 of pregnancy^{140, 141}. This is in agreement with studies reporting increases of peripheral maternal/placentally-derived cytokines including IFN γ , IL-6 and TNF^{120, 142, 143, 144}, as well as fetal cells^{145, 146}, and other placental particles (e.g. microvesicles and exosomes)^{147, 148}, across gestation. These changes result in a state of gradually increasing maternal systemic sterile inflammation, and elevation of circulating innate immune cells with enhanced phagocytic activity, activation, and pro-inflammatory cytokine production^{130, 139, 142, 144, 149, 150, 151, 152, 153, 154, 155}. This state of cellular inflammation is not dissimilar in some respects to that observed in non-pregnant women with acute inflammatory sepsis¹⁴². However, this maternal inflammation does not cause harm. Rather, it seems to be a necessary physiological adaptation. An increase in systemic maternal inflammation augments innate immune defense against pathogens, and is thought to facilitate tissue remodelling and changes to maternal metabolism, perhaps by

activation of inflammatory pathways to induce insulin resistance^{28, 29, 156}. This systemic inflammation, with features of both acute and chronic inflammation, is confined to the period of pregnancy and possibly lactation, though limited data exist regarding inflammation during lactation. However, this inflammation must be balanced against other pregnancy adaptations and maternal-fetal tolerance, so pre-existing chronic inflammatory disorders, including obesity, have a detrimental impact.

Globally, over half of women enter pregnancy overweight or obese^{35, 157}, and/or gain excess gestational weight¹⁵⁸. A study that included over 500 women from Southwestern Ontario, including clinics in Hamilton, found that over half of women gain more weight than is medically recommended during pregnancy¹⁵⁹. Epidemiological data supports a synergistic relationship between obesity and pregnancy, as women with pregravid obesity are more likely to develop metabolic complications like gestational diabetes mellitus (GDM), as well as complications antenatally (e.g. congenital abnormalities, pre-eclampsia, pre-term birth), intrapartum (e.g. stillbirth, surgery), and postpartum (e.g. hemorrhage, infection)^{160, 161, 162, 163}. Pregravid obesity is associated with an increased maternal and child lifelong risk of obesity, as well as cardiovascular, neurological, and metabolic disorders, often associated with chronic inflammation^{164, 165, 166, 167, 168}. The mechanisms by which obesity has negative impacts on maternal and child health remain poorly understood.

From a metabolic perspective, early pregnancy adaptations in healthy individuals promote an anabolic state, involving an increase in maternal pancreatic β -cell mass, lowering the threshold for glucose-stimulated insulin production, and increasing circulating insulin levels^{125, 169, 170, 171}, as well as augmenting lipid storage in adipose

tissue, leading to an increase in body weight and adiposity¹⁷², and accumulation of glycogen in the liver^{171, 173}. There is a gradual increase in maternal appetite despite elevation of circulating levels of leptin and insulin^{169, 174}. In the latter half of pregnancy, there is a partial reversal of earlier adaptations, including a decrease in maternal insulin sensitivity in liver, skeletal muscle, and adipose tissue, as well as an increase in hepatic gluconeogenesis and adipose tissue lipolysis, to maximize glucose and lipid availability for the fetus^{125, 126, 170, 171}.

When women are overweight or obese prior to pregnancy, or gain excess weight during gestation, crosstalk between maternal and placental cytokines and other endocrine and immune signalling factors appears to become dysregulated^{28, 29, 175, 176, 177, 178, 179, 180}. In obese women and experimental animals, the metabolic responses to pregnancy are often exaggerated, with a greater degree of hyperglycemia and hyperinsulinemia in late gestation^{181, 182, 183}. Research suggests that pregnancy in obese individuals, similar to the obese non-pregnant state, increases circulating pro-inflammatory cytokines and chemokines^{184, 185, 186}, and adipose and placental tissue inflammation^{175, 178, 179, 187, 188, 189}. Therefore, pre-gravid obesity and/or excess gestational weight gain may dysregulate maternal physiological, metabolic, and immunological adaptations, with the potential for lifelong detrimental effects on maternal and child health.

1.2 Macrophages

Macrophage Discovery and Functions

Elie Metchnikoff described macrophages in 1892 after he inserted thorns into starfish larvae and observed cells that surrounded and engulfed the foreign material¹⁹⁰.

Metchnikoff's later research identified that macrophages internalize and kill bacteria as part of the host defense against pathogens, eliminate vestigial cells in embryogenesis, and maintain tissue homeostasis through phagocytosis of senescent and damaged host cells^{191, 192, 193, 194}. He also recognized that macrophages could recruit other leukocytes to sites of tissue injury or infection. Macrophages are now recognized as innate immune cells that are found in the majority of tissues in the body.

The importance of macrophages in host homeostasis and the inflammatory response is clear from their high conservation across species, despite having evolved over 500 million years ago¹⁹⁵. However, macrophages also exhibit considerable heterogeneity in their functions and regulation. They sense and respond to microenvironment cues including metabolic changes, tissue damage, and microorganisms, while supporting surrounding cells and tissue structures. Macrophages are multitaskers, and perform a variety of functions including those described by Metchnikoff in the inflammatory response (e.g. phagocytosis, secretion of soluble mediators of inflammation (i.e. cytokines and chemokines, NO and ROS), antigen presentation, and lymphocyte activation), resolution of inflammation and routine tissue maintenance (e.g. phagocytosis of apoptotic and necrotic cells and cellular debris, and production of factors to promote tissue proliferation, remodelling, and angiogenesis), and/or regulation of vascular, smooth muscle, and neuronal networks^{195, 196}. Mice with systemic genetic knockout of macrophage growth and differentiation factors, such as CSF1, have severe developmental defects within organs, tissues, and bone marrow^{197, 198, 199, 200, 201}. Therefore, macrophages have diverse and critical tissue-specific roles in homeostasis, as well as in initiation and resolution of the acute inflammatory response to pathogens.

Macrophage Ontogeny – RES and MPS

In the early 20th century, over 30 different names were used to identify phagocytic cells, in part due to their diverse morphologies and tissue localization within anatomically distinct locations. Karl Albert Ludwig Aschoff proposed in 1924 that mononuclear phagocytic cells, like monocytes and macrophages, could be classified within a Reticuloendothelial System (RES) by their appearance after staining with various histological dyes²⁰². The RES proposed that phagocytes and endothelial cells shared a common tissue-derived progenitor. However, it became apparent that the morphology and functions of cell populations within the RES were highly heterogeneous^{203, 204}. In addition, subsequent *in vivo* studies of radioisotope labelling, monocyte transfer, parabiosis, and radiation chimeras, and *in vitro* studies of blood monocyte differentiation, showed that circulating monocytes could extravasate and differentiate into tissue macrophages^{203, 205, 206, 207, 208, 209}.

A new classification system, the Mononuclear Phagocyte System, was developed in 1972. The premise of the MPS was that adult tissue macrophages are continuously and solely replenished by bone marrow-derived monocytes that infiltrate and differentiate into macrophages incapable of proliferation²⁰⁵. The MPS proposed that hematopoietic stem cells in the bone marrow differentiate into precursors of mononuclear phagocytes, and then circulating monocytes, which are precursors for tissue macrophages. However, Metchnikoff had noted far earlier that phagocytes were present in starfish embryos¹⁹⁰, and this was later also observed in mouse embryos²¹⁰, implying an origin independent of blood monocytes, but neither the RES nor MPS fully explained this observation.

Macrophage Ontogeny – MPS, Embryonic Origins and Core Programming

In the past decade there has been a reconsideration of tissue macrophage ontogeny. Using a combination of parabiosis, genetic fate mapping, chemical or antibody-based depletion methods, radiation chimeras, adoptive transfer, and Cre-recombinase lineage tracing techniques, researchers have conclusively shown that most adult tissues contain a significant proportion of long-lived macrophages of embryonic origin, derived from the fetal yolk sac or fetal liver, that may be maintained through self-proliferation^{211, 212, 213, 214}. These tissue macrophages seed the entire embryo *in utero* once the circulatory system is established. While an embryonic origin of macrophages is in opposition to the MPS²⁰⁵, most adult tissues also contain macrophage populations from blood monocytes derived from bone marrow after birth²¹⁴.

There are temporal and spatial components to the post-birth accumulation of bone marrow monocyte-derived macrophages in tissues under homeostasis. Most tissues have mixed populations of macrophages of distinct ontogeny, with specific tissue niche requirements for monocyte recruitment and tissue-resident macrophage self-renewal²¹⁴. Adult tissues have macrophage populations that are not replenished by steady-state monocyte recruitment (e.g. microglia of the brain^{215, 216, 217}, alveolar macrophages of the lungs^{218, 219, 220}, Langerhans cells of the epidermis^{221, 222, 223}, certain cardiac macrophages^{224, 225, 226}, and Kupffer cells of the liver^{227, 228, 229}), macrophages replaced by low steady-state monocyte recruitment (e.g. pancreas²³⁰, heart^{224, 226}, kidney²³¹, spleen^{228, 229}, peritoneum²³²), and other tissues have fast steady-state replenishment of some macrophage populations by monocyte recruitment (e.g. dermis^{233, 234}, gut^{235, 236}).

Comparative transcriptomic studies of tissue macrophages led by the Immunological Genome Project Consortium have identified core or lineage ‘macrophage programming’ genes and accompanying transcription factors^{237, 238, 239, 240, 241, 242}. These lineage-determining transcription factors mediate gene expression of common macrophage surface markers (e.g. CD64, F4/80, MerTK, CSF1R), and expression of genes required for common macrophage functions, such as phagocytosis. This programming is thought to help macrophages of bone marrow origin acquire the same tissue niche-specific functional specialization, transcriptional profiles, enhancer landscapes and epigenetic regulation (i.e. through DNA methylation, chromatin structure, and histone modifications), and self-maintenance capacity, of the embryonic origin tissue-resident macrophages that they may replace^{212, 218, 238, 239, 243, 244, 245, 246, 247}. These findings have been corroborated with whole-tissue transplantation studies, which have shown that macrophages within donor heart²⁴⁸, liver²⁴⁹, and lung^{249, 250} tissues can self-maintain for years, though there is gradual replacement with recipient monocyte-derived macrophages. Studies on peritoneal macrophages suggest that biological sex may influence the composition of adult and embryonic origin tissue macrophage populations²³².

Comparative transcriptomic studies also highlighted significant differences in macrophage gene expression between tissues, irrespective of embryonic or monocyte origin, suggesting that local environmental stimuli are crucial in modulating macrophage fate in addition to transcription factors and enhancers that control conserved macrophage programming^{212, 239, 240, 242, 243, 245, 251}. Environmental stimuli include any entity that is capable of being ‘recognized’ by a macrophage, including immune complexes, apoptotic cells, oxygen and nutrients, glucocorticoids, growth factors, hormones and cytokines,

microbes and microbial products, and nucleotide derivatives. Macrophage interactions with surrounding stromal, epithelial, or endothelial cells, and the size and structural complexity of the tissue itself, also influence their characteristics^{211, 252}.

Accordingly, when isolated and cultured, tissue macrophages rapidly lose their tissue-specific transcriptomic signatures and phenotype²⁴⁵. This transcriptional plasticity has also been confirmed by *in vitro* experiments polarizing macrophages to pro-inflammatory or anti-inflammatory states and *vice versa*²⁵³. Transplanted healthy macrophages or bone marrow progenitors can fulfill tissue-specific functions in treatment of mouse models of hereditary pulmonary alveolar proteinosis^{254, 255}, further supporting the concepts that local immune cell and tissue-derived factors, and cell-cell interactions, regulate macrophage population recruitment, prevalence, proliferative capacity, and heterogeneous functions, between tissues and within tissue-specific niches^{211, 252}. However, it is important to note that adult and embryonic origin macrophages may have different functions during homeostasis or inflammation within the same tissue, as has been reported from studies of cardiac macrophages^{224, 225}.

Macrophage Identification

Macrophages are classically described in mice as being F4/80⁺ sessile mononuclear cells that contain an abundant cytoplasm with large vacuoles and lysosomal granules²⁵⁶. *In vitro* studies of bone marrow-derived macrophages showed that macrophage phenotype and activation (as indicated by changes in cytokine production) is altered in response to cytokines like IFN γ , IL-4, or IL-13^{257, 258, 259}, bacterial products like LPS²⁶⁰, growth factors like GM-CSF or CSF1²⁶¹, hormones²⁶¹, and manipulation of cellular metabolism^{257, 260, 262}. These studies led to the widespread use of descriptors of

macrophage activation including M1/M2, pro-/anti-inflammatory, classical/alternate, ‘metabolically activated’, or subdivisions thereof, according to experimental procedures²⁶³. While the M1/M2 dichotomy is ubiquitous in scientific literature, it has been increasingly acknowledged by the research community that tissue macrophage characteristics are quite different *in vitro* compared to *in vivo*^{263, 264, 265}. Moreover, these classification schemes were defined prior to the consensus that most tissue macrophage populations are of mixed embryonic and adult bone marrow origin.

Genome-wide transcriptional profiling techniques, multiparameter flow cytometry analysis, and histological and intravital imaging techniques, in addition to identifying core genes and functions, have recently revealed unique surface markers and morphological characteristics that can be used to identify and differentiate macrophages in distinct anatomical locations^{237, 240, 241, 242, 244, 266, 267, 268}. Simultaneously, there has been more consideration of environmental signals that may influence tissue macrophage characteristics and maintenance, as well as metabolism. As a consequence, there has been more focus on tissue-specific identification of phenotype and functions of macrophage populations in homeostasis and disease, while acknowledging macrophage ontogeny and the monocyte origins of adult bone marrow-derived macrophages.

1.3 Monocytes

Monocyte Discovery and Ontogeny

The word ‘monocyte’ was coined by Artur Pappenheim 110 years ago to describe a non-granular phagocytic mononuclear cell population in blood smears²⁶⁹. Monocytes are now often characterized as innate immune cells that arise from hematopoietic

progenitors within the adult bone marrow, egress into peripheral blood, and replenish tissue macrophage populations¹⁹⁶. Following the MPS, within the bone marrow a Common Myeloid Progenitor (CMP), from an unidentified hematopoietic stem cell (HSC) precursor, is thought to give rise to all myeloid cell lineages (Figure 1.1).

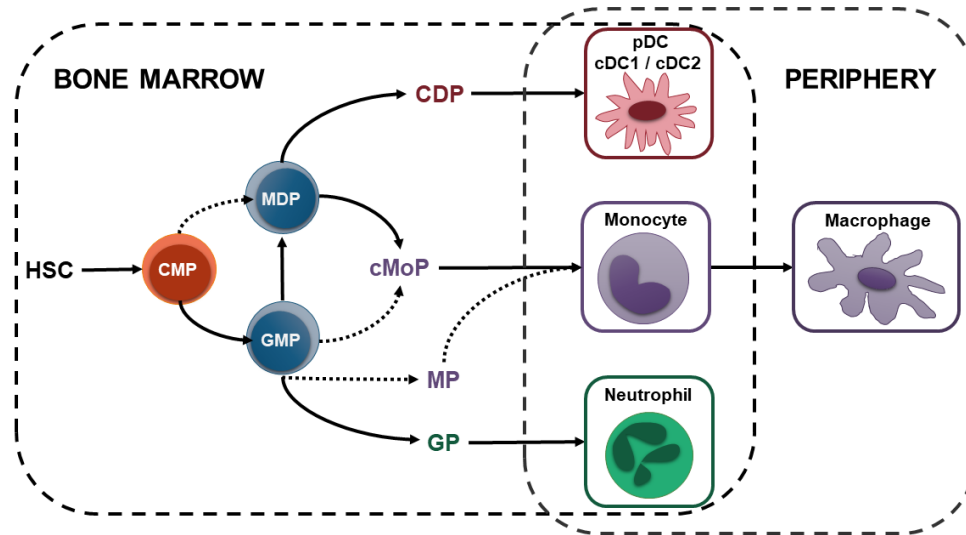


Figure 1.1. Myeloid cell differentiation in the steady state.

As described in the text, monocytes are derived from cMoPs which arise from hematopoietic stem cells. Solid lines indicate broadly accepted pathways of myeloid cell differentiation, and dotted lines indicate possible other pathways of HSCs to monocytes based on more recent publications. CDP – common dendritic cell progenitor; cDC – conventional dendritic cell; pDC – plasmacytoid dendritic cell; MP – monocyte progenitor; GP – granulocyte progenitor.

The general hierarchy of differentiation is: HSC to CMP to granulocyte-monocyte progenitor (GMP) to monocyte-dendritic cell progenitor (MDP) to common monocyte progenitor (cMoP) to monocyte^{270, 271, 272}, though there has been discussion as to whether MDPs are a distinct population²⁷³, and it has been proposed that monocytes arise from cMoPs via GMPs, from MDPs independent from GMPs, and/or *vice versa*^{214, 274}. Monopoiesis can be induced under inflammatory conditions within extramedullary sites including the spleen, liver, and kidneys^{101, 275, 276, 277}, and there may be preferential use of certain monocyte progenitor differentiation pathways under specific conditions of

infection or inflammation^{274, 278, 279, 280, 281}. Regardless, it is well-recognized that cMoPs and monocytes, like macrophages, require epigenetic regulation of their development and CSF1R/CSF1 signalling for survival^{239, 240, 282, 283}.

Monocyte Identification

In humans, monocytes are typically divided into three subsets: CD14⁺CD16⁻ (classical), which transition into CD14⁺CD16⁺⁺ (intermediate), and then CD14⁻CD16⁺⁺ (non-classical) in the steady state^{270, 284}. Blood monocytes in mice are divided into two or three subsets, according to their expression of Ly6C. Specifically, Ly6C⁺: Ly6C^{high} (inflammatory) and Ly6C^{low} (also referred to as Ly6C^{int} or Ly6C^{mid}), and Ly6C⁻ (also confusingly referred to as Ly6C^{low})^{285, 286, 287}. Ly6C⁺ monocytes have primarily been studied by examining the Ly6C^{high} subset, but distinct transcriptional control and chemotactic and functional responses have been recently described for Ly6C^{low} monocytes^{270, 286, 288, 289}. Ly6C^{high} monocytes are often considered phenotypically and functionally equivalent to human classical monocytes (CD14⁺CD16⁻), while Ly6C⁻ monocytes are often compared to human non-classical monocytes (CD14⁻CD16⁺⁺)²⁹⁰.

Studies of mice and humans have revealed that fetal, neonatal, young and old adult monocytes have distinct transcriptional profiles under steady-state conditions, and exhibit differential responses to cytokines and microbial stimulation^{212, 291, 292}. In adult mice, only ~8% of active genes are differentially expressed between Ly6C^{high} and Ly6C⁻ monocytes in the steady state²⁸⁶, but each monocyte subset has specific roles in maintaining homeostasis, as well as during infection or inflammation. Ly6C^{high} monocytes have a half-life of approximately 19 hours (overall lifespan of ~4 days), while Ly6C⁻ monocytes are retained for ~11 days under steady-state conditions^{270, 293, 294}. Like

their bone marrow progenitors, monocytes have a differentiation series from Ly6C^{high} to Ly6C⁻, regulated by transcription factors including C/EBP β ^{286, 295}, KLF4²⁹⁶, Notch2²⁹⁷, and Nr4a1^{298, 299}. Other studies have proposed that Ly6C⁻ monocytes may also develop independently of Ly6C⁺ monocytes^{296, 300}. The Ly6C⁺ to Ly6C⁻ transition may occur via return of Ly6C⁺ monocytes to the bone marrow in a CXCR4-regulated manner^{301, 302}, or within circulation due to time-dependent loss of bone marrow signalling^{286, 295, 299}.

Monocyte Movement

Monocyte egress from the bone marrow, their movement within blood vessels and lymphatic vessels, and their extravasation from circulation into tissues, is dependent on chemokine signalling and adhesion molecule-receptor interactions. In the steady state, Ly6C^{high} monocyte retention in the bone marrow is dependent on CXCR4 and CX₃CR₁^{301, 302, 303, 304}, and egress from bone marrow is regulated by CCR2 signalling initiated by CCL2/CCL7^{305, 306, 307, 308}. Ly6C^{high} monocyte surface expression of CD11b/CD18, CD62L, PSGL1, PECAM1, VLA1, and LFA1 facilitates vascular rolling, adhesion, and transendothelial migration^{309, 310, 311}. Ly6C⁻ monocytes express low levels of CCR2 and their egress from bone marrow is thought to depend on S1PR5³¹². Ly6C⁻ monocytes patrol along the endothelium to survey the luminal surface to scavenge microparticles and necrotic debris to help maintain the integrity of the endothelial barrier. This slow crawling depends on their expression of CD11b/CD18, as well as CX₃CR₁-CX₃CL₁, and LFA-1/ICAM-1 or LFA-1/ICAM-2 interactions^{287, 298, 313, 314}.

Monocyte Functions – Steady-State

Ly6C^{high} monocytes are often referred to as ‘classical’ or ‘inflammatory’ monocytes. Under conditions of homeostasis, if they do not transition into Ly6C⁻

monocytes, Ly6C^{high} monocytes can extravasate into tissues to replenish tissue macrophage and dendritic cell populations^{208, 285, 286, 287}. While Ly6C^{high} monocytes do not interact closely with the endothelium of blood vessels, they can form ‘marginal pools’ in vascular beds of peripheral organs, including within the lung, liver, and kidney^{266, 315, 316, 317}. Ly6C^{high} monocytes can also enter lymph nodes and non-lymphoid tissues like the lung in a CCR2-dependent manner without differentiation into macrophages in the steady state, acting as effector cells or surveillance cells that sample antigens to bring them to draining lymph nodes^{224, 294}.

Ly6C⁻ monocytes are often referred to as ‘patrolling’ monocytes, as under conditions of homeostasis they remain within and patrol the vasculature by crawling on the luminal side of the endothelium³¹⁴. They have been identified through adoptive transfer experiments to also be present in the spleen, liver, lung, and brain, though they are absent from the peritoneum and lymph nodes²⁸⁷. Ly6C⁻ monocytes identify and remove damaged cells and debris, oxidized lipids, and potential pathogens, as well as promote angiogenesis and endothelial cell proliferation^{313, 314}. Ly6C⁻ monocytes may mediate antibody-dependent cellular cytotoxicity as they express Fcγ receptors³¹⁸. Ly6C⁻ monocytes are less proliferative than Ly6C^{high} monocytes, and can be recruited to non-inflamed tissues in a CX₃CR₁-dependent manner and differentiate into resident macrophages^{270, 289, 313, 314}.

Monocyte Functions - Inflammation

Monocytes are amongst the first responders to an inflammatory response. When tissue homeostasis is disrupted, Ly6C⁻ monocytes arrive within an hour and produce TNF and IL-1β³¹⁴, but they soon afterward change their gene expression to participate in

resolution of inflammation in tissues by facilitating wound healing, angiogenesis, and tissue remodelling, often differentiating into tissue macrophages with anti-inflammatory properties^{314, 319, 320}. CX₃CR₁/CX₃CL₁ interaction can mediate recruitment of Ly6C⁻ monocytes into tissues during infection and to atherosclerotic plaques^{321, 322, 323}. Ly6C^{high} monocyte numbers rapidly increase in blood in response to acute infection or injury³²². Ly6C^{high} monocyte recruitment to injured tissue typically occurs within 24-48 hours³²⁴, though microhemorrhages allow Ly6C^{high} monocytes to exit blood vessels within 4 hours of injury³²⁵. A reservoir of bone marrow-derived circulating Ly6C^{high} monocytes is also found within the subcapsular red pulp of the spleen in the steady state^{326, 327}. These splenic monocytes are recruited to tissues in an Angiotensin II-dependent manner in response to inflammation, which is thought to provide time for the initiation of increased bone marrow monopoiesis^{326, 328, 329}. Under conditions of inflammation, the CCR2/CCL2 axis is used for recruitment of Ly6C^{high} monocytes, but it has also been reported that expression of other chemokine receptors, including CCR1, CCR5, CCR7, CXCL1 and CCR8, may control monocyte trafficking to unique tissue sites³²². Ly6C^{high} monocytes may differentiate into tissue macrophages, inflammatory TNF/iNOS-producing dendritic cells (Tip-DCs), or other macrophage populations, according to specific cues from the tissue microenvironment^{322, 330, 331}. Circulating Ly6C^{high} monocytes can also take on effector functions in the blood and at peripheral sites throughout the body. Ly6C^{high} monocytes have phagocytic activity and are sensitive to endogenous and exogenous stimuli, producing ROS and pro-inflammatory cytokines including TNF, IL-1 β , and IFN γ , to propagate inflammatory responses^{196, 285, 286, 306, 332}.

Once inflammation is resolved, monocytes that extravasated into tissues may undergo apoptosis in the absence of cytokines and growth factors, or may differentiate into tissue-resident macrophages^{208, 270, 272, 322, 333}. Inflammation-elicited macrophages may similarly undergo apoptosis, or remain within the tissue, especially if tissue-resident macrophages have been depleted. Regulation of this process seems to rely on tissue-specific transcriptional regulation and the type and extent of macrophage depletion, as well as whether the depleted macrophages are of embryonic or adult origin^{214, 224, 240, 334, 335}. Therefore, specific activation signals, in combination with other environmental factors, may start the transition from monocyte to macrophage.

Monocytes and Macrophages in Chronic Inflammation

As mentioned, peripheral organs and tissues in the steady state have differential requirements for monocyte recruitment to replenish resident macrophage populations^{211, 214}. Some tissues have essentially no monocyte recruitment, while others such as the gastrointestinal tract, which has been described as the largest immune organ in the body, have rapid recruitment^{235, 236}. The systemic nature of chronic low grade inflammation impacts peripheral monocyte characteristics, their recruitment into tissues, as well as their differentiation into, and functions as, tissue macrophages. Alterations to peripheral and tissue-localized monocyte or macrophage populations have accordingly been implicated in the pathology of inflammaging^{101, 336, 337}, and in non-communicable diseases characterized by chronic inflammation including autoimmune disorders like multiple sclerosis, rheumatoid arthritis, and lupus erythematosus³³⁸, localized and metastatic cancers³³⁹, metabolic disorders including obesity, coronary artery disease, and type 2 diabetes²⁵, as well as tissue-localized inflammatory disorders like lung fibrosis and

inflammatory bowel disease³³⁸. Research into the roles of monocytes and macrophages in inflammation is essential to understand how chronic inflammation arises, its effects on peripheral organ systems, and how it can be treated to reduce risk of disease burden.

1.4 Structure and Functions of the Gastrointestinal Tract

The gastrointestinal tract comprises the esophagus, the stomach, the small intestine, and the large intestine, from the mouth to the anus. Digestion and transcellular transport of bile salts, nutrients like proteins, fats, and some vitamins and sugars, occurs in the small intestine^{340, 341, 342, 343}, whereas water and electrolyte absorption are primary roles of the colon³⁴⁴. The gastrointestinal tract is associated with other organ systems, including the liver, pancreas, gall bladder and salivary glands, lymphatics, vasculature, and autonomic and sensory neurons, all of which support specialized gut functions³⁴⁵. Intestinal function is impacted by changes to any of its supporting organ systems, or changes to intestinal epithelium structure or function.

A single layer of epithelial cells separates the intestinal lumen from the underlying lamina propria. Lgr5⁺ cells interspersed among Paneth cells at the bottom of the crypts divide to become proliferating transit-amplifying cells that differentiate into the absorptive (i.e. enterocytes) or secretory (i.e. mucus and hormones: enteroendocrine, Paneth, tuft, M, and goblet) cell lineages that comprise the intestinal epithelium^{346, 347, 348}. The organization of these cells varies according to the region of the gut, to fulfill distinct functional requirements. The entire intestinal epithelium is continuously replaced by new cells (in the mouse every 3-5 days in the small intestine and every 5-7 days in the colon)^{348, 349}. The intestinal barrier must be permeable to essential ions, nutrients, and

water, but must restrict the movement of microorganisms, and immune-stimulating compounds such as endotoxins, allergens, and antigens³⁴⁵. Molecules and cells that cross the intestinal epithelial barrier may have a direct impact on local immune cells and tissue structures, or may access lymphatic or blood vessels and travel to other sites in the body. Maintenance of the intestinal barrier between the lumen and the lamina propria is essential for homeostasis, and there are multiple mechanisms in place to ensure that the physical, biochemical, and immunological aspects of the barrier are maintained.

Intestinal epithelial cells are overlaid with a mucus barrier, preventing direct interaction of bacteria with the epithelial cells³⁵⁰. The mucus layer of the small intestine contains bicarbonate ions and antimicrobial peptides (e.g. defensins, cathelicidins, lysozyme, antimicrobial lectins secreted by Paneth cells), which form a gradient from the epithelium to the lumen to trap and kill microbes^{351, 352, 353}. Mucus can also detach to be removed from the intestines^{352, 354}. In the colon there are two layers of mucus, and the outer layer contains peptides that bind and aggregate commensal bacteria to support their production of metabolites like short chain fatty acids (SCFAs) and vitamins^{352, 355, 356, 357}. Throughout the intestine IgA secreted by plasma cells also induces aggregation of bacteria^{358, 359}, and enzymes like alkaline phosphatase dephosphorylate ATP (high ATP inhibits growth of commensal bacteria) and bacterial substrates capable of stimulating PRRs on innate immune cells (e.g. LPS, flagellin, CpG DNA)^{360, 361}.

Transport of molecules across the epithelial layer occurs in three ways: the transcellular pathway (passive diffusion across the cell membranes), the receptor-mediated transcellular pathway, and the paracellular pathway (passive diffusion through the spaces between adjacent cells)³⁶². Paracellular movement is regulated by

transmembrane or cytoplasmic tight junction proteins (e.g. occludin, claudins, junction adhesion molecules) on the apical ends of intestinal epithelial cells (i.e. closer to the lumen) that interact with intracellular proteins (e.g. zonulin) attached to the underlying actin cytoskeleton, anchoring adjacent cells together^{362, 363, 364}. Epithelial tight junctions, along with adherens junctions and desmosomes, seal the paracellular space between epithelial cells, preventing bacteria and luminal antigens from entering the lamina propria, but selectively allow paracellular movement of nutrients³⁶². Specialized M cells and goblet cells within the intestinal epithelium can also facilitate movement of luminal antigens and even live bacteria across the epithelial barrier^{365, 366, 367, 368}.

1.5 The Microbiome and Immunity

In the late 19th century, investigations into the germ theory of disease by Louis Pasteur³⁶⁹, and the development of Robert Koch's postulates³⁷⁰, established that microorganisms are the cause of many communicable diseases. It was subsequently proposed by Elie Metchnikoff that toxins produced by microorganisms in the intestines may contribute to aging, and that manipulating the intestinal microbiota directly, or via diet and nutrition, and could improve an individual's health³⁷¹. With advances in culture-independent genomic sequencing methods, combined with refinements of culture-dependent methods, there has been a more recent expansion of research into the composition of the microbiome (the collective genetic material of all microbes, i.e. bacteria, viruses, protozoa, archaea, and fungi) and host-microbe interactions. It is now well-recognized that microorganisms contribute to host homeostasis, and interactions between microbes and the host can be harmful, beneficial, have no effect, or may be

essential for host health³⁷². Within the intestine the microbiota has important roles in mediating host nutrient uptake and metabolism^{356, 373}, maintenance of the gut barrier³⁷⁴, intestinal vasculature^{268, 375}, and enteric neuronal networks^{376, 377}, as well as mucosal immunity^{235, 236, 372, 374}. There is also evidence that the intestinal microbiome modulates whole-body health and both communicable and non-communicable disease risk and outcomes^{374, 378, 379}.

Commensal intestinal microorganisms have an evolutionarily adapted symbiotic relationship with host cells³⁸⁰. Studies of mice without any microbiota (germ free), a limited microbiota, or after antibiotic treatment, have shown that specific commensal microbial species and their metabolites have direct effects on immune cell development and functions under conditions of homeostasis. For example, *Clostridium* genus bacteria promote development of intestinal T_{regs}^{381, 382}, and segmented filamentous bacteria induce development of intestinal Th17 cells^{383, 384, 385}. In addition, bacterial metabolites including the SCFA butyrate promote goblet cell production of mucus, plasma cell secretion of IgA, immune-mediated epithelial tissue repair processes, and suppress macrophage NfκB-mediated pro-inflammatory cytokine expression^{356, 373}.

Commensal bacteria and their metabolites also affect immunity beyond the gastrointestinal tract³⁸⁶. For example, SCFAs are required for the maturation and function of microglia in the brain^{387, 388}. Furthermore, microbial products like LPS, or LPS-containing bacteria themselves, have been reported (in the context of diet-induced obesity) to translocate to peripheral blood and adipose tissue^{389, 390}, activating peripheral adipocyte and adipose tissue macrophage signalling pathways^{75, 83}. In fact, ablation of bacterial product sensing in mice by genetic knockout of PRRs for flagellin (TLR5)^{391, 392},

lipoproteins (TLR2)³⁹³, peptidoglycan (NOD1 or NOD2)^{394, 395}, LPS (TLR4)^{391, 396}, as well as coreceptors like CD14^{83, 397}, or downstream adaptor molecules like MyD88^{397, 398}, or partial or complete removal of the microbiota by use of antibiotic-treated or germ-free mice^{83, 398, 399}, have all been reported to be protective against the development of obesity, chronic systemic inflammation, and/or hyperglycemia and insulin resistance. Therefore, the intestinal microbiota and microbial products alter local and peripheral immune responses and can contribute to chronic inflammation.

The composition of the microbiota is influenced by host biological sex, age, health status, genetics, diet, antibiotic and probiotic exposure, and inflammation³⁷². The majority of bacteria within the gut of healthy humans and mice are part of two phyla, the Firmicutes and the Bacteroidetes^{400, 401, 402}. Alterations to microbial composition are referred to as microbial dysbiosis, and may involve the loss or reduction of the abundance of microbial species that promote immunological tolerance and homeostasis, as well as outgrowth of those that induce inflammation³⁷². As a consequence, changes in the gut microbiota can contribute to the development of acute infection or chronic inflammation. Shifts in microbial composition are now well-established to be associated with changes to gut structure and mucosal immune defense, as well as systemic immunity and metabolism⁴⁰³, so disentangling their relationships is of considerable interest in order to identify new approaches to prevent and treat chronic inflammatory disorders.

1.6 Intestinal Macrophages

Like other tissue macrophages, intestinal macrophages perform ‘housekeeping’ functions of phagocytic removal of cellular debris and tissue remodelling⁴⁰⁴, but have

considerable phenotypic and functional heterogeneity that likely facilitates their roles within specific niches of intestinal tissue layers. Intestinal macrophages have roles in maintenance of the intestinal epithelial barrier and vascular and neuronal networks, and establishment of tolerance to innocuous food antigens and commensal bacteria, but are also able to effectively respond to and eliminate pathogens. Intestinal macrophages under conditions of homeostasis are typically described as being highly bactericidal and phagocytic, yet anti-inflammatory and tolerogenic^{405, 406, 407}.

Intestinal Macrophages - Ontogeny

In accordance with the MPS classification of macrophages, it was thought until recently that the intestines are seeded with embryonic macrophages that are rapidly replaced by bone marrow origin monocyte-derived macrophages after birth, coinciding with establishment of the microbiota^{223, 235}. The persistent exposure of intestinal macrophages to microbes and luminal antigens, and the continual requirement for phagocytic removal of cells and debris due to the rapid turnover of the intestinal epithelium, were proposed to increase tissue niche accessibility, and require that intestinal macrophages also have a high turnover rate^{196, 211, 252}. As described earlier, global and transcriptomic analyses of tissue-resident macrophage differentiation and maturity recently prompted a re-evaluation of macrophage identity in many tissues^{218, 237, 242}. In 2018, two papers using complementary approaches of flow cytometry and immunofluorescence microscopy in mice definitively showed that, in addition to adult monocyte-derived macrophages of bone marrow-origin, embryonic origin long-lived tissue-resident macrophages are found within the small intestine^{408, 409}, and colon⁴⁰⁹. Research on human small intestinal macrophages has also recently identified within the

jejunum a subset of macrophages with rapid turnover from blood monocytes, and two longer-lived macrophage populations^{410, 411}.

Mouse intestinal macrophages with unique morphology, gene expression and cytokine production profiles, localization characteristics, and turnover rates assessed by adoptive bone marrow transfer and fate-mapping, can be identified according to their expression of CD4 and TIM4: CD4⁻TIM4⁻, CD4⁺TIM4⁻, and CD4⁺TIM4⁺^{408, 409}.

CD4⁻TIM4⁻ macrophages are solely derived from adult bone marrow-origin monocytes. CD4⁺TIM4⁻ macrophages have a much slower turnover rate but are also replaced by monocytes. CD4⁺TIM4⁺ macrophages are long-lived embryonic origin macrophages. A recent study that performed scRNAseq on Lin⁻MHCII^{high} cells from the colon also found that cells with the highest expression of TIM4 were the most developmentally ‘advanced’ in comparison to blood monocytes⁴¹². BrdU labelling experiments confirmed that long-lived macrophages can locally proliferate⁴⁰⁸, though mature intestinal macrophages can also upregulate expression of *ccl7* and *ccl8* genes, which may mediate recruitment of monocyte replacements²⁴². Monocyte migration into intestinal tissues under homeostatic conditions relies on their expression of CCR2 and β 7-integrin for chemotaxis^{236, 306, 413, 414}. Once Ly6C^{high} blood monocytes enter the intestine they progressively increase their expression of MHCII and downregulate their expression of Ly6C, CCR2, and extravasation markers^{223, 233, 235, 236, 415, 416}. Multiple adoptive transfer experiments have shown that as intestinal macrophages mature, they also increase their expression of CX₃CR₁, so most mature gut macrophages are described as Ly6C^{-/low}CCR2^{-/low}MHCII⁺CX₃CR₁^{high}. Maturation of intestinal macrophages leads to progressive upregulation of other surface markers such as CD64, F4/80, MHCII, CD11c,

CD163, and MerTK, as well as expansion of cell size^{223, 233, 235, 236, 408, 409, 415, 416, 417}.

Newly recruited monocytes replenish CD4⁺TIM4⁺ macrophage populations under homeostatic conditions (Figure 1.2).

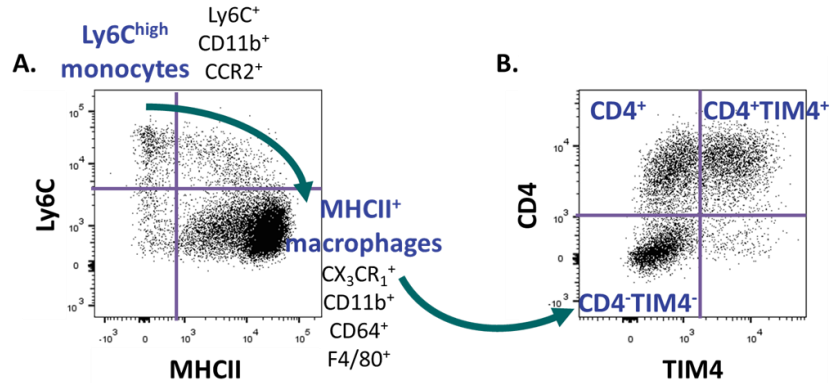


Figure 1.2. Monocyte and macrophage populations in the intestines.

(A) Monocyte to macrophage differentiation in the intestines.

(B) Intestinal macrophage populations identified by expression of CD4 and TIM4.

More recently, monocyte-to-macrophage differentiation in the intestines has been verified through intravital imaging of cell surface marker and morphological changes²⁶⁸, as well as by assessment of monocyte-to-macrophage differentiation in studies of bulk RNAseq and scRNAseq transcriptomes of FACS-purified monocytes and macrophages^{242, 418}. Differentiation of monocytes into intestinal macrophages is thought to occur quickly, as monocytes that have crossed the endothelial barrier into the intestines are already transcriptionally distinct from blood monocytes^{242, 294, 418}, and adoptively transferred Ly6C^{high} monocytes can enter the colon and begin differentiation into macrophages within 24 hours²³⁵, although intravital imaging suggests that differentiation can begin within an hour around blood vessels²⁶⁸. Experiments using transgenic mice, and adoptive transfer and parabiosis techniques, have reported that intestinal monocyte-derived CD4⁺TIM4⁺ macrophages have a half-life of ~4-8 weeks (4-6 weeks in the small intestine and 6-8 weeks in the colon)^{223, 235, 236, 242, 409, 419}.

Intestinal Macrophages – Localization

Macrophages are present along the entire length and within all structural layers of the gastrointestinal tract^{256, 420}. As in other tissues, intestinal macrophages organize within and interact with non-immune cell structures, and core macrophage programming, in combination with local trophic factors, including microorganisms, microbial products, nutrients, and food antigens within the intestinal lumen, supports their self-maintenance and functions within intestinal tissue niches^{372, 373, 408, 421}. Numbers of macrophages assessed by immunohistochemistry or stereology have shown that macrophages are more concentrated in the distal small intestine, and especially the colon, which contains the highest quantities of bacteria, whereas they are less prevalent in the upper areas of the small intestine, which mainly contain stomach acid, bile, and pancreatic secretions^{256, 420, 422, 423, 424, 425}. Our own flow cytometry data also indicates that the composition of the CD4⁻TIM4⁻, CD4⁺, and CD4⁺TIM4⁺ macrophage populations differs along the length of the intestines, with a higher prevalence of monocyte-derived CD4⁻TIM4⁻ macrophages with increasing microbial load from the duodenum to the colon (Figure 1.3).

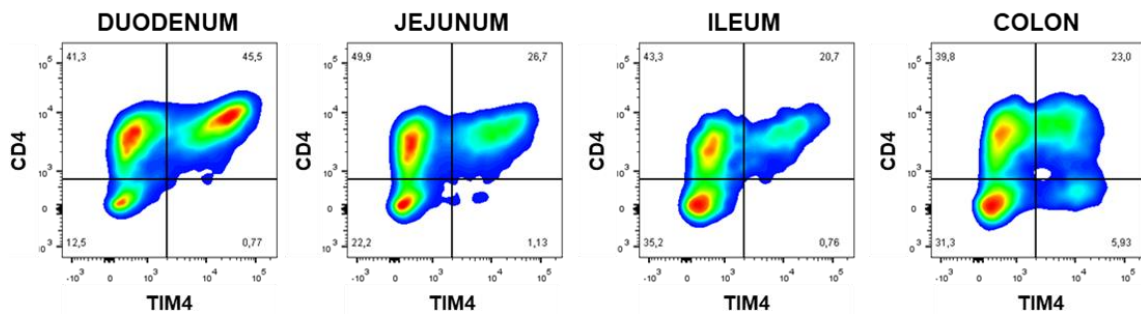


Figure 1.3. CD4⁻TIM4⁻, CD4⁺, and CD4⁺TIM4⁺ macrophage prevalence along the intestines.

The tissue layers of the intestines are organized into four compartments surrounding the lumen: the mucosa, the submucosa, the muscularis externa, and the serosa³⁴⁵. The single-layered epithelium covered with mucus (in contact with the lumen

and organized into crypts (and villi in the small intestine)) separates the lumen from the underlying mucosa and submucosal regions containing irregular connective tissue, a blood capillary network, lymphatic vessels, and extrinsic neuronal processes. The muscularis externa of circular and longitudinal smooth muscle layers is alternated with the submucosal plexus and myenteric plexus containing enteric neurons. Though the basic structure is the same, the thickness of tissue layers and their cellular composition and functions differ according to their location along the length of the intestines.

Analysis of macrophage morphology and localization has also revealed distinct tissue niche behaviours within the layers of the intestines. De Schepper and colleagues identified that over a period of 35 weeks in the small intestine, F4/80⁺ macrophages have ~95% turnover from bone marrow-derived monocytes in the mucosa, ~45% turnover in the submucosa, and ~60% turnover in the muscularis externa, indicating that monocyte-derived and embryonic origin macrophages have differential localization within the intestinal wall⁴⁰⁸. Accordingly, macrophage localization corresponds to different transcriptional profiles and functions (Figure 1.4)⁴²⁶.

Lamina propria Macrophages

Within the lamina propria (a layer of connective tissue that separates the intestinal epithelium from the underlying smooth muscle tissue), immunohistochemistry and intravital and electron microscopy imaging have shown that there is a dense network of macrophages in association with capillaries, lymphatic vessels, and neurons that run through villi and in the mucosa^{267, 268, 408, 422, 423, 427}. Macrophages are also found within crypts and lymphoid tissues including Peyer's patches^{428, 429}.

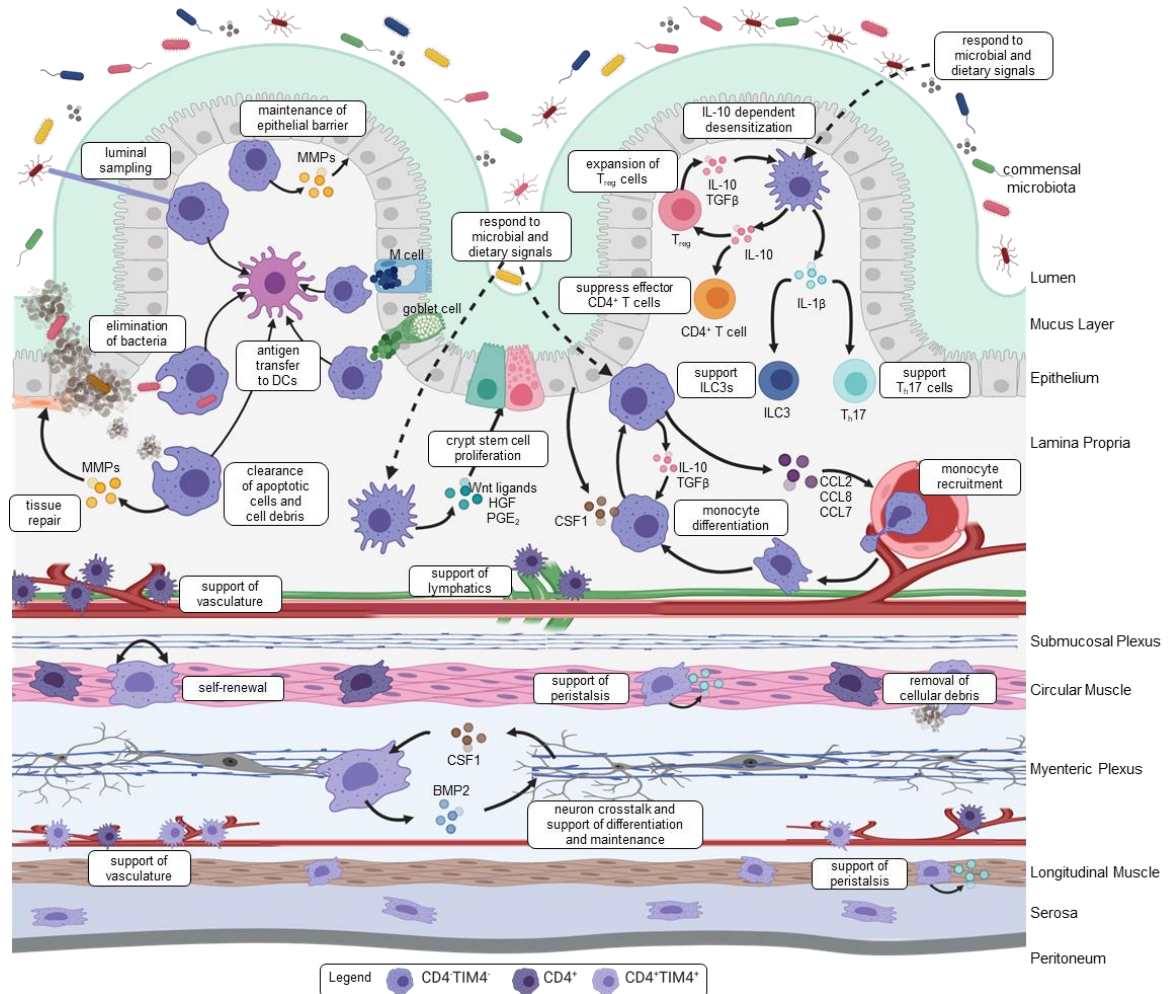


Figure 1.4. Summary of intestinal macrophage localization and functions.

Lamina propria macrophages have a more pro-inflammatory transcriptome compared to macrophages from the muscularis region, consistent with their role in being part of the ‘first-line’ defense against invading bacteria due to their close proximity to the gut lumen^{405, 407, 415, 430, 431, 432, 433}. Monocyte-derived CD4⁺ TIM4⁻ macrophages are primarily found within villi and regions of the lamina propria close to the intestinal epithelium. *In vitro* studies have reported that CD4⁺ TIM4⁻ intestinal macrophages are highly phagocytic^{223, 236, 434}, and scRNAseq analysis has shown an enrichment of genes associated with antigen processing and presentation, specialized innate immune responses

(e.g. suppression of IL-1 β and PRR signalling, enhanced expression of TGF β -dependent genes), and bactericidal activity⁴¹². Lamina propria macrophages support maintenance of the intestinal epithelial barrier via efferocytosis of apoptotic cells and cellular material^{236, 242, 404, 417, 435}, secretion of trophic factors to stimulate stem cell proliferation and differentiation^{429, 436}, including Wnt ligands^{437, 438}, hepatocyte growth factor (HGF)⁴³⁹, and PGE₂^{433, 440}, and secretion of matrix metalloproteinases (MMPs) to promote epithelial cell repair and tissue remodelling^{441, 442}. Macrophages sense and phagocytose luminal antigens by extension of transepithelial dendrites across the intestinal barrier^{242, 431, 443, 444}, or via M cell and goblet cell antigen transport^{365, 366, 367, 368}, and can transfer antigens to migratory dendritic cells (DCs) that travel to mesenteric lymph nodes to elicit adaptive immune responses to pathogens or tolerogenic responses to dietary antigens^{431, 445, 446}. Lamina propria macrophages also directly and indirectly support recruitment, proliferation, and survival of T_{regs}^{447, 448, 449}, Th17 cells^{446, 450}, ILC3 cells⁴⁵¹, as well as DCs, monocytes, and other immune cells^{415, 449, 450, 452, 453, 454}, recruit replacement monocytes^{223, 235}, and suppress effector CD4⁺ T cells through secretion of anti-inflammatory cytokines^{374, 446, 455}. Therefore, lamina propria macrophages have roles in mediating interactions between the intestinal epithelium, the microbiota, luminal antigens, and other immune cells, to support immunological tolerance and host defense.

Submucosal and Muscularis Macrophages

Macrophages within the submucosal and muscularis regions are generally CD4⁺ (i.e. CD4⁺ or CD4⁺TIM4⁺) and have a more tissue-protective transcriptomic profile with enrichment of genes associated with cell-cell adhesion, wound healing, tissue protection, and neuronal development^{242, 267, 408}. scRNAseq analysis has shown that intestinal

macrophages with the highest expression of TIM4 similarly have transcriptional profiles enriched for genes involved in cell recruitment, scavenging and apoptotic cell clearance, and tissue regeneration⁴¹². Mouse models of macrophage depletion (*Csf1*^{-/-}), or disruption of monocyte recruitment (*Ccr2*^{-/-}) or differentiation (*Nr4a1*^{-/-}), as well as germ free or antibiotic-treated mice, have altered blood vessel morphology and abundance, and increased vascular leakiness^{268, 408}. Macrophage depletion also alters the distribution and proliferation of enteric neurons in the submucosa and myenteric plexus^{267, 456, 457}, and dysregulates ion secretion, neuronal calcium signalling, muscle contraction, and peristalsis^{267, 408, 456, 457}. Therefore, submucosa and muscularis macrophages primarily support the vasculature, smooth muscle activity, and the enteric nervous system.

Intestinal Macrophages - Anti-inflammatory Character

Intestinal macrophages express TLRs3-9, NOD-like receptors, and TREM2, but associated adaptor and downstream signalling proteins (e.g. CD14, NOD2, MyD88, and TRAF6) are downregulated^{236, 415, 434, 458}, and I κ B proteins are upregulated^{459, 460}, which prevents downstream signalling and NF κ B-mediated expression of pro-inflammatory cytokines. IL-10/IL10R^{435, 448, 458, 461, 462, 463} and TGF- β /TGF β R^{464, 465} signalling, which can be induced by intestinal epithelial cells or other immune cells, help maintain intestinal macrophage anti-inflammatory properties. This is also thought to be supported by continual turnover of the intestinal epithelium (phagocytic activity suppresses pro-inflammatory gene expression)^{404, 466}, commensal bacteria themselves^{412, 421, 467}, intestinal epithelial cell production of TSLP, TGF β , and retinoic acid^{467, 468, 469}, dietary metabolites (promoting IL-10 production and reprogramming metabolism)^{421, 445, 470, 471}, and CX₃CR₁-CX₃CL₁ interactions^{446, 472, 473}. However, when homeostasis is disrupted, PRR signalling

can elicit phagocytic and bactericidal activities of resident macrophages, and an acute inflammatory response via recruited monocytes.

Intestinal Macrophages - Response to Inflammation

The single-cell layer design of the intestinal epithelium maximizes its absorption of nutrients, but also arguably increases its susceptibility to damage and infection. Intestinal inflammation due to infection from bacteria such as *Citrobacter rodentium*⁴⁷⁴ or *Salmonella enterica* serovar Typhimurium⁴⁷⁵, the protozoan parasite *Toxoplasma gondii*^{476, 477}, or helminths^{433, 476, 478}, elicits rapid CCR2-dependent recruitment of inflammatory Ly6C^{high} monocytes into intestinal tissues. Ly6C^{high} monocyte recruitment can also be induced by inflammation associated with colitis (i.e. inflammatory bowel disease; induced by DSS (dextran sulphate sodium)^{236, 415, 479, 480}, TNBS (2,4,6-Trinitrobenzenesulfonic acid)^{481, 482}, T-cell transfer^{223, 417, 483}, or *Helicobacter hepaticus* with anti-IL10R treatment^{484, 485}), or by sterile tissue injury²⁶⁸. These inflammation-elicited monocytes differentiate into intestinal macrophages with high expression of MHCII and hyperresponsiveness to PRR activation^{223, 236, 413, 415, 458, 486, 487}. The inflammation-elicited monocyte-derived macrophages produce pro-inflammatory cytokines including TNF, IL-6, IL-12, and IL-23, inflammasome cytokines IL-1 β and IL-18, as well as NO and ROS, to promote local inflammation, and chemokines like CCL4, CCL5, CCL8, and CCL11, to facilitate further recruitment of Ly6C^{high} monocytes and other effector cells. Accumulation of pro-inflammatory Ly6C^{high} monocytes and monocyte-derived macrophages is increased in intestinal lesion areas of IBD patients^{411, 488, 489}, and the frequency of immature macrophages, but not mature resident macrophages, has also been positively correlated with endoscopic score of disease

severity in Crohn's patients⁴⁹⁰. Due to the non-specific attributes of an acute inflammatory response, bystander host cells within the intestinal epithelium can become damaged, which may compromise the integrity of the intestinal epithelium^{415, 489, 491, 492}. Infiltration of luminal contents, including bacteria, bacterial products, and other antigens into the lamina propria, can further perpetuate local inflammation, recruitment, and activation of other pro-inflammatory immune cells, leading to tissue pathology^{372, 493}. Once inflammation is resolved, monocyte-derived macrophages may remain, especially if there is depletion of tissue-resident macrophages, which could elevate the basal level of intestinal inflammation^{214, 408}.

Though it has been reported that tissue-resident lamina propria macrophages can extravasate into the intestinal lumen during *Salmonella enterica* infection and phagocytose pathogenic bacteria⁴⁹⁴, tissue-resident macrophages are typically thought to retain their anti-inflammatory characteristics in response to infection or injury^{233, 236, 415, 417, 485, 495}. Depletion or dysfunction of resident macrophage populations^{405, 406, 407}, or disruption of macrophage-specific TGF β ⁴⁶⁵, IL-10R⁴⁹⁶, or MyD88 signalling⁴⁹⁷, can lead to chronic inflammation independent of infection or injury. Consequently, through local proliferation, and secretion of cytokines like IL-10 (which has a bystander effect on other immune cell populations), and TNF (to promote enterocyte growth), as well as tissue repair factors, tissue-resident macrophages may help prevent pathology from inflammation-elicited immune cells and participate in the resolution of inflammation, facilitating a return to homeostasis.

1.7 Rationale

Inflammation is a complex biological process required to maintain host homeostasis¹, yet over half of global deaths can be attributed to diseases associated with chronic sterile inflammation⁴⁹⁸. Obesity is increasingly prevalent worldwide³⁰, and its comorbidities have a negative impact on an individual's health and quality of life^{31, 34, 46}. Included here is also pregravid obesity¹⁵⁷, and excess gestational weight gain¹⁵⁸, which are both associated with short and long-term detrimental effects on maternal health^{160, 162}. Effects of chronic inflammation are modified by biological sex, age, and health status^{1, 2}. Superimposed upon these circumstances is the fact that chronic inflammation is also an intrinsic component of biological aging²⁶, complicating the role that inflammation plays in our lifelong risk of chronic disease⁴⁹⁹.

Current research endeavours have identified common features of chronic inflammatory disorders in both humans and mice, which interact in a feed-forward cycle. These components include intestinal microbial dysbiosis, an increase in intestinal permeability, elevation of soluble pro-inflammatory cytokines like TNF in peripheral blood and tissues, changes to the phenotype and functions of immune cells in circulation and within tissues, local pathology from cellular damage and/or tissue restructuring, as well as metabolic dysfunction⁴⁹⁹. Monocytes and macrophages have essential roles in acute inflammation, but in chronic inflammation they often contribute to pathology^{1, 2}.

In obesity, the relationships between adiposity, chronic inflammation, circulating monocytes, and metabolic dysfunction, remain poorly defined. The cellular inflammatory response differs by biological sex, but most preclinical animal studies that have examined

cellular aspects of chronic inflammation in obesity have used male animals, so it is often unclear if these data are also applicable to females. To date, few studies have examined the effects of maternal obesity on peripheral blood immune cell populations in pregnancy, and no studies have been done during lactation. Though there are similar reports of microbial dysbiosis, intestinal permeability, and local inflammation within the gut in obesity, pregnancy, and aging, it is unclear how these changes affect intestinal monocyte-derived and tissue-resident macrophage populations.

Despite the many advancements in our knowledge of how immune cells contribute to inflammation and disease, a better understanding of how monocytes and macrophages change in response to chronic inflammation under different biological conditions will help identify novel approaches for intervention.

Central Hypothesis

We hypothesize that chronic inflammation alters peripheral monocyte and intestinal macrophage prevalence, phenotype, and functions. We hypothesize that these effects are modulated by different biological conditions and can be mediated by TNF and the intestinal microbiota.

Central Aim

We aim to understand effects of biological sex on peripheral immune cell numbers in homeostasis, and effects of chronic inflammation in the context of obesity, pregnancy, and/or biological aging, on peripheral blood and intestinal monocyte and macrophage prevalence, phenotype, and functions (Figure 1.5).

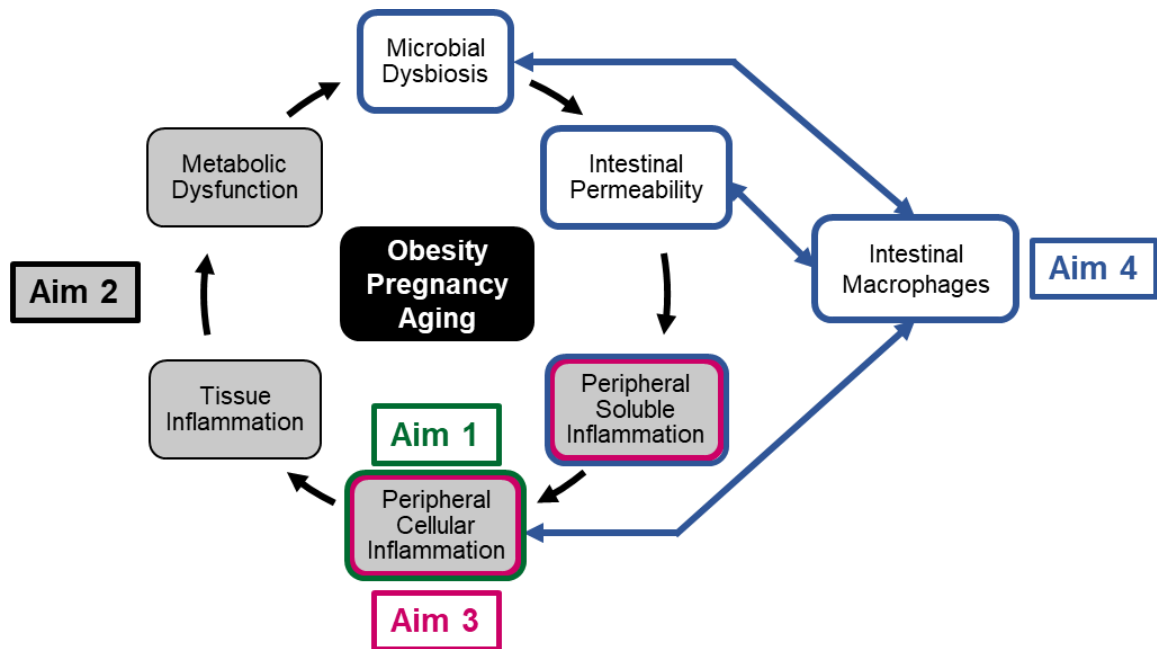


Figure 1.5. Central thesis aims to investigate effects of chronic inflammation.

Specific Aims

- 1** - Characterize the effects of biological sex and the female reproductive cycle on numbers of monocytes (and other immune cells) in peripheral blood. (**Chapter 3**)
- 2** - Disentangle the relationships between peripheral monocytes and obesity, TNF-mediated inflammation, hyperinsulinemia, and hyperglycemia, in male mice. (**Chapter 4**)
- 3** - Determine the longitudinal effects of obesity and TNF-mediated inflammation on peripheral monocytes in female mice and assess effects of pregravid obesity and excess gestational weight gain on peripheral immunological adaptations during pregnancy and lactation. (**Chapter 5**)
- 4** - Determine the effects of chronic inflammation and the microbiota on intestinal macrophages in obesity and aging, and assess effects of excess gestational weight gain on intestinal macrophages in lactation. (**Chapter 6**)

Chapter 2. Materials & Methods

Note that all materials and methods for Chapters 3 and 4 are within the manuscripts included in those chapters. All materials and methods for Chapters 5 and 6 are described below

2.1 Animal experiments

Wildtype C57BL/6J female and male mice (WT; cat#00064, The Jackson Laboratory), and TNF^{-/-} C57BL/6J female and male mice (TNF^{-/-}; cat#003008, The Jackson Laboratory), were bred at the McMaster University Central Animal Facility under specific-pathogen free (SPF) conditions. The pathogen-free status of mice was ensured through continuous monitoring of sentinel mice and specific testing of fecal samples for common murine pathogens. For all experiments, mice were housed in sterile vent/rack cages with *ad libitum* access to food and water, at constant ambient temperature (22°C) on a 12 hour light-dark cycle. Mouse diets are summarized in Table 2.1.

Table 2.1. Mouse diet allocation and composition by experiment cohort.

Experiment Cohort	Diet Name	Source	Energy	Composition
Young SPF (WT and TNF ^{-/-} non-pregnant, pregnant, and lactation study)	‘standard chow’ Teklad 22/5 Rodent Diet	8640, Envigo	3.4 kcal/g	17% kcal fat 29% kcal protein 54% kcal carbohydrates
Young SPF (WT and TNF ^{-/-} non-pregnant and pregnant)	60% high fat diet	D12492, Research Diets, Inc.	5.2 kcal/g	60% kcal fat 20% kcal protein 20% kcal carbohydrates
Lactation Study	45% high fat diet	D12451, Research Diets, Inc.	4.7 kcal/g	45% kcal fat 20% kcal protein 35% kcal carbohydrates
Aging Studies (WT young and old SPF)	‘aging diet’ Teklad irradiated global 14% protein diet	2914, Envigo	2.9 kcal/g	13% kcal fat 20% kcal protein 67% kcal carbohydrates
Germ Free Mice (non-pregnant and pregnant)	S-2335 Mouse Breeder Sterilizable Diet	7004, Envigo	3.5 kcal/g	29% kcal fat 20% kcal protein 51% kcal carbohydrates

Littermate $TNF^{+/+}$ and $TNF^{-/-}$ mice were generated from F2 $TNF^{+/-}$ heterozygotes⁵⁰⁰, and genotyping was performed by PCR (see below). Male and female adult germ free (GF) C57BL/6N mice, originally from Taconic Biosciences, were obtained from the Axenic Gnotobiotic Unit at McMaster University.

All animal experiments were performed in accordance with Institutional Animal Utilization Protocols approved by McMaster University's Animal Research Ethics Board following the recommendations of the Canadian Council on Animal Care.

Genotyping

Tail tissue samples were collected at weaning and flash frozen in liquid nitrogen. Samples were incubated overnight at 37°C in lysis buffer (100 mM Tris-Cl pH 8.0, 5 mM EDTA pH 8.0, 200 mM NaCl, 0.2% (w/v) SDS, 0.5 mg/mL proteinase K (cat#P2308, Sigma-Aldrich)). Samples were mixed by inversion, centrifuged (13,000 rpm, 20 minutes), and genomic DNA was precipitated in 100% isopropanol, and pelleted (13,000 rpm, 5 minutes). The cell pellet was washed twice with 75% ethanol and centrifuged (13,000 rpm, 5 minutes), air dried, resuspended in nuclease-free water, and dissolved at 55°C. DNA concentration was determined by NanoDrop (ThermoFisher Scientific) and diluted to 100-200 ng/μL. The PCR protocol and primers (Table 2.2) were based on The Jackson Laboratory Protocol 22433: Standard PCR Assay - Tnf<tm1Gkl> version 2.3 (from <https://www.jax.org/Protocol?stockNumber=003008&protocolID=22433>).

Table 2.2. TNF genotyping PCR primers.

Description	Primer Sequence
Common TNF genotyping forward primer	5'-TAG CCA GGA GGG AGA ACA GA-3'
Wildtype reverse TNF genotyping primer	5'-AGT GCC TCT GCC AGT TC-3'
Mutant reverse TNF genotyping primer	5'-CGT TGG CTA CCC GTG ATA TT-3'

The PCR master mix was prepared with 10X PCR buffer (cat#10342020, Invitrogen), 50 μ M MgCl₂ (cat#10342020, Invitrogen), 10 μ M dNTPs (cat#18-427-088, ThermoFisher Scientific), 10 μ M common TNF genotyping forward primer, 10 μ M wildtype reverse TNF genotyping primer, 10 μ M mutant reverse TNF genotyping primer, 1U Taq polymerase (cat#10342020, Invitrogen), and 100-200 ng genomic DNA, in nuclease free water, to a total volume of 25 μ L. Samples were run on a Mastercycler Pro5 (Eppendorf) using a touchdown program, with initial denaturation at 94°C for 5 minutes, then 10 cycles at 94°C for 45 seconds, 65°C for 30 seconds, and 68°C for 40 seconds, with the melting temperature of 65°C decreasing by 0.5°C every cycle, followed by 25 cycles at 94°C for 45 seconds, 55°C for 30 seconds, and 72°C for 40 seconds, with a final elongation step at 72°C for 7 minutes before cooling to 4°C. Samples were electrophoresed on a 1.5% agarose gel (in TAE buffer, pH 8.3). Genotype was identified as wildtype (TNF^{+/+}) with a product band of 183 bp, knockout (TNF^{-/-}) with a product band of 318 bp, or heterozygous (TNF^{+/-}) with product bands of 183 bp and 318 bp.

Model of diet-induced obesity in non-pregnant mice: SPF WT and TNF^{-/-}
(Chapter 5: section 5.1; Chapter 6: sections 6.1 to 6.3)

WT mice were fed a standard chow diet upon weaning (cat#8640, Envigo). Littermate WT and TNF^{-/-} mice were fed Teklad irradiated global 14% protein diet (cat#2914, Envigo) upon weaning. At either 5 weeks of age (WT mice), or 8 weeks of age after genotyping (littermate mice), mice were fed a standard chow diet (17% kcal from fat, cat#8640, Envigo), or were placed on an obesogenic, low fibre, high fat diet (60% kcal from fat, cat#D12492, Research Diets, Inc.) until endpoint. Mice were provided with a plastic tube and cotton and paper bedding material for enrichment. Food intake and body weight were monitored weekly.

Young germ free mouse colonization with chow and high fat diet microbiota*(Chapter 6; section 6.3)*

Donor WT SPF female mice were fed their respective standard chow diet or 60% high fat diet for 7-12 weeks prior to the start of the experiment. Female WT GF mice were exported at 8-10 weeks of age from the Axenic-Gnotobiotic Unit at McMaster University. GF mice were housed under the same SPF conditions as donor mice after export, with *ad libitum* water and standard chow diet (cat#8640, Envigo). The colonized ex-GF mice received dirty cage bottoms (with fecal pellets and enrichment plastic tube and cotton/paper bedding material) from the SPF donor mice on a weekly basis. Cage bottoms were inspected to remove any food prior to transfer. Body weight and food intake were monitored on a weekly basis.

Model of diet-induced obesity in pregnant mice: SPF WT and TNF^{-/-}*(Chapter 5, sections 5.2.2 and 5.2.3)*

At 5 weeks of age, female WT or non-littermate TNF^{-/-} mice were cohoused two per cage and allocated to a standard chow diet (17% kcal from fat, cat#8640, Envigo) or a 60% high fat diet (cat#D12492, Research Diets, Inc.). Mice were provided with a plastic tube and cotton and paper bedding material for enrichment. After 6 weeks diet allocation, mating was performed by cohousing the wildtype female mice with a wildtype male mouse fed the standard chow diet (or TNF^{-/-} female mice with a TNF^{-/-} male mouse) at the end of the light cycle. Successful mating was identified the next morning by the presence of a vaginal plug (designated embryonic day E0.5 of gestation) and female mice were thereafter individually housed. Mouse body weight and food intake were monitored weekly pre-pregnancy and at E0.5, E6.5, E10.5, E14.5, and/or E18.5. Mice were sacrificed at E14.5 or E18.5 by cervical dislocation after an overnight fast.

Model of excess gestational weight gain in lactation: SPF WT

(Chapter 5, section 5.2.4; Chapter 6, section 6.5)

Lactating dams were obtained from a cohort study collaboration between the Bowdish and Sloboda labs, and were used in this thesis to examine changes in immune cell populations during lactation. WT C57BL/6J female and male mice were purchased from The Jackson Laboratory (cat#00064). Following 1 week of acclimation after arrival, female mice were cohoused two per cage. All mice were initially maintained on the standard chow diet (cat#8640, Envigo), with food and water provided *ad libitum*. Mating was performed by cohousing two female mice with a wildtype C57BL/6J male mouse (fed standard chow diet) at the end of the light cycle. Successful mating was identified the next morning by the presence of a vaginal plug. Upon confirmation of pregnancy, female mice were individually housed. The same male mouse for each pair of female mice was used for successive matings for each pregnancy. First pregnancy litters were sacrificed upon birth. One week later, dams were randomly allocated to continue on the standard chow diet or were placed on a high fat diet (45% kcal from fat, cat#D12451, Research Diets Inc.). Following two weeks of dietary intervention, female mice were mated by individual housing with a male mouse (fed standard chow diet) overnight as described above. Pregnant mice were maintained on the standard chow or high fat diet throughout pregnancy and lactation. Mouse weight and/or food intake was monitored weekly pre-pregnancy and at E0.5, E6.5, E10.5, E14.5, and E18.5, as well as post-natal day 21 (P21). Dams were checked daily after E18.5 for the presence of a litter. Once a litter was noted, this was designated as postnatal day 1 or P1. As litter size influences intestinal physiological changes during lactation¹²², at P7 we standardized all litters to six offspring with an equal sex ratio when possible. Dams with litters of less than 6 pups were

excluded. Offspring were weaned in the morning at P21. Assessments were carried out within 24 hours after weaning. Dams were sacrificed by cervical dislocation. Dams were ~4.5-5 months of age upon sacrifice.

Note regarding diet selection: In the other pregnancy studies in this thesis that examined effects of pregravid diet-induced obesity, dams were fed a 60% kcal from fat diet for 6 weeks prior to mating. Dams fed this diet prior to mating and pregnancy, even for a shorter period of two weeks, have poor litter survival. For this study, we used a lower fat content diet (45% kcal from fat) that had been previously used by the Sloboda lab^{501, 502, 503}, and dams were fed the diet for a shorter period of time prior to mating to generate second pregnancies. These decisions allowed us in this thesis to examine lactating dams and effects of excess gestational weight gain on immune cells in the periphery and intestines, and to generate offspring for the other cohort study collaboration.

Germ free pregnant mice
(Chapter 6: section 6.5)

GF were fed *ad libitum* S-2335 Mouse Breeder Sterilizable Diet (cat#7004, Envigo). Female and male germ free mice were paired every Monday evening and females were checked for the presence of a vaginal plug Tuesday through Friday mornings (E0.5). If no vaginal plug was observed, mice were separated and paired again the following week. Upon visualization of a vaginal plug, which was designated as confirmation of pregnancy, female mice were individually housed and exported from the Axenic Gnotobiotic Unit on E14.5. Mice were fasted for 6 hours (10 am – 4 pm). Intestinal samples were obtained for analysis by flow cytometry.

Aging studies – young and old SPF and GF experiments and colonization*(Chapter 6: section 6.4)*

Young (3-5 months of age) and old (18-24 months of age) WT female and male SPF and GF mice were used. SPF mice were fed *ad libitum* a standard aging diet (cat#2914, Envigo), and provided with an exercise wheel mounted on a hut for cage enrichment. GF mice were obtained from the Axenic Gnotobiotic Unit at McMaster University. In the facility GF mice were fed *ad libitum* the S-2335 Mouse Breeder Sterilizable Diet (cat#7004, Envigo). For SPF cohousing experiments, young adult SPF mice (4-7 months) were cohoused with old SPF mice (20-22 months) for 8-10 weeks. For GF colonization experiments, adult GF mice (9-12 months) were colonized with microbiota by placing them in dirty cage bottoms from young SPF WT mice (3-4 months) or old SPF WT mice (19-20 months). The colonized mice were fed the standard aging diet. Dirty cage bottoms from the SPF donor mice were replaced on a weekly basis for 6 weeks, and then the colonized mice were aged for ~10 months (to 20-22 months).

2.2 *In vivo* experiments**2.2.1 Metabolic and body composition assessments***(Chapter 5: section 5.1.1)*

Blood glucose was measured via tail vein using the Accu-Chek Inform II system glucometer and test strips (Roche Diagnostics). Caloric intake was calculated based on the amount of food consumed and individual mouse weight per experiment cage ($[(\text{Food eaten}/\# \text{ of mice in cage}) * (\text{g/kcal food energy density})]/\text{mouse weight}$). Adiposity was measured as percent body fat calculated from whole-body Echo-MRI imaging (Bruker Minispec LF90-II).

2.2.1.1 Glucose tolerance test

Mice were fasted for 6 hours (9 am – 3 pm). Blood glucose concentrations were measured via tail nick samples using a glucometer (described above) before intraperitoneal (i.p.) injection of 1.5 g/kg glucose (cat#G-7528, Sigma Aldrich) in sterile 0.9% saline, and after 20, 30, 40, 60, 90, and 120 minutes, as previously described^{504, 505}.

2.2.1.2 Glucose stimulated insulin secretion test

Mice were fasted for 12 hours (9 pm – 9 am). Blood was collected from a tail nick using a heparinized capillary tube (~70 µL) before and at 10, 60, and 120 minutes after i.p. injection of 3 g/kg glucose (cat#G-7528, Sigma Aldrich) in sterile 0.9% saline. All blood samples were placed on ice during the test. Samples were centrifuged for 10 minutes at 8000xg, and serum was removed and frozen at -80°C. Insulin concentrations were measured using a commercial ELISA kit by the manufacturer's instructions (cat#33270, AIS Toronto Biosciences). Assay results were recorded using the BioPlex 200 system and BioPlex Manager software version 6.1 (Bio-Rad Laboratories, Inc.).

2.2.1.3 Insulin tolerance test

Mice were fasted for 6 hours (9 am – 3 pm). Blood glucose concentrations were measured via tail nick samples using a glucometer as described above before i.p. injection of 1U/mL/kg insulin (cat#G-7528, Sigma Aldrich) in sterile 0.9% saline, and post-injection after 20, 30, 40, 60, 90, and 120 minutes, as previously described^{504, 505}.

2.2.2 CCL2-elicited monocyte response assay

Sterile saline, or 200 nM of recombinant murine CCL2 (endotoxin-free, cat#250-10, PeproTech) diluted in sterile saline, were administered i.p. as previously described³³⁶. Blood and femur bone marrow were collected four hours later for assessment by flow cytometry (see sections 2.5.1 and 2.5.2).

2.2.3 Intestinal permeability

2.2.3.1 *In vivo* intestinal permeability

(Chapter 6: sections 6.1 to 6.3 and 6.5)

Mice were placed in a clean cage and fasted for 6 hours (3 am – 9 am), or for 4 hours after weaning (lactation study: 8 am – 12 pm) and during the assay. Blood was collected via tail nick in a heparinized capillary tube prior to gavage with 4 kDa fluorescein isothiocyanate-conjugated dextran (FITC-dextran; cat#46944, Sigma-Aldrich) diluted in PBS (pH 7.4) (80 mg/kg body weight or 8 mg/kg for lactation study), and post-gavage at 30, 60, 90, 120, and 240 minutes. Acid-citrate dextrose (15% v/w; cat#C3821, Sigma-Aldrich) was added to blood samples after collection to prevent clotting. Plasma was collected post-centrifugation (8000 rpm, 10 minutes) after each time point and stored at 4°C until all samples were collected. Whole-intestine permeability was assessed by measuring fluorescence in plasma diluted 1:10 in PBS in duplicate on a plate reader with excitation at 585 nm and emission at 530 nm (Synergy H4 Hybrid Microplate Reader, BioTek Instruments, Inc.). Intestinal permeability was calculated by subtracting the average baseline fluorescence values and average fluorescence of triplicate wells of PBS (sample blank) from the average post-gavage fluorescence values at each time point in each mouse, and was expressed as relative fluorescence units.

2.2.3.2 *In vitro* intestinal permeability

(Chapter 6: sections 6.1 and 6.3)

In vitro intestinal permeability experiments were performed by Jennifer Jury, in collaboration with Dr. Elena Verdú at McMaster University. Sections of intestinal tissue were obtained from young female mice in feeding experiments (section 6.1) or after microbiota colonization (section 6.3). The proximal colon and distal ileum were excised, opened along the mesenteric border, stripped of the external muscularis layer, and mounted into Ussing chambers (World Precision Instruments), as previously described^{506, 507}. In brief, samples were equilibrated in oxygenated Krebs buffer containing 10 mM glucose (serosal side) or 10 mM mannitol (luminal side) at 37°C for ~30 minutes before baseline potential difference and short circuit current were recorded to calculate tissue conductance (G; mS/cm²) by Ohm's law. Short circuit current (I_{sc}) was measured after equilibration as an indication of active ion transport. Mucosal-to-serosal flux (%flux/cm²/hr) of the small inert probe ⁵¹Cr-EDTA (360 Da; 6 µCi/mL) (Perkin Elmer), as a measure of paracellular permeability, was assessed by taking an initial radiolabelled sample of mucosal buffer and then samples from the serosal compartment every 30 minutes for 2 hours, with addition of fresh buffer to maintain a constant volume. Samples were assessed in a liquid scintillation counter (LS6500 Multi Purpose Scintillation Counter, Beckman Coulter, Inc.), with counts from each 30 minute time point averaged and compared to the initial radiolabelled sample.

2.3 Cytokine ELISA

(Chapter 5: section 5.1)

Whole blood was collected retro-orbitally into heparin, centrifuged at 10000xg for 10 minutes, and plasma was frozen until analysis. Plasma levels of TNF and IL-6 were

assessed with a high sensitivity Milliplex MAP Kit, as per the manufacturer's instructions (cat#MCYTOMAG-70K, EMD Millipore). Assay results were recorded using the BioPlex 200 system and BioPlex Manager software v6.1 (Bio-Rad Laboratories, Inc.).

2.4 Adipose tissue histology and immunohistochemistry

(Chapter 5: section 5.1)

Adipose tissue from gonadal fat was fixed in 10% neutral-buffered formalin at room temperature for 24 hours, and processed and embedded into paraffin by the Core Histology Facility, McMaster University Research Centre. Sections of 5 µm were cut at 50 µm intervals and mounted on charged glass slides. For both adipocyte quantification and macrophage immunohistochemistry, slides were visualized with the Nikon Eclipse NI microscope (960122, Nikon Eclipse NI-S-E). Images were captured using the Nikon DS-Qi2 Colour Microscope Camera and Nikon NIS Elements Imaging Software (v4.30.02).

2.4.1 Quantification of adipocyte cross-sectional area

Slides were stained with hematoxylin and eosin at the Core Histology Facility, McMaster Immunology Research Centre. Images were taken at 20x magnification. For each mouse, three sections of adipose tissue were used for analysis, and three fields of view were captured per section such that at least 30 adipocytes could be measured within each image. Measurement of cross-sectional area was performed with ImageJ (National Institutes of Health)⁵⁰⁸. Cross-sectional area was averaged per section and per animal.

2.4.2 Localization and count of adipose tissue macrophages

As previously described¹⁷⁸, slides of adipose tissue were deparaffinized in Histo-Clear (cat#50-329-50, Fisher Scientific), blocked with 5% normal rabbit serum, and stained with anti-F4/80 monoclonal antibody (1:100; rabbit anti-rat; cat#ab6640, Abcam Inc.) overnight at 4°C for 16-18 hours. Endogenous peroxidase was inhibited with 3% H₂O₂ incubation prior to secondary antibody incubation (1:100; cat#BA-4001, Vector Laboratories Inc.), avidin-biotin peroxidase labelling (VectaStain Elite ABC-Peroxidase Kit; cat# PK-6101, Vector Laboratories Inc.), and DAB reaction (cat#BA-4001, Vector Laboratories Inc.), and samples were counterstained with Meyer's hematoxylin (cat#MHS1, Sigma Aldrich). For each mouse, two sections of adipose tissue were used for analysis, and four fields of view were captured per section at 20x magnification. The total number of nuclei and the number of nuclei of F4/80⁺ cells were counted for each field of view. The fraction of F4/80⁺ cells was calculated as the sum of the number of nuclei of F4/80⁺ cells divided by the total number of nuclei for each field of view, and ratios were averaged across each section and for each mouse and expressed as a percentage of F4/80⁺ cells per total cells⁵⁰.

2.5 Flow cytometry analysis of immune cells

2.5.1 Peripheral blood

Peripheral whole blood was collected retro-orbitally in heparinized capillary tubes under isoflurane anesthesia (non-pregnant SPF and GF mice and lactation study dams), or from tail vein nick (SPF pregnancies). All blood samples were collected in the morning to minimize effects of diurnal variation⁵⁰⁹. Whole blood (100 µL) was stained with 50 µL

antibody mix at room temperature for 30 minutes, incubated with 1x eBioscience 1-step Fix/Lyse Solution (cat#00-5333-54, ThermoFisher Scientific) for 10 minutes with frequent inversion, centrifuged at 2,000 rpm at room temperature, washed with FACs buffer (0.5% w/v BSA, 1% EDTA, PBS pH 7.6), and resuspended in FACs buffer.

Monoclonal antibodies with the following specificities were used to assess **monocytes and neutrophils** by surface staining: CCR2 (475301; PE) from R&D Systems, CD3 (17A2; Alexa Fluor 700), CD11b (M1/70; PE-Cy7), CD19 (eBio1D3; Alexa Fluor 700), CD45 (30-F11; eFluor 450), F4/80 (17-4801-82; APC), Ly6G (1A8; Alexa Fluor 700) and NK1.1 (PK136; Alexa Fluor 700), all from eBioscience, and CX₃CR₁ (SA011F11; BV650) and Ly6C (HK1.4; Alexa Fluor 488) from BioLegend. **B cells, T cells and NK cells** were identified using monoclonal antibodies with the following specificities: CD3 (17A2; Brilliant Violet 605) from BioLegend, and CD4 (RM4-5; APC-eFluor780), CD8 (53-6.7; APC), CD11b (M1/70; PE-Cy7), CD19 (eBio1D3; Alexa Fluor 700), CD45 (30-F11; eFluor 450), and NK1.1 (PK136; PE), all from eBioscience.

Intracellular staining was performed on 100 µL whole blood in complete RPMI 1640 supplemented with 10% fetal calf serum and 2x eBioscience Protein Transport Inhibitor Cocktail (cat#00-4980-03, ThermoFisher Scientific) without (unstimulated) or with lipopolysaccharide (200 ng/mL; cat#tlrl-pb5lps, InvivoGen) (stimulated) in a total volume of 200 µL. Samples were incubated for 4 hours in a tissue culture incubator (5% CO₂) at 37°C, surface stained with antibodies as described above, and then intracellular staining was performed after 30 minutes permeabilization at room temperature with 1x eBioscience Permeabilization Buffer (cat#88-8824-00, ThermoFisher Scientific) as

previously described³³⁶. Samples were surface stained with monoclonal antibodies with the following specificities: CD3 (17A2; Alexa Fluor 700), CD11b (M1/70; PE-Cy7), CD19 (eBio1D3; Alexa Fluor 700), CD45 (30-F11; eFluor 450), Ly6G (1A8; Alexa Fluor 700), and NK1.1 (PK136; Alexa Fluor 700), all from eBioscience, and Ly6C (HK1.4; Alexa Fluor 488) from BioLegend. Intracellular staining was done with monoclonal antibodies specific for TNF (MP6-XT22; Brilliant Violet 650; BioLegend), and/or IL-6 (MP5-20F3; PerCP-eFluor 710; eBioscience).

2.5.2 Bone marrow

Bone marrow was extracted from femurs and prepared as previously described¹⁰¹. The whole blood monocyte and neutrophil population surface stain antibody mix and protocol as described in section 2.5.1 were used for surface staining. Bone marrow progenitor surface staining and intracellular staining for Ki67 expression were performed using the whole blood protocols in section 2.5.1. Intracellular staining was performed without stimulation or incubation, with permeabilization immediately after surface staining. Monoclonal antibodies from BioLegend with the following specificities were used to assess myeloid progenitors by surface staining: Sca-1/Ly-6A/E (D7; PE-Dazzle 594), CD117/c-Kit (2B8; Brilliant Violet 421), CD135/Flt-3 (A2F10; PE), CD127/IL7R α (A7R34; PerCP-Cy5.5), CD34 (HM34; AF647), CD16/32 (93; Brilliant Violet 711), CD11b (M1/70; APC-Cy7), CD115 (AFS98; Alexa Fluor 488), Ly6G (1A8; Alexa Fluor 700), CD3 (145-2C11; PE-Cy7), Ter119 (TER-119; PE-Cy7), and B220/CD45R (RA3-6B2; PE-Cy7), all from eBioscience. A monoclonal antibody for Ki67 (16A8; Brilliant Violet 605; BioLegend) was used for intracellular staining.

2.5.3 Intestinal tissue

Intestinal ileum and colon tissues were removed and processed for flow cytometry based on previous protocols^{409, 510}. The distal 25% of the small intestine, adjacent to the caecum, was considered ileal tissue.

After dissection, intestinal tissue was immediately placed in ice-cold PBS. Mesenteric fat and Peyer's patches (in the small intestine) were removed and the tissue was longitudinally cut open and washed with PBS to remove contents. The tissue was cut into ~2 cm pieces and incubated in pre-warmed 'Stir Media' (RPMI 1640 supplemented with 3% FBS, 100 U/mL penicillin, 100 µg/mL streptomycin, 20 mM HEPES, 5 mM EDTA pH 8.0, and 1 mM DTT (cat#D0632, Sigma-Aldrich)) at 37°C for 20 minutes with constant stirring (~550 rpm) to remove the mucus layer.

Tissues were washed 3x by shaking for 30 seconds in serum-free pre-warmed RPMI 1640 supplemented with 100 U/mL penicillin, 100 µg/mL streptomycin, 2 mM EDTA, and 20 mM HEPES, and rinsed with pre-warmed PBS. The tissue was finely minced with scissors and incubated by stirring in serum-free pre-warmed 'Complete Media' (RPMI 1640 supplemented with 100 U/mL penicillin, 100 µg/mL streptomycin, 20 mM HEPES, 1% (v/v) non-essential amino acids, 1% (v/v) sodium pyruvate, 1% (v/v) L-glutamine, 0.01% (v/v) β-mercaptoethanol), with 0.5 mg/mL DNase I (cat#10104159001, Sigma-Aldrich) and 0.1 mg/mL Liberase TL (cat#05401020001, Sigma-Aldrich) added immediately prior to incubation for 30 minutes at 37°C (stirring at ~550 rpm), to dissociate intestinal epithelial cells and leukocytes.

Digested tissue was homogenized, washed with ice-cold Stir Media, passed through a 70 µm filter, centrifuged at 1500 rpm for 10 minutes, resuspended in ice-cold

Stir Media, passed through a 40 μm filter, and centrifuged again. The pellet was resuspended in ice-cold Complete Media supplemented with 3% FBS until staining. Live cells were counted manually under a light microscope with a hemocytometer and trypan blue stain (cat#MT25900CI, Corning).

Single cell suspensions of 5×10^5 - 2×10^6 cells were stained in a v-well plate, with all centrifugation steps at 2000 rpm for 2 minutes. Samples were washed in PBS and were incubated at 4°C with CD16/32 Fc block (cat#101302, BioLegend) in PBS for 10 minutes before staining with 50 μL antibody mix in PBS for 20 minutes at 4°C (see below). Samples were washed twice in PBS and fixed for 10 minutes in 1x eBioscience Fix-Lyse buffer (cat#00-5333-52, ThermoFisher Scientific) before washing in PBS with final resuspension in 200 μL PBS for flow cytometer analysis.

Monoclonal antibodies with the following specificities were used to assess macrophage populations in the intestines by surface staining: CD4 (R4.5; APC), Ly6C (HK1.4; Alexa Fluor 488), TIM4 (RMT4-54; PE), CD64 (X54-5/7.1; PE-Dazzle 594), CCR2 (SA203G11; Brilliant Violet 421), CD45 (30-F11; Brilliant Violet 510), F4/80 (BM8; Brilliant Violet 605), all from BioLegend, and CD11b (M1/70; PerCP-Cy5.5), MHCII (M5/114.15.2; Alexa Fluor 700), CD3 (145-2C11; PE-Cy7), B220/CD45R (RA3-6B2; PE-Cy7), and Ly6G (M1/70; PE-Cy7), all from eBioscience, and SiglecF (E50-2440; Brilliant Violet 711) from BD Biosciences. Dead cells were excluded using the LIVE/DEAD™ Fixable Near-IR Dead Cell Stain Kit, for 633 or 635 nm excitation (cat#L34975, Invitrogen).

For intracellular staining without stimulation, samples were stained as described above in a 50 μL volume with a modified surface stain. Monoclonal antibodies with the

following specificities were used for surface staining: CD4 (R4.5; APC), TIM4 (RMT4-54; PE), CD64 (X54-5/7.1; PE-Dazzle 594), CD45 (30-F11; Brilliant Violet 510), all from BioLegend, CD11b (M1/70; PE-Cy7) and MHCII (M5/114.15.2; Alexa Fluor 700) from eBioscience, and SiglecF (E50-2440; Brilliant Violet 711) from BD Biosciences. Dead cells were excluded using the LIVE/DEAD™ Fixable Near-IR Dead Cell Stain Kit, for 633 or 635 nm excitation (cat#L34975, Invitrogen). Samples were permeabilized in 200 µL of 1x eBioscience Permeabilization Buffer (cat#88-8824-00, ThermoFisher Scientific) for 30 minutes at room temperature, stained in 50 µL intracellular antibody mix with 1x Permeabilization Buffer for 30 minutes, washed twice in PBS, and resuspended in 200 µL PBS for analysis. Monoclonal antibodies with the following specificities were used for intracellular staining without stimulation: Ki67 (16A8; Brilliant Violet 605; BioLegend), TNF (MP6-XT22; Alexa Fluor 488; eBioscience), and IL-10 (JES5-16E3; PerCP-Cy5.5; eBioscience).

For intracellular staining with stimulation, samples were incubated with and without stimulation with lipopolysaccharide (200 ng/mL) in complete RPMI supplemented with 10% FBS and 2x eBioscience Protein Transport Inhibitor Cocktail (cat#00-4980-03, ThermoFisher Scientific) in a total volume of 200 µL, for 2.5 hours in a tissue culture incubator (5% CO₂) at 37°C. Surface and intracellular staining was performed as described previously for macrophage expression of TNF, IL-6, and IL-10⁵¹¹.

2.5.4 Data collection and analysis

All antibodies were titrated to determine optimal concentrations. Stained samples were assessed with unstained, isotype, and/or fluorescence-minus-one controls. Samples were run on a BD Biosciences LSRII or BD Biosciences Fortessa flow cytometer (BD

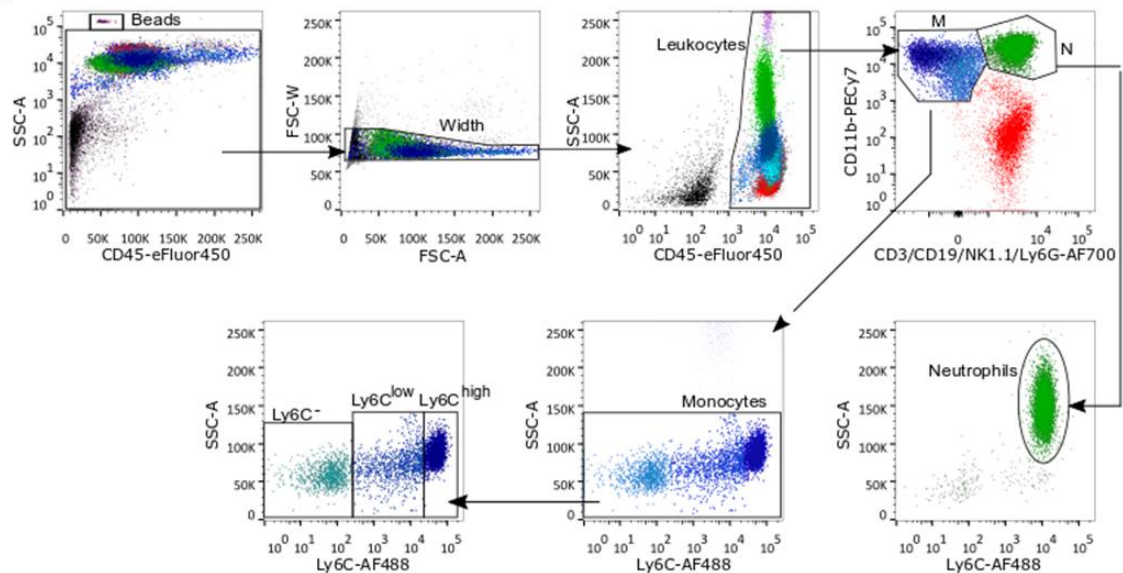
Biosciences). Data were analyzed using the FlowJo v9 software (Tree Star). Flow cytometry data for myeloid and lymphocyte populations in peripheral blood were analyzed as outlined in Appendix I, bone marrow immune cells and progenitor populations as in Appendix II, and intestinal immune cells as in Appendix III. Total cell counts were determined with CountBright Absolute Counting Beads (cat#C3650, Life Technologies). Expression of surface markers was quantified by measuring geometric mean fluorescence intensity of each fluorescence marker and subtracting background geometric mean fluorescence intensity of isotype or fluorescence-minus-one controls.

2.6 Statistical analysis

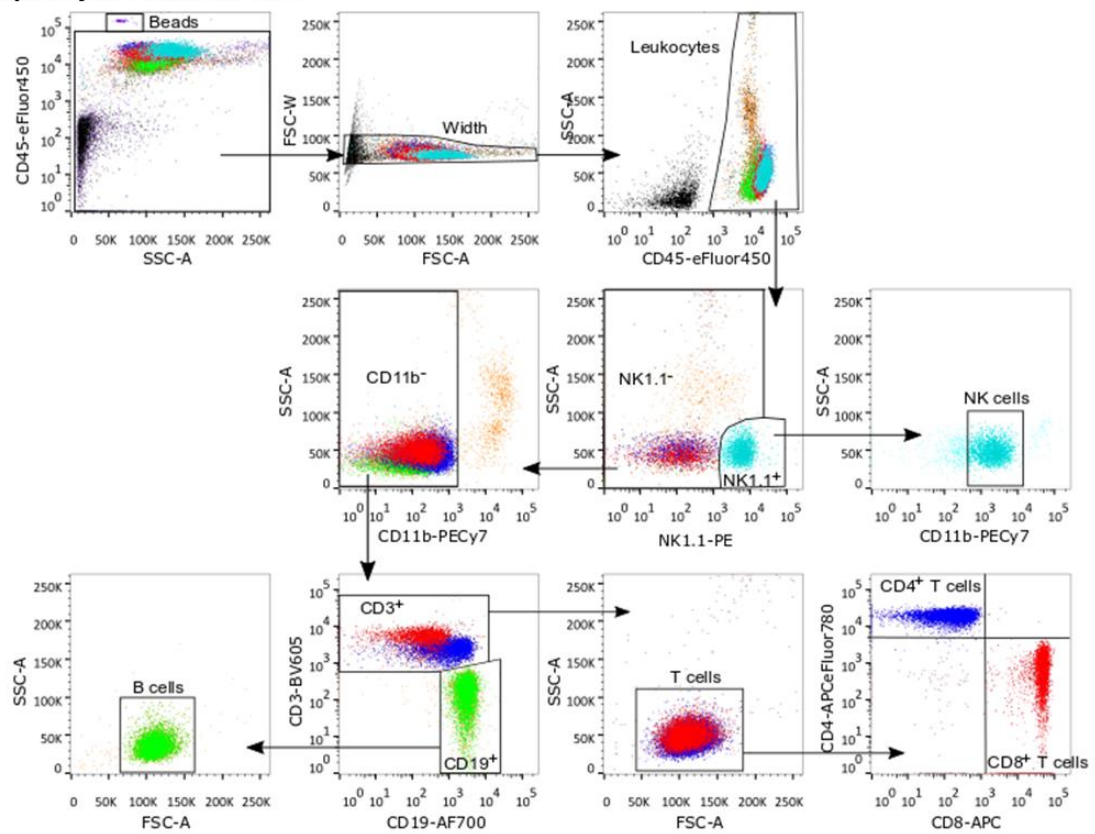
Details of specific statistical tests are included in figure legends. Data normality and variance were considered, and most data were analyzed and plotted with GraphPad Prism version 8 (GraphPad Software). More robust analyses of within-group and between-group composition and variation were performed using the *vegan*, *lme4*, and *sjstats* packages and default functions in R (v.3.3.4). Differences in peripheral immune cell composition were examined by permutational multivariate analysis of variance (PERMANOVA) with the *adonis* function. Immune cell variation was assessed using a permutation test for homogeneity of multivariate dispersions (PERMDISP) with the *betadisper* and *permutest* functions to compare the median distance-to-centroid of each group. Principal Component Analysis (PCA) ordination plots were generated using the *prcomp* function and *devtools* and *ggbiplot* packages. Data was processed to avoid overemphasis on high mean values (mean centering) and to account for value range (variance scaling). Statistical significance was defined as a *P* value of <0.05.

Appendix I. Flow Cytometry Analysis - Myeloid and Lymphocyte Gating

Myeloid Surface Stain

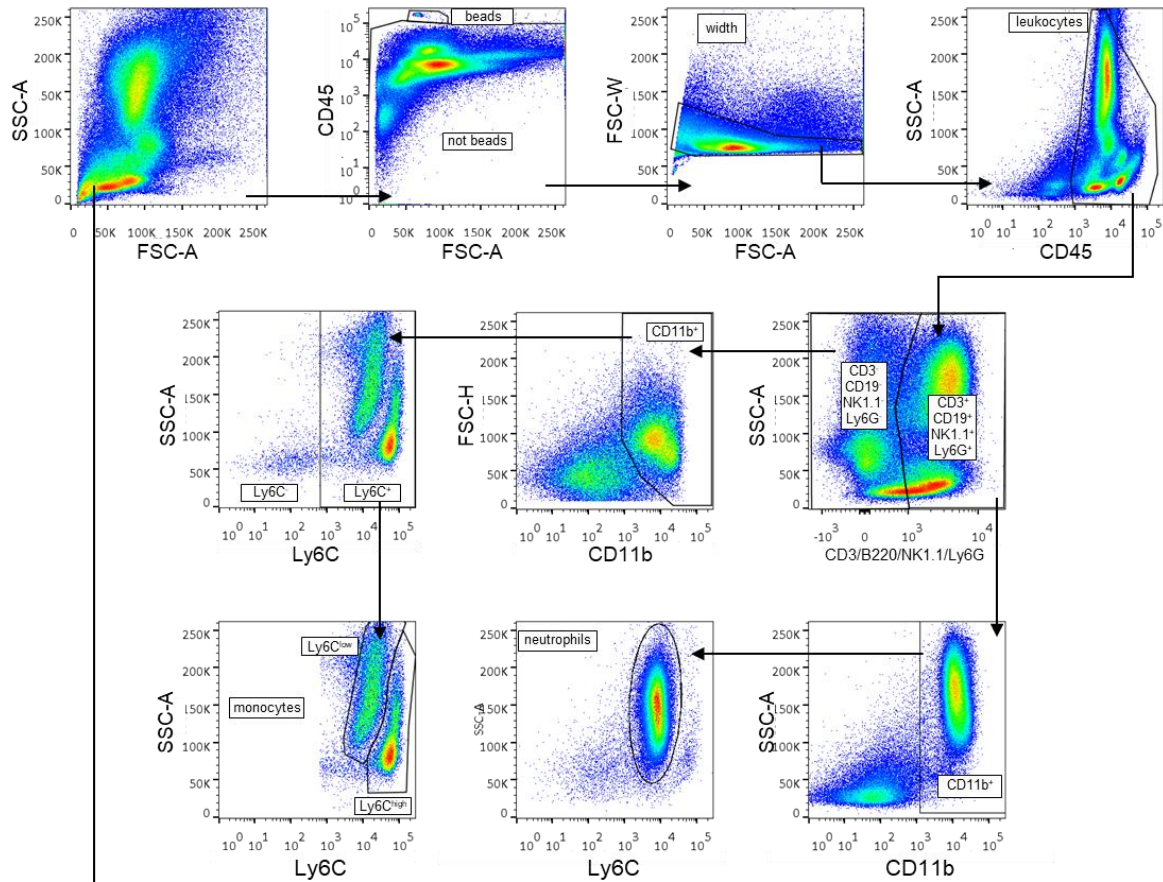


Lymphocyte Surface Stain

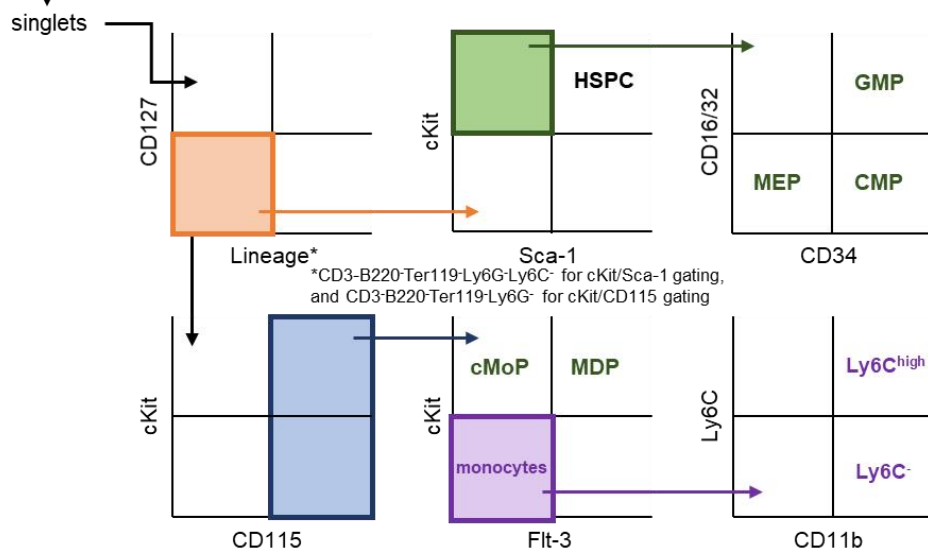


Appendix II. Flow Cytometry Analysis - Bone Marrow Gating

Bone Marrow Surface Stain

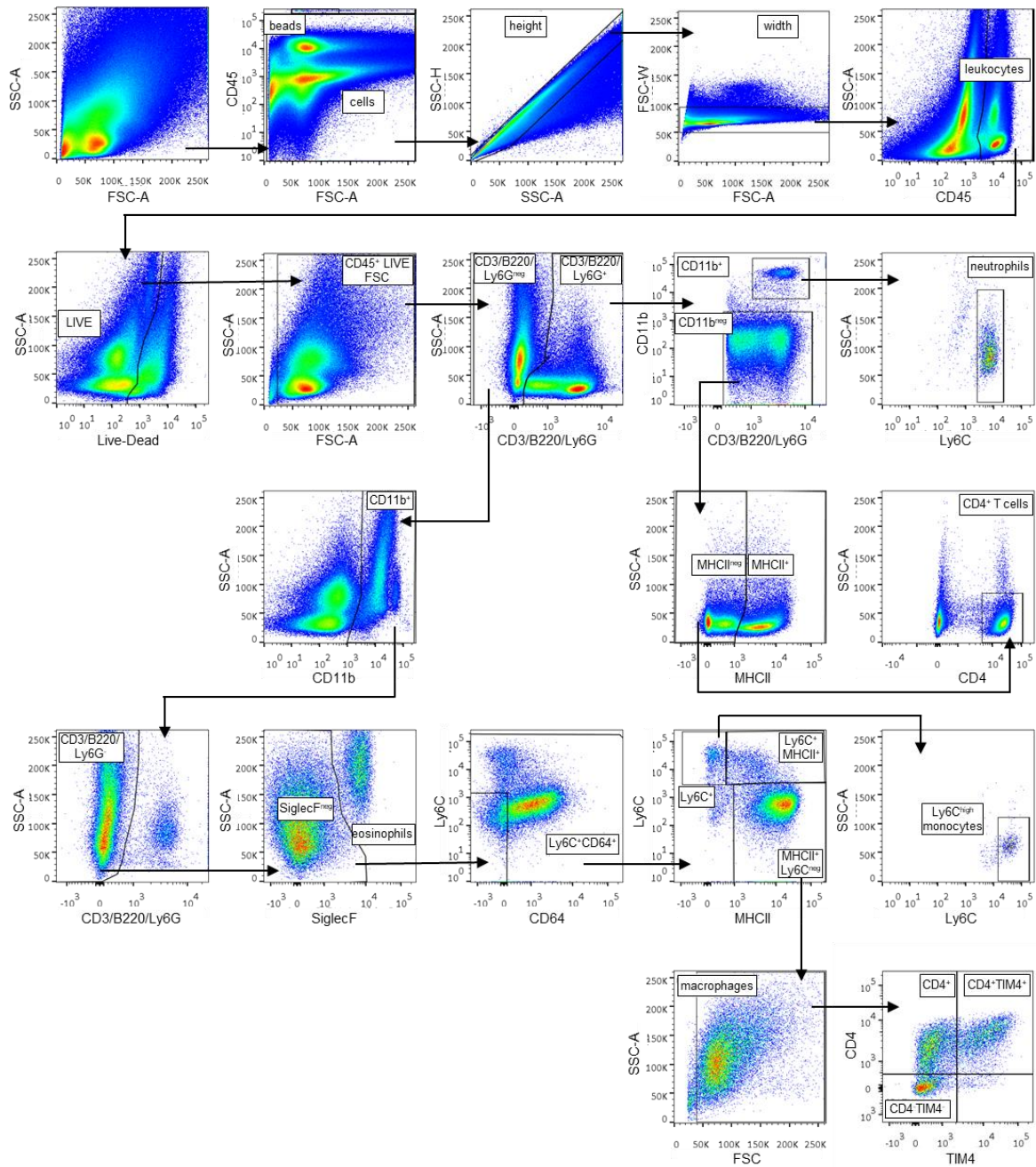


Bone Marrow Progenitor Stain



Appendix III. Flow Cytometry Analysis - Intestinal Tissue Gating

Intestine Surface Stain



Chapter 3. Biological sex, not reproductive cycle, influences peripheral blood immune cell prevalence in mice

This chapter contains a manuscript recently submitted for publication.

A broader awareness of sex-based differences and similarities in health and disease has increased acknowledgement of the importance and value of considering biological sex in basic research. Accordingly, the CIHR, NIH and other grant funding agencies have issued mandates for inclusion of male and female mice or subjects to ensure that research is applicable to both sexes. This manuscript addresses common concerns about the effects of biological sex and the female reproductive cycle when quantifying immune cells in peripheral blood (immunophenotyping). We found under routine experimental conditions with C57BL/6J mice that circulating immune cell prevalence and variability in female mice are not influenced by reproductive cycle stage. However, immune cell populations have a distinct composition by biological sex and are more variable in male mice compared to female mice. Body weight was a significant contributor to variability in male mice. Using publicly available CBC data from the JaxPhenome database, we also showed that immune cell composition and variability are not consistent between common inbred laboratory mouse strains. The flow cytometry data used in this study was collated from experiments across a three-year period, which gave us a large dataset (up to n=67 for male mice and up to n=120 for female mice for some immune cell populations), and prompted the creation of summary statistics and resource tables for researchers, to facilitate experiment planning and sample size calculations.

Biological sex, not reproductive cycle, influences peripheral blood immune cell prevalence in mice

Jessica A. Breznik^{*†}, Christian Schulz^{*†}, Jinhui Ma[‡], Deborah M. Sloboda^{§¶#}, Dawn M. E. Bowdish^{*†}

^{*}Department of Pathology and Molecular Medicine, McMaster Immunology Research Centre, McMaster University, Hamilton, Ontario, Canada.

[†]Michael G. DeGroote Institute for Infectious Disease Research, McMaster University, Hamilton, Ontario, Canada.

[‡]Department of Health Research Methods, Evidence, and Impact, McMaster University, Hamilton, Ontario, Canada

[§]Department of Biochemistry and Biomedical Sciences, McMaster University, Hamilton, Ontario, Canada.

[¶]Farncombe Family Digestive Health Research Institute, McMaster University, Hamilton, Ontario, Canada.

[#]Department of Pediatrics, McMaster University, Hamilton, Ontario, Canada.

Corresponding Author:

Dawn M. E. Bowdish

M. G. DeGroote Institute for Infectious Disease Research

McMaster Immunology Research Centre

McMaster University, MDCL 4020

1280 Main Street West

Hamilton, Ontario, Canada L8S 4K1

Phone: +1-905-525-9140, ext 22313

Fax: +1-905-522-6750

Email: bowdish@mcmaster.ca

Key Points Summary

- Traditionally the female sex, compared to the male sex, has been perceived as having greater variability in many physiological traits including within the immune system.
- We show that biological sex, but not female reproductive cyclicity, has a significant effect on immune cell prevalence and variability, and that sex differences were not consistent amongst common inbred laboratory mouse strains.
- We found that male C57BL/6J mice compared to female mice had greater variability in peripheral blood immunophenotype, and that this was influenced by body weight.
- We created summary tables for researchers to facilitate experiment planning and sample size calculations for peripheral immune cells that consider effects of biological sex.

Abstract

Immunophenotyping (i.e. quantifying the number and types of circulating leukocytes) is used to characterize immune changes during health and disease, and in response to pharmacological and other interventions. Despite the importance of biological sex in immune function, there is considerable uncertainty amongst researchers as to the extent to which biological sex or the female reproductive cycle influence blood immunophenotype. We quantified circulating leukocytes by multicolour flow cytometry in young C57BL/6J mice and assessed effects of the reproductive cycle, biological sex, and other experimental and biological factors on data variability. We found that there are no significant effects of the female reproductive cycle on the prevalence of B cells, NK cells, CD4⁺ T cells, CD8⁺ T cells, monocytes, or neutrophils. Immunophenotype composition and variability do not significantly change between stages of the female reproductive cycle. There are, however, sex-specific differences in immune cell prevalence, with fewer monocytes, neutrophils, and NK cells in female mice. Surprisingly, immunophenotype is more variable in male mice, and weight is a significant contributing factor. We show that immunophenotype varies between inbred mouse strains, and that using equal sample sizes of male and female mice is not always appropriate for evaluations of all immune cell populations in peripheral blood.

Introduction

Inclusion and distinction of biological sex in research enriches opportunities for scientific discovery, knowledge, and application (Ritz *et al.*, 2014; Klein *et al.*, 2015; Clayton, 2016); however, traditional gender biases and stereotypes have had a profound influence on how biomedical scientists approach preclinical animal research (Ritz *et al.*, 2014; Clayton, 2016). Traditionally, there has been an imbalance in the consideration of biological sex (and often the exclusion of females) in experiment design, data interpretation, and peer review and publication, which has had a negative impact on clinical developments and human health (Correa-De-Araujo, 2006; Fish, 2008; Check Hayden, 2010; Beery & Zucker, 2011; Clayton & Collins, 2014; Beery, 2018; Geller *et al.*, 2018). Less than 10% of published articles in four leading preclinical immunology journals in 2009 reported using animals from both sexes, and more than 60% of articles did not specify sex (Beery & Zucker, 2011). Biomedical funding agencies, including the National Institutes of Health, the Canadian Institutes of Health Research, and the European Commission, have recently established guidelines to encourage the consideration of sex as a basic biological variable. These guidelines aim to improve the rigor and reproducibility of research by rectifying the historical under-reporting of biological sex, generalization of male data to females and *vice versa*, and exclusion of female subjects (Clayton & Collins, 2014; Clayton, 2016; Tannenbaum *et al.*, 2016). A follow-up study of the same immunology journals in 2019 accordingly showed improvements in sex inclusion, as ~40% of articles included animals from both sexes and only ~25% of articles did not specify sex (Woitowich *et al.*, 2020). However, across biological disciplines, almost a third of studies that provided rationale for use of a single

sex still cited the potential for increased experimental variability in females (Woitowich *et al.*, 2020).

Rationale for exclusion of female animal models from preclinical research often comes from the biased belief that data variability is increased in females as a result of fluctuations in circulating ovarian hormones across the reproductive cycle, requiring a larger sample size and perhaps even monitoring of these hormones or reproductive cyclicity (Becker *et al.*, 2005; Wald & Wu, 2010; Fields, 2014). Yet, 43% of leading immunology journal articles in 2019 did not provide a description of sample size by biological sex (Woitowich *et al.*, 2020). A common approach by researchers is to propose using equal numbers of subjects for both sexes, though this practice is not necessarily appropriate if variability differs by sex (Festing & Altman, 2002; Nakagawa & Cuthill, 2007; Piper *et al.*, 2019). There is variation in endogenous sex hormone production in humans, whether as a result of intra-individual changes (e.g. across the lifespan or female reproductive cycle) or inter-individual factors (e.g. genetics or environment), though current pharmacological or immunological interventions are not routinely administered in ways that account for this natural variation (Jasienska *et al.*, 2017). Epidemiological and clinical data document unequivocal sex differences in susceptibility to infectious disease and cancer, vaccine responses, and the incidence of autoimmune disorders (Fish, 2008; Pennell *et al.*, 2012). Concerns about variability do not justify deliberate exclusion of either biological sex, but failing to consider data variation can have unintended consequences for study outcomes.

To date, we still lack sufficient empirical data to overturn the bias in using female subjects in immunological studies, and to address sample size by biological sex. Herein we investigated effects of biological sex on peripheral blood immune cell composition and variability. We quantified circulating leukocytes by flow cytometry (Ly6C^{high} and Ly6C^{low} monocytes, neutrophils, NK cells, B cells, CD4⁺ T cells and CD8⁺ T cells) in young adult wildtype C57BL/6J male and female mice under typical experimental conditions, and investigated sources of variation including reproductive cyclicity (in females), weight, age, seasonality, and cage effects. We determined that reproductive cyclicity does not have a significant effect on immunophenotype in female mice and rather, there are sex-specific differences in immune cell composition and variability. In particular, we found that variability in immunophenotype was greater in male mice, and that weight was a significant covariate that contributed to male, but not female, data variation. Based on our results, we also provide summary statistics and reference tables for researchers to perform sample size calculations that consider differences in both immune cell composition and variation by biological sex.

Methods

Ethical approval. All animal experiments were performed in accordance with Institutional Animal Utilization Protocols approved by McMaster University's Animal Research Ethics Board (Animal Utilization Protocol 17-05-19) following the recommendations of the Canadian Council on Animal Care and the ethical principles of the Journal of Physiology (Grundy, 2015).

Animals. Wildtype C57BL/6J mice were originally purchased from The Jackson Laboratory (RRID:IMSR JAX:000664) and bred at the McMaster University Central Animal Facility. All mice were cohoused 2-5 mice per cage (by sex) under specific pathogen-free conditions with constant ambient temperature (22°C) on a 12 hour light-dark cycle. Mice were fed a standard chow diet (8640 Teklad 22/5 Rodent Diet, Envigo) *ad libitum* and provided water *ad libitum*. Mice were sacrificed by cervical dislocation after blood collection, or if mice were used in further experiments, mice were given a subcutaneous injection of normal saline solution (0.9% NaCl) and eye gel following blood collection, and were monitored to ensure recovery. All sample sizes in the study indicate the number of individual mice. Female mice ~2-5 months of age (8-21 weeks; mean 12.4 weeks; $n = 120$) and male mice ~2.5-5 months of age (11-19 weeks; mean 14.1 weeks; $n = 67$), i.e. sexually mature young adults, were used in this study. All mice were virgins. Recorded mean weights were 20.1 g for female mice (range: 16.9-23.9 g) and 30.3 g for male mice (range: 26.3-37.3 g). Experimental groups are described in figures and tables.

Reproductive cycle stage determination. Hormonal fluctuations across the murine reproductive cycle correspond to distinct changes to the vaginal epithelium, in terms of cell morphology and prevalence. Vaginal cytology is a well-established and accurate method for identifying female murine estrous cycle stage and the functional status of the hypothalamic-pituitary-ovarian axis (Byers *et al.*, 2012; Cora *et al.*, 2015; Chan *et al.*, 2018; Wallace *et al.*, 2018). Vaginal cytological preparations were obtained from virgin female mice coincident with blood collection. Cells were collected with a cotton swab

moistened with sterile ambient temperature normal saline solution (0.9% NaCl), using a rolling motion against the vaginal epithelial wall, and transferred onto a dry glass microscope slide. Slides were air dried and stained with Gill Method Hematoxylin Stain (CS401-1D, Fisher Chemical) for 5 minutes to provide contrast. Slides were rinsed with tap water and air dried prior to histological assessment under a bright field microscope. All cytology assessments were performed by one individual to ensure consistency (Cora *et al.*, 2015). Estrous stage was identified by examining cellular morphology and relative abundance of nucleated vaginal epithelial cells, cornified vaginal epithelial cells, and leukocytes, as previously described (Byers *et al.*, 2012; Cora *et al.*, 2015; Wallace *et al.*, 2018). Each cytological preparation was assigned to one of four estrous stages: *diestrus* (predominantly leukocytes), *proestrus* (predominantly nucleated epithelial cells), *estrus* (predominantly anucleated cornified epithelial cells), or *metestrus* (equal proportions of anucleated cornified epithelial cells, nucleated epithelial cells, and leukocytes). Representative images of each reproductive cycle stage are shown in Figure 2A.

Blood collection and flow cytometry analysis. Peripheral blood was collected retro-orbitally under isoflurane anesthesia for analysis by flow cytometry. Blood samples were collected in the morning to minimize effects of diurnal variation (Pick *et al.*, 2019). Monoclonal antibodies with the following specificities were used with isotype and unstained controls to assess monocyte and neutrophil populations in 100 μ L of whole blood: CD3 (1:750; 17A2; Alexa Fluor 700, RRID:AB_529508), CD11b (1:1200; M1/70; PE-Cy7, RRID:AB_469587), CD19 (1:750; eBio1D3; Alexa Fluor 700, RRID:AB_837082), CD45 (1:440; 30-F11; eFluor 450, RRID:AB_1518807), Ly6G

(1:1500; 1A8; Alexa Fluor 700, RRID:AB_2802355) and NK1.1 (1:750; PK136; Alexa Fluor 700, RRID:AB_2574504), all from eBioscience, and Ly6C (1:1200; HK1.4; Alexa Fluor 488; RRID:AB_10639728) from BioLegend. B cell, T cell and NK cell populations were identified using monoclonal antibodies and unstained and isotype controls with the following specificities in 100 μ L of whole blood: CD3 (1:300; 17A2; Brilliant Violet 605; RRID:AB_2562039) from BioLegend, and CD4 (1:750; RM4-5; APC-eFluor780, RRID:AB_1272219), CD8 (1:750; 53-6.7; APC, RRID:AB_469334, or Alexa Fluor 488, RRID:AB_469896), CD11b (1:1200; M1/70; PE-Cy7, RRID:AB_469587), CD19 (1:750; eBio1D3; Alexa Fluor 700, RRID:AB_837082), CD45 (1:440; 30-F11; eFluor 450, RRID:AB_1518807), and NK1.1 (1:750; PK136; PE, RRID:AB_466048), all from eBioscience. All antibodies were titrated to determine optimal concentrations, and stains were prepared in 50 μ L volumes. Reported dilutions for each antibody include total blood and antibody stain volume (i.e. 150 μ L). Samples were stained with antibodies at room temperature for 30 minutes, incubated with 1x 1-step Fix/Lyse Solution (00-5333-54, eBioscience) for 10 minutes with frequent inversion, centrifuged at 2,000 rpm at room temperature, washed with FACs buffer (PBS, 0.5% w/v BSA, 1% EDTA, pH 7.6), and resuspended in FACs buffer for analysis. Samples were run on a BD Biosciences LSR II or BD Biosciences Fortessa flow cytometer (BD Biosciences). Data were analyzed using the FlowJo v9 software (Tree Star). Gating strategies are summarized in Figure 1. Total cell counts were determined with CountBright Absolute Counting Beads (C3650, Life Technologies).

Data curation. Female mouse data were collated from 9 experiments with $n = 4$ -13 mice per experiment (all cell populations) and 6 experiments with $n = 5$ -8 mice per experiment (monocyte and neutrophil stain only), from 2016 – 2019. Male mouse data were collated from 6 separate experiments with $n = 4$ -8 mice per experiment, one experiment with $n = 5$ mice (monocyte and neutrophil stain only) and one experiment with $n = 30$ mice, from 2017 – 2019. The publicly available Jackson Laboratories Mouse Phenome Database (MPD; RRID:SCR_003212, www.phenomejax.org) (Bogue *et al.*, 2018) was used to access the data set Jaxpheno4 (The Jackson Laboratory, 2007), which contains CBC (complete blood count) data from male and female mice 8 to 16 weeks of age. These data were obtained from 200 μ L retro-orbital whole blood analyzed with a Bayer ADVIA 120 Hematology Analyzer; further details are available from the online database. Data was accessed for C57BL/6J, BALB/cJ, C3H/HeJ, CBA/J, DBA/2J, FVB/NJ, and NOD/ShiLtJ classical inbred laboratory mouse strains. Jaxpheno4 data were used to examine peripheral lymphocyte, neutrophil, and total leukocyte population composition and variation by biological sex.

Statistical analysis

Leukocytes in the four reproductive cycle stages in female mice were analyzed by parametric one-way ANOVA if the leukocyte population was normally distributed (assessed by either Shapiro-Wilk test for normality or Brown-Forsythe test for equal variance) and the Brown-Forsythe test was not significant. Data that were not normally distributed were analyzed by non-parametric Kruskal-Wallis test. As no tests were statistically significant, post-hoc multiple comparison tests were not performed.

Comparisons of leukocyte populations between male and female mice were analyzed by unpaired two-tailed Student's *t* test (parametric) with Welch's correction (assuming unequal variances between male and female mice) or Mann-Whitney *U* test (non-parametric) according to normality. Comparisons of CBC data from C57BL/6J mice and other inbred mouse strains were performed by two-way ANOVA with correction for multiple comparisons between C57BL/6J mice and other strains by Dunnett's test. Data were analyzed and plotted with GraphPad Prism version 6 (GraphPad Software, RRID:SCR_002798). Effect size and sample size calculations were performed in G*Power (Faul *et al.*, 2007) (v.3.1.9.4, RRID:SCR_013726), with $\alpha = 0.05$ and 80% power. Two-group two-tailed comparisons were calculated using the statistical test Means: Difference between two independent means (two groups). Calculations of sample sizes for immune cell population comparisons within each sex were performed using immune cell population mean, calculated mean based on a set percent change, and equal standard deviation. More robust analyses of within-group and between-group composition and variation were performed using the *vegan*, *lme4*, and *sjstats* packages and default functions available from CRAN (<https://cran.r-project.org/>) using the R programming language in RStudio (v.3.3.4, RRID:SCR_000432). Differences in immune cell population composition between reproductive cycle stages in female mice and by biological sex were examined by permutational multivariate analysis of variance (PERMANOVA) with the *adonis* function. Immune cell population variation within reproductive cycle stages and within a biological sex was assessed using a permutation test for homogeneity of multivariate dispersions (PERMDISP) with the *betadisper* and *permutest* functions to compare the median distance-to-centroid of each group. Principal

Component Analysis (PCA) ordination plots were generated using the *prcomp* function and *devtools* and *ggbiplot* packages. Data was processed prior to performing PCA to avoid overemphasis on variables with high mean values (mean centering), and to account for populations with a greater range of values (variance scaling). The intraclass correlation coefficient (ICC) was calculated for immune cell populations using the mixed effect model with sex and age as the fixed effects and cage as the random effect (Fleiss & Cohen, 1973; Moen *et al.*, 2016). The design effect (DE) was calculated as $DE = 1 + ICC(m-1)$, where *m* is the average number of mice per cage (mean \pm SD: 3.91 ± 1.10). Statistical significance was defined as a *P* value of <0.05 .

Data availability

Data from this study are available from the corresponding author upon request.

Results

Reproductive cycle stage does not significantly change peripheral immune cell prevalence or variability in female mice

We quantified leukocytes in peripheral whole blood of young female mice by flow cytometry. We identified reproductive cycle stage in each individual mouse by examination of vaginal smear epithelial and immune cell prevalence and morphology (Figure 2A). Vaginal cytology is a non-invasive accepted standard method for determination of reproductive cycle stage in female mice, as it provides an indirect yet accurate assessment of ovarian hormone fluctuations (Byers *et al.*, 2012; Cora *et al.*,

2015; Chan *et al.*, 2018; Wallace *et al.*, 2018). Myeloid immune cells (Figure 2, B to F), lymphocytes (Figure 2, G to L), their ratio (Figure 2M), and total leukocyte counts (Figure 2N), were not significantly different between reproductive cycle stages. Mouse weight was not significantly different between the reproductive stage groups (Figure 2O; mean \pm SD: proestrus, 20.4 ± 1.38 g; estrus 20.2 ± 1.52 g; metestrus, 20.5 ± 1.78 g; diestrus, 20.2 ± 1.22 g), nor was age (Figure 2P). Reproductive cycle stage therefore did not alter any of the leukocyte populations examined, whether as a proportion of total CD45⁺ leukocytes (Figure 2) or as absolute cell counts (data not shown).

We next assessed whether there were significant changes in whole population immunophenotype between each reproductive cycle stage. We plotted our data by estrous stage using PCA (Principal Component Analysis) (Figure 2Q), with PC1 and PC2 illustrating 76.9% of variance in the dataset. We determined using a whole-population analysis approach (i.e. considering all individual leukocyte populations simultaneously) that immunophenotype was similar in each stage of the female reproductive cycle (PERMANOVA: $P = 0.467$, $R^2 = 0.04856$). Leukocyte population variance was also not altered by reproductive cycle stage (PERMDISP: $P = 0.882$, $F = 0.2315$; Figure 2R). We repeated these analyses using absolute cell counts, and likewise found that data composition and variation were similar in each stage of the reproductive cycle (Figure 2S; PERMANOVA: $P = 0.213$, $R^2 = 0.07242$; PERMDISP: $P = 0.510$, $F = 0.8152$). These results indicate that inter-individual female mouse leukocyte populations, and immunophenotype as a whole, are not altered by reproductive cycle stage, either in terms of their composition or variation.

We also considered a simplified approach to characterize reproductive cyclicity, grouping data from proestrus and estrus (absence of leukocytes in vaginal smears; estradiol-dominant stages analogous to human follicular phase) and metestrus and diestrus (presence of leukocytes in vaginal smears; progesterone-dominant stages analogous to human luteal phase) (Byers *et al.*, 2012; Cora *et al.*, 2015). When our data were separated into these two groups, we again found no differences in peripheral leukocyte population composition or variation, whether we considered proportional data (Figure 2T; PERMANOVA: $P = 0.561$, $R^2 = 0.01007$; PERMDISP: $P = 0.416$, $F = 0.7168$) or absolute cell counts (Figure 2U; PERMANOVA: $P = 0.200$, $R^2 = 0.02419$; PERMDISP: $P = 0.231$, $F = 1.6276$). In summary, female mouse reproductive cyclicity does not significantly alter inter-individual peripheral leukocyte population prevalence, nor does it increase peripheral leukocyte variation under normal physiological and experimental conditions.

Peripheral immunophenotype is not more variable in C57BL/6J female mice compared to male mice

For many years, researchers assumed that data obtained from male mouse models were representative of data from female mouse models, and *vice versa* (Beery, 2018; Shansky, 2019). Using data collected for our reproductive cycle stage assessments in female mice, and additional immunophenotyping data from young adult male (~2.5-5 months of age; 11-19 weeks; mean 14.1 weeks) and female mice (~2-5 months of age; 8-21 weeks; mean 12.4 weeks), we performed pairwise comparisons of immune cell populations by biological sex (Figure 3, Tables 1 to 3). We confirmed that female and male peripheral

blood immune cell profiles are not the same. Male mice had higher proportions (of CD45⁺ leukocytes) of monocytes (Figure 3A), neutrophils (Figure 3B), and NK cells (Figure 3C), whereas female mice had higher proportions of B cells (Figure 3D), CD4⁺ T cells (Figure 3E), and CD8⁺ T cells (Figure 3F). Absolute cell count data also demonstrated significant sex differences (Table 3). It is important to note that although mean values are different by biological sex, the range of data values for most immune cell populations overlaps between male and female mice for both proportional data and absolute counts, in particular for NK cells, CD4⁺ T cells, and CD8⁺ T cells. For example, although the mean prevalence of CD8⁺ T cells is higher in female mice (mean \pm SD: 7.06 \pm 1.74% as a proportion of total leukocytes) in comparison to male mice (5.89 \pm 1.10%), the range of male mouse CD8⁺ T cell prevalence is from 3.44 to 8.24%, which is completely within the identified range of CD8⁺ T cells in female mice (2.24 to 9.96%) (Table 2). These observations of overlapping data ranges, rather than completely distinct distributions, suggest that assessing biological sex-associated variation would be more informative than comparison of absolute means, when considering sex differences in peripheral immune cells.

There is a widely held assumption across biomedical research disciplines that reproductive cyclicity increases the variability of data generated in females (Wald & Wu, 2010; Beery, 2018; Shansky, 2019). We found that reproductive cycle stage did not contribute to variation in female mouse immunophenotype. We next investigated whether there was any merit to the belief that female data is more variable than male data. We initially considered variation in each of the leukocyte populations in terms of standard

deviation (i.e. actual dispersion of data) and coefficient of variation (CV; i.e. scaled dispersion), which differed according to immune cell subset. For example, while B cells had a higher coefficient of variation in male mice (male CV 25.4%; female CV 8.4%), CD8⁺ T cells were more variable in female mice (male CV 18.7%; female CV 24.6%), yet the coefficient of variation of CD4⁺ T cells was similar in male mice and female mice (male CV 20.4%; female CV 20.2%) (Table 2).

We then assessed whole-population leukocyte changes and variability by biological sex. Immunophenotype data were plotted using PCA for leukocyte subsets as proportions of CD45⁺ leukocytes (Figure 3G) and as absolute cell counts (Figure 3H). Consistent with our analysis of individual leukocyte subsets, we found a sex-specific effect on the prevalence of all leukocyte populations (PERMANOVA: $P = 0.001$; $R^2 = 0.35224$), and their absolute cell counts (PERMANOVA: $P = 0.001$, $R^2 = 0.1590$). We found that biological sex explains 35.2% of variance in the immune cell populations (by proportions; 15.9% by absolute cell counts). Analysis of homogeneity showed a difference in variance of leukocyte populations by biological sex (Figure 3I; PERMDISP; proportions: $P = 0.001$, $F = 36.673$; absolute cell counts: $P = 0.023$, $F = 4.990$), which was greater in male mice compared to female mice.

Peripheral immunophenotype is influenced by weight in male mice

We further considered experimental and biological factors that may have contributed to variability in our data. All blood was collected, processed, and analyzed in a similar manner, to minimize effects of circadian rhythm and day-to-day experiment variation

(Pick *et al.*, 2019). The mice were all derived from an in-house breeding program, were of the same genotype, were separated by sex and unmated, and were maintained with similar cage conditions (bedding, enrichment, food, cohousing). Using univariate analysis, we evaluated whether factors like age, weight, social dominance, and time of year (season), contributed to variation in our data on a population-level basis (Table 4). Time of year (grouped by season) and social dominance (using within-cage weight differences as a proxy) did not contribute to data variation in either male or female mice. We found that both weight (grouped according to standard deviation or 95% confidence interval) and age (in weeks) contributed to overall leukocyte immunophenotype variation in male mice. Female mouse data showed a similar (though cumulatively smaller) effect of age on data variation (Table 4). There were no associations between female immunophenotype variation and weight, social dominance, or time of year. Overall, our data demonstrate that age, even within the small age range of our ‘young adult mouse’ dataset (~2-5 months of age), influences female and male immunophenotype variation, whereas weight may also affect immunophenotype variation in male mice.

Flow cytometry and complete blood count peripheral immune cell data show greater variability in male mice

Flow cytometry is a common method to identify immune cells in peripheral blood, but CBC data are also widely used in preclinical and clinical research (Hoggatt *et al.*, 2016). Our flow cytometry data showed a large range of cell counts and proportional values for B cell and neutrophil populations in male mice (Figure 3; Tables 1 to 3), so we next compared our data with CBC data from the publicly available Jaxpheno4 dataset (see

Methods; Figure 4, Tables 5 and 6). While overall cell proportions and counts were slightly different as a result of cell population identification methods (i.e. flow cytometry identifies leukocytes using antigen-specific fluorophore-conjugated monoclonal antibodies whereas CBC identifies leukocytes by size using electrical resistance) (Hoggatt *et al.*, 2016), similar observations were apparent. Neutrophil cell counts and proportional prevalence were higher in male mice compared to female mice (Figure 4, A to B and E to F). Lymphocyte cell counts were higher in female mice compared to male mice by CBC, but not flow cytometry analysis (Figure 4, C to D), while female mice had higher proportions of lymphocytes by CBC and flow cytometry analysis compared to male mice (Figure 4, G to H). As well, the range of values and variance were consistently greater in male mice compared to female mice for the CBC-derived and flow cytometry-derived prevalence data for lymphocytes (CBC % white blood cells: male CV 31.3%, female CV 4.6%; flow cytometry % leukocytes: male CV 20.8%, female CV 4.23%) and neutrophils (CBC % white blood cells: male CV 82.3%; female CV 43.5%, flow cytometry % leukocytes: male CV 68.2%, female CV 36.8%) (Tables 5 and 6). These CBC data corroborated our flow cytometry results showing that peripheral blood lymphocyte and neutrophil prevalence is indeed more variable in male mice compared to female mice.

Peripheral blood immune cell prevalence and variability are not consistent across classical inbred laboratory mouse strains

We used C57BL/6J mice in our experiments, which is the most common inbred mouse strain used by biomedical researchers and is widely used for the generation of knockout and transgenic mouse models. To investigate whether our observations are also applicable

to other mouse strains, we accessed CBC and differential count data from the Jaxpheno4 dataset for a subset of other common laboratory strains of wildtype inbred mice: BALB/cJ, C3H/HeJ, CBA/J, DBA/2J, FVB/NJ, and NOD/ShiLtJ (Figure 5, Tables 5 and 6). While C57BL/6J lymphocyte and neutrophil prevalence data had the highest variation (assessed from standard deviation and coefficient of variation) in male mice, some mouse strains had either similar variation between sexes (e.g. C3H/HeJ), or higher variation in females (e.g. CBA/J). Effects of biological sex and strain on these CBC measurements were assessed by two-way ANOVA for lymphocyte and neutrophil mean population cell counts and prevalence. As summarized in Tables 5 and 6, there was a significant interaction between the effects of sex and strain on neutrophil prevalence, lymphocyte prevalence, and cell counts of neutrophils and lymphocytes. Simple main effects analysis showed that there was a significant effect of strain for all cell populations, while an effect of biological sex was significant for lymphocyte cell counts and prevalence, and neutrophil prevalence, but not neutrophil cell counts. These data show that despite similar genetic origins and limited haplotype diversity (Yang *et al.*, 2007; Yang *et al.*, 2011), inbred laboratory mouse strains have considerable strain and sex-specific variability in peripheral blood immune cell characteristics.

Individual peripheral leukocyte populations have distinct sample size requirements

We have shown that sex-specific differences exist in immunological data from peripheral blood, so using equal sample sizes of male and female subjects (at least in mice) is not optimal to determine whether there are differences in specific traits or treatment outcomes within a biological sex (Festing & Altman, 2002; Nakagawa & Cuthill, 2007; Piper *et al.*,

2019). Although sample sizes should be determined by a calculated effect size (e.g. after performing a pilot study), this is not always feasible. Our flow cytometry data for young adult C57BL/6J female and male mice was collected under normal physiological conditions (Tables 1 to 3), and can be used to perform *a priori* calculations for experiment planning (Festing & Altman, 2002). To illustrate, we used our calculations of mean and standard deviation for leukocyte populations, based on a predicted percent change in population prevalence, to generate a table of possible sample sizes for commonly used two-group comparisons (Table 7). For example, using the mean and standard deviation of the prevalence of CD4⁺ T cells in female mice (Table 2), we calculated that an experiment with two independent groups (e.g. control and treatment), with an expected 30% change in CD4⁺ T cell prevalence after treatment (Cohen's $d = 1.48$), would require a sample size of 9 female mice in each group. In addition, we calculated sample sizes for two-group comparisons of neutrophils and total lymphocytes using CBC data, which were similar or even greater than sample sizes calculated from our flow cytometry data (Table 8). These tables illustrate that leukocyte populations have distinct sex-specific requirements for sample size determination to assess a similar magnitude change. In accordance with our observations of sex-specific differences of data variation within leukocyte populations, our calculations show that male and female mice often have separate sample size recommendations for the same expected percent change or effect size.

Group housing of multiple mice within a single cage is widely used to ensure animal welfare while optimizing experimental design and cost (Horii *et al.*, 2017; Kappel *et al.*,

2017). Though dependent on study design, the standard practice is often to assume that potential effects of mouse housing cage are irrelevant for a given level of statistical power for a study, so each mouse is considered as an independent sample and the dependence of mice in the same cage is largely ignored (Basson *et al.*, 2020). We therefore calculated the required sample size (n_0), assuming that mice are independent, for each immune cell population (Tables 7 and 8). However, the clustering effect of housing cage may be an important contributor to the estimation of statistical power and sample size (Collins & Tabak, 2014; Parker & Browne, 2014; Baker, 2016; Basson *et al.*, 2020). To assess the impact of using data from mice within the same cage compared to different cages on our sample size and statistical power calculations due to the intra-cage (clustering) effects, we also calculated the intraclass correlation coefficient and design effect (Table 9). These factors can be applied to adjust the required sample size (adjusted sample size $n = n_0 * DE$) to account for the similarity of mice within the same cage, for each immune cell population (Fleiss & Cohen, 1973; Moen *et al.*, 2016).

Discussion

Blood immune cell composition is reflective of whole-body immunological status (Kaczorowski *et al.*, 2017). Blood immunophenotype is modified by sex, gender, genetics and environmental factors, as well as other conditions that impact the endocrine-immune axis, including obesity, physical activity, pregnancy, and age (Fish, 2008; Pennell *et al.*, 2012; Brodin *et al.*, 2015; Brodin & Davis, 2017; Mangino *et al.*, 2017). While these factors contribute to significant inter-individual variation, repeated assessments across weeks to months, and even years, suggest that the peripheral immune cell composition of

a healthy adult individual is fairly stable in the absence of perturbations such as vaccination or an acute infection (Orri *et al.*, 2013; Tsang *et al.*, 2014; Carr *et al.*, 2016; Shen-Orr *et al.*, 2016). However, there remains considerable uncertainty regarding the effects of the female reproductive cycle on immunophenotype (Becker *et al.*, 2005; Wald & Wu, 2010; Fields, 2014). Multiple studies have attempted to document changes in the prevalence, phenotype, and/or function of peripheral immune cells in relation to the menstrual cycle in humans (Bain & England, 1975; Mathur *et al.*, 1979; Northern *et al.*, 1994; Faas *et al.*, 2000; Bouman *et al.*, 2001a, b; Darmochwal-Kolarz *et al.*, 2003; Lee *et al.*, 2010; Prasad *et al.*, 2014; Nowak *et al.*, 2016). These studies vary widely in design, in terms of blood collection and assessment procedures, how the menstrual cycle is tracked, the number of cycles evaluated, when blood is collected during the day and when during the reproductive cycle, group size, as well as subject demographics including age and weight. Perhaps it is not then surprising that there is no agreement as to whether immunophenotype changes in relation to the female reproductive cycle. The lack of consensus in human data may be due to the general inter-individual variation of immunophenotype, independent of reproductive cyclicity (Orri *et al.*, 2013; Tsang *et al.*, 2014; Carr *et al.*, 2016; Shen-Orr *et al.*, 2016; Kaczorowski *et al.*, 2017), or could be indicative of combined effects of differences in genetics and environmental-social context on endocrine-immune interactions in study populations (Demas & Carlton, 2015). Experimental animal models used to assess the physiological effects of ovarian hormones often administer supraphysiological levels of exogenous sex-steroids, deplete endogenous hormone production through surgery (ovariectomy) or use pharmacological intervention (Diaz Brinton, 2012). Consequently, there was little evidence to indicate whether changes

to immunophenotype occur due to normal endogenous hormone variations within the reproductive cycle. We investigated the effects of reproductive cyclicity on inter-individual immunophenotype composition and variability using genetically identical C57BL/6J inbred female mice under controlled environmental and experimental conditions to mitigate sources of variation. Reproductive stage was determined by an accepted standard, vaginal cytology, at the time of blood collection in individual mice. To our knowledge, this is the first study to examine associations between murine peripheral immune cell populations and estrous cycle stage by flow cytometry.

Our data show that large shifts in immunophenotype do not occur between the four stages of the mouse estrous cycle, or between estradiol or progesterone-dominant stages. These results are consistent with previous studies that quantified leukocytes in blood smears across successive estrous cycles in the same group of BALB/c mice over 4 months (total leukocytes and lymphocytes) (Mysliwska *et al.*, 1975), and by CBC in white rats over 2.5 months (total leukocytes, lymphocytes, neutrophils and eosinophils) (Gloskowska-Moraczewska & Sitarska, 1973). Our study was not designed to assess whether immune cell activation or function differs across the reproductive cycle, as has been suggested by observations of changes to lymphocyte size and nuclear structure in blood smears collected from mice across successive estrous cycles (Mysliwska *et al.*, 1975). While direct manipulation of ovarian function and/or exposure of mice to supraphysiological levels of ovarian sex hormones was not within the scope of our investigation, a recent study found that there was no effect of exogenous estradiol-hemisuccinate or medroxyprogesterone-acetate treatment on total leukocytes in bone marrow, spleen, or

peripheral blood, compared to pre-injection assessments or measurements from control mice in estrus (estradiol-high) or diestrus (progesterone-high) reproductive stages (De Gregorio *et al.*, 2018). Lymphocyte and granulocyte differential counts from blood smears were likewise unaffected by estradiol-hemisuccinate or medroxyprogesterone-acetate treatment (De Gregorio *et al.*, 2018). These previous studies are consistent with our observations that peripheral leukocyte composition is similar between stages of the reproductive cycle in young female mice. Therefore, if a researcher is not specifically interested in studying the effects of female sex hormones, or intra-individual effects, under typical experimental conditions there is no need to track the estrous cycle, measure hormones, or chemically/physically alter female mice to assess peripheral blood immunophenotype. Female mammals, including mice and humans, rely on the proper function of the hypothalamus-pituitary-ovarian axis for successful reproduction, and accordingly there are analogous, though different, patterns of hormone fluctuations across the ~4-5 day estrous cycle in mice and the ~28 day menstrual cycle in humans (Becker *et al.*, 2005). Our data, from a clinical perspective, therefore suggests that inter-individual changes in peripheral blood immunophenotype may not be significant across the menstrual cycle. While we found that reproductive cyclicity did not alter peripheral blood immunophenotype, it is also important to note that both estrogen and testosterone modulate behaviour (McEwen *et al.*, 2015; Gobinath *et al.*, 2017), and accordingly estrous stage has been reported to impact some behavioural traits in female mice (ter Horst *et al.*, 2012), just as testosterone also impacts some behaviours in male mice (Celec *et al.*, 2015).

We characterized distinct sex-specific effects on peripheral blood leukocyte prevalence in C57BL/6J mice (Figure 3). Despite this, we also found that there were similarities in the range and distribution of male and female immune cell populations, whether expressed as absolute counts or as a proportion (of total leukocytes). Thus, we further considered whether there existed a sex-specific effect on the variability of data. We identified that male immunophenotype was significantly more variable than female immunophenotype in C57BL/6J mice, which contradicts the widely held assumption that reproductive cyclicity increases the variability of data collected from females (Wald & Wu, 2010; Beery, 2018; Shansky, 2019). Our experimental data is consistent with observations of Prendergast and colleagues, who reviewed 9932 mouse traits from 293 published articles and found that male traits had a broader distribution of variability than female traits, although the estrous cycle was not considered in their study (Prendergast *et al.*, 2014).

Immunophenotype variability in male, but not female mice, was found by univariate analysis to be significantly influenced by weight (Table 4). Mouse weight is affected by many factors including sex, age, diet, behaviour, and metabolism (Bartke & Dalterio, 1975; Horii *et al.*, 2017; Ingvorsen *et al.*, 2017). While we did not further explore this observation, it may indicate that multivariate methods of analysis, such as linear mixed models, would be useful to consider in study design and analysis where weight is a potential confounding factor (Oellrich *et al.*, 2016; Ingvorsen *et al.*, 2017). Weights of mice within a cage have been used as a marker of social dominance, which is known to influence male mouse sex hormone levels (Bartke & Dalterio, 1975; Machida *et al.*, 1981; Horii *et al.*, 2017), though we did not see any effects on immunophenotype. Testosterone

is often assumed to be non-fluctuating, but there is considerable intra- and inter-individual variation in peripheral testosterone (up to a 40-fold increase) in young sexually mature male mice, due to spontaneous release every 3-4 hours even in the absence of mating interactions (Bartke & Dalterio, 1975; Coquelin & Desjardins, 1982; Nyby, 2008). Whether male sex hormones may influence mouse immunophenotype variability under normal physiological conditions has never been tested to our knowledge. Testosterone has been reported to suppress B cell lymphopoiesis in the bone marrow, and B cell maturation in the spleen, resulting in decreased circulating B cells (Viselli *et al.*, 1997; Wilhelmson *et al.*, 2018), and has also been reported to stimulate neutrophil production (Chuang *et al.*, 2009). However, those experiments were performed by surgical manipulation (orchiectomy) or generation of transgenic androgen receptor knockout mice, and consideration of male sex hormones was outside the scope of our current study. Irrespective of whether male or female sex hormones influence immunophenotype, identifying potential sources of variation does not justify deliberate exclusion of either biological sex, but should guide experimental design.

We compared our flow cytometry immunophenotype data with publicly available CBC data, and found considerable variation in neutrophil and total lymphocyte populations amongst several inbred mouse strains (Figure 5; Tables 5 and 6). We showed a continuum of immunological variation across classical inbred laboratory mouse strains and identified that immune cell counts, prevalence, and effects of biological sex are not consistent across multiple strains. Despite this, trends of immune cell prevalence in C57BL/6J mice (i.e. female mice have a higher proportion of lymphocytes and a lower proportion of

neutrophils) were also apparent in FVB/NJ, BALB/cJ, and DBA/2J mouse strains, and lower variability was likewise observed in neutrophil and lymphocyte populations of FVB/NJ and BALB/cJ female mice. Our data emphasize the importance of recording characteristics including mouse strain and source, sex, age and weight, and support the use of PREPARE (Planning Research and Experimental Procedures on Animals: Recommendations for Excellence) and ARRIVE (Animal Research: Reporting of *In Vivo* Experiments) guidelines when planning, conducting, and reporting experiments to improve critical analysis of data and reproducibility (Kilkenny *et al.*, 2009; Clayton, 2016; Smith *et al.*, 2018).

There has been increasing acknowledgement of a ‘reproducibility crisis’ in science (Collins & Tabak, 2014; Baker, 2016). This realization has reaffirmed the importance of power calculations and selection of appropriate sample size, which is hampered by the lack of biological data available for thoughtful and informed calculations (Nakagawa & Cuthill, 2007; Halsey *et al.*, 2015; Higginson & Munafo, 2016; Piper *et al.*, 2019).

Reliable power calculations would minimize cost, ensure minimal and humane use of animals, and refine sensitivity and reproducibility of scientific data (Festing & Altman, 2002; Shaw *et al.*, 2002; Kilkenny *et al.*, 2009; Burden *et al.*, 2015). We used our flow cytometry data and publicly available CBC data to calculate sample sizes for two-group assessments (Tables 7 and 8). Our calculations illustrate that the often-standard practice of using equivalent sample sizes of male and female mice may be well-intentioned, but flawed (Festing & Altman, 2002). Sample size was almost equivalent for both sexes when considering total lymphocytes, total monocytes, and CD4⁺ T cells, but in contrast,

neutrophils and B cell measurements required fewer female mice, and fewer male mice were required for assessments of CD8⁺ T cells and NK cells. In addition, we demonstrated that the intra-cage clustering and the design effect (Table 9) for immune cell populations in peripheral blood are not insignificant (Fleiss & Cohen, 1973; Nakagawa & Cuthill, 2007). We expect this information can be of use in planning future immunophenotype experiments. These data illustrate the importance of considering male and female data by sex when there are sex-specific differences in data distribution, and support the use of factorial designs to evaluate effects of treatment and biological sex (Festing & Altman, 2002; Shaw *et al.*, 2002; Beery, 2018).

Our data complement those in meta-analyses demonstrating that categorical and continuous measures of behavioural, morphological, physiological, and molecular traits in female rodents are no more variable, or even less variable, than those of male rodents (Mogil & Chanda, 2005; Prendergast *et al.*, 2014; Itoh & Arnold, 2015; Becker *et al.*, 2016; Dayton *et al.*, 2016). Our study emphasizes the importance of reporting animal characteristics and their influence on experiment outcomes, addresses long-held assumptions about physiological effects of biological sex, and contributes to demystifying the influence, or lack thereof, of the female mouse reproductive cycle on routine blood immunophenotyping.

Additional Information

Competing interests: The authors declare that they have no competing interests.

Author contributions: JAB, DMS, and DMEB designed the study. JAB and CS performed the experiments. JAB, DMS, DMEB, and JM contributed to the analysis of data. JAB, DMB and DMEB contributed to the interpretation of data and writing and editing of the manuscript. All authors have approved the final version of the manuscript and agree to be accountable for all aspects of the work. All persons listed as authors qualify for authorship.

Funding: JAB was supported by a Queen Elizabeth II Graduate Scholarship in Science and Technology (QEII-GSST). CS was supported by a postdoctoral fellowship from the Deutsche Forschungsgemeinschaft (SCHU3131/1-1) and an Ontario Lung Association Team Breathe Award Grant-in-Aid awarded to DMEB. DMS is the Canada Research Chair in Perinatal Programming. This research is supported by a CIHR Team Grant led by DMS and a CIHR Geroscience Demonstration Grant led by DMS and DMEB. DMEB is the Canada Research Chair in Aging and Immunity. The Bowdish lab is supported by the McMaster Immunology Research Centre and the M. G. DeGroote Institute for Infectious Disease Research.

Acknowledgements: The authors thank Katherine Kennedy for her advice regarding data analysis.

References

- Bain BJ & England JM. (1975). Variations in leucocyte count during menstrual cycle. *British medical journal* **2**, 473-475.
- Baker M. (2016). 1,500 scientists lift the lid on reproducibility. *Nature* **533**, 452-454.
- Bartke A & Dalterio S. (1975). Evidence for episodic secretion of testosterone in laboratory mice. *Steroids* **26**, 749-756.
- Basson AR, LaSalla A, Lam G, Kulpins D, Moen EL, Sundrud MS, Miyoshi J, Ilic S, Theriault BR, Cominelli F & Rodriguez-Palacios A. (2020). Artificial microbiome heterogeneity spurs six practical action themes and examples to increase study power-driven reproducibility. *Scientific reports* **10**, 5039.
- Becker JB, Arnold AP, Berkley KJ, Blaustein JD, Eckel LA, Hampson E, Herman JP, Marts S, Sadee W, Steiner M, Taylor J & Young E. (2005). Strategies and Methods for Research on Sex Differences in Brain and Behavior. *Endocrinology* **146**, 1650-1673.
- Becker JB, Prendergast BJ & Liang JW. (2016). Female rats are not more variable than male rats: a meta-analysis of neuroscience studies. *Biology of sex differences* **7**, 34.
- Beery AK. (2018). Inclusion of females does not increase variability in rodent research studies. *Current opinion in behavioral sciences* **23**, 143-149.
- Beery AK & Zucker I. (2011). Sex bias in neuroscience and biomedical research. *Neuroscience and biobehavioral reviews* **35**, 565-572.
- Bogue MA, Grubb SC, Walton DO, Philip VM, Kolishovski G, Stearns T, Dunn MH, Skelly DA, Kadakkuzha B, TeHennepe G, Kunde-Ramamoorthy G & Chesler EJ. (2018). Mouse Phenome Database: an integrative database and analysis suite for curated empirical phenotype data from laboratory mice. *Nucleic acids research* **46**, D843-d850.
- Bouman A, Moes H, Heineman MJ, de Leij LF & Faas MM. (2001a). Cytokine production by natural killer lymphocytes in follicular and luteal phase of the ovarian cycle in humans. *American journal of reproductive immunology (New York, NY : 1989)* **45**, 130-134.
- Bouman A, Moes H, Heineman MJ, de Leij LF & Faas MM. (2001b). The immune response during the luteal phase of the ovarian cycle: increasing sensitivity of human monocytes to endotoxin. *Fertility and sterility* **76**, 555-559.

- Brodin P & Davis MM. (2017). Human immune system variation. *Nature Reviews Immunology* **17**, 21-29.
- Brodin P, Jojic V, Gao T, Bhattacharya S, Angel CJ, Furman D, Shen-Orr S, Dekker CL, Swan GE, Butte AJ, Maecker HT & Davis MM. (2015). Variation in the human immune system is largely driven by non-heritable influences. *Cell* **160**, 37-47.
- Burden N, Chapman K, Sewell F & Robinson V. (2015). Pioneering better science through the 3Rs: an introduction to the national centre for the replacement, refinement, and reduction of animals in research (NC3Rs). *Journal of the American Association for Laboratory Animal Science : JAALAS* **54**, 198-208.
- Byers SL, Wiles MV, Dunn SL & Taft RA. (2012). Mouse estrous cycle identification tool and images. *PLoS One* **7**, e35538.
- Carr EJ, Dooley J, Garcia-Perez JE, Lagou V, Lee JC, Wouters C, Meyts I, Goris A, Boeckxstaens G, Linterman MA & Liston A. (2016). The cellular composition of the human immune system is shaped by age and cohabitation. *Nature immunology* **17**, 461-468.
- Celec P, Ostatníková D & Hodosy J. (2015). On the effects of testosterone on brain behavioral functions. *Frontiers in neuroscience* **9**, 12-12.
- Chan KA, Jazwiec PA, Gohir W, Petrik JJ & Sloboda DM. (2018). Maternal nutrient restriction impairs young adult offspring ovarian signaling resulting in reproductive dysfunction and follicle loss. *Biology of reproduction* **98**, 664-682.
- Check Hayden E. (2010). Sex bias blights drug studies. *Nature* **464**, 332-333.
- Chuang KH, Altuwaijri S, Li G, Lai JJ, Chu CY, Lai KP, Lin HY, Hsu JW, Keng P, Wu MC & Chang C. (2009). Neutropenia with impaired host defense against microbial infection in mice lacking androgen receptor. *The Journal of experimental medicine* **206**, 1181-1199.
- Clayton JA. (2016). Studying both sexes: a guiding principle for biomedicine. *FASEB journal : official publication of the Federation of American Societies for Experimental Biology* **30**, 519-524.
- Clayton JA & Collins FS. (2014). Policy: NIH to balance sex in cell and animal studies. *Nature* **509**, 282-283.
- Collins FS & Tabak LA. (2014). Policy: NIH plans to enhance reproducibility. *Nature* **505**, 612-613.
- Coquelin A & Desjardins C. (1982). Luteinizing hormone and testosterone secretion in young and old male mice. *The American journal of physiology* **243**, E257-263.

- Cora MC, Kooistra L & Travlos G. (2015). Vaginal Cytology of the Laboratory Rat and Mouse: Review and Criteria for the Staging of the Estrous Cycle Using Stained Vaginal Smears. *Toxicologic pathology* **43**, 776-793.
- Correa-De-Araujo R. (2006). Serious gaps: how the lack of sex/gender-based research impairs health. *Journal of women's health (2002)* **15**, 1116-1122.
- Darmochwal-Kolarz D, Rolinski J, Tabarkiewicz J, Leszczynska-Gorzelak B, Buczkowski J, Wojas K & Oleszczuk J. (2003). Blood myeloid and lymphoid dendritic cells are stable during the menstrual cycle but deficient during mid-gestation. *Journal of reproductive immunology* **59**, 193-203.
- Dayton A, Exner EC, Bukowy JD, Stodola TJ, Kurth T, Skelton M, Greene AS & Cowley AW, Jr. (2016). Breaking the Cycle: Estrous Variation Does Not Require Increased Sample Size in the Study of Female Rats. *Hypertension (Dallas, Tex : 1979)* **68**, 1139-1144.
- De Gregorio PR, Salva S, Tomás MST & Nader-Macias MEF. (2018). Effects of exogenous sex hormones on mouse estrous cycle, vaginal microbiota and immune cells. *Scandinavian Journal of Laboratory Animal Science* **44**, 14.
- Demas GE & Carlton ED. (2015). Ecoimmunology for psychoneuroimmunologists: Considering context in neuroendocrine-immune-behavior interactions. *Brain, behavior, and immunity* **44**, 9-16.
- Diaz Brinton R. (2012). Minireview: translational animal models of human menopause: challenges and emerging opportunities. *Endocrinology* **153**, 3571-3578.
- Faas M, Bouman A, Moesa H, Heineman MJ, de Leij L & Schuiling G. (2000). The immune response during the luteal phase of the ovarian cycle: a Th2-type response? *Fertility and sterility* **74**, 1008-1013.
- Faul F, Erdfelder E, Lang AG & Buchner A. (2007). G*Power 3: a flexible statistical power analysis program for the social, behavioral, and biomedical sciences. *Behavior research methods* **39**, 175-191.
- Festing MFW & Altman DG. (2002). Guidelines for the Design and Statistical Analysis of Experiments Using Laboratory Animals. *ILAR Journal* **43**, 244-258.
- Fields RD. (2014). NIH policy: Mandate goes too far. *Nature* **510**, 340-340.
- Fish EN. (2008). The X-files in immunity: sex-based differences predispose immune responses. *Nat Rev Immunol* **8**, 737-744.

- Fleiss JL & Cohen J. (1973). The equivalence of weighted kappa and the intraclass correlation coefficient as measures of reliability. *Educational and Psychological Measurement* **33**, 613-619.
- Geller SE, Koch AR, Roesch P, Filut A, Hallgren E & Carnes M. (2018). The More Things Change, the More They Stay the Same: A Study to Evaluate Compliance With Inclusion and Assessment of Women and Minorities in Randomized Controlled Trials. *Academic medicine : journal of the Association of American Medical Colleges* **93**, 630-635.
- Gloskowska-Moraczewska Z & Sitarska E. (1973). [Blood pattern in white rats in the course of sexual cycle]. *Acta haematologica Polonica* **4**, 117-121.
- Gobinath AR, Choleris E & Galea LA. (2017). Sex, hormones, and genotype interact to influence psychiatric disease, treatment, and behavioral research. *Journal of neuroscience research* **95**, 50-64.
- Grundy D. (2015). Principles and standards for reporting animal experiments in The Journal of Physiology and Experimental Physiology. *The Journal of physiology* **593**, 2547-2549.
- Halsey LG, Curran-Everett D, Vowler SL & Drummond GB. (2015). The fickle P value generates irreproducible results. *Nat Methods* **12**, 179-185.
- Higginson AD & Munafo MR. (2016). Current Incentives for Scientists Lead to Underpowered Studies with Erroneous Conclusions. *PLoS biology* **14**, e2000995.
- Hoggatt J, Hoggatt AF, Tate TA, Fortman J & Pelus LM. (2016). Bleeding the laboratory mouse: Not all methods are equal. *Experimental hematology* **44**, 132-137.e131.
- Horii Y, Nagasawa T, Sakakibara H, Takahashi A, Tanave A, Matsumoto Y, Nagayama H, Yoshimi K, Yasuda MT, Shimoi K & Koide T. (2017). Hierarchy in the home cage affects behaviour and gene expression in group-housed C57BL/6 male mice. *Scientific reports* **7**, 6991.
- Ingvorsen C, Karp NA & Lelliott CJ. (2017). The role of sex and body weight on the metabolic effects of high-fat diet in C57BL/6N mice. *Nutr Diabetes* **7**, e261-e261.
- Itoh Y & Arnold AP. (2015). Are females more variable than males in gene expression? Meta-analysis of microarray datasets. *Biology of sex differences* **6**, 18.
- Jasienska G, Bribiescas RG, Furberg A-S, Helle S & Núñez-de la Mora A. (2017). Human reproduction and health: an evolutionary perspective. *The Lancet* **390**, 510-520.

- Kaczorowski KJ, Shekhar K, Nkulikiyimfura D, Dekker CL, Maecker H, Davis MM, Chakraborty AK & Brodin P. (2017). Continuous immunotypes describe human immune variation and predict diverse responses. *Proceedings of the National Academy of Sciences* **114**, E6097.
- Kappel S, Hawkins P & Mendl MT. (2017). To Group or Not to Group? Good Practice for Housing Male Laboratory Mice. *Animals (Basel)* **7**, 88.
- Kilkenny C, Parsons N, Kadyszewski E, Festing MF, Cuthill IC, Fry D, Hutton J & Altman DG. (2009). Survey of the quality of experimental design, statistical analysis and reporting of research using animals. *PLoS One* **4**, e7824.
- Klein SL, Schiebinger L, Stefanick ML, Cahill L, Danska J, de Vries GJ, Kibbe MR, McCarthy MM, Mogil JS, Woodruff TK & Zucker I. (2015). Opinion: Sex inclusion in basic research drives discovery. *Proceedings of the National Academy of Sciences* **112**, 5257.
- Lee S, Kim J, Jang B, Hur S, Jung U, Kil K, Na B, Lee M, Choi Y, Fukui A, Gilman-Sachs A & Kwak-Kim JY. (2010). Fluctuation of Peripheral Blood T, B, and NK Cells during a Menstrual Cycle of Normal Healthy Women. *The Journal of Immunology* **185**, 756.
- Machida T, Yonezawa Y & Noumura T. (1981). Age-associated changes in plasma testosterone levels in male mice and their relation to social dominance or subordination. *Hormones and behavior* **15**, 238-245.
- Mangino M, Roederer M, Beddall MH, Nestle FO & Spector TD. (2017). Innate and adaptive immune traits are differentially affected by genetic and environmental factors. *Nature communications* **8**, 13850.
- Mathur S, Mathur RS, Goust JM, Williamson HO & Fudenberg HH. (1979). Cyclic variations in white cell subpopulations in the human menstrual cycle: correlations with progesterone and estradiol. *Clinical immunology and immunopathology* **13**, 246-253.
- McEwen BS, Gray JD & Nasca C. (2015). 60 YEARS OF NEUROENDOCRINOLOGY: Redefining neuroendocrinology: stress, sex and cognitive and emotional regulation. *J Endocrinol* **226**, T67-T83.
- Moen EL, Fricano-Kugler CJ, Luikart BW & O'Malley AJ. (2016). Analyzing Clustered Data: Why and How to Account for Multiple Observations Nested within a Study Participant? *PloS one* **11**, e0146721-e0146721.
- Mogil JS & Chanda ML. (2005). The case for the inclusion of female subjects in basic science studies of pain. *Pain* **117**, 1-5.

- Mysliwska J, Stech J, Skassa W & Mysliwski A. (1975). [Peripheral blood lymphocytes in female mice during successive phases of the sexual cycle]. *Acta haematologica Polonica* **6**, 37-43.
- Nakagawa S & Cuthill IC. (2007). Effect size, confidence interval and statistical significance: a practical guide for biologists. *Biological reviews of the Cambridge Philosophical Society* **82**, 591-605.
- Northern AL, Rutter SM & Peterson CM. (1994). Cyclic changes in the concentrations of peripheral blood immune cells during the normal menstrual cycle. *Proceedings of the Society for Experimental Biology and Medicine Society for Experimental Biology and Medicine (New York, NY)* **207**, 81-88.
- Nowak J, Borkowska B & Pawlowski B. (2016). Leukocyte changes across menstruation, ovulation, and mid-luteal phase and association with sex hormone variation. *American journal of human biology : the official journal of the Human Biology Council* **28**, 721-728.
- Nyby JG. (2008). Reflexive testosterone release: a model system for studying the nongenomic effects of testosterone upon male behavior. *Frontiers in neuroendocrinology* **29**, 199-210.
- Oellrich A, Meehan TF, Parkinson H, Sarntivijai S, White JK & Karp NA. (2016). Reporting phenotypes in mouse models when considering body size as a potential confounder. *Journal of biomedical semantics* **7**, 2.
- Orru V, Steri M, Sole G, Sidore C, Virdis F, Dei M, Lai S, Zoledziwska M, Busonero F, Mulas A, Floris M, Mentzen WI, Urru SA, Olla S, Marongiu M, Piras MG, Lobina M, Maschio A, Pitzalis M, Urru MF, Marcelli M, Cusano R, Deidda F, Serra V, Oppo M, Pili R, Reinier F, Berutti R, Pireddu L, Zara I, Porcu E, Kwong A, Brennan C, Tarrier B, Lyons R, Kang HM, Uzzau S, Atzeni R, Valentini M, Firinu D, Leoni L, Rotta G, Naitza S, Angius A, Congia M, Whalen MB, Jones CM, Schlessinger D, Abecasis GR, Fiorillo E, Sanna S & Cucca F. (2013). Genetic variants regulating immune cell levels in health and disease. *Cell* **155**, 242-256.
- Parker RM & Browne WJ. (2014). The place of experimental design and statistics in the 3Rs. *Ilar j* **55**, 477-485.
- Pennell LM, Galligan CL & Fish EN. (2012). Sex affects immunity. *Journal of autoimmunity* **38**, J282-291.
- Pick R, He W, Chen C-S & Scheiermann C. (2019). Time-of-Day-Dependent Trafficking and Function of Leukocyte Subsets. *Trends in immunology* **40**, 524-537.

- Piper SK, Grittner U, Rex A, Riedel N, Fischer F, Nadon R, Siegerink B & Dirnagl U. (2019). Exact replication: Foundation of science or game of chance? *PLoS biology* **17**, e3000188.
- Prasad A, Mumford SL, Buck Louis GM, Ahrens KA, Sjaarda LA, Schliep KC, Perkins NJ, Kissell KA, Wactawski-Wende J & Schisterman EF. (2014). Sexual activity, endogenous reproductive hormones and ovulation in premenopausal women. *Hormones and behavior* **66**, 330-338.
- Prendergast BJ, Onishi KG & Zucker I. (2014). Female mice liberated for inclusion in neuroscience and biomedical research. *Neuroscience and biobehavioral reviews* **40**, 1-5.
- Ritz SA, Antle DM, Cote J, Derooy K, Fraleigh N, Messing K, Parent L, St-Pierre J, Vaillancourt C & Mergler D. (2014). First steps for integrating sex and gender considerations into basic experimental biomedical research. *FASEB journal : official publication of the Federation of American Societies for Experimental Biology* **28**, 4-13.
- Shansky RM. (2019). Are hormones a “female problem” for animal research? *Science* **364**, 825.
- Shaw R, Festing MF, Peers I & Furlong L. (2002). Use of factorial designs to optimize animal experiments and reduce animal use. *Ilar j* **43**, 223-232.
- Shen-Orr SS, Furman D, Kidd BA, Hadad F, Lovelace P, Huang YW, Rosenberg-Hasson Y, Mackey S, Grisar FA, Pickman Y, Maecker HT, Chien YH, Dekker CL, Wu JC, Butte AJ & Davis MM. (2016). Defective Signaling in the JAK-STAT Pathway Tracks with Chronic Inflammation and Cardiovascular Risk in Aging Humans. *Cell systems* **3**, 374-384.e374.
- Smith AJ, Clutton RE, Lilley E, Hansen KEA & Brattelid T. (2018). PREPARE: guidelines for planning animal research and testing. *Lab Anim* **52**, 135-141.
- Tannenbaum C, Schwarz JM, Clayton JA, de Vries GJ & Sullivan C. (2016). Evaluating sex as a biological variable in preclinical research: the devil in the details. *Biology of sex differences* **7**, 13.
- ter Horst JP, de Kloet ER, Schächinger H & Oitzl MS. (2012). Relevance of stress and female sex hormones for emotion and cognition. *Cellular and molecular neurobiology* **32**, 725-735.
- The Jackson Laboratory. (2007). Hematological survey of 11 strains of mice. MPD:Jaxpheno4. The Jackson Laboratory, Mouse Phenome Database web resource.

- Tsang JS, Schwartzberg PL, Kotliarov Y, Biancotto A, Xie Z, Germain RN, Wang E, Olnes MJ, Narayanan M, Golding H, Moir S, Dickler HB, Perl S & Cheung F. (2014). Global analyses of human immune variation reveal baseline predictors of postvaccination responses. *Cell* **157**, 499-513.
- Viselli SM, Reese KR, Fan J, Kovacs WJ & Olsen NJ. (1997). Androgens alter B cell development in normal male mice. *Cellular immunology* **182**, 99-104.
- Wald C & Wu C. (2010). Of Mice and Women: The Bias in Animal Models. *Science* **327**, 1571.
- Wallace JG, Potts RH, Szamosi JC, Surette MG & Sloboda DM. (2018). The murine female intestinal microbiota does not shift throughout the estrous cycle. *PloS one* **13**, e0200729-e0200729.
- Wilhelmson AS, Lantero Rodriguez M, Stubelius A, Fogelstrand P, Johansson I, Buechler MB, Lianoglou S, Kapoor VN, Johansson ME, Fagman JB, Duhlin A, Tripathi P, Camponeschi A, Porse BT, Rolink AG, Nissbrandt H, Turley SJ, Carlsten H, Martensson IL, Karlsson MCI & Tivesten A. (2018). Testosterone is an endogenous regulator of BAFF and splenic B cell number. *Nature communications* **9**, 2067.
- Woitowich NC, Beery A & Woodruff T. (2020). A 10-year follow-up study of sex inclusion in the biological sciences. *eLife* **9**.
- Yang H, Bell TA, Churchill GA & Pardo-Manuel de Villena F. (2007). On the subspecific origin of the laboratory mouse. *Nature genetics* **39**, 1100-1107.
- Yang H, Wang JR, Didion JP, Buus RJ, Bell TA, Welsh CE, Bonhomme F, Yu AH, Nachman MW, Pialek J, Tucker P, Boursot P, McMillan L, Churchill GA & de Villena FP. (2011). Subspecific origin and haplotype diversity in the laboratory mouse. *Nature genetics* **43**, 648-655.

Table 1. Whole blood myeloid cell prevalence by biological sex in C57BL/6J mice.

Leukocyte Population	<i>P value</i> ^A	Sex	<i>n</i>	Mean (95% CI)	Median (95% CI)	SD	Min.	Max.	CV (%)
% CD45 ⁺ Leukocytes									
Neutrophils	<0.0001	Female	120	5.73	5.27	2.11	1.58	15.1	36.8
				(5.35 – 6.11)	(4.92 – 5.52)				
		Male	67	19.0	12.9	13.0	5.26	55.9	68.2
(15.9 – 22.2)	(11.2 – 18.8)								
Monocytes	<0.0001	Female	120	5.51	5.21	1.62	2.29	9.50	29.4
				(5.21 – 5.80)	(4.94 – 5.50)				
		Male	67	9.70	9.05	3.03	5.43	17.6	31.2
(8.96 – 10.4)	(7.97 – 9.91)								
Ly6C ^{high} Monocytes	<0.0001	Female	120	2.60	2.44	1.04	0.94	5.67	39.8
				(2.41 – 2.79)	(2.22 – 2.66)				
		Male	67	5.82	4.76	3.18	2.03	15.6	54.6
(5.05 – 6.60)	(4.39 – 5.58)								
Ly6C ^{low} Monocytes	<0.0001	Female	120	1.26	1.23	0.34	0.62	2.22	27.0
				(1.20 – 1.32)	(1.16 – 1.30)				
		Male	67	1.61	1.48	0.61	0.69	3.91	37.9
(1.46 – 1.76)	(1.36 – 1.65)								
Ly6C ^{high} : Ly6C ^{low} Ratio	<0.0001	Female	120	2.05	1.96	0.52	1.04	3.94	25.4
				(1.95 – 2.14)	(1.85 – 2.07)				
		Male	67	4.43	2.05	3.63	1.30	20.3	81.9
(3.51 – 5.35)	(2.68 – 3.58)								
Ly6C ⁻ Monocytes	<0.0001	Female	120	1.65	1.53	0.51	0.63	3.06	30.8
				(1.56 – 1.74)	(1.44 – 1.68)				
		Male	67	2.39	2.17	0.81	1.01	4.91	34.0
(2.19 – 2.59)	(2.09 – 2.42)								
% Monocytes									
Ly6C ^{high} Monocytes	<0.0001	Female	120	46.4	46.7	7.41	23.9	63.6	16.0
				(45.0 – 47.7)	(44.8 – 48.4)				
		Male	67	57.0	54.2	14.0	33.7	88.7	24.5
(53.6 – 60.4)	(50.7 – 59.9)								
Ly6C ^{low} Monocytes	<0.0001	Female	120	23.2	23.1	2.76	15.8	29.8	11.9
				(22.7 – 23.7)	(22.4 – 23.6)				
		Male	67	17.2	18.1	5.45	4.37	30.1	31.8
(15.8 – 18.5)	(16.8 – 19.3)								
Ly6C ⁻ Monocytes	0.0142	Female	120	30.6	30.1	6.86	17.3	53.9	22.5
				(29.3 – 31.8)	(27.6 – 31.2)				
		Male	67	26.6	26.9	9.82	7.01	48.7	37.0
(24.2 – 29.0)	(24.3 – 29.7)								
% Ly6C ⁺ Monocytes									
Ly6C ^{high} Monocytes	<0.0001	Female	120	66.4	66.3	5.22	51.2	79.8	7.86
				(65.5 – 67.3)	(65.0 – 67.5)				
		Male	67	76.6	75.4	8.92	56.5	95.4	11.6
(74.4 – 78.8)	(73.1 – 77.7)								

^A*P* values are for non-parametric Mann-Whitney *U* tests.

Table 2. Whole blood lymphocyte prevalence by biological sex in C57BL/6J mice.

Leukocyte Population	P value ^A	Sex	n	Mean	Median	SD	Min.	Max.	CV (%)
				(95% CI)	(95% CI)				
% CD45 ⁺ Leukocytes									
Total Lymphocytes	<0.0001 ^{MW}	Female	77	83.7	84.9	3.54	75.2	91.1	4.23
				(82.9 - 84.5)	(84.4 - 85.4)				
		Male	62	68.1	73.0	14.2	30.9	85.2	20.8
				(64.5 - 71.7)	(68.4 - 76.0)				
NK cells	<0.0001 ^{MW}	Female	77	2.34	2.26	0.85	0.53	4.49	36.3
				(2.15 – 2.54)	(2.05 – 2.49)				
		Male	62	2.95	2.86	0.82	1.59	5.67	27.7
				(2.75 – 3.16)	(2.52 – 3.13)				
B cells	<0.0001 ^{MW}	Female	81	63.8	63.2	5.35	51.9	78.6	8.4
				(62.6 – 65.0)	(62.0 – 64.9)				
		Male	62	50.6	53.8	12.9	20.1	70.2	25.4
				(47.4 – 53.9)	(49.8 – 56.7)				
CD4 ⁺ T cells	<0.0001 ST	Female	81	9.85	10.1	1.99	4.12	14.7	20.2
				(9.41 – 10.3)	(9.55 – 10.5)				
		Male	62	8.01	7.97	1.64	4.51	13.0	20.4
				(7.60 – 8.43)	(7.52 – 8.32)				
CD8 ⁺ T cells	<0.0001 ^{MW}	Female	81	7.06	7.18	1.74	2.24	9.96	24.6
				(6.68 – 7.45)	(6.55 – 7.75)				
		Male	62	5.89	5.99	1.10	3.44	8.24	18.7
				(5.61 – 6.17)	(5.56 – 6.30)				
CD4 ⁺ : CD8 ⁺ Ratio	0.0654 ST	Female	81	1.43	1.40	0.20	0.93	2.04	14.0
				(1.38 – 1.47)	(1.35 – 1.48)				
		Male	62	1.37	1.37	0.16	0.93	1.78	11.9
				(1.33 – 1.41)	(1.32 – 1.42)				
% Lymphocytes									
NK cells	<0.0001 ^{MW}	Female	77	2.82	2.65	1.09	0.615	5.48	38.5
				(2.58 - 3.07)	(2.46 - 2.99)				
		Male	62	4.56	4.33	1.63	2.33	9.44	35.7
				(4.14 – 4.97)	(3.79 – 4.77)				
B cells	0.0385 ^{MW}	Female	77	76.0	75.0	4.80	67.0	91.3	6.32
				(74.9 - 77.1)	(73.8 - 76.5)				
		Male	62	73.5	74.0	5.34	57.1	83.3	7.26
				(72.1 – 74.8)	(72.8 – 75.4)				
CD4 ⁺ T cells	0.4172 ST	Female	77	11.8	12.0	2.47	4.78	17.3	20.9
				(11.2 - 12.4)	(11.6 - 12.7)				
		Male	62	12.2	11.9	2.83	7.26	20.0	23.3
				(11.4 – 12.9)	(10.8 – 12.9)				
CD8 ⁺ T cells	0.6827 ^{MW}	Female	77	8.46	8.85	2.11	2.60	12.4	25.0
				(7.99 - 8.94)	(8.02 - 9.27)				
		Male	62	8.87	8.64	1.68	5.20	14.8	19.0
				(8.44 – 9.29)	(8.48 – 9.14)				

^A*P* values are for parametric Student's *t* (ST) or non-parametric Mann-Whitney *U* (MW) tests.

Table 3. Whole blood immune cell population counts by biological sex in C57BL/6J mice.^A

Leukocyte Population	<i>P</i> value ^B	Sex	<i>n</i>	Mean	Median	SD	Min.	Max.	CV (%)
				(95% CI)	(95% CI)				
Neutrophils	<0.0001	Female	115	183	157	88	23	390	48.2
				(167 - 200)	(144 - 182)				
		Male	30	754	524	604	125	2288	80.1
				(529 - 980)	(322 - 963)				
Monocytes	<0.0001	Female	115	185	166	86	32	496	46.7
				(169 - 201)	(154 - 190)				
		Male	30	301	257	158	107	814	52.6
				(242 - 361)	(215 - 330)				
Ly6C ^{high} Monocytes	<0.0001	Female	115	86	77	47	11	306	54.4
				(77 - 94)	(69 - 84)				
		Male	30	186	149	135	42	659	72.5
				(135 - 236)	(117-198)				
Ly6C ^{low} Monocytes	<0.0001	Female	115	42	39	18	9	115	43.5
				(39 - 46)	(36 - 45)				
		Male	30	46	42	21	15	93	46.3
				(38 - 54)	(33 - 61)				
Ly6C ⁻ Monocytes	<0.0001	Female	115	57	55	29	10	176	50.6
				(51 - 62)	(49 - 60)				
		Male	30	70	62	30	25	143	43.6
				(58 - 81)	(49 - 85)				
NK cells	0.0521	Female	72	77	68	41	18	206	53.5
				(68 - 87)	(60 - 81)				
		Male	30	95	83	49	26	215	52.1
				(76 - 113)	(64 - 98)				
B cells	0.0897	Female	76	2082	1891	770	778	4464	37.0
				(1906 - 2258)	(1751 - 2165)				
		Male	30	1802	1712	954	318	4650	52.9
				(1446 - 2158)	(1230 - 2159)				
T cells	0.0205	Female	76	581	529	245	200	1394	42.2
				(525 - 638)	(478 - 596)				
		Male	30	478	393	209	192	982	43.7
				(400 - 556)	(358 - 485)				
CD4 ⁺ T cells	0.0201	Female	76	321	296	130	123	727	40.5
				(292 - 351)	(257 - 336)				
		Male	30	264	229	113	107	552	42.7
				(222 - 306)	(196 - 283)				
CD8 ⁺ T cells	0.0303	Female	76	234	212	108	62	610	46.1
				(209 - 259)	(185 - 234)				
		Male	30	193	158	88	79	392	45.6
				(160 - 226)	(140 - 191)				

^AAll cell counts are cells/ μ L.^B*P* values are for non-parametric Mann-Whitney *U* tests.

Table 4. Assessments of factors affecting immune cell population variance and distribution in young female and male C57BL/6J mice.

Assessment Factor ^A	Male					Female				
	<i>n</i>	PERMANOVA		PERMDISP		<i>n</i>	PERMANOVA		PERMDISP	
		<i>P</i>	<i>R</i> ²	<i>P</i>	<i>F</i>		<i>P</i>	<i>R</i> ²	<i>P</i>	<i>F</i>
Age^B	62	0.001	0.34476	0.245	1.3856	81	0.001	0.31340	0.232	1.4269
Weight – SD^{C,H}	30	0.015	0.24394	0.192	1.7401	67	0.193	0.04590	0.554	0.6710
Weight - 95% CI^{D,H}	30	0.001	0.50791	0.054	3.3152	67	0.899	0.00930	0.600	0.5063
Dominance^{E,H}	30	0.565	0.04554	0.674	0.4099	67	0.802	0.01400	0.234	1.4252
Estrous Stage^F	NA	NA	NA	NA	NA	58	0.467	0.04856	0.882	0.2315
Time of Year^G	62	0.0679	0.07456	0.379	1.0578	81	0.152	0.04137	0.590	0.5117

^AStatistical significance was assessed using the R functions *adonis* (PERMANOVA for immunophenotype composition) and *permdisp* (assessment of homogeneity for immunophenotype variance) on immunophenotype data.

^BAge in weeks.

^CMice were divided into three groups according to standard deviation (SD) from the mean: weight lower than mean–1SD, weight within mean±SD, and weight greater than mean+1SD.

^DMice were divided into three groups according to the 95% confidence interval (CI) of the mean: weight less than the 95% CI, weight within the 95% CI, and weight greater than the 95% CI.

^ESocial dominance was assessed by using mouse weight as a proxy measure (Machida *et al.*, 1981; Horii *et al.*, 2017) to divide mice within a cage into three groups. The heaviest mouse in each cage was identified as ‘most dominant’, the lightest mouse in each cage was identified as ‘least dominant’, and the other mice in the cage were identified as ‘intermediate’.

^FReproductive cycle (estrous) stage as determined by vaginal cytology; from Figure 2.

^GTime of Year was divided into 3-month seasons: Winter (December – February), Spring (March – May), Summer (June-August), and Autumn (September – November).

^HWeight data was not available for all mice, resulting in smaller sample size for those calculations.

Table 5. CBC cell counts of neutrophils and lymphocytes in whole blood of female and male mice of classical laboratory inbred strains.

		CBC Cell Count (x10 ³ cells/μl) ^A										
		n	Neutrophils					Lymphocytes				
Strain	Sex	n	Mean	SD	95% CI	CV (%)	vs C57BL/6J P value ^B	Mean	SD	95% CI	CV (%)	vs C57BL/6J P value ^B
C57BL/6	Female	77	0.2419	0.1599	0.206 – 0.278	66.1	na	2.734	1.293	2.440 – 3.027	47.3	na
	Male	64	0.8245	0.9107	0.597 – 1.052	110.5	na	1.899	0.838	1.690 – 2.108	44.1	na
BALB/cJ	Female	22	0.4873	0.1929	0.402 – 0.573	39.6	0.0801	2.613	0.527	2.380 – 2.847	20.2	0.9928
	Male	21	0.6033	0.2899	0.471 – 0.735	48.0	0.1707	2.142	1.428	1.492 – 2.792	66.7	0.8307
C3H/HeJ	Female	23	0.6630	0.1427	0.601 – 0.725	21.5	0.0001	2.068	0.681	1.774 – 2.363	32.9	0.0122
	Male	22	0.6523	0.2642	0.535 – 0.769	40.5	0.3999	1.847	0.615	1.574 – 2.120	33.3	0.9997
CBA/J	Female	43	0.4709	0.3233	0.371 – 0.570	68.7	<0.0001	1.917	0.630	1.723 – 2.110	32.9	<0.0001
	Male	46	0.3439	0.1150	0.310 – 0.378	33.5	0.0030	1.456	0.553	1.292 – 1.620	38.0	0.0158
DBA/2J	Female	34	0.9350	0.5856	0.731 – 1.139	62.6	<0.0001	3.757	1.346	3.287 – 4.227	35.8	<0.0001
	Male	31	0.6684	0.2286	0.585 – 0.752	34.2	0.0463	2.485	0.787	2.196 – 2.773	31.7	0.2813
FVB/NJ	Female	21	0.2824	0.1217	0.227 – 0.338	43.1	0.9982	2.390	1.003	1.933 – 2.846	42.0	0.5071
	Male	25	0.6168	0.5119	0.405 – 0.828	83.0	0.1696	1.794	0.838	1.448 – 2.140	46.7	0.9952
NODShiLtJ	Female	41	0.6307	0.2215	0.561 – 0.701	35.1	<0.0001	1.626	0.697	1.406 – 1.846	42.9	<0.0001
	Male	47	0.5234	0.1825	0.470 – 0.577	34.9	0.0011	1.174	0.498	1.028 – 1.320	42.4	0.0002
Source of Variation		Sex		F(1,503) = 3.507			0.0617	Sex		F(1,503) = 50.18		0.0302
		Strain		F(6,503) = 6.758			<0.0001	Strain		F(6,503) = 27.72		<0.0001
		Interaction		F(6,503) = 12.70			<0.0001	Interaction		F(6,503) = 2.345		<0.0001
		Flow Cytometry Cell Count (x10 ³ cells/μL) ^C										
		Neutrophils						Lymphocytes				
Strain	Sex	n	Mean	SD	95% CI	CV (%)		n	Mean	SD	95% CI	CV (%)
C57BL/6J	Female	115	0.1833	0.0884	0.167 – 0.200	48.2		72	2.721	1.02	2.510 – 2.966	37.5
	Male	30	0.7543	0.6044	0.529 – 0.980	80.1	30	2.374	1.17	1.937 – 2.811	49.3	

^ACBC data is from the Jaxpheno4 dataset of the Jax Phenome Database.^BComparison between C57BL/6J mouse CBC data and other strain CBC data, performed by two-way ANOVA (with sex and strain as main effects) with Dunnett's test for multiple comparisons of strains to C57BL/6J mouse data for each sex.^CFlow cytometry data is from this study (Table 3).

Table 6. CBC prevalence of neutrophils and lymphocytes in whole blood of female and male mice of classical laboratory inbred strains.

		CBC Prevalence (%WBCs) ^A										
		n	Neutrophils					Lymphocytes				
Strain	Sex	n	Mean	SD	95% CI	CV (%)	vs C57BL/6J P value ^B	Mean	SD	95% CI	CV (%)	vs C57BL/6J P value ^B
C57BL/6	Female	77	7.8	3.4	7.02 – 8.56	43.5	na	87.7	4.1	86.8 – 88.7	4.6	na
	Male	64	25.7	21.2	20.5 – 31.0	82.3	na	69.6	21.8	64.2 – 75.1	31.3	na
BALB/cJ	Female	22	14.8	3.2	13.4 – 16.3	21.8	0.0220	80.6	3.7	79.0 – 82.2	4.7	0.0310
	Male	21	23.1	8.4	19.3 – 26.9	36.6	0.8411	71.9	9.8	67.4 – 76.4	13.7	0.9322
C3H/HeJ	Female	23	23.7	4.0	21.9 – 25.4	16.9	<0.0001	70.7	4.3	68.8 – 72.5	6.2	<0.0001
	Male	22	24.5	4.0	22.7 – 26.3	16.5	0.9952	69.4	4.6	67.4 – 71.5	6.6	>0.9999
CBA/J	Female	43	18.9	8.2	16.4 – 21.4	43.2	0.0223	76.5	8.3	74.0 – 79.1	10.9	<0.0001
	Male	46	19.0	5.1	17.5 – 20.5	26.8	<0.0001	75.8	5.8	74.0 – 77.5	7.6	0.0631
DBA/2J	Female	34	18.6	5.3	16.7 – 20.4	28.8	<0.0001	76.0	5.6	74.0 – 77.9	7.4	<0.0001
	Male	31	19.9	3.4	18.7 – 21.2	17.0	0.3740	74.0	4.2	75.5 – 72.4	5.7	0.0185
FVB/NJ	Female	21	10.7	4.2	8.74 – 12.6	39.8	0.7803	84.1	5.6	81.6 – 86.7	6.7	0.6185
	Male	25	24.8	18.2	17.3 – 32.3	73.2	0.9981	70.1	19.4	62.1 – 78.2	27.7	0.9997
NODShiLtJ	Female	41	27.0	8.5	24.3 – 29.7	31.6	<0.0001	65.8	8.4	63.1 – 68.4	12.8	<0.0001
	Male	47	29.8	7.5	27.6 – 32.0	25.1	0.1824	63.1	8.0	60.8 – 65.5	12.7	0.0077
	Source of Variation		Sex	F(1,503) = 45.60			<0.0001	Sex	F(1,503) = 45.12			<0.0001
			Strain	F(6,503) = 14.51			<0.0001	Strain	F(6,503) = 19.38			<0.0001
			Interaction	F(6,503) = 11.88			<0.0001	Interaction	F(6,503) = 10.32			<0.0001
		Flow Cytometry Prevalence (%CD45 ⁺ leukocytes) ^C										
		Neutrophils						Lymphocytes				
Strain	Sex	n	Mean	SD	95% CI	CV (%)		n	Mean	SD	95% CI	CV (%)
C57BL/6J	Female	120	5.73	2.11	5.35 – 6.11	36.8		77	83.7	3.54	92.9 – 84.5	4.23
	Male	67	19	13	15.9 – 22.2	68.2		62	68.1	14.2	64.5 – 71.7	20.8

^ACBC data is from the Jaxpheno4 dataset of the Jax Phenome Database (as a proportion of total white blood cell count).

^BStatistical comparison between C57BL/6J mouse CBC data and other strain CBC data, performed by two-way ANOVA (with sex and strain as main effects) with Dunnett's test for multiple comparisons of strains to C57BL/6J mouse data for each sex.

^CFlow cytometry data is from this study (Tables 1 and 2).

Table 7. Sample size calculations for immune cell populations in whole blood of female and male C57BL/6J mice.

Cell Population	Sex	Test ^A	Change in Leukocyte Population													
			5%	10%	15%	20%	25%	30%	35%	40%	45%	50%	60%	70%	80%	90%
Neutrophils	Female	<i>t</i>	853	214	96	55	36	25	19	15	12	10	8	6	5	4
		<i>U</i>	893	224	101	57	37	26	20	16	13	11	8	6	5	5
		<i>d</i>	0.14	0.27	0.41	0.54	0.68	0.81	0.95	1.09	1.22	1.36	1.63	1.90	2.17	2.44
	Male	<i>t</i>	2920	731	326	184	118	83	61	47	38	31	22	16	13	11
		<i>U</i>	3057	765	341	193	124	86	64	49	39	32	23	17	14	11
		<i>d</i>	0.07	0.15	0.22	0.29	0.37	0.44	0.51	0.59	0.66	0.73	0.88	1.03	1.17	1.32
Monocytes	Female	<i>t</i>	544	137	62	35	23	17	13	10	8	7	5	4	4	4
		<i>U</i>	569	143	65	37	24	17	13	10	9	7	6	5	4	4
		<i>d</i>	0.17	0.34	0.51	0.68	0.85	1.02	1.19	1.36	1.53	1.70	2.04	2.38	2.72	3.06
	Male	<i>t</i>	613	154	69	40	26	19	14	11	9	8	6	5	4	4
		<i>U</i>	642	162	73	42	27	19	15	12	10	8	6	5	4	4
		<i>d</i>	0.16	0.32	0.48	0.64	0.80	0.96	1.12	1.28	1.44	1.60	1.92	2.24	2.56	2.88
B cells	Female	<i>t</i>	46	13	7	4	4	3	3	3	3	2	2	2	2	2
		<i>U</i>	48	13	7	5	4	3	3	3	3	3	2	2	2	2
		<i>d</i>	0.60	1.19	1.79	2.38	2.98	3.58	4.17	4.77	5.36	5.96	7.15	8.35	9.54	10.7
	Male	<i>t</i>	406	103	46	27	18	13	10	8	7	6	5	4	3	3
		<i>U</i>	425	107	49	28	19	13	10	8	7	6	5	4	4	3
		<i>d</i>	0.20	0.39	0.59	0.79	0.98	1.18	1.38	1.58	1.77	1.97	2.36	2.76	3.15	3.54
CD4 ⁺ T cells	Female	<i>t</i>	258	66	30	18	12	9	7	5	5	4	4	3	3	3
		<i>U</i>	270	69	31	18	12	9	7	6	5	4	4	3	3	3
		<i>d</i>	0.25	0.49	0.74	0.99	1.24	1.48	1.73	1.98	2.23	2.47	2.97	3.46	3.96	4.45
	Male	<i>t</i>	263	67	31	18	12	9	7	6	5	4	4	3	3	3
		<i>U</i>	275	70	32	19	13	9	7	6	5	5	4	3	3	3
		<i>d</i>	0.24	0.49	0.73	0.98	1.22	1.47	1.71	1.96	2.20	2.45	2.94	3.43	3.92	4.41
CD8 ⁺ T cells	Female	<i>t</i>	382	97	44	25	17	12	9	8	6	5	4	4	3	3
		<i>U</i>	400	101	46	26	17	13	10	8	7	6	5	4	3	3
		<i>d</i>	0.20	0.41	0.61	0.81	1.02	1.22	1.42	1.63	1.83	2.03	2.44	2.84	3.25	3.66
	Male	<i>t</i>	222	57	26	15	10	8	6	5	4	4	3	3	3	3
		<i>U</i>	232	59	27	16	11	8	6	5	5	4	4	3	3	3
		<i>d</i>	0.27	0.53	0.80	1.07	1.33	1.60	1.87	2.13	2.40	2.67	3.20	3.74	4.27	4.80
NK cells	Female	<i>t</i>	827	208	93	53	35	24	18	14	12	10	7	6	5	4
		<i>U</i>	1433	359	161	91	59	41	31	24	19	16	12	9	7	6
		<i>d</i>	0.14	0.28	0.41	0.55	0.69	0.83	0.97	1.10	1.24	1.38	1.65	1.93	2.21	2.48
	Male	<i>t</i>	483	122	55	32	21	15	11	9	8	6	5	4	4	3
		<i>U</i>	506	128	58	33	22	16	12	10	8	7	5	4	4	3
		<i>d</i>	0.18	0.36	0.54	0.72	0.90	1.08	1.26	1.44	1.62	1.81	2.17	2.53	2.89	3.25

^ASample sizes are shown for two-tailed Student's *t* tests (*t*) and two-tailed Mann-Whitney tests (*U*) with Cohen's effect size (*d*). Calculations were performed with data of leukocyte prevalence mean and standard deviation from Tables 1 and 2, assuming equal group sizes and consistent standard deviation for each group, and were based on a percentage 'change in leukocyte population' from our reference population mean, assuming $\alpha = 0.05$ and 80% power. Sample size calculations did not account for intra-cage clustering effects (Table 9). Shaded cells indicate when sample size for each group is approximately 10 or fewer mice.

Table 8. Comparison of sample size calculations for neutrophils and lymphocytes in whole blood of female and male C57BL/6J mice based on CBC and flow cytometry data.

Leukocyte Population	Sex	Analysis	Mean	SD	Test ^A	Change in Leukocyte Population													
						5%	10%	15%	20%	25%	30%	35%	40%	45%	50%	60%	70%	80%	90%
Neutrophils	Female	CBC	7.80	3.39	<i>t</i>	1191	299	134	76	49	35	26	20	16	13	10	8	6	5
					<i>U</i>	1427	313	140	79	51	36	27	21	17	14	10	8	7	6
		Flow	5.73	2.11	<i>t</i>	853	214	96	55	36	25	19	15	12	10	8	6	5	4
					<i>U</i>	893	224	101	57	37	26	20	16	13	11	8	6	5	5
	Male	CBC	25.7	21.2	<i>t</i>	4249	1063	473	267	171	119	88	68	54	44	31	23	18	15
					<i>U</i>	4449	1113	496	279	179	125	92	71	56	46	32	24	19	15
		Flow	19.0	13.0	<i>t</i>	2920	731	326	184	118	83	61	47	38	31	22	16	13	11
					<i>U</i>	3057	765	341	193	124	86	64	49	39	32	23	17	14	11
Lymphocytes	Female	CBC	87.7	4.05	<i>t</i>	15	5	3	3	3	2	2	2	2	2	2	2	2	2
					<i>U</i>	16	5	3	3	3	2	2	2	2	2	2	2	2	2
		Flow	83.7	3.54	<i>t</i>	13	5	3	3	2	2	2	2	2	2	2	2	2	2
					<i>U</i>	21	7	4	3	3	3	3	2	2	2	2	2	2	2
	Male	CBC	69.6	21.8	<i>t</i>	616	155	70	40	26	19	14	11	9	8	6	5	4	4
					<i>U</i>	645	162	73	42	27	19	15	12	10	8	6	5	4	4
		Flow	68.1	14.2	<i>t</i>	273	69	32	18	12	9	7	6	5	4	4	3	3	3
					<i>U</i>	286	73	33	19	13	10	7	6	5	5	4	3	3	3

^ASample sizes are shown for two-tailed Student's *t* tests (*t*) and two-tailed Mann-Whitney tests (*U*). Sample size calculations were performed with *a priori* CBC data from the Jaxpheno4 dataset of the Jax Phenome database (for 'CBC') summarized in Table 6, and flow cytometry leukocyte prevalence data from Tables 1 and 2 (for 'Flow'). Calculations were done assuming the same standard deviation from the mean of each group and a percentage 'change in leukocyte population' from the reference population mean, assuming $\alpha = 0.05$ and 80% power. Sample size calculations did not account for intra-cage clustering effects (Table 9). Shaded cells indicate when sample size for each group is approximately 10 or fewer mice.

Table 9. Immune cell population cage variance effects

Cell Population	Intraclass Correlation Coefficient (ICC)^A	Design Effect (DE)^B
Neutrophils	0.336	1.946
Monocytes	0.186	1.524
B cells	0.341	2.013
CD4 ⁺ T cells	0.274	1.814
CD8 ⁺ T cells	0.261	1.776
NK cells	0.326	1.969

^AThe intraclass correlation coefficient compares variance between clusters (cages) to variance within clusters (ICC range is 0 to 1, where 1 indicates all data in the cluster is identical).

^BThe design effect estimates the extent to which sample size should be altered due to clustering of data. The design effect can be used to approximate the effective sample size (n) using $n = n_0(DE)$, where n_0 = sample size assuming there is no clustering effect (i.e. mice are independent from each other, as calculated in Tables 6 and 7) and DE is the design effect.

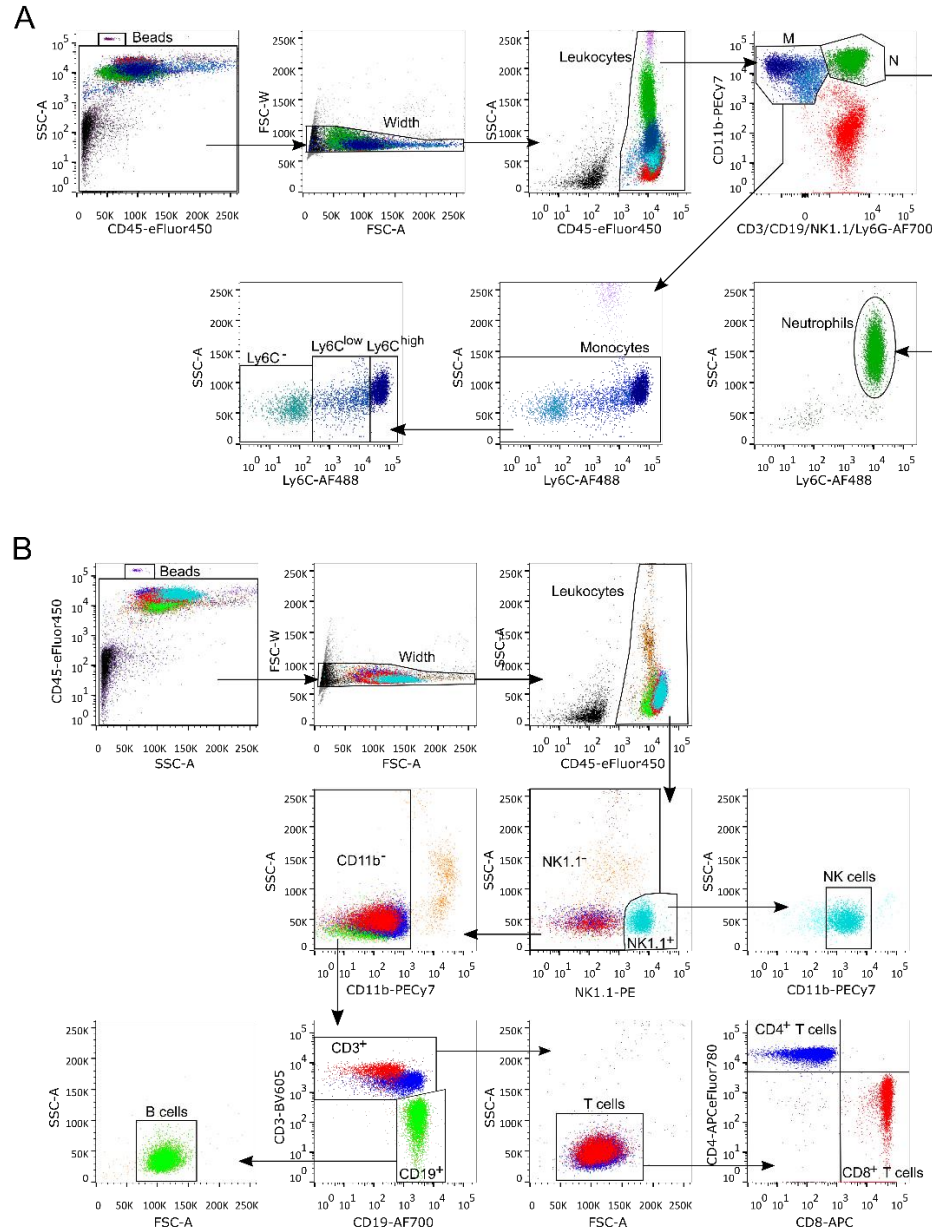


Figure 1. Flow cytometry data gating strategies for peripheral whole blood immunophenotyping.

(A) Identification of monocyte and neutrophil populations with a 4-fluorophore stain: Count beads were removed from the cell population. A width gate (FSC-W by FSC-A) was created to remove immune cell aggregates. CD45⁺ cells (leukocytes) were gated. Axes of CD11b⁺ and AF700⁺ (conjugated to antibodies specific for CD3, CD19, NK1.1 or Ly6G) were selected to separate CD11b⁺Ly6G⁻ (M), CD11b⁺Ly6G⁺ (N), and CD11b^{mid}CD3⁺CD19⁺NK1.1⁺ (lymphocytes: T cells, B cells, NK cells) cell populations. Neutrophils were confirmed as CD45⁺CD11b⁺Ly6G⁺Ly6C^{high} cells, and the CD45⁺CD11b⁺Ly6G⁺Ly6C^{low} monocytes were divided into subsets by their expression of Ly6C: Ly6C⁺ (Ly6C^{high} and Ly6C^{low}), and Ly6C⁻.

(B) Identification of NK cells, B cells, and T cell populations with a 7-fluorophore stain: Count beads were removed from the cell population. A width gate (FSC-W by FSC-A) was used to remove cell aggregates. CD45⁺ cells (leukocytes) were gated. The population was separated into NK1.1⁺ cells and NK1.1⁻ cells. NK cells were identified as NK1.1⁺CD11b^{mid}SSC^{low}. The NK1.1⁻CD11b⁻ population was gated on CD19 and CD3. B cells were identified as CD45⁺NK1.1⁻CD11b⁻CD19⁺SSC^{low} cells. T cells were identified as CD45⁺NK1.1⁻CD11b⁻CD3⁺SSC^{low} cells, and divided into CD4⁺ and CD8⁺ subsets.

Count beads were included in both stains for absolute quantitation of cell populations. FSC, front-scatter. SSC, side-scatter.

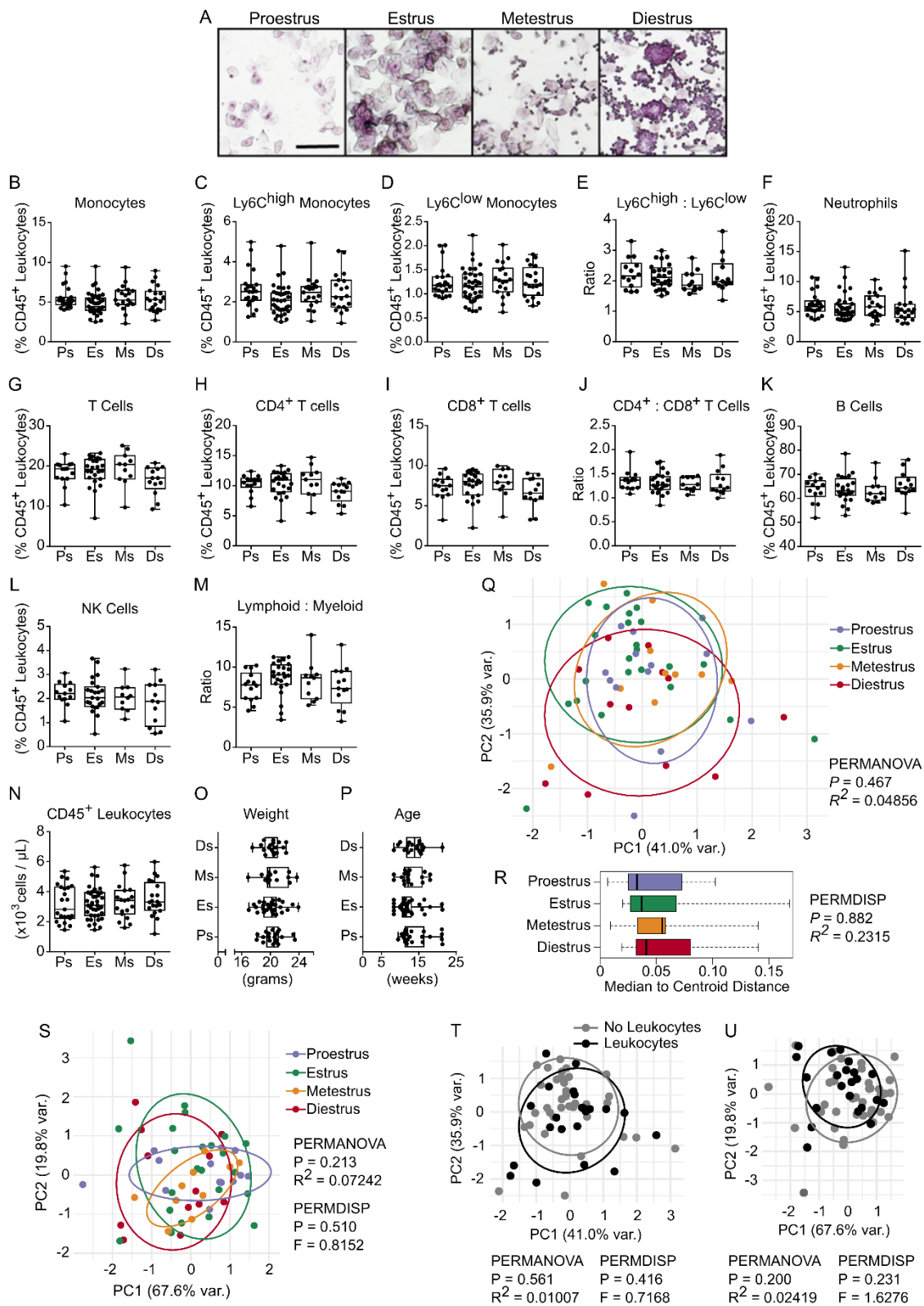


Figure 2. Peripheral blood leukocytes are not altered by female reproductive cycle stage in C57BL/6J mice.

(A) Representative images of vaginal smears stained with hematoxylin (to provide contrast) for each of the reproductive cycle stages in young female C57BL/6J mice. Proestrus is characterized by a predominance of nucleated epithelial cells, estrus by a predominance of anucleated cornified cells, metestrus by equal proportions of anucleated cornified epithelial cells, nucleated epithelial cells, and leukocytes, and diestrus is characterized by a predominance of leukocytes. Scale bar indicates 100 μm . (B to U) Flow cytometry data of peripheral blood leukocyte populations in young female C57BL/6J mice was stratified by female reproductive cycle stage. Reproductive cycle stage did not alter leukocyte prevalence (as a proportion of total CD45^+ leukocytes): total monocytes (B), $\text{Ly6C}^{\text{high}}$ monocytes (C), Ly6C^{low} monocytes (D), the ratio of $\text{Ly6C}^{\text{high}}$ to Ly6C^{low} monocytes (E), neutrophils (F), total T cells (G), CD4^+ T cells (H), CD8^+ T cells (I), the ratio of CD4^+ to CD8^+ T cells (J), B cells (K), NK cells (L) or the ratio of lymphoid to myeloid cells (M). Total leukocyte counts were likewise not significantly different in each reproductive cycle stage (N). Mouse weight (O) and age (P) were similar across all stages. PCA of immunophenotype data showed a differential influence of immune cell populations on data characteristics, but no significant differences associated with female reproductive cycle stage (Q). (R) Median to centroid distances for each reproductive cycle stage were not statistically significant, indicating that there were no differences in leukocyte population variability between each reproductive cycle stage. (S) PCA of absolute counts of immunophenotype data likewise showed no significant shifts associated with female reproductive cycle stage. Data was also considered in terms of a simpler definition of the presence or absence of leukocytes in vaginal smears. There were no significant differences in population composition or variability by cell prevalence (as a proportion of total CD45^+ leukocytes) (T) or absolute cell counts (U). For B-F, N and P, $n = 101$ (Ps=23, Es=39, Ms=19, Ds=20). For G-K, $n = 62$ (Ps=14, Es=24, Ms=11, Ds=13). For L-M and Q-R, $n = 58$ (Ps=13, Es=23, Ms=10, Ds=12). For O and S, $n = 84$ (Ps=20, Es=31, Ms=15, Ds=18). For T-U, $n = 84$ (no leukocytes (proestrus and estrus) $n = 51$, leukocytes (metestrus and diestrus) $n = 33$). Data are shown as a dot for each mouse. Data in B-P and R are presented as box and whiskers plots, minimum to maximum, where the centre line represents the median. Data in Q and S-U were plotted on PC1 and PC2. Statistical significance was assessed by one-way ANOVA for E, K-L, and N-O, or Kruskal-Wallis test of variance for B-D and F-J, M, and P, or using the R functions *adonis* (Q, S-U) and *permdisp* (R, S-U). Reproductive cycle stages: proestrus (Ps), estrus (Es), metestrus (Ms), diestrus (Ds).

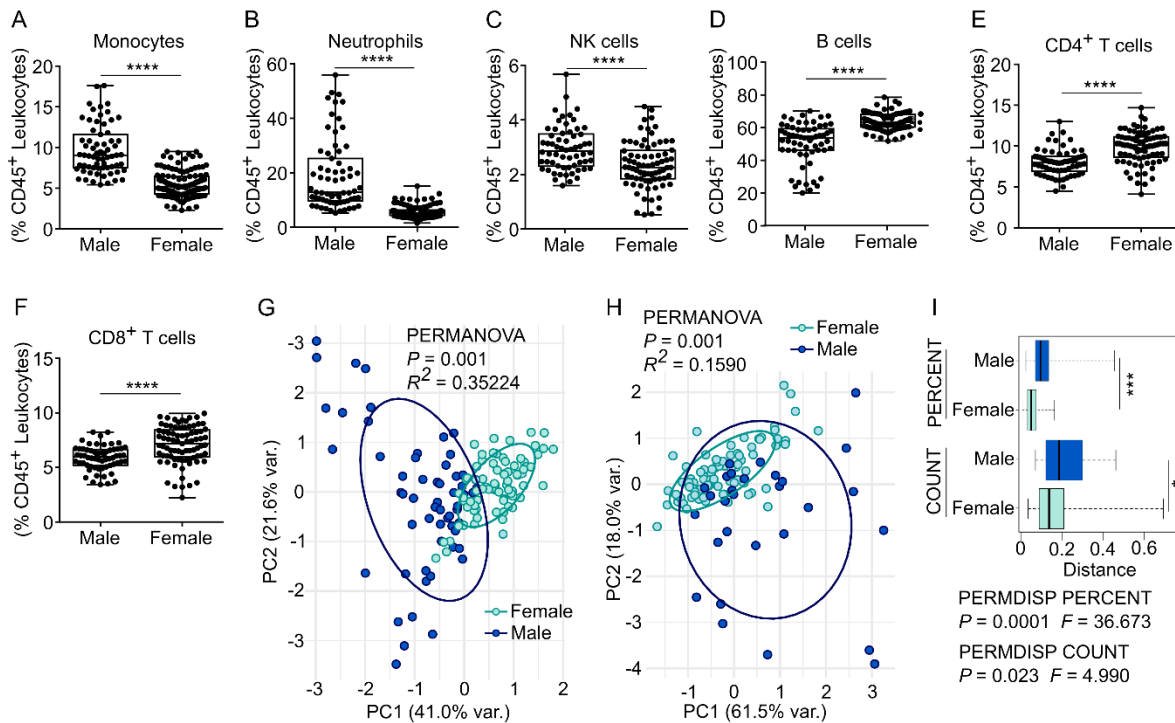


Figure 3. Biological sex has a significant effect on peripheral blood immune cell population composition and variability in C57BL/6J mice.

Flow cytometry analysis of peripheral blood revealed that female mice compared to male mice had lower quantities (as a proportion of total CD45⁺ leukocytes) of monocytes (A), neutrophils (B) and NK cells (C), whereas B cells (D), CD4⁺ T cells (E), and CD8⁺ T cells (F) were more prevalent in female mice. PCA of immunophenotype data by sex confirmed a significant shift in leukocyte composition associated with biological sex, whether data are expressed as a proportion of total CD45⁺ leukocytes (G) or absolute cell counts (H). Data were significantly more variable in male mice for proportional data (percent) and cell count data (count) (I). For A-B, $n = 67$ for male mice and $n = 120$ for female mice. For C and G-I, male mice $n = 62$ and female mice $n = 77$. For D-F, $n = 62$ for male mice and $n = 81$ for female mice. Data are shown as a dot for each mouse. Data in A-F and I are presented as box and whiskers plots, minimum to maximum, where the centre line represents the median. Data in G and H were plotted on PC1 and PC2. Statistical significance was assessed by two-tailed Mann-Whitney U test (A-D, F) or Student's t test (E) according to normality, or using the R functions *adonis* (G-H) and *permdisp* (I).

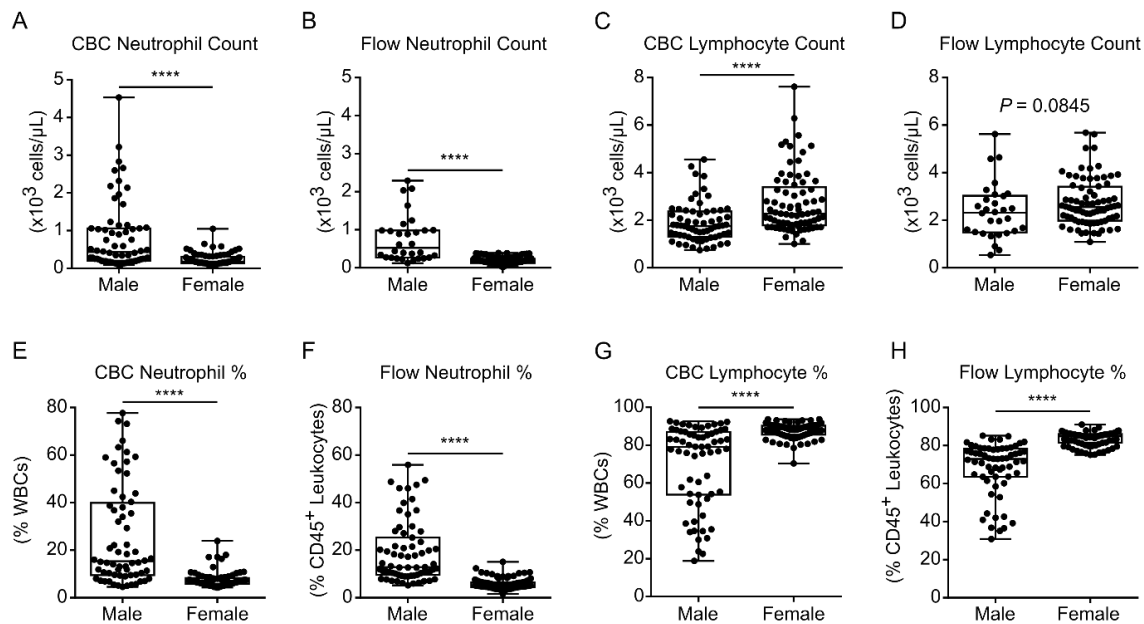


Figure 4. Peripheral blood neutrophil and lymphocyte populations assessed by CBC or flow cytometry in young female and male C57BL/6J mice.

CBC data from the Jax Phenome Database (see Methods) was compiled to examine data values and variability in male and female mice 8-16 weeks of age from multiple inbred mouse strains. CBC data from C57BL/6J male ($n = 77$) and female ($n = 64$) mice 8-16 weeks of age was compared to the flow cytometry data from this study (female $n = 76-120$, male $n = 30-67$). Total cell counts of neutrophils by CBC (A) and flow cytometry (B), and lymphocytes by CBC (C) and flow cytometry (D). Prevalence of neutrophils by CBC (E) and flow cytometry (F), and lymphocytes by CBC (G) and flow cytometry (H). For A, C, E and G, $n = 64$ for male mice and $n = 77$ for female mice. For B, $n = 30$ for male mice and $n = 115$ for female mice. For D, $n = 30$ for male mice and $n = 76$ for female mice. For F, $n = 67$ for male mice and $n = 120$ for female mice. For H, $n = 62$ for male mice and $n = 81$ for female mice. Data are presented as box and whiskers plots, minimum to maximum, where the centre line represents the median. Data are shown as a dot for each mouse. Statistical significance was assessed by two-tailed Mann-Whitney U test.

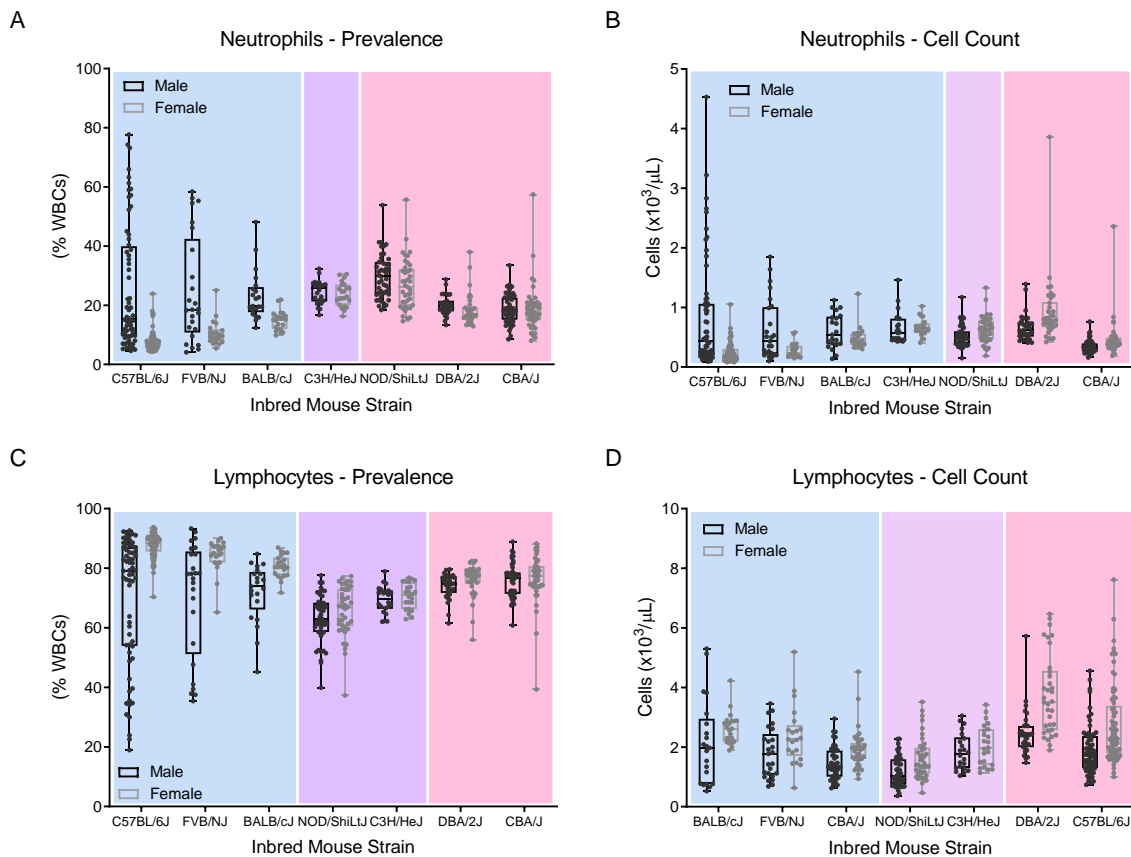


Figure 5. Peripheral blood neutrophil and lymphocyte populations in young female and male classical inbred mouse strains.

CBC data from the Jax Phenome Database (see Methods) was compiled to examine data values and variability in male and female mice 8-16 weeks of age from multiple inbred mouse strains. Neutrophil prevalence (A) and total counts (B), as well as lymphocyte prevalence (C) and total counts (D) were assessed. Strains with greater variability (assessed by coefficient of variation (CV)) in male mice are shaded in blue (left), strains with a CV within 1% for males and females are shaded in purple (middle), and strains with a greater CV in female mice are shaded in pink (right). See Tables 5 and 6 for sample size information. Data are shown as a dot for each mouse. Data are shown as box and whiskers plots, minimum to maximum, where the centre line represents the median.

Chapter 4. TNF, but not hyperinsulinemia or hyperglycemia, is a key driver of obesity-induced monocytosis revealing that inflammatory monocytes correlate with insulin in obese male mice


This chapter contains a published manuscript from *Physiological Reports**.

In obesity, macrophages that accumulate within adipose tissue produce pro-inflammatory cytokines including TNF, which contribute to metabolic dysregulation. The underlying relationships between peripheral monocytosis and obesity, inflammation, and regulation of glucose and insulin metabolism, have remained unclear. The purpose of this manuscript was to investigate the effects of obesity on peripheral monocyte prevalence, phenotype, and functions in a mouse model of obesity, and to assess if obesity itself, or the accompanying changes in glucose, insulin, and inflammatory status, contribute to monocyte prevalence. We used male mice to assess monocyte populations in diet-induced obesity without and with manipulation of insulin resistance (by antibiotic depletion of the intestinal microbiota), hyperglycemia (Akita mice) and hyperinsulinemia (sub-cutaneous insulin pellets) in the absence of obesity, and in context of reduced inflammation and insulin resistance (TNF^{-/-} mice). We confirmed that diet-induced obesity alters bone marrow and peripheral myeloid cell populations, found that obesity increases circulating immature inflammatory Ly6C^{high} monocytes, and showed that inflammation mediated by TNF, not glucose or insulin, correlated with Ly6C^{high} monocytes and insulin resistance, in male mice.

*Originally published in *Physiological Reports*: Breznik, J.A., Naidoo, A., Foley, K. P., Schulz, C., Lau, T.C., Loukov, D. Sloboda, D.M., Bowditch, D.M.E., & Schertzer, J.D. TNF, but not hyperinsulinemia or hyperglycemia, is a key driver of obesity-induced monocytosis revealing that inflammatory monocytes correlate with insulin in obese male mice. *Physiol Rep.* 2018 Dec;6(23):e13937. doi: 10.14814/phy2.13937. Copyright © 2018 by The Authors. *Physiological Reports* published by Wiley Periodicals, Inc. on behalf of The Physiological Society and the American Physiological Society.

ORIGINAL RESEARCH

TNF, but not hyperinsulinemia or hyperglycemia, is a key driver of obesity-induced monocytosis revealing that inflammatory monocytes correlate with insulin in obese male mice

Jessica A. Breznik^{1,2,3,a}, Avee Naidoo^{1,2,3,a}, Kevin P. Foley^{4,5,a}, Christian Schulz^{1,2,3}, Trevor C. Lau^{4,5}, Dessi Loukov^{1,2,3}, Deborah M. Sloboda^{4,5,6}, Dawn M. E. Bowdish^{1,2,3*} & Jonathan D. Schertzer^{4,5*} 

1 Department of Pathology and Molecular Medicine, McMaster University, Hamilton, Canada

2 McMaster Immunology Research Centre, McMaster University, Hamilton, Canada

3 Michael G. DeGroote Institute for Infectious Disease Research, McMaster University, Hamilton, Canada

4 Department of Biochemistry and Biomedical Sciences, McMaster University, Hamilton, Canada

5 Farncombe Family Digestive Health Research Institute, McMaster University, Hamilton, Canada

6 Department of Obstetrics and Gynecology and Pediatrics, McMaster University, Hamilton, Canada

Keywords

inflammation, insulin, monocyte, obesity, TNF.

Correspondence

Jonathan D. Schertzer, Biochemistry and Biomedical Sciences, McMaster University, 1280 Main Street West, HSC 4H19, Hamilton, ON L8S 4K1.
Tel: 905-525-9140, ext. 22254
Fax: 905-522-9033
E-mail: schertze@mcmaster.ca

Funding Information

AN and DL were supported by the Canadian Institutes of Health Research (CIHR) Doctoral Research Award. KPF was supported by a Natural Sciences and Engineering Council (NSERC) postdoctoral fellowship. JAB was funded by a Queen Elizabeth II Graduate Scholarship in Science and Technology. CS was supported by a postdoctoral fellowship from the Deutsche Forschungsgemeinschaft (SCHU3131/1-1). TCL was funded by a Frederick Banting and Charles Best Canada Graduate Scholarship. DMS is the Canada Research Chair in Perinatal Programming. Work in the Sloboda lab is in part funded by the CIHR. DMEB is the Canada Research Chair in Aging and Immunity. Work in the Bowdish lab is supported in part by the McMaster Immunology Research Centre and the M. G. DeGroote Institute for Infectious Disease Research. JDS is the Canada Research Chair in Metabolic Inflammation and held CDA Scholar and CIHR New Investigator awards. Work in the Schertzer lab was supported by NSERC. This research is

Abstract

Inflammation contributes to obesity-related hyperinsulinemia and insulin resistance, which often precede type 2 diabetes. Inflammation is one way that obesity can promote insulin resistance. It is not clear if the extent of obesity, hyperinsulinemia, or hyperglycemia, underpins changes in cellular immunity during diet-induced obesity. In particular, the requirement for obesity or directionality in the relationship between insulin resistance and monocyte characteristics is poorly defined. Inflammatory cytokines such as tumor necrosis factor (TNF) can contribute to insulin resistance. It is unclear if TNF alters monocytosis or specific markers of cellular immunity in the context of obesity. We measured bone marrow and blood monocyte characteristics in WT and TNF^{-/-} mice that were fed obesogenic, high fat (HF) diets. We also used hyperglycemic Akita mice and mice implanted with insulin pellets in order to determine if glucose or insulin were sufficient to alter monocyte characteristics. We found that diet-induced obesity in male mice increased the total number of monocytes in blood, but not in bone marrow. Immature, inflammatory (Ly6C^{high}) monocytes decreased within the bone marrow and increased within peripheral blood of HF-fed mice. We found that neither hyperinsulinemia nor hyperglycemia was sufficient to induce the observed changes in circulating monocytes in the absence of diet-induced obesity. In obese HF-fed mice, antibiotic treatment lowered insulin and insulin resistance, but did not alter circulating monocyte characteristics. Fewer Ly6C^{high} monocytes were present within the blood of HF-fed TNF^{-/-} mice in comparison to HF-fed wild-type (WT) mice. The prevalence of immature Ly6C^{high} monocytes in the blood correlated with serum insulin and insulin resistance irrespective of the magnitude of adipocyte or adipose tissue hypertrophy in obese mice. These data suggest that diet-induced obesity instigates a TNF-dependent increase in circulating inflammatory monocytes, which predicts increased blood insulin and insulin resistance independently from markers of adiposity or adipose tissue expansion.

supported by a CIHR Team Grant led by DMS
and a NSERC discovery grant held by JDS.

Received: 4 November 2018; Revised: 8
November 2018; Accepted: 11 November
2018

doi: 10.14814/phy2.13937

Physiol Rep, 6 (23), 2018, e13937,
<https://doi.org/10.14814/phy2.13937>

^aThese authors contributed equally to this
work.

*These authors are both corresponding
authors.

Introduction

Obesity is associated with chronic, low-grade systemic inflammation that also impacts endocrine control of metabolism (McPhee and Schertzer 2015). This metabolic inflammation (or metaflammation) can impair insulin action in tissues that participate in blood glucose control. The consequent insulin resistance is often matched by hyperinsulinemia, which independently promotes obesity and insulin resistance that generally precedes hyperglycemia and type 2 diabetes (T2D) (Mehran et al. 2012). In combination with other environmental and genetic factors, prolonged hyperinsulinemia, insulin resistance and metaflammation during obesity, coupled with insufficient insulin secretion, can lead to elevated blood glucose and the development of T2D (Ashcroft and Rorsman 2012).

Obesity alters endocrine and immunological communication between cells and tissues. For example, increased inflammatory mediators in adipose tissue contribute to reduced insulin sensitivity within adipocytes and other tissues that help control blood glucose. Endocrine and paracrine actions of cytokines, chemokines and adipokines produced by expanding adipose tissue and tissue-localized immune cells during obesity contribute to local and systemic inflammation and the development of insulin resistance (Weisberg et al. 2006; Lumeng et al. 2007a,b). The molecular mechanisms that connect insulin resistance and inflammatory cytokines/chemokines are widely studied. Comparatively little is known about how cellular immunity relates to compartmentalized, tissue-specific inflammatory cues and insulin resistance during obesity.

Accumulation of pro-inflammatory polarized macrophages within metabolic tissues is a key component of metabolic inflammation, as ablation or inhibition of macrophage inflammatory signaling can attenuate obesity-induced insulin resistance in adipose and liver tissue

(Arkan et al. 2005; Cai et al. 2005; Han et al. 2013; Revelo et al. 2016; Desai et al. 2017). Adipose tissue macrophages in particular are derived from local proliferation, resident hematopoietic stem cells, and infiltration of peripheral blood monocytes (macrophage precursors) (Weisberg et al. 2003; Xu et al. 2003; Oh et al. 2012; Amano et al. 2014; Luche et al. 2017). Murine monocytes can be divided into subsets by their surface expression of the glycoprotein Ly6C: Ly6C[−] (also referred to as Ly6C^{low}) and Ly6C⁺ (Ly6C^{int} and Ly6C^{high}) (Geissmann et al. 2003; Gordon and Taylor 2005). Ly6C^{high} monocytes mature into Ly6C[−] patrolling monocytes in the steady state but migrate to sites of acute inflammation during infection via CCL2/CCR2-dependent chemotaxis, extravasate into tissues, and differentiate into macrophages (Geissmann et al. 2003; Gordon and Taylor 2005; Serbina and Pamer 2006; Tsou et al. 2007). The pro-inflammatory cytokine TNF contributes to monocyte migration during infection by promoting CCR2 expression (Boekhoudt et al. 2003). CCR2^{−/−} mice are protected against obesity-induced macrophage accumulation, inflammation, hyperinsulinemia, and insulin resistance (Chen et al. 2005; Weisberg et al. 2006; Ito et al. 2008). TNF is produced by tissue-localized macrophages in obese mice, and its neutralization improves insulin sensitivity (Hotamisligil et al. 1995; Uysal et al. 1997). Thus, we hypothesized that during diet-induced obesity there is a TNF-dependent egress of Ly6C^{high} monocytes from bone marrow into circulation, these monocytes contribute to tissue-associated macrophage accumulation, and they are associated with metaflammation and insulin resistance.

We initially assessed the effects of diet-induced obesity on monocyte prevalence in bone marrow and blood and their expression of inflammatory and maturity markers (Ly6C, F4/80) in wild-type (WT) male mice. We found that monocyte reprogramming during obesity begins in the

bone marrow and is marked by increased circulating Ly6C[−], Ly6C^{int}, and Ly6C^{high} monocytes in HF-fed mice. Using TNF^{−/−} male mice as a model of reduced systemic inflammation, we demonstrated that despite diet-induced obesity in TNF^{−/−} mice there was a reduction in circulating Ly6C^{high} inflammatory monocytes and macrophage accumulation in adipose tissue in comparison to WT mice. More importantly, this discovery allowed for an assessment of insulin resistance characteristics in obese mice that had different levels of circulating Ly6C^{high} monocytes. We determined that during diet-induced obesity the TNF-dependent prevalence of blood monocytes, and inflammatory Ly6C^{high} monocytes in particular, were better predictors of indices of insulin resistance than body weight or parameters of adiposity, such as adipocyte size. We found no evidence that this relationship is bidirectional since manipulation of insulin levels, insulin resistance, or blood glucose did not alter monocyte characteristics.

Importantly, obesity-induced increases in circulating Ly6C^{high} monocytes directly correlated with blood insulin levels irrespective of adipose tissue/cell expansion in obese mice.

Materials and Methods

Animals

WT C57BL/6J male mice and TNF^{−/−} male mice on a C57BL/6J background were originally purchased from The Jackson Laboratory (WT no. 00064; TNF^{−/−} no. 003008; Bar Harbor, ME) and bred at the McMaster Central Animal Facility (Hamilton, ON, Canada), as described (Zganiacz *et al.* 2004; Puchta *et al.* 2016). Heterozygous C57BL/6-Ins2^{Akita}/J (Akita^{+/-}) male mice were purchased from The Jackson Laboratory (no. 003548). All animals were housed under specific pathogen-free conditions with a 12-hour light/dark cycle. Diets were manipulated at 8 weeks of age. WT and TNF^{−/−} male mice (not littermates) were allocated to either *ad libitum* standard chow diet (18% kcal from fat; Envigo Teklad Diets 7913, Madison, WI) or an obesogenic, low fiber, high fat (HF) diet (60% kcal from fat; Research Diets Inc. D12492, New Brunswick, NJ) for 18–24 weeks. Akita^{+/-} male mice and WT male mice were used for hyperglycemia experiments at 8 weeks of age. WT male mice used for hyperinsulinemia experiments were maintained on an *ad libitum* standard chow diet. To induce hyperinsulinemia, subcutaneous implantation of insulin pellets, or sham surgery was performed on WT male mice at 10–12 weeks of age as recommended by the manufacturer (~0.1U/day release; LinBit for Mice Pr-1-B, LinShin Canada Inc., Toronto, ON, Canada). WT male mice used for antibiotic microbiota depletion experiments were maintained on HF diet for 20 weeks prior to antibiotic

treatment, which consisted of 1 g/L ampicillin (Sigma A6140) and 0.5 g/L neomycin (Sigma N1878) in drinking water. Antibiotics were changed every 2 days over 4 weeks. All experiments were performed in accordance with Institutional Animal Utilization Protocols approved by McMaster University's Animal Research Ethics Board following the recommendations of the Canadian Council for Animal Care. Data from each individual mouse are indicated by a single symbol in all figures.

Metabolic assessments

Mice were fasted for 6 h with *ad libitum* water. Blood glucose and insulin were measured to calculate HOMA-IR as we have done previously (Cavallari *et al.* 2017). Fasting blood glucose was measured via tail vein using the Accu-Chek Inform II system glucometer and test strips (Roche Diagnostics, Mississauga, ON, Canada). Blood (50 μ L) was collected via tail vein, incubated at room temperature for 20 min, and spun at 7500g for 5 min at 4°C. Insulin was quantified in serum by ELISA according to the manufacturer's instructions (Fig. 3 - AIS Toronto Biosciences 32270, Toronto, ON, Canada; Figs. 4 and 6 - EMD Millipore EZRMI-13K, Billerica, MA).

Flow cytometry

Bone marrow flushed from a femur and disrupted with an 18-gauge needle, or peripheral blood collected retro-orbitally (100 μ L), was analyzed by flow cytometry to identify monocyte populations, as previously published (Puchta *et al.* 2016). Monoclonal antibodies with the following conjugated fluorophores were used in this study with isotype controls: CD3 (Alexa Fluor 700), CD11b (PE-Cy7), CD19 (Alexa Fluor 700), CD45 (eFluor 450), F4/80 (APC), IL-6 (PerCP-eFluor 710), Ly6G (Alexa Fluor 700), and NK1.1 (Alexa Fluor 700), all from eBioscience (San Diego, CA), as well as CCR2 (PE; R&D Systems, Minneapolis, MA) and Ly6C (FITC; BioLegend, San Diego, CA). Intracellular staining was performed on blood in unstimulated conditions and following stimulation with lipopolysaccharide (200 ng/mL) in complete RPMI supplemented with 10% fetal calf serum and 2x Protein Transport Inhibitor (eBioscience 00-4980-03). Samples were initially surface stained with antibodies and then intracellular staining was performed after 30 min permeabilization at room temperature with 1x Intracellular Staining Permeabilization Wash Buffer (BioLegend 421002) as previously described (Puchta *et al.* 2016). Flow cytometry was performed on a BD Biosciences LSRFortessa and analyzed using the FlowJo v9 software (Tree Star). Total cell counts were determined with CountBright Absolute Counting Beads (Life Technologies C36950).

Immunohistochemistry

Adipose tissue macrophages were analyzed as published (Denou et al. 2015). Epididymal fat pads were fixed in 10% formalin at room temperature and embedded in paraffin. 5- μ m sections cut at 50- μ m intervals were mounted on positively charged glass slides, deparaffinized in xylene, treated with proteinase K, and stained with an anti-F4/80 (1:500) monoclonal antibody (Bio-Rad Antibodies MCA-497) on the Leica Bond RX automated staining system. Adipocyte size and total number of F4/80-expressing cells (macrophages) were assessed using ImageJ (Schneider et al. 2012).

Statistical analyses

Monocyte population prevalence and phenotype differences (for individual monocyte populations) were evaluated with the Mann-Whitney U test or Student's *t* test according to normality by the D'Agostino and Pearson omnibus test. Differences in HF-fed TNF^{-/-} and WT adipose tissue macrophages, adipocyte cross-sectional area, and fasting blood glucose were evaluated with the Mann-Whitney U test or Student's *t* test according to normality. Body mass and metabolic parameter comparisons by genotype and diet were performed by two-way ANOVA with Tukey's post hoc test. Correlation analyses between adipose tissue characteristics, monocytes, and metabolic parameters, were performed using Spearman's rank correlation rho or Pearson correlation according to normality. Data were analyzed with GraphPad Prism version 6 (GraphPad Software, La Jolla, CA). A *P* < 0.05 was considered statistically significant.

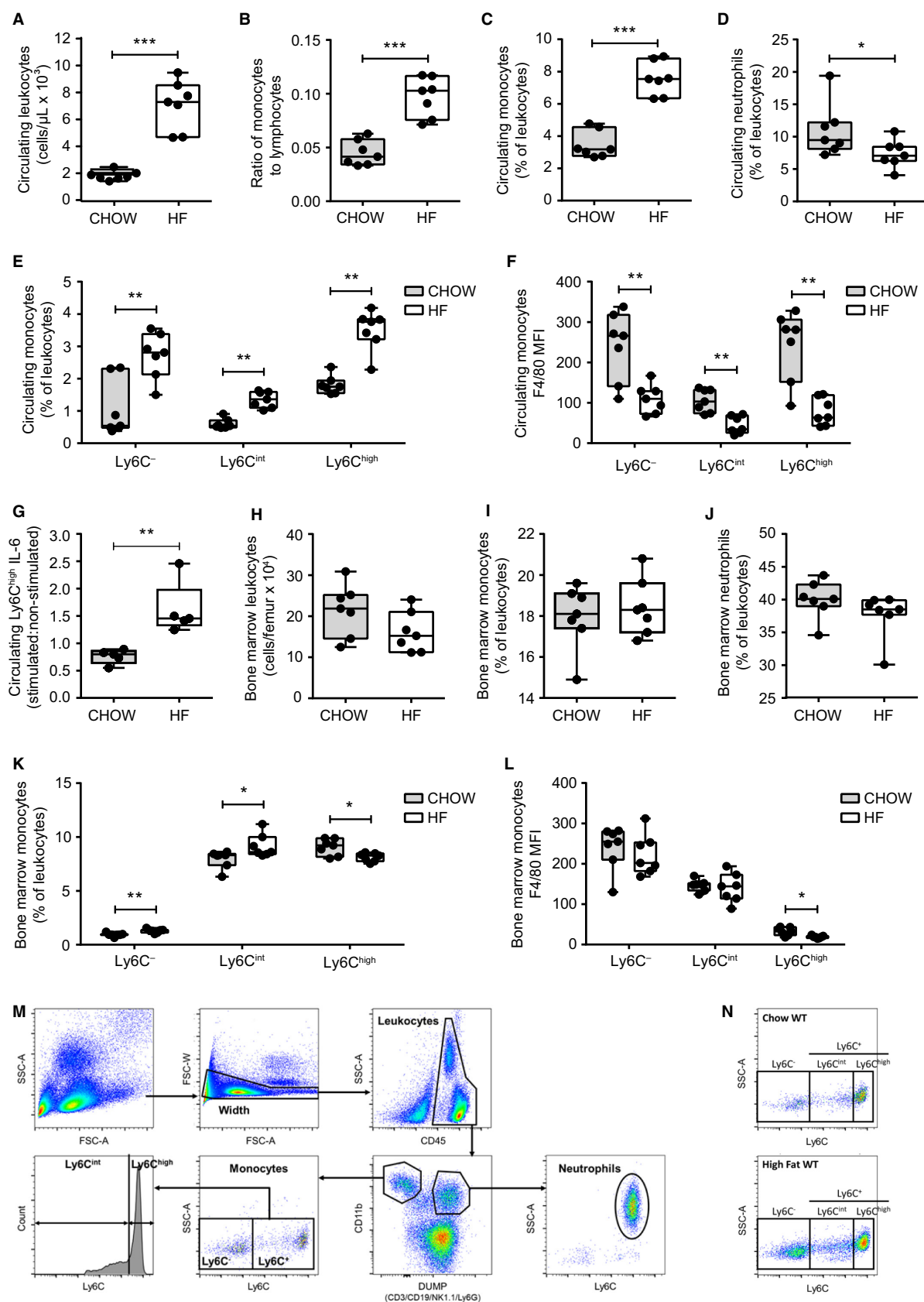
Results

Diet-induced obesity alters monocyte populations in bone marrow and blood

Leukocytosis, an increase in white blood cells, occurs in obese and/or diabetic humans (Kullo et al. 2002; Ohshita

et al. 2004; Tong et al. 2004). More recently, an elevation in circulating monocytes (monocytosis) has been associated with poorly controlled T2D, cardiovascular disease, and increased adiposity (Poitou et al. 2011; Barrett et al. 2017). Similar to Nagareddy and colleagues (Nagareddy et al. 2014), we found that WT male mice fed a HF diet for 18 weeks had a significant increase in circulating leukocytes in peripheral whole blood (Fig. 1A). HF-fed mice had an elevated ratio of circulating monocytes to lymphocytes in comparison to chow-fed control mice (Fig. 1B), due to a disproportionate increase in the prevalence of circulating monocytes (Fig. 1C) and a small decrease in the prevalence of circulating neutrophils (Fig. 1D). To further investigate the effect of diet-induced obesity on monocyte characteristics, we assessed their prevalence and expression of surface markers of inflammation (Ly6C) and maturity (F4/80). When we assessed the circulating monocyte subsets according to their expression of Ly6C it was apparent that male mice on a HF diet had elevated circulating populations of Ly6C⁻, Ly6C^{int}, and Ly6C^{high} monocytes (Fig. 1E). All monocyte subsets were increased more than twofold (as a proportion of total leukocytes) in the circulation of HF-fed mice. Absolute cell counts were also elevated in HF-fed mice (data not shown). Ly6C^{high} monocytes were significantly less mature (decreased F4/80 expression) in HF-fed mice (Fig. 1F) and Ly6C^{high} had higher surface expression of CCR2 in comparison to the other monocyte subsets (data not shown) (Chen et al. 2005; Tsou et al. 2007). Intracellular staining also indicated that circulating Ly6C^{high} monocytes from HF-fed mice produced higher levels of the pro-inflammatory cytokine IL-6 in response to LPS stimulation (Fig. 1G). Thus, diet-induced obesity in male mice is accompanied by an increase in circulating, immature inflammatory Ly6C^{high} monocytes. It was previously demonstrated that HF-fed mice have increased proliferation of the hematopoietic common myeloid progenitors within bone marrow (Nagareddy et al. 2014). We

Figure 1. Diet-induced obesity increases circulating monocyte populations. Peripheral whole blood was analyzed in chow-fed (*n* = 7) and HF-fed (*n* = 7) WT male mice after 18 weeks diet allocation. (A) absolute count of circulating leukocytes (CD45⁺ cells). (B) proportion of monocytes to lymphocytes. (C) circulating monocytes. (D) circulating neutrophils. (E) proportions of Ly6C⁻, Ly6C^{int}, and Ly6C^{high} subsets of monocytes in chow-fed and HF-fed mice. (F) expression of maturity marker F4/80 in circulating monocyte subsets from chow-fed and HF-fed mice. (G) IL-6 levels within Ly6C^{high} monocytes in response to LPS stimulation in chow-fed (*n* = 5) and HF-fed (*n* = 5) mice. (H) absolute count of bone marrow leukocytes. (I) bone marrow monocytes. (J) bone marrow neutrophils. (K) proportions of Ly6C⁻, Ly6C^{int}, and Ly6C^{high} subsets of monocytes. (L) expression of maturity marker F4/80 in bone marrow monocyte subsets. Each data point indicates a single mouse. Statistical significance was determined by Mann-Whitney tests. Data are presented as box and whiskers plots, minimum to maximum, where the center line represents the median. **P* ≤ 0.05, ***P* ≤ 0.01, ****P* ≤ 0.001. MFI – Geometric Mean Fluorescence Intensity. (M) flow cytometry gating strategy for the identification of leukocytes, neutrophils, and monocytes (bone marrow-resident and circulating). Representative images from a blood sample are shown. A width gate was created to exclude cell aggregates. CD45⁺ cells (leukocytes) were first gated. Subsequently, CD11b^{+/−} and AF700^{+/−} population gating allowed separation of CD11b⁺Ly6G[−] (monocytes), CD11b⁺Ly6G⁺ (neutrophils), and CD11b^{mid/−}CD3⁺CD19⁺NK1.1⁺ (lymphocytes: T cells, B cells, NK cells) cell populations. The CD45⁺CD11b⁺Ly6G⁺Ly6C⁺SSC^{high} cells were identified as neutrophils and the CD45⁺CD11b⁺Ly6G[−]Ly6C⁺SSC^{low} monocyte cells were divided into subsets by their expression of Ly6C: Ly6C⁻, Ly6C^{int}, and Ly6C^{high}. (N) Representative flow plots of monocyte populations in chow-fed and HF-fed wild-type male mice.



determined that leukocyte numbers and monocyte prevalence, as well as the prevalence of neutrophils, were unchanged within bone marrow of HF-fed mice (Fig. 1H–J). However, Ly6C^{int} and Ly6C^{high} monocytes were elevated whereas Ly6C^{high} monocytes were decreased in the bone marrow of HF-fed mice (Fig. 1K). In addition, bone marrow-resident Ly6C^{high} monocytes in HF-fed mice had lower expression of the F4/80 maturity marker (Fig. 1L). These data are consistent with the concept that diet-induced obesity promotes egress of immature, inflammatory Ly6C^{high} monocytes from the bone marrow into circulation. The flow cytometry gating strategy is illustrated in Figure 1M, and representative plots of monocyte populations in chow-fed and HF-fed mice are shown in Figure 1N. We subsequently assessed whether specific metabolic factors (such as glucose, insulin, insulin resistance or extent of obesity/adiposity) were associated with elevated circulating Ly6C^{high} monocytes.

Elevated blood glucose or insulin alone is insufficient to alter Ly6C^{high} monocytes

The HF diet model used leads to increased adiposity, blood glucose, insulin, and insulin resistance (Cavallari et al. 2017). We next tested if elevation of blood glucose or insulin alone could increase circulating inflammatory monocytes. Chow-fed Akita^{+/-} mice (C57BL/6-Ins2^{Akita}/J) were used to model diabetes to test the effect of hyperglycemia on monocyte characteristics, in the absence of obesity (Yoshioka et al. 1997; Gurley et al. 2006). Random fed blood glucose was significantly elevated in chow-fed Akita^{+/-} mice in comparison to chow-fed WT mice (Fig. 2A). No differences were identified in the percentage of circulating total monocytes or monocyte subsets (Fig. 2B and C). Ly6C^{high} monocyte surface expression of F4/80 was unchanged in hyperglycemic Akita^{+/-} mice (Fig. 2D). CCR2 expression was also unchanged in hyperglycemic Akita^{+/-} mice (Fig. 2E). However, hyperglycemic Akita^{+/-} mice had significantly elevated neutrophils in circulation (Fig. 2F). We next tested the effects of short-term hyperinsulinemia that was sustained for 2 weeks after implanting slow release insulin pellets in WT chow-fed mice. The increased insulin load reduced random fed blood glucose (Fig. 2G), but monocyte percentages were similar between sham and insulin pellet implanted mice (Fig. 2H and I). Expression of F4/80 and CCR2 on Ly6C^{high} monocytes was also unchanged in mice with insulin pellets (Fig. 2J and K). To contrast, we observed that mice implanted with insulin pellets had decreased circulating neutrophils (Fig. 2L). These results suggest that overt hyperglycemia, and (short-term) chronic hyperinsulinemia are not sufficient to account for the increase in circulating immature,

inflammatory Ly6C^{high} monocytes that we observed in HF diet-fed mice.

Antibiotic-mediated lowering of glucose and insulin during obesity are insufficient to alter circulating Ly6C^{high} monocytes

We also considered whether circulating Ly6C^{high} monocytes can be modulated by glucose and insulin in the context of diet-induced obesity. We used our previously established antibiotic treatment protocol in mice that modestly reduces peripheral glucose and insulin within 4 weeks (Denou et al. 2015). Mice with established diet-induced obesity after 20 weeks of HF diet feeding were allocated to receive water as usual or drinking water supplemented with antibiotics for 4 weeks. Antibiotic treatment did not alter body weight (Fig. 3A) or adiposity (Fig. 3B). Fasting blood glucose was lower after 4 weeks of antibiotic treatment (Fig. 3C). Further, fasting blood insulin decreased at 2 weeks and 4 weeks of antibiotic treatment (Fig. 3D). Insulin resistance, measured by the homeostatic model assessment of insulin resistance (HOMA-IR), was lower at 2 weeks and 4 weeks of antibiotic treatment (Fig. 3E). Total circulating leukocyte numbers were unaffected by antibiotic treatment (data not shown). The prevalence of circulating Ly6C^{high} monocytes was not altered by antibiotics at 2 and 4 weeks (Fig. 3F). These results were consistent with our previous data showing that manipulation of glucose and insulin is not sufficient to alter the prevalence of circulating Ly6C^{high} monocytes.

TNF contributes to inflammatory Ly6C^{high} monocyte prevalence during diet-induced obesity

We used TNF^{-/-} mice to examine the role of TNF in mediating obesity-associated changes to inflammatory Ly6C^{high} monocytes. Consistent with previous studies (Uysal et al. 1997; Ventre et al. 1997; Koulmanda et al. 2012), we initially confirmed that TNF^{-/-} mice are partially protected from a HF diet-induced increase in body mass, as well as insulin resistance assessed by HOMA-IR (Fig. 4A and B). Lower insulin resistance was due to lower fasting serum insulin rather than changes in blood glucose in HF-fed TNF^{-/-} mice (Fig. 4C and D). We next showed that HF diet-fed TNF^{-/-} mice had significantly fewer adipose tissue-resident macrophages compared to HF diet-fed WT mice (Fig. 4E). When we examined peripheral monocyte populations, we found there was a twofold reduction in the proportion of circulating monocytes relative to lymphocytes in HF-fed TNF^{-/-} mice (Fig. 5A). This difference in the ratio of

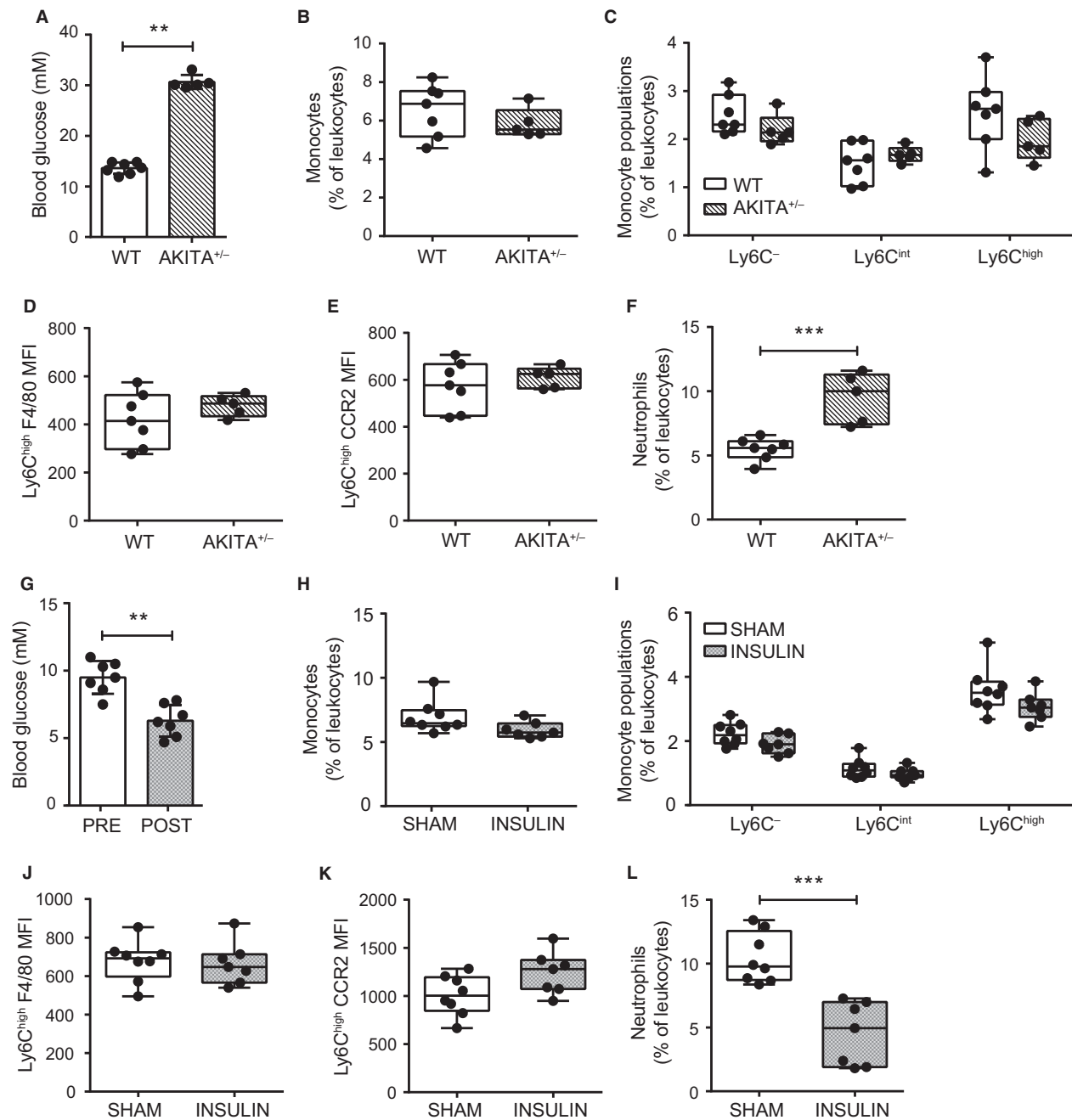


Figure 2. Ly6C^{high} prevalence and phenotype are independent of glucose and insulin in absence of obesity. Peripheral blood monocytes were assessed in chow fed, male WT ($n = 7$) and Akita^{+/-} ($n = 5$) mice. (A) random fed blood glucose in WT and Akita^{+/-} mice. (B and C) total monocytes and Ly6C⁻, Ly6C^{int}, and Ly6C^{high} monocyte subsets as a percentage of total leukocytes (CD45⁺ cells) in WT and Akita^{+/-} mice. (D and E) Ly6C^{high} monocyte F4/80 and CCR2 surface expression in WT and Akita^{+/-} mice. (F) total neutrophils as a percentage of total leukocytes in WT and Akita^{+/-} mice. Effects of hyperinsulinemia on circulating monocytes were assessed in peripheral blood of sham ($n = 8$) and insulin pellet implanted ($n = 7$) chow-fed, WT male mice. (G) random fed blood glucose preimplantation and 2-weeks post-insulin pellet implantation. (H and I) total monocytes and Ly6C-expressing monocyte subsets as a percentage of total leukocytes (CD45⁺ cells) in mice 2 weeks after sham and post-insulin pellet implantation. (J and K) Ly6C^{high} monocyte F4/80 and CCR2 surface expression. (L) total neutrophils as a proportion of total leukocytes in mice 2 weeks after sham and post-insulin pellet implantation. Each data point indicates a single mouse. Two-tailed Mann-Whitney U tests were used to assess statistical significance between diet groups. Data are presented as box and whiskers plots, minimum to maximum, where the center line represents the median. ** $P \leq 0.01$, *** $P \leq 0.001$. MFI: Geometric Mean Fluorescence Intensity.

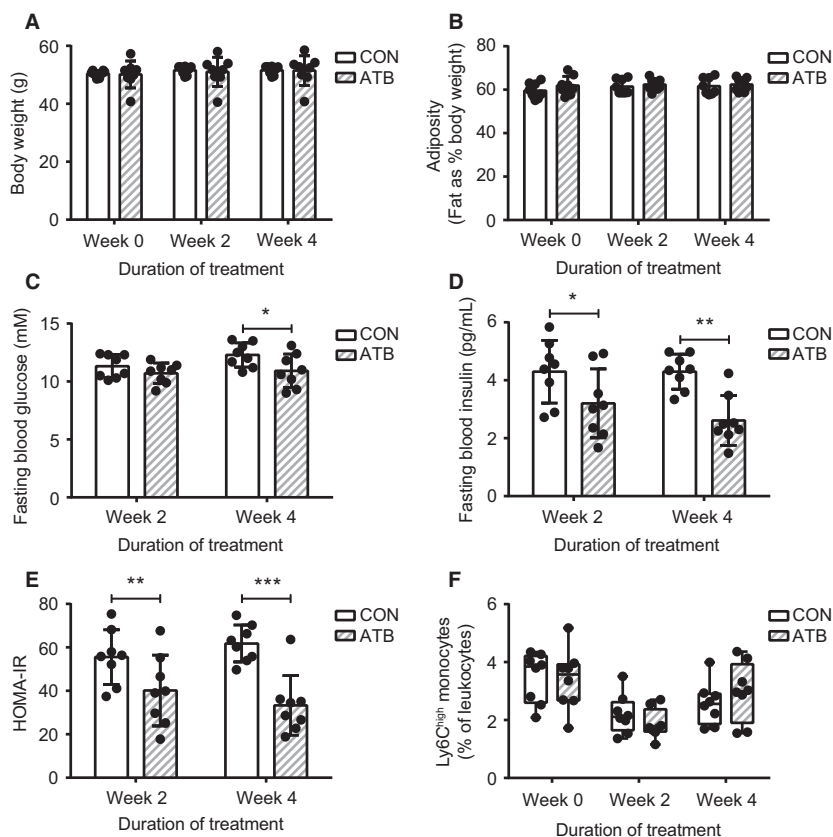


Figure 3. Ly6C^{high} prevalence in obesity is not altered by antibiotic-mediated lowering of glucose and insulin. WT male mice were allocated to HF diet for 20 weeks and maintained on HF diet following allocation to usual drinking water (CON, $n = 8$) or antibiotics in drinking water (ATB, $n = 8$) for 4 weeks. Assessments occurred before allocation to antibiotic treatment (week 0) and after 2 and 4 weeks of treatment. (A) body weight. (B) adiposity. (C) fasting blood glucose. (D) fasting blood insulin. (E) HOMA-IR. (F) circulating Ly6C^{high} monocytes as a percentage of total leukocytes (CD45⁺ cells). Each data point indicates a single mouse. Two-tailed Student's t tests or Mann-Whitney U tests were used to assess statistical significance between diet groups at each timepoint according to normality. Data are presented as bar graphs with mean \pm standard deviation (A to E) or box and whiskers plots, minimum to maximum, where the center line represents the median (F).

* $P \leq 0.05$, ** $P \leq 0.01$, *** $P \leq 0.001$.

monocytes/lymphocytes in HF-fed WT mice versus HF-fed TNF^{-/-} mice is analogous to the ratio of monocytes/lymphocytes in HF-fed WT mice compared to chow-fed WT mice (Fig. 1B). Accordingly, total and Ly6C^{high} monocytes were lower in the circulation of HF-fed TNF^{-/-} mice compared to HF-fed WT mice (Fig. 5B and C), though Ly6C^{high} monocyte prevalence was similar in HF-fed WT and TNF^{-/-} mouse bone marrow (Fig. 5D). No differences were observed in circulating Ly6C^{high} monocyte maturity (Fig. 5E) or CCR2 expression between HF-fed WT and TNF^{-/-} mice (Fig. 5F). These data indicate that TNF contributes to obesity-associated changes in circulating Ly6C^{high} monocyte prevalence in addition to hyperinsulinemia and macrophage accumulation in metabolic tissues. Indeed, we observed a strong positive correlation in these HF-fed mice between circulating monocytes and body weight, as well as circulating

monocytes and macrophage accumulation in adipose tissue (Fig. 5G and H).

Ly6C^{high} monocytes correlate with insulin during obesity

The relationship between adiposity and insulin sensitivity is complicated by many factors, including the lipid storage location (Wagenknecht et al. 2003; Muller et al. 2012). In mice, the mass of specific fat pads and adipocyte cross-sectional area have previously been shown to mark specific aspects of diet-induced adiposity (Weisberg et al. 2003; Chusyd et al. 2016). We assessed if body weight, gonadal adipose tissue mass, or adipocyte hypertrophy (i.e., cross-sectional area of adipocytes), correlated with serum insulin levels in HF-fed WT and TNF^{-/-} mice (Fig. 6A–C). We combined HF-fed WT and TNF^{-/-}

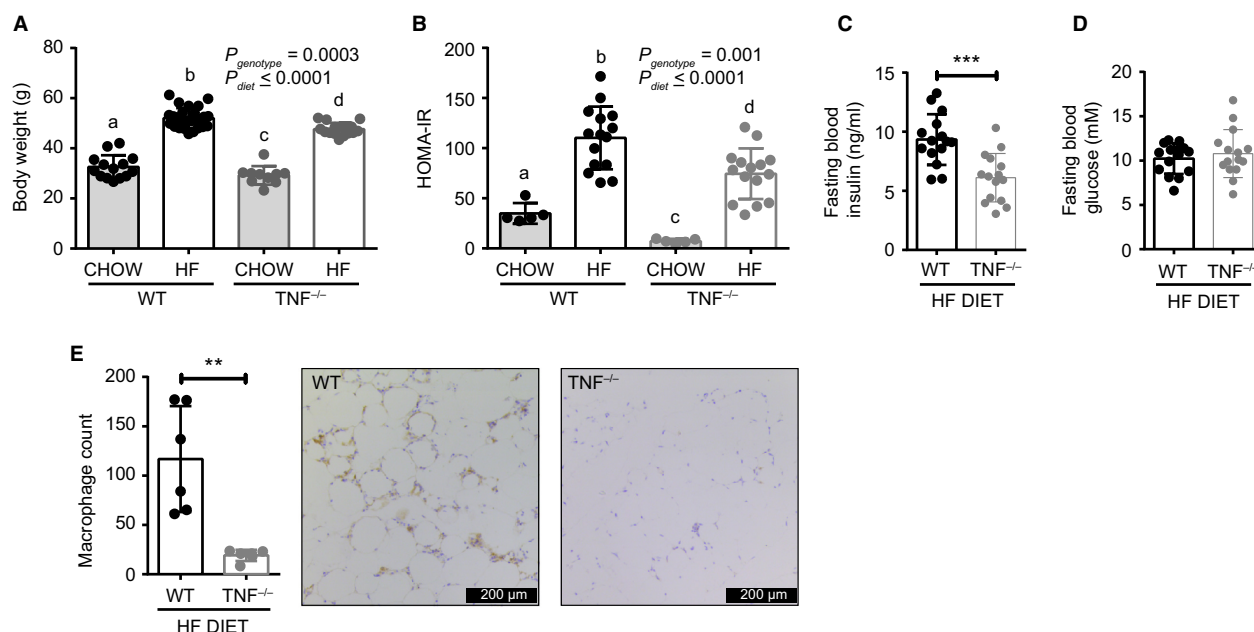


Figure 4. TNF contributes to insulin resistance and adipose inflammation during obesity. WT and $TNF^{-/-}$ male mice were allocated to a chow or HF diet for 24 weeks. Body weight (A) and HOMA-IR (B) determined at endpoint for chow-fed and HF-fed WT and $TNF^{-/-}$ mice. Fasting blood insulin (C) and glucose (D) in HF-fed mice WT and $TNF^{-/-}$ mice. (E) quantification of adipose tissue-resident macrophages and representative images of immunohistochemistry staining for macrophages (F4/80-positive cells) in gonadal adipose tissue of HF-fed WT and $TNF^{-/-}$ mice. Data were derived from two independent cohorts of mice, where $n = 5-9$ mice per group. Each data point indicates a single mouse. Two-way ANOVA with Tukey's post test was performed for A and B, where inset P values represent main effects and bars with different letters indicate significant differences. Significance was assessed by Mann-Whitney test for C to E. Data in C to E are shown as bar graphs with mean \pm standard deviation. $**P \leq 0.01$, $***P \leq 0.001$.

data and observed that there was a positive correlation between total body weight and insulin. In contrast, neither epididymal adipose tissue mass nor adipocyte cross-sectional area, as markers of adiposity, correlated with fasting blood insulin. In fact, adipocyte cross-sectional area was not different in the gonadal fat pads of HF-fed WT and $TNF^{-/-}$ mice (Fig. 6D). Given the importance of adipose tissue macrophages in driving obesity and metabolic dysfunction (Olefsky and Glass 2010; Osborn and Olefsky 2012), and our observations of the effects of HF diet on the prevalence of circulating monocytes, we next examined whether macrophage and monocyte characteristics related to insulin. The number of adipose tissue macrophages did not correlate with fasting blood insulin (Fig. 6E). However, the prevalence of blood $Ly6C^{high}$ monocytes positively correlated with fasting blood insulin (Fig. 6F and Table 1). Given the direct correlation of insulin and blood $Ly6C^{high}$ monocytes it was logical that we also found an association between $Ly6C^{high}$ monocytes and HOMA-IR (Table 1). Correlations were also identified between total, $Ly6C^{-}$ and $Ly6C^{int}$ monocytes and fasting blood insulin. We did not observe an association between $Ly6C^{high}$ monocytes and fasting blood glucose

(Fig. 6G and Table 1). These data indicate that there is a direct association between serum insulin and the prevalence of circulating immature inflammatory $Ly6C^{high}$ monocytes rather than markers of adiposity such as fat pad mass or adipocyte size in obese male mice.

Discussion

In this study we examined the effects of diet-induced obesity on monocyte prevalence and phenotype. We found that our model of long-term diet-induced obesity elevates circulating leukocytes and results in an expansion of peripheral monocytes. We identified that alterations to $Ly6C^{high}$ monocyte phenotype during obesity are TNF-dependent, begin in the bone marrow, and lead to a higher prevalence of circulating immature and migration-primed inflammatory $Ly6C^{high}$ monocytes that positively correlate with serum insulin, linking peripheral immune function with endocrine dysregulation.

Monocytosis, an increase in peripheral blood monocytes, has been recognized for many years to coincide with inflammation (Dutta and Nahrendorf 2014), and it has been more recently recognized to contribute to chronic

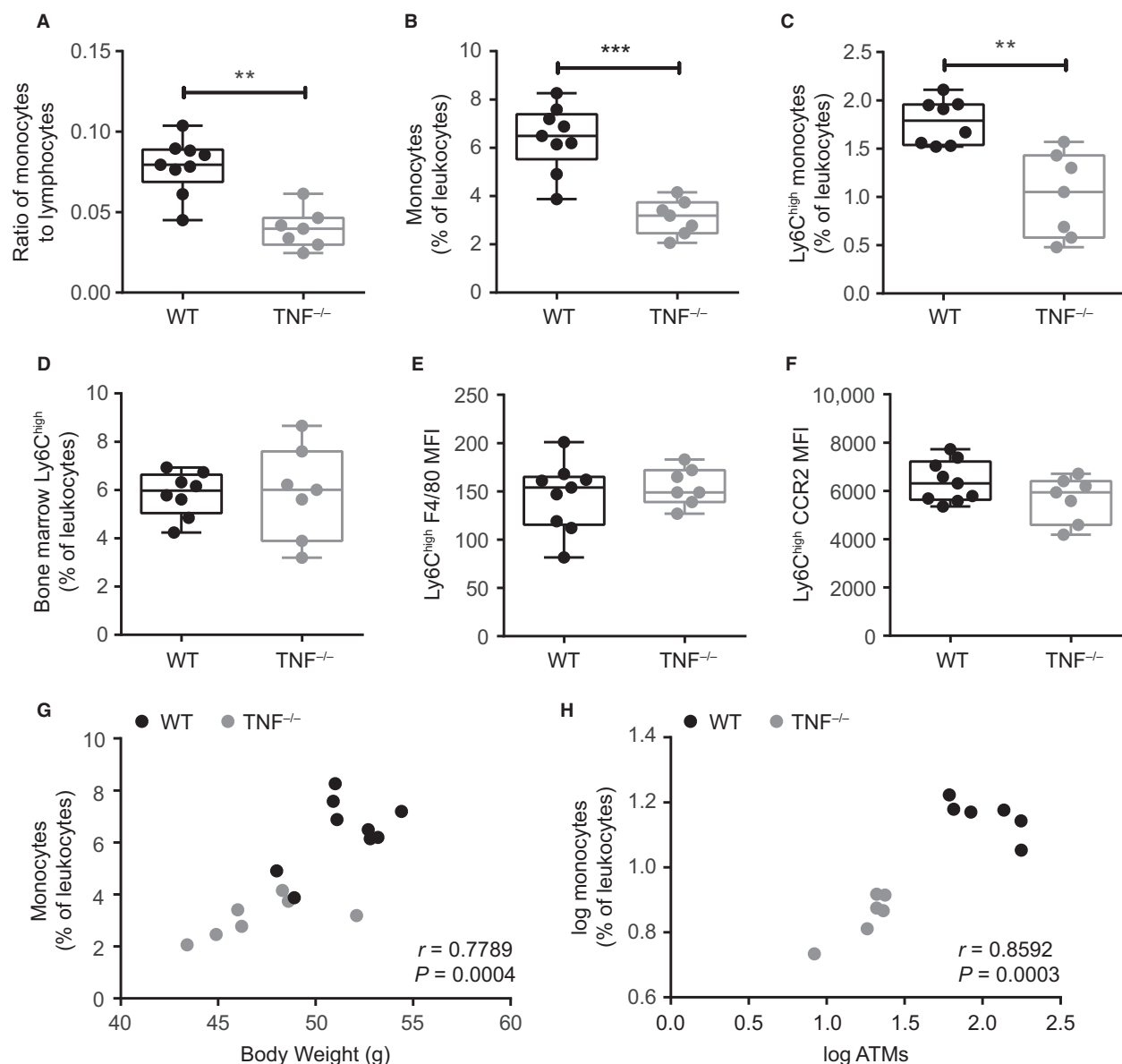


Figure 5. TNF contributes to the egress of monocytes during obesity. Monocyte populations were compared in $TNF^{-/-}$ and WT male mice allocated to HF diet for 24 weeks. (A) proportion of circulating monocytes to lymphocytes. (B and C) total monocytes and $Ly6C^{high}$ monocytes as a proportion of total leukocytes (CD45⁺ cells). (D) bone marrow $Ly6C^{high}$ monocytes expressed as a proportion of leukocytes. (E and F) circulating $Ly6C^{high}$ surface expression of F4/80 and CCR2. (G) correlation of monocyte prevalence and body weight. (H) correlation of monocyte prevalence and adipose tissue macrophages (ATMs). Data in A to E are representative of two independent cohorts of HF-fed mice ($n = 7-9$ /genotype). Each dot is a mouse. Statistical significance determined by Mann-Whitney tests. Data in A to E are presented as box and whiskers plots, minimum to maximum, where the center line represents the median. Correlations for G-H were determined by Pearson's tests. ** $P \leq 0.01$, *** $P \leq 0.001$. MFI – Geometric Mean Fluorescence Intensity.

low-grade inflammation during obesity (Schmidt et al. 1999; Ford 2002; Kullo et al. 2002). We observed a decrease in $Ly6C^{high}$ monocytes in the bone marrow and an increase in this population in circulation in HF diet-fed obese male mice that are well known to have mild hyperglycemia and hyperinsulinemia. Circulating monocytosis, and a

particular elevation of $Ly6C^{high}$ monocytes, has also been reported in Ob/Ob mice (Nagareddy et al. 2014). $Ly6C^{high}$ mouse monocytes are comparable to human classical (CD14⁺CD16⁻) and intermediate (CD14⁺CD16⁺) monocytes (Gordon and Taylor 2005). Classical monocytes both in circulation and adipose tissue increase with obesity

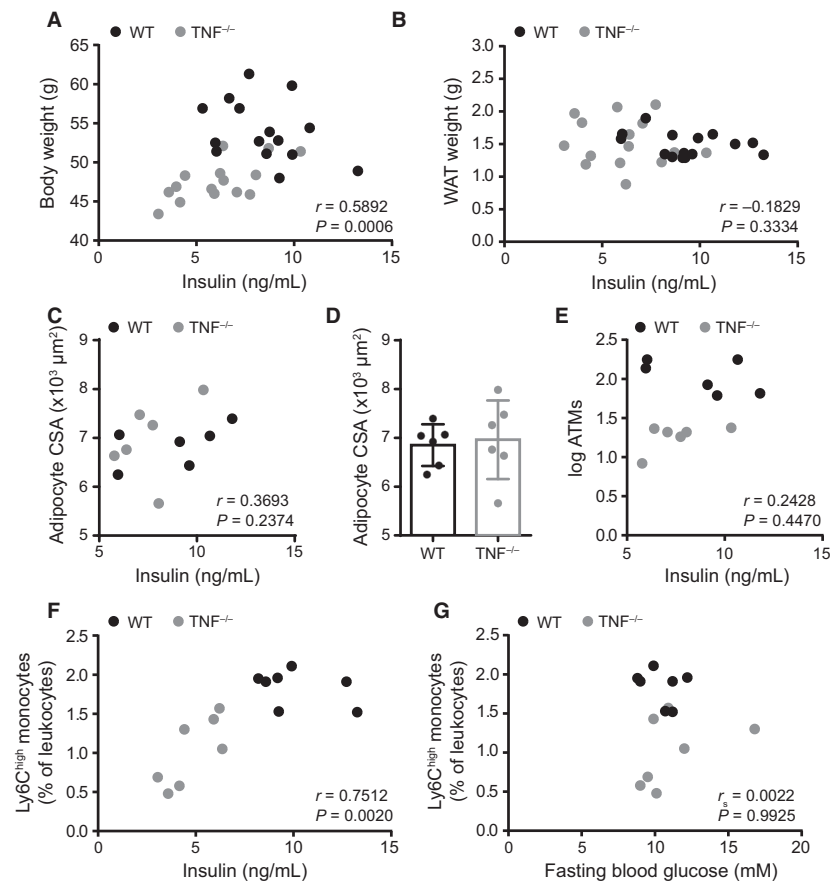


Figure 6. Circulating inflammatory monocytes may predict insulin during obesity. Correlations in HF-fed $TNF^{-/-}$ and WT mice. (A) correlation of body weight and fasting insulin. (B) correlation of fasting blood insulin and epididymal adipose tissue weight (WAT). (C) correlation of fasting blood insulin and adipocyte cross-sectional area (CSA). (D) quantification of adipocyte CSA in HF-fed WT and $TNF^{-/-}$ mice. (E) correlation of fasting blood insulin and adipose tissue macrophages (ATMs). (F) correlation of fasting blood insulin and the prevalence of circulating $Ly6C^{high}$ monocytes in all HF-fed mice. (G) correlation of fasting blood glucose and the prevalence of circulating $Ly6C^{high}$ monocytes in all HF-fed mice. Data in A and B are from two independent cohorts of HF-fed mice ($n = 7-9/\text{genotype}$). Data in C–E are from a subset of HF-fed mice from those cohorts ($n = 6/\text{genotype}$). Data in F and G are from one cohort of HF-fed mice ($n = 7/\text{genotype}$). Each dot is a mouse. Data in D are shown as a bar graph with mean \pm standard deviation. Correlations for A–C and E–G were determined by Spearman or Pearson's tests and Mann-Whitney U test was used to assess D.

Table 1. Correlations of monocyte populations with body weight and metabolic parameters in obese male mice.

	Total monocytes	$Ly6C^{-}$	$Ly6C^{int}$	$Ly6C^{high}$
Body weight	$r = 0.7790$ $P = 0.0004$	$r = 0.6942$ $P = 0.0029$	$r = 0.7423$ $P = 0.0010$	$r = 0.7526$ $P = 0.0008$
Fasting blood glucose	$r_s = -0.07517$ $P = 0.7729$	$r_s = -0.02063$ $P = 0.9322$	$r_s = -0.2137$ $P = 0.4173$	$r_s = 0.0022$ $P = 0.9925$
Fasting blood insulin	$r = 0.6861$ $P = 0.0067$	$r = 0.5680$ $P = 0.0341$	$r = 0.6418$ $P = 0.0134$	$r = 0.7247$ $P = 0.0034$
HOMA-IR	$r = 0.6076$ $P = 0.0212$	$r = 0.5070$ $P = 0.0643$	$r = 0.4968$ $P = 0.0707$	$r = 0.7512$ $P = 0.0020$

Text in bold denotes statistical significance at $P < 0.05$.

(Wouters et al. 2017), and their activation has also been reported in diabetics (Cipolletta et al. 2005). An increase in intermediate monocytes in obese humans has been linked to an increased risk of subclinical atherosclerosis and cardiovascular events (Seidler et al. 2010; Poitou et al. 2011; Rogacev et al. 2012; Ziegler-Heitbrock 2015), as well as insulin resistance (Krininger et al. 2014). Expansion of the circulating intermediate monocyte population has also been reported in T1D and T2D patients (Mysliwska et al. 2012; Terasawa et al. 2015; Ren et al. 2017).

In addition to assessing circulating monocyte prevalence, we assessed how obesity affected their progression toward a mature tissue macrophage phenotype by examining their expression of F4/80, a surface marker related to maturity. Our observations of decreased F4/80 expression on the surface of Ly6C^{high} monocytes in bone marrow and blood of HF-fed mice suggest that these monocytes are less mature. These immature monocytes are known to migrate to tissues in the context of infection via the CCR2/CCL2 chemotactic axis and thus may be primed for migration into metabolic tissues (Weisberg et al. 2006; Tsou et al. 2007; Ito et al. 2008). There were lower Ly6C^{high} monocytes in the bone marrow and higher Ly6C^{high} monocytes in blood, indicating that diet-induced obesity may alter egress of inflammatory monocytes from the bone marrow into circulation.

We have previously demonstrated a role for TNF in mediating dysfunction of monocyte development and function with aging, as well as increasing susceptibility to infection (Puchta et al. 2016). In addition to their association with increased circulating inflammatory CD14⁺CD16⁺ intermediate monocytes, high levels of circulating TNF are characteristic of obesity as well as chronic inflammatory conditions. Anti-TNF therapies used to treat rheumatoid arthritis can decrease risk of developing T2D (Klaasen et al. 2011; Solomon et al. 2011; Gremese et al. 2013). We expanded on the pleiotropic role of this pro-inflammatory cytokine by demonstrating its involvement in inflammatory Ly6C^{high} monocyte egress from the bone marrow into circulation and accumulation of macrophages in metabolic tissues during obesity. TNF may induce NLRP3 inflammasome priming and activation (Alvarez and Munoz-Fernandez 2013; McGeough et al. 2017). Our data illustrating the importance of TNF in obesity-associated monocytosis agree with that of Nagareddy and colleagues, who found that obesity-associated changes in adiposity and monocytosis are dependent on the NLRP3 inflammasome, and in particular NLRP3-dependent production of IL-1 β (Alvarez and Munoz-Fernandez 2013; Nagareddy et al. 2014; McGeough et al. 2017). The changes we observed to monocyte phenotype in TNF^{-/-} mice were coincident with attenuation of hyperinsulinemia and insulin resistance and a slight reduction in body mass. Lower insulin levels underpinned lower

insulin resistance (measured by HOMA-IR) in the HF-fed TNF^{-/-} mice. This was expected as TNF is known to promote insulin resistance during obesity (Uysal et al. 1997; Ventre et al. 1997; Hivert et al. 2010; Koulmanda et al. 2012), but this mouse model also provided a unique model to correlate insulin and inflammatory monocytes during diet-induced obesity. Deletion of TNF reduced accumulation of macrophages in adipose tissue despite similar levels of adipocyte hypertrophy during HFD-fed feeding. Therefore, our data show that TNF is a key regulator of diet-induced changes to monocyte/macrophage-driven inflammation in obesity, and that TNF can contribute to metaflammation in a manner that is independent of adipocyte hypertrophy and regulation of glucose. These data also reinforced the concept that obesity-induced changes in inflammatory monocytes correlated with insulin rather than markers of adiposity such as adipocyte size.

Our data indicated that tissue-specific effects of the Ly6C^{high} monocytes and/or metabolic tissue changes predicted the development of some aspects of insulin resistance, which led us to examine the association of monocyte phenotype and insulin levels. Comparisons of blood monocyte characteristics and circulating insulin levels in HF-fed WT and TNF^{-/-} mice during diet-induced obesity demonstrated that circulating immature inflammatory Ly6C^{high} monocytes were more strongly associated with serum insulin levels compared to indices of adiposity, total body weight, and other monocyte populations in male mice. Circulating Ly6C^{high} monocytes appear positioned to predict or propagate hyperinsulinemia or insulin resistance during diet-induced obesity. A recent publication examining the role of CX3CR1 and Gr1^{low} monocytes (equivalent to our Ly6C⁻ monocyte population) in diet-induced obesity, by using female mice deficient for CX3CR1 in blood or hematopoietic compartments, reported a negative association between Gr1^{low} monocytes and HOMA-IR (Béliard et al. 2017). Our data in male mice show an association between Ly6C⁻ monocytes and insulin levels rather than HOMA-IR. Our data were determined through modulation of TNF-related inflammation in obesity rather than directly modifying monocytes, which may explain this discrepancy. In addition, there are likely sex-specific differences that alter monocyte characteristics in obesity that warrant further study.

Hyperglycemia and hyperinsulinemia have both previously been shown to alter monocyte epigenetic programming and function in conditions of infection and stress (Xiu et al. 2014), and it has recently been reported that insulin signaling in obesity has a significant role in mediating adaptive T cell inflammatory responses (Tsai et al. 2018). Consequently, the positive correlation that we observed of an increasing prevalence of inflammatory

Ly6C^{high} monocytes with increasing insulin resistance in male mice suggested insulin may mediate phenotypic changes to Ly6C^{high} monocytes in obesity. We found that raising insulin was not sufficient to alter circulating Ly6C^{high} monocytes in the absence of obesity. In surprising contrast to a previous study (Nagareddy *et al.* 2013), we found that hyperglycemic Akita^{+/-} mice did not have changes to circulating Ly6C^{high} monocytes. Our Akita^{+/-} mice were assessed at 8 weeks of age whereas the previous study performed measures on mice at 12–16 weeks of age (Nagareddy *et al.* 2013). Longer exposure to elevated peripheral glucose may explain this discrepancy. We did confirm that circulating neutrophils were significantly higher in hyperglycemic Akita^{+/-} mice (Nagareddy *et al.* 2013), and further showed that ongoing low-dose insulin exposure (*i.e.*, from a slow-release implant) can reduce the proportion of circulating neutrophils, likely due to the accompanying reduction in blood glucose. We further demonstrated that reduction of peripheral glucose and insulin via antibiotic treatment in obese wild-type mice does not alter Ly6C^{high} monocyte populations in circulation. We acknowledge *in vivo* manipulation of glucose and insulin is interdependent. Nevertheless, our data suggest that elevated blood glucose or insulin in the absence of cellular mediators, hormones, hyperlipidemia, and other factors that accompany obesity, are insufficient to alter monocyte prevalence or measurements of maturity (F4/80) or chemotactic potential (CCR2). We cannot exclude the possibility that dyslipidemia or hyperleptinemia may also contribute to the changes in monocyte maturity and phenotype that we observed with HF diet (Desai *et al.* 2017; Rahman *et al.* 2017; Short *et al.* 2017). A significant limitation of our data is that our WT and TNF^{-/-} experiments were not conducted in littermate mice. Although metabolic data were consistent with previous data, our study design cannot rule out the possibility that differences in genetic background, microbiota composition, or husbandry may have influenced the results (Hotamisligil *et al.* 1995; Uysal *et al.* 1997; Ventre *et al.* 1997). The use of non-littermate mice is a weakness of this study to provide a direct role of TNF, but the association of inflammatory monocytes with insulin may span a diverse genetic background and should be further investigated in humans. Our current data support a model where obesity-related cellular mediators alter monocyte characteristics, which contribute to cellular inflammation and hormone regulation within metabolic tissues. Our data suggest directionality in the relationship between insulin and monocyte changes during obesity, where diet-induced changes in Ly6C^{high} monocytes predict insulin and insulin resistance, but neither glucose, insulin, nor insulin resistance appears to alter these inflammatory monocytes during obesity.

Monocyte prevalence and phenotype have been proposed as biomarkers in cardiovascular disease and chronic inflammatory disorders (Yang *et al.* 2014; Chara *et al.* 2015; Meeuwse *et al.* 2017; Loukov *et al.* 2018). Our data links monocyte/macrophage phenotype to changes in whole body insulin regulation due to diet-induced obesity and suggests that monocyte characteristics in obese individuals could serve as predictive biomarkers of diabetes risk and may represent a mechanism linking inflammation and insulin regulation. Modulation of low-grade inflammation through selectively targeting monocyte populations in obese individuals may therefore improve insulin sensitivity. Examining the role of all monocyte subsets in driving peripheral and tissue-specific meta-inflammation will improve our understanding of the development of hyperinsulinemia, insulin resistance, and type 2 diabetes in obese individuals.

Conflict of Interest

The authors have no conflicts of interest, financial, or otherwise, to be declared.

References

- Alvarez, S., and M. A. Munoz-Fernandez. 2013. TNF-Alpha may mediate inflammasome activation in the absence of bacterial infection in more than one way. *PLoS ONE* 8:e71477.
- Amano, S. U., J. L. Cohen, P. Vangala, M. Tencerova, S. M. Nicoloso, J. C. Yaw, *et al.* 2014. Local proliferation of macrophages contributes to obesity-associated adipose tissue inflammation. *Cell Metab.* 19:162–171.
- Arkan, M. C., A. L. Hevener, F. R. Greten, S. Maeda, Z. W. Li, J. M. Long, *et al.* 2005. IKK-beta links inflammation to obesity-induced insulin resistance. *Nat. Med.* 11:191–198.
- Ashcroft, F. M., and P. Rorsman. 2012. Diabetes mellitus and the beta cell: the last ten years. *Cell* 148:1160–1171.
- Barrett, T. J., A. J. Murphy, I. J. Goldberg, and E. A. Fisher. 2017. Diabetes-mediated myelopoiesis and the relationship to cardiovascular risk. *Ann. N. Y. Acad. Sci.* 1402:31–42.
- Béiard, S., W. Le Goff, F. Saint-Charles, L. Poupel, V. Deswaerte, L. Bouchareychas, *et al.* 2017. Modulation of Gr1low monocyte subset impacts insulin sensitivity and weight gain upon high-fat diet in female mice. *Int. J. Obes.* 41:1805.
- Boekhoudt, G. H., Z. Guo, G. W. Beresford, and J. M. Boss. 2003. Communication between NF-kappa B and Sp1 controls histone acetylation within the proximal promoter of the monocyte chemoattractant protein 1 gene. *J. Immunol.* 170:4139–4147.
- Cai, D., M. Yuan, D. F. Frantz, P. A. Melendez, L. Hansen, J. Lee, *et al.* 2005. Local and systemic insulin resistance resulting from hepatic activation of IKK-beta and NF-kappaB. *Nat. Med.* 11:183–190.

- Cavallari, J. F., M. D. Fullerton, B. M. Duggan, K. P. Foley, E. Denou, B. K. Smith, et al. 2017. Muramyl dipeptide-based postbiotics mitigate obesity-induced insulin resistance via IRF4. *Cell Metab.* 25:1063–1074.e1063.
- Chara, L., A. Sánchez-Atrio, A. Pérez, E. Cuende, F. Albarrán, A. Turrión, et al. 2015. The number of circulating monocytes as biomarkers of the clinical response to methotrexate in untreated patients with rheumatoid arthritis. *J. Transl. Med.* 13:2.
- Chen, A., S. Mumick, C. Zhang, J. Lamb, H. Dai, D. Weingarh, et al. 2005. Diet induction of monocyte chemoattractant protein-1 and its impact on obesity. *Obes. Res.* 13:1311–1320.
- Chusyd, D. E., D. Wang, D. M. Huffman, and T. R. Nagy. 2016. Relationships between rodent white adipose fat pads and human white adipose fat depots. *Front. Nutr.* 3:10.
- Cipolletta, C., K. E. Ryan, E. V. Hanna, and E. R. Trimble. 2005. Activation of peripheral blood CD14⁺ monocytes occurs in diabetes. *Diabetes* 54:2779–2786.
- Denou, E., K. Lomède, L. Garidou, C. Pomie, C. Chabo, T. C. Lau, et al. 2015. Defective NOD2 peptidoglycan sensing promotes diet-induced inflammation, dysbiosis, and insulin resistance. *EMBO Mol. Med.* 7:259–274.
- Desai, H. R., T. Sivasubramaniam, X. S. Revelo, S. A. Schroer, C. T. Luk, P. R. Rikkala, et al. 2017. Macrophage JAK2 deficiency protects against high-fat diet-induced inflammation. *Sci. Rep.* 7:7653.
- Dutta, P., and M. Nahrendorf. 2014. Regulation and consequences of monocytosis. *Immunol. Rev.* 262:167–178.
- Ford, E. S. 2002. Leukocyte count, erythrocyte sedimentation rate, and diabetes incidence in a national sample of US adults. *Am. J. Epidemiol.* 155:57–64.
- Geissmann, F., S. Jung, and D. R. Littman. 2003. Blood monocytes consist of two principal subsets with distinct migratory properties. *Immunity* 19:71–82.
- Gordon, S., and P. R. Taylor. 2005. Monocyte and macrophage heterogeneity. *Nat. Rev. Immunol.* 5:953–964.
- Gremese, E., A. Carletto, M. Padovan, F. Atzeni, B. Raffeiner, A. R. Giardina, et al. 2013. Obesity and reduction of the response rate to anti-tumor necrosis factor alpha in rheumatoid arthritis: an approach to a personalized medicine. *Arthritis Care Res. (Hoboken)* 65:94–100.
- Gurley, S. B., S. E. Clare, K. P. Snow, A. Hu, T. W. Meyer, and T. M. Coffman. 2006. Impact of genetic background on nephropathy in diabetic mice. *Am. J. Physiol. - Renal Physiol.* 290:F214–F222.
- Han, M. S., D. Y. Jung, C. Morel, S. A. Lakhani, J. K. Kim, R. A. Flavell, et al. 2013. JNK expression by macrophages promotes obesity-induced insulin resistance and inflammation. *Science* 339:218–222.
- Hivert, M. F., L. M. Sullivan, P. Shrader, C. S. Fox, D. M. Nathan, R. B. Sr D'Agostino, et al. 2010. The association of tumor necrosis factor alpha receptor 2 and tumor necrosis factor alpha with insulin resistance and the influence of adipose tissue biomarkers in humans. *Metabolism* 59:540–546.
- Hotamisligil, G. S., P. Arner, J. F. Caro, R. L. Atkinson, and B. M. Spiegelman. 1995. Increased adipose tissue expression of tumor necrosis factor-alpha in human obesity and insulin resistance. *J. Clin. Invest.* 95:2409–2415.
- Ito, A., T. Suganami, A. Yamauchi, M. Degawa-Yamauchi, M. Tanaka, R. Kouyama, et al. 2008. Role of CC chemokine receptor 2 in bone marrow cells in the recruitment of macrophages into obese adipose tissue. *J. Biol. Chem.* 283:35715–35723.
- Klaasen, R., C. A. Wijbrandts, D. M. Gerlag, and P. P. Tak. 2011. Body mass index and clinical response to infliximab in rheumatoid arthritis. *Arthritis Rheum.* 63:359–364.
- Koulmanda, M., M. Bhasin, Z. Awdeh, A. Qipo, Z. Fan, D. Hanidziar, et al. 2012. The Role of TNF- α in Mice with Type 1- and 2- Diabetes. *PLoS ONE* 7:e33254.
- Krinninger, P., R. Ensenaer, K. Ehlers, K. Rauh, J. Stoll, S. Krauss-Etschmann, et al. 2014. Peripheral monocytes of obese women display increased chemokine receptor expression and migration capacity. *J. Clin. Endocrinol. Metab.* 99:2500–2509.
- Kullo, I. J., D. D. Hensrud, and T. G. Allison. 2002. Comparison of numbers of circulating blood monocytes in men grouped by body mass index (<25, 25 to <30, > or =30). *Am. J. Cardiol.* 89:1441–1443.
- Loukov, D., S. Karampatos, M. R. Maly, and D. M. E. Bowdish. 2018. Monocyte activation is elevated in women with knee-osteoarthritis and associated with inflammation, BMI and pain. *Osteoarthritis and Cartilage* 26:255–263.
- Luche, E., V. Robert, V. Cuminetti, C. Pomié, Q. Sastourné-Arrey, A. Waget, et al. 2017. Corrupted adipose tissue endogenous myelopoiesis initiates diet-induced metabolic disease. *ELife* 6:e23194.
- Lumeng, C. N., J. L. Bodzin, and A. R. Saltiel. 2007a. Obesity induces a phenotypic switch in adipose tissue macrophage polarization. *J. Clin. Invest.* 117:175–184.
- Lumeng, C. N., S. M. Deyoung, J. L. Bodzin, and A. R. Saltiel. 2007b. Increased inflammatory properties of adipose tissue macrophages recruited during diet-induced obesity. *Diabetes* 56:16–23.
- McGeough, M. D., A. Wree, M. E. Inzaugarat, A. Haimovich, C. D. Johnson, C. A. Peña, et al. 2017. TNF regulates transcription of NLRP3 inflammasome components and inflammatory molecules in cryopyrinopathies. *J. Clin. Invest.* 127:4488–4497.
- McPhee, J. B., and J. D. Schertzer. 2015. Immunometabolism of obesity and diabetes: microbiota link compartmentalized immunity in the gut to metabolic tissue inflammation. *Clin. Sci. (Lond.)* 129:1083–1096.
- Meeuwssen, J. A. L., M. Wesseling, I. E. Hoefer, and S. C. A. de Jager. 2017. Prognostic value of circulating inflammatory cells in patients with stable and acute coronary artery disease. *Front. Cardiovasc. Med.* 4:44.

- Mehran, A. E., N. M. Templeman, G. S. Brigidi, G. E. Lim, K. Y. Chu, X. Hu, et al. 2012. Hyperinsulinemia drives diet-induced obesity independently of brain insulin production. *Cell Metab.* 16:723–737.
- Muller, M. J., M. Lagerpusch, J. Enderle, B. Schautz, M. Heller, and A. Bosy-Westphal. 2012. Beyond the body mass index: tracking body composition in the pathogenesis of obesity and the metabolic syndrome. *Obes. Rev.* 13(Suppl 2):6–13.
- Mysliwska, J., M. Smardzewski, N. Marek-Trzonkowska, M. Mysliwiec, and K. Raczynska. 2012. Expansion of CD14+CD16+ monocytes producing TNF- α in complication-free diabetes type 1 juvenile onset patients. *Cytokine* 60:309–317.
- Nagareddy, P. R., A. J. Murphy, R. A. Stirzaker, Y. Hu, S. Yu, R. G. Miller, et al. 2013. Hyperglycemia promotes myelopoiesis and impairs the resolution of atherosclerosis. *Cell Metab.* 17:695–708.
- Nagareddy, P. R., M. Kraakman, S. L. Masters, R. A. Stirzaker, D. J. Gorman, R. W. Grant, et al. 2014. Adipose tissue macrophages promote myelopoiesis and monocytoysis in obesity. *Cell Metab.* 19:821–835.
- Oh, D. Y., H. Morinaga, S. Talukdar, E. J. Bae, and J. M. Olefsky. 2012. Increased macrophage migration into adipose tissue in obese mice. *Diabetes* 61:346–354.
- Ohshita, K., K. Yamane, M. Hanafusa, H. Mori, K. Mito, M. Okubo, et al. 2004. Elevated white blood cell count in subjects with impaired glucose tolerance. *Diabetes Care* 27:491–496.
- Olefsky, J. M., and C. K. Glass. 2010. Macrophages, inflammation, and insulin resistance. *Annu. Rev. Physiol.* 72:219–246.
- Osborn, O., and J. M. Olefsky. 2012. The cellular and signaling networks linking the immune system and metabolism in disease. *Nat. Med.* 18:363–374.
- Poitou, C., E. Dalmat, M. Renovato, V. Benhamo, F. Hajdouch, M. Abdenour, et al. 2011. CD14dimCD16+ and CD14+CD16+ monocytes in obesity and during weight loss: relationships with fat mass and subclinical atherosclerosis. *Arterioscler. Thromb. Vasc. Biol.* 31:2322–2330.
- Puchta, A., A. Naidoo, C. P. Verschoor, D. Loukov, N. Thevaranjan, T. S. Mandur, et al. 2016. TNF drives monocyte dysfunction with age and results in impaired anti-pneumococcal immunity. *PLoS Pathog.* 12:e1005368.
- Rahman, M. S., A. J. Murphy, and K. J. Woollard. 2017. Effects of dyslipidaemia on monocyte production and function in cardiovascular disease. *Nat. Rev. Cardiol.* 14:387–400.
- Ren, X., W. Mou, C. Su, X. Chen, H. Zhang, B. Cao, et al. 2017. Increase in peripheral blood intermediate monocytes is associated with the development of recent-onset type 1 diabetes mellitus in children. *Int. J. Biol. Sci.* 13:209–218.
- Revelo, X. S., M. Ghazarian, M. H. Chng, H. Luck, J. H. Kim, K. Zeng, et al. 2016. Nucleic acid-targeting pathways promote inflammation in obesity-related insulin resistance. *Cell Rep.* 16:717–730.
- Rogacev, K. S., B. Cremers, A. M. Zawada, S. Seiler, N. Binder, P. Ege, et al. 2012. CD14++CD16+ monocytes independently predict cardiovascular events: a cohort study of 951 patients referred for elective coronary angiography. *J. Am. Coll. Cardiol.* 60:1512–1520.
- Schmidt, M. I., B. B. Duncan, A. R. Sharrett, G. Lindberg, P. J. Savage, S. Offenbacher, et al. 1999. Markers of inflammation and prediction of diabetes mellitus in adults (Atherosclerosis Risk in Communities study): a cohort study. *Lancet* 353:1649–1652.
- Schneider, C. A., W. S. Rasband, and K. W. Eliceiri. 2012. NIH Image to ImageJ: 25 years of image analysis. *Nat. Methods* 9:671.
- Seidler, S., H. W. Zimmermann, M. Bartneck, C. Trautwein, and F. Tacke. 2010. Age-dependent alterations of monocyte subsets and monocyte-related chemokine pathways in healthy adults. *BMC Immunol.* 11:30.
- Serbina, N. V., and E. G. Pamer. 2006. Monocyte emigration from bone marrow during bacterial infection requires signals mediated by chemokine receptor CCR2. *Nat. Immunol.* 7:311–317.
- Short, J. D., S. Tavakoli, H. N. Nguyen, A. Carrera, C. Farnen, L. A. Cox, et al. 2017. Dyslipidemic diet-induced monocyte “priming” and dysfunction in non-human primates is triggered by elevated plasma cholesterol and accompanied by altered histone acetylation. *Front Immunol.* 8:958.
- Solomon, D. H., E. Massarotti, R. Garg, J. Liu, C. Canning, and S. Schneeweiss. 2011. Association between disease-modifying antirheumatic drugs and diabetes risk in patients with rheumatoid arthritis and psoriasis. *JAMA* 305:2525–2531.
- Terasawa, T., Y. Aso, K. Omori, M. Fukushima, A. Momobayashi, and T. Inukai. 2015. Bezafibrate, a peroxisome proliferator-activated receptor α agonist, decreases circulating CD14(+)CD16(+) monocytes in patients with type 2 diabetes. *Transl. Res.* 165:336–345.
- Tong, P. C., K.-F. Lee, W.-Y. So, M. H. Ng, W.-B. Chan, M. K. Lo, et al. 2004. White blood cell count is associated with macro- and microvascular complications in Chinese patients with type 2 diabetes. *Diabetes Care* 27:216–222.
- Tsai, S., X. Clemente-Casares, A. C. Zhou, H. Lei, J. J. Ahn, Y. T. Chan, et al. 2018. Insulin receptor-mediated stimulation boosts T cell immunity during inflammation and infection. *Cell Metab.* pii: S1550-4131(18)30504-7. [Epub ahead of print]. <https://doi.org/10.1016/j.cmet.2018.08.003>.
- Tsou, C. L., W. Peters, Y. Si, S. Slaymaker, A. M. Aslanian, S. P. Weisberg, et al. 2007. Critical roles for CCR2 and MCP-3 in monocyte mobilization from bone marrow and recruitment to inflammatory sites. *J. Clin. Invest.* 117:902–909.

- Uysal, K. T., S. M. Wiesbrock, M. W. Marino, and G. S. Hotamisligil. 1997. Protection from obesity-induced insulin resistance in mice lacking TNF- α function. *Nature* 389:610–614.
- Ventre, J., T. Doebber, M. Wu, K. MacNaul, K. Stevens, M. Pasparakis, et al. 1997. Targeted disruption of the tumor necrosis factor- α Gene: metabolic consequences in obese and nonobese mice. *Diabetes* 46:1526.
- Wagenknecht, L. E., C. D. Langefeld, A. L. Scherzinger, J. M. Norris, S. M. Haffner, M. F. Saad, et al. 2003. Insulin sensitivity, insulin secretion, and abdominal fat: the Insulin Resistance Atherosclerosis Study (IRAS) Family Study. *Diabetes* 52:2490–2496.
- Weisberg, S. P., D. McCann, M. Desai, M. Rosenbaum, R. L. Leibel, and A. W. Jr Ferrante. 2003. Obesity is associated with macrophage accumulation in adipose tissue. *J. Clin. Invest.* 112:1796–1808.
- Weisberg, S. P., D. Hunter, R. Huber, J. Lemieux, S. Slaymaker, K. Vaddi, et al. 2006. CCR2 modulates inflammatory and metabolic effects of high-fat feeding. *J. Clin. Invest.* 116:115–124.
- Wouters, K., K. Gaens, M. Bijnen, K. Verboven, J. Jocken, S. Wetzels, et al. 2017. Circulating classical monocytes are associated with CD11c⁺ macrophages in human visceral adipose tissue. *Sci. Rep.* 7:42665.
- Xiu, F., M. Stanojic, L. Diao, and M. G. Jeschke. 2014. Stress hyperglycemia, insulin treatment, and innate immune cells. *Int. J. Endocrinol.* 2014:486403.
- Xu, H., G. T. Barnes, Q. Yang, G. Tan, D. Yang, C. J. Chou, et al. 2003. Chronic inflammation in fat plays a crucial role in the development of obesity-related insulin resistance. *J. Clin. Invest.* 112:1821–1830.
- Yang, J., L. Zhang, C. Yu, X.-F. Yang, and H. Wang. 2014. Monocyte and macrophage differentiation: circulation inflammatory monocyte as biomarker for inflammatory diseases. *Biomarker Res.* 2:1–1.
- Yoshioka, M., T. Kayo, T. Ikeda, and A. Koizumi. 1997. A Novel Locus, Mody4 Distal to D7Mit189 on Chromosome 7 Determines Early-Onset NIDDM in Nonobese C57BL/6 (Akita) Mutant Mice. *Diabetes* 46:887–894.
- Zganiacz, A., M. Santosuosso, J. Wang, T. Yang, L. Chen, M. Anzulovic, et al. 2004. TNF- α is a critical negative regulator of type 1 immune activation during intracellular bacterial infection. *J. Clin. Invest.* 113:401–413.
- Ziegler-Heitbrock, L. 2015. Blood monocytes and their subsets: established features and open questions. *Front Immunol.* 6:423.

Chapter 5. Peripheral immunophenotype and obesity-associated chronic inflammation in female mice

In this chapter, we aimed to assess effects of obesity-associated low-grade chronic inflammation on peripheral blood immune cell populations, focussing on monocytes. We used a model of high fat diet feeding in young female mice to examine longitudinal effects of diet-induced obesity on peripheral blood immunophenotype and monocyte phenotype and activation (section 5.1). We subsequently examined peripheral immune cells in pregnancy and lactation, and effects of maternal obesity and excess gestational weight gain (section 5.2). These studies also investigated if modulation of inflammation via TNF would ameliorate effects of diet-induced obesity on peripheral immunophenotype.

5.1 Peripheral immunophenotype and diet-induced obesity in non-pregnant female mice

5.1.1 Introduction

Obesity-associated inflammation has primarily been studied by quantifying cytokines, including TNF, in the periphery or within metabolic tissues such as adipose, wherein there is significant accumulation of pro-inflammatory macrophages^{50, 51, 58, 512}. As described previously, the majority of adipose tissue macrophages are derived from precursor Ly6C^{high} monocytes in the blood, via CCR2/CCL2-mediated chemotaxis^{51, 55, 57}, though there is some local proliferation of established tissue macrophage populations^{52, 512}. Accordingly, studies in mice employing genetic global or hematopoietic ablation of CCR2 or CCL2^{56, 57, 513}, treatment with a CCR2 antagonist^{54, 514}, or genetic ablation of MIF (macrophage migration inhibitory factor)^{515, 516}, which reduce accumulation of monocyte-derived macrophages in adipose tissue, have been reported to reduce adiposity, tissue inflammation, and metabolic dysfunction. Monocytosis, an increase in circulating monocytes, occurs in obesity in humans^{517, 518, 519, 520, 521, 522}. Male mice in models of diet-induced obesity have an increased prevalence of circulating Ly6C^{high} monocytes (similar to human classical monocytes) within 6 weeks⁵²³, and this is also apparent after 12 weeks⁵²⁴, 18 weeks (Chapter 4), 20 weeks⁵²⁵, and 24 weeks (Chapter 4). We also found increases in Ly6C^{low} and Ly6C⁻ monocytes (similar to human non-classical monocytes) in high fat (HF)-fed male mice and showed that Ly6C^{high} monocytes had increased expression of IL-6 in response to LPS stimulation. Increased surface expression of chemotactic antigens and enhanced cytokine responses to bacterial LPS or viral ssRNA

stimulation have also been reported in classical and non-classical monocytes from obese humans compared to lean controls⁵¹⁸.

Multiple studies in male rodents have shown that genetic ablation of TNF^{526, 527, 528}, and antibody-mediated^{529, 530, 531, 532} or siRNA-mediated⁵³³ blockade of TNF, can improve glucose homeostasis and insulin resistance in male models of obesity, whereas administration of TNF has the opposite effect^{534, 535, 536}. Genetic knockout of the TNF receptors TNFR1 and/or TNFR2 has also been found to mediate insulin sensitivity in models of diet-induced obesity^{537, 538, 539}. Our data from Chapter 4 showed that in male mice peripheral blood Ly6C^{high} monocytes correlate with insulin resistance, and that modulation of obesity-associated inflammation via TNF reduces circulating Ly6C^{high} monocytes. There may be sex differences in the role of monocytes in diet-induced obesity, as there is sexual dimorphism in innate immune signalling pathways and their epigenetic regulation^{540, 541, 542}.

As described in Chapter 3, biological sex is an important factor to consider in any aspect of physiology. Despite epidemiological data showing that the global incidence of obesity is similar between both sexes, if not greater in females³¹, and evidence that biological sex has an impact on fat deposition, metabolism, and energy balance^{543, 544, 545}, most preclinical studies in rodents that use a diet-induced obesity model have evaluated the adverse effects of high fat diet consumption in males^{546, 547}. C57BL/6J male mice are commonly used for these studies, likely in part because C57BL/6J mice are considered to be highly susceptible to effects of high fat diet feeding, and males generally show more extreme phenotypes of adiposity, metabolic dysfunction, and inflammation than female

mice^{546, 548, 549}. Severity of obesity, inflammation, and metabolic dysfunction, also differs according to the length of diet allocation^{550, 551, 552, 553, 554}.

We performed longitudinal studies in female mice to assess changes to peripheral immune cell population dynamics in response to diet-induced obesity, and the effects of immunomodulation by TNF. Based on our previous findings in male mice (Chapter 4), we hypothesized that feeding female mice a high fat diet would result in peripheral monocytosis, particularly of Ly6C^{high} monocytes, and that these monocytes would be more pro-inflammatory compared to monocytes from blood of chow-fed mice. We predicted that TNF^{-/-} female mice fed a high fat diet would be partially protected from diet-induced obesity and changes to overall immunophenotype and Ly6C^{high} monocytes.

5.1.2 Results

High fat diet induces obesity in female mice

We placed young female wildtype C57BL/6J mice on either a standard chow diet or high fat diet (60% kcal from fat) for up to 30 weeks. On a weekly basis we monitored body weight (Figure 5.1.1A), and calculated energy consumption from food intake (Figure 5.1.1B). HF-fed mice began to consume less kilocalories than chow-fed mice after 12 weeks of diet (Figure 5.1.1B), despite continued increases in body weight and adiposity (Figure 5.1.1A,C). Within 6 weeks we observed that HF-fed mice had ~20% greater adiposity than chow-fed mice (Figure 5.1.1C; Chow: 15.0 ± 3.2%; HF: 35.9 ± 8.6%). HF-fed mice compared to chow-fed mice had an increase in liver weight after 18 weeks (Figure 5.1.1D), as well as increased weights of gonadal (Figure 5.1.1E) and mesenteric fat depots (Figure 5.1.1F), and adipocyte size (Figure 5.1.1G), within 6 weeks.

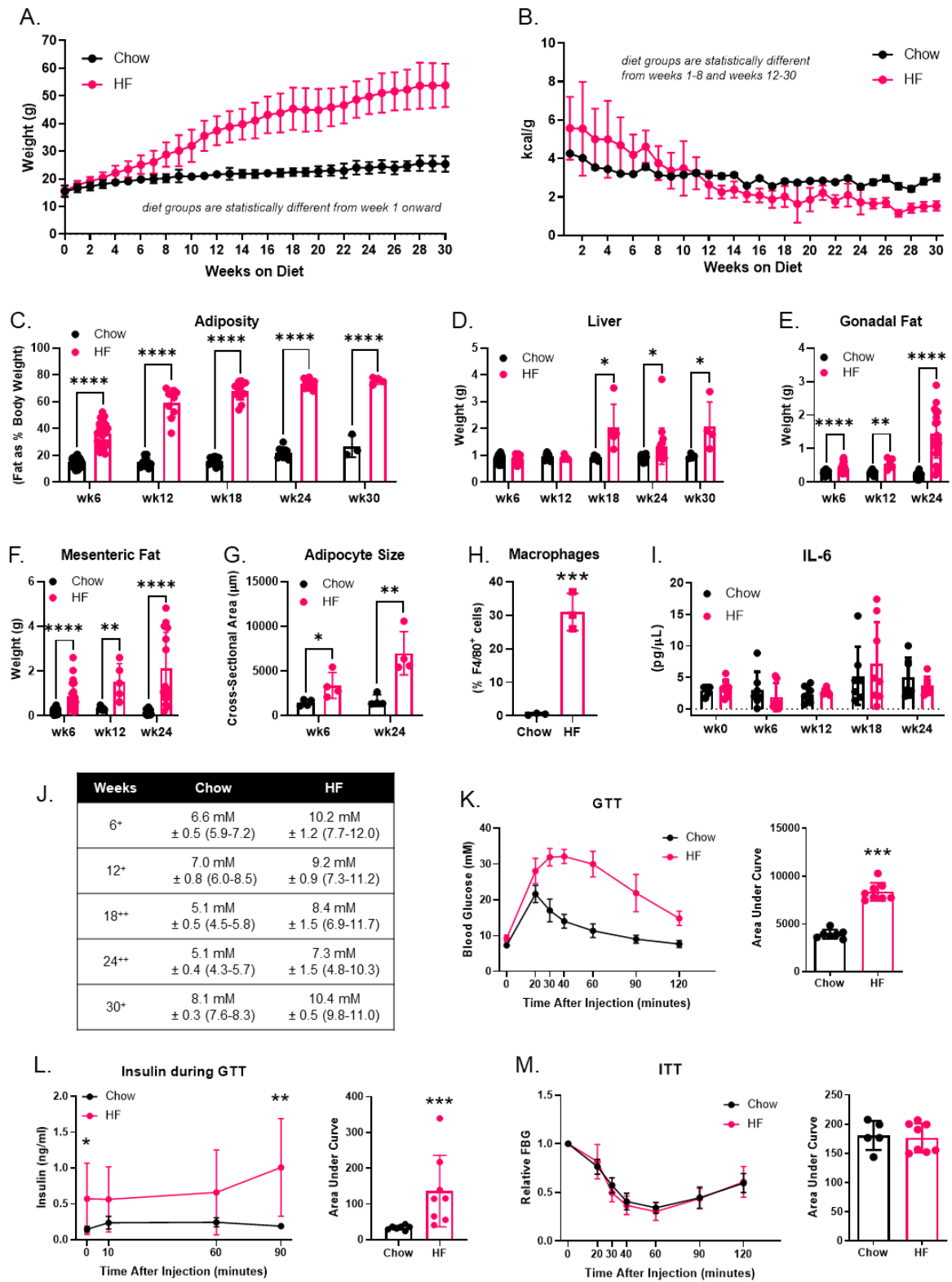


Figure 5.1.1. Model phenotype - female mice fed standard chow or HF diet.

Mice were placed on standard chow diet (Chow) or 60% high fat (HF) diet. Physiological, inflammation-associated and metabolic features were assessed between 6 and 30 weeks diet allocation. Body weight (A) and energy consumption from food (B) were assessed weekly. (C) adiposity assessed after 6, 12, 18, 24, and 30 weeks diet allocation by Echo-MRI. Weights of liver (D), gonadal fat (E), and mesenteric fat (F). (G) cross-sectional area of adipocytes in gonadal fat. (H) macrophages (F4/80⁺ cells) in gonadal adipose tissue after 24 weeks diet allocation. (I) IL-6 assessed by ELISA from serum collected pre-diet through to 24 weeks diet allocation. Metabolic phenotype: (J) fasting blood glucose; + = 6 hour fast; ++ = 12 hour fast; $p < 0.001$ at each assessed time point between diet groups. (K) glucose tolerance test. (L) glucose stimulated insulin secretion test. (M) insulin tolerance test. Data in A-B and K-M are shown as a dot at the mean with error bars at \pm standard deviation. Data in C-I and area under the curve in K-M are shown with box height at the mean with error bars at \pm standard deviation, with each data point indicating an individual mouse. Data in A-F and J were pooled from 1-4 independent experiments of $n=3-8$ mice per diet. Data in G and H are from a subset of mice from one independent cohort. Data in I and K-M are from one independent cohort with Chow $n=7$ and HF $n=8$. Statistical significance was assessed by two-tailed Student's *t* test between diet groups at each time point. * $p < 0.05$, ** $p < 0.01$, *** $p < 0.001$, **** $p < 0.0001$.

HF diet feeding led to increased accumulation of F4/80⁺ macrophages in adipose tissue (Figure 5.1.1H), compared to chow-fed mice. We attempted to measure TNF and IL-6 cytokine levels longitudinally in serum as an indication of soluble inflammation. We were only able to detect TNF in 10/78 assessed samples (data not shown). Although we detected IL-6 in 75/78 samples (Figure 5.1.1I), there were no statistically significant differences between diet groups.

While not a primary aspect of our study, we also assessed metabolic parameters to provide context for our data. We observed that by 6 weeks HF-fed mice compared to chow-fed mice had significantly increased fasting blood glucose levels, which persisted through to 30 weeks of HF diet feeding (Figure 5.1.1J). Between 14 and 18 weeks diet allocation, we examined glucose and insulin management by glucose tolerance tests (Figure 5.1.1K-L) and insulin tolerance tests (Figure 5.1.1M). Female mice with HF diet-induced obesity had a slower rate of glucose clearance compared to chow-fed mice, despite having significantly greater insulin secretion, suggesting that HF-fed mice were glucose intolerant and hyperinsulinemic. Insulin tolerance was similar between diet

groups. In summary, feeding female mice a HF diet induced changes to body composition within 6 weeks that were characteristic of obesity, including increases in adiposity, adipocyte hypertrophy, and hyperglycemia, in comparison to chow-fed mice, and these changes continued through to 30 weeks of diet allocation.

Peripheral leukocyte populations

We assessed the prevalence of peripheral leukocytes in whole blood after 3, 6, 12, 18, 24, and 30 weeks diet allocation (Figure 5.1.2). Although neutrophil prevalence (as a proportion of total leukocytes) was similar between diet groups (Figure 5.1.2A), the prevalence of total monocytes and the prevalence of Ly6C^{high} monocytes were lower in HF-fed mice compared to chow-fed mice after 3 weeks diet allocation (Figure 5.1.2B-C and F). Monocyte prevalence was similar between HF-fed and chow-fed mice after 6 weeks, and then increased in HF-fed mice from 12 weeks onward. The prevalence of Ly6C^{low} monocytes was similar between diet groups for the first 12 weeks of diet allocation (Figure 5.1.2D), but over time, the increase in Ly6C^{high} monocytes meant that there was a proportional decrease in Ly6C^{low} monocytes (Figure 5.1.2F). The prevalence of Ly6C⁻ monocytes also increased in HF-fed mice compared to chow-fed mice, from 6 through 30 weeks diet allocation (Figure 5.1.2E). B cell (Figure 5.1.2G), NK cell (Figure 5.1.2H), and T cell (Figure 5.1.2I-K) prevalence, as a proportion of total leukocytes, were different at discrete time points. There was a general trend toward a decrease in T cells in HF-fed mice compared to chow-fed mice, though the prevalence of CD4⁺ T cells (Figure 5.1.2J,L) and CD8⁺ T cells were not consistently different (Figure 5.1.2K).

While these data are informative about the dynamics of monocytes in relation to other immune cell populations, the proportional increase in monocyte populations that we

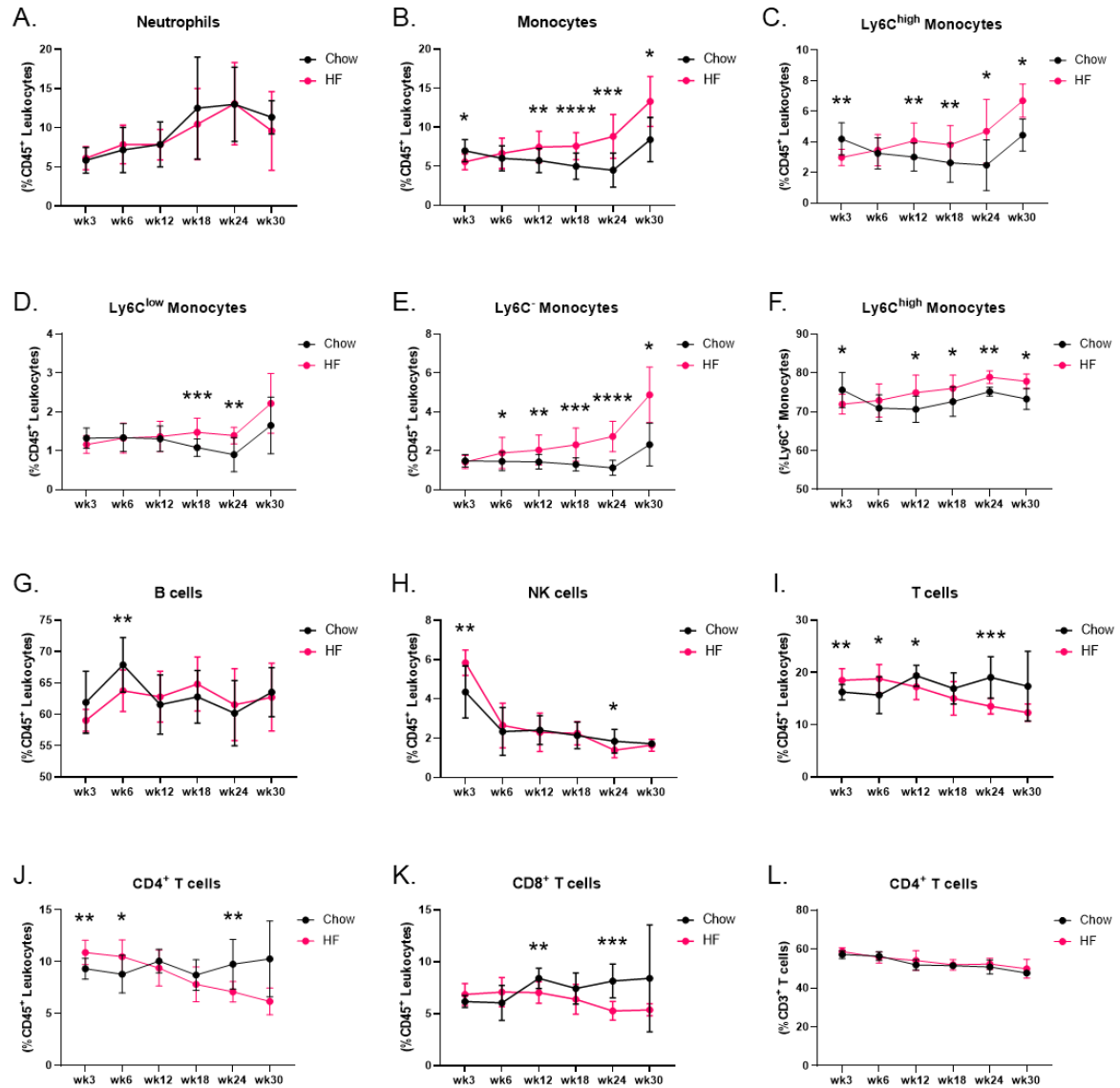


Figure 5.1.2. Peripheral blood immune cell prevalence in mice fed chow or HF diet.

Flow cytometry analysis of peripheral blood leukocytes in wildtype mice on standard chow (Chow) or 60% high fat (HF) diet from 6 weeks (wk6) through 30 weeks (wk30) diet allocation. Prevalence (as a proportion of CD45⁺ leukocytes) of: (A) neutrophils, (B) total monocytes, (C) Ly6C^{high} monocytes, (D) Ly6C^{low} monocytes, (E) Ly6C⁺ monocytes. (F) Ly6C^{high} monocytes as a proportion of Ly6C⁺ monocytes. Prevalence (as a proportion of CD45⁺ leukocytes) of: (G) B cells, (H) NK cells, (I) T cells, (J) CD4⁺ T cells, (K) CD8⁺ T cells. (L) CD4⁺ T cells as a proportion of total CD3⁺ T cells. Data are presented with a dot at the mean with error bars of \pm standard deviation. Data are pooled from 1-3 independent experiments with a total of $n=3-8$ mice per diet. Statistical significance was assessed by two-tailed Student's *t* test between diet groups at each time point. * $p<0.05$, ** $p<0.01$, *** $p<0.001$, **** $p<0.0001$.

observed in HF-fed mice could have been due to a decrease in cell numbers in another leukocyte population, so we next considered absolute cell counts (Figure 5.1.3).

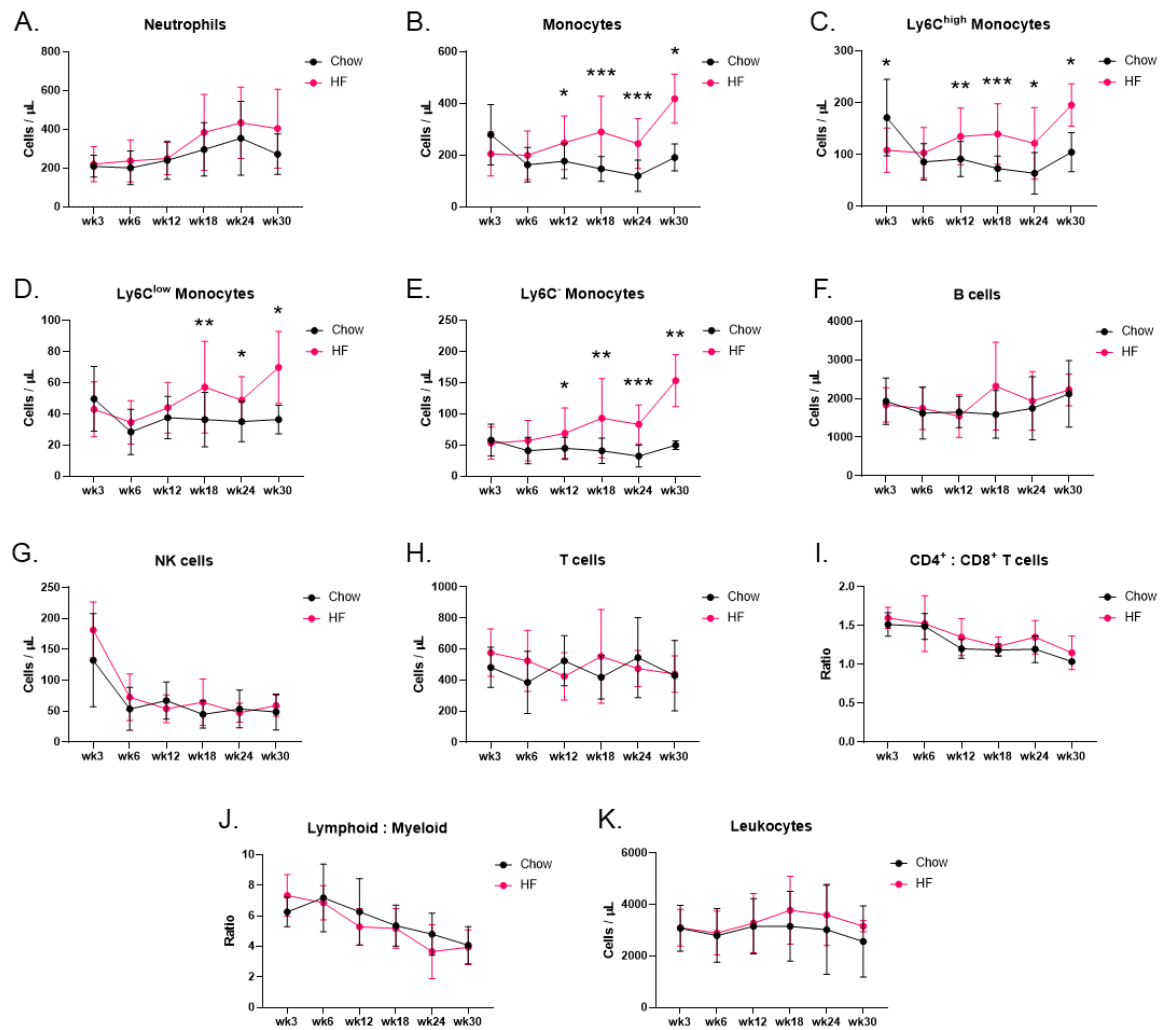


Figure 5.1.3. Peripheral blood absolute cell counts in mice fed chow or HF diet.

Flow cytometry analysis of peripheral blood leukocytes in wildtype mice on standard chow (Chow) or 60% high fat (HF) diet from 6 weeks (wk6) through 30 weeks (wk30) diet allocation. Absolute cell counts of: (A) neutrophils, (B) total monocytes, (C) Ly6C^{high} monocytes, (D) Ly6C^{low} monocytes, (E) Ly6C⁻ monocytes, (F) B cells, (G) NK cells, (H) T cells. (I) ratio of CD4⁺ to CD8⁺ T cells. (J) ratio of lymphoid to myeloid cells. (K) total leukocytes. Data are presented with a dot at the mean with error bars of \pm standard deviation. Data are pooled from 1-4 independent experiments with a total of $n=3-8$ mice per diet group. Statistical significance was assessed by two-tailed Student's t test between diet groups at each time point. * $p < 0.05$, ** $p < 0.01$, *** $p < 0.001$.

There were no statistically significant differences in cell counts of neutrophils (Figure 5.1.3A), B cells (Figure 5.1.3F), NK cells (Figure 5.1.3G), T cells (Figure 5.1.3H), or the ratio of CD4⁺ and CD8⁺ T cells (Figure 5.1.3I) between diet groups, and the ratio of lymphocytes (B cells, T cells, and NK cells) to myeloid cells (monocyte and neutrophils) (Figure 5.1.3J), and total leukocyte counts (Figure 5.1.3K), remained similar between diet groups. However, total monocytes and monocyte subset cell counts in HF-fed mice from 12 weeks (total monocytes, Ly6C^{high} and Ly6C^{low} monocytes) or 18 weeks (Ly6C^{low}) diet allocation onward (Figure 5.1.3B-E) were higher compared to chow-fed mice, similar to the increasing trend in monocyte prevalence (Figure 5.1.2C-F). Therefore, HF diet feeding in female mice altered immunophenotype dynamics, with a significant longitudinal increase in peripheral blood monocyte cell counts, in particular of Ly6C^{high} monocytes, in comparison to immunophenotype of female mice fed a standard chow diet.

Blood monocyte phenotype, function, and inflammatory response

We also assessed monocyte surface phenotype (Table 5.1.1; Appendix I). We measured expression of Ly6C, CCR2, F4/80, CX₃CR₁, and CD11b. We observed that Ly6C^{high} monocytes generally had higher expression of Ly6C, and decreased expression of F4/80 and CX₃CR₁, in HF-fed mice compared to chow-fed mice, and expression of CD11b was higher on Ly6C^{high} monocytes after 3 and 6 weeks diet allocation in HF-fed mice. We observed in HF-fed mice compared to chow-fed mice that Ly6C^{low} monocytes had increased expression of Ly6C after 3 and 6 weeks, though this decreased by 18 and 24 weeks. Ly6C^{low} expression of CCR2, F4/80, and CX₃CR₁ was initially decreased after 3 weeks, but this was not consistently observed thereafter. Ly6C^{low} monocytes had similar surface expression as Ly6C^{low} monocytes, but had increased CX₃CR₁ expression after 18

and 24 weeks. Our observations indicate that expression of surface markers in the Ly6C^{high} to Ly6C^{low} transition was altered in HF-fed mice compared to chow-fed mice.

Table 5.1.1. Peripheral blood monocyte surface phenotype in WT mice fed HF vs chow diet.

Surface Marker	Population	Weeks of 60% High Fat Diet Allocation				
		3	6	12	18	24
Ly6C	Ly6C ^{high}	↑ **** <0.0001	↑ **** <0.0001	↑ ** p=0.0041	↑ **** <0.0001	↑ **** <0.0001
	Ly6C ^{low}	↑ **** p=0.0006	↑ **** p=0.0021	ns	↓ * p=0.0424	↓ * p=0.0218
CCR2	Ly6C ^{high}	ns	ns	ns	ns	ns
	Ly6C ^{low}	↓ * p=0.0452	ns	ns	↓ * p=0.0104	ns
	Ly6C ^{low}	↓ * p=0.0383	ns	ns	↓ *** p=0.0067	ns
F4/80	Ly6C ^{high}	↓ ** p=0.0064	↓ **** <0.0001	↓ * p=0.0156	↓ ** p=0.0063	ns
	Ly6C ^{low}	↓ ** p=0.0093	↓ **** <0.0001	ns	ns	ns
	Ly6C ^{low}	ns	↓ ** p=0.0048	ns	ns	ns
CX ₃ CR ₁	Ly6C ^{high}	↓ * p=0.0248	↓ * p=0.0303	↓ **** p=0.0003	↓ **** p<0.0001	↓ ** p=0.0018
	Ly6C ^{low}	↓ ** p=0.0020	ns	ns	ns	ns
	Ly6C ^{low}	↓ * p=0.0160	ns	ns	↑ * p=0.0439	↑ ** p=0.0026
CD11b	Ly6C ^{high}	↑ * p=0.0123	↑ ** p=0.0035	ns	↓ ** p=0.0087	ns
	Ly6C ^{low}	ns	ns	ns	ns	ns
	Ly6C ^{low}	ns	ns	ns	ns	ns

(e.g. Ly6C^{high} monocytes from HF-fed mice compared to chow-fed mice consistently have higher Ly6C expression) Geometric mean expression of each marker was combined from 2-4 independent experiments of n=3-8 mice per group by normalizing the data from each mouse to the mean of the chow diet mouse group in each independent experiment. This approach was taken to account for variation in cytometer settings between experiments. ns – not significant.

Ly6C^{high} monocytes migrate to obese adipose tissue by CCR2/CCL2-mediated chemotaxis^{56, 57}. As we detected increased accumulation of F4/80⁺ macrophages within adipose tissue of the HF-fed female mice (Figure 5.1.1H), we expected that HF-fed mouse Ly6C^{high} monocytes would exhibit increased expression of CCR2, but there was similar surface expression of CCR2 on Ly6C^{high} monocytes from HF-fed and chow-fed mice. To ensure that Ly6C^{high} monocytes from HF mice were responsive to CCL2, we injected chow and HF-fed mice i.p. with CCL2 or saline, and assessed changes in peripheral monocyte populations four hours later (Figure 5.1.4)³³⁶.

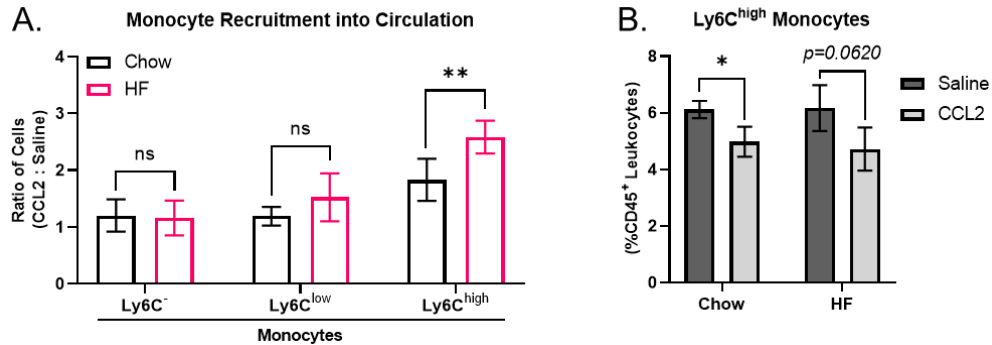


Figure 5.1.4. Response of peripheral monocyte populations to chemotactic ligand CCL2.

Mice fed with standard chow diet or 60% high fat diet were injected i.p. with CCL2 or saline, and 4 hours later blood (A) and/or femur bone marrow (B) were collected for assessment by flow cytometry. Data in A are shown as fold differences in immune cell numbers between mice injected with CCL2 and the mean of mice injected with saline for both of the diet groups. Data are shown with box height at the mean with error bars indicating \pm standard deviation. Data are from one independent experiment, with CCL2 $n=6$ and saline $n=4$, for both diet groups in blood. Bone marrow was collected from $n=3-4$ mice per treatment for both diet groups. Statistical significance was assessed by two-tailed Student's t test between diet groups at each time point. * $p<0.05$, ** $p<0.01$.

We observed that within 6 weeks diet allocation there was a significantly higher fold difference in circulating Ly6C^{high} monocytes between CCL2 and saline-treated HF-fed mice (2.58 ± 0.29), compared to the fold difference in CCL2 and saline-treated chow-fed mice (1.83 ± 0.37) (Figure 5.1.4A). The fold differences of Ly6C⁻ monocytes were similar between diet groups, as expected, given that they do not use CCR2/CCL2 for bone marrow egress or migration³¹², and the fold differences of Ly6C^{low} monocytes were also similar. When we examined bone marrow, we observed a trend toward a decrease in the prevalence of Ly6C^{high} monocytes chow-fed and HF-fed mice treated with CCL2 compared to saline (Figure 5.1.4B), suggesting that there is egress of Ly6C^{high} monocytes from bone marrow into circulation. This experiment showed that the Ly6C^{high} monocytes from HF-fed mice, despite similar surface expression of CCR2 as Ly6C^{high} monocytes from chow-fed mice, are more responsive to CCL2 in the periphery. We next assessed intracellular production of TNF and IL-6 in Ly6C^{high} monocytes (Figure 5.1.5).

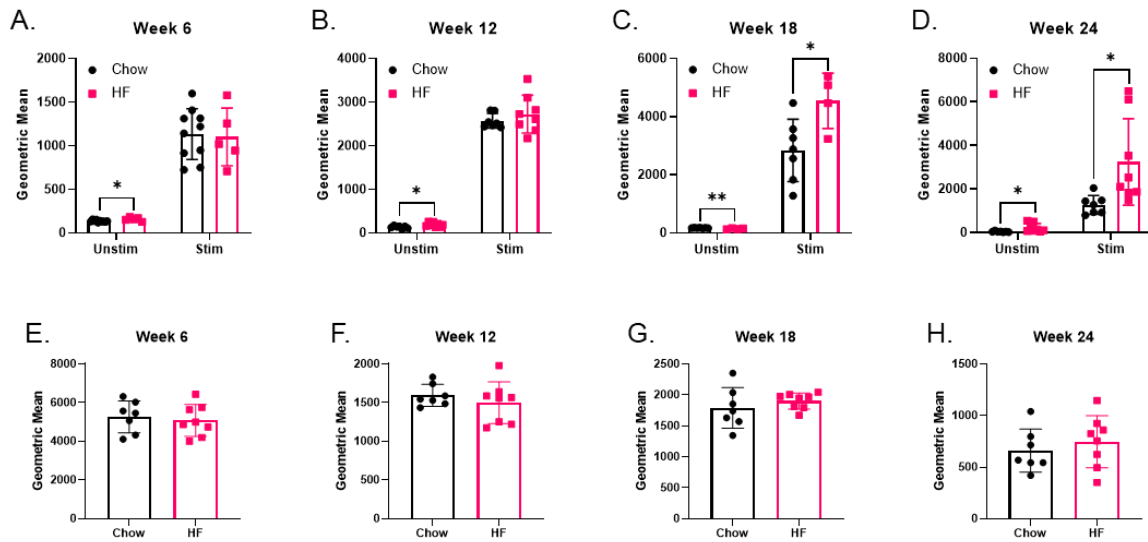


Figure 5.1.5. Ly6C^{high} monocyte production of TNF and IL-6 in mice fed chow or HF diet. Flow cytometry analysis of Ly6C^{high} monocyte production of TNF and IL-6 in response to whole blood stimulation with LPS in mice fed with standard chow diet (Chow) or 60% high fat diet (HF). Production of TNF after: (A) 6 weeks, (B) 12 weeks, (C) 18 weeks, (D) 24 weeks in unstimulated (Unstim) and stimulated (Stim) whole blood. Production of IL-6 after stimulation: (E) 6 weeks, (F) 12 weeks, (G) 18 weeks, (H) 24 weeks. Data are shown with box height at the mean with error bars at \pm standard deviation. Each data point indicates an individual mouse. Data in A-D are representative of 1-4 independent experiments of n=4-8 mice per group, and data in E-H are each from one independent experiment of Chow n=7 and HF n=8. Statistical significance was assessed by two-tailed Student's t test between diet groups at each time point. * $p < 0.05$, ** $p < 0.01$.

We observed slightly higher levels of TNF production in unstimulated blood Ly6C^{high} monocytes in HF-fed mice after 6, 12, 18, and 24 weeks diet allocation, though response to LPS stimulation was only significantly different between diet groups after 18 and 24 weeks (Figure 5.1.5A-D). There were no significant differences in IL-6 production between diet groups (Figure 5.1.5E-H).

Therefore, HF-fed female mice, in comparison to chow-fed mice, had a higher prevalence of circulating Ly6C^{high} monocytes with an altered surface phenotype, which were more responsive to CCL2, and had higher LPS-stimulated production of the pro-inflammatory cytokine TNF.

Bone marrow monocyte and progenitor populations

Acute and chronic inflammation elicit myelopoiesis²⁷⁶. We predicted that the increased numbers of circulating monocytes were due to enhanced production of monocytes and progenitor populations in bone marrow, and we assessed those populations by flow cytometry (Figure 5.1.6).

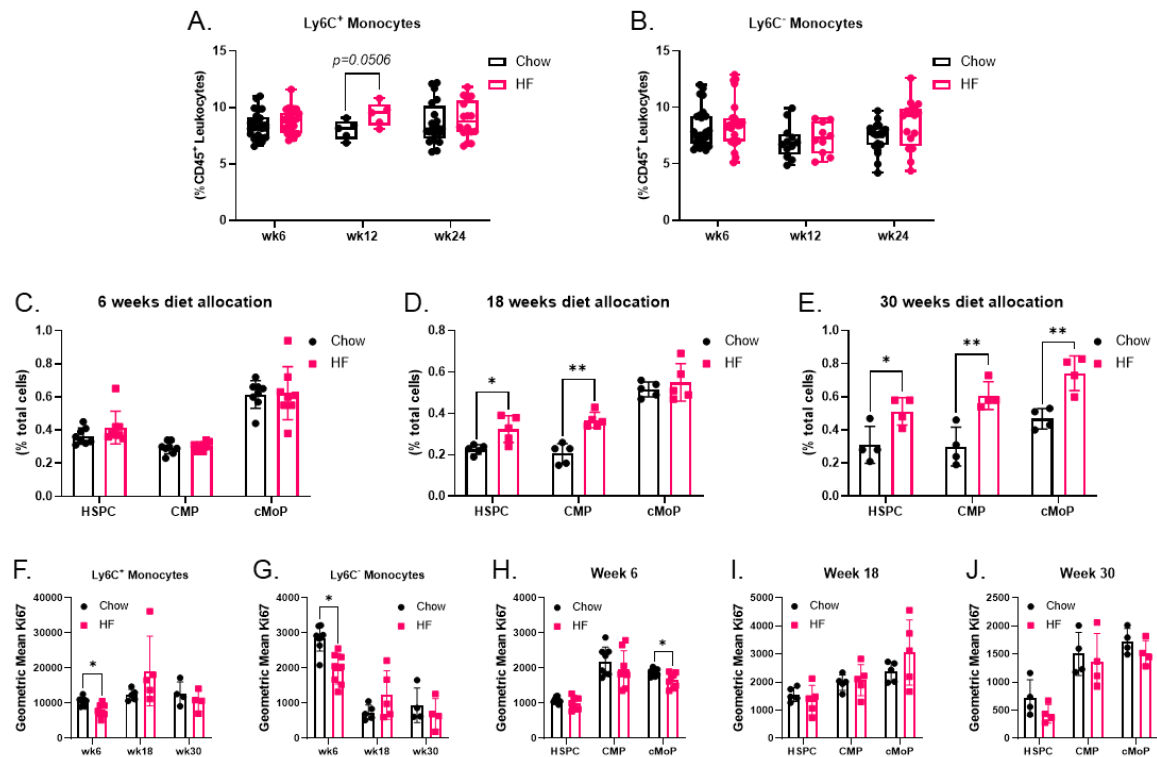


Figure 5.1.6. Bone marrow monocytes and precursors in mice fed chow or HF diet.

Flow cytometry analysis of femur bone marrow from mice fed with standard chow diet (Chow) or 60% high fat diet (HF) for 6-30 weeks. Prevalence (as a proportion of total leukocytes) of: (A) Ly6C⁺ monocytes, (B) Ly6C⁻ monocytes. Prevalence (as a proportion of total cells) of hematopoietic stem cell precursor (HSPC), common myeloid progenitor (CMP) and common monocyte progenitor (cMoP) cells after: (C) 6 weeks, (D) 18 weeks, or (E) 30 weeks diet allocation. Geometric mean expression of proliferation marker Ki67: (F) Ly6C⁺ monocytes, (G) Ly6C⁻ monocytes, and HSPC, CMP, and cMoP cells after: (H) 6 weeks, (I) 18 weeks, and (J) 30 weeks diet allocation. Data in A-B are shown as box plots, minimum to maximum, with the center line at the median, and data in C-J are shown with box height at the mean with error bars indicating \pm standard deviation. Each data point indicates an individual mouse. Data in A-B are pooled from 1-3 independent experiments of $n=3-8$, and data in C-I are each from one independent experiment of $n=4-8$ per diet group. Statistical significance was assessed by two-tailed Student's t test between diet groups at each time point. * $p < 0.05$, ** $p < 0.01$.

We did not observe any changes to Ly6C⁺ or Ly6C⁻ monocyte prevalence in bone marrow after 6, 12, or 24 weeks of high fat diet feeding (Figure 5.1.6A-B). Hematopoietic stem and multipotential progenitor cells (HSPCs) give rise to a common myeloid progenitor (CMP), which becomes a common monocyte progenitor (cMoP) before differentiation into a monocyte^{270, 271, 272}. HF-fed mice compared to chow-fed mice did not have an increase in HSPCs, CMPs, or cMoPs after 6 weeks of diet allocation, but HSPC and CMP populations were increased by 18 weeks, and cMoP populations were increased by 30 weeks (Figure 5.1.6C-E). We also measured expression of Ki67, which stains actively proliferating cells (Figure 5.1.6F-J). There was a transient decrease in Ki67 expression (implying a reduction in proliferation) in cMoP, Ly6C⁺, and Ly6C⁻ monocyte populations after 6 weeks in HF-fed mice compared to chow-fed mice, but this was not observed at later time points.

We measured surface expression of Ly6C, CCR2, F4/80, CX₃CR₁, and CD11b on bone marrow monocytes (Table 5.1.2; Appendix I). Although there were some similarities between diet groups with monocytes in peripheral blood (Table 5.1.1), Ly6C expression was only found to be higher on Ly6C⁺ monocytes in the bone marrow of HF-fed mice after 12 weeks, whereas its expression was increased on blood Ly6C^{high} monocytes from 3 weeks diet allocation. Bone marrow Ly6C⁺ monocytes had lower expression of CX₃CR₁, as in peripheral blood, while Ly6C⁻ monocytes had lower expression of CCR2. With an extended period of HF diet (i.e. by 24 weeks) there was a decrease in expression of CD11b on Ly6C⁺ and Ly6C⁻ monocytes, and decreased expression of F4/80 on Ly6C⁺ monocytes of HF-fed mice compared to chow-fed mice.

Table 5.1.2. Bone marrow monocyte surface phenotype in WT mice fed HF vs chow diet.

Surface Marker	Population	Weeks Diet Allocation		
		6	12	24
Ly6C	Ly6C ⁺	ns	↑ ^{**} p=0.0052	ns
	Ly6C ⁻	ns	ns	ns
CCR2	Ly6C ⁺	ns	ns	ns
	Ly6C ⁻	↓ ^{**} p=0.0023	ns	↓ [*] p=0.0100
F4/80	Ly6C ⁺	ns	ns	↓ ^{***} p=0.0005
	Ly6C ⁻	↓ ^{**} p=0.0093	ns	ns
CX ₃ CR ₁	Ly6C ⁺	↓ ^{**} p=0.0012	↓ [*] p=0.0115	NA
	Ly6C ⁻	ns	ns	NA
CD11b	Ly6C ⁺	ns	ns	↓ ^{****} p<0.0001
	Ly6C ⁻	ns	ns	↓ ^{****} p<0.0001

(e.g. HF-fed mice compared to chow-fed mice have higher expression of Ly6C on Ly6C⁺ monocytes after 12 weeks) Geometric mean surface expression was combined from 2-3 independent experiments of n=4-8 mice per group by normalizing the data from each mouse to the mean of the chow mouse group in each independent experiment. This approach was taken to account for variation in cytometer settings between experiments. NA – not available. ns – not significant.

Effects of TNF on peripheral immunophenotype in diet-induced obesity in non-pregnant female mice

After performing baseline measurements at 8 weeks of age, TNF^{-/-} and WT (TNF^{+/+}) littermate mice were placed on a high fat diet (60% kcal from fat) for up to 30 weeks. TNF^{-/-} and WT mice had similar body weight throughout the experiment, as summarized every 6 weeks (Figure 5.1.7A). Both genotype groups gained over 10 grams by 12 weeks diet allocation (WT: 29.2 ± 4.8 g; KO: 28.8 ± 3.6 g), and over 20 grams by 30 weeks diet allocation (WT: 46.9 ± 4.8 g; KO: 41.6 ± 6.8 g). The total increase in whole body adiposity was similar between genotypes (Figure 5.1.7B). Fasting blood glucose was also similar between diet groups after 12 weeks (WT: 9.5 ± 0.8 mM; KO: 9.6 ± 0.5 mM), or 28 weeks (WT: 9.6 ± 0.5 mM; KO: 9.2 ± 0.7 mM) (Figure 5.7.1C).

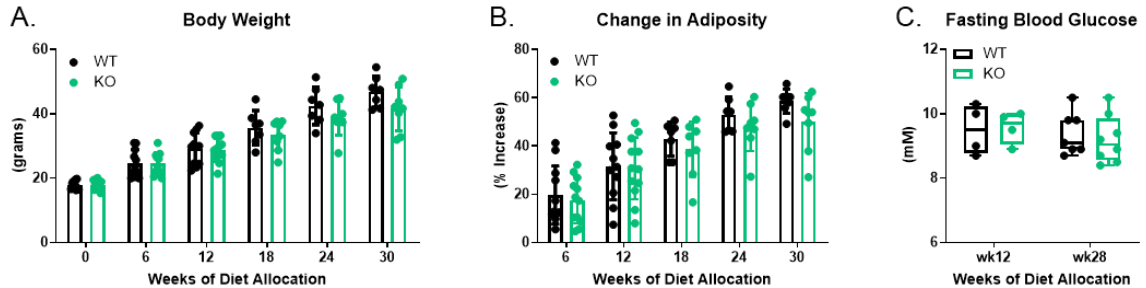


Figure 5.1.7. Body weight, adiposity, and fasting blood glucose in WT and TNF^{-/-} mice on HF diet.

Wildtype (WT) and TNF^{-/-} (KO) mice were placed on 60% high fat diet at 8 weeks of age. Body weight and adiposity were assessed prior to diet allocation and every 6 weeks thereafter. (A) body weight. (B) increase in adiposity from baseline. (C) Fasting blood after a 6 hour fast after 12 or 28 weeks diet allocation. Data in A and B are presented with box height at the mean with error bars indicating \pm standard deviation. Data in C are presented in box and whisker plots, minimum to maximum, where the center line indicates the median. Data are pooled from 1-2 independent experiments of n=4-8 mice per group. Statistical significance was assessed by Student's two-tailed t test at each time point.

We assessed peripheral blood immune cells longitudinally by flow cytometry.

There was a statistically significant difference in global immunophenotype composition (Figure 5.1.8), from baseline through to 30 weeks in both WT and TNF^{-/-} mice (PERMANOVA, $p = 0.001$, $R^2 = 0.30499$), driven by a small but significant increase in data variability with increasing time of HF diet feeding (PERMDISP, $p = 0.037$, $F = 1.9496$). Between-genotype comparisons showed that immunophenotype composition was different at baseline (PERMANOVA, $p = 0.035$, $R^2 = 0.11536$), with small but significant differences persisting between WT and TNF^{-/-} mice after 12 weeks (PERMANOVA, $p = 0.037$, $R^2 = 0.1281$) and 30 weeks (PERMANOVA, $p = 0.048$, $R^2 = 0.2132$). No differences were found in variability (assessed by PERMDISP) between genotypes at any assessed time point.

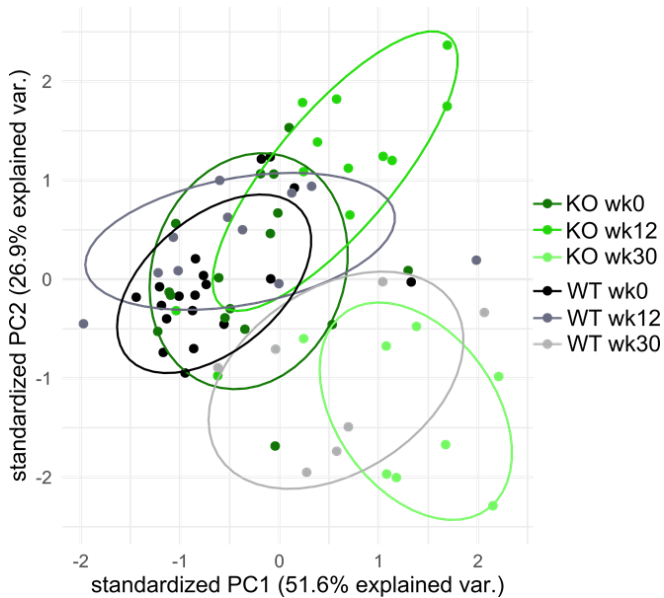


Figure 5.1.8. Effects of HF diet feeding on immunophenotype of WT and TNF^{-/-} mice.

PCA plot of immunophenotype data (absolute cell counts) of wildtype and TNF^{-/-} mice fed a 60% high fat diet plotted on PC1 and PC2. For clear visualization, only data from baseline, 12 weeks, and 30 weeks diet allocation are shown.

While the prevalence of neutrophils (Figure 5.1.9A), total monocytes (Figure 5.1.9B), and Ly6C^{high}, Ly6C^{low}, and Ly6C⁻ subsets (Figure 5.1.9C-E) increased with longer time of high fat diet feeding in WT mice, this was also found in the TNF^{-/-} mice, with no consistent statistical differences between genotypes. In addition, the prevalence of Ly6C^{high} monocytes as a proportion of Ly6C⁺ monocytes was similar between genotypes (Figure 5.1.9F). We found that the prevalence of NK cells (Figure 5.1.9G) and T cells (Figure 5.1.9I) remained similar between genotypes, though B cell prevalence in TNF^{-/-} mice was higher than in WT mice (Figure 5.1.9H).

Numbers of neutrophils (Figure 5.1.10A), total monocytes (Figure 5.1.10B), and monocyte subsets (Figure 5.1.10C-E), were not consistently different between WT and TNF^{-/-} mice. Likewise, NK cell counts were not consistently different (Figure 5.1.10F), nor were T cells (Figure 5.1.10H) or the ratio of CD4⁺ to CD8⁺ T cells (Figure 5.1.10I). The ratio of lymphocytes to myeloid cells was significantly different after 6 weeks HF diet allocation between genotypes, but not at other assessed time points (Figure 5.1.10J).

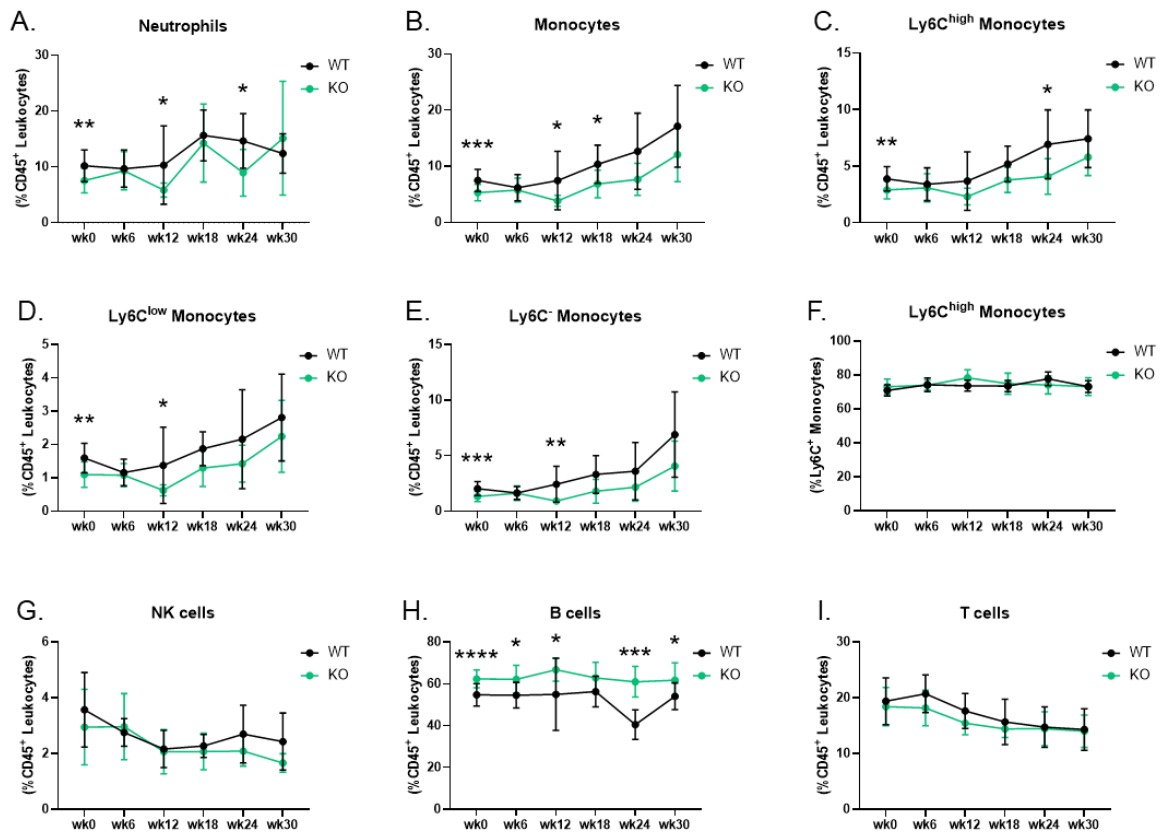


Figure 5.1.9. Peripheral blood immune cell prevalence in WT and TNF^{-/-} mice on HF diet.

Flow cytometry analysis of peripheral blood leukocytes in wildtype (WT) and TNF^{-/-} (KO) mice on 60% high fat diet prior to diet allocation (wk0) and every 6 weeks through to 30 weeks diet allocation (wk30). Prevalence (as a proportion of CD45⁺ leukocytes) of: (A) neutrophils, (B) total monocytes, (C) Ly6C^{high} monocytes, (D) Ly6C^{low} monocytes, (E) Ly6C⁺ monocytes. (F) Ly6C^{high} monocytes as a proportion of Ly6C⁺ monocytes. Prevalence (as a proportion of CD45⁺ leukocytes) of: (G) NK cells, (H) B cells, (I) T cells. Data are presented with a dot at the mean with error bars of \pm standard deviation. Data are pooled from 1-3 independent experiments with a total of n=7-19 mice per genotype at each time point. Statistical significance was assessed by two-tailed Student's t test between genotypes at each time point. * $p<0.05$, ** $p<0.01$, *** $p<0.001$, **** $p<0.0001$.

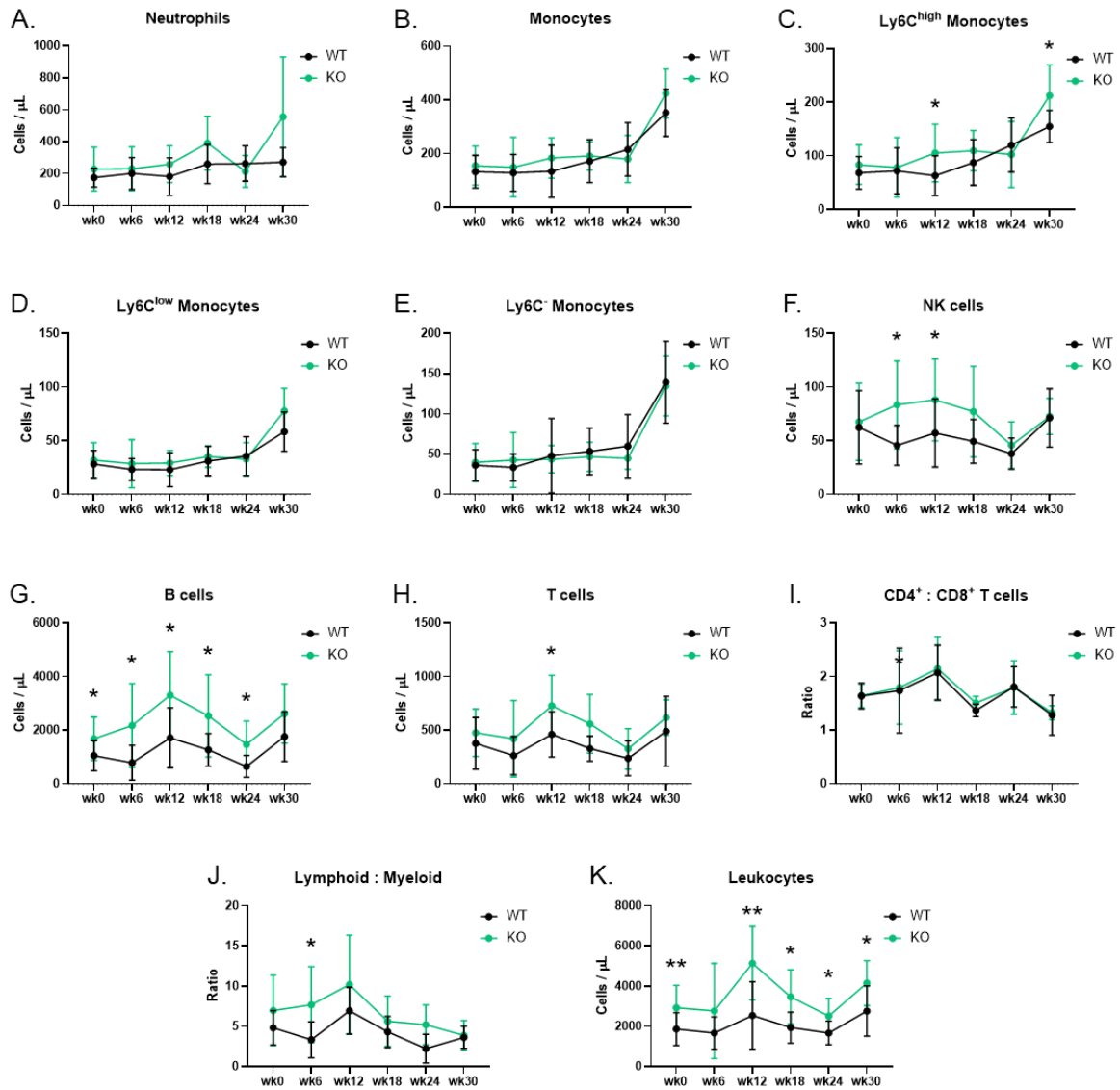


Figure 5.1.10. Peripheral blood immune cell absolute cell counts in WT and TNF^{-/-} mice on HF diet.

Flow cytometry analysis of peripheral blood leukocytes in wildtype (WT) and TNF^{-/-} (KO) mice on 60% high fat diet prior to diet allocation (wk0) and every 6 weeks through to 30 weeks diet allocation (wk30). Absolute cell counts of: (A) neutrophils, (B) total monocytes, (C) Ly6C^{high} monocytes, (D) Ly6C^{low} monocytes, (E) Ly6C⁻ monocytes, (F) NK cells, (G) B cells, (H) T cells. (I) ratio of CD4⁺ to CD8⁺ T cells. (J) ratio of lymphocytes to myeloid cells. (K) absolute cell count of leukocytes. Data are presented with a dot at the mean with error bars of \pm standard deviation. Data are pooled from 1-3 independent experiments with a total of n=7-19 mice per genotype at each time point. Statistical significance was assessed by two-tailed Student's t test between genotypes at each time point. * $p < 0.05$, ** $p < 0.01$.

Compared to WT mice, total leukocytes were elevated in TNF^{-/-} mice at baseline through to 30 weeks (Figure 5.1.10K), as were cell counts of B cells, at baseline through to 24 weeks (Figure 5.1.10G). An elevated number of B cells has been previously reported in chow-fed TNF^{-/-} mice compared to chow-fed littermate WT siblings^{555, 556, 557, 558}.

Therefore, while HF-fed TNF^{-/-} mice appeared to have a lower prevalence of monocytes in comparison to HF-fed WT mice, this was not statistically significant at all time points, and this was due to an increase in B cell counts (and thus prevalence of B cells), rather than changes to the absolute numbers of monocytes. In summary, HF diet feeding altered peripheral blood immunophenotype in both WT and TNF^{-/-} mice, but monocyte numbers remained similar between genotypes.

We also examined phenotypic changes to blood monocytes in HF-fed WT and TNF^{-/-} mice (Table 5.1.3; Appendix I). Once mice were placed on the high fat diet, there was some variability in monocyte surface marker expression over time, though Ly6C^{high} monocyte surface phenotype became more similar between WT and TNF^{-/-} mice with increasing diet exposure. Ly6C^{low} and Ly6C⁻ monocytes in particular retained lower expression of CX₃CR₁ in HF-fed TNF^{-/-} mice compared to HF-fed WT mice through to 24 or 30 weeks of diet allocation.

Table 5.1.3. Blood monocyte surface phenotype in WT and TNF^{-/-} mice fed HF diet.

Surface Marker	Population	Weeks of 60% High Fat Diet Allocation					
		0	6	12	18	24	30
Ly6C	Ly6C ^{high}	ns	ns	↓** p=0.001	ns	ns	ns
	Ly6C ^{low}	ns	ns	ns	↑* p=0.0185	ns	↑** p=0.002
CCR2	Ly6C ^{high}	↓** p=0.0018	ns	↓* p=0.0305	ns	ns	ns
	Ly6C ^{low}	ns	ns	ns	ns	ns	ns
	Ly6C ⁻	↑* p=0.0413	ns	ns	ns	ns	ns
F4/80	Ly6C ^{high}	↓** p=0.0014	ns	ns	ns	ns	ns
	Ly6C ^{low}	↓**** p<0.0001	ns	ns	↓** p=0.0095	ns	ns
	Ly6C ⁻	↓** p=0.001	↓* p=0.0472	ns	↓* p=0.0112	ns	ns
CX ₃ CR ₁	Ly6C ^{high}	ns	ns	ns	↓* p=0.0183	ns	ns
	Ly6C ^{low}	↓** p=0.008	↓** p=0.0016	↓* p=0.0305	↓**** p<0.0001	↓* p=0.0102	ns
	Ly6C ⁻	↓* p=0.012	↓* p=0.0186	↓* p=0.0182	↓* p=0.0187	ns	↓** p=0.0015
CD11b	Ly6C ^{high}	↓* p=0.0106	ns	ns	ns	ns	ns
	Ly6C ^{low}	↓*** p=0.0002	ns	ns	ns	ns	ns
	Ly6C ⁻	↓*** p=0.0001	ns	ns	ns	ns	ns

Data are shown comparing TNF^{-/-} mouse monocyte surface expression to WT mouse monocyte surface expression (e.g. Ly6C^{high} monocytes in TNF^{-/-} mice have lower expression of CCR2 at baseline (week 0), in comparison to Ly6C^{high} monocytes in WT mice). Geometric mean expression of each marker was combined from 1-3 independent experiments of n=4-8 mice per group by normalizing the data from each mouse to the mean of the chow mouse group in each independent experiment. This approach was taken to account for variation in cytometer settings between experiments. ns – not significant.

5.1.3 Discussion

To our knowledge, this is the first study to perform a longitudinal assessment of peripheral leukocytes by flow cytometry in the context of diet-induced obesity in WT or TNF^{-/-} female mice. We found in WT mice that Ly6C^{high} monocytes, Ly6C⁻ monocytes, and Ly6C^{low} monocytes, are more prevalent with increasing time of HF diet feeding, both as a proportion of total CD45⁺ leukocytes, and as absolute cell numbers (Figures 5.1.2B-E

and 5.1.3B-E), compared to chow-fed mice. Our observations were consistent with previous data, including our own, from male mice fed a high fat diet for 12-24 weeks^{523, 524, 525} (Chapter 4), and with a recent study in humans that reported increases in all monocyte subsets in obese individuals compared to individuals of a healthy BMI⁵²².

We observed that there are progressive and temporal changes to the proportional prevalence and numbers of peripheral Ly6C^{high} monocytes in diet-induced obesity (Figure 5.1.2C and Figure 5.1.3C), which emphasizes the importance of choosing an appropriate length of HF diet feeding for intervention studies. HF-fed WT mice had an acute reduction in circulating monocytes after 3 weeks of diet compared to chow-fed mice. This may have been due to increased retention of monocytes within the bone marrow, as there was a transient decrease in monocyte and cMoP proliferation in HF fed mice at 6 weeks, though their prevalence remained similar to chow-fed mice. We observed that Ly6C^{high} monocytes from HF-fed female mice were more responsive to CCL2-elicited egress into circulation within 6 weeks in comparison to chow-fed mouse Ly6C^{high} monocytes. Increased chemotactic activity of non-classical monocytes has also been reported in obese female humans^{518, 520}. After 3 and 6 weeks of diet, the surface phenotype of Ly6C^{high} monocytes in our HF-fed mice suggested that they were less mature (in terms of monocyte-to-macrophage progression as they had lower F4/80 and higher Ly6C), and that they were less likely to re-enter the bone marrow and transition into Ly6C⁻ monocytes (lower CX₃CR₁, higher CD11b) compared to Ly6C^{high} monocytes from chow-fed mice (Table 5.1.1; Appendix I). It was recently shown in male mice that within one week of diet feeding that HF-fed mice, compared to chow-fed mice, have a decrease in circulating monocytes, with increased *ccl2* gene expression and accumulation of macrophages in

adipose tissue⁵⁵⁹. Our data may therefore indicate that an early effect of HF diet is that Ly6C^{high} monocytes preferentially travel to adipose (or other metabolic tissues).

We observed a recovery in blood monocyte numbers and proportional prevalence by 6 weeks, with a subsequent increase in circulating Ly6C^{high} monocytes in HF fed mice, as well as Ly6C^{low} and Ly6C⁻ subsets, which remained significantly higher in HF mice through to 30 weeks of diet allocation (Figures 5.1.2 and 5.1.3). At 12 weeks there was also a change in CD11b expression on Ly6C^{high} monocytes from HF-fed mice compared to chow-fed mice, as they had higher expression of CD11b at 3 and 6 weeks, but lower expression at 18 weeks, and Ly6C⁻ monocytes began to express higher levels of CX₃CR₁, at 18 weeks, which together may indicate changes in movement of monocytes in the periphery (Table 5.1.1; Appendix I). After 18 and 24 weeks diet allocation, circulating Ly6C^{high} monocytes of HF-fed mice compared to chow-fed mice produced more intracellular TNF after LPS stimulation (Figure 5.1.5C-D). Therefore, diet-induced obesity increased circulating TNF-producing pro-inflammatory yet immature Ly6C^{high} monocytes, which are primed for CCR2/CCL2-mediated migration to peripheral tissues.

We did not observe changes in the prevalence of monocytes between diet groups after 6, 12, or 24 weeks in the bone marrow (Figure 5.1.6A-B). These results were not completely unexpected, since we did not observe changes to total monocytes in bone marrow in male mice after 24 weeks of HF diet (Chapter 4). After 6 weeks of diet allocation, we observed no changes to bone marrow progenitors of HF-fed mice compared to chow-fed mice (Figure 5.1.6C), despite increased HSPCs, CMPs, and cMoPs by 18 weeks (Figure 5.1.6D) and at 30 weeks (Figure 5.1.6E). It has previously been reported (in male mice) that 3 weeks of HF diet did not impact HSPCs or CMPs⁵⁵⁹, but

those populations expanded after 20 weeks^{525, 560}. The stability in bone marrow monocyte levels in the present study may indicate that monocytes from HF-fed mice compared to chow-fed mice rapidly egress and are less likely to return to the bone marrow, consistent with our observations of changes to blood Ly6C^{high} monocyte surface phenotype within 3 weeks of diet allocation (i.e. higher expression of Ly6C and lower expression of CX₃CR₁ and F4/80), and with our observation that at early time points of diet allocation Ly6C⁻ monocytes have lower expression of CX₃CR₁ in the bone marrow in HF-fed mice.

While we expected to see an increase in pro-inflammatory cytokines in the circulation of HF-fed mice compared to chow-fed mice, IL-6 levels remained similar between diet groups from 6 weeks through to 24 weeks of diet allocation. This was in accord with data from another study in female mice⁵⁶¹. Overt obesity-associated soluble inflammation in female mice is generally more subtle than that observed in male mice after a similar length of diet allocation^{561, 562, 563, 564}. Although we were not able to consistently detect TNF in serum, our data showed that Ly6C^{high} monocytes from HF-fed mice have the capacity to produce more TNF in response to LPS stimulation.

We observed that genetic ablation of TNF does not protect against diet-induced adiposity, hyperglycemia, or changes to peripheral Ly6C^{high} monocytes and overall immunophenotype even after 30 weeks of HF diet feeding. Before diet allocation, Ly6C^{high} monocytes from TNF^{-/-} mice had a phenotype that appeared less mature (lower F4/80 and CCR2), with reduced capacity for retention in bone marrow or interaction with CX₃CL₁ within blood vessels (lower CX₃CR₁), and adhesion and transmigration in blood vessels (lower CD11b), compared to Ly6C^{high} monocytes from WT mice (Table 5.1.3; Appendix I). Interestingly, Ly6C^{low} and Ly6C⁻ monocytes from TNF^{-/-} mice retained their

lower expression of CX₃CR₁ after HF diet allocation. TNF treatment can induce CX₃CR₁ expression on macrophage-like THP-1 cells, and expression of its receptor CX₃CL₁ on endothelial cells^{565, 566, 567}, so without tonic stimulation of TNF, expression of tissue CX₃CL₁ and monocyte CX₃CR₁ may be lower. With increasing time of HF diet feeding, monocyte surface phenotype in WT and TNF^{-/-} mice became more similar, indicating that TNF^{-/-} mice are not protected from HF diet-induced changes to monocyte phenotype.

It has been suggested that the absence of TNF helps maintain insulin sensitivity in the first few weeks of HF diet feeding in male mice, and may attenuate later development of adiposity and inflammation, protecting against insulin resistance⁵²⁸, consistent with our observations in Chapter 4. While fasting blood glucose and adiposity were similar, we did not further characterize metabolic parameters between the HF-fed TNF^{-/-} and WT female mice. However, comparisons of HF-fed and chow-fed mice from our WT cohort indicate that female HF-fed WT mice were not insulin resistant by ITT after 16 weeks, though they were glucose intolerant and produced higher insulin by GTT compared to chow-fed female mice (Figure 5.1.1K-M). These data were consistent with studies using similar models in female mice after 12-15 weeks of HF diet^{561, 563, 564}, though male mice are glucose and insulin intolerant within 9-12 weeks of HF diet^{394, 547, 563, 568, 569}. Therefore, WT female mice remained insulin sensitive for longer than male mice, suggesting sex differences in effects of TNF, and/or that female mice are more “resistant” to the metabolic consequences of diet-induced obesity. Overall, our longitudinal study of diet-induced obesity in WT and TNF^{-/-} mice emphasizes the importance of considering appropriate time points for experimental analysis, and that data from male mouse models is not always applicable to female mouse models or *vice versa*.

5.2 Peripheral immunophenotype, diet-induced obesity, and excess gestational weight gain, in female mice during pregnancy and lactation

5.2.1 Introduction

Healthy pregnancy requires an increase in innate immune mechanisms to provide protection against infection, with selective suppression of adaptive immune responses toward fetal/paternal antigens^{570, 571}. Studies of maternal peripheral blood in humans generally report increases in circulating granulocytes (including neutrophils, basophils, eosinophils, and mast cells) during pregnancy^{142, 149, 155, 572}, and these cells exhibit an activated phenotype with enhanced phagocytic function, respiratory burst activity, and cytokine production^{120, 142, 152, 573, 574, 575, 576, 577}. Complement factors and acute phase proteins are also elevated in circulation^{578, 579, 580, 581}. To contrast, NK cells and B cells tend to decrease during gestation⁵⁸², though B cell antibody production increases in the third trimester^{571, 583}. Studies of cellular and cell-free transcriptomes in maternal circulation have reported a gradual decrease of gene expression related to B cell function across gestation, as well as fluctuations in T cell-associated gene expression, with a decrease in the first and second trimesters, and an increase in the third trimester^{139, 140, 584, 585}. The cytokines produced by T cells change during pregnancy, with increased Th2/T_{reg} responses in the second trimester^{586, 587, 588, 589}. There is also evidence of corresponding changes in immune cells within the thymus and the spleen^{590, 591, 592}.

Specific alterations to peripheral immunophenotype and enhanced inflammatory responses during normal pregnancy have been associated with pregnancy complications including preeclampsia^{130, 142, 147, 573, 574, 575, 593, 594} and preterm labor^{152, 573, 584}.

Consequently, there has been considerable effort to identify blood biomarkers of

physiological and pathological complications of pregnancy, as this could be a fairly non-invasive approach for early detection of problems that could threaten maternal and fetal health.

In healthy weight individuals, pregnancy leads to alterations in endocrine and immune functions that promote insulin resistance, increased adiposity, alterations to microbiota composition, and progressive low-grade systemic inflammation^{118, 119, 120, 121, 122, 123, 180}. Pre-gravid obesity and/or excess weight gain during pregnancy have been reported to interfere with these adaptations^{28, 29, 175, 176, 177, 178, 179, 180}, which may have long-term implications for maternal and fetal health. Women with excess gestational weight gain have a 3-fold increase in risk of obesity at 8 years postpartum⁵⁹⁵, and are at elevated risk of developing type 2 diabetes and other comorbidities like glucose intolerance, dyslipidemia, and cardiovascular disease, later in life^{164, 165, 166, 167, 168}. As the postpartum period of one pregnancy often becomes the preconception period of the next pregnancy, a higher BMI pre- and post-pregnancy increases maternal risk of gestational weight gain across successive pregnancies^{596, 597, 598, 599}.

It is generally accepted that pregravid obesity results in increased systemic inflammation during pregnancy, with an imbalance toward production of Th1 cytokines, such as TNF²⁹. As previously described, TNF has pleiotropic roles in modulation of systemic inflammation and metabolism²⁵. The balance between IL-10 (a Th2 cytokine) and TNF is important in implantation, placental development, embryogenesis, and parturition^{588, 600}. Even in uncomplicated pregnancies TNF has been reported to increase in maternal circulation across gestation^{150, 601}. However, maternal TNF levels in mid-to-late pregnancy correlate with insulin resistance⁶⁰¹, and above-normal levels are associated

with preeclampsia^{602, 603, 604}, and premature labour⁶⁰⁴. We have previously reported that TNF is increased in serum at E18.5 in mice with diet-induced obesity¹⁷⁹, and it has also been reported that PBMC production of pro-inflammatory cytokines including TNF was significantly increased in obese pregnant women, in comparison to healthy weight pregnant women, in the third trimester¹⁸⁶.

Research to date on maternal obesity and excess weight gain during pregnancy has primarily focussed on modifications to maternal metabolism or placental structure and function during pregnancy, or offspring health. Markers of soluble inflammation, especially pro-inflammatory cytokines, have been extensively used to consider effects of obesity-associated inflammation, but results from those studies are often conflicting¹⁸⁴. Even though there are critical cellular immunological adaptations during pregnancy, there has been little consideration of circulating immune cells. We aimed to examine effects of diet-induced obesity and excess gestational weight gain on peripheral blood immune cells in pregnancy and lactation, and to assess if immunomodulation by genetic ablation of TNF would prevent changes to maternal immunophenotype. We predicted that typical pregnancy-induced changes to maternal immune cells, including increases in neutrophils and decreases in lymphocytes, would be blunted by maternal obesity, and that the absence of TNF may be protective. We predicted that excess gestational weight gain would also alter maternal immunophenotype during lactation.

5.2.2 Maternal peripheral immunophenotype and diet-induced obesity at E14.5

Using our model of diet-induced obesity, female mice were fed a standard chow diet or 60% high fat diet for 6 weeks prior to mating and were retained on their respective

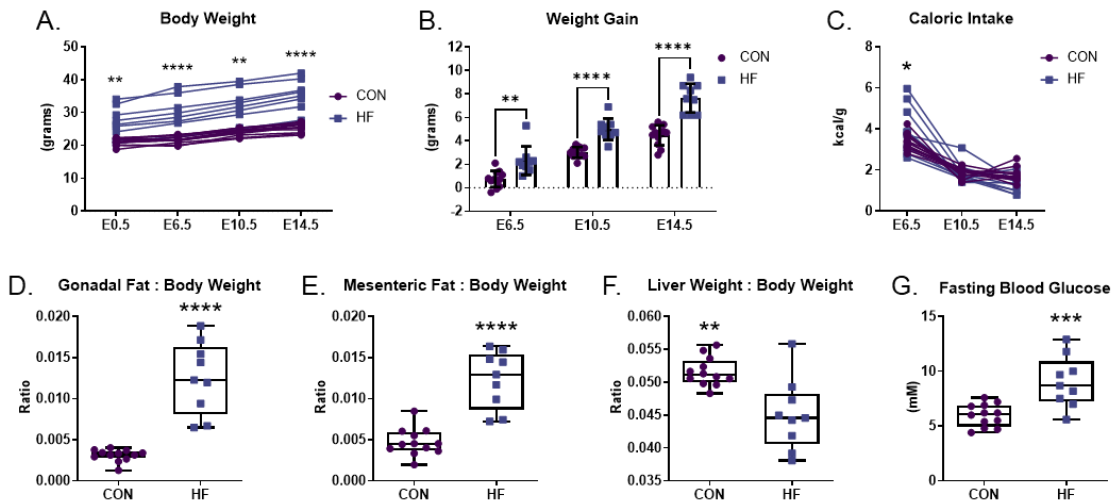
diets through to endpoint at E14.5 (mid-gestation). HF-fed female mice were significantly heavier compared to chow-fed mice throughout gestation to E14.5 (Figure 5.2.1A-B), consistent with previous work in similar mouse models^{178, 179, 180, 605, 606}. Caloric intake was increased in mice fed high fat diet early in pregnancy and normalized by E10.5 (Figure 5.2.1C), consistent with published data¹⁷⁸. At E14.5, the ratios of gonadal fat and mesenteric fat weight to body weight were increased in HF fed mice compared to chow-fed mice (Figure 5.2.1D-E), while liver weight to body weight was decreased (Figure 5.2.1F). Consistent with our previous data¹⁷⁸, HF-fed dams had increased fasting blood glucose compared to chow-fed dams (Figure 5.2.1G). Litter size, reabsorptions, fetal blood glucose, as well as fetal and placental weights, and their ratio, remained similar between diet groups (Figure 5.2.1H-M), also in agreement with our previous data¹⁷⁸.

Peripheral blood immunophenotype was assessed by flow cytometry. Dams with diet-induced obesity had an increased prevalence of B cells compared to chow-fed dams (Figure 5.2.2A). NK cell prevalence was similar between diet groups (Figure 5.2.2B), although the prevalence of total T cells and both CD4⁺ and CD8⁺ T cell subsets were decreased in dams with HF diet-induced obesity compared to chow-fed dams (Figure 5.2.2C-D). Absolute cell counts of B cells were increased in HF-fed dams compared to chow-fed dams (Figure 5.2.2E), although cell counts of NK cells and total T cells, and the ratio of CD4⁺ to CD8⁺ T cells, were not different (Figure 5.2.2F-H).

Significant changes to peripheral blood myeloid cell populations were also identified. HF-fed dams had a lower prevalence of neutrophils compared to chow-fed dams (Figure 5.2.2I). We also observed that dams with diet-induced obesity had an

increased proportion of total monocytes (Figure 5.2.2J) and Ly6C^{high} monocytes (Figure 5.2.2K), and Ly6C^{high} monocytes as a proportion of total monocytes (Figure 5.2.2L).

Maternal measurements



Fetal and Placental measurements

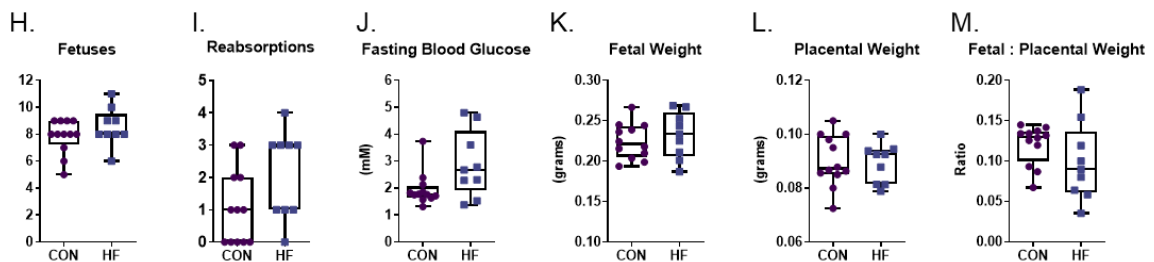


Figure 5.2.1. Maternal, fetal, and placental physiological measurements.

Maternal (A-G), fetal (H-K), and placental (L-M) physiological parameters were measured during gestation and/or at E14.5 endpoint. (A) weight at E0.5, E6.5, E10.5, and E14.5. (B) weight gain from E0.5 to E6.5, E10.5, and E14.5. (C) kilocalorie consumption at E6.5, E10.5, and E14.5. (D) ratio of gonadal fat weight to body weight. (E) ratio of mesenteric fat weight to body weight. (F) ratio of liver weight to body weight. (G) fasting blood glucose. (H) number of fetuses. (I) number of reabsorptions. (J) fetal fasting blood glucose. (K) fetal weight. (L) placental weight. (M) ratio of fetal to placental weight. Each data point in A-I indicates an individual mouse (dam), and in J-M fetal/placental data for each fetus is averaged per dam. Data in A and C are shown with lines connecting time points for individual mice. Data in B are presented as a box plot where the top line indicates the mean, with bars at \pm standard deviation. Data in D-M are presented as box and whisker plots, min to max, with the center line at the median. CON – standard chow diet, n=12, HF – 60% high fat diet, n=9. Statistical significance was assessed by Student's t test. * $p<0.05$, ** $p<0.01$, *** $p<0.001$, **** $p<0.0001$.

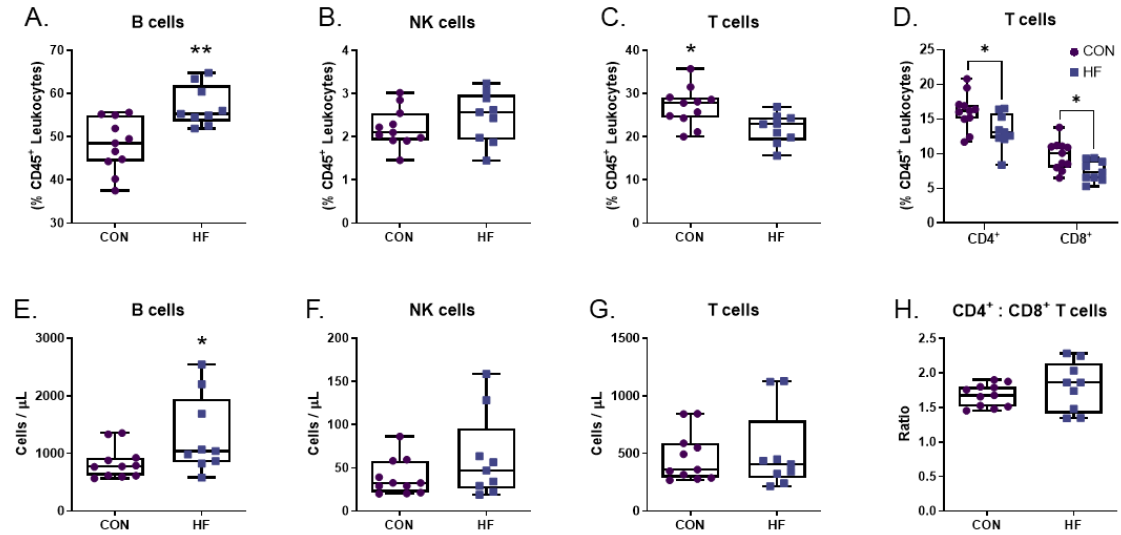
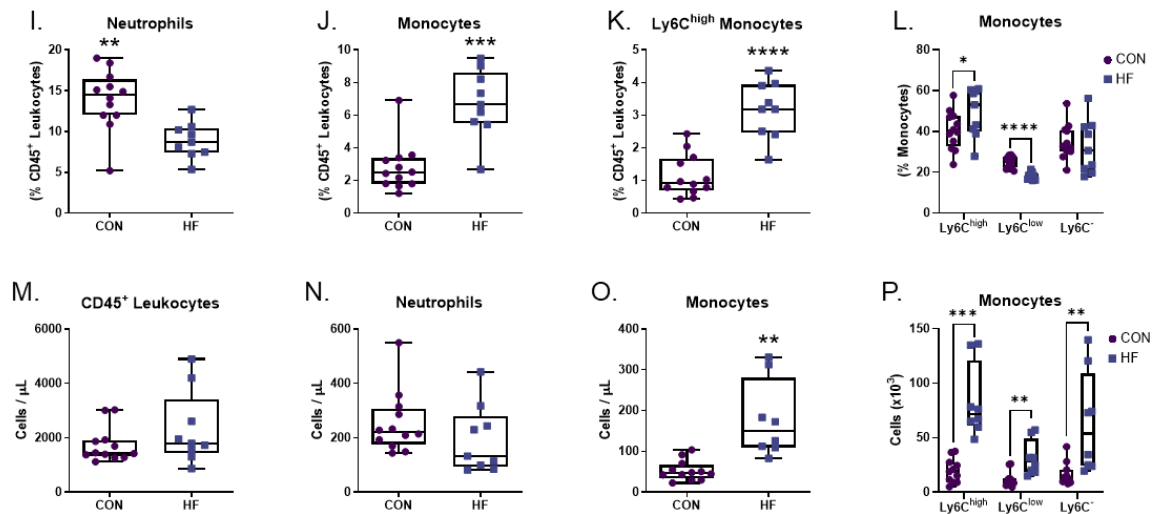
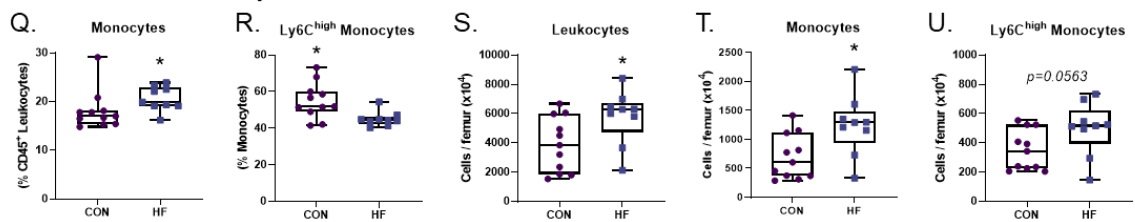
Blood – Lymphocytes*Blood – Myeloid Cells**Bone Marrow - Monocytes*

Figure 5.2.2. Effects of diet-induced obesity on peripheral blood and bone marrow immune cells at E14.5.

Maternal peripheral blood and femur bone marrow immune cell populations were assessed by flow cytometry at E14.5. Prevalence (as a proportion of CD45⁺ leukocytes) of: (A) B cells, (B) NK cells, (C) T cells, (D) CD4⁺ and CD8⁺ T cells. Absolute cell counts of: (E) B cells, (F) NK cells, (G) T cells. (H) ratio of CD4⁺ to CD8⁺ T cells. Prevalence (as a proportion of CD45⁺ leukocytes) of: (I) neutrophils, (J) monocytes, (K) Ly6C^{high} monocytes. (L) Prevalence of Ly6C^{high}, Ly6C^{low}, and Ly6C⁻ monocytes as a proportion of total monocytes. Blood absolute cell counts of: (M) CD45⁺ leukocytes, (N) neutrophils, (O) monocytes, (P) Ly6C^{high}, Ly6C^{low}, and Ly6C⁻ monocytes. Bone marrow prevalence of: (Q) monocytes, (R) Ly6C^{high} monocytes. Bone marrow absolute cell counts of: (S) total leukocytes, (T) monocytes, (U) Ly6C^{high} monocytes. Each data point indicates an individual mouse. Data are presented as box and whisker plots, min to max, with the center line at the median. CON – standard chow diet, n=11-12, HF – 60% high fat diet, n=9. Statistical significance was assessed by Student's t test. * $p < 0.05$, ** $p < 0.01$, *** $p < 0.001$, **** $p < 0.0001$.

The absolute cell counts of leukocytes were similar between diet groups (Figure 5.2.2M), as were cell counts of neutrophils (Figure 5.2.2N), but monocyte cell counts were elevated in dams with HF diet-induced obesity compared to chow-fed dams (Figure 5.2.2O-P). We also assessed bone marrow monocyte cell populations. The prevalence of monocytes was significantly increased in dams with diet-induced obesity (Figure 5.2.2Q), though the proportion of Ly6C^{high} monocytes (of total monocytes) was decreased (Figure 5.2.2R). Absolute cell counts of CD45⁺ leukocytes and monocytes were significantly increased in bone marrow of dams with diet-induced obesity compared to chow-fed dams (Figure 5.2.2S-T), and there was a trend toward an increase in Ly6C^{high} monocytes (Figure 5.2.2U). Overall, these data indicate that blood immunophenotype is significantly different in dams with HF diet-induced obesity compared to lean chow-fed dams, in particular B cell and monocyte populations, which had increased prevalence (as a proportion of total leukocytes) as well as cell numbers. Bone marrow monocyte populations were likewise increased in HF-fed dams compared to chow-fed dams.

5.2.3 Maternal immunophenotype, TNF, and diet-induced obesity at E18.5

To assess if peripheral immune effects of diet-induced obesity in pregnancy are regulated by increased TNF-mediated systemic inflammation, we performed a pilot study in WT and TNF^{-/-} female mice. Following the same model of diet-induced obesity described for the E14.5 study (section 5.2.2) and in non-pregnant mice (section 5.1.1), female mice were fed standard chow diet or 60% high fat diet for 6 weeks prior to mating, and were maintained on their respective diets through to endpoint at E18.5 (late gestation). We observed no differences in placental efficiency, fetus number, weight, or sex ratio, in WT and TNF^{-/-} mice on chow or HF diet (data not shown). Peripheral blood immune cells were characterized by flow cytometry (Figure 5.2.3).

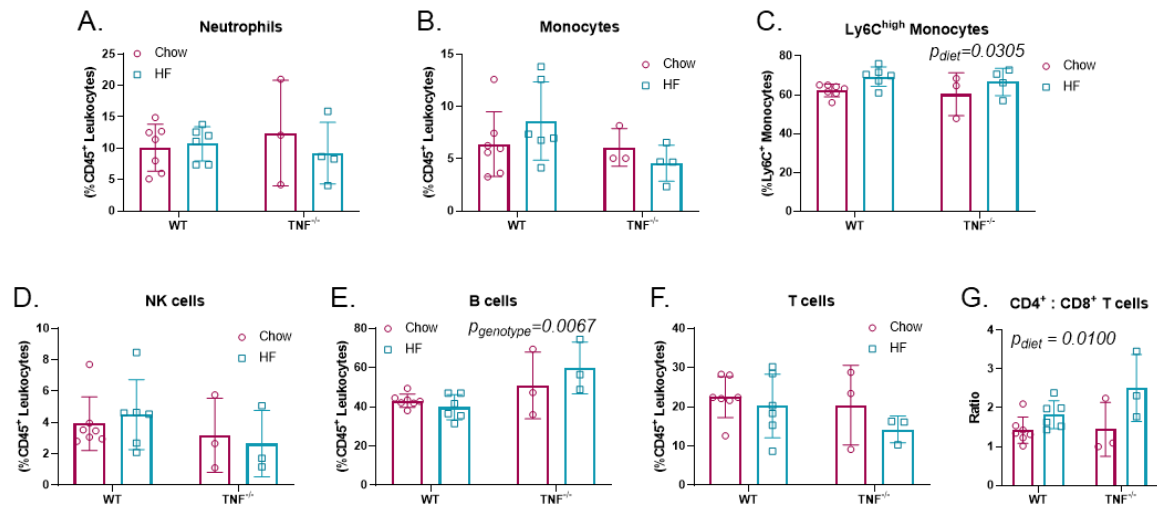


Figure 5.2.3. Effects of diet-induced obesity and TNF on peripheral blood immunophenotype at E18.5.

Maternal peripheral blood immune cell populations were assessed by flow cytometry at E18.5 in wildtype (WT) and TNF^{-/-} mice fed standard chow diet (Chow) or 60% high fat diet (HF). Prevalence (as a proportion of CD45⁺ leukocytes) of: (A) neutrophils, (B) monocytes. (C) Ly6C^{high} monocytes as a proportion of Ly6C⁺ monocytes. Blood prevalence (as a proportion of CD45⁺ leukocytes) of: (D) NK cells, (E) B cells, (F) T cells. (G) ratio of CD4⁺ to CD8⁺ T cells. Each data point indicates an individual mouse. Data are presented as box plots with the box height at the mean and bars at \pm standard deviation. WT n=6-7, TNF^{-/-} n=3-4. Statistical significance was assessed by two-way ANOVA.

We observed no main effects of diet or genotype on neutrophils (Figure 5.2.3A), total monocytes (Figure 5.2.3B), NK cells (Figure 5.2.3D), or total T cells (Figure 5.2.3F). There was a main effect of diet on Ly6C^{high} monocyte prevalence in HF-fed dams (Figure 5.2.3C), and the ratio of CD4⁺ to CD8⁺ T cells (due to a decrease in prevalence of CD8⁺ T cells) at E18.5 (Figure 5.2.3G). We also observed an effect of genotype on B cell prevalence (i.e. TNF^{-/-} mice had an increased prevalence of B cells) (Figure 5.2.3E), consistent with our observations in HF-fed non-pregnant TNF^{-/-} and WT mice (Figure 5.1.9). Therefore, these pilot data suggest that TNF^{-/-} mice, compared to WT mice, were not protected from effects of diet-induced obesity on immunophenotype at E18.5.

5.2.4 Maternal excess gestational weight gain and peripheral immunophenotype during lactation

We aimed to investigate effects of excess gestational weight gain on changes to maternal immunophenotype during lactation, with a particular focus on monocytes. To induce gestational weight gain, female mice were placed on a 45% (kcal from fat) high fat diet for two weeks prior to and throughout pregnancy and lactation. Although maternal weight between diet groups was similar upon confirmation of a vaginal plug (i.e. at E0.5), HF-fed dams gained more weight during pregnancy at all assessed time points (E6.5, E10.5, E14.5, and E18.5) (Figure 5.2.4A). HF-fed dams retained this excess gestational weight during lactation and were heavier at weaning compared to standard chow-fed mice (P21; Chow: 29.3 ± 1.3 g; HF: 31.5 ± 2.9 g). Mice that were fed the high fat diet gained ~20% more weight from E0.5 through to P21 (mean: 6.10 g) than mice that were on the chow diet (mean: 4.85 g). Litter size, offspring weights, and offspring sex ratios (assessed at P7) were not statistically different between diet groups (Figure 5.2.4B-D).

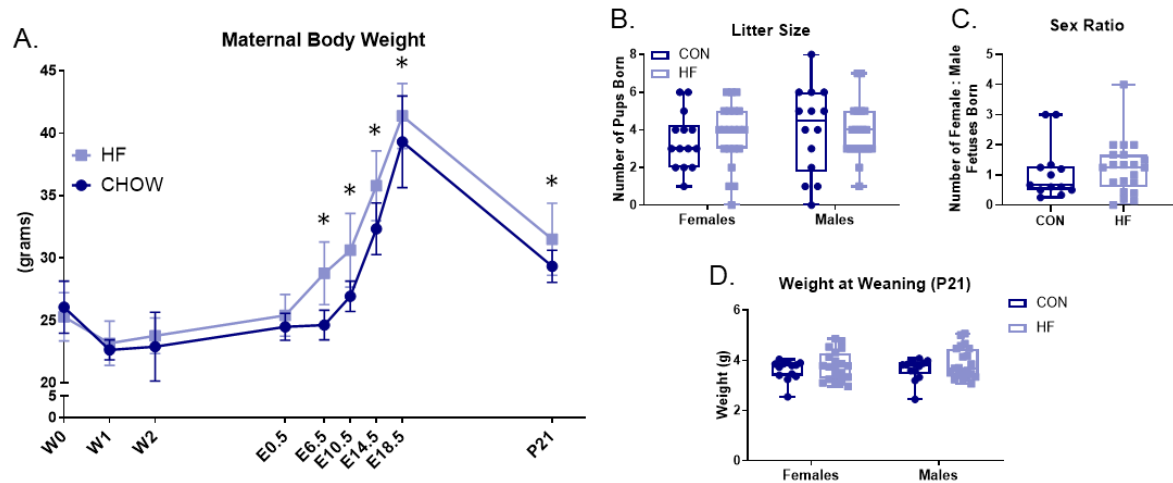
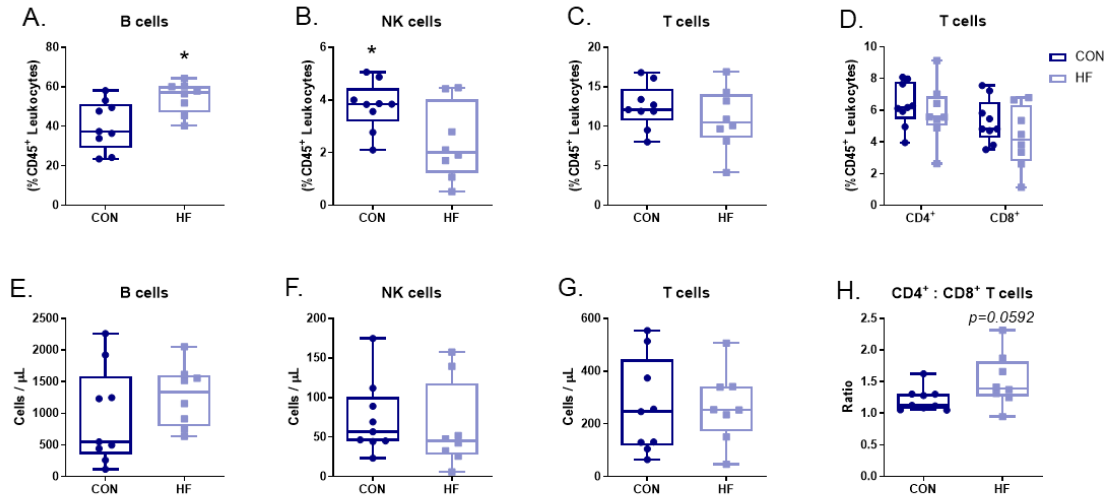


Figure 5.2.4. Effects of excess gestational weight gain on dam and offspring measurements. (A) Body weight of female mice allocated to standard chow (CON) or 45% high fat diet (HF) was measured at the start of diet allocation (W0), after 1 week (W1) and 2 weeks (W2), during pregnancy (at gestational days E0.5, E6.5, E10.5, E14.5, E18.5), and during lactation at P21. (B) number of female and male offspring at P7. (C) female to male sex ratio of offspring. (D) weight of offspring at P21 (average weight of female and male offspring per dam). Data in A are shown with a dot at the mean with error bars at \pm standard deviation. Data in B-D are presented as box and whisker plots, minimum to maximum, where the center line indicates the median. Each data point in B-D represents one dam (i.e. offspring measures were averaged per dam). For A, CON n=11-14, HF n=20-25. For B-D, CON n=14, HF n=21. Statistical significance was assessed by Student's t test (A,C) or two-way ANOVA (B,D). * $p < 0.05$.

We assessed peripheral blood immune cells by flow cytometry. We found that HF-fed dams compared to chow-fed dams had an increase in the prevalence of B cells (as a proportion of total leukocytes) (Figure 5.2.5A), a decrease in NK cell prevalence (Figure 5.2.5B), but no changes to the prevalence of total T cells (Figure 5.2.5C), CD4⁺ T cells, or CD8⁺ T cells (Figure 5.2.5D). Absolute cell counts of B cells (Figure 5.2.5E), NK cells (Figure 5.2.5F), and total T cells (Figure 5.2.5G), were not significantly different, though there was a trend toward an increase in the ratio of CD4⁺ to CD8⁺ T cells in HF-fed dams (Figure 5.2.5H). There were no significant differences in the prevalence (as a proportion of total leukocytes) of neutrophils (Figure 5.2.5I), total monocytes (Figure 5.2.5J), or Ly6C^{high} monocytes (Figure 5.2.5K), though there was a significant increase in the prevalence of Ly6C^{high} monocytes within all monocytes (Figure

5.2.5L). Total cell counts of leukocytes, neutrophils, monocytes, or Ly6C^{high}, Ly6C^{low}, or Ly6C⁻ monocytes, were not significantly different between diet groups (Figure 5.2.5M-P).

Lymphocytes



Myeloid Cells

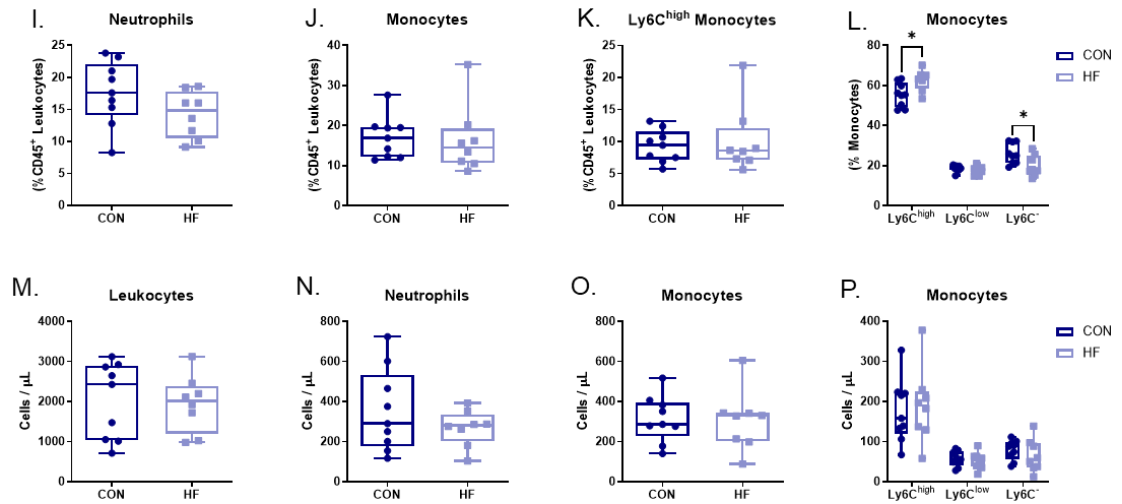


Figure 5.2.5. Effects of excess gestational weight gain on maternal blood leukocytes at P21.

Flow cytometry analysis of peripheral whole blood leukocytes of dams at P21 fed standard chow diet (CON) or 45% high fat diet (HF). Prevalence (as a proportion of CD45⁺ leukocytes) of: (A) B cells, (B) NK cells, (C) T cells, (D) CD4⁺ and CD8⁺ T cells. Absolute cell counts of: (E) B cells, (F) NK cells, (G) T cells. (H) ratio of CD4⁺ and CD8⁺ T cells. Prevalence (as a proportion of CD45⁺ leukocytes) of: (I) neutrophils, (J) total monocytes, (K) Ly6C^{high} monocytes. (L) prevalence of Ly6C^{high}, Ly6C^{low}, and Ly6C⁻ monocytes as a proportion of total monocytes. Absolute cell counts of: (M) leukocytes, (N) neutrophils, (O) total monocytes, (P) Ly6C^{high}, Ly6C^{low}, and Ly6C⁻ monocytes. Data are presented as box and whisker plots, minimum to maximum, with the center line at the median. Each data point indicates an individual mouse. CON n=9, HF n=8. Statistical significance was assessed by two-tailed Student's t test. * $p<0.05$.

We further assessed monocyte populations by examining their surface expression of Ly6C, F4/80, CX₃CR₁, CCR2, and CD11b (Figure 5.2.6; Appendix I). Ly6C^{high} monocytes in chow and HF-fed dams had similar expression of Ly6C (Figure 5.2.6A) and F4/80 (Figure 5.2.6B), though Ly6C^{high} monocytes in HF-fed dams compared to chow-fed dams exhibited lower expression of CX₃CR₁ (Figure 5.2.6C) and higher expression of CCR2 (Figure 5.2.6D) as well as CD11b (Figure 5.2.6E). Ly6C^{low} monocytes had similar expression of F4/80 (Figure 5.2.6B) and CD11b (Figure 5.2.6E) between diet groups, but HF-fed dams compared to chow-fed dams had lower expression of CX₃CR₁ and increased expression of CCR2 (Figure 5.2.6C-D). Ly6C⁻ monocyte surface expression of F4/80, CX₃CR₁, and CD11b was not significantly different between the diet groups (Figure 5.2.6B-C, E), though CCR2 expression on Ly6C⁻ monocytes was elevated in HF-fed dams compared to chow-fed dams (Figure 5.2.6D).

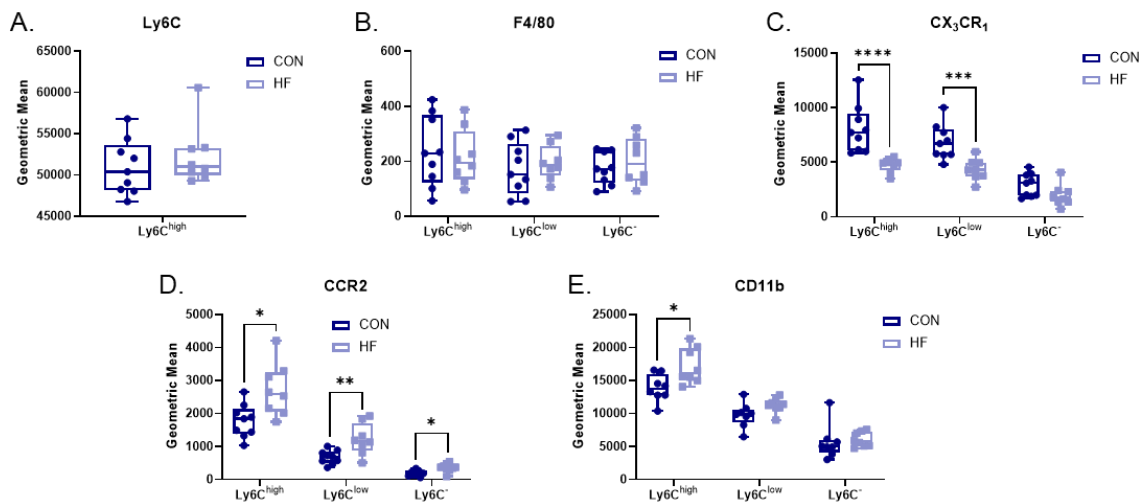


Figure 5.2.6. Effects of excess gestational weight gain on maternal peripheral blood monocyte surface phenotype at P21.

Flow cytometry analysis of peripheral whole blood monocytes at P21 of dams fed standard chow diet (CON) or 45% high fat diet (HF). Monocyte geometric mean surface expression: (A) Ly6C, (B) F4/80, (C) CX₃CR₁, (D) CCR2, (E) CD11b. Data are presented as box and whisker plots, minimum to maximum, where the center line indicates the median. Each data point indicates an individual mouse. CON n=9, HF n=8. Statistical significance was assessed by two-tailed Student's t test. * $p < 0.05$, ** $p < 0.01$, *** $p < 0.001$, **** $p < 0.0001$.

We also examined monocyte populations within the bone marrow. Bone marrow monocytes were not significantly different by total cell counts or as a proportion of total leukocytes between the diet groups (Figure 5.2.7A-E), but Ly6C^{high} monocytes exhibited higher expression of chemotactic marker CCR2 (Figure 5.2.7G) in HF-fed dams compared to chow-fed dams. These data suggested that excess gestational weight gain does not have a major impact on bone marrow monocyte populations, though it may increase their CCR2-mediated migration into blood. Overall, there were changes to bone marrow monocyte phenotype and peripheral blood immunophenotype during lactation in mice with diet-induced excess gestational weight gain.

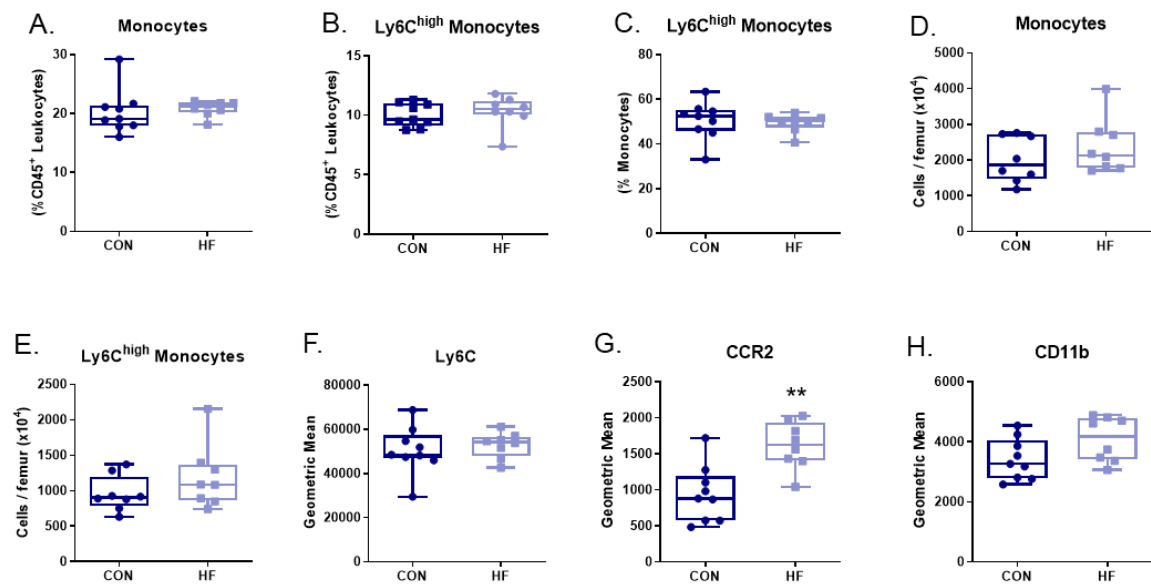


Figure 5.2.7. Effects of excess gestational weight gain on bone marrow monocytes at P21.

Flow cytometry analysis of bone marrow monocytes at P21 of dams fed standard chow diet (CON) or 45% high fat diet (HF). Prevalence (as a proportion of CD45⁺ leukocytes) of: (A) monocytes, (B) Ly6C^{high} monocytes. (C) prevalence of Ly6C^{high} monocytes as a proportion of monocytes. Absolute cell counts of: (D) monocytes, (E) Ly6C^{high} monocytes. Ly6C^{high} monocyte geometric mean surface expression of: Ly6C (F), CCR2 (G), and CD11b (H). Data are presented as box and whisker plots, minimum to maximum, where the center line indicates the median. Each data point indicates an individual mouse. CON n=9, HF n=8. Statistical significance was assessed by two-tailed Student's t test. ** $p < 0.01$.

5.2.5 Discussion

Similar to data from human pregnancies^{149, 152, 607, 608, 609, 610, 611, 612}, over the course of pregnancy in chow-fed mice we observed an increase in the prevalence of myeloid cells (monocytes and neutrophils; Figure 5.2.8A), with a reduction of lymphocytes (B cells, T cells, NK cells; Figure 5.2.8B), resulting in an increasing ratio of myeloid cells to lymphocytes (Figure 5.2.8C). In particular, the prevalence of neutrophils in chow-fed dams at E14.5 (mean \pm SD, $13.93 \pm 3.71\%$ of total leukocytes; Figure 5.2.2I) and at E18.5 ($10.1 \pm 3.72\%$; Figure 5.2.3A), was higher than in chow-fed non-pregnant mice ($5.73 \pm 2.11\%$; Chapter 3), and the prevalence of B cells in chow-fed dams was significantly lower during pregnancy at E14.5 ($48.1 \pm 6.11\%$; Figure 5.2.2A) and at E18.5 ($43.2 \pm 3.40\%$; Figure 5.2.3E) than in non-pregnant chow-fed mice of similar age ($63.8 \pm 5.35\%$; Chapter 3).

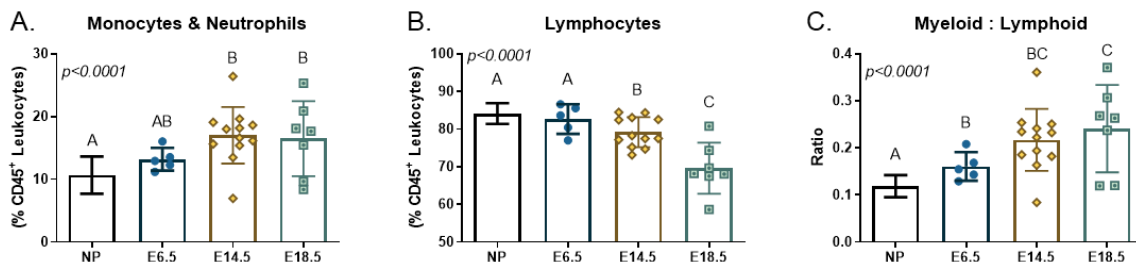


Figure 5.2.8. Comparison of blood leukocyte populations in non-pregnant and pregnant mice.

Leukocytes in peripheral whole blood were assessed by flow cytometry from non-pregnant (NP) mice (age-matched, Chapter 3) and pregnant mice in early pregnancy (E6.5, n=5), mid-pregnancy (E14.5, n=12), or term pregnancy (E18.5, n=7). All mice were fed standard chow diet. Prevalence as a proportion of CD45⁺ leukocytes: (A) myeloid cells (monocytes and neutrophils), (B) lymphocytes (B cells, T cells, NK cells). (C) ratio of myeloid to lymphoid cells. Data are shown as box plots with the top of the box at the mean and error bars at \pm standard deviation. Dots represent individual mice at each time point. Data were assessed by one-way ANOVA or non-parametric Kruskal-Wallis test. Letters indicate similarities or differences that are of statistical significance.

To our knowledge, there are no publications on maternal peripheral immune cells during lactation in mice, so we compared our data of peripheral immune cell prevalence and numbers from the chow-fed lactational dams to that of age-matched non-pregnant

chow-fed female mice (Appendix II). These comparisons revealed significant differences in blood immunophenotype, and in particular showed that the increase in myeloid cells and decrease in lymphocytes that occurs during pregnancy in mice persists into lactation (Appendix II-H). Interestingly, studies of maternal blood in cows show similar trends as our data between mid-pregnancy and lactation, with a decrease in B cells, an increase in monocytes, and a slight decrease in CD4⁺ T cells and CD8⁺ T cells⁶¹³. Our observations from our studies on maternal immunophenotype in pregnancy and lactation are summarized in Table 5.2.1.

Table 5.2.1. Summary of effects of HF diet feeding in female mice.

Immune Cell Population	Non-Pregnant Mice (12 weeks)	Pregnancy E14.5	Pregnancy E18.5	Lactation P21
Ly6C ^{high}	↑	↑	↑	↑
Monocytes	↑	↑	---	---
Neutrophils	---	↓	---	---
B cells	---	↑	---	↑
NK cells	---	---	---	↓
T cells	↓	↓	---	---
CD4 ⁺ : CD8 ⁺	---	---	↑	~↑

Effects of high fat diet feeding are summarized from week 12 data of Figure 5.1.2 (non-pregnant mice, 60% HF diet), Figure 5.2.2 (E14.5 pregnancy, 60% HF diet), Figure 5.2.3 (E18.5 pregnancy, 60% HF diet), and Figure 5.2.5 (P21 lactation, 45% HF diet). Arrows indicate changes in HF-fed mice compared to chow-fed mice according to immunophenotype data of the proportions of peripheral immune cells (prevalence as a proportion of total leukocytes, or as a proportion of total monocytes for Ly6C^{high} monocytes).

We assessed effects of pregravid HF diet-induced obesity on maternal immunophenotype at E14.5. As noted above, the prevalence of lymphocytes in our chow-fed dams at E14.5 was lower than in non-pregnant mice of a similar age, particularly as B cells were less prevalent (mean \pm SD, pregnant: $48.1 \pm 6.1\%$; non-pregnant: $63.8 \pm 5.35\%$), but this adaptation was not observed in dams with diet-induced obesity ($57.1 \pm 4.67\%$) (Figure 5.2.2A). We also observed that CD4⁺ and CD8⁺ T cell prevalence was decreased in dams with diet-induced obesity (Figure 5.2.2D). Consistent with these data,

an increased prevalence of B cells and decreased prevalence of CD8⁺ T cells has been reported in the second trimester in women with pregravid obesity compared to women with a healthy pre-pregnancy BMI⁵⁸⁶. Future studies examining numbers, phenotype, and cytokine production profiles of specific subsets of B cells (e.g. naïve, transitional, memory), as well as subsets of CD4⁺ and CD8⁺ T cells (e.g. CD4⁺ Th subsets, and naïve or memory cells), would provide further insight as to whether these changes could have a detrimental impact on the adaptive immune response to infection, or effectiveness of vaccination, as has been reported in non-pregnant obese individuals^{614, 615, 616, 617}.

In non-pregnant mice with diet-induced obesity, we observed significant increases in the prevalence and numbers of total and Ly6C^{high} monocytes (section 5.1), and we similarly found that Ly6C^{high} monocytes were increased in HF-dams at E14.5 compared to chow-fed dams (Figure 5.2.2L,P). We did not further characterize monocyte phenotype or cytokine production in pregnancy due to technical constraints, but monocytes in pregnancy typically have a more activated phenotype and altered cytokine responses^{142, 144, 152, 573, 594}. Monocytes are recruited from blood into maternal endometrial tissue as it becomes the decidua at the beginning of pregnancy^{618, 619, 620}. These monocytes mature into macrophages that support implantation⁶²¹, remodeling of uterine connective tissues and blood vessels^{622, 623, 624}, and regulation of trophoblast invasion^{622, 624}. Once the placenta is formed, maternal macrophages are involved in antigen presentation and immunomodulation of other leukocytes^{625, 626, 627}, infection defense⁶²⁸, fetal antigen tolerance^{620, 629}, and parturition⁶³⁰. Combining studies of monocyte and decidual macrophage cytokine responses to PRR stimulation, with transcriptomic and metabolomic techniques that have recently been used to study immune and metabolic changes in

healthy pregnancy^{120, 129, 130, 139}, would provide further insight into the effects of pregravid obesity on tissue-localized and peripheral immunological adaptations early in pregnancy and at mid-gestation.

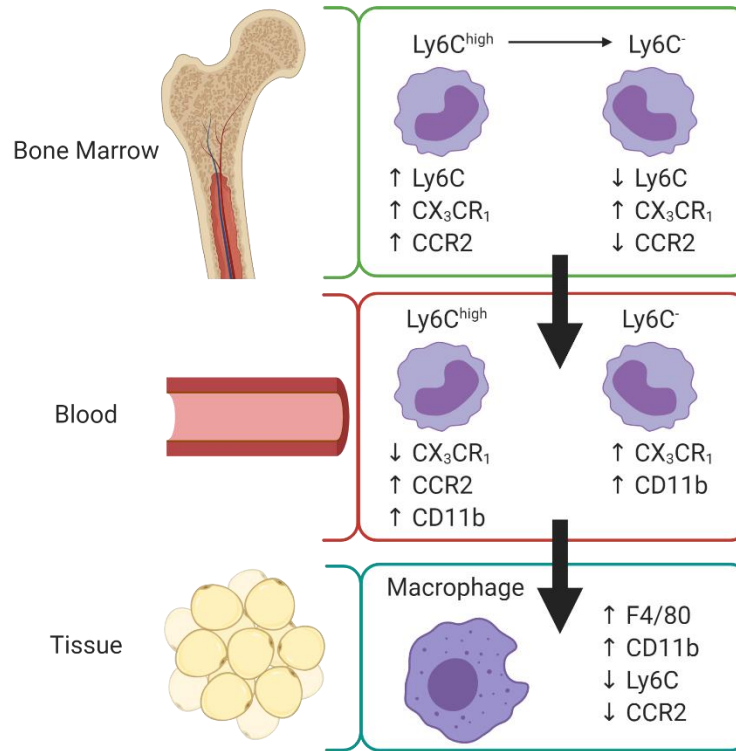
Our pilot study on the effects of genetic ablation of TNF on maternal immunophenotype suggested that at E18.5 HF-fed TNF^{-/-} dams compared to HF-fed WT dams were not protected from effects of diet-induced obesity (Figure 5.2.3). In addition, differences that we observed in maternal immunophenotype between HF-fed and chow-fed dams at E14.5, such as an increased prevalence of monocytes and B cells (Figure 5.2.2A,J), were not apparent at E18.5 (Figure 5.2.3B,E). These data are in agreement with a recent study that reported that third trimester peripheral blood of normal weight and pregravid obese women had no significant differences in the frequency of total monocytes, NK cells, B cells, and total CD4⁺ T cells and CD8⁺ T cells¹⁸⁶. In other work, a model of pre-pregnancy HF diet allocation (with different diet composition) reported that there were no differences in the prevalence of total circulating monocytes in chow-fed and HF-fed dams at E18.5⁶³¹. Levels of circulating pro-inflammatory cytokines decrease in women with pregravid obesity late in gestation⁶³², and studies in mice have also reported lower inflammation within adipose^{631, 633} or liver tissue⁶³¹ of HF-fed dams late in gestation, in comparison to HF-fed non-pregnant mice. Thus, the similarities in immunophenotype between chow-fed and HF-fed mice at E18.5, whether WT or TNF^{-/-} genotype, could suggest that pregnancy attenuates obesity-associated changes to tissue-localized and peripheral inflammation, and consequently circulating immune cells, particularly late in gestation. Alternatively, there may be a ‘catch-up’ of required immunological changes in pregnancy that results in a similar end-of-pregnancy

immunophenotype in lean and obese women, or chow-fed and HF-fed mice. This may occur concurrently with other metabolic or physiological adaptations. For example, glucose intolerance and elevated secretion of insulin in response to glucose at E14.5 in HF-fed dams, compared to chow-fed dams, is no longer apparent at E18.5⁶³³. In obese women compared to lean women, increased trajectories of weight gain, insulin resistance, and circulating triglyceride levels are more apparent within the first and second trimesters of pregnancy^{634, 635, 636}. Gradual attenuation of obesity-associated inflammation, or late-gestation adjustment of maternal immune, metabolic, or physiological traits to meet required pregnancy adaptations, may be a protective measure for fetal development.

We also considered effects of excess gestational weight gain in lactation. B cell prevalence in non-pregnant female mice was more comparable to the B cell prevalence in dams with excess gestational weight gain at P21 (mean \pm SD, NP: $58.2 \pm 5.6\%$; HF: $54.5 \pm 8.15\%$), than the chow-fed dams at P21 (Chow Lac: $40.4 \pm 12.4\%$). NK cell prevalence was also more similar between non-pregnant mice and HF-fed dams during lactation at P21 (mean \pm SD, NP: $2.09 \pm 0.57\%$; HF: $2.38 \pm 1.45\%$) than chow-fed dams during lactation (Chow Lac: $3.77 \pm 0.92\%$). While monocyte prevalence was similar between the diet groups in lactation at P21, peripheral blood Ly6C^{high} monocytes may more readily migrate into tissues, as they expressed lower CX₃CR₁ and higher CCR2 and CD11b in HF-fed dams compared to chow-fed dams (Figure 5.2.6).

These data collectively indicate that there are temporal changes to maternal blood immunophenotype across pregnancy and lactation, and support our overall hypotheses that maternal peripheral blood immune cell adaptations are modified in pregnancy by pregravid obesity, and in lactation by excess gestational weight gain.

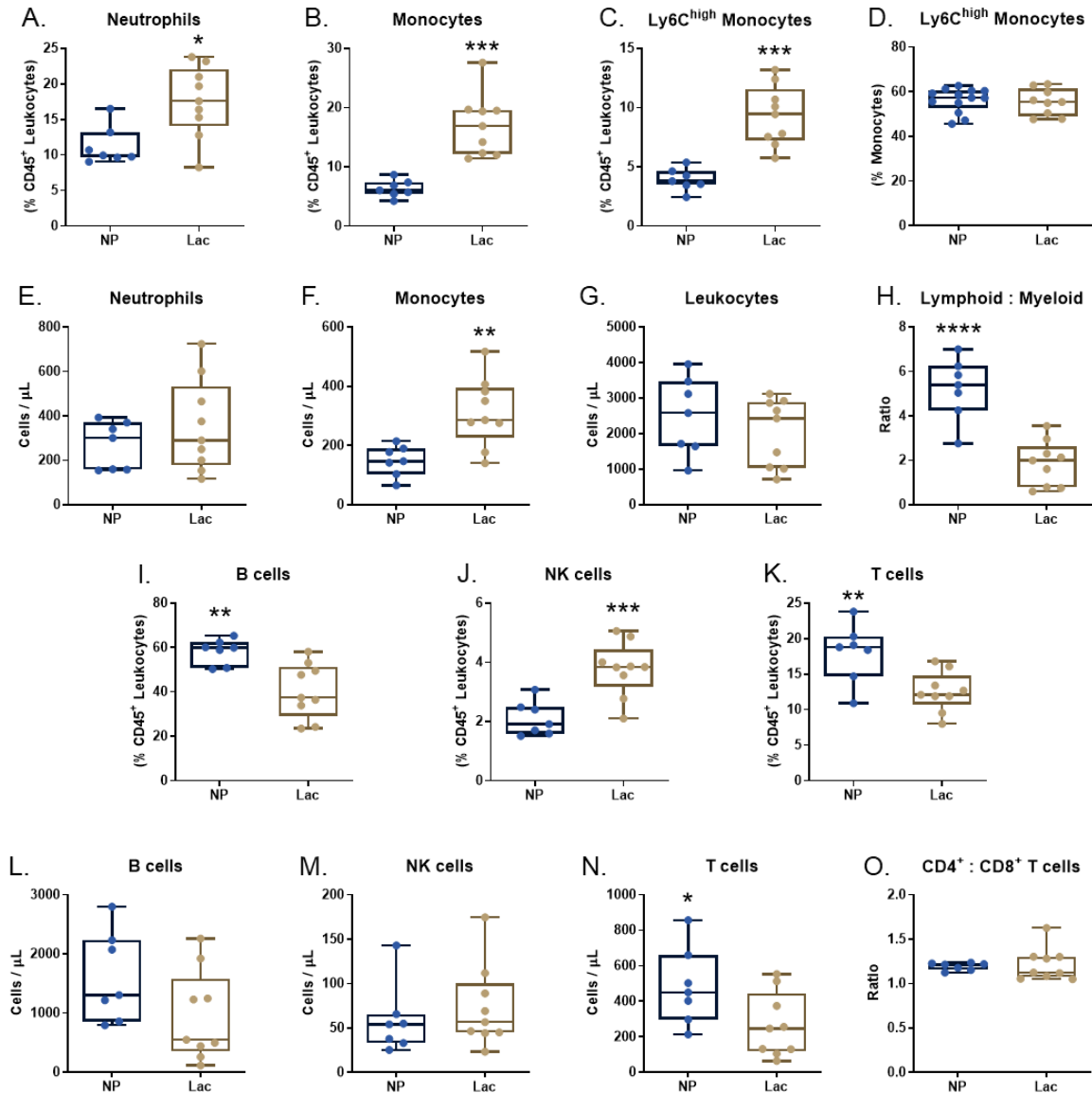
Appendix I.



Surface phenotype changes of the $Ly6C^{high}$ to $Ly6C^{-}$ monocyte transition in the bone marrow, monocyte migration in blood, and monocyte to macrophage differentiation.

As described in Chapter 1, as monocytes transition from $Ly6C^{high}$ to $Ly6C^{-}$ in the bone marrow, they lose expression of $Ly6C$ and $CCR2$ ²⁸⁷. $Ly6C^{high}$ monocyte retention in the bone marrow is dependent on CX_3CR_1 ^{286, 301, 302}. $Ly6C^{high}$ monocyte egress from bone marrow is regulated by $CCR2$ signalling initiated by $CCL2/CCL7$ ^{305, 306, 307, 308}. $Ly6C^{-}$ monocytes use CX_3CR_1 - CX_3CL_1 interactions to patrol the blood vessel endothelium^{287, 298, 313, 314}. $CD11b$ is involved in vascular movement and endothelial transmigration^{637, 638}. As monocytes transition into tissue macrophages, they increase their surface expression of $F4/80$ and expression of $Ly6C$ and $CCR2$ is reduced^{272, 322}. For simplicity, $Ly6C^{low}$ monocytes are not shown in this figure.

Appendix II.



Comparison of peripheral blood immunophenotype in age-matched non-pregnant non-lactating female mice and dams in lactation at P21.

Flow cytometry analysis of peripheral whole blood leukocytes of chow-fed age-matched non-pregnant mice (NP) and chow-fed dams at P21 (Lac). Prevalence (as a proportion of CD45⁺ leukocytes) of: (A) neutrophils, (B) monocytes, (C) Ly6C^{high} monocytes. (D) Prevalence of Ly6C^{high} monocytes (as a proportion of total monocytes). Absolute cell counts of: (E) neutrophils, (F) monocytes, (G) total leukocytes. (H) ratio of lymphocytes to myeloid cells. Prevalence (as a proportion of CD45⁺ leukocytes) of: (I) B cells, (J) NK cells, (K) T cells. Absolute cell counts of: (L) B cells, (M) NK cells, (N) T cells. (O) ratio of CD4⁺ and CD8⁺ T cells. Data are presented as box and whisker plots, minimum to maximum, where the center line indicates the median. Each data point indicates an individual mouse. NP n=7, Lac n=9. Statistical significance was assessed by two-tailed Student's t test. * $p < 0.05$, ** $p < 0.01$, *** $p < 0.001$, **** $p < 0.0001$.

Chapter 6. Intestinal macrophages in chronic inflammation

In this chapter, we aimed to assess effects of chronic inflammation on intestinal macrophages. We began by using the model of diet-induced obesity in female mice established in Chapter 5, examining longitudinal effects on macrophage prevalence, phenotype, and functions due to obesity-associated inflammation (section 5.1). We considered whether modulation of TNF would prevent effects of diet-induced obesity (section 5.2), and the role of the microbiome (section 5.3). We then assessed effects of age-associated chronic inflammation, and the aging microbiome (section 5.4). We also investigated effects of intestinal adaptations and excess maternal weight gain during lactation (section 5.5).

6.1 Intestinal macrophages in diet-induced obesity

6.1.1 Introduction

Changes to intestinal homeostasis in diet-induced obesity have been linked to inflammation and metabolic dysregulation in the liver, skeletal muscle, and adipose tissue, as well as systemic inflammation and insulin resistance^{375, 639 75, 83, 89, 640, 641, 642}. Many researchers have reported that diet-induced obesity causes the development of a pro-inflammatory environment in the small intestines and colons of mice^{89, 390, 643, 644, 645}. Mouse models have accordingly demonstrated that a high fat diet exacerbates inflammation and intestinal pathology in genetic mouse models of IBD^{646, 647}, and exacerbates chemically-induced DSS colitis by increasing pro-inflammatory macrophage accumulation^{648, 649}. In contrast, when mice with diet-induced obesity are treated with the anti-inflammatory drug 5-aminosalicylic acid (which has limited systemic effects), intestinal permeability is reduced, as is systemic soluble inflammation, adipose tissue inflammation, and insulin resistance⁶⁴¹.

Diet-induced obesity is associated with impairment of the gut vascular barrier³⁷⁵, dysregulation of enteric neuron activity and gastrointestinal motility^{650, 651}, dysregulation of intestinal stem cell crypt proliferation^{652, 653}, and impaired lymphatic function⁶⁵⁴. Macrophages have been implicated in regulation of all of those processes in conditions of homeostasis. As previously discussed, macrophages are involved in maintenance of an anti-inflammatory tolerogenic environment and epithelial barrier integrity in the intestines. Microbial dysbiosis, disruptions to the intestinal epithelial barrier, and increased inflammatory tone of the lamina propria and underlying tissues, can influence recruitment, phenotype, and functions of monocytes and macrophages^{267, 405, 407}.

Treatment of the macrophage cell line RAW 264.7 with metabolites produced in the intestines of mice fed HF diet induces gene expression and secretion of IL-1 β , IL-6, and TNF⁶⁵⁵. These cytokines can remodel the actin-myosin cytoskeleton within intestinal epithelial cells, disrupting tight junction protein interactions and increasing paracellular permeability^{492, 656, 657}, as well as alter transcription of claudin molecules that form tight junctions and pores³⁶⁴. Accordingly, *in vitro* co-culture models have shown that human primary monocytes or monocyte-derived macrophages expressing inflammasome cytokines like IL-1 β and IL-18, or TNF, can reduce transepithelial resistance (i.e. increase intestinal permeability) in Caco-2, HT-29B/6, and T84 intestinal epithelial cell lines by altering epithelial cell localization of tight junction protein claudin-2, and inducing epithelial cell apoptosis⁴⁸⁹. Studies that depleted intestinal epithelial cell *cc12* (involved in chemotactic recruitment of monocytes), or treated mice with anti-CSF1 (required for differentiation and maintenance of tissue macrophages) have suggested that macrophages, and monocyte-derived macrophages in particular, also contribute to intestinal inflammation and systemic metabolic dysregulation in diet-induced obesity^{89, 658}.

In Chapter 5 we identified that HF diet-induced obesity in non-pregnant female mice increases circulating immature pro-inflammatory Ly6C^{high} monocytes, and that these monocytes are more sensitive to CCL2-elicited chemotaxis. Acute intestinal inflammation due to infection, colitis, or sterile injury, elicits rapid CCR2/CCL2-mediated recruitment of pro-inflammatory Ly6C^{high} monocytes into intestinal tissues, which develop into immature, pro-inflammatory macrophages^{236, 405, 415, 433}. It was unclear whether these observations would apply in the context of diet-induced obesity, in which inflammation is characterized as low-grade and chronic.

Conflicting data has been reported from studies that have examined intestinal macrophages in the context of diet-induced obesity. Immunohistochemistry data from Kawano and colleagues suggested that there is an increase in CD68⁺ macrophages in the colon lamina propria within 4 weeks of HF diet in male mice in comparison to chow-fed mice. Flow cytometry data also identified an increase in CD11b⁺F4/80⁺CD11c⁻ cells in the colon but not small intestine of HF-fed male mice in comparison to chow-fed mice⁸⁹. In contrast, Luck *et al.* reported that there is a trend toward a decrease in the prevalence of colon CX₃CR₁⁺MHCII⁺ macrophages and a significant decrease in total cell numbers in mice with diet-induced obesity, in comparison to lean chow-fed mice, after 14 weeks diet allocation⁶⁴⁰. Using immunofluorescence staining in the small intestine, it was found that villus CD11b⁺MHCII⁺ cells (but not CX₃CR₁⁺ cells by flow cytometry) decreased after one week in mice fed a HF diet compared to a chow diet, but this difference disappeared after 16 weeks⁶⁵⁹. Garidou and colleagues reported no changes to the prevalence of ileum CD19⁻MHCII⁺ antigen presenting cells in male mice after 30 days HF diet in comparison to chow-fed mice⁶⁶⁰. It had also been reported after 10 weeks that male mice fed HF diet compared to chow diet had a similar prevalence of small intestine CX₃CR₁⁺ macrophages, but there was an increase in CD103⁻CX₃CR₁⁺CD11c^{hi} macrophages and a decrease in CD103⁻CX₃CR₁⁺CD11c^{lo} macrophages⁶⁶¹. Therefore, while there was some evidence to suggest that macrophage populations are altered in both the colon and small intestine as a result of diet-induced obesity, there was no consensus amongst published data. It was also unclear whether there is increased infiltration of monocytes and accumulation of monocyte-derived macrophages, and whether resident macrophage population prevalence, phenotype and/or functions are affected.

We hypothesized that recruitment of immature inflammatory Ly6C^{high} monocytes into the intestines would contribute to intestinal inflammation, and that they would differentiate into macrophages with pro-inflammatory properties. We predicted that these pro-inflammatory macrophages would disrupt normal tissue-resident macrophage population prevalence, proliferation, phenotype, and functions, and that these changes contribute to increased intestinal permeability. We assessed Ly6C^{high} monocytes, transitional Ly6C⁺MHCII⁺ cells, and macrophages (total and CD4⁻TIM4⁻, CD4⁺, and CD4⁺TIM4⁺ populations) in the colons and small intestines of female mice, using a model of diet-induced obesity. Based on studies of turnover rates of intestinal macrophages^{214, 408, 409}, we performed assessments after 6, 12, and 18 weeks of diet allocation.

6.1.2 Results

Intestine length and permeability

After allocating young female mice to standard chow diet or a high fat diet (60% kcal from fat) for 6, 12, or 18 weeks, we measured body weight and lengths of the small intestine and colon (Figure 6.1.1A-C). Diet-induced obesity was observed in mice fed the HF diet, with an ~23% increase in body weight in HF-fed mice compared to chow-fed mice after 6 weeks (chow mean: 20.39 g; HF mean: 26.44 g) and an ~46% increased body weight in HF-fed mice compared to chow-fed mice after 18 weeks (chow mean: 22.74 g; HF mean: 42.29 g) (Figure 6.1.1A). Consistent with previous reports from male mice^{89, 662, 663}, after 6 weeks small intestine length was decreased in female mice fed the HF diet (mean \pm SD: 31.6 \pm 1.6 cm) in comparison to chow-fed mice (35.5 \pm 2.8 cm) (Figure 6.1.1B). There was also a main effect of time of diet allocation, though a similar ~4 cm

difference in length was observed between diet groups after 6, 12, and 18 weeks. By 6 weeks, colon length was significantly decreased in mice fed the HF diet (mean \pm SD: 6.2 ± 0.4 cm) compared to mice fed the chow diet (7.6 ± 1.2 cm), and colon length remained shorter in HF-fed mice in comparison to chow-fed mice after 12 and 18 weeks (Figure 6.1.1C). These results may seem counterintuitive as the intestines use energy for growth, but when energy is in excess, a smaller epithelial surface area is required to maximize energy absorption, and the intestinal epithelium is energetically costly to maintain, so intestinal length decreases⁶⁶⁴. Decreased intestinal length may also be an indication of inflammation, as has been reported in mouse models of colitis^{435, 480, 642, 665}.

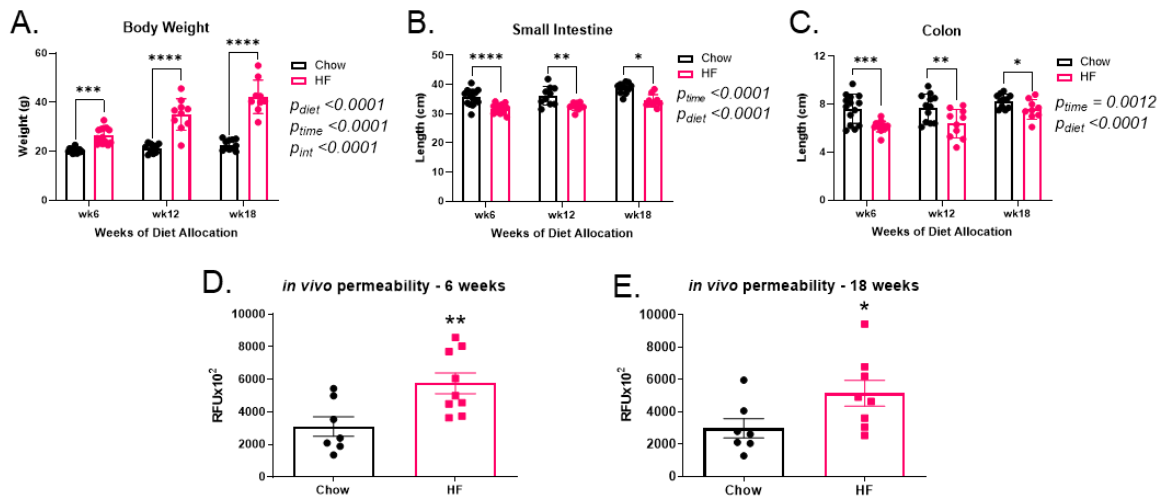


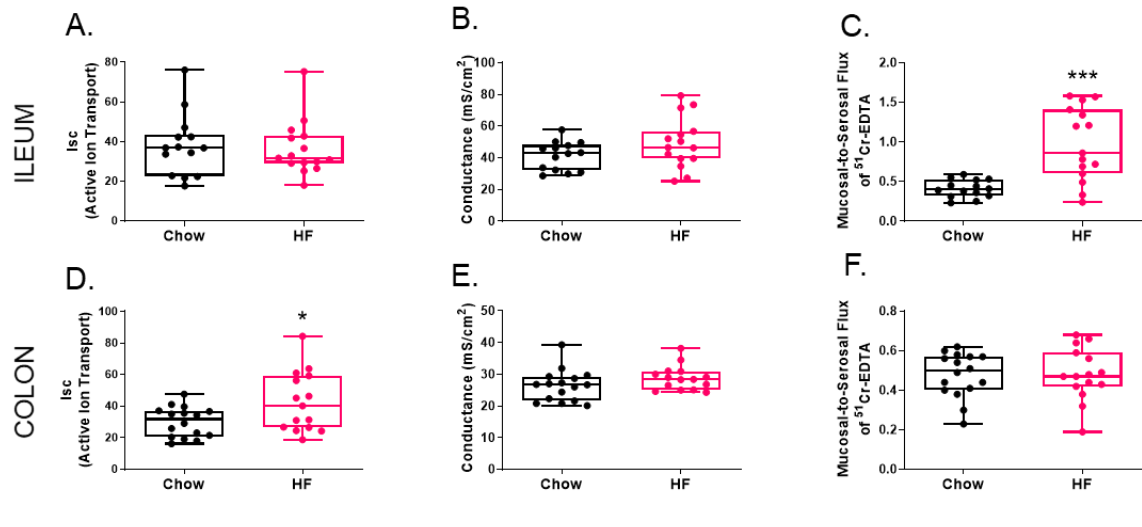
Figure 6.1.1. Intestinal lengths and permeability in chow and HF-fed mice.

Intestinal permeability and physiology were assessed after 6, 12, or 18 weeks allocation to standard chow (Chow) or 60% high fat (HF) diet. (A) body weight. (B) small intestine length. (C) colon length. An *in vivo* FITC-dextran assay of intestinal permeability was performed 6 weeks (D) and 18 weeks (E) after diet allocation. Each data point indicates an individual mouse. Data in A-E are presented with box height at the mean with error bars indicating \pm standard deviation. Data in A to C are pooled from 2-3 independent experiments of $n=4-5$ mice per group ($n=9-14$ per time point). Data in D are representative of two independent experiments of $n=7-10$ mice per diet group. Data in E are from one independent experiment of $n=7-8$ mice per diet group. Statistical significance was assessed by two-way ANOVA with Tukey's post-hoc test for between-diet comparisons for A-C and by two-tailed Student's *t* test for D-E. RFU – relative fluorescence units. * $p < 0.05$, ** $p < 0.01$, *** $p < 0.001$, **** $p < 0.0001$.

Studies of diet-induced obesity in male mice have reported increases in intestinal permeability^{89, 390, 660}. However, it has been observed that male mice have greater intestinal permeability than female mice fed a Western diet (40% kcal from fat) for 20 weeks⁶⁶⁶, and it has been reported that estrogen may have protective effects on intestinal permeability^{667, 668}. To ascertain if diet-induced obesity affected intestinal permeability in our female mouse model, we initially performed an *in vivo* assay and measured plasma fluorescence after gavaging mice with FITC-conjugated dextran. We found that there was an increase in post-gavage plasma fluorescence in HF-fed mice compared to chow-fed mice by 6 weeks of diet allocation (Figure 6.1.1D), which persisted after 18 weeks (Figure 6.1.1E). These data suggested that an increase in intestinal permeability occurs within 6 weeks in female mice fed a HF diet compared to a chow diet, coincident with our measurements of decreased small intestine and colon lengths in the HF-fed mice.

The FITC-dextran assay provides an indication of whether there are changes in intestinal permeability, but it does not show where or how changes occur. We used Ussing chambers, a short-term organ culture method, to examine tissue permeability in the distal ileum and proximal colon after 6 weeks or 20 weeks of diet allocation (Figure 6.1.2). We measured conductance (i.e. an indicator of tissue integrity), short-circuit current (I_{sc}; i.e. total ion transport), and mucosal-to-serosal flux of ⁵¹Cr-EDTA (i.e. paracellular permeability)^{669, 670}. These experiments identified no differences in conductance between the diet groups in either ileal or colon tissues after 6 weeks diet allocation (Figure 6.1.2B and E), but HF-fed mice, in comparison to chow-fed mice, had an increase in ileal conductance after 20 weeks (Figure 6.1.2H), suggestive of disruption of tissue structure^{669, 670}. After 6 weeks, short-circuit current was slightly increased in

6 weeks diet allocation



20 weeks diet allocation

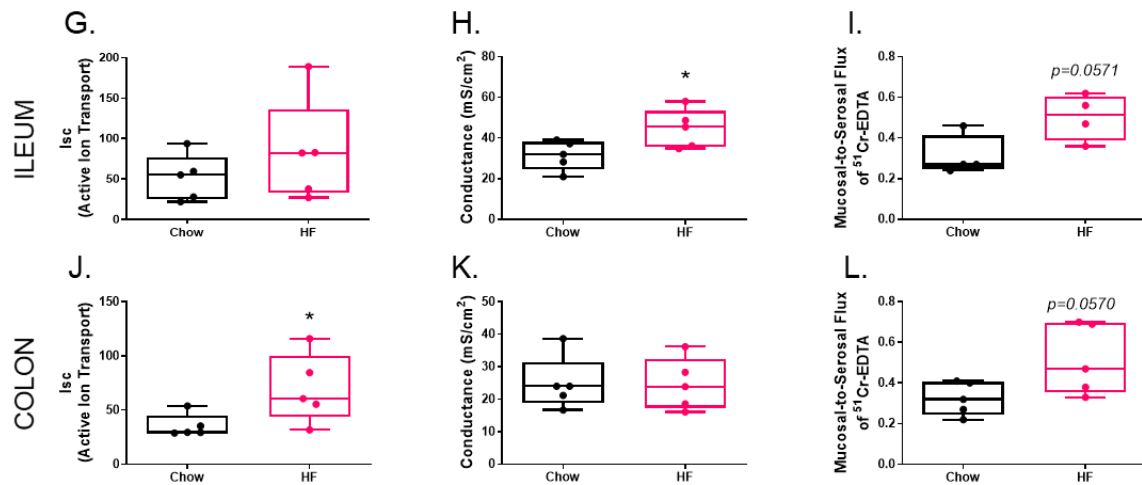


Figure 6.1.2. Ussing chamber assessments of intestines in chow and HF-fed mice.

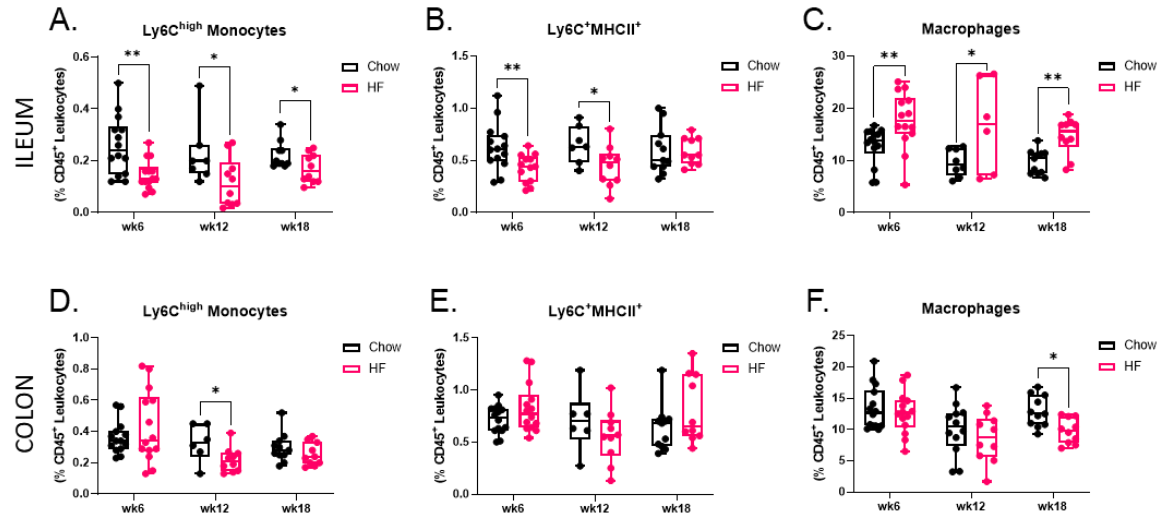
Intestinal permeability and physiology were assessed by *in vitro* Ussing chamber assay after 6 weeks (A-F) or 20 weeks (G-L) allocation to standard chow (Chow) or 60% high fat (HF) diet. Ileum tissue: (A,G) ion short current, (B,H) conductance, (C,I) paracellular permeability. Colon tissue: (D,J) ion short current, (E,K) conductance, (F,L) paracellular permeability. Each data point indicates an individual mouse. Data are presented as box and whisker plots, minimum to maximum, where the center line indicates the median. Data in A-F are pooled from two independent experiments of n=8 mice per group. Data in G-L are from one independent experiment of n=4-5 mice per group. Statistical significance was assessed by two-tailed Student's t test. * $p < 0.05$, *** $p < 0.001$.

colons of HF-fed mice in comparison to chow-fed mice (Figure 6.1.2D). Paracellular permeability, measured by mucosal-to-serosal flux of ^{51}Cr -EDTA, was not different in colon tissues after 6 weeks between diet groups (Figure 6.1.2F), but there was a significant increase in paracellular permeability of the ileum tissues of HF-fed mice compared to chow-fed mice (Figure 6.1.2C), which implied that the observed increase in intestinal permeability in HF-fed mice in comparison to chow-fed mice at 6 weeks by *in vivo* FITC-dextran assay (Figure 6.1.1D) is primarily due to loss of ileum tight junction barrier integrity. After 20 weeks, short-circuit current in HF-fed mouse colons was increased in comparison to chow-fed mouse colons (Figure 6.1.2J), as we had observed after 6 weeks (Figure 6.1.2D), indicative of a sustained difference in active ion transport. While not significant, likely due to limited sample size, there was a trend toward increased *in vitro* paracellular flux of ^{51}Cr -EDTA in both the ileum (as observed at 6 weeks) and the colon after 20 weeks (Figure 6.1.2I and 6.1.2L) in HF-fed mice compared to chow-fed mice, suggesting that both colon and ileum intestinal epithelium barrier changes may contribute to the higher intestinal permeability observed in HF-fed mice compared to chow-fed mice by the *in vivo* FITC-dextran assay at 18 weeks (Figure 6.1.1E). These experiments collectively showed that intestinal lengths, tissue integrity, and paracellular permeability, are altered between chow-fed and HF-fed mice within 6 weeks of diet allocation, and that these changes persist or even become exacerbated with increasing adiposity and HF diet exposure after 12 and 18 weeks.

Intestinal macrophages – prevalence and absolute cell counts

We used flow cytometry to assess monocyte and macrophage populations in whole tissue digestions of the ileum and colon. We began by examining the prevalence of

the monocyte-to-macrophage transition populations of Ly6C⁺MHCII⁻, Ly6C⁺MHCII⁺, and MHCII⁺ immune cells (Figure 6.1.3).



Intestinal monocyte and macrophage populations were assessed by flow cytometry in the colon and ileum after 6, 12, or 18 weeks of diet allocation to standard chow (Chow) or 60% high fat (HF) diet. Ileum prevalence (as a proportion of total CD45⁺ leukocytes) of: (A) Ly6C^{high} monocytes, (B) Ly6C⁺MHCII⁺ cells, (C) total MHCII⁺ macrophages. Colon prevalence (as a proportion of total CD45⁺ leukocytes) of: (D) Ly6C^{high} monocytes, (E) Ly6C⁺MHCII⁺ cells, (F) total MHCII⁺ macrophages. Each data point indicates an individual mouse. Data are presented as box and whisker plots, minimum to maximum, where the center line indicates the median. Data are pooled from 1-3 independent experiments of n=4-5 mice per group. Statistical significance was assessed by Student's two-tailed t test at each time point. **p* < 0.05, ***p* < 0.01.

In the ileum, we observed that Ly6C^{high} monocytes (as a proportion of total leukocytes) were consistently decreased in mice with HF diet-induced obesity compared to chow-fed mice (Figure 6.1.3A), with a reduction of Ly6C⁺MHCII⁺ transitional monocytes at 6 and 12 weeks in HF-fed mice in comparison to chow-fed mice (Figure 6.1.3B). MHCII⁺ macrophages (as a proportion of total leukocytes) in the ileum were increased at all time points in HF-fed mice in comparison to chow-fed mice (Figure 6.1.3C). In the colon, we observed that Ly6C^{high} monocytes (as a proportion of total leukocytes) in the HF-fed mice were no different from chow-fed mice after 6 weeks or 18 weeks, though there was a decrease after 12 weeks (Figure 6.1.3D). There were no

differences in the proportions of colon $\text{Ly6C}^+\text{MHCII}^+$ cells between diet groups at any time point (Figure 6.1.3E). Colon MHCII^+ macrophage prevalence was not different at 6 or 12 weeks, and was decreased at 18 weeks in HF-fed mice in comparison to chow-fed mice (Figure 6.1.3F).

We also considered absolute cell counts (i.e. numbers of cells). $\text{Ly6C}^{\text{high}}$ monocyte, transitional $\text{Ly6C}^+\text{MHCII}^+$ cells, and MHCII^+ macrophage cell counts were not significantly increased in either the ileums (Figure 6.1.4A-C) or colons (Figure 6.1.4G-I) of HF-fed mice compared to chow-fed mice. Cell counts of all three populations in HF-fed mice compared to chow-fed mice were consistently decreased at 6, 12, and 18 weeks in the ileums, despite an increase in the prevalence of MHCII^+ macrophages (Figure 6.1.3C). In the colons of HF-fed mice compared to chow-fed mice, $\text{Ly6C}^{\text{high}}$ monocytes and total MHCII^+ macrophages were decreased after 6 weeks, and $\text{Ly6C}^{\text{high}}$ monocytes and transitional $\text{Ly6C}^+\text{MHCII}^+$ cells were decreased after 12 weeks. As we had observed that the lengths of the small intestine and colon were decreased in mice with HF diet-induced obesity in comparison to chow-fed mice, we also adjusted cell counts by the tissue length (though it must be noted that this approach does not account for changes in tissue diameter and overall surface area). We found similar trends in the ileum (Figure 6.1.4D-F) and colon (Figure 6.1.4J-L). Therefore, in contrast to our hypothesis, compared to chow-fed mice, mice with HF diet-induced obesity did not have increased infiltration of circulating $\text{Ly6C}^{\text{high}}$ monocytes into ileum or colon tissues, nor an increase in the number of transitional $\text{Ly6C}^+\text{MHCII}^+$ cells or MHCII^+ macrophages.

We further examined macrophage populations by considering the prevalence (as a proportion of total macrophages) and numbers (as absolute cell counts) of $\text{CD4}^-\text{TIM4}^-$,

CD4⁺, and CD4⁺TIM4⁺ macrophages (as illustrated in Figure 1.2), in the ileum (Figure 6.1.5), and the colon (Figure 6.1.6).

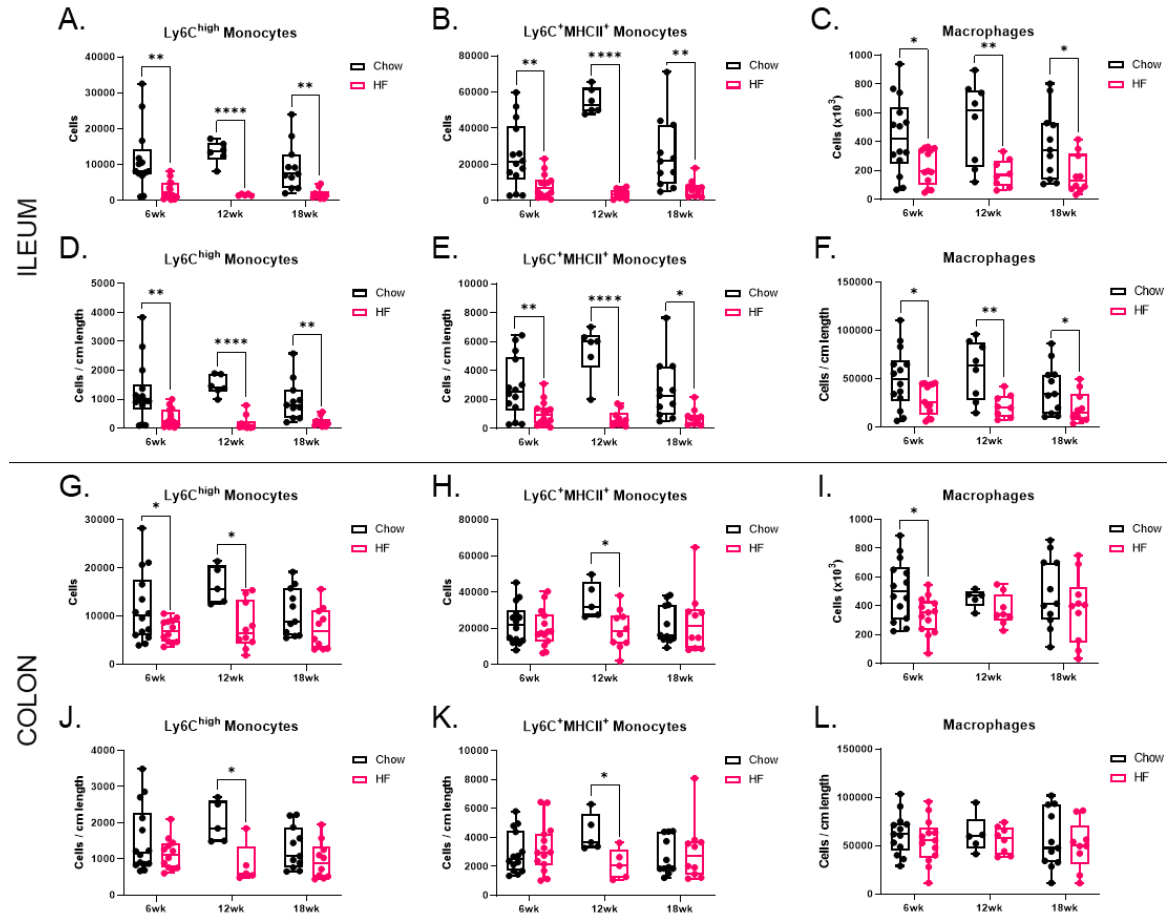


Figure 6.1.4. Intestinal monocyte and macrophage cell counts in chow and HF-fed mice.

Intestinal macrophage populations were assessed by flow cytometry in the colon and ileum after 6, 12, or 18 weeks of diet allocation to standard chow (Chow) or 60% high fat (HF) diet. Ileum absolute cell counts of: (A) Ly6C^{high} monocytes, (B) Ly6C⁺MHCII⁺ cells, (C) total MHCII⁺ macrophages. Ileum absolute cell counts per cm tissue length of: (D) Ly6C^{high} monocytes, (E) Ly6C⁺MHCII⁺ cells, (F) total MHCII⁺ macrophages. Colon absolute cell counts of: (G) Ly6C^{high} monocytes, (H) Ly6C⁺MHCII⁺ cells, (I) total MHCII⁺ macrophages. Colon absolute cell counts per cm tissue length of: (J) Ly6C^{high} monocytes, (K) Ly6C⁺MHCII⁺ cells, (L) total MHCII⁺ macrophages. Each data point indicates an individual mouse. Data are presented as box and whisker plots, minimum to maximum, where the center line indicates the median. Data are pooled from 1-3 independent experiments of n=4-5 mice per group. Statistical significance was assessed by Student's two-tailed t test at each time point. **p*<0.05, ***p*<0.01, ****p*<0.001, *****p*<0.0001.

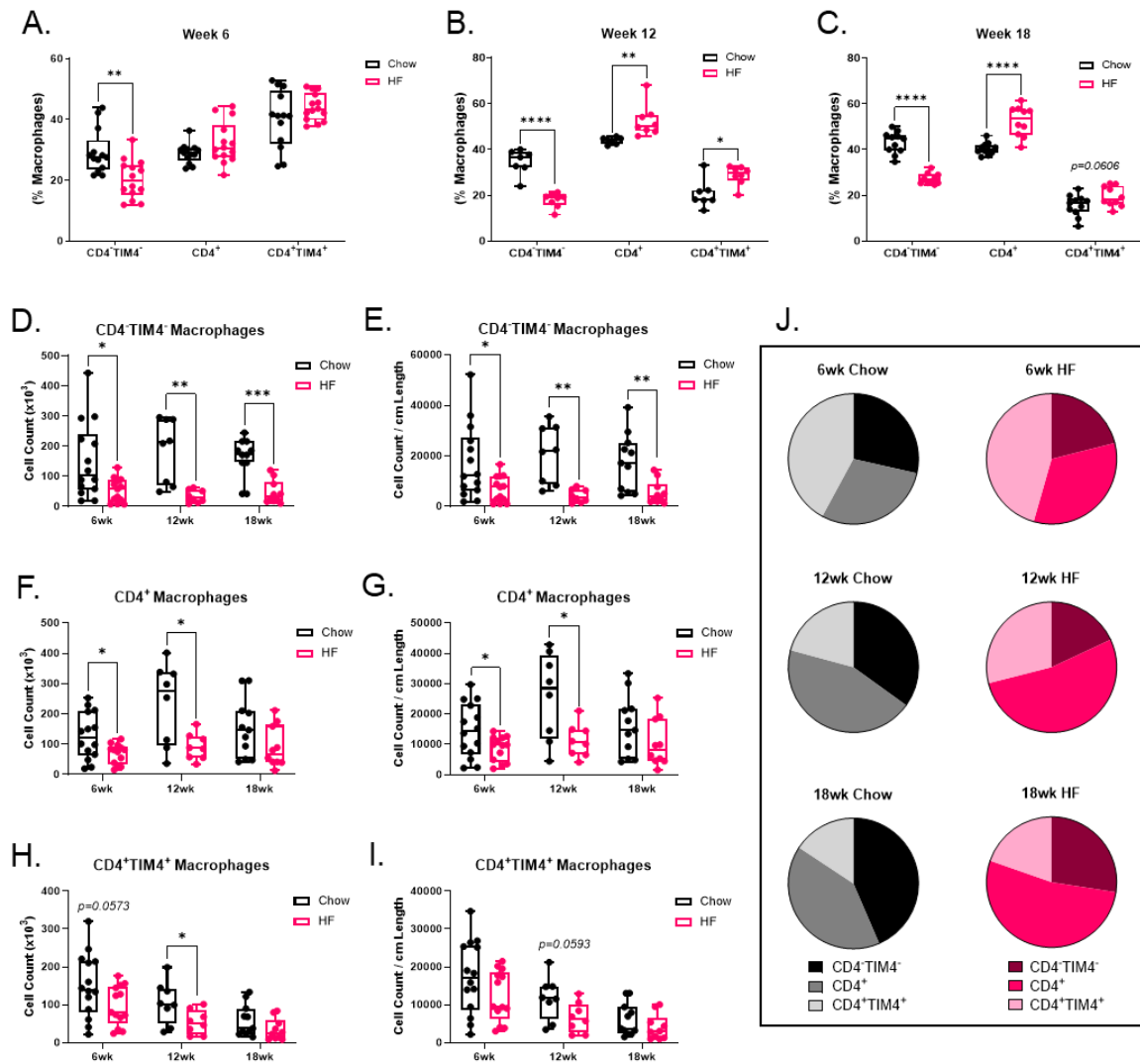


Figure 6.1.5. Ileum macrophage populations in chow and HF-fed mice.

Ileum CD4⁺TIM4⁻, CD4⁺, and CD4⁺TIM4⁺ macrophage populations were assessed by flow cytometry after 6, 12, or 18 weeks allocation to standard chow (Chow) or 60% high fat (HF) diet. Ileum CD4⁺TIM4⁻, CD4⁺, and CD4⁺TIM4⁺ macrophages (as a proportion of total macrophages) after: (A) 6 weeks, (B) 12 weeks, (C) 18 weeks. (D,F,H) absolute cell counts of ileum macrophage populations. (E,G,I) absolute cell counts of macrophages normalized by ileum length. (J) Pie graph summaries of mean prevalence of each macrophage population by assessed time point. Each data point in A-I indicates an individual mouse and data are presented as box and whisker plots, minimum to maximum, with the center line at the median. Data are pooled from 2-3 independent experiments of n=4-5 mice per group. Statistical significance was assessed by Student's two-tailed t test at each time point. * $p < 0.05$, ** $p < 0.01$, *** $p < 0.001$, **** $p < 0.0001$.

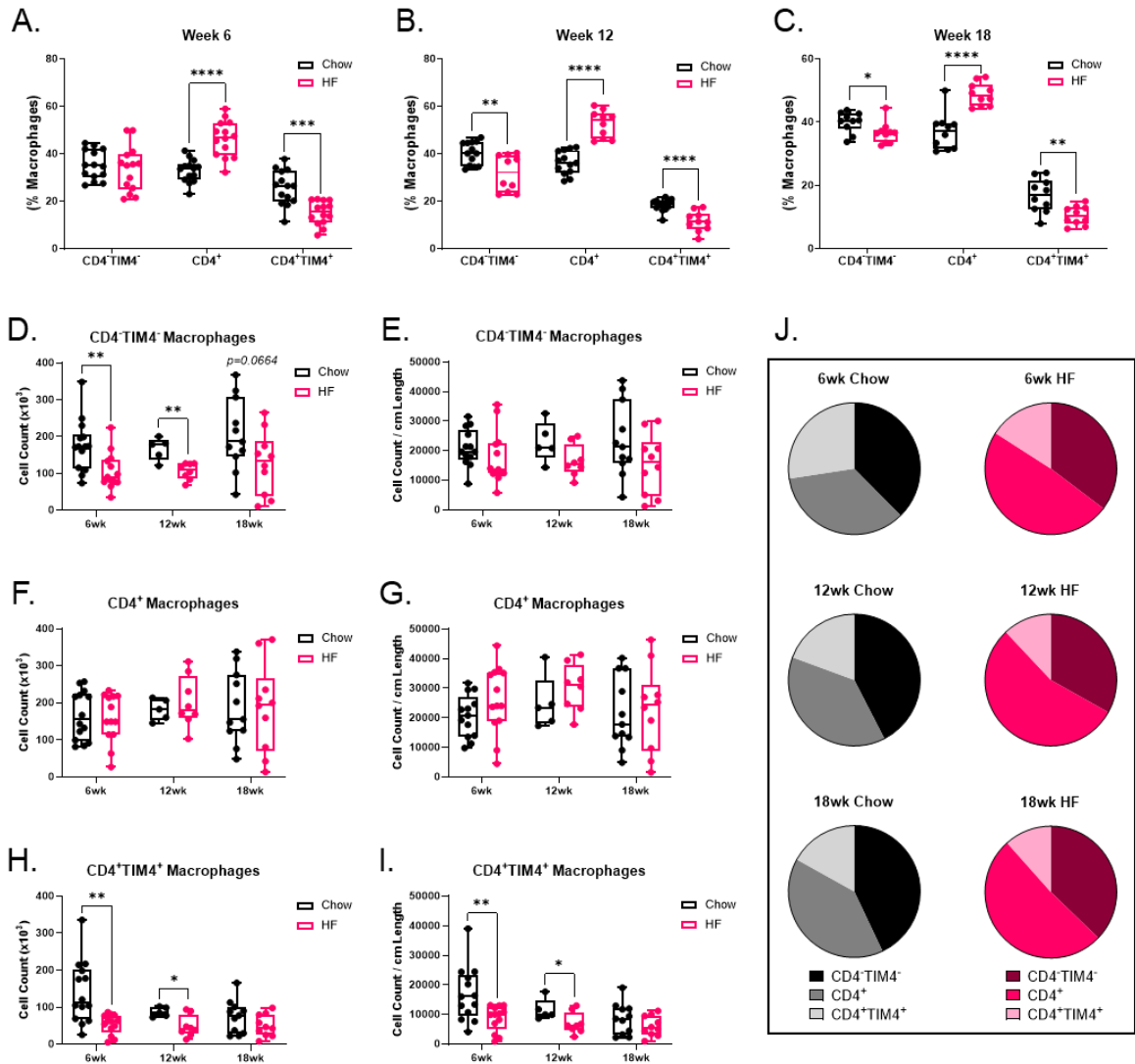


Figure 6.1.6. Colon macrophage populations in chow and HF-fed mice.

Colon CD4⁺TIM4⁻, CD4⁺, and CD4⁺TIM4⁺ macrophage populations were assessed by flow cytometry after 6, 12, or 18 weeks allocation to standard chow (Chow) or 60% high fat (HF) diet. Colon CD4⁺TIM4⁻, CD4⁺, and CD4⁺TIM4⁺ macrophages after: (A) 6 weeks, (B) 12 weeks, (C) 18 weeks. (D,F,H) absolute cell counts of colon macrophage populations. (E,G,I) absolute cell counts of macrophages normalized by colon length. (J) Pie graph summaries of mean prevalence of each macrophage population by assessed time point. Each data point in A-I indicates an individual mouse and data are presented as box and whisker plots, minimum to maximum, with the center line at the median. Data are pooled from 2-3 independent experiments of n=4-5 mice per group. Statistical significance was assessed by Student's two-tailed t test at each time point. **p*<0.05, ***p*<0.01, ****p*<0.001, *****p*<0.0001.

In the ileums of HF-fed mice in comparison to chow-fed mice, there was a consistent decrease in CD4⁻TIM4⁻ macrophage prevalence (Figure 6.1.5A-C), absolute cell counts (Figure 6.1.5D), and absolute cell counts adjusted to tissue length (Figure 6.1.5E) at 6, 12 and 18 weeks, consistent with our observations of decreases in Ly6C^{high} monocyte and transitional and Ly6C⁺MHCII⁺ cell populations (Figures 6.1.3A-B; 6.1.4A-B, D-E). In HF-fed mice the proportions of ileum CD4⁺ and CD4⁺TIM4⁺ macrophages were both increased at 12 weeks in comparison to chow-fed mice (Figure 6.1.5B), though total cell counts of these populations were decreased (Figure 6.1.5F-I). CD4⁻TIM4⁻, CD4⁺, and CD4⁺TIM4⁺ macrophage population dynamics were also altered in the colon. In comparison to chow-fed mice, HF-fed mice had a significantly reduced prevalence of CD4⁺TIM4⁺ macrophages and an increase in CD4⁺ macrophages (as a proportion of total macrophages) after 6, 12, and 18 weeks (Figure 6.1.6A-C). Assessment of absolute cell counts indicated that the number of CD4⁺ macrophages in the colon was similar between chow-fed and HF-fed mice after all assessed time points (Figure 6.1.6F-G), while CD4⁻TIM4⁻ and CD4⁺TIM4⁺ cell counts were decreased in HF-fed mice compared to chow-fed mice at 6 and 12 weeks (Figure 6.1.6D-E; H-I).

Intestinal macrophages – proliferation

As we consistently observed decreases in cell counts of Ly6C^{high} monocytes, transitional Ly6C⁺MHCII⁺ macrophages, and CD4⁻TIM4⁻ macrophages in the ileums of HF-fed mice in comparison to chow-fed mice (Figures 6.1.3 to 6.1.5), our data suggested that there may be reduced recruitment of monocytes to the ileum to replenish macrophage populations in response to effects of diet-induced obesity. The reduction of intestinal macrophage numbers could also be due to a concomitant decrease in local self-renewal

of macrophages or loss of proliferative capacity of newly recruited monocyte-derived macrophages^{214, 220}. We assessed chow-fed and HF-fed mouse macrophage proliferation in the ileum and colon by flow cytometry, combining surface staining with intracellular staining of nuclear cell proliferation marker Ki67 (Figure 6.1.7).

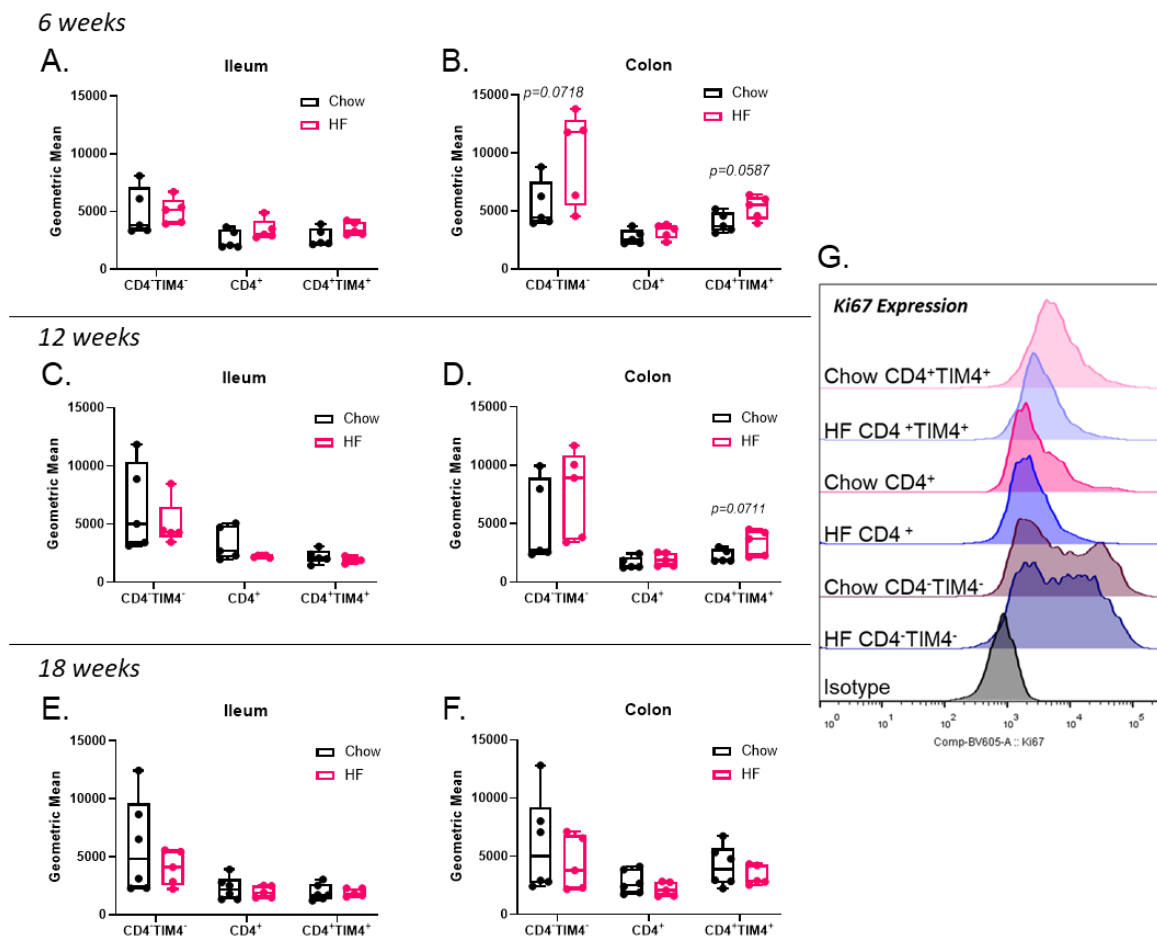


Figure 6.1.7. Colon and ileum macrophage proliferation in chow and HF-fed mice.

Macrophage proliferation was assessed by flow cytometry analysis of intracellular Ki67 expression in CD4⁺TIM4⁻, CD4⁺, and CD4⁺TIM4⁺ macrophages of mice fed standard chow (Chow) or 60% high fat (HF) diet for 6, 12 or 18 weeks. Ileum: (A) 6 weeks, (C) 12 weeks, (E) 18 weeks. Colon: (B) 6 weeks, (D) 12 weeks, (F) 18 weeks. (G) Representative histograms of Ki67 staining in CD4⁺TIM4⁻, CD4⁺, and CD4⁺TIM4⁺ macrophages from mice fed chow or high fat diet. Data are reported as geometric mean fluorescence intensity. Each data point indicates an individual mouse. Data are presented as box and whisker plots, minimum to maximum, where the center line indicates the median. Data are from one independent experiment at each time point of n=5-6 mice per group. Statistical significance was assessed by Student's two-tailed t test at each time point.

We observed that the Ki67 staining pattern was different according to CD4 and TIM4 expression, with CD4⁻TIM4⁻ macrophages of both chow-fed and HF-fed mice showing the highest levels of staining (Figure 6.1.7G), consistent with their more recent recruitment from monocyte precursors to replace tissue macrophages^{214, 408, 409}. There were no significant differences of Ki67 staining after 6, 12 or 18 weeks diet allocation between chow or HF diet groups in CD4⁻TIM4⁻, CD4⁺, or CD4⁺TIM4⁺ macrophages in the ileum (Figure 6.1.7A,C,E) or colon (Figure 6.1.7B,D,F). Therefore, HF diet-induced obesity did not appear to alter the self-renewal rate of longer-lived embryonic origin CD4⁺TIM4⁺ macrophages or longer-lived monocyte-derived CD4⁺ macrophages. Nor was the proliferation of rapidly recruited monocyte-derived CD4⁻TIM4⁻ macrophages changed in HF-fed mice compared to chow-fed mice. These results suggested that reduced monocyte recruitment, rather than a reduction in local macrophage proliferation, is a significant contributor to the sustained reduction in macrophage cell counts observed in the ileums of mice with HF diet-induced obesity in comparison to chow-fed mice.

Intestinal macrophages – surface phenotype

We further assessed macrophage surface expression of Ly6C, CD11b, CD64, CCR2, F4/80, and MHCII, as well as the intestinal tissue macrophage markers CD4 and TIM4, in the ileum (Table 6.1.1) and the colon (Table 6.1.2). As shown in Figure 1.2, as monocytes become intestinal tissue macrophages, they progressively lose expression of Ly6C and CCR2 while increasing their expression of CD64, F4/80, and MHCII. Additional details about these cell surface proteins are provided in Appendix I.

Table 6.1.1. Surface marker expression of ileum macrophages from chow and HF-fed mice.

Marker	CD4 ⁺ TIM4 ⁻			CD4 ⁺			CD4 ⁺ TIM4 ⁺		
	6wk	12wk	18wk	6wk	12wk	18wk	6wk	12wk	18wk
Ly6C	↓ * p=0.0234	↓ * p=0.0167	↓ * p=0.0380	↓ *** p=0.0008	↓ ** p=0.0035	↓ ** p=0.0091	↓ ** p=0.0026	↓ * p=0.0120	↓ * p=0.0323
CD11b	↓ *** p<0.0001	↓ *** p<0.0001	↓ *** p<0.0001	↓ *** p<0.0001	↓ *** p<0.0001	↓ *** p<0.0001	↓ *** p<0.0001	↓ *** p<0.0001	↓ *** p<0.0001
CD64	ns	↓ * p=0.0139	↓ * p=0.0242	↓ ** p=0.0032	↓ ** p=0.0016	↓ *** p=0.0004	↓ *** p<0.0001	↓ ** p=0.0025	↓ *** p=0.0001
CCR2	↓ ** p=0.0016	↓ *** p<0.0001	↓ *** p=0.0001	↓ ** p=0.0054	↓ *** p<0.0001	↓ *** p=0.0005	↓ ** p=0.0016	↓ *** p<0.0001	↓ *** p=0.0006
F4/80	ns	ns	ns	ns	↑ * p=0.0141	ns	ns	↑ * p=0.0200	ns
MHCII	ns	↑ *** p=0.0001	↑ ** p=0.0030	↑ ** p=0.0082	↑ *** p<0.0001	↑ *** p<0.0001	↑ ** p=0.0028	↑ *** p<0.0001	↑ *** p<0.0001
CD4	--	--	--	ns	ns	ns	↓ * p=0.0173	ns	ns
TIM4	--	--	--	--	--	--	↓ ** p=0.0015	↓ * p=0.0236	↓ * p=0.0369

Data are shown comparing HF to Chow mouse macrophages (e.g. CD4⁺TIM4⁻ macrophages from HF-fed mice in comparison to chow-fed mice have significantly lower expression of Ly6C after 6 weeks diet allocation). Geometric mean expression of each surface marker was combined from 2-3 independent experiments of n=4-5 mice per group by normalizing the data from each mouse to the mean of the chow mouse group in each independent experiment. This approach was taken to account for variation in cytometer settings between experiments.

Table 6.1.2. Surface marker expression of colon macrophages from chow and HF-fed mice.

Marker	CD4 ⁺ TIM4 ⁻			CD4 ⁺			CD4 ⁺ TIM4 ⁺		
	6wk	12wk	18wk	6wk	12wk	18wk	6wk	12wk	18wk
Ly6C	ns	ns	ns	ns	ns	ns	↑ * p=0.0236	ns	ns
CD11b	↓ *** p<0.0001	↓ *** p<0.0001	↓ *** p<0.0001	↓ *** p<0.0001	↓ *** p<0.0001	↓ *** p<0.0001	↓ * p=0.0220	↓ * p=0.0339	↓ *** p<0.0001
CD64	ns	ns	ns	ns	↓ * p=0.0181	↓ * p=0.01121	ns	ns	ns
CCR2	ns	↓ ** p=0.0037	ns	ns	ns	ns	↓ ** p=0.0055	ns	ns
F4/80	ns	ns	ns	ns	ns	↓ ** p=0.0085	ns	ns	ns
MHCII	↑ ** p=0.0298	ns	ns	↑ *** p<0.0001	↑ * p=0.0159	↑ *** p=0.0007	↑ ** p=0.0062	↑ * p=0.0437	↑ *** p<0.0001
CD4	--	--	--	ns	ns	↓ *** p=0.0004	↓ ** p=0.0078	ns	↓ *** p<0.0001
TIM4	--	--	--	--	--	--	ns	↓ * p=0.0293	↓ *** p=0.0001

Data are shown comparing HF to Chow mouse macrophages (e.g. CD4⁺TIM4⁻ macrophages from HF-fed mice in comparison to chow-fed mice have significantly lower expression of CD11b after 6 weeks diet allocation). Geometric mean expression of each surface marker was combined from 2-3 independent experiments of n=4-5 mice per group by normalizing the data from each mouse to the mean of the chow mouse group in each independent experiment. This approach was taken to account for variation in cytometer settings between experiments.

Assessment of surface expression revealed that CD4⁻TIM4⁻, CD4⁺, and CD4⁺TIM4⁺ macrophages at almost all time points in the ileums of HF-fed mice, in comparison to chow-fed mice, had reduced surface expression of Ly6C, CD11b, CD64, and CCR2. In comparison to macrophages in chow-fed mice, MHCII expression was increased on all ileum macrophage populations from HF-fed mice, and TIM4 expression was decreased on CD4⁺TIM4⁺ macrophages. As in the ileum, all colon macrophage populations of HF-fed mice consistently had lower expression of CD11b, whereas CD4⁺ and CD4⁺TIM4⁺ macrophages had higher MHCII expression, in comparison to colon macrophages from chow-fed mice. In HF-fed mice compared to chow-fed mice, colon CD4⁺ macrophages had decreased CD64 expression at 12 and 18 weeks, and at 18 weeks both CD4 and TIM4 expression were decreased on CD4⁺ and CD4⁺TIM4⁺ populations. These data collectively indicated that there are tissue-specific effects of HF diet-induced obesity on intestinal macrophage surface phenotype.

Intestinal macrophages – intracellular cytokine expression

A critical characteristic of intestinal macrophage maintenance of homeostasis is their constitutive expression of IL-10, which supports an anti-inflammatory and tolerogenic intestinal environment^{236, 461, 483, 496, 671}. Intestinal macrophages also produce low levels of TNF²³⁶, which is involved in maintenance of the intestinal epithelium^{672, 673}. We predicted that intestinal macrophages from mice with diet-induced obesity would have reduced expression of IL-10, and increased expression of TNF, in comparison to macrophages from lean mice fed the standard chow diet. We assessed intracellular expression of these cytokines in ileum and colon macrophages by flow cytometry. Intestinal macrophages are typically hyporesponsive to PRR stimuli like LPS^{223, 236, 433, 459},

⁴⁸³, and we also found this to be the case in pilot experiments (Appendix II A-B). We showed that intestinal permeability is increased in mice with HF diet-induced obesity in comparison to lean chow-fed mice (Figures 6.1.1 and 6.1.2), so we assumed that any bacteria or antigens that crossed the epithelial barrier due to increased permeability would have already influenced macrophage polarization and inflammatory character, and accordingly decided to examine basal cytokine production in the absence of stimulation.

In both the colon and ileum, we observed that CD4⁻TIM4⁻, CD4⁺, and CD4⁺TIM4⁺ macrophages generally had differential expression of IL-10 and TNF, irrespective of diet, with the greatest cytokine expression in CD4⁺TIM4⁺ macrophages (Figure 6.1.8). However, our hypothesis was not true for any macrophage population after 6, 12, or 18 weeks diet allocation. IL-10 production was similar in ileum macrophages from chow-fed and HF-fed mice after 6 weeks (Figure 6.1.8A), but in mice with HF diet-induced obesity in comparison to chow-fed lean mice, IL-10 was increased in ileum CD4⁻TIM4⁻ and CD4⁺ macrophages after 12 weeks (Figure 6.1.8B), and in CD4⁻TIM4⁻ macrophages after 18 weeks (Figure 6.1.8C). TNF expression was significantly decreased in all ileum macrophages of HF-fed mice in comparison to chow-fed mice after 6 weeks (Figure 6.1.8D), and in CD4⁺ and CD4⁺TIM4⁺ macrophages after 12 weeks (Figure 6.1.8E), but no differences were detected by 18 weeks (Figure 6.1.8F). In the colon, there was also evidence of temporal changes in IL-10 and TNF expression within all macrophage populations. After 6 and 12 weeks diet allocation, colon macrophages from chow-fed mice generally had lower expression of IL-10 (Figure 6.1.8G-H), and higher expression of TNF (Figure 6.1.8J-K), in comparison to HF-fed mice.

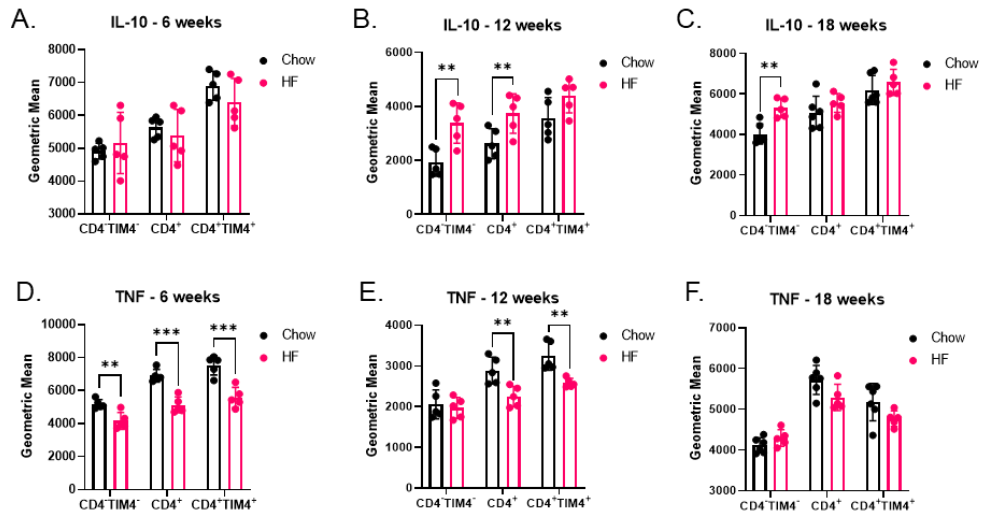
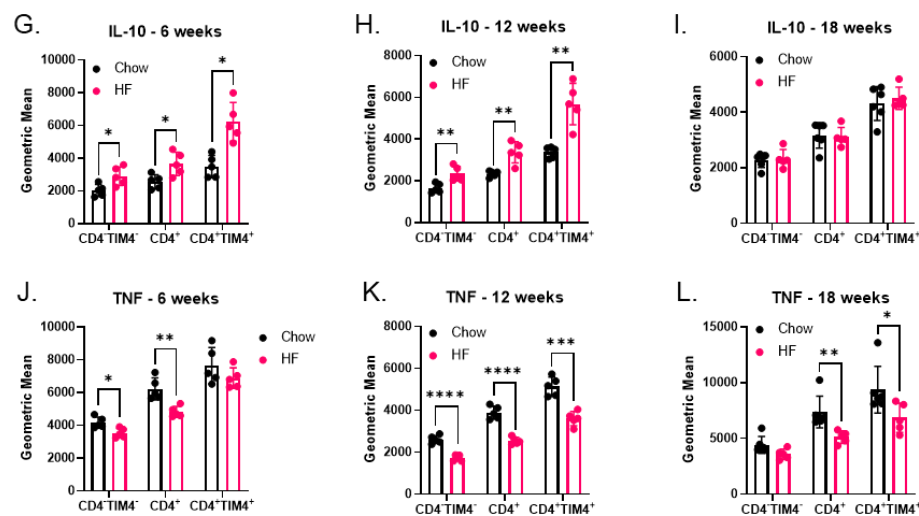
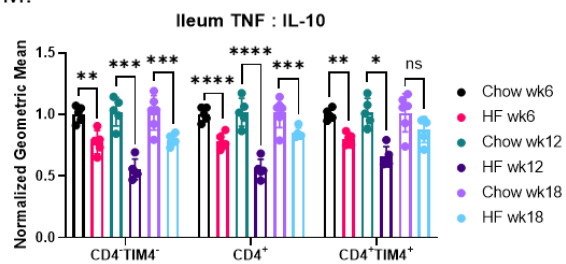
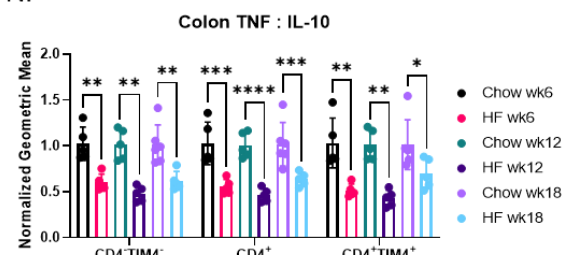
Ileum*Colon***M.****N.**

Figure 6.1.8. TNF and IL-10 expression in ileum and colon macrophages of chow and HF-fed mice.

Ileum and colon CD4⁻TIM4⁻, CD4⁺, and CD4⁺TIM4⁺ macrophage intracellular expression of TNF and IL-10 was assessed by flow cytometry after 6, 12, or 18 weeks of allocation to standard control chow (Chow) or 60% high fat (HF) diet. Ileum macrophage intracellular expression of IL-10 after: (A) 6 weeks, (B) 12 weeks, (C) 18 weeks. Ileum macrophage intracellular expression of TNF after: (D) 6 weeks, (E) 12 weeks, (F) 18 weeks. Colon macrophage intracellular expression of IL-10 after: (G) 6 weeks, (H) 12 weeks, (I) 18 weeks. Colon macrophage intracellular expression of TNF after: (J) 6 weeks, (K) 12 weeks, (L) 18 weeks. The ratio of TNF : IL-10 expression was compared across experiments by normalizing the geometric mean data from each mouse to the mean of the chow mouse group for each macrophage population in each independent experiment for (M) ileum macrophages and (N) colon macrophages. Each data point indicates an individual mouse. Data in A-L are reported as geometric mean fluorescence intensity. Data are from one independent experiment at each time point of n=5-6 mice per group. Data in A-L are presented as box and whisker plots, minimum to maximum, where the center line indicates the median. Data in M and N are presented with box height at the mean with error bars at \pm standard deviation. Statistical significance was assessed by Student's two-tailed t test for each macrophage subset at each time point. * $p < 0.05$, ** $p < 0.01$, *** $p < 0.001$, **** $p < 0.0001$.

After 18 weeks, there were no differences in production of IL-10 within colon macrophages between the diet groups (Figure 6.1.8I), and TNF expression was similar in CD4⁻TIM4⁻ macrophages (Figure 6.1.8L), though mice with HF diet-induced obesity had lower expression of TNF in CD4⁺ and CD4⁺TIM4⁺ colon macrophages in comparison to lean chow-fed mice. We also plotted our data as a ratio of TNF to IL-10 expression (Figure 6.1.8M-N). These comparisons further illustrated that the intestinal macrophages from mice with diet-induced obesity have altered cytokine expression profiles, though there are temporal differences in expression. Overall, these data showed that intestinal macrophages from mice with HF diet-induced obesity, in comparison to lean chow-fed mice, generally had higher basal-level expression of IL-10, and lower expression of TNF, though there were temporal and tissue-specific changes between and within diet groups.

Intestinal eosinophils, neutrophils, and CD4⁺ T cells

As macrophages communicate directly and indirectly with other immune cell populations in the intestines to maintain homeostasis⁴⁰⁵, we also examined the prevalence of eosinophils, neutrophils, and CD4⁺ T cells in the ileum and colon (Figure 6.1.9).

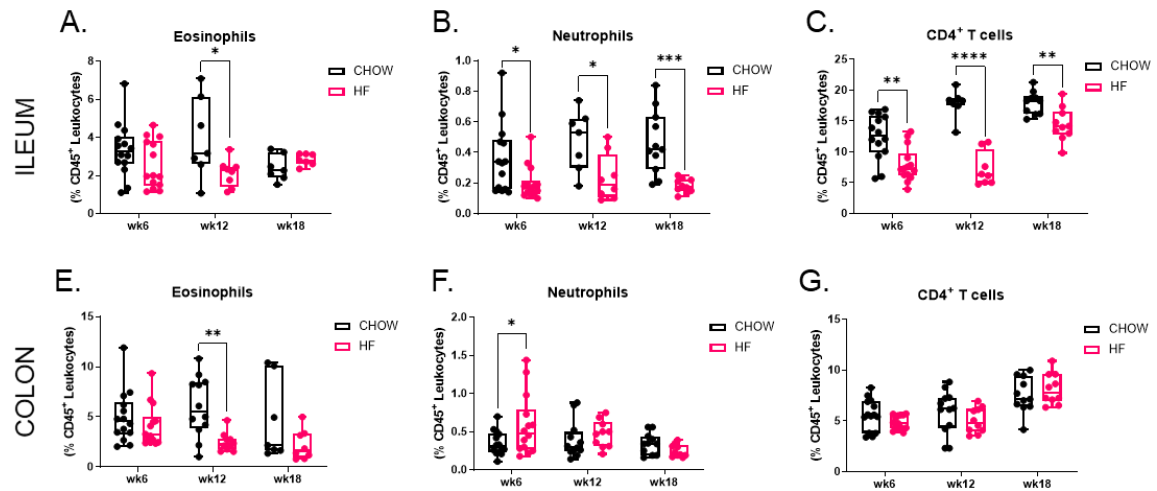


Figure 6.1.9. Colon and ileum eosinophils, neutrophils, and CD4⁺ T cells.

Intestinal immune cell populations were assessed after 6, 12, or 18 weeks of allocated chow (Chow) or 60% high fat (HF) diet. Ileum prevalence (as a proportion of total CD45⁺ leukocytes) of: (A) eosinophils, (B) neutrophils, (C) CD4⁺ T cells. Colon prevalence (as a proportion of total CD45⁺ leukocytes) of: (E) eosinophils, (F) neutrophils, (G) CD4⁺ T cells. Each data point indicates an individual mouse. Data are presented as box and whisker plots, minimum to maximum, where the center line indicates the median. Data are pooled from 2-3 independent experiments of $n=4-5$ mice per group. Statistical significance was assessed by Student's two-tailed t test at each time point. * $p < 0.05$, ** $p < 0.01$, *** $p < 0.001$, **** $p < 0.0001$.

In the ileum, the prevalence of eosinophils was decreased in mice on HF diet compared to mice on chow diet after 12 weeks (Figure 6.1.9A), while the prevalence of neutrophils (Figure 6.1.9B) and CD4⁺ T cells was decreased at all time points in HF-fed mice compared to chow-fed mice (Figure 6.1.9C). In the colon, we observed that HF-fed mice likewise had a reduced prevalence of eosinophils in comparison to chow-fed mice after 12 weeks (Figure 6.1.9E) but not the other time points, and that the prevalence of neutrophils (Figure 6.1.9F) was increased in HF-fed mice compared to chow-fed mice after 6 weeks, but was not significantly different after 12 or 18 weeks. The prevalence of CD4⁺ T cells in the colon was not affected at any time point (Figure 6.1.9G). Absolute cell counts showed the same trends (data not shown). These data demonstrate, as we observed for intestinal monocytes and macrophages, that there are dynamically regulated changes in intestinal immune cell populations due to diet-induced obesity.

6.1.3 Discussion

Our data showed that female mice with HF diet-induced obesity, in comparison to chow-fed lean mice, had decreased small intestine and colon lengths within 6 weeks diet allocation. Whole-intestine *in vivo* permeability was increased after 6 weeks, as well as 18 weeks, in HF-fed mice compared to chow-fed mice (Figure 6.1.1). Ussing chamber *in vitro* assessments showed that mice with diet-induced obesity, in comparison to lean mice, had increased colon active ion transport after 6 and 20 weeks, increased ileum paracellular permeability within 6 weeks, increased ileum conductance after 20 weeks, and a trend toward increased paracellular permeability in the colon and ileum within 20 weeks (Figure 6.1.2). HF-fed mice, in comparison to chow-fed mice, had tissue and time-dependent changes in the prevalence of eosinophil, neutrophil, and CD4⁺ T cell populations (Figure 6.1.9). Intestinal macrophages (total and CD4⁻TIM4⁻, CD4⁺, and CD4⁺TIM4⁺ populations) had similar proliferation in HF-fed and chow-fed mice, but there were obesity-associated changes to their proportional prevalence, numbers, surface phenotype, and intracellular production of cytokines IL-10 and TNF, and these changes occurred in a tissue-specific and time-dependent manner (Figures 6.1.3 to 6.1.8). Therefore, intestinal physiology, permeability, and immune cell populations were altered in female mice fed a high fat diet compared to female mice fed a standard chow diet.

We observed in the ileum tissue in HF-fed female mice, in comparison to chow-fed mice, that there was a depletion of CD4⁻TIM4⁻ and CD4⁺ macrophage numbers within 6 weeks, and CD4⁻TIM4⁻ macrophage numbers remained lower even after 18 weeks in HF-fed mice in comparison to chow-fed mice. Macrophage proliferation rates remained similar between chow and HF-fed mice, but there was a significant reduction in the

numbers of Ly6C^{high} monocytes in the ileums of HF-fed mice compared to chow-fed mice, suggesting that the reduction of CD4⁻TIM4⁻ macrophages occurred because they were not being replenished from monocytes. In addition, ileum CD4⁺TIM4⁺ macrophages had lower expression of CD64 and TIM4 in HF-fed mice compared to chow-fed mice. Both TIM4 and CD64 have been independently implicated in phagocytic activities of macrophages^{674, 675, 676, 677}, so decreased expression of either marker could have a detrimental impact on phagocytosis, and in particular efferocytosis of apoptotic cells. As monocytes mature into macrophages, they reduce their expression of Ly6C and CCR2, and increase their expression of MHCII, F4/80, and CD64 (Appendix I). We observed that ileum CD4⁻TIM4⁻ macrophages from HF-fed mice, in comparison to chow-fed mice, consistently had lower expression of Ly6C and CCR2, which may also indicate that they are not replenished from blood monocytes at the same rate as CD4⁻TIM4⁻ macrophages in chow-fed mice. In the colon, we observed that CD4⁻TIM4⁻ and CD4⁺TIM4⁺ macrophage numbers were decreased in HF-fed mice in comparison to chow-fed mice within 6 weeks, but CD4⁺ macrophages remained similar through to 18 weeks. Similar to the ileum, proliferation assessed by Ki67 was not different between diet groups at any time point in the colon, so the decrease in CD4⁻TIM4⁻ macrophages was likely due to reduced Ly6C^{high} monocyte recruitment, as we observed after 6 weeks and 12 weeks in HF-fed mice compared to chow-fed mice.

One of the most interesting findings from these experiments was that all intestinal macrophages in HF-fed mice had similar or significantly increased expression of IL-10, and similar or decreased expression of TNF, in comparison to macrophages from chow-fed mice, whereas we had predicted the opposite. Macrophages decrease their surface

expression of CD64 after treatment with IL-10⁶⁷⁸, and we observed that ileal macrophages in particular consistently had lower expression of CD64 in HF-fed mice in comparison to chow-fed mice, so there may be autocrine effects of the increased IL-10 production in macrophages of HF-fed mice. The ratio of TNF to IL-10 expression remained lower for all macrophage populations at all timepoints (except for CD4⁺TIM4⁺ macrophages in the ileum after 18 weeks). MHCII was consistently higher on CD4⁺ and CD4⁺TIM4⁺ macrophages in the colons and ileums of HF-fed mice compared with chow-fed mice. MHCII is typically upregulated on macrophages in response to local inflammation^{679, 680}. Future studies should directly measure intestinal tissue inflammatory cytokine expression and also consider functional assays of macrophage phagocytic activities after cell-sorting CD4⁻TIM4⁻, CD4⁺, and CD4⁺TIM4⁺ macrophages, to further interpret the changes in macrophage surface phenotype that we observed between chow-fed and HF-fed mice. In addition, further studies with IL-10-deficient (IL10^{-/-}) mice may help to disentangle the effects of IL-10 and diet-induced obesity on intestinal inflammation, permeability, and macrophage populations. IL10^{-/-} mice spontaneously develop chronic intestinal inflammation⁶⁸¹. It has also been reported that specific knockout of hematopoietic cell-derived IL-10 does not increase adipose or liver tissue inflammation or insulin resistance in mice fed a HF diet⁶⁸², but effects within the intestines have not been evaluated.

By considering several time points in our assessments, we observed that there were changes to macrophage population dynamics even in chow-fed mice between 6 and 18 weeks diet allocation (Figures 6.1.5 and 6.1.6). These changes were not unexpected, as under conditions of homeostasis, there is a gradual accumulation of monocyte-derived

macrophages post-birth that has been reported to stabilize at ~12 weeks of age in the colon and at ~20 weeks of age in the small intestine²¹⁴. The chow-fed mice were ~11 weeks of age after 6 weeks diet allocation, and ~23 weeks of age after 18 weeks diet allocation. It has been generally proposed that there is a limited space within tissue niches for macrophages, so while total macrophage numbers remain similar, the proportion of monocyte-derived macrophages gradually increases post-birth until, as mentioned, a plateau is reached after ~12-20 weeks, depending on localization within the intestines^{196, 211, 252}. Our observations are in accord with those data and concepts. Total macrophage numbers remained similar across 6, 12, and 18 weeks diet allocation in chow-fed mice. We observed that there were changes in the CD4⁻TIM4⁻, CD4⁺, and CD4⁺TIM4⁺ macrophage populations (as a proportion of total macrophages) between 6 and 12 weeks diet allocation (in the colon and ileum), and 12 and 18 weeks diet allocation (particularly in the ileum), with a decrease in embryonic origin CD4⁺TIM4⁺ macrophages and an increase in monocyte-derived CD4⁻TIM4⁻ macrophages. Macrophage population dynamics did not change as much over time in the colons of HF-fed mice compared to chow-fed mice (Figure 6.1.6J), remaining similar after 6, 12, and 18 weeks diet allocation, whereas CD4⁺TIM4⁺ and CD4⁻TIM4⁻ macrophage dynamics continued to change in the ileums of HF-fed mice between 12 and 18 weeks diet allocation (Figure 6.1.5J). Given these changes in macrophage population composition, and the reduction in numbers of macrophages in HF-fed mice compared to chow-fed mice, particularly in the ileum, it would be interesting in future experiments to determine if placing mice on a high fat diet once intestinal macrophage populations are stabilized (i.e. after 20 weeks of age) would have similar effects on monocyte recruitment and macrophage population

characteristics. Given the post-birth recruitment of macrophages, diet-induced obesity in young mice could have more severe long-term effects on intestinal function than in more mature mice.

Overall, our observations on the effects of diet-induced obesity on macrophage populations in the ileum and the colon are distinct from previous reports^{89, 640, 659, 660, 661}, but likely reflect differences in diet composition and length of feeding prior to assessment, macrophage identification methods, and/or biological sex (the previous studies used male mice or sex was not specified). Our data are also distinct from reports of changes to macrophage populations in other metabolic tissues in the context of diet-induced obesity, such as increased macrophage accumulation and pro-inflammatory cytokine production in adipose tissue^{50, 51}, as well as the pancreas⁸⁷, liver⁵⁶, and skeletal muscle^{72, 86}. Furthermore, our data suggest that effects of (diet-induced) obesity-associated chronic inflammation on intestinal monocyte and macrophage populations are unique from effects due to inflammatory responses to intestinal infection or genetic or chemically-induced colitis.

6.2 The role of TNF in diet-induced obesity

6.2.1 Introduction

TNF is constitutively produced within the intestines at low levels by enterocytes within the intestinal epithelium, stromal cells, and by macrophages and other immune cells^{683, 684}, and has roles in homeostatic maintenance and repair of the intestinal epithelial barrier^{656, 672, 684, 685, 686}, and immune function^{673, 687}. However, elevated levels of TNF are well-documented in intestinal parasitic and bacterial infections in humans and mice^{433, 475, 477, 686}, inflammatory bowel disease in humans^{688, 689}, and genetic (e.g. IL10^{-/-}, Casp8 Δ IEC) and chemically-induced (e.g. DSS, TNBS) mouse models of intestinal sterile inflammation^{435, 665, 690, 691, 692}.

As described in Chapter 1, monocytes that infiltrate into the intestinal mucosa in response to inflammation, and monocyte-derived macrophages, are potent sources of TNF^{433, 686, 692}. *In vitro* studies have shown that TNF secreted by human macrophage-like THP-1 cells can induce intestinal epithelial cell apoptosis and necrosis⁴⁹¹. Excess TNF can disrupt the intestinal epithelial barrier by inducing immune cell activation^{489, 673, 686, 687}, increasing epithelial cell turnover and cell death^{686, 692, 693}, downregulating mucus production^{694, 695}, and disrupting tight junction proteins^{492, 656}. Accordingly, mice with chronic overproduction of TNF (TNF $\Delta^{\text{ARE/+}}$ mice) spontaneously develop colitis in the small intestine⁶⁹⁶. While our experiments in section 6.1 showed that intestinal macrophages do not increase their expression of TNF in HF-fed mice compared to chow-fed mice, and that monocyte infiltration into intestinal tissues is not increased, it is generally reported that whole-tissue inflammation and gene expression of TNF are increased in the small intestine and colon of mice with diet-induced obesity^{364, 639, 643, 645}.

The Bowdish lab has previously demonstrated, using $\text{TNF}^{-/-}$ mice and anti-TNF treatment, that reduction of TNF protects old mice from age-associated chronic inflammation, intestinal permeability, microbial dysbiosis, and peripheral monocyto^{336, 337, 511}. In section 6.1, we documented that WT mice with diet-induced obesity have increased intestinal permeability and altered intestinal macrophage populations in the ileum and colon. As TNF has been identified as an important pro-inflammatory cytokine in the pathophysiology of chronic inflammation in obesity²⁵, and inflammatory disorders of the intestines, as described above, we hypothesized that $\text{TNF}^{-/-}$ mice fed a HF diet would be protected from increased intestinal permeability and changes to intestinal macrophages that accompany HF diet-induced obesity in WT mice.

6.2.2 Results

Intestinal physiology and permeability

Littermate $\text{TNF}^{-/-}$ and $\text{TNF}^{+/+}$ wildtype female mice were placed on a high fat diet (60% kcal from fat) at 8 weeks of age after baseline measurements, as described in Chapter 5 (Section 5.1). To determine if $\text{TNF}^{-/-}$ mice were protected from intestinal permeability associated with diet-induced obesity, mice were gavaged with FITC-dextran after diet allocation for 12 weeks (Figure 6.2.1A) or 28 weeks (Figure 6.2.1B), and plasma fluorescence was measured up to 4 hours post-gavage. There were no significant differences by genotype in plasma fluorescence at any assessed time point, nor by calculated area under the curve, suggesting that HF-fed $\text{TNF}^{-/-}$ mice have similar intestinal permeability as HF-fed WT mice. At endpoint, we measured intestinal tissue lengths and compared them to intestine lengths of 8 week old $\text{TNF}^{-/-}$ and WT chow-fed

mice (i.e. equivalent to baseline, prior to diet allocation of HF-fed mice). We observed that there were main effects of diet feeding time, as well as genotype, on small intestine length (Figure 6.2.1C), which decreased in HF-fed WT mice (mean \pm SD, 30 weeks: 32.1 ± 1.5 cm) in comparison to baseline chow-fed WT mice (baseline: 36.3 ± 0.3 cm), and in HF-fed TNF^{-/-} mice (30 weeks: 33.1 ± 1.4 cm) in comparison to baseline chow-fed TNF^{-/-} mice (baseline: 37.9 ± 2.2 cm), though post-hoc tests were not significant between genotypes. There was no significant effect of genotype on colon length, though there was a trend toward a decrease in length over time (Figure 6.2.1D). Therefore, both TNF^{-/-} and WT mice fed a HF diet had similar intestinal permeability up to 28 weeks after diet allocation and reductions in intestinal tissue lengths up to 30 weeks of HF diet allocation.

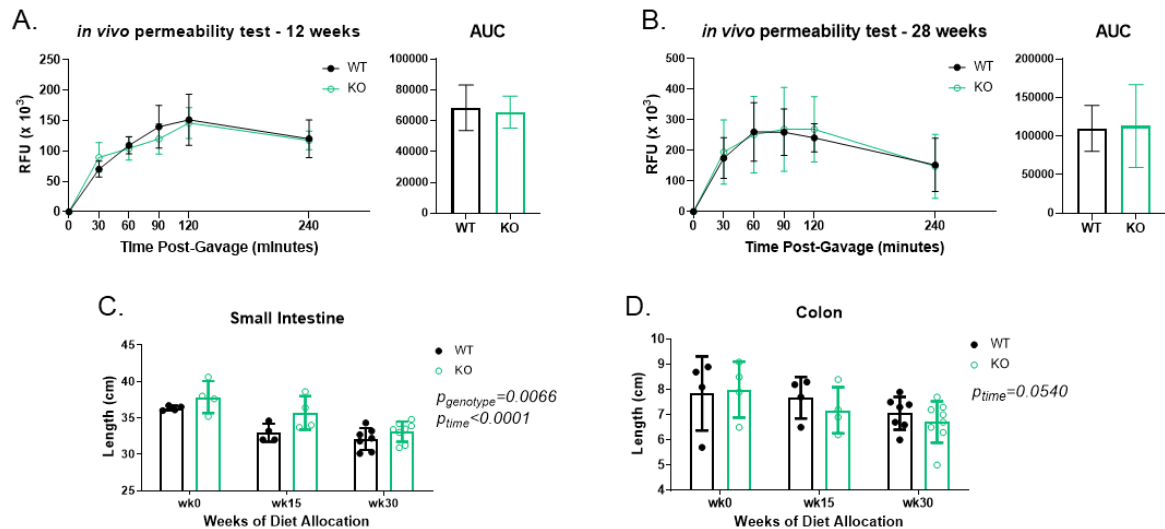


Figure 6.2.1. Intestine lengths and permeability in littermate WT and TNF^{-/-} mice.

Littermate wildtype (WT) and TNF^{-/-} (KO) mice were assessed at 8 weeks of age prior to diet allocation (wk0) and after allocation to 60% high fat diet. *In vivo* FITC-dextran intestinal permeability assay plasma fluorescence: (A) 12 weeks diet allocation, (B) 28 weeks diet allocation. (C) small intestine length. (D) colon length. Data in A and B are presented as mean \pm standard deviation with area under the curve (AUC) presented with box height at the mean with error bars indicating \pm standard deviation. Data in C-D are presented with box height at the mean and error bars at \pm standard deviation. Data are from one independent experiment at each time point of n=4-8 mice per genotype. RFU – relative fluorescence units. Statistical significance was assessed by two-tailed Student's t test for A-B and by two-way ANOVA with Tukey's post-hoc test for C-D.

Intestinal macrophages – prevalence, absolute cell counts, and surface phenotype

We assessed Ly6C^{high} monocytes, total MHCII⁺ macrophages, and CD4⁻TIM4⁻, CD4⁺, and CD4⁺TIM4⁺ macrophage populations by flow cytometry in the ileums (Figure 6.2.2) and colons (Figure 6.2.3) of chow-fed WT and TNF^{-/-} mice at 8 weeks of age, and WT and TNF^{-/-} mice after 15 and 30 weeks of HF diet allocation. In ileum tissues there were no significant differences by genotype in the prevalence (as a proportion of total leukocytes) of Ly6C^{high} monocytes (Figure 6.2.2A), or macrophages (Figure 6.2.2B), or macrophage cell counts (Figure 6.2.2C). We also assessed the prevalence of CD4⁻TIM4⁻, CD4⁺, and CD4⁺TIM4⁺ macrophages (as a proportion of total macrophages) (Figure 6.2.2D). As we found that there were significant main effects of genotype and time of diet feeding for CD4⁺ and CD4⁺TIM4⁺ populations, we normalized data collected after 15 and 30 weeks of diet allocation to the mean of the baseline dataset for each macrophage population (Figure 6.2.2E). This allowed us to determine that the effects of HF diet on ileum macrophage prevalence were similar after 15 weeks in WT and TNF^{-/-} mice, but that there was a divergence after 30 weeks, when TNF^{-/-} mice in particular had a higher prevalence of ileum CD4⁻TIM4⁻ and CD4⁺ macrophages in comparison to WT mice, relative to pre-diet baseline. However, absolute cell counts of the macrophage populations (Figure 6.2.2G-I) were not significantly different between the WT and TNF^{-/-} mice at baseline or at 15 or 30 weeks after HF diet allocation.

There were no significant differences in colon macrophage numbers (Figure 6.2.3B), or the prevalence of macrophages (Figure 6.2.3C) between HF-fed TNF^{-/-} and WT mice. There was a decrease in Ly6C^{high} monocytes within the colons of TNF^{-/-} mice compared to WT mice after 15 weeks, but this was not observed at 30 weeks.

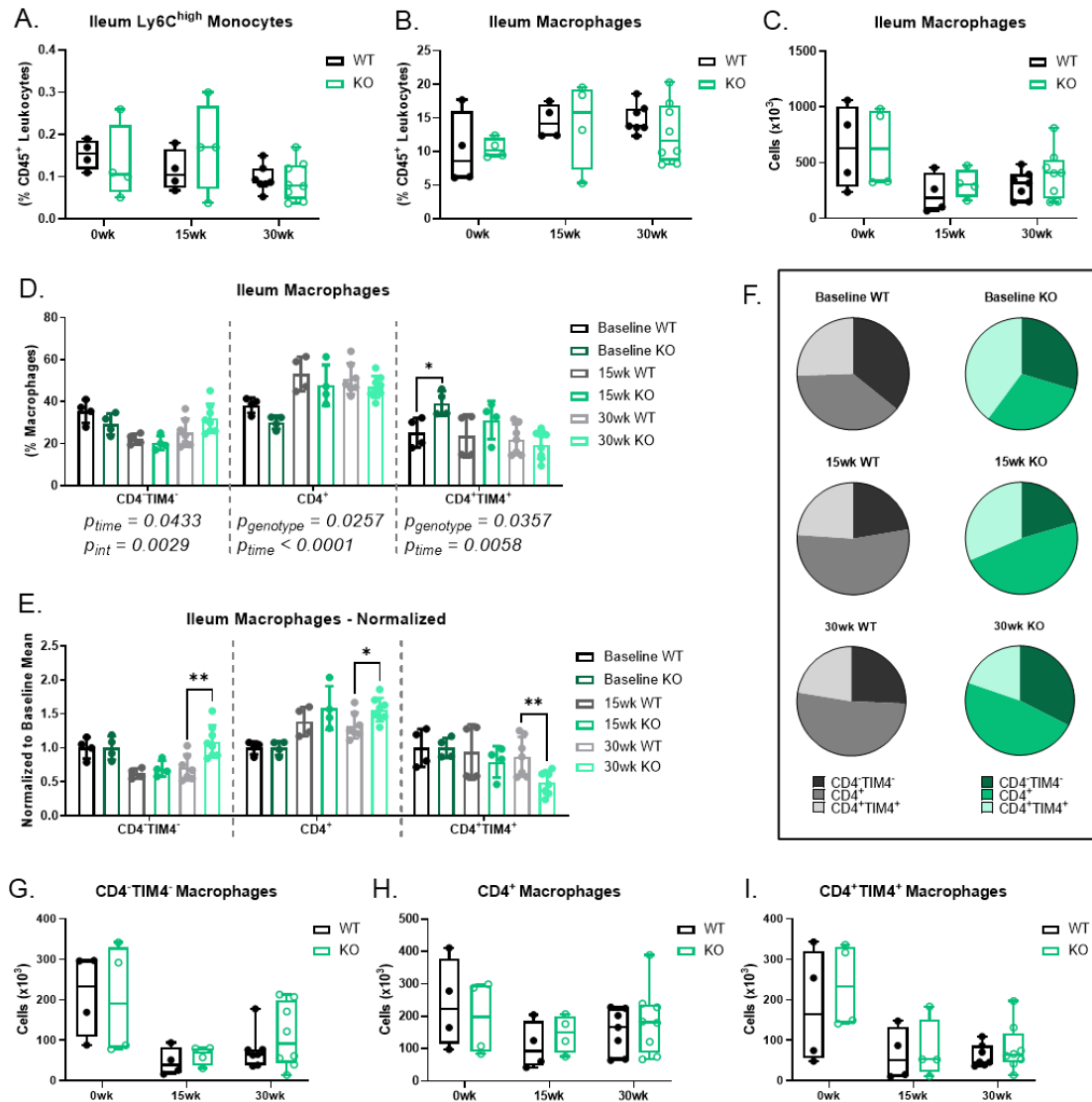


Figure 6.2.2. Ileum monocytes and macrophages in littermate WT and TNF^{-/-} mice.

Ileum immune cells were assessed by flow cytometry in wildtype (WT) and TNF^{-/-} (KO) mice at 8 weeks of age (0wk/Baseline), and after 15 weeks (15wk) or 30 weeks (30wk) of high fat diet allocation. Prevalence (as a proportion of CD45⁺ leukocytes) of: (A) Ly6C^{high} monocytes, (B) total macrophages. (C) absolute cell count of total macrophages. (D) prevalence of CD4⁻TIM4⁻, CD4⁺, and CD4⁺TIM4⁺ macrophages. (E) prevalence of CD4⁻TIM4⁻, CD4⁺, and CD4⁺TIM4⁺ macrophages normalized to the mean of the baseline data to adjust for between-genotype differences. (F) Pie graph summaries of mean prevalence of each macrophage population by genotype and assessed time point. Absolute cell counts of macrophages: (G) CD4⁻TIM4⁻, (H) CD4⁺, (I) CD4⁺TIM4⁺. Each data point indicates an individual mouse. Data in A-C and G-I are presented as box and whisker plots, minimum to maximum, with the center line at the median. Data in D-E are presented with box height at the mean with error bars indicating \pm standard deviation. Data are from one independent experiment of 4-8 mice per genotype at each time point. Statistical significance was assessed by Student's two-tailed t test between genotypes at each time point for A-C, E, and G-I, and by two-way ANOVA with Tukey's post-hoc test for D. * $p < 0.05$, ** $p < 0.01$.

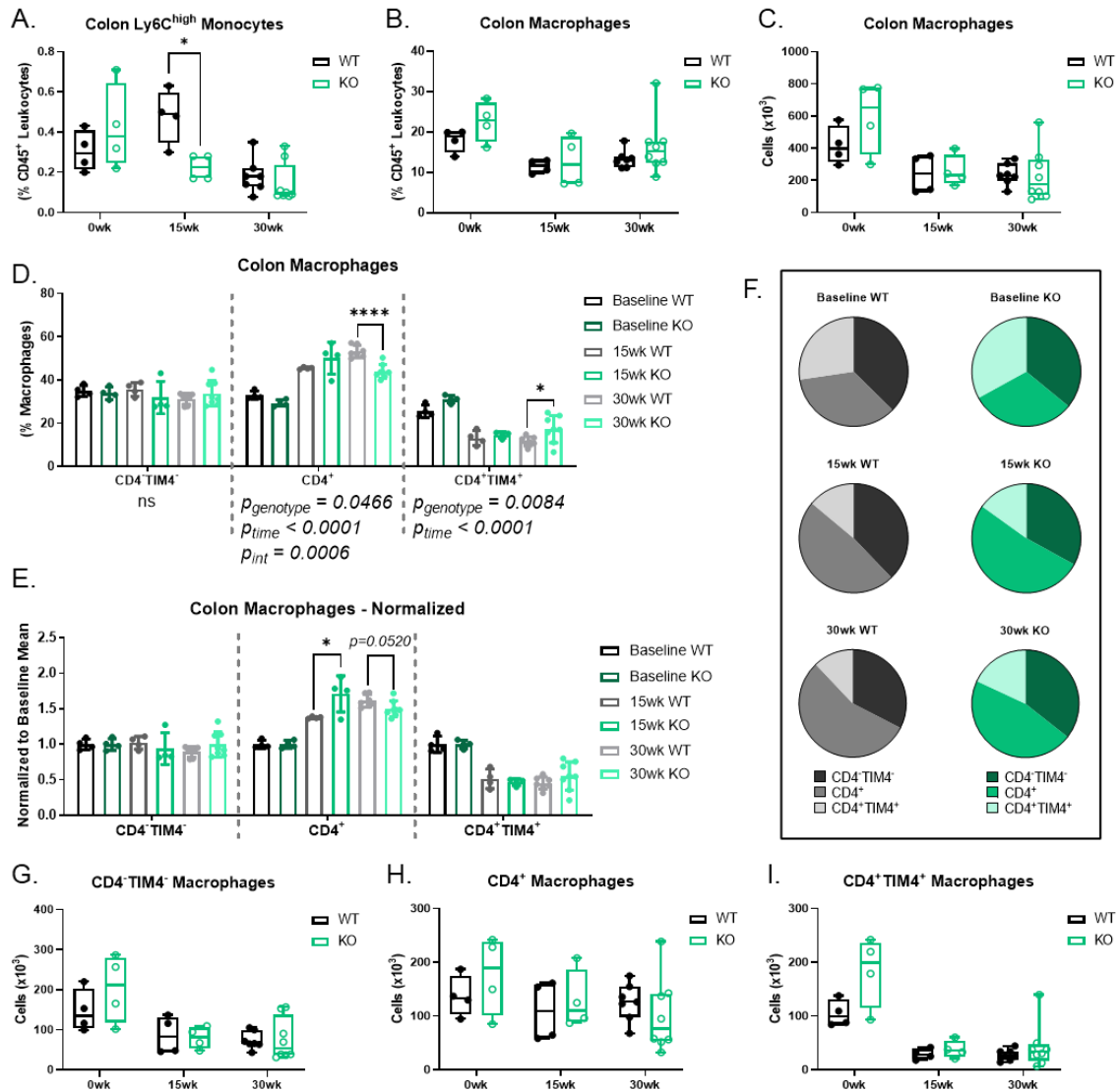


Figure 6.2.3. Colon monocytes and macrophages in littermate WT and TNF^{-/-} mice.

Colon immune cells were assessed by flow cytometry in wildtype (WT) and TNF^{-/-} (KO) mice at 8 weeks of age (0wk/Baseline), and after 15 weeks (15wk) or 30 weeks (30wk) of high fat diet allocation. Prevalence (as a proportion of CD45⁺ leukocytes) of: (A) Ly6C^{high} monocytes, (B) total macrophages. (C) absolute cell count of total macrophages. (D) prevalence of CD4⁻TIM4⁻, CD4⁺, and CD4⁺TIM4⁺ macrophages. (E) prevalence of CD4⁻TIM4⁻, CD4⁺, and CD4⁺TIM4⁺ macrophages normalized to the mean of the baseline data to adjust for between-genotype differences. (F) Pie graph summaries of mean prevalence of each macrophage population by genotype and assessed time point. Absolute cell counts of macrophages: (G) CD4⁻TIM4⁻, (H) CD4⁺, (I) CD4⁺TIM4⁺. Each data point indicates an individual mouse. Data in A-C and G-I are presented as box and whisker plots, minimum to maximum, with the center line at the median. Data in D-E are presented with box height at the mean with error bars indicating \pm standard deviation. Data are from one independent experiment of 4-8 mice per genotype at each time point. Statistical significance was assessed by Student's two-tailed t test between genotypes at each time point for A-C, E, and G-I, and by two-way ANOVA with Tukey's post-hoc test for D. * $p < 0.05$, *** $p < 0.0001$.

There were main effects of genotype and time on CD4⁺ and CD4⁺TIM4⁺ macrophages in the colon (Figure 6.2.3D). Normalizing the 15 and 30 week data to the baseline data revealed that there is an increase in the prevalence of colon CD4⁺ macrophages after 15 weeks in TNF^{-/-} mice in comparison to WT mice, but no other significant differences were observed (Figure 6.2.3E). Absolute cell counts of colon CD4⁻TIM4⁻, CD4⁺ and CD4⁺TIM4⁺ macrophages were also not significantly different between WT and TNF^{-/-} mice at any assessment time point (Figure 6.2.3G-I).

We also examined the surface expression of monocyte-macrophage markers Ly6C, CD11b, CD64, CCR2, F4/80, MHCII, CD4, and TIM4 on the CD4⁻TIM4⁻, CD4⁺, and CD4⁺TIM4⁺ macrophages in HF-fed WT and TNF^{-/-} mice (ileums - Figure 6.2.4; colons - Figure 6.2.5; Appendix I). Colon CD4⁺TIM4⁺ macrophages in TNF^{-/-} mice compared to WT mice had decreased expression of CD11b after 15 weeks (Figure 6.2.5B), and decreased expression of CD64 after 30 weeks (Figure 6.2.5K), but there were no other statistically significant differences in surface marker expression on colon macrophages between WT and TNF^{-/-} mice. There were no significant differences of surface marker expression between TNF^{-/-} and WT mouse ileum macrophages after 15 or 30 weeks of HF diet feeding.

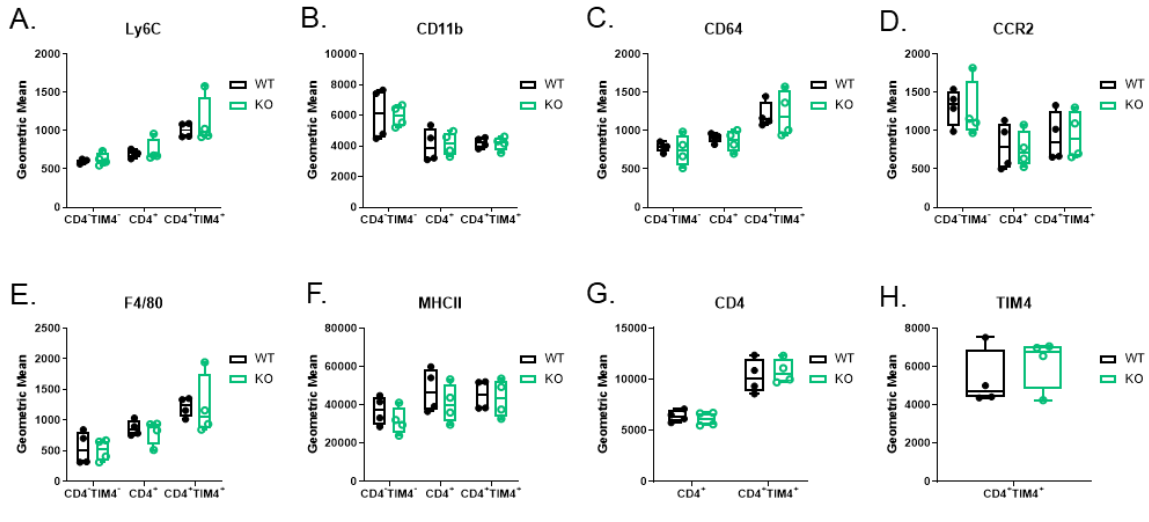
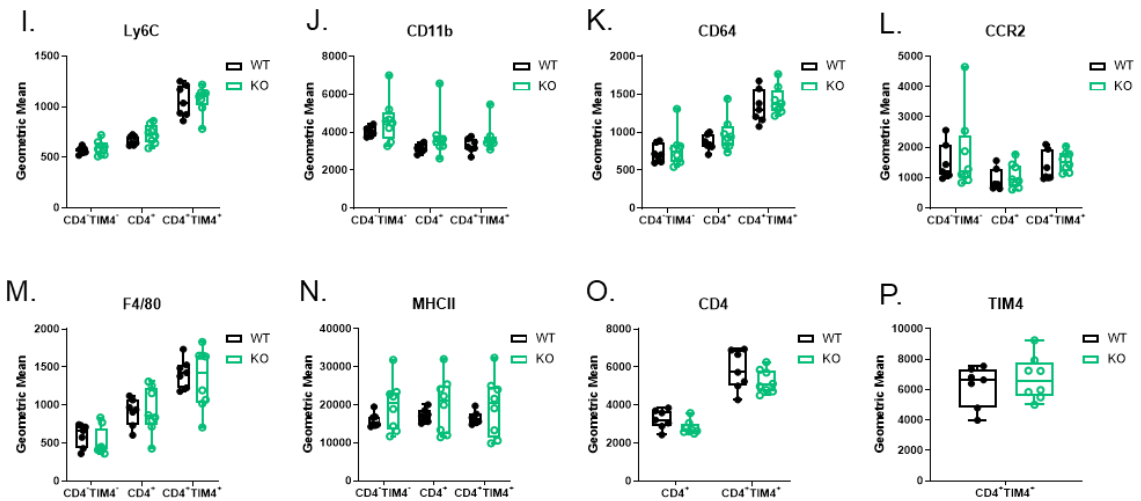
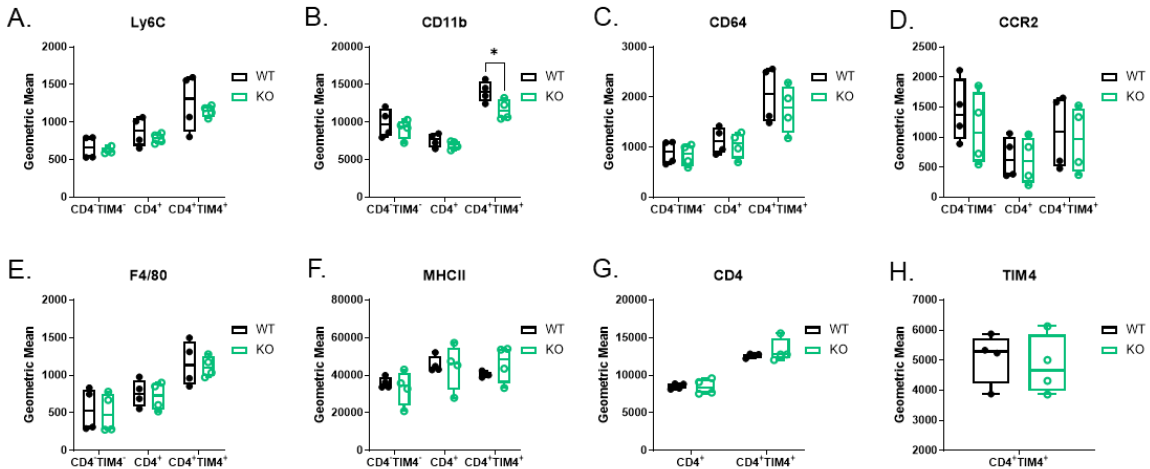
Ileum Macrophages – 15 weeks*Ileum Macrophages – 30 weeks*

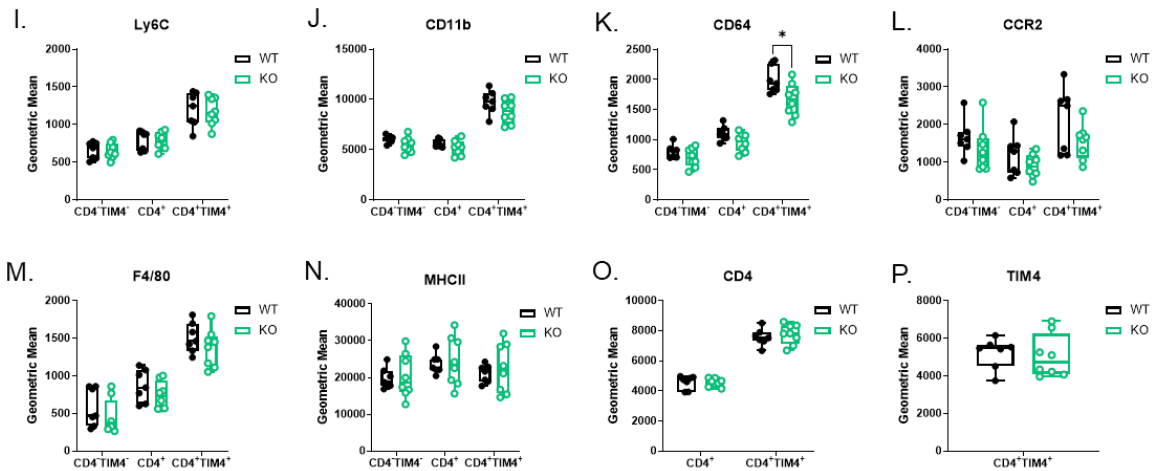
Figure 6.2.4. Ileum macrophage surface phenotype in littermate WT and $TNF^{-/-}$ mice.

Flow cytometry analysis of CD4⁺TIM4⁻, CD4⁺, and CD4⁺TIM4⁺ macrophage populations in the ileums of littermate wildtype (WT) and $TNF^{-/-}$ (KO) female mice on 60% high fat diet for 15 weeks (A-H) or 30 weeks (I-P). Geometric mean expression of Ly6C (A,I), CD11b (B,J), CD64 (C,K), CCR2 (D,L), F4/80 (E,M), MHCII (F,N), CD4 (G,O), and TIM4 (H,P). Data are reported as geometric mean fluorescence intensity. Data are from one experiment of n=4-8 at each time point. Data are presented as box and whisker plots, minimum to maximum, where the center line indicates the median. Statistical significance was assessed by two-tailed Student's t test between genotypes for each macrophage population.

Colon Macrophages – 15 weeks



Colon Macrophages – 30 weeks

**Figure 6.2.5. Colon macrophage surface phenotype in littermate WT and $TNF^{-/-}$ mice.**

Flow cytometry analysis of $CD4^{-}TIM4^{-}$, $CD4^{+}$, and $CD4^{+}TIM4^{+}$ macrophage populations in the colons of littermate wildtype (WT) and $TNF^{-/-}$ (KO) female mice on 60% high fat diet for 15 weeks (A-H) or 30 weeks (I-P). Geometric mean expression of Ly6C (A,I), CD11b (B,J), CD64 (C,K), CCR2 (D,L), F4/80 (E,M), MHCII (F,N), CD4 (G,O), and TIM4 (H,P). Data are reported as geometric mean fluorescence intensity. Data are from one experiment of $n=4-8$ at each time point. Data are presented as box and whisker plots, minimum to maximum, where the center line indicates the median. Statistical significance was assessed by two-tailed Student's t test between genotypes for each macrophage population. $*p < 0.05$.

6.2.3 Discussion

In these experiments the data from WT mice, comparing effects of HF diet feeding to baseline assessments, showed similar trends to our earlier experiments comparing WT mice fed HF or chow diet (section 6.1). HF diet feeding induced decreases in intestinal length, decreases in cell counts of ileum and colon macrophages, in particular $CD4^+TIM4^+$ populations, and a relative increase in the prevalence of $CD4^+$ macrophages (as a proportion of total macrophages). WT and $TNF^{-/-}$ mice fed HF diet had similar effects between genotypes, suggesting that genetic ablation of TNF in female mice is not protective against HF diet-induced intestinal permeability, decreases in intestinal length, or changes to macrophage population dynamics or surface phenotype. In the ileum, macrophages in $TNF^{-/-}$ mice may even have greater changes in response to HF diet relative to baseline data, as after 30 weeks we observed a significant increase in $CD4^-TIM4^-$ and $CD4^+$ macrophages in the ileum, and an accompanying decrease in the prevalence of $CD4^+TIM4^+$ macrophages, in $TNF^{-/-}$ mice compared to WT mice, though total cell counts were unchanged between genotypes. Therefore, these data may indicate that TNF, unlike in intestinal infection or IBD, does not have a major role in regulation of intestinal macrophage populations in response to diet-induced obesity.

These data were unexpected because, as mentioned, previous research suggests that TNF contributes to intestinal inflammation in diet-induced obesity^{364, 639, 643, 645}. However, multiple studies also suggest that TNF has pleiotropic effects in acute and chronic inflammation in the intestines. $TNF\Delta^{ARE/+}$ mice, which overexpress TNF, spontaneously develop IBD-like pathology in the terminal ileum^{696, 697}, and have lower body weight and adiposity in comparison to wildtype mice⁶⁹⁸. In contrast, it has been

reported that $\text{TNF}^{-/-}$ mice are more susceptible to pathology from acute DSS-induced colitis, and use of anti-TNF therapy similarly leads to worse tissue damage^{699, 700}. However, anti-TNF therapy reduces intestinal inflammation in chronic DSS-induced colitis⁷⁰⁰, and $\text{TNF}^{-/-}$ mice are not susceptible to acute or chronic TNBS-induced colitis^{692, 699}. It has also been reported that anti-TNF treatment reduces pathology from infection with *Salmonella enterica* serovar Typhimurium⁷⁰¹, yet increases pathology in *Citrobacter rodentium* or *Clostridium difficile* infection^{702, 703}. In addition, treatment failure of anti-TNF therapy is also documented in IBD, with both primary non-response or loss of response after initially successful treatment⁷⁰⁴, which suggests that there may be different etiologies of intestinal inflammation that are not TNF-dependent.

Feeding $\text{Tnf}\Delta^{\text{ARE}/+}$ mice a palm oil-based high fat diet accelerates intestinal inflammation, with worse pathology, reduction of tight junction protein expression and increased endotoxin translocation, but the mice do not develop obesity, adipose tissue inflammation, or impaired glucose tolerance, in comparison to WT mice⁶⁴⁶. Future studies with $\text{Tnf}\Delta^{\text{ARE}/+}$ and $\text{TNF}^{-/-}$ mice and their WT littermates, and treatment with 5-aminosalicylic acid (which as mentioned reduces intestinal permeability and systemic soluble inflammation in models of diet-induced obesity)⁶⁴¹, may help to disentangle the effects, or lack thereof, of TNF and diet-induced obesity on intestinal inflammation, permeability, and macrophage population dynamics. Overall, our data indicate that the absence of TNF does not prevent changes to intestinal permeability or macrophage populations in response to diet-induced obesity in female mice.

6.3 Immunological effects of the microbiome

6.3.1 Introduction

It is well-established that mice fed an obesogenic diet, such as the primarily lard-based 60% kcal fat diet that has been used in this chapter, a similar 45% kcal fat diet, ‘cafeteria’ or ‘Western’ diets, or other high fat content diets, have intestinal microbial dysbiosis^{75, 83, 569, 705}. Studies from humans and mice have reported that obesity changes bacterial diversity and taxa distribution by 16S rRNA sequencing (e.g. increased Firmicutes to Bacteroides ratio, decreased microbial diversity, decreased richness)^{75, 83, 84, 401, 402, 706, 707, 708, 709}, and alters the metaproteome and metabolome^{710, 711, 712}. As mentioned in Chapter 1, there is strong evidence that bacterial products and PRR signalling contribute to the development of obesity, chronic systemic inflammation, and metabolic dysregulation^{75, 83, 391, 392, 393, 394, 395, 396, 397, 399}, which implies that the intestine and its microbiota have an important role in the etiology and progression of obesity.

Chronic inflammation and metabolic dysfunction in mouse models of diet-induced obesity have in particular been associated with the bacterial cell wall component LPS. Modulation of the microbiota by antibiotic treatment in mice with diet-induced obesity reduces intestinal permeability, circulating LPS, adipose tissue inflammation, and insulin resistance (as we also observed in Chapter 4)^{75, 83, 84, 707, 713}. In the previous sections of this chapter, we showed that there are effects of HF diet-induced obesity on intestinal macrophages and intestinal permeability (section 6.1), and HF-fed TNF^{-/-} and WT mice exhibited similar changes (section 6.2). We considered that microbial dysbiosis, rather than TNF-mediated effects on obesity-associated inflammation, may be sufficient to alter intestinal homeostasis.

A common approach to examine mechanisms of host-microbe interactions, and causative effects of intestinal microorganisms in health and disease, is to use gnotobiotic mice that completely lack a microbiota (i.e. germ free mice)^{714, 715}. Colonization of germ free (GF) mice may be accomplished with use of a complex microbiota, a simplified microbiota, or even a single bacterial species. Colonization of a GF mouse with the microbiota from non-obese mice on a standard chow diet is sufficient to increase body-fat content, insulin resistance, and macrophage accumulation in adipose tissue, in comparison to a naïve GF mouse^{399, 713, 716, 717, 718}. Gavage of caecal microbiota from *ob/ob* donor mice (which have increased food consumption and adiposity due to leptin deficiency) into adult wildtype GF recipient mice on a standard chow diet resulted in an ~20% increase in fat mass within two weeks, in comparison to microbiota transfer from a wildtype donor mouse⁷⁰⁵. Intestinal expression of NfκB has also been reported to be elevated 2 weeks post-colonization in GF mice colonized with microbiota from donor HF-fed but not chow-fed mice³⁹⁰. In addition, the microbiota of humans can also influence mouse adiposity. Transplantation of human faecal microbiota into GF mice led to increased adiposity in mice that received microbiota from obese donors, but not lean donors⁷⁰⁹. Colonization of GF mice with microbiota of twins discordant for obesity led to increased adiposity in mice that received the microbiota from the obese twin⁷¹⁷. Transfer of obese human donor microbiota into mice, followed by a second mouse-to-mouse transfer, also increased recipient mouse weight gain⁷¹⁷. These data collectively suggest that the presence of a dysbiotic ‘obesogenic’ microbiota, in absence of a HF diet, is sufficient to induce intestinal inflammation and impact systemic metabolism.

While several studies had suggested that transfer of microbiota from genetically or diet-induced obese mice to GF mice can cause elevation of circulating or tissue-localized pro-inflammatory cytokines in comparison to microbiota transfer from lean mice^{390, 392}, the immunological impact of colonization with microbiota from mice with diet-induced obesity had not been studied in detail. Whether the microbiota could transfer local and systemic cellular inflammation was unknown. We were specifically interested in investigating if the microbiota of HF-fed mice in our diet-induced obesity model was sufficient to induce intestinal and peripheral immunological changes described earlier in this thesis (section 5.1; section 6.1). We hypothesized that GF mice colonized with the microbiota from mice with HF diet-induced obesity, in comparison to microbiota from lean chow-fed mice, would have increased adiposity, intestinal permeability, circulating pro-inflammatory monocytes, and altered intestinal macrophage prevalence and phenotype.

6.3.2 Results

A minimally invasive approach was used to colonize young female GF mice 8-10 weeks of age with microbiota from chow-fed and HF-fed donor mice, through environmental exposure and coprophagy^{719, 720, 721}. The GF mice were placed in a ‘dirty’ cage from SPF donor mice containing bedding and fecal pellets, and the donor cage was replaced with a new ‘dirty’ cage bottom from the donor mice on a weekly basis³³⁷. We transferred microbiota from female donors to female GF mice to avoid effects of biological sex on microbial engraftment^{719, 722}. Body weight and food intake were measured weekly, and other assessments were performed at baseline and at 6, 12 and/or

18 weeks post-microbial exposure. We chose these extended time points based on reports that colonization itself can induce an inflammatory response within the intestines that requires up to 30 days for resolution^{723, 724, 725}, that structural features of the epithelium including the mucus layer require 5-6 weeks to develop^{724, 726}, and that microbial engraftment requires up to 9 weeks for stabilization^{726, 727, 728}.

Physiological measurements and food consumption

Body weights between the chow and HF microbiota groups were not different throughout the experiment (Figure 6.3.1A). Energy intake from food was also consistently similar between the microbiota groups (Figure 6.3.1B). Although body weight and adiposity increased significantly in both microbiota groups, total weight gain (Figure 6.3.1C) and adiposity (Figure 6.3.1D; measured by Echo-MRI) were not significantly different between the microbiota groups at 6, 12, or even 18 weeks post-microbial exposure. Fasting blood glucose after 12 weeks was likewise not different between microbiota groups (Figure 6.3.1E), though fasting blood glucose levels were significantly lower in the colonized ex-GF recipient mice compared to the donor chow-fed mice, as well as compared to the donor HF-fed mice. The microbiota groups also had similar liver weights at endpoint (Figure 6.3.1F). In summary, recipient mice in the chow and HF microbiota groups had similar physiological changes post-colonization, with no significant differences in body weight, adiposity, liver weight, food consumption, or fasting blood glucose.

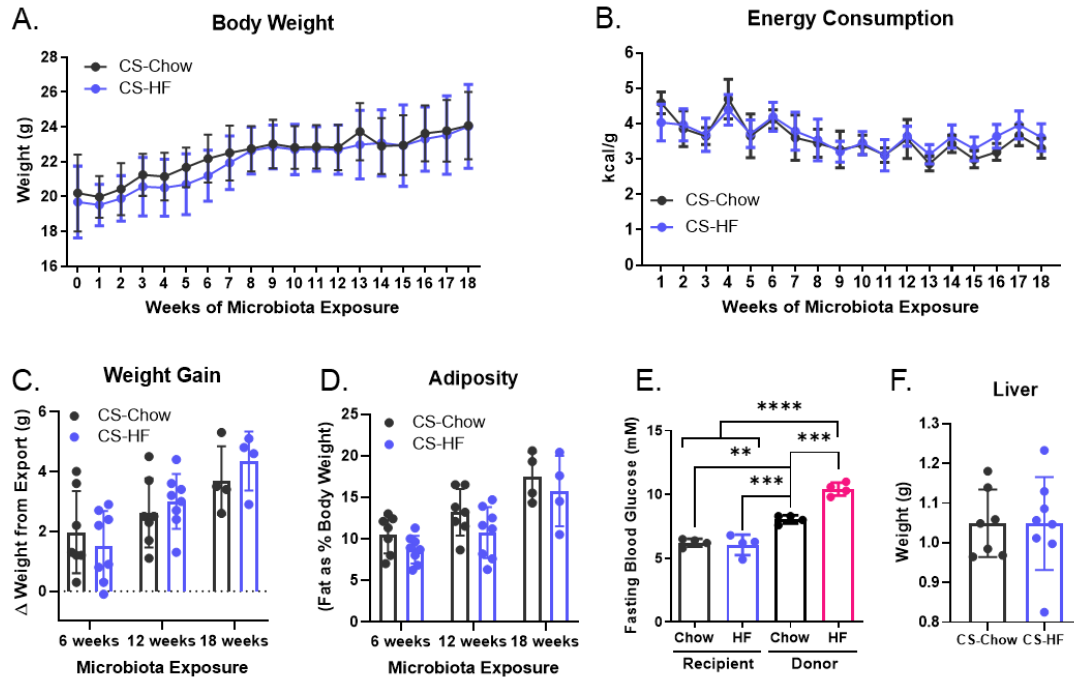


Figure 6.3.1. Chow and HF microbiota effects on physiological measurements.

Young germ free mice were colonized with microbiota from chow-fed or HF-fed mice. (A) body weight measured at export and on a weekly basis thereafter. (B) total weekly food kilocalorie consumption. At 6, 12, and/or 18 weeks: (C) weight gain after colonization, (D) adiposity. (E) fasting blood glucose after 12 weeks. (F) liver weight at endpoint. Data in A and B are shown as mean \pm standard deviation. Each data point in C-F indicates an individual mouse and data are presented with box height at the mean with error bars at \pm standard deviation. Data in A-D and F are pooled from two independent experiments with $n=3-4$ mice per group. Data in E are from one independent experiment of $n=4$ mice per group. CS-Chow: ex-germ free mice with microbiota from chow-fed SPF mice. CS-HF: ex-germ-free mice with microbiota from 60% high fat-fed SPF mice. Statistical analyses were performed using Student's *t* test between microbiota groups at each time point for A-D and F, and by two-way ANOVA for E ($p_{\text{microbiota}} = 0.0013$, $p_{\text{RvsD}} < 0.0001$, $p_{\text{int}} = 0.0004$). ** $p < 0.01$, *** $p < 0.001$, **** $p < 0.0001$.

Intestinal physiology and permeability

In vivo intestinal permeability was assessed 12 weeks post-microbiota colonization. Permeability was similar between the recipient chow and HF microbiota groups and chow-fed donor group (Figure 6.3.2A), as was total area under the curve (Figure 6.3.2B), but permeability was significantly higher in the HF-fed donor mice compared to the chow-fed donor mice and both microbiota recipient groups.

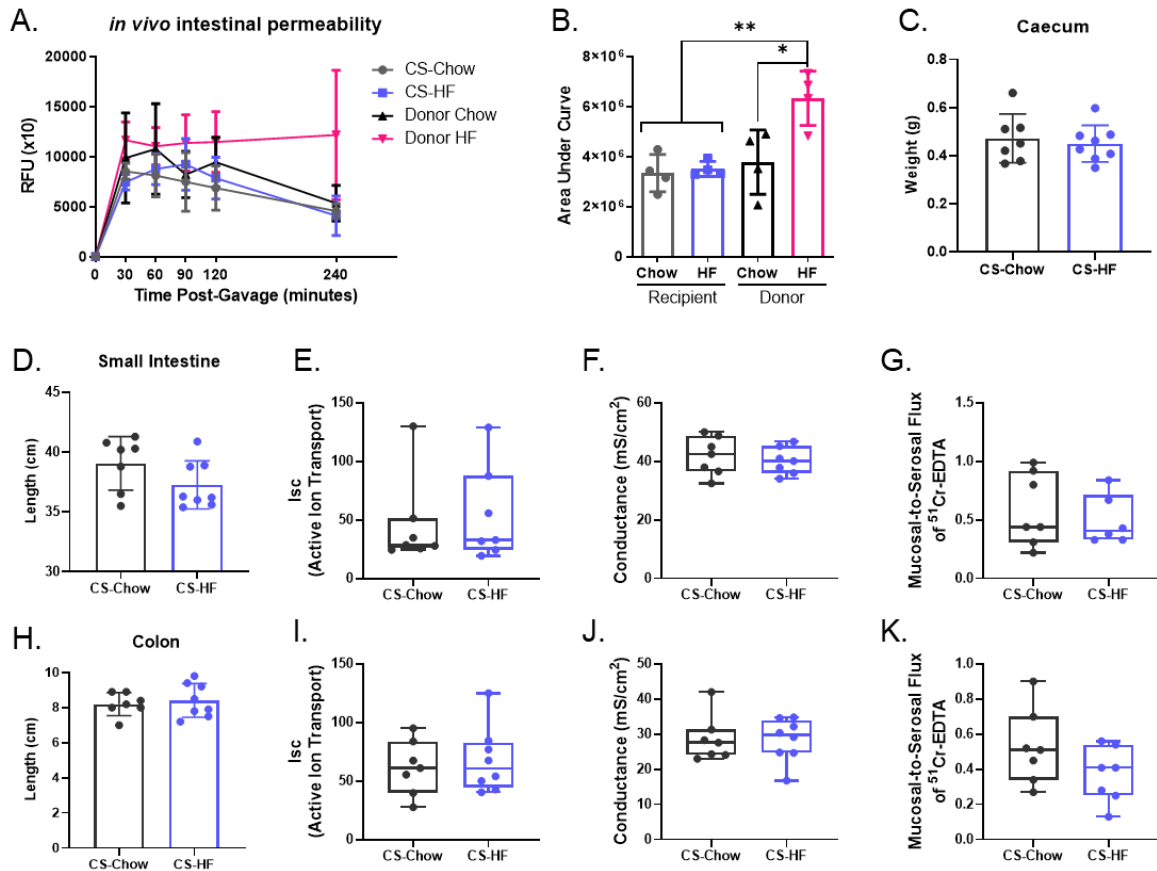


Figure 6.3.2. Chow and HF microbiota effects on intestinal permeability and physiology.

Young germ free mice were colonized with microbiota from chow-fed or HF-fed mice. (A) *in vivo* FITC-dextran intestinal permeability assay plasma fluorescence and (B) area under the curve of recipient and donor mice. (C) caecal weight. (D) small intestine length. *In vitro* Ussing chamber assay of ileum tissue ion short current (E), conductance (F), and paracellular permeability (G). (H) colon length. *In vitro* Ussing chamber assay of colon tissue ion short current (I), conductance (J), and paracellular permeability (K). Data in A are shown as mean \pm standard deviation. Each data point in B-K indicates a single mouse. Data in B-D and H are presented with box height at the mean with error bars indicating \pm standard deviation. Data in E-G and I-K are presented as box and whisker plots, minimum to maximum, with the center line at the median. Data in A-B are from one experiment of $n=4$ mice per group. Data in C to K are pooled from two independent experiments of $n=3-4$ mice per group. CS-Chow: ex-germ free mice with microbiota from chow-fed SPF mice. CS-HF: ex-germ-free mice with microbiota from 60% high fat-fed SPF mice. RFU – relative fluorescence units. Statistical significance was assessed by two-way ANOVA with Tukey's post-hoc test for B ($p_{\text{microbiota}} = 0.0129$, $p_{\text{RvsD}} = 0.0044$, $p_{\text{int}} = 0.0251$) and by two-tailed Student's t test for C-K. * $p < 0.05$, ** $p < 0.01$.

We also examined ileum and colon tissues using *in vitro* Ussing chambers. There were no statistically significant differences in ileum ion short current (Figure 6.3.2E), conductance (Figure 6.3.2F), or paracellular permeability (Figure 6.3.2G) between chow or HF microbiota recipient mice. Analysis of colon tissue likewise detected no differences in those parameters (Figure 6.3.2I-K). Measurements of caecal weight (Figure 6.3.2C), the length of the small intestine (Mean \pm SD, Chow: 39.1 ± 2.2 cm; HF: 37.3 ± 2.0 cm) (Figure 6.3.2D), and colon length (Chow: 8.2 ± 0.6 cm; HF: 8.4 ± 1.0 cm) (Figure 6.3.2H), were not significantly different between recipient microbiota groups. These data indicated that mice that received the chow or HF microbiota had similar intestinal physiology (caecal weight and tissue lengths), total intestinal permeability (by FITC-dextran assay), as well as paracellular permeability (by mucosal-to-serosal flux), active ion transport (by ion short-current), and tissue structural integrity (from conductance) in ileum and colon tissues.

Intestinal macrophages

We characterized macrophages and other immune cell populations in the ileum and colon in the recipient chow and HF microbiota mice by flow cytometry. The prevalence of Ly6C^{high} monocytes, total macrophages, eosinophils, or CD4⁺ T cells in the ileum (Figure 6.3.3A-D) and colon (Figure 6.3.3E-H) were similar between recipient microbiota groups. The prevalence of CD4⁻TIM4⁻, CD4⁺, and CD4⁺TIM4⁺ macrophages was also similar in the ileum (Figure 6.3.3I) and colon (Figure 6.3.3J) of the chow microbiota and HF microbiota groups. There were no significant differences in CD4⁻TIM4⁻, CD4⁺, or CD4⁺TIM4⁺ macrophage surface marker expression of Ly6C, CCR2, CD11b, F4/80, MHCII, CD64, CD4, or TIM4, in either the ileum (Figure 6.3.4A-

H), or colon (Figure 6.3.4I-P), between microbiota groups (Appendix I). These data suggested that the chow and HF microbiota had similar effects on intestinal macrophage prevalence and phenotype in the recipient mice. We also compared intestinal macrophage populations and tissue lengths of the recipient chow and HF microbiota mice to data from age-matched naïve GF mice and chow-fed SPF mice (Appendix III). This confirmed that intestinal macrophage population dynamics in the recipient mice changed in response to colonization, being distinct from naïve GF mice and more similar to SPF mice.

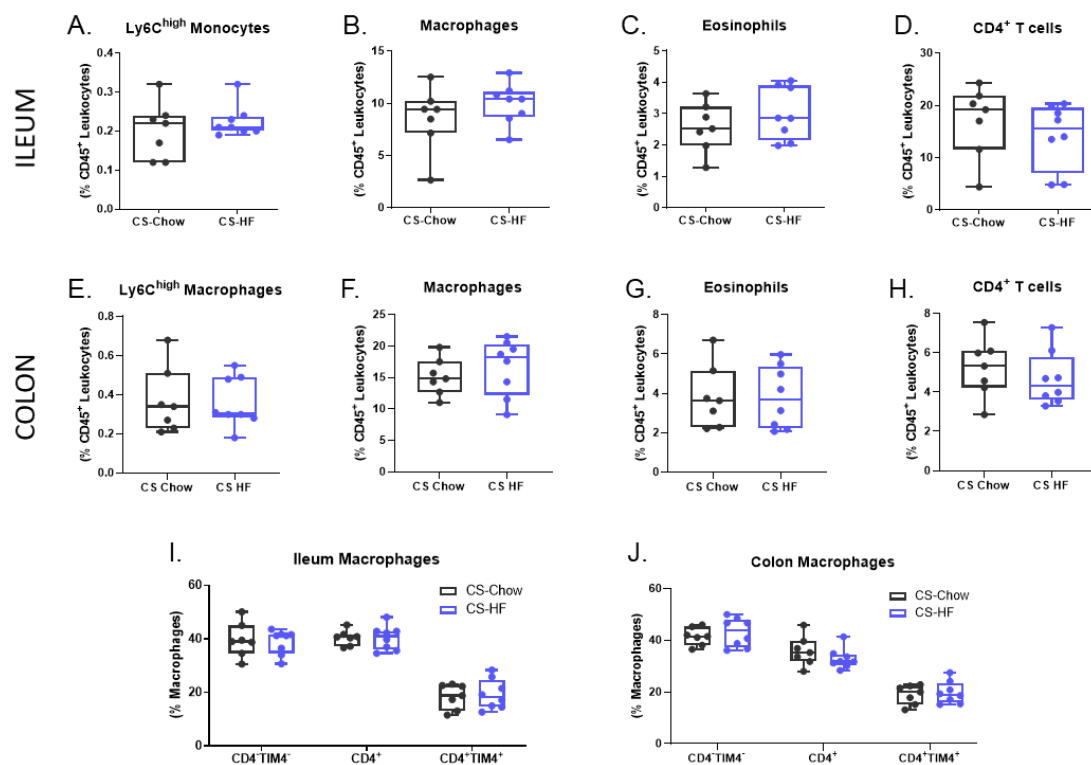


Figure 6.3.3. Chow and HF microbiota effects on prevalence of ileum or colon immune cells.

Young germ free mice were colonized with microbiota from chow-fed or HF-fed mice. Intestinal immune cell populations from colon and ileum tissue were assessed by flow cytometry after 12-18 weeks microbiota colonization. Ileum: (A) Ly6C^{high} monocytes, (B) total macrophages, (C) eosinophils, (D) CD4⁺ T cells. Colon: (E) Ly6C^{high} monocytes, (F) total macrophages, (G) eosinophils, (H) CD4⁺ T cells. CD4⁺TIM4⁻, CD4⁺, and CD4⁺TIM4⁺ macrophage populations in the ileum (I) and colon (J). Data are presented as box and whisker plots, minimum to maximum, where the center line indicates the median. Each data point indicates a single mouse. Data are pooled from two independent experiments of n=3-4 mice per group. CS-Chow: ex-germ free mice with microbiota from chow-fed SPF mice. CS-HF: ex-germ-free mice with microbiota from 60% high fat-fed SPF mice. Statistical significance was assessed between microbiota groups by two-tailed Student's t test.

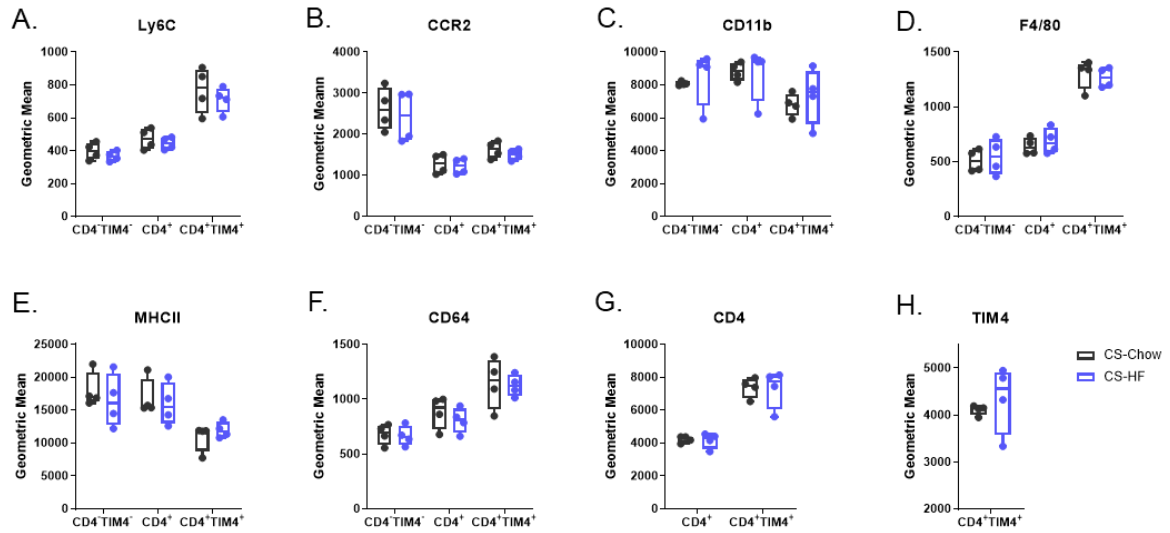
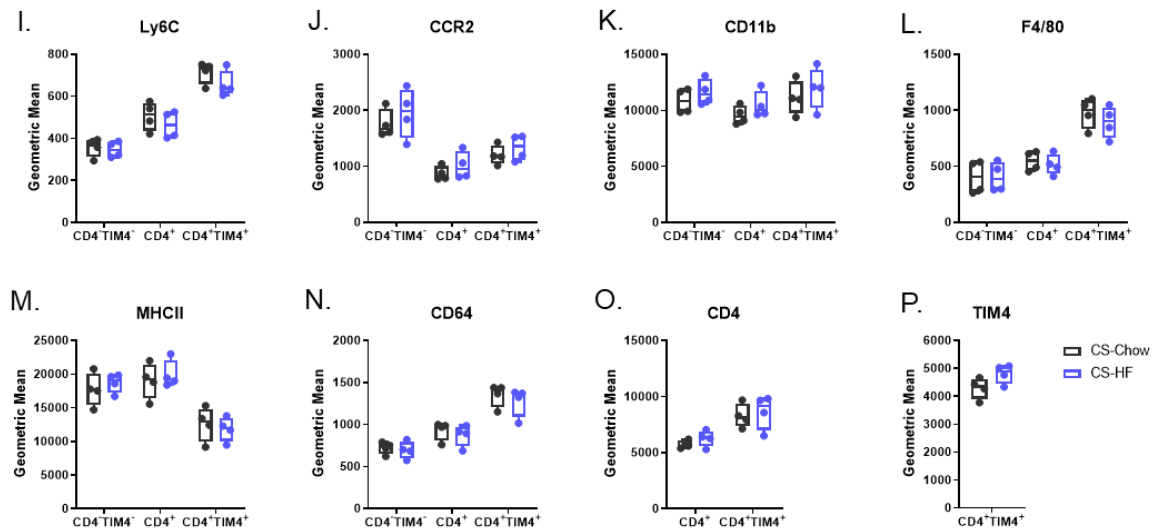
Ileum*Colon*

Figure 6.3.4. Chow and HF microbiota effects on ileum and colon macrophage surface phenotype.

Young germ free mice were colonized with microbiota from chow-fed or HF-fed mice. Flow cytometry analysis of CD4⁻TIM4⁻, CD4⁺, and CD4⁺TIM4⁺ macrophage populations in the ileum (A-H) and colon (I-P). Geometric mean expression of Ly6C (A,I), CCR2 (B,J), CD11b (C,K), F4/80 (D,L), MHCII (E,M), CD64 (F,N), CD4 (G,O), and TIM4 (H,P). Data are reported as geometric mean fluorescence intensity. Data are presented as box and whisker plots, minimum to maximum, where the center line indicates the median. Data are representative of two independent experiments of n=3-4 mice per microbiota group. CS-Chow: ex-germ free mice with microbiota from chow-fed SPF mice. CS-HF: ex-germ-free mice with microbiota from 60% high fat-fed SPF mice. Statistical significance was assessed by two-tailed Student's t test for each macrophage population.

Peripheral immunophenotype

Peripheral immune cells in whole blood were quantified by flow cytometry immediately after export of GF mice (i.e. prior to exposure to donor microbiota) and after 6, 12, and 18 weeks microbial exposure (Figures 6.3.5 and 6.3.6). We initially examined the composition and variability of all immune cell populations (i.e. overall immunophenotype) between time points and by microbiota type (Figure 6.3.5A; Table 6.3.1). Immunophenotype composition was not significantly different between microbiota recipient groups at baseline, 6, 12, or 18 weeks, though there was a significant change in composition in comparison to baseline at 6, 12, and 18 weeks post-colonization (PERMANOVA $p = 0.001$, $R^2 = 0.51371$), indicating that colonization induced changes to peripheral immunophenotype. Immunophenotype variability was modestly increased in the HF microbiota group at 12 weeks, but not at other time points. There were no significant differences at baseline, or after 6, 12, or 18 weeks, between the chow and HF recipient microbiota groups, in the prevalence of monocytes, neutrophils, NK cells, B cells, total T cells, $CD4^+$ T cells, $CD8^+$ T cells, or the ratio of $CD4^+$ and $CD8^+$ T cells (Figure 6.3.5B-I). The ratio of lymphocytes to myeloid cells (Figure 6.3.6A), and absolute cell counts of leukocytes, monocytes, neutrophils, NK cells, B cells, total T cells, $CD4^+$ T cells, and $CD8^+$ T cells, were not different between recipient groups (Figure 6.3.6B-I).

Table 6.3.1. Composition and variability of peripheral immunophenotype at export and after colonization of recipient chow and HF microbiota groups.

	Baseline	Week 6	Week 12	Week 18
Composition (PERMANOVA)	ns $p = 0.820$ $R^2 = 0.01667$	ns $p = 0.818$ $R^2 = 0.02107$	ns $p = 0.627$ $R^2 = 0.03992$	ns $p = 0.508$ $R^2 = 0.13573$
Variability (PERMDISP)	ns $p = 0.913$ $F = 0.0124$	ns $p = 0.871$ $F = 0.021$	* ↑ HF $p = 0.014$ $F = 4.806$	ns $p = 0.513$ $F = 0.591$

Data in Figure 6.3.5 were assessed for changes in composition (PERMANOVA) and variability (PERMDISP) in R.

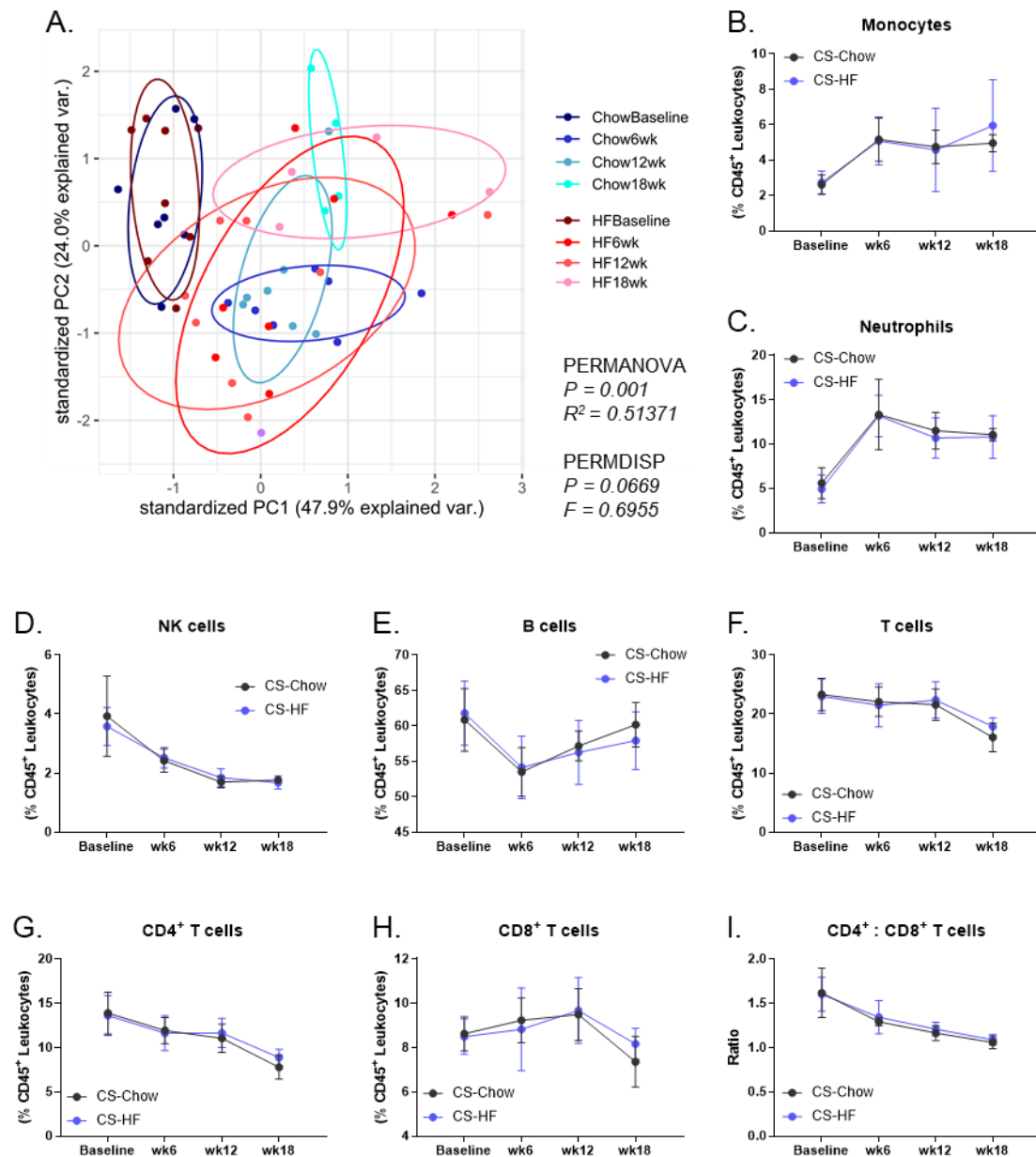


Figure 6.3.5. Peripheral immunophenotype of recipient chow and HF microbiota groups - prevalence.

Young germ free mice were colonized with microbiota from chow-fed or HF-fed mice. Peripheral blood immunophenotype was assessed by flow cytometry at export and at 6, 12, and/or 18 weeks post-microbiota exposure. (A) PCA plot of immunophenotype data on PC1 and PC2. Prevalence of: (B) total monocytes, (C) neutrophils, (D) NK cells, (E) B cells, (F) T cells, (G) CD4⁺ T cells, (H) CD8⁺ T cells. (I) ratio of CD4⁺ to CD8⁺ T cells. Data are pooled from two independent experiments of n=3-4 mice per group. Data in A are shown with dots indicating individual mice at each time point. Data in B-I are presented with a dot at the mean and error bars at \pm standard deviation. CS-Chow: ex-germ free mice with microbiota from chow-fed SPF mice. CS-HF: ex-germ-free mice with microbiota from 60% high fat-fed SPF mice. Data in A were assessed for changes in composition (PERMANOVA) and variability (PERMDISP) in R. Statistical significance for B-I was assessed by two-tailed Student's t test at each time point.

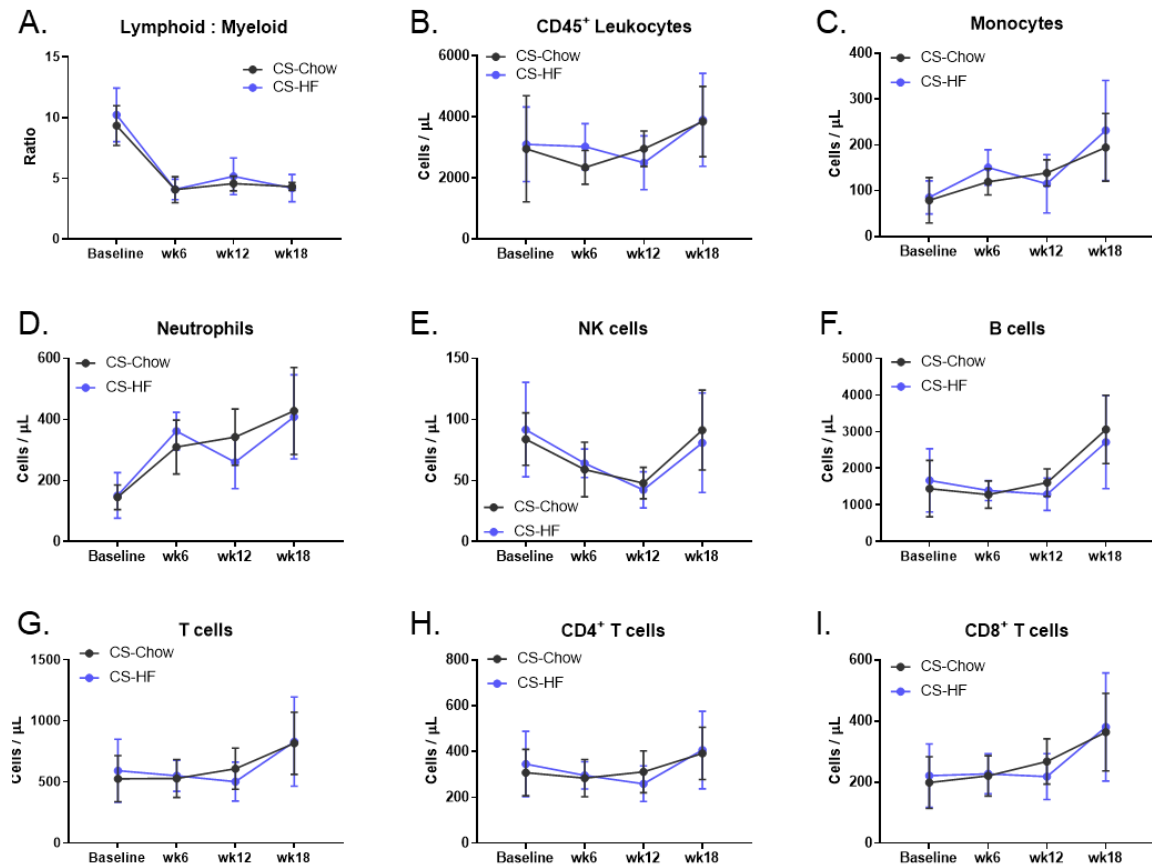


Figure 6.3.6. Peripheral immunophenotype of recipient chow and HF microbiota groups – absolute cell counts.

Young germ free mice were colonized with microbiota from chow-fed or HF-fed mice. Peripheral blood immunophenotype was assessed by flow cytometry at export and at 6, 12, and/or 18 weeks post-microbiota exposure. (A) ratio of lymphoid to myeloid cells. Absolute counts of: (B) CD45⁺ leukocytes, (C) monocytes, (D) neutrophils, (E) NK cells, (F) B cells, (G) T cells, (H) CD4⁺ T cells, (I) CD8⁺ T cells. Data are presented with a dot at the mean and error bars at \pm standard deviation. CS-Chow: ex-germ free mice with microbiota from chow-fed SPF mice. CS-HF: ex-germ-free mice with microbiota from 60% high fat-fed SPF mice. Data are pooled from two independent experiments of $n=3-4$ mice per group. Statistical significance was assessed by two-tailed Student's *t* test at each time point.

As Ly6C^{high} monocyte characteristics in particular were found to change with HF diet-induced obesity in our previous experiments (section 5.1), and as we observed a significant shift in total monocyte prevalence and cell counts between baseline and post-colonization assessments (Figure 6.3.5B; 6.3.6C), we further characterized peripheral blood Ly6C^{high} monocytes (Figure 6.3.7).

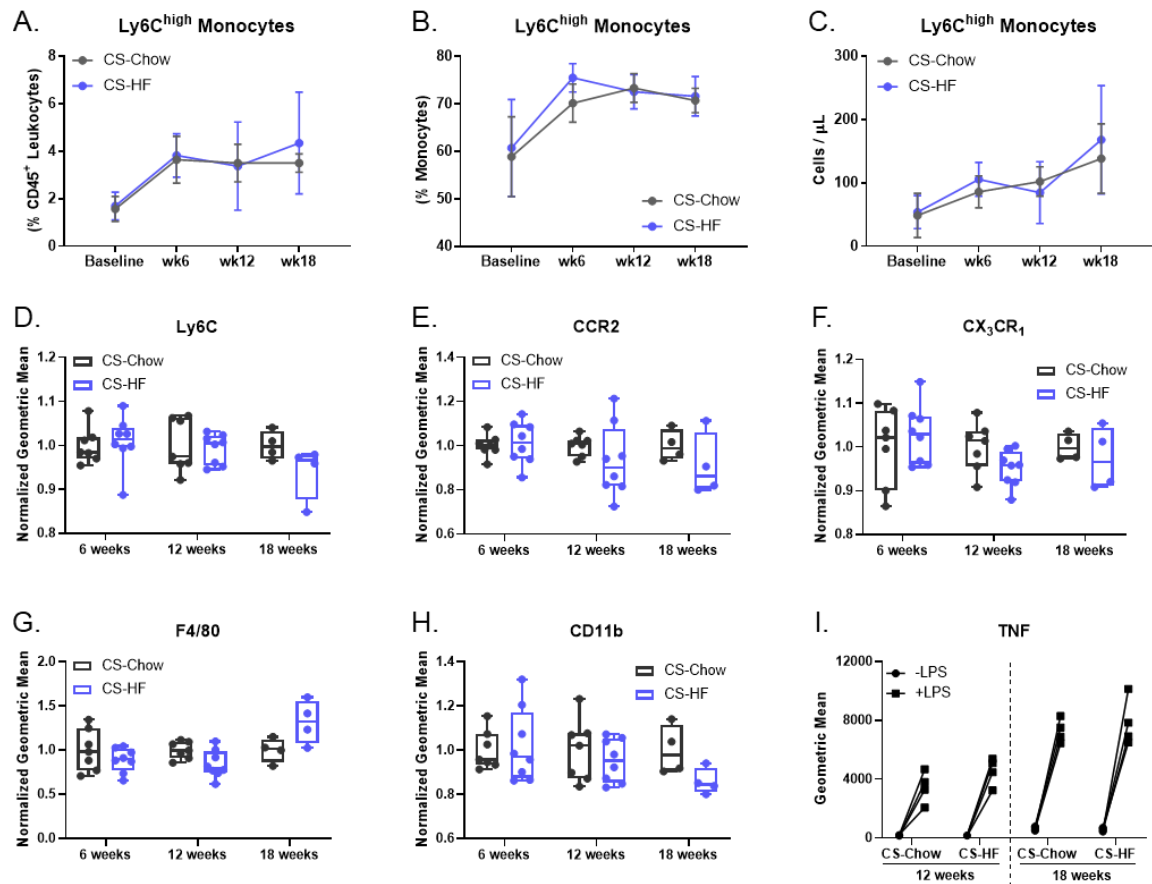


Figure 6.3.7. Peripheral blood Ly6C^{high} monocyte characteristics in recipient chow and HF microbiota groups.

Young germ free mice were colonized with microbiota from chow-fed or HF-fed mice. Peripheral blood Ly6C^{high} monocytes at export (baseline), 6 weeks, 12 weeks, and/or 18 weeks after microbiota exposure were assessed by flow cytometry. Ly6C^{high} monocyte prevalence as a proportion of: (A) CD45⁺ leukocytes, (B) monocytes. (C) absolute cell counts of Ly6C^{high} monocytes. Ly6C^{high} monocyte surface expression of: (D) Ly6C, (E) CCR2, (F) CX₃CR₁, (G) F4/80, (H) CD11b. (I) Intracellular production of TNF without LPS stimulation (-LPS) and with LPS stimulation (+LPS) after 12 and 18 weeks microbiota exposure. Data in A-C are presented with a dot at the mean and error bars at \pm standard deviation. Data in D to H are presented as box and whisker plots, minimum to maximum, with the center line at the median. Each data point indicates an individual mouse. Geometric mean expression of each marker was combined from two independent experiments of n=3-4 mice per group by normalizing the data from each mouse to the mean of the chow mouse group in each independent experiment. Data in (I) are of one independent experiment at each time point of n=4 mice per group. CS-Chow: ex-germ free mice with microbiota from chow-fed SPF mice. CS-HF: ex-germ-free mice with microbiota from 60% high fat-fed SPF mice. Statistical significance was assessed by two-tailed Student's t test at each time point.

We found no statistically significant differences between microbiota recipient groups at any of the assessed time points for peripheral blood Ly6C^{high} monocyte prevalence (Figure 6.3.7A-B) or absolute cell counts (Figure 6.3.7C). Surface expression of Ly6C, CCR2, CX₃CR₁, F4/80, or CD11b (Figure 6.3.7D-H), was likewise not different between microbiota groups. We further considered that the response of Ly6C^{high} monocytes to a stimulus may be different between the microbiota recipient groups. Using flow cytometry, we assessed peripheral blood Ly6C^{high} monocyte intracellular production of TNF in the absence of and in response to stimulation with LPS (Figure 6.3.7I). While there was an increase in TNF production in response to LPS stimulation, there were no significant differences in TNF expression between microbiota groups after 12 weeks or 18 weeks microbial exposure. These data collectively suggested that microbial colonization altered peripheral blood immune cell numbers and proportional distributions, but there were no significant differences after colonization with microbiota from chow-fed donor mice compared to colonization with microbiota from HF-fed donor mice.

Bone marrow myeloid cell progenitors

The microbiota has been shown to influence bone marrow immune cells via microbial metabolites that travel from the gut to the periphery, either directly through the bloodstream, or via the lymphatics^{322, 729, 730}. To ascertain whether bone marrow progenitors of peripheral monocytes were altered without apparent peripheral or intestinal tissue effects, we characterized the prevalence of Ly6C^{high} monocytes and precursors in femur bone marrow (Figure 6.3.8A-C), as well as proliferation and maturity characteristics of progenitors. We found no statistically significant changes in proliferation or maturity characteristics of monocyte progenitor CMP (Figure 6.3.8D-E),

GMP (Figure 6.3.8F-G), MDP (Figure 6.3.8H-K), or cMoP (Figure 6.3.8L-N) populations between the recipient chow or HF microbiota groups.

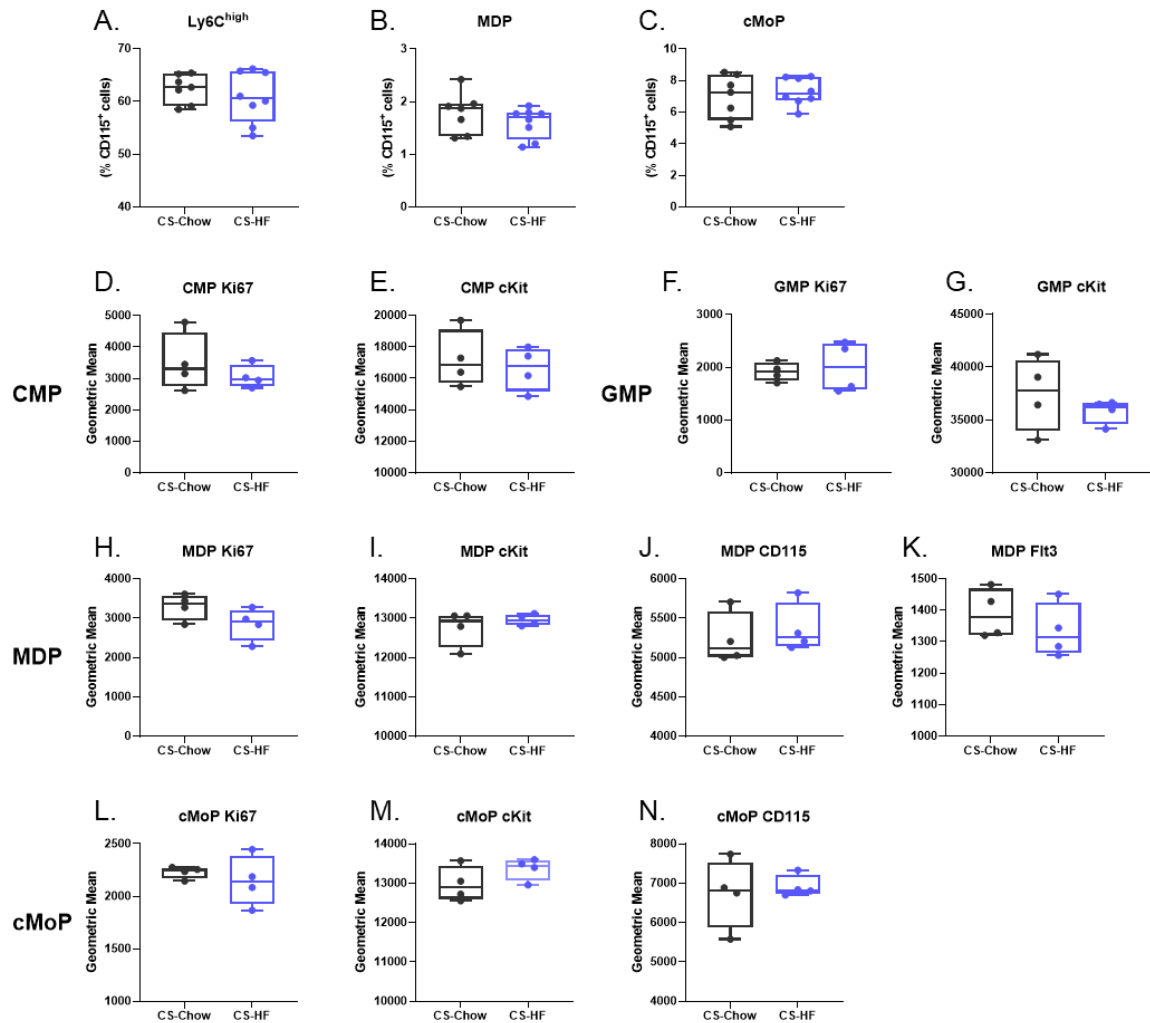


Figure 6.3.8. Bone marrow myeloid progenitors in chow and HF microbiota groups.

Young germ free mice were colonized with microbiota from chow-fed or HF-fed mice. Flow cytometry was performed at endpoint to assess monocyte bone marrow progenitor prevalence, proliferation, and maturity. Prevalence of Ly6C^{high} monocytes (A) and MDP (B) and cMoP (C) progenitors. Proliferation and maturity: CMP expression of Ki67 (D) and cKit (E); GMP expression of Ki67 (F) and cKit (G); MDP expression of Ki67 (H), cKit (I), CD115 (J), and Flt3 (K). cMoP expression of Ki67 (L), cKit (M), and CD115 (N). Data are presented as box and whisker plots, minimum to maximum, where the center line indicates the median. Data are representative of two independent experiments at 12-18 weeks post-microbiota exposure and each data point indicates a single mouse. Data in D-N are reported as geometric mean fluorescence intensity. CS-Chow: ex-germ free mice with microbiota from chow-fed SPF mice. CS-HF: ex-germ-free mice with microbiota from 60% high fat-fed SPF mice. Statistical significance was assessed by two-tailed Student's t test between microbiota groups. See Figure 1.1 for reference.

6.3.3 Discussion

We used GF mice to conduct a thorough investigation of the immunological effects of colonization with the microbiota of lean mice fed a chow diet in comparison to colonization with the microbiota of mice with HF diet-induced obesity. Our data showed that colonization of GF mice with chow-fed mouse donor microbiota or HF-fed mouse donor microbiota induced changes in peripheral and intestinal tissue immune cell populations. However, even with weekly re-exposure to the donor microbiota via cage bottom transfers, the HF microbiota was insufficient to induce physiological and immunological traits that we characterized in our model of HF diet-induced obesity in SPF mice. Specifically, we showed that there were no statistically significant differences between chow and HF microbiota recipient groups for measures of body weight, adiposity, liver weight, fasting blood glucose, energy consumption, intestinal permeability, intestine lengths, intestinal immune cell populations, caecal weight, peripheral blood immunophenotype, peripheral blood Ly6C^{high} monocyte surface phenotype and production of TNF in response to LPS, or bone marrow myeloid progenitor prevalence and expression of proliferation markers. These data collectively imply that the presence of a microbiota, rather than its composition, altered immunological and physiological characteristics in the recipient mice.

While the data from these experiments disproves our initial hypotheses about the causative role of the microbiota in obesity, and may seem contrary to more ‘classic’ research on microbiota colonization of germ free mice outlined in the introduction, evidence from more recent experiments supports our findings and suggests that microbiota-diet interactions may explain our results. For example, Rodriguez and

colleagues examined interactions of the microbiota, diet, and obesity by transplanting gut microbiota from lean or obese human donors into mice with antibiotic-depleted microbiota, and then mice were fed one of three diets for 22 weeks: a standard chow diet, a high fat high sugar Western diet, or a high fat diet. Despite mice having a distinct microbiota according to their microbiota donor, all mice on a specific diet had similar final body weight, adiposity, overall weight gain, and glucose tolerance, with distinct alterations to their microbiota associated with the allocated diet⁷³¹. In addition, studies have shown that diet-microbiota interactions after colonization of GF or antibiotic-treated mice contribute to adiposity and adipose tissue inflammation^{398, 707, 732}, and tissue pathology in DSS-elicited colitis^{733, 734}. It has also been reported that distinct microbiota can produce similar bacterial metabolites that induce similar effects on body weight and glucose tolerance^{655, 735}. These studies collectively suggest that obesity, and accompanying metabolic dysfunction and tissue inflammation, are associated with diet-microbiota interactions that result in the production of specific microbial metabolites and common bacterial products like LPS or peptidoglycan, and are not just a consequence of the intestinal microbiota and the presence or absence of specific genera or species of bacteria (or other microorganisms).

We did not expect the effects of diet to be sufficiently large to eradicate any differences between colonization with chow or HF microbiota in the recipient mice, especially with weekly re-exposure from donor mice (though it is unclear how much the microbiota of the recipient mice would change with re-exposure to the donor microbiota). Analysis of both the intestinal microbiome and metabolite profiles from the donor and recipient mice in these experiments may therefore provide more insight into the

development of obesity-associated inflammation and its effects on local intestinal and peripheral immune cell populations. Future experiments could also examine whether the HF diet, specific components of the diet, or an external challenge such as infection, has differential effects in chow and HF microbiota recipient mice.

While we assumed, based on previous unpublished and published data from our lab that used a similar colonization methodology³³⁷, that the donor microbiome would be transferred to the recipient mice, we were not able to confirm this. Fecal pellets and caecal contents were collected from recipient and donor mice for 16S rRNA sequencing, but at the time of submission of this thesis, the sequencing results were not available. However, to our knowledge, this is still the first report of an extended assessment of peripheral immunophenotype and intestinal macrophage changes that occur after colonization of germ free mice, and this data by itself is of potential interest to the scientific community. In summary, while we observed that colonization of germ free mice altered peripheral, bone marrow, and intestinal immune cell populations, results were similar in mice that received microbiota from chow-fed or HF-fed donors, and this may be due to diet-microbiota interactions.

6.4 Intestinal macrophages in aging

6.4.1 Introduction

Intestinal microbiota-derived immune and metabolic factors may induce local and systemic inflammation in aging. Studies have shown that age-associated inflammation, similar to obesity-associated inflammation, is linked with microbial dysbiosis and increased intestinal permeability in humans^{736, 737, 738}, and in a variety of model organisms including *Drosophila melanogaster*⁷³⁹, *Caenorhabditis elegans*⁷⁴⁰, non-human primates^{741, 742}, rats^{743, 744}, and mice^{337, 745, 746}. Elevated intestinal permeability with increasing biological age is thought to contribute to higher translocation of pro-inflammatory bacterial products, bacteria themselves, and food antigens, into the lamina propria, which can then enter the vasculature and lymphatics, contributing to systemic inflammation as well as metabolic dysfunction⁷⁴⁷. Accordingly, circulating LBP and soluble CD14 (co-receptor for TLR4) in humans correlate with poor health outcomes with increasing biological age⁷³⁸. Old mice fed a HF diet compared to a chow diet also have greater microbial dysbiosis, intestinal permeability, and systemic inflammation^{748, 749}.

A causal relationship between microbial dysbiosis and ‘inflammaging’ has been shown through microbiota colonization experiments in GF mice. The Bowdish lab has reported that colon paracellular permeability and circulating pro-inflammatory cytokines were elevated in young GF mice colonized with microbiota from old SPF mice, in comparison to young GF mice colonized with microbiota from young SPF mice³³⁷. It has also been reported that young GF mice colonized with microbiota from old mice, in comparison to colonization with microbiota from young mice, have increased circulating TLR2-stimulating bacterial products, and higher frequencies of Th1 cells in Peyer’s

patches and Th2 and T_{reg} populations in the spleen⁷⁵⁰. These studies suggested that transfer of a dysbiotic microbiota is sufficient to promote systemic inflammation, intestinal permeability, and changes to tissue immune cell populations. Furthermore, treatment of old mice with probiotics has shown success in preventing microbial dysbiosis, increased intestinal permeability, systemic inflammation, and/or metabolic dysfunction^{740, 751, 752}. It has also been demonstrated that cohousing young and old mice for 30-40 days has an ‘immune boosting’ effect on local adaptive immunity in the gut, rescuing an age-associated reduction of intestinal germinal centre B cells and T follicular helper cells in Peyer’s patches, though there were no functional differences in the systemic adaptive immune response to immunization between old mice and cohoused old mice⁷⁵³. Similarly, housing old mice for 6 weeks in cages containing used bedding from young mice improved intestinal immunosurveillance by increasing IgA production and functional maturation and antigen sampling activities of M cells⁷⁵⁴. The changes in those papers were attributed to factors in the young microbiota that were able to ‘rescue’ age-associated losses in immune function and cell proliferation, but it is unclear if there is a similar effect on innate immune cells like monocytes and macrophages.

As in obesity, monocytes are particularly sensitive to the effects of age-associated chronic inflammation. Increased myelopoiesis in aging elevates the prevalence of circulating CD16⁺ intermediate and/or non-classical monocytes in humans^{755, 756, 757, 758} and Ly6C^{high} monocytes in mice^{336, 337}, which produce more pro-inflammatory cytokines in comparison to biologically young monocytes. Chronic exposure of young mice to low doses of LPS induces changes in myelopoiesis similar to those observed in old mice⁷⁵⁹. Effects of aging on macrophages include decreased phagocytic and bactericidal

activity^{336, 760, 761, 762, 763}, altered TLR expression and activation^{764, 765}, and antigen-presentation^{766, 767}, as well as an increase in pro-inflammatory cytokine production^{336, 337, 764}, and dysregulation of tissue repair mechanisms⁷⁶⁸. Circulating pro-inflammatory cytokine levels are decreased in old TNF^{-/-} mice compared to old WT mice^{336, 337, 769}, and in old WT mice treated with anti-TNF therapy³³⁶ or clodronate liposomes⁷⁶⁹, compared to untreated old WT mice, indicating that monocytes and macrophages are both influenced by, and contribute to, age-associated chronic inflammation. Age-associated changes in monocyte and macrophage function also affect survival, activation, and proliferation of other immune cells, compromising adaptive immunity⁷⁶⁸.

Recruitment of monocytes to intestinal tissues to replenish short-lived macrophage populations under conditions of homeostasis presumably occurs throughout the lifespan of a mouse^{214, 235}, so age-associated changes to peripheral monocytes and bone marrow-derived macrophages could influence monocyte-derived intestinal macrophage populations. There may also be age-associated changes to tissue-resident long-lived intestinal macrophages programmed by both intrinsic factors and extrinsic factors, given their sensitivity to microenvironment stimuli from surrounding immune cells, the microbiota and microbial products, and structural tissues. For example, aging is associated with dysregulation of intestinal blood perfusion and oxygenation, which can induce hypoxia⁷⁷⁰, and HIF-1 α (hypoxia inducible factor-1 α) has been reported to induce pro-inflammatory cytokine expression within intestinal macrophages^{771, 772}. It was reported that the number of CD11c⁺ cells (presumptive macrophages or dendritic cells) decreased in Peyer's patches in old mice compared to young mice⁷⁵⁴, but it was also reported that the number of myeloperoxidase-producing cells (monocytes/neutrophils)

was increased in small intestine epithelial crypts of old mice compared to young mice⁷⁷³. Microarray analysis of colon and ileum tissue homogenates in young mice (3 months) and old mice (19 months) identified age-associated changes in Ingenuity Pathway Analysis categories, including ‘recruitment of macrophages’ and ‘activation of phagocytes/macrophages’⁷⁷⁴. However, there had been no direct investigation of effects of age on intestinal macrophage populations, nor on the effects of age-associated microbial dysbiosis in mediating those changes.

We aimed to characterize intestinal macrophage populations in the colon, as previous data from our lab identified a significant increase in paracellular permeability in colon tissue, but not ileum tissue, of old mice³³⁷. We predicted, based on the parallels between obesity and aging, with observations of chronic low-grade inflammation, peripheral monocytes, microbial dysbiosis, and increased intestinal permeability, that intestinal macrophage populations would have similar changes between young and old mice as we observed in lean mice and mice with diet-induced obesity in section 6.1.

6.4.2 Results

Effects of aging on colon macrophages in SPF mice

We examined colon tissues and colon macrophage populations in young (3-5 months) and old (18-24 months) female SPF mice. There were no differences in colon length between young and old SPF mice (Figure 6.4.1A), though overall tissue weight increased (Figure 6.4.1B), likely as older colons were generally observed to have increased fecal contents and a distended appearance. We assessed colon macrophages in young and old SPF mice by flow cytometry. Total cell counts of macrophages were

similar between young and old mice (Figure 6.4.1C). There was a significant increase in the prevalence of macrophages (as a proportion of total leukocytes) in old mice compared to young mice (Figure 6.4.1D), and there was a significant increase in the prevalence of $CD4^-TIM4^-$ macrophages and a decrease in $CD4^+TIM4^+$ macrophages with age (as a proportion of total macrophages; Figure 6.4.1E). The number of $CD4^+TIM4^+$ macrophages was lower in old mice compared to young mice (Figure 6.4.1F).

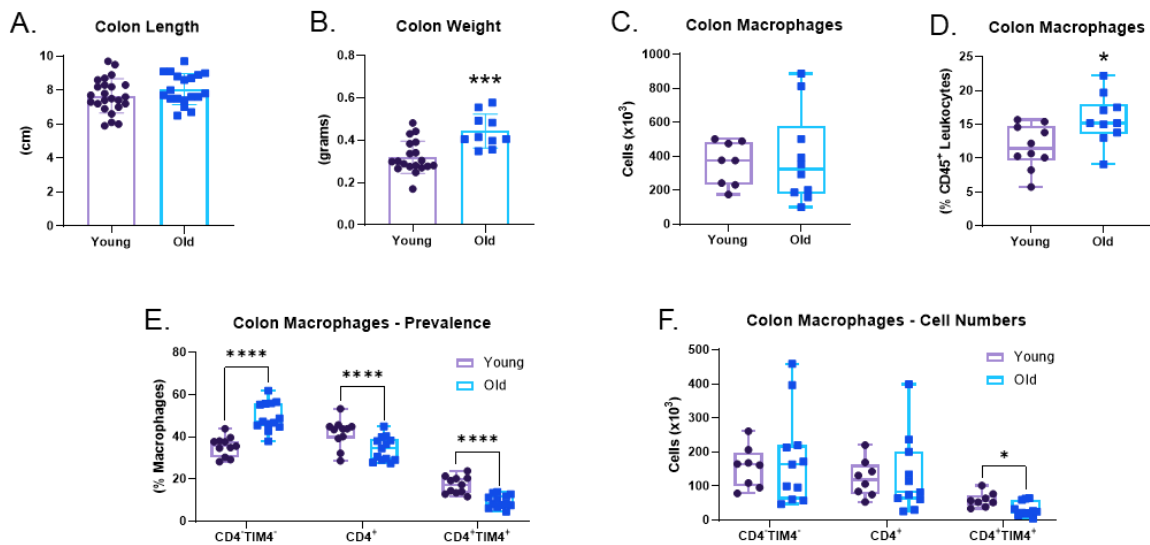


Figure 6.4.1. Young and old SPF mouse colon physiology and macrophage populations.

SPF young (3-5 months) and old (18-24 months) mouse colons were processed and stained for flow cytometry analysis. (A) colon length. (B) colon weight. (C) absolute cell counts of macrophages. (D) prevalence of macrophages (as a proportion of total $CD45^+$ leukocytes). $CD4^-TIM4^-$, $CD4^+$, and $CD4^+TIM4^+$ macrophages: (E) as a proportion of total macrophages, (F) absolute cell counts. Data in A-B are presented with box height at the mean with error bars indicating \pm standard deviation. Data in C-G are presented as box and whisker plots, minimum to maximum, where the center line indicates the median. Each data point indicates an individual mouse. Data are combined from multiple independent experiments of $n=1-4$ mice per group: (A) Young $n=24$, Old $n=19$; (B) Young $n=19$, Old $n=10$; (C) and (F) Young $n=8$, Old $n=11$; (D) and (E) Young $n=10$, Old $n=10$. Statistical significance between age groups was assessed by Student's two-tailed t test. * $p<0.05$, *** $p<0.001$, **** $p<0.0001$.

We next assessed macrophage intracellular cytokine production by flow cytometry. From initial assessments of total $MHCII^+$ macrophages, we found that production of IL-10 (Figure 6.4.2A) and IL-6 (Figure 6.4.2B) was similar between young

and old mice, with or without LPS stimulation, but that production of TNF was increased even in the absence of LPS stimulation in old mouse macrophages (Figure 6.4.2C). We further assessed intracellular production of IL-10 and TNF in $CD4^-TIM4^-$, $CD4^+$, and $CD4^+TIM4^+$ macrophages in the absence of stimulation. We did not observe differences in expression of IL-10 (Figure 6.4.2D), but all macrophage populations in old mice compared to young mice had increased expression of TNF (Figure 6.4.2E). We also assessed whether proliferation was affected by age (Figure 6.4.2F). Expression of Ki67 was highest in $CD4^-TIM4^-$ macrophages, as observed previously (Figure 6.1.7G). Proliferation was similar in $CD4^-TIM4^-$ and $CD4^+$ macrophages in young and old mice, but decreased significantly in old mouse $CD4^+TIM4^+$ macrophages.

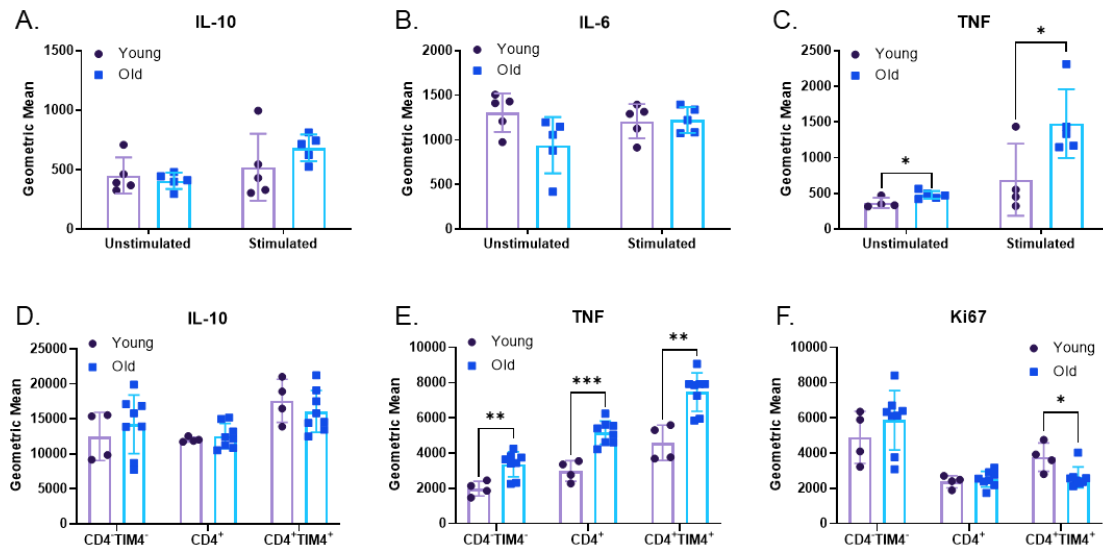


Figure 6.4.2. Young and old SPF mouse colon macrophage intracellular cytokines.

SPF young (3-5 months) and old (18-24 months) mouse colon tissue was processed and stained for flow cytometry analysis. Colon macrophage intracellular production of: (A) IL-10, (B) IL-6, and (C) TNF without LPS stimulation (Unstimulated) and with LPS stimulation (Stimulated). $CD4^-TIM4^-$, $CD4^+$, and $CD4^+TIM4^+$ macrophage intracellular expression of: (D) IL-10, (E) TNF, and (F) Ki67 assessed without stimulation. Data are reported as geometric mean fluorescence intensity. Data are presented with box height at the mean with error bars indicating \pm standard deviation. Each dot indicates an individual mouse. Data in A-C are from a single experiment of $n=5$ mice per group, and data in D-E are from a single experiment of Young $n=4$ and Old $n=8$. Statistical significance was determined using an unpaired Student's t-test for each experimental condition in A-C and for each macrophage subset in D-F. * $p<0.05$, ** $p<0.01$, *** $p<0.001$.

In summary, young and old SPF mice had similar colon lengths and total numbers of intestinal macrophages, and their macrophages expressed similar intracellular levels of IL-10, but old mouse macrophages had higher intracellular production of the pro-inflammatory cytokine TNF in comparison to young mouse macrophages. In comparison to young mice, old mice had an increased prevalence of CD4⁻TIM4⁻ macrophages (as a proportion of total macrophages), whereas there was a decrease in CD4⁺TIM4⁺ macrophage total cell numbers, relative prevalence, and proliferation.

Effects of aging on colon macrophages in the absence of the microbiome

We subsequently considered whether aging itself alters intestinal immune cell populations in the absence of the microbiome, by assessing colon macrophage populations in female young (3-5 months) and old (18-22 months) germ free mice. GF mice had similar colon lengths irrespective of age (Figure 6.4.3A), though caecal weight was ~5-fold greater in old mice (Figure 6.4.3B), consistent with previous observations⁷⁷⁵. The absolute numbers of colon macrophages (Figure 6.4.3C), numbers of colon macrophages adjusted by tissue length (Figure 6.4.3D), and the prevalence of macrophages (Figure 6.4.3E), were also not different between young and old GF mice. However, we observed that the prevalence of CD4⁻TIM4⁻ macrophages was increased and the prevalence of CD4⁺ macrophages was decreased in old GF mice compared to young GF mice (Figure 6.4.3F). These data suggest that age, independent of the microbiome, has an impact on colon macrophage population dynamics.

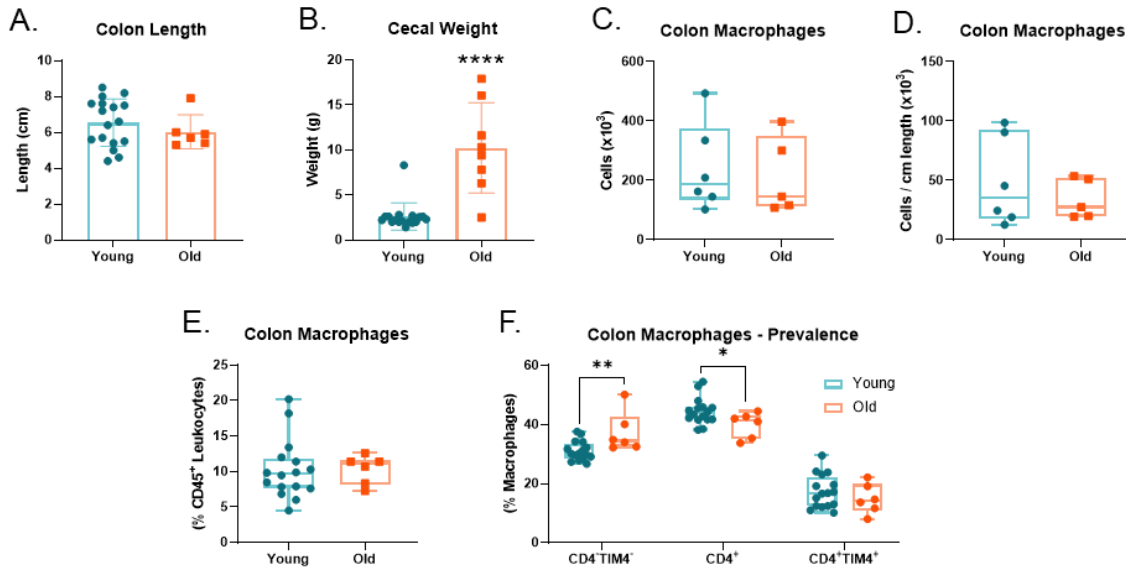


Figure 6.4.3. Young and old germ free mouse intestinal physiology and colon macrophage prevalence.

Young (3-5 months) and old (18-24 months) germ free mouse colon macrophages were assessed by flow cytometry. (A) colon length. (B) caecal weight. (C) absolute cell counts of total macrophages. (D) total macrophage counts normalized by tissue length. (E) prevalence of total macrophages (as a proportion of CD45⁺ leukocytes). (F) prevalence of CD4⁺TIM4⁻, CD4⁺, and CD4⁺TIM4⁺ macrophages (as a proportion of total macrophages). Each data point indicates an individual mouse. Data in A-B are presented with box height at the mean with error bars indicating \pm standard deviation. Data in C-F are presented as box and whisker plots, minimum to maximum, with the center line at the median. Data are combined from multiple independent experiments of n=1-3 mice per group. Young n=6-16, Old n=5-6. Statistical significance was assessed by Student's two-tailed t test. * $p < 0.05$, ** $p < 0.01$, **** $p < 0.0001$.

Cohousing young and old SPF mice – effects on old mouse colon macrophages

We next considered whether exposure of old mice to a young microbiota can alter their colon macrophage population dynamics. Old SPF mice (20-22 months of age) were cohoused with young SPF mice (4-7 months of age) for 8-10 weeks, and then we assessed colon macrophage populations by flow cytometry (Figure 6.4.4). We compared data from non-cohoused young and old SPF mice with data from the old cohoused mice. The total prevalence of macrophages in the old cohoused mice remained more similar to old non-cohoused control mice than young non-cohoused control mice (Figure 6.4.4A).

Macrophage cell counts were similar in all groups (Figure 6.4.4B). The absolute cell

counts of CD4⁺TIM4⁺ macrophages were decreased in the colons of old cohoused mice, like the old non-cohoused controls, in comparison to the young non-cohoused controls (Figure 6.4.4C). Assessment of the prevalence of CD4⁺TIM4⁺, CD4⁺, and CD4⁺TIM4⁺ macrophages (as a proportion of total macrophages) showed that they were more similar between old cohoused mice and old non-cohoused control mice (Figure 6.4.4D-F) than old cohoused mice and young non-cohoused control mice. These observations showed that short-term cohousing with young SPF mice does not affect colon macrophage numbers or prevalence in old SPF mice. This implied that the young microbiota cannot ‘rescue’ age-associated changes to colon macrophage dynamics.

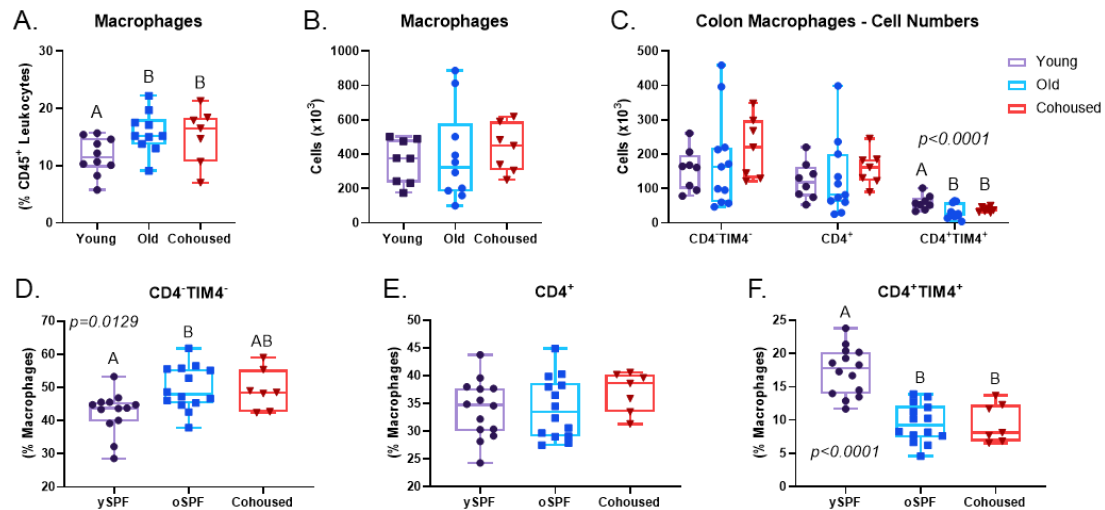


Figure 6.4.4. Cohousing young and old SPF mice does not alter colon macrophage dynamics in old mice.

Old SPF mice (20-22 months) were cohoused with young SPF mice (4-7 months) for 8-10 weeks prior to assessment of colon macrophages by flow cytometry. (A) prevalence of total macrophages. (B) absolute cell counts of macrophages. (C) absolute cell counts of CD4⁺TIM4⁺, CD4⁺, and CD4⁺TIM4⁺ macrophages. Prevalence of: (D) CD4⁺TIM4⁺, (E) CD4⁺, (F) CD4⁺TIM4⁺ macrophages (as a proportion of total macrophages). Data are plotted with young SPF (ySPF) and old SPF (oSPF) controls for comparison to old cohoused SPF mice (Cohoused). Each data point indicates an individual mouse. Data are presented as box and whisker plots, minimum to maximum, where the center line indicates the median. Data for ‘Cohoused’ is from one independent experiment of n=7 mice. Data for ‘ySPF’ and ‘oSPF’ are pooled from multiple independent experiments of n=1-4 mice per group, with ySPF n=8-14 and oSPF n=11-14. Statistical significance for each immune cell population was assessed by one-way ANOVA with Tukey’s post-hoc test, and letters indicate statistical similarities or differences.

Colonization of young GF mice with young and old microbiota

To assess effects of age-associated microbial dysbiosis on intestinal macrophage populations, we colonized adult middle-aged GF mice (~9-12 months of age) with young microbiota (from mice 3-4 months of age), or old microbiota (from mice 19-20 months of age), by exposing the GF mice to cage bottoms from the donor mice with weekly cage changing. Donor and recipient mice were maintained on the same diet. After colonization, mice were aged to ~20-22 months. We predicted that GF mice colonized with the old ‘dysbiotic’ microbiota would exhibit the age-related changes to intestinal macrophages that we identified (Figure 6.4.1), whereas intestinal macrophages from GF mice colonized with the young microbiota would more closely resemble those of young SPF mice.

There was a main effect of microbiota type, i.e. whether mice received ‘young’ or ‘old’ microbiota, on mouse weight (Figure 6.4.5A), but post-hoc tests were not significantly different between microbiota groups at baseline or endpoint. Mice that were colonized with the ‘old’ microbiota compared to mice that were colonized with the ‘young’ microbiota had increased caecal weight (Figure 6.4.5B) and reduced colon length (Figure 6.4.5C), though small intestine length was similar (Figure 6.4.5D). There were no differences in the prevalence (as a proportion of total leukocytes) or absolute cell counts of eosinophils (Figure 6.4.4E and I), CD4⁺ T cells (Figure 6.4.5F and J), Ly6C^{high} monocytes (Figure 6.4.5G and K), or total macrophages (Figure 6.4.5H and L), or cell counts of those populations normalized to colon length (data not shown) between microbiota groups. Furthermore, populations of CD4⁻TIM4⁻, CD4⁺, and CD4⁺TIM4⁺ macrophages were unaffected by the type of microbiota colonization, whether by

prevalence (Figure 6.4.6A-B), cell counts (Figure 6.4.6C), or cell counts normalized to colon length (Figure 6.4.6D).

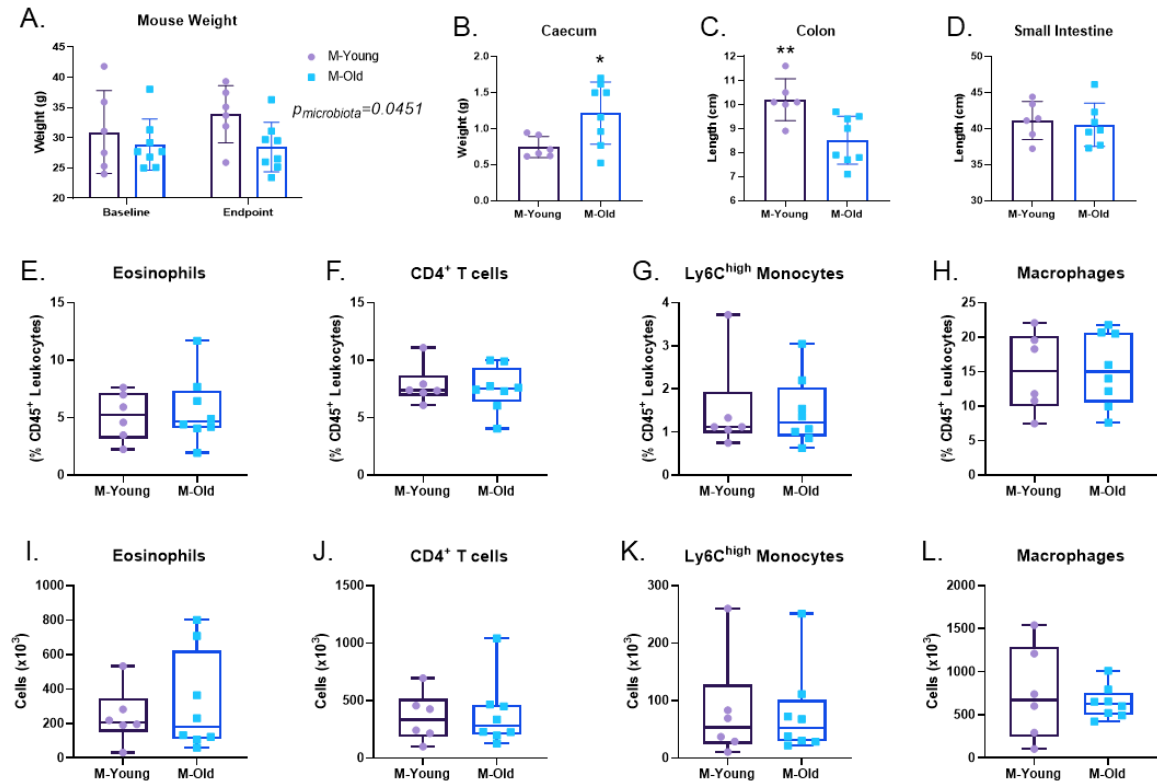


Figure 6.4.5. Effects of young and old microbiota colonization on intestinal physiology and colon immune cell populations.

Germ free mice 9-12 months of age were colonized with young SPF microbiota (3-4 months; ‘M-Young’) or old SPF microbiota (19-20 months; ‘M-Old’) and then aged for ~10 months prior to assessment of intestinal physiology and immune cell populations by flow cytometry (i.e. at 19-22 months of age). (A) body weight. (B) caecal weight. (C) colon length. (D) small intestine length. Colon immune cell populations were assessed by flow cytometry. Prevalence (as a proportion of CD45⁺ leukocytes) of: (E) eosinophils, (F) CD4⁺ T cells, (G) Ly6C^{high} monocytes, (H) total macrophages. Absolute cell counts of: (I) eosinophils, (J) CD4⁺ T cells, (K) Ly6C^{high} monocytes, (L) total macrophages. Data in A-D are presented with box height at the mean with error bars indicating \pm standard deviation. Data in E-L are presented as box and whisker plots, minimum to maximum, with the center line at the median. Data are from one independent experiment. Young n=6, Old n=8. Statistical significance was assessed in A by two-way ANOVA, and in B-L by two-tailed Student’s t test. * $p < 0.05$, ** $p < 0.01$.

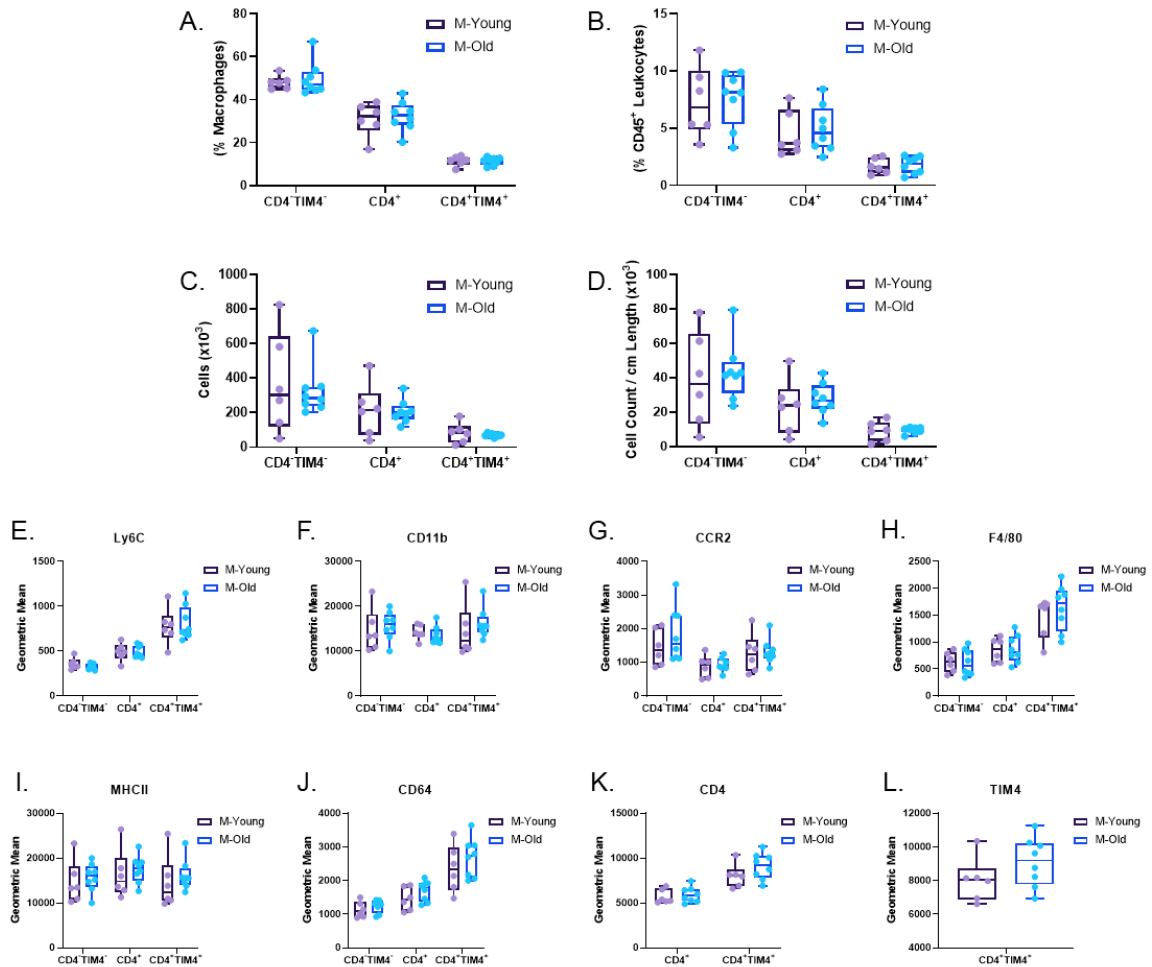


Figure 6.4.6. Effects of young and old microbiota colonization on colon macrophages.

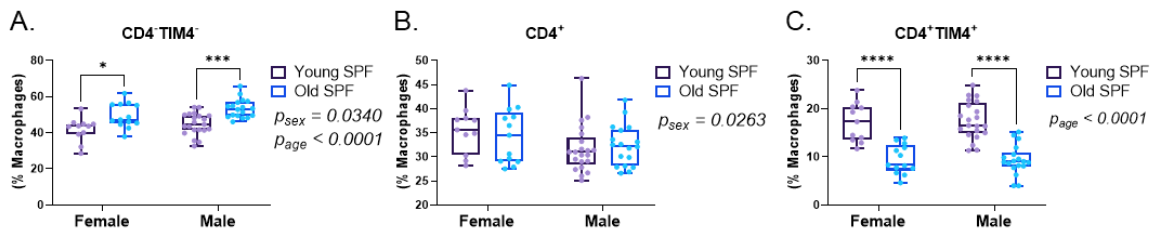
Germ free mice 9-12 months of age were colonized with young SPF microbiota (3-4 months; 'M-Young') or old SPF microbiota (19-20 months; 'M-Old') and then aged for ~10 months prior to assessment of intestinal macrophages by flow cytometry (i.e. at 19-22 months of age). CD4⁺TIM4⁻, CD4⁺, and CD4⁺TIM4⁺ macrophages as a proportion of: (A) total macrophages, (B) total leukocytes. CD4⁺TIM4⁻, CD4⁺, and CD4⁺TIM4⁺ macrophages: (C) absolute cell counts, (D) cell counts normalized by colon length. Geometric mean surface expression of: (E) Ly6C, (F) CD11b, (G) CCR2, (H) F4/80, (I) MHCII, (J) CD64, (K) CD4, (L) TIM4. Each data point indicates an individual mouse. Data are presented as box and whisker plots, minimum to maximum, where the center line indicates the median. Data are from one independent experiment. M-Young n=6, M-Old n=8. Statistical significance was assessed by two-tailed Student's t test between microbiota groups for each macrophage population.

Macrophage population dynamics in both microbiota groups were more similar to those of old SPF mice than young SPF mice (Appendix IV). CD4⁻TIM4⁻, CD4⁺, and CD4⁺TIM4⁺ surface expression of monocyte-to-macrophage markers Ly6C, CD11b, CCR2, F4/80, MHCII, CD64, CD4 and TIM4 was not different between the microbiota groups (Figure 6.4.6E to L). Therefore, colonization of middle-aged GF mice with young or old microbiota, followed by aging of the mice to ~20-22 months, had a similar effect on intestinal macrophage prevalence, cell numbers, and surface phenotype.

Age, sex, the microbiome, and colon macrophages

While conducting our comparisons of colon macrophages in female young and old SPF and GF mice, we also assessed macrophages in male mice (Figure 6.4.7). In SPF mice, we observed significant effects of biological sex on CD4⁻TIM4⁻ macrophages (slightly higher in males; Figure 6.4.7A) and CD4⁺ macrophages (slightly lower in males; Figure 6.4.7B), though the prevalence of CD4⁺TIM4⁺ macrophages was similar (Figure 6.4.7C). We found that biological age had similar effects in both SPF female and male mice (i.e. an increase in the prevalence of CD4⁻TIM4⁻ macrophages and a decrease in CD4⁺TIM4⁺ macrophages). In GF mice, like SPF mice, there was a significant effect of sex on CD4⁻TIM4⁻ macrophages (slightly higher in male mice; Figure 6.4.7D), but there were no effects of biological sex on CD4⁺ macrophages (Figure 6.4.7E) or CD4⁺TIM4⁺ macrophages (Figure 6.4.7F). There was a main effect of age on CD4⁻TIM4⁻, CD4⁺, and CD4⁺TIM4⁺ macrophage populations in GF mice. While there may be functional differences by sex which we did not evaluate, these data indicate that biological sex affects macrophage dynamics within the colon, and that there are similar trends of age effects in both sexes under conditions of homeostasis in either SPF or GF mice.

SPF Mice



Germ Free Mice

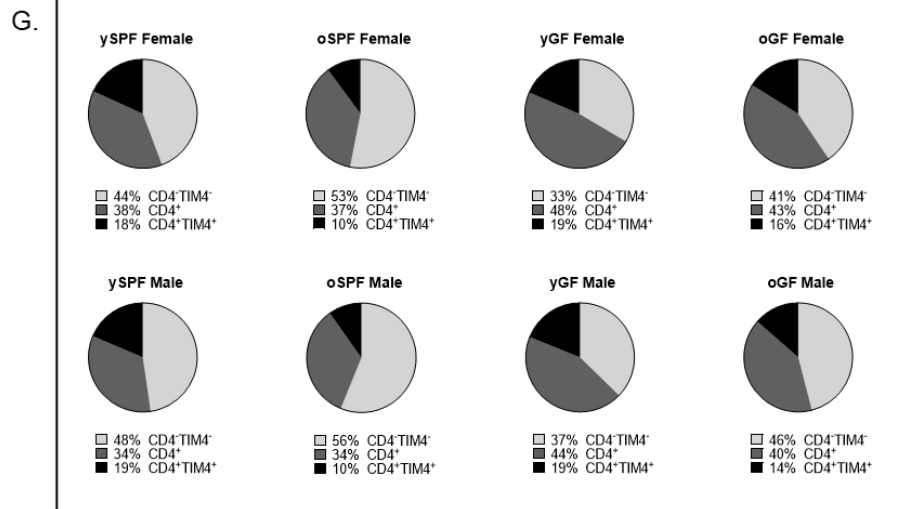
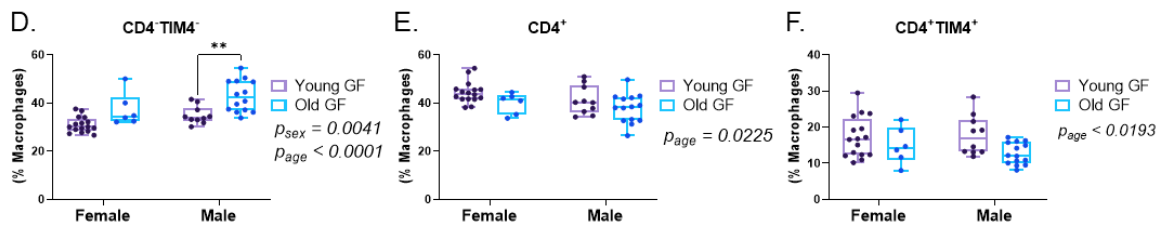


Figure 6.4.7. Comparison of colon macrophage populations by biological sex and age in SPF and GF mice.

SPF and GF young (3-5 months) and old (18-24 months) female and male mouse colons were processed for flow cytometry analysis of tissue macrophages. Prevalence of macrophages in SPF mice: (A) CD4⁺TIM4⁻, (B) CD4⁺, and (C) CD4⁺TIM4⁺ (as a proportion of total macrophages). Prevalence of macrophages in GF mice: (D) CD4⁺TIM4⁻, (E) CD4⁺, and (F) CD4⁺TIM4⁺ (as a proportion of total macrophages). (G) pie chart summaries of macrophage populations in A-F. Data in A-F are presented as box and whisker plots, minimum to maximum, where the center line indicates the median. Each data point indicates an individual mouse. Data are combined from multiple independent experiments of n=1-4 mice per group. (A-C and G) SPF: Female Young n=11; Female Old n=13; Male Young n=21; Male Old n=18. (D-F and G) GF: Female Young n=16; Female Old n=6; Male Young n=10; Male Old n=14. Statistical significance between age groups in A-F was assessed by two-way ANOVA with Tukey's post-hoc test. **p*<0.05, ***p*<0.01, ****p*<0.001, *****p*<0.0001.

6.4.3 Discussion

In these experiments, we observed that age influences colon macrophage dynamics. There was an increase in the prevalence of macrophages in the colons of old SPF mice (as a proportion of total leukocytes), though cell numbers did not change with age (Figure 6.4.1). Of particular interest were the $CD4^+TIM4^+$ macrophages in old mice, which, in comparison to young mice, had decreased prevalence, total cell numbers, and proliferation, as well as significantly increased TNF production even in the absence of stimulation, though they retained the capacity to produce similar levels of IL-10 (Figures 6.4.1 and 6.4.2). These data could indicate that the self-renewal capacity of $CD4^+TIM4^+$ macrophages decreases with age, and that this causes a gradual reduction in $CD4^+TIM4^+$ macrophage numbers. As long-lived macrophages like the $CD4^+TIM4^+$ population are often found in association with mucosal endothelial cells, lymphatic vessels, and enteric neurons⁴⁰⁸, the gradual loss of this population, and its more pro-inflammatory phenotype, may be related to age-associated changes that disrupt blood vessel and lymphatic barriers^{771, 772}, and dysregulate neuronal signalling⁷⁷⁶ and smooth muscle contraction⁷⁷⁷. As the total macrophage cell counts also did not change with age, it is possible that less mature $CD4^+$ and $CD4^-TIM4^-$ macrophages may take on some of those roles, as it has been reported that $TIM4^+$ macrophages in the peritoneal cavity are replaced with increasing age by $TIM4^-$ macrophages that are functionally indistinguishable²³². The $CD4^+$ and $TIM4^-CD4^-$ colon macrophages also had higher intracellular expression of TNF in old mice compared to young mice. Similar to our data, it was reported that the prevalence of $CD45^+F4/80^+$ macrophages in the muscularis region of the small intestine was similar in young and old mice, but that the macrophages in old mice lost their anti-

inflammatory phenotype and increased their pro-inflammatory cytokine production, promoting a decrease in neuron proliferation and an increase in neuronal apoptosis⁷⁷⁸.

We also observed that age in the absence of the microbiota has an impact on colon macrophage populations in both male and female mice. There were changes to CD4⁺TIM4⁺ and CD4⁺ macrophage dynamics in young and old GF mice, though the prevalence of total macrophages and CD4⁺TIM4⁺ macrophages remained similar (Figure 6.4.3). In combination with our observations in section 6.3, these data suggested that both chronological age and microbial colonization influence macrophage dynamics in the colon. To further explore the effects of the microbiota and aging on colon macrophage populations, we cohoused old SPF mice with young SPF mice, and colonized GF mice with young or old mouse microbiota. Cohousing young and old SPF mice for 8-10 weeks did not change colon macrophage population characteristics in the old SPF mice (Figure 6.4.4). GF mice that were colonized with young or old microbiota at ~9-12 months of age and subsequently aged to ~20-22 months likewise had similar colon macrophage and other immune cell population dynamics between recipient microbiota groups (Figures 6.4.5 and 6.4.6). 16S rRNA sequencing data from the cohousing and colonization experiments were unavailable at the time of writing this thesis, so we cannot comment on how similar or different the mouse microbiomes were between the experiment groups. While macrophage and other intestinal immune cell populations were similar between the microbiota groups, the GF mice colonized with young microbiota had a reduced caecal weight and increased colon length in comparison to the GF mice colonized with the old microbiota. These data could be an indication of reduced fermentation or production of SCFAs, in combination with changes in energy absorption, due to differences in

microbiota composition^{664, 779}. Irrespective, any differences in the microbial or metabolite composition between the ‘young’ and ‘old’ microbiota groups were not sufficient to alter immune cell composition in the colon.

As previously discussed, colonization itself, rather than microbiota composition, could be the defining factor dictating macrophage population composition in recipient mice. However, as mentioned, it was reported that exposure of old SPF mice to a young microbiota was sufficient to improve aspects of intestinal adaptive immunity^{753, 754}, and elevated Th1 cells in Peyer’s patches have been reported in GF mice colonized with old microbiota in comparison to GF mice colonized with young microbiota⁷⁵⁰. It seems unlikely that innate immune cells like macrophages would be unaffected by changes to the composition of the intestinal microbiota. As mentioned, we have previously shown that there is an increase in colon paracellular permeability in old mice compared to young mice³³⁷, but even if the intestinal epithelial barrier is maintained, intestinal macrophages can be exposed to luminal antigens directly via extension of transepithelial dendrites^{242, 431, 443, 444} or indirectly via M cell or goblet cell antigen transport^{365, 366, 367, 368}, and macrophages also communicate with surrounding epithelial and immune cells^{405, 407}.

Another interpretation of these data is that biological age also impacts the intestinal epithelium, chronic inflammation, and intestinal immune cell populations, in addition to microbiota composition. Previous work from the Bowdish lab has shown that old GF mice colonized with young microbiota had more similar colon paracellular permeability and peripheral circulating TNF levels to young GF mice colonized with old microbiota, as opposed to young GF mice colonized with young microbiota³³⁷, suggesting that biological tissue age influenced effects of the microbiota on intestinal permeability

and circulating soluble inflammation and *vice versa*. Interestingly, when Fransen and colleagues investigated short-term temporal changes to the microbiome after transfer of young and old microbiota to young GF mice, they found that within 4 weeks the young recipient colonized mice that received the old microbiota had a more similar microbiome to young mice that received the young donor microbiota, compared to the microbiome of their donor old mice⁷⁵⁰. These observations suggest that there may be age-specific adaptations of the microbiota after initial colonization of GF mice.

As we chose to age our GF mice for ~10 months after colonization with the donor microbiota, natural physiological changes that occur to the intestines with age, and the accompanying age-associated changes to tissue microenvironment cells and secreted cytokines, chemokines and growth factors, may have confounded effects of colonization with ‘young’ or ‘old’ microbiota on intestinal immune cells. Previous work from the Bowdish lab with age-discordant bone marrow chimeras has shown that changes to peripheral blood Ly6C^{high} monocyte prevalence and phenotype, and bone marrow-derived macrophage phagocytic and bactericidal activities, were largely dependent on the host microenvironment⁷⁸⁰. Another recent chimera study similarly reported that both biological age and external ‘inflammaging’ factors influence small intestine muscularis macrophage phenotype⁷⁷⁸. We observed that there are age-related changes to CD4⁻TIM4⁻ and CD4⁺ macrophage dynamics in the absence of the microbiota (i.e. in GF mice), so age-intrinsic features of macrophages, even independent of the microbiota, and/or factors in the surrounding aging tissue microenvironment, could have led to similar changes to macrophage populations in both recipient groups. It is possible that there may have been differences in intestinal immune cells in our ‘old’ and ‘young’ microbiota groups if the

recipient mice were assessed at an earlier point after initial colonization, before physiological changes from aging, or influences of aging on the microbiota, may have become more important in dictating immune cell composition than the initial donor microbiota. Accordingly, a recent short-term study (4 weeks) of GF mice colonized with young or old microbiota reported that GF mice colonized with the old microbiota had alterations to intestinal macrophage phenotype and intestinal transit⁷⁸¹. As the intestinal microbiota influences both peripheral^{322, 729, 730} and tissue-localized immune cell populations^{372, 405}, assessment of peripheral soluble and cellular inflammation in our mice could provide more insight into whether the young and old recipient mouse groups have similar characteristics of chronic age-associated inflammation, such as elevated peripheral blood levels of TNF and Ly6C^{high} monocytes.

In summary, our data suggest that endogenous stimulatory signals (e.g. ‘self’ signals from cellular senescence or genetic programming), and exogenous ‘non-self’ stimulatory signals influenced by factors in the external environment (e.g. senescent mesenchymal cells, changes to secreted cytokines, chemokines or growth factors, or microbial dysbiosis), may contribute to age-associated changes to colon macrophages.

6.5 Intestinal macrophages in lactation with excess weight gain

6.5.1 Introduction

During pregnancy, changes to intestinal structure in humans, ruminants, and rodents are necessary to augment nutrient absorption capacity to ensure adequate energy is extracted for maternal and fetal requirements. These adaptations involve increases in intestinal length^{122, 782, 783}, weight¹²², and villus height^{784, 785, 786}, increased expression of nutrient transporters^{122, 782, 785, 786, 787, 788, 789}, and expansion of vascular networks^{790, 791}. These physiological changes may contribute to increased intestinal permeability in late pregnancy^{179, 792}. Pregnancy also changes the intestinal microbiome across gestation in humans^{793, 794} and mice^{178, 179, 180, 590}. Late in gestation (E18.5), Elderman and colleagues identified in the proximal colon 789 differentially expressed genes between non-pregnant and pregnant mice, including pathways corresponding to immune development, signalling, and function, which correlated to changes in the microbiome⁵⁹⁰. However, whether the microbiota has a direct role in mediating maternal immune adaptations within the intestines is currently unknown.

Many of the physiological and anatomical changes that occur during pregnancy are also required for the energetically costly process of lactation. During lactation, the gut, liver, and mammary glands have high nutrient exposure, while the rest of the body experiences a state of chronic undernutrition⁷⁹⁵. Extensive remodelling of the intestines as described above is required to ensure adequate nutrition and energy absorption to support maternal and offspring requirements. In small rodents like mice, changes to the intestinal tract vary according to litter size, presumably to maximize energy extraction for maternal

and fetal needs while balancing the energetic requirements of intestinal tissue maintenance¹²².

Studies in humans and animal models have suggested that pregnancy and lactation-related intestinal adaptations and increases in body weight are retained for a significant period of time post-weaning. In mice, lactation-enhanced transport capacity of nutrients like glucose and proline was retained up to 70 days after birth, small intestine villus height remained higher for up to 200 days, and length and weight of the small intestine, as well as body weight, was maintained up to 300 days⁷⁸⁵. Considering that a typical laboratory mouse can live for ~2 years, that represents almost a third of its lifespan. Epidemiological evidence suggests that body composition changes that occur during pregnancy in humans are often retained in the postpartum period, and a higher BMI pre-pregnancy, or post-pregnancy due to excess gestational weight gain, increases a woman's risk of being overweight or obese later in life^{158, 596, 597, 598, 599}.

Recent publications using mouse models have reported that diet-induced obesity, which is often associated with excess weight gain during pregnancy, alters maternal intestinal adaptations in pregnancy. Diet-induced obesity changes the composition of the microbiota across pregnancy, reducing SCFA-producing bacteria in particular, and alters mRNA expression of genes associated with nutrient transport, intestinal inflammation, and epithelial barrier integrity^{178, 179, 180, 796}.

As previously described, intestinal macrophages have a multitude of roles in supporting intestinal functions, including tissue remodelling, epithelial cell growth, neuronal networks, and immune protection and tolerance^{405, 406, 407}, so they likely participate in and support the intestinal adaptations that occur during pregnancy and

lactation. As shown in Chapter 5 (section 5.2.4), excess weight gain during pregnancy alters maternal peripheral blood immunophenotype adaptations during lactation. We considered whether diet-induced excess gestational weight gain would influence maternal intestinal adaptations during lactation, and the role of the microbiota in mediating those changes.

6.5.3 Results

To induce excess gestational weight gain, as described in Chapter 5 (section 5.2.4), female mice were placed on a high fat diet (45% kcal from fat) for two weeks prior to mating and were maintained on that diet during pregnancy and lactation. This short term exposure resulted in ~20% greater weight gain in HF-fed mice, compared to standard chow-fed mice, from E0.5 through to P21 (Figure 5.2.4).

Intestinal physiology and permeability

At P21, we measured lengths of the small intestine (Figure 6.5.1A) and colon (Figure 6.5.1B). Small intestines were longer in chow-fed dams compared to HF-fed dams (mean \pm SD, Chow: 41.13 ± 2.98 cm; HF: 37.78 ± 3.25 cm), as were colon lengths (Chow: 8.30 ± 0.65 cm; HF: 7.10 ± 0.53 cm). Caecal weight was ~3-fold lower in HF-fed dams compared to chow-fed dams (Figure 6.5.1C). Mesenteric fat weight was increased in the HF-fed dams compared to the chow-fed dams (Figure 6.5.1D). We also found that HF-fed dams had a modest increase in intestinal permeability (Figure 6.5.1E). These data identified that HF-fed dams, compared to chow-fed dams, had excess gestational weight gain, reduced colon and small intestine lengths, reduced caecal weight, and increased mesenteric fat weight and intestinal permeability, at P21 during lactation.

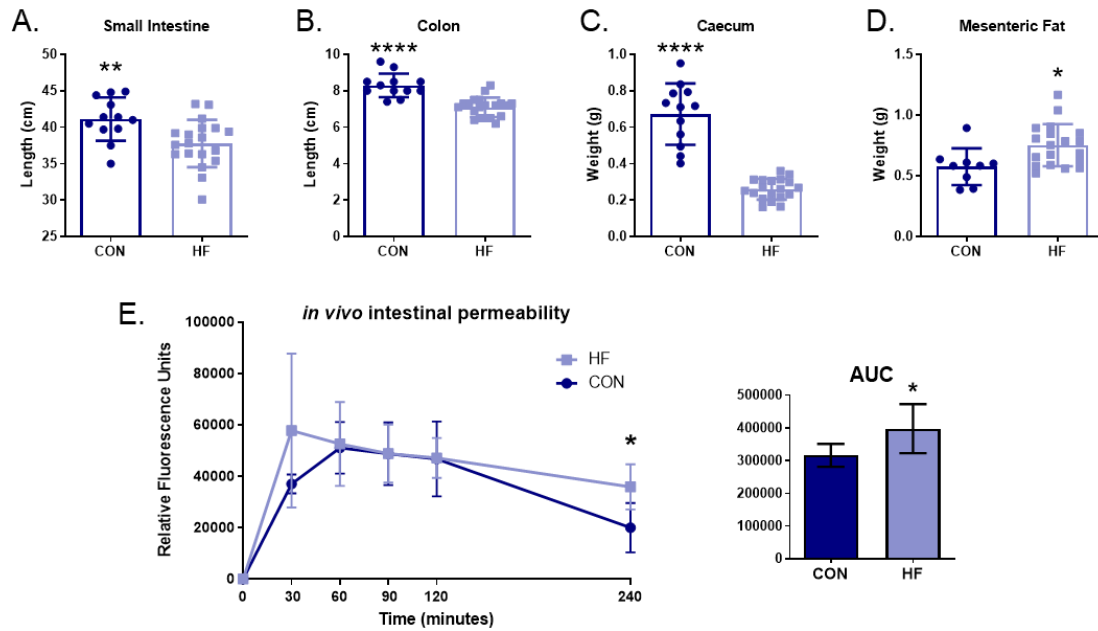


Figure 6.5.1. Maternal intestinal physiological measurements and permeability.

Maternal physiological parameters were measured during lactation at P21. (A) small intestine length. (B) colon length. (C) caecal weight. (D) mesenteric fat weight. (E) *in vivo* FITC-dextran assay fluorescence in plasma post-gavage. Data in A-D and AUC are presented with box height at the mean with error bars indicating \pm standard deviation. Data in E are shown as mean \pm standard deviation. Each data point in A-D indicates an individual mouse. For A-D, CON n=12 and HF n=19. For E, CON n=3 and HF n=11. Statistical significance was assessed by Student's t test. CON – standard chow diet, HF – 45% high fat diet. * $p < 0.05$, ** $p < 0.01$, **** $p < 0.0001$.

Intestinal eosinophils, neutrophils, and CD4⁺ T cells

We assessed intestinal immune cell populations in the ileum and colon by flow cytometry. In the ileum there was a trend toward a decrease in the prevalence of eosinophils in HF-fed dams compared to chow-fed dams (Figure 6.5.2A), though neutrophil prevalence was similar between chow and HF-fed dams (Figure 6.5.2B). CD4⁺ T cell prevalence was significantly reduced in the ileums of HF-fed dams compared to chow-fed dams (Figure 6.5.2C). HF-fed dam colons had a reduction in the prevalence of eosinophils (Figure 6.5.2G), but no differences to neutrophils (Figure 6.5.2H) or CD4⁺ T cells (Figure 6.5.2I), in comparison to chow-fed dams. Total cell counts were not different between diet groups for these immune cell populations in either the ileum

(Figure 6.5.2D-F) or the colon (Figure 6.5.2J-L). As small intestine and colon lengths were decreased in HF-fed dams, we also assessed immune cell numbers by tissue length, but there were no significant differences between diet groups (data not shown).

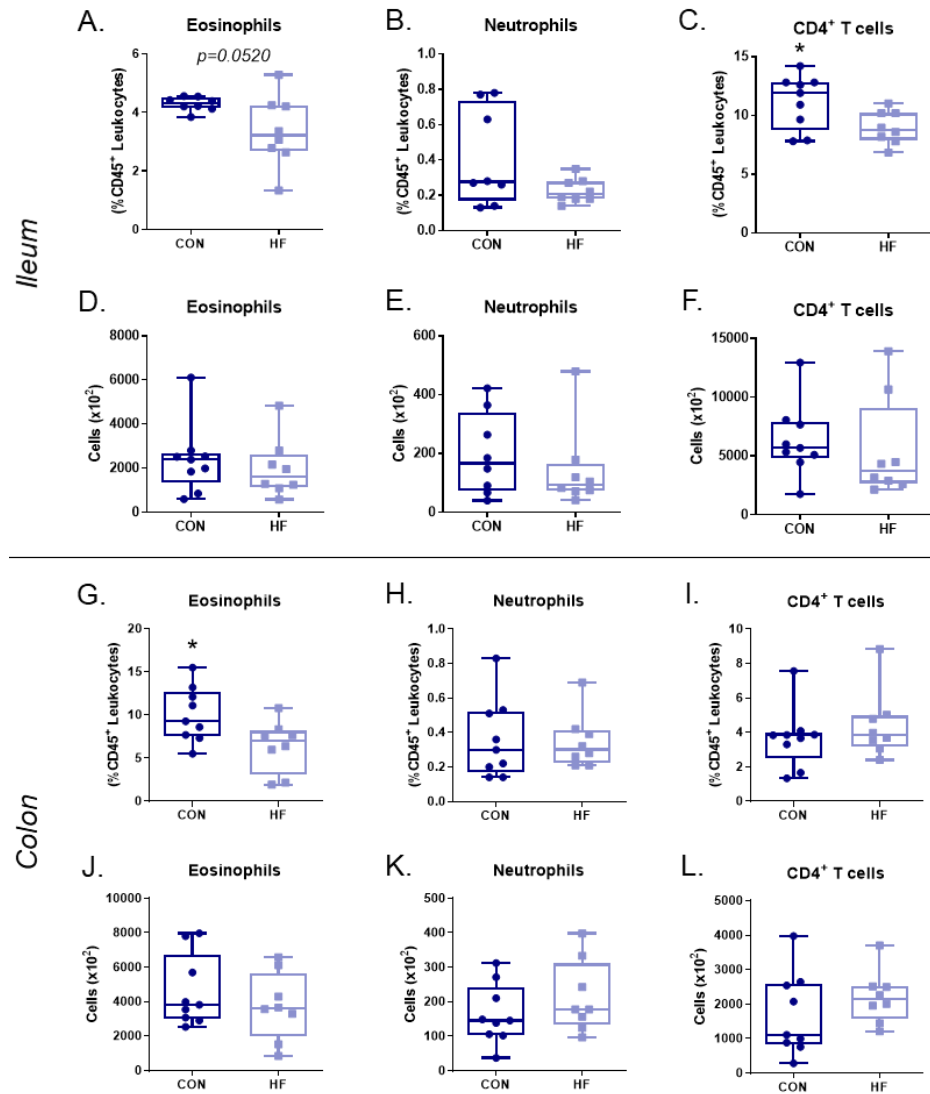


Figure 6.5.2. Maternal ileum and colon eosinophils, neutrophils, and CD4⁺ T cells.

Flow cytometry analysis of maternal intestinal immune cell populations in the ileum (A-F) and colon (G-L) during lactation at P21. Ileum prevalence of: (A) eosinophils, (B) neutrophils, (C) CD4⁺ T cells. Ileum absolute cell counts of: (D) eosinophils, (E) neutrophils, (F) CD4⁺ T cells. Colon prevalence of: (G) eosinophils, (H) neutrophils, (I) CD4⁺ T cells. Colon absolute cell counts of: (J) eosinophils, (K) neutrophils, (L) CD4⁺ T cells. Each data point indicates an individual mouse. Data are presented as box and whisker plots, minimum to maximum, where the center line indicates the median. CON n=9, HF n=8. Statistical significance was assessed by two-tailed Student's t test. CON – standard chow diet, HF – 45% high fat diet. * $p < 0.05$.

Intestinal monocytes and macrophages –prevalence, cell counts, and surface phenotype

Monocyte and macrophage populations in the ileum and colon were assessed by flow cytometry. In comparison to chow-fed dams, Ly6C^{high} monocyte prevalence in the ileums of the HF-fed dams was decreased (Figure 6.5.3A), though cell counts were similar (Figure 6.5.3C). There were no changes to Ly6C^{high} monocyte prevalence or cell counts in the colons between diet groups (Figure 6.5.3E and 6.5.3G). Total macrophage prevalence and absolute counts in the ileums (Figure 6.5.3B and 6.5.3D) and colons (Figure 6.5.3F and 6.5.3H) were likewise not different between chow and HF-fed dams.

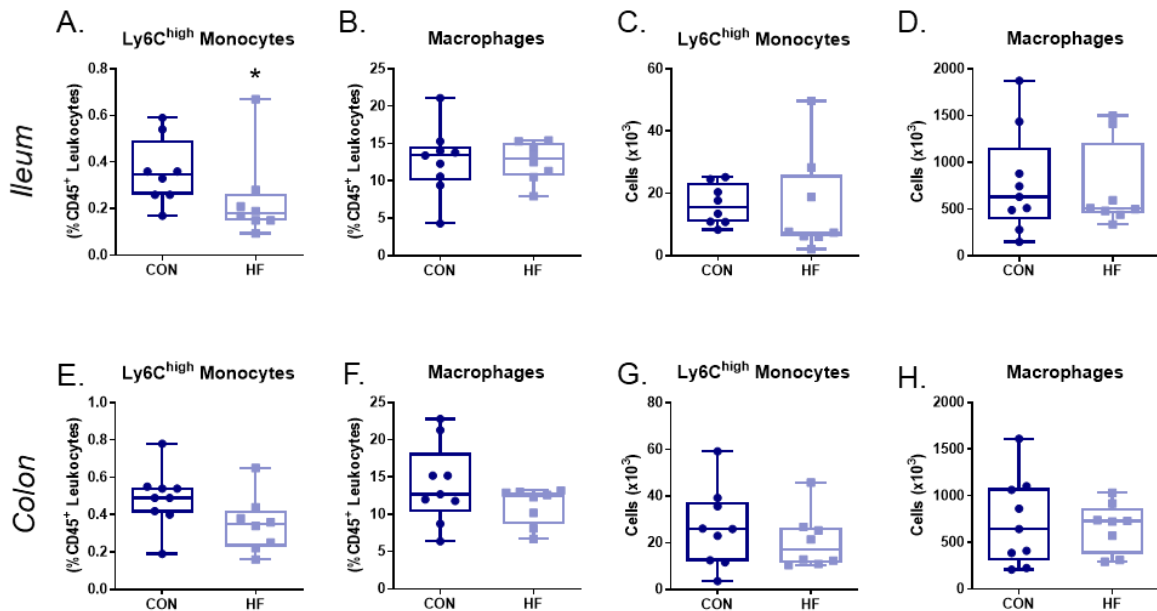


Figure 6.5.3. Maternal ileum and colon Ly6C^{high} monocytes and total macrophages.

Flow cytometry analysis of maternal intestinal immune cell populations in the ileum (A-D) and colon (E-G) during lactation at P21. Ileum prevalence (as a proportion of CD45⁺ leukocytes) of: (A) Ly6C^{high} monocytes, (B) total macrophages. Ileum absolute cell counts of: (C) Ly6C^{high} monocytes, (D) total macrophages. Colon prevalence (as a proportion of CD45⁺ leukocytes) of: (E) Ly6C^{high} monocytes, (F) total macrophages. Colon absolute cell counts of: (G) Ly6C^{high} monocytes, (H) total macrophages. Each data point indicates an individual mouse. Data are presented as box and whisker plots, minimum to maximum, where the center line indicates the median. CON n=9, HF n=8. Statistical significance was assessed by two-tailed Student's t test. CON – standard chow diet, HF – 45% high fat diet. **p*<0.05.

We next examined CD4⁻TIM4⁻, CD4⁺ and CD4⁺TIM4⁺ macrophages. The prevalence of CD4⁻TIM4⁻ macrophages in the ileums was significantly reduced in HF-fed dams compared to chow-fed dams, while the prevalence of CD4⁺ and CD4⁺TIM4⁺ populations increased (Figure 6.5.4A-B). Ileum CD4⁺ macrophage cell counts (Figure 6.5.4C), and counts normalized to tissue length (Figure 6.5.4D), were likewise increased in HF-fed dams compared to chow-fed dams. In the colons of HF-fed dams, there was a significant increase in the proportion of CD4⁺ macrophages and a corresponding decrease in CD4⁺TIM4⁺ macrophages, with a trend toward a decrease in CD4⁻TIM4⁻ macrophages compared to chow-fed dams (Figure 6.5.4E-F). There were no differences in cell counts in the colon (Figure 6.5.4G), but there was a significant increase in CD4⁺ macrophage cell counts by tissue length in HF-fed dams compared to chow-fed dams (Figure 6.5.4H).

We also assessed macrophage surface phenotype (Table 6.5.1; Appendix I). Compared to chow-fed dams, expression of CD64 and CD11b was lower on CD4⁻TIM4⁻, CD4⁺, and CD4⁺TIM4⁺ macrophage populations in HF-fed dams in the ileum, and TIM4 was also decreased on CD4⁺TIM4⁺ macrophages in HF-fed dams. In HF-fed dams compared to chow-fed dams, Ly6C expression remained higher and MHCII was lower on CD4⁻TIM4⁻ macrophages in the ileum, while CCR2 was higher on CD4⁺ and CD4⁺TIM4⁺ macrophages. Colon macrophages of HF-fed dams, compared to chow-fed dams, had higher expression of Ly6C and F4/80, and the CD4⁺ and CD4⁺TIM4⁺ macrophages had higher expression of CCR2, as well as CD4, though there were no differences in MHCII expression. Overall, these data indicated that there were changes to intestinal monocyte and macrophage dynamics and surface phenotype, with tissue-specific effects, between dams with HF diet-induced excess weight gain and chow-fed dams in lactation at P21.

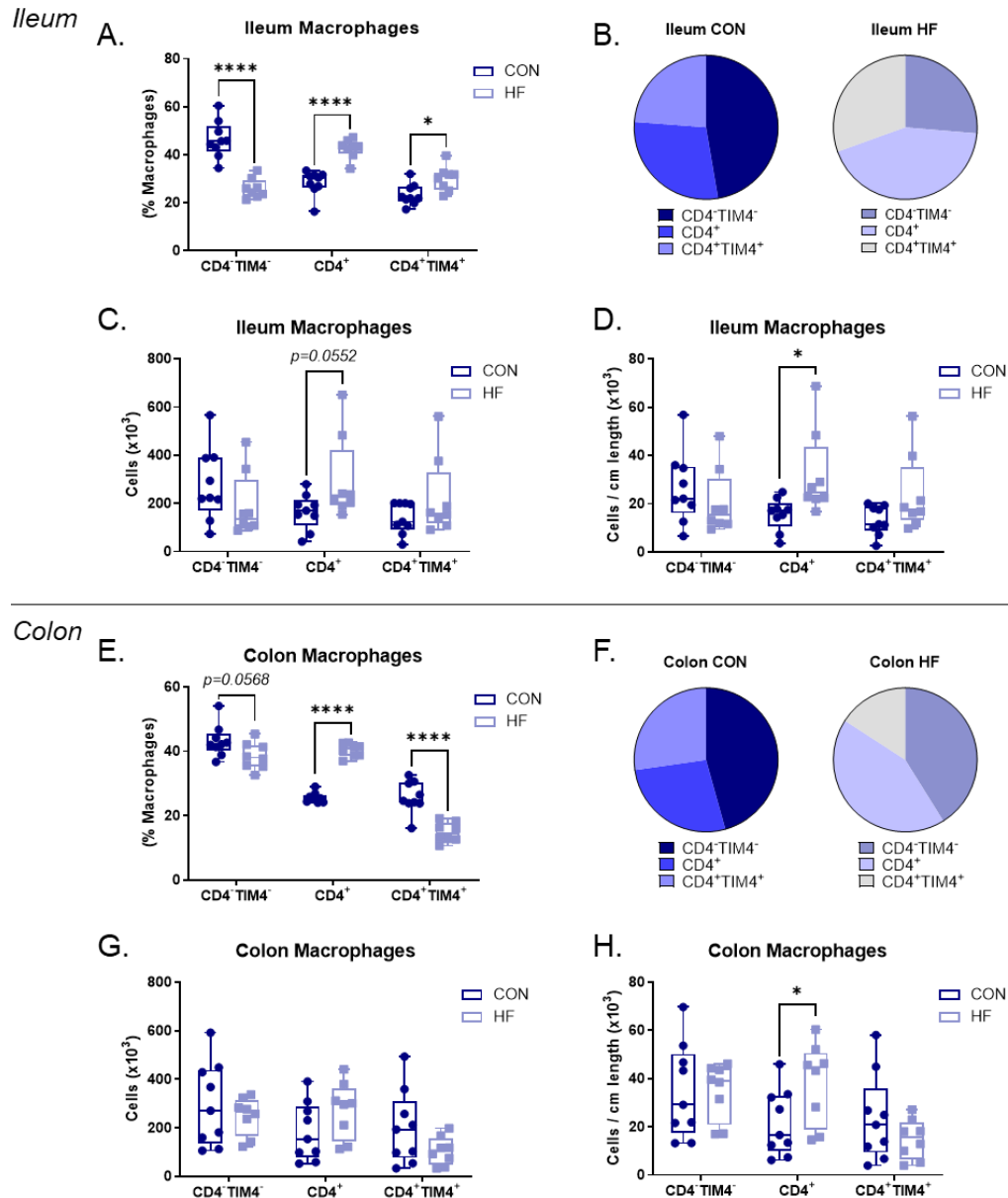


Figure 6.5.4. Maternal ileum and colon macrophage prevalence and cell counts.

Flow cytometry analysis of maternal CD4⁻TIM4⁻, CD4⁺, and CD4⁺TIM4⁺ macrophages in the ileum (A-D) and colon (E-H) during lactation at P21. Ileum CD4⁻TIM4⁻, CD4⁺, and CD4⁺TIM4⁺ macrophages: (A) prevalence (as % of total macrophages), (B) summary pie graphs of mean prevalence, (C) absolute cell counts, (D) absolute cell counts by tissue length. Colon CD4⁻TIM4⁻, CD4⁺, and CD4⁺TIM4⁺ macrophages: (E) prevalence (as % of total macrophages), (F) summary pie graphs of mean prevalence, (G) absolute cell counts, (H) absolute cell counts by tissue length. Each data point indicates an individual mouse. Data in A, C-E and G-H are presented as box and whisker plots, minimum to maximum, where the center line indicates the median. Data in B and F show mean values from A and E, respectively. CON n=9, HF n=8. Statistical significance was assessed by two-tailed Student's t test for each macrophage population. CON – standard chow diet, HF – 45% high fat diet. * $p < 0.05$, **** $p < 0.0001$.

Table 6.5.1. Summary of intestinal macrophage surface expression changes between HF-fed and chow-fed dams at P21.

Marker	ILEUMS			COLONS		
	CD4 ⁻ TIM4 ⁻	CD4 ⁺	CD4 ⁺ TIM4 ⁺	CD4 ⁻ TIM4 ⁻	CD4 ⁺	CD4 ⁺ TIM4 ⁺
Ly6C	↑ ** p = 0.0034	ns	ns	↑ *** p = 0.0004	↑ ** p = 0.0014	↑ ** p = 0.0018
CD11b	↓ **** p < 0.0001	↓ **** p < 0.0001	↓ **** p < 0.0001	↓ *** p = 0.0002	ns	↑ *** p = 0.0008
CD64	↓ **** p < 0.0001	↓ **** p < 0.0001	↓ **** p < 0.0001	ns	ns	↑ **** p < 0.0001
CCR2	ns	↑ *** p = 0.0001	↑ *** p = 0.0001	ns	↑ **** p < 0.0001	↑ **** p < 0.0001
F4/80	ns	ns	ns	↑ **** p < 0.0001	↑ **** p < 0.0001	↑ *** p = 0.0003
MHCII	↓ * p = 0.0174	ns	ns	ns	ns	ns
CD4	--	↑ * p = 0.0125	ns	--	↑ **** p < 0.0001	↑ * p = 0.0193
TIM4	--	--	↓ **** p < 0.0001	--	--	ns

Data show changes in geometric mean surface expression between HF-fed and chow-fed dams.

(e.g. Ileum CD4⁻TIM4⁻ macrophages from HF-fed dams had higher expression of Ly6C compared to ileum CD4⁻TIM4⁻ macrophages from chow-fed dams.)

Intestinal macrophages – effect of the microbiota on maternal adaptations

We next considered whether the microbiota may have a role in inducing changes to intestinal macrophage populations during pregnancy/lactation by examining intestinal macrophages in germ free mice. By mid-pregnancy (E14.5), along with an increase in body weight (Figure 6.5.5A) and caecal weight (Figure 6.5.5B), there was a 15% increase in the length of the small intestine in comparison to GF non-pregnant mice (Figure 6.5.5C), though colon length was similar (Figure 6.5.5D). These data indicated that at mid-pregnancy there are changes to intestinal physiology, even in the absence of the microbiota. The prevalence of total macrophages (as a proportion of total leukocytes) was similar in the ileum (Figure 6.5.5E) and colon (Figure 6.5.5G) of non-pregnant GF mice and GF mice at E14.5. CD4⁻TIM4⁻, CD4⁺, and CD4⁺TIM4⁺ macrophage prevalence (as a proportion of total macrophages) was also similar between non-pregnant GF mice or GF mice at E14.5 in both the ileum (Figure 6.5.5F) and the colon (Figure 6.5.5H). Therefore,

in the absence of the microbiota, macrophage population dynamics in the ileum and colon remained similar between non-pregnant mice and at mid-gestation (E14.5).

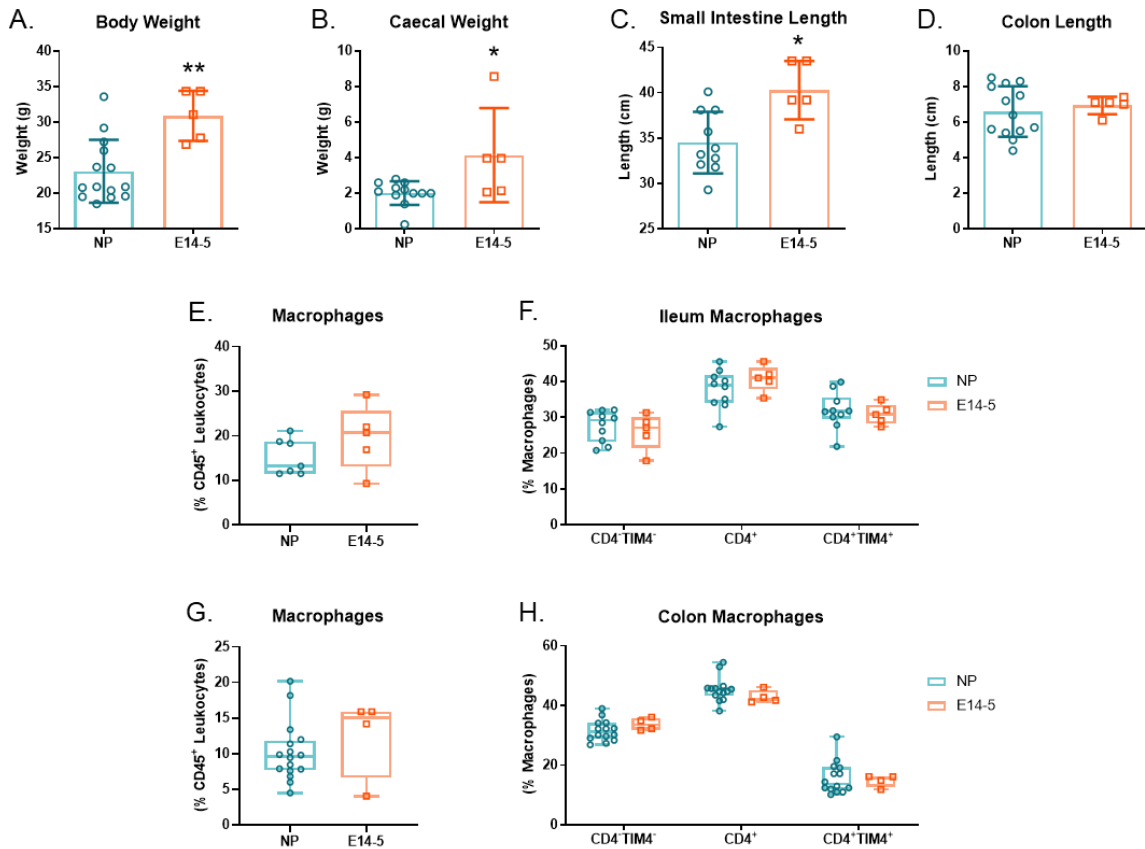


Figure 6.5.5. Intestinal physiology and macrophage prevalence in non-pregnant GF mice and GF mice at E14.5.

Intestinal macrophage populations were assessed by flow cytometry from age-matched germ-free non-pregnant (NP) and E14.5 pregnant female mice (E14.5). (A) body weight. (B) caecal weight. (C) small intestine length. (D) colon length. Ileum: (E) total macrophages as a proportion of CD45⁺ leukocytes, (F) CD4⁺TIM4⁻, CD4⁺, and CD4⁺TIM4⁺ macrophages as a proportion of total macrophages. Colon: (G) total macrophages as a proportion of CD45⁺ leukocytes, (H) CD4⁺TIM4⁻, CD4⁺, and CD4⁺TIM4⁺ macrophages as a proportion of total macrophages. Each data point indicates an individual mouse. Data in A-D are presented with box height at the mean with error bars indicating \pm standard deviation. Data in E-H are presented as box and whisker plots, minimum to maximum, where the center line indicates the median. Data are from multiple independent experiments of $n=1-3$ per group. NP $n=7-16$; E14.5 $n=4-5$. Statistical significance was assessed by two-tailed Student's t test for between-group comparisons, and for each macrophage population. * $p<0.05$, ** $p<0.01$.

6.5.4 Discussion

Our data showed that HF-fed dams with excess gestational weight gain, in comparison to chow-fed dams, had modestly increased intestinal permeability, reduced small intestine and colon tissue lengths, and altered intestinal macrophage prevalence and surface phenotype, in a tissue-specific manner at P21 during lactation. To our knowledge, this is the first report on intestinal immune cells during lactation in mice. To provide further context for our observations, we compared the intestinal data from the chow-fed dams in lactation to age matched non-pregnant female mice on the same standard chow diet (Appendix V). During lactation, the intra-macrophage prevalence of CD4⁺ macrophages was significantly decreased, and CD4⁺TIM4⁺ prevalence was significantly increased, in both the ileum (Appendix V-D) and colon (Appendix V-J). In the ileum, these changes appeared to be due to increases in numbers of CD4⁺TIM4⁺ and especially CD4⁺TIM4⁺ macrophages (Appendix V-E and V-F), while CD4⁺TIM4⁺ macrophages numbers were increased in the colon (Appendix V-K and V-L). As CD4⁺TIM4⁺ macrophages are newly derived from monocytes, these comparisons imply that there may be increased recruitment of monocytes into ileum tissue during lactation, while the long-lived CD4⁺TIM4⁺ population, which is found deeper within the gut wall, may self-proliferate, to support restructuring of vascular, lymphatic, and neuronal networks^{783, 791}.

Our data also showed that excess weight gain from a HF diet has distinct tissue-specific effects on maternal intestinal adaptations, which are different from effects of diet-induced obesity in non-pregnant mice. In particular there was an increase in cell numbers of CD4⁺ macrophages (normalized to intestinal length) in both the ileums and the colons of HF-fed dams compared to chow-fed dams, and CD4⁺ macrophages in HF-

fed dams compared to chow-fed dams also had higher surface expression of CD4. It has been proposed that CD4⁻TIM4⁻ macrophages may mature into CD4⁺ macrophages²⁵², so the decreased prevalence of Ly6C^{high} monocytes (within the ileum) and CD4⁻TIM4⁻ macrophages (in the ileum and colon), and increased prevalence and numbers of CD4⁺ macrophages in the ileum and colon tissues of HF-fed dams, could indicate less monocyte recruitment (as observed in the ileum) and more maturation from CD4⁻TIM4⁻ to CD4⁺ macrophages. These data could alternatively reflect an increase in local proliferation of CD4⁺ macrophages. Interestingly, it was previously reported in E18.5 dams fed a HF diet (60% kcal from fat) prior to and during pregnancy, compared to chow-fed dams, that there were significant increases in gene expression of *Cd4* and *F4/80* in ileum tissues¹⁷⁹, which may indicate that the increase in ileum CD4⁺ macrophages that we observed in lactation is also apparent earlier in pregnancy in mice with diet-induced obesity.

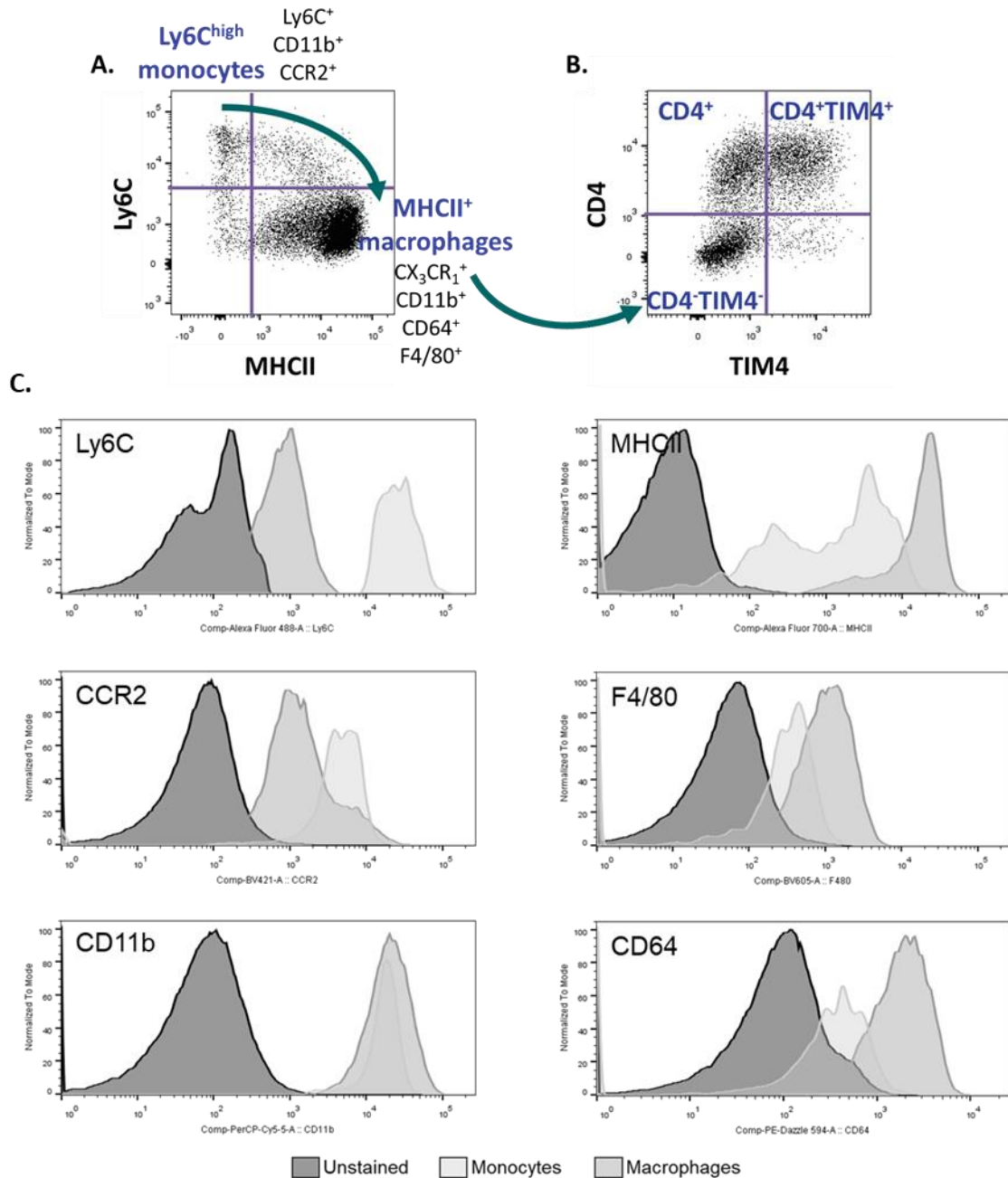
We observed significant differences in surface marker expression on intestinal macrophages in dams with excess gestational weight gain in comparison to chow-fed dams (Table 6.5.1). There were changes in HF-fed mice compared to chow-fed mice suggestive of a reduced capacity for efferocytosis (decreased CD64 and TIM4 on CD4⁺TIM4⁺ ileal macrophages), and especially dysregulation of monocyte-to-macrophage differentiation, including higher Ly6C and lower CD64 and MHCII expression on ileum CD4⁻TIM4⁻ macrophages, and higher Ly6C and F4/80 expression on colon CD4⁻TIM4⁻ macrophages, as well as changes to macrophage activation, including increased CD11b, CD64, CD4 and F4/80 expression on colon CD4⁺TIM4⁺ macrophages. Future experiments could assess if macrophage cytokine production, proliferation, and functions within the intestines, are altered in the dams with excess gestational weight

gain, to better understand how cell numbers of CD4⁺ macrophages increase, and if macrophages retain their anti-inflammatory characteristics, as we observed in non-pregnant mice with diet-induced obesity. Previous studies reported that dams with HF diet-induced obesity, compared to chow-fed dams, had decreased colon gene expression of mucus barrier protein *Muc2* at E14.5¹⁷⁸, and tight junction protein zonulin (*Zo1*) in the ileum at E18.5, and increased expression of occludin in the ileum at E18.5¹⁷⁹. Further studies in lactation should also examine if there are similar changes in expression of tight junction or mucus barrier proteins, and the overall structure of the intestines (e.g. villus height, crypt depth, numbers of goblet cells), that may contribute to the increase in intestinal permeability that we observed in HF-fed dams compared to chow-fed dams.

We also observed that macrophage population dynamics were not significantly different in the small intestines and colons of non-pregnant GF mice and GF mice at E14.5. As we observed significant changes in intestinal macrophage dynamics between non-pregnant SPF mice and SPF mice in lactation (Appendix V), these data may indicate that the microbiota has a role in mediating those changes. It is certainly possible that the change in macrophage dynamics only occurs later in pregnancy or during lactation itself, independent of the microbiota, but those are considerations for future experiments.

Overall, these data provide support for further research into maternal intestinal immunological adaptations during pregnancy and lactation, as we showed that there are distinct changes to immune cells in lactation, which are altered by excess gestational weight gain, and our data suggested that the microbiome may have a role in mediating those adaptations.

Appendix I.



Monocyte and macrophage progression of surface marker expression.

(A) Monocyte to macrophage transition in the intestines. (B) Intestinal macrophage populations (CD4⁻TIM4⁻, CD4⁺, CD4⁺TIM4⁺). (C) Representative images of intestinal Ly6C⁺ monocyte and CD64⁺MHCII⁺ macrophage surface expression of monocyte-macrophage maturity markers: Ly6C, CCR2, CD11b, MHCII, F4/80 and CD64.

Appendix I.

Macrophage Surface Markers

Note that the associated functions of most of these markers have not been studied specifically in the context of intestinal monocyte recruitment or intestinal macrophages.

Ly6C refers to two separate genes (Ly6C1 and Ly6C2), but they are highly similar and cannot be distinguished by currently available antibodies, so they are referred to collectively as Ly6C⁷⁹⁷. Ly6C is expressed by monocytes, neutrophils, dendritic cells, subsets of CD4⁺ and CD8⁺ T cells, NK cells, and plasma cells^{797, 798}. Ly6C is implicated in signal transduction in the inflammatory response leading to production of pro-inflammatory cytokines, as well as regulation of uptake of apoptotic cells by macrophages^{797, 798}. It is often used to identify monocyte subsets in mice. Under conditions of homeostasis, elevated expression of Ly6C on monocytes is regarded as a marker of immaturity as Ly6C^{high} monocytes lose their expression of Ly6C as they transition into Ly6C^{low} monocytes in bone marrow, and reduce Ly6C expression when they differentiate into tissue macrophages^{233, 236, 286, 287}. More information about Ly6C^{high}, Ly6C^{low}, and Ly6C⁻ monocytes is within Chapter 1 – see section 1.3.

CD64 (FcγRI) is a member of the Fcγ receptor (FcγR) family expressed on CD34⁺ hematopoietic progenitor cells including activated neutrophils, monocytes, and macrophages²²³. It is a major receptor for IgG-mediated phagocytosis and antibody-dependent cellular cytotoxicity⁶⁷⁶. Binding and internalization via CD64 contributes to macrophage pro-inflammatory characteristics, including secretion of TNF and IL-6⁷⁹⁹, and CD64 is highly expressed on macrophages treated with IFNγ and LPS⁸⁰⁰. Elevation of CD64 expression on macrophages is often associated with infection and chronic inflammatory conditions⁷⁹⁹. Monocytes that express CD64 have increased phagocytic activity and superoxide production⁴¹³. Macrophages decrease CD64 expression after treatment with IL-10⁶⁷⁸.

CCR2 is a chemokine receptor for CCL2 (MCP-1). It is expressed on monocytes, macrophages, basophils, dendritic cells, memory T cells, NK cells, and MDSCs^{301, 305, 801}.

CCR2-CCL2 interaction is essential for recruitment of monocytes into tissues under inflammatory conditions, as well as during homeostasis^{287, 301}. Monocyte migration to adipose and liver tissues via the CCR2-CCL2 axis contributes to development of tissue-specific and systemic inflammation and increasing insulin resistance that accompanies obesity⁵⁷. CCR2 expression decreases upon extravasation of monocytes into intestinal tissue as part of monocyte-to-macrophage maturation^{223, 235, 433}. Upregulation of CCR2 on Ly6C^{high} is regarded as promoting their migration to tissues²⁸⁷.

CD4 is a glycoprotein member of the immunoglobulin superfamily best recognized to be found on the surface of T cells, though it is also expressed on dendritic cells, monocytes, and macrophages^{242, 802}. The function of CD4 on intestinal macrophages is currently unknown. However, CD4 is a known receptor on T cells and macrophages for HIV^{803, 804}. The conserved and widespread expression of CD4 in long-lived resident intestinal macrophages capable of self-proliferation, as opposed to rapidly replaced monocyte-derived macrophages, would support its use as a receptor for viral infection.

TIM4 (T-cell immunoglobulin and mucin domain containing 4) is a type I transmembrane protein. Members of the ‘TIM’ family have roles in immune regulation in allergy, asthma, and autoimmunity⁸⁰⁵. TIM4 is primarily expressed on antigen-presenting cells like macrophages and dendritic cells, and is a common marker of tissue macrophages of embryonic origin^{242, 675}. TIM4 is implicated as a receptor for exosome-dependent cellular entry of HIV⁸⁰⁶. TIM4 expression on macrophages has been implicated in maintenance of homeostasis via regulation of T cell expansion and survival, efferocytosis, and regulation of macrophage activation^{805, 807, 808}. *timd4*^{-/-} mice or mice treated with anti-TIM4 have increased development of antibody-mediated autoimmune conditions (due to reduced macrophage-mediated efferocytosis and/or modulation of effector CD4⁺ T cells functions)^{809, 810}, yet anti-TIM4 treatment can reduce inflammation in late-stage mouse models of arthritis⁸¹⁰. Human SNPs have been associated with rheumatoid arthritis and systemic lupus erythematosus, as well as lipid dysregulation⁸¹¹. TIM4-associated efferocytosis has been implicated in protection against atherosclerosis⁸¹², and TIM4 can also inhibit NLRP3 inflammasome activation⁸¹³.

F4/80

F4/80, more traditionally referred to as EMR-1 (EGF-like module-containing mucin-like hormone receptor-like 1) or ADGRE1, is highly and constitutively expressed on most resident tissue macrophages in mice, and also has low expression on monocytes^{229, 256}. Embryonic origin macrophages typically have higher F4/80 expression than monocyte-derived macrophages²²⁹. Expression of F4/80 increases as monocytes mature into macrophages. Though it is not required for development of mouse tissue macrophages⁸¹⁴, it has been found to be important in cell-cell adhesion and macrophage activation. F4/80 expression is downregulated on macrophages in response to IFN γ ⁸¹⁵, as well as activated macrophages in context of infection⁸¹⁶. F4/80 may have roles in cell adhesion and signal transduction⁸¹⁴.

MHCII

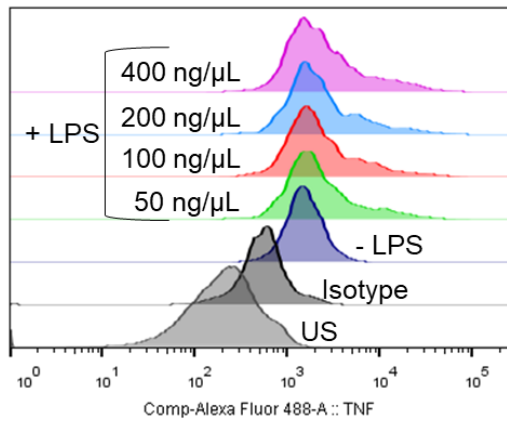
MHC II (major histocompatibility complex class II) proteins are expressed constitutively by antigen-presenting cells such as B cells, dendritic cells, macrophages, and thymic epithelial cells. Macrophages express low levels of MHCII under basal conditions. Its expression on the surface of macrophages can be increased *in vitro* by treatment with LPS and IFN γ , which also promotes production of pro-inflammatory factors like TNF, IL-6 and nitric oxide, as well as phagocytic activity, whereas IL-10 treatment promotes its intracellular sequestration^{261, 263}. Intestinal macrophages express MHCII but do not appear to use it for antigen presentation⁴⁰⁵.

CD11b

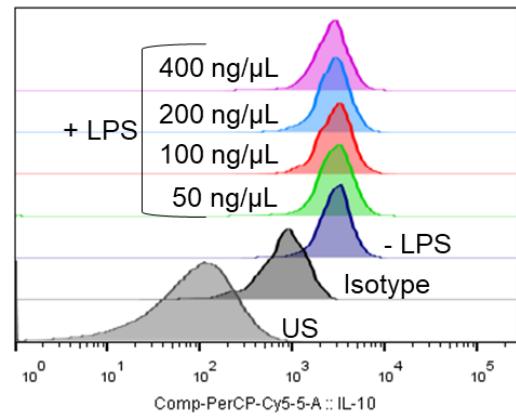
CD11b, also known as Mac-1 or integrin α M, is an integrin adhesion molecule primarily expressed on monocytes, macrophages, and neutrophils. CD11b combines with integrin β 2 (CD18) to form MAC-1 (integrin α M β 2), which is involved in transmigration of immune cells like monocytes through endothelial cells⁸¹⁷. CD11b prevents *in situ* proliferation of adipose tissue macrophages (i.e. its absence promotes more local proliferation rather than monocyte recruitment) and promotes a Th2 cytokine expression profile⁶³⁸. CD11b is also involved in modulation of immune responses and may suppress TLR signalling in macrophages⁸¹⁸.

Appendix II.

A. *TNF Expression*



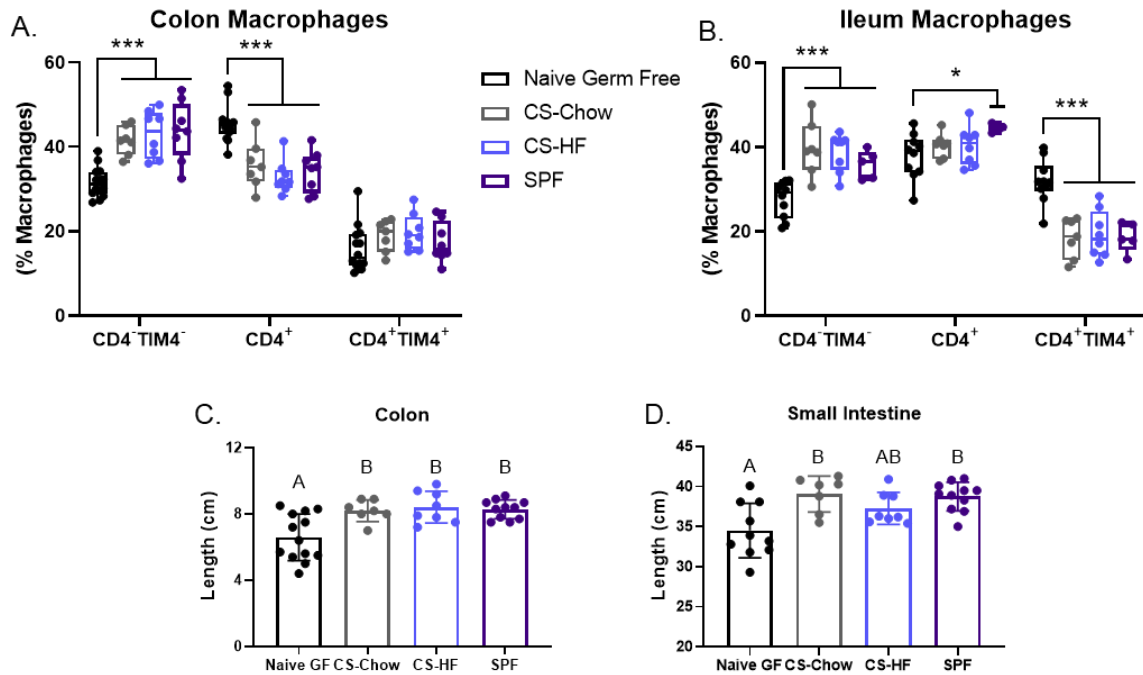
B. *IL-10 Expression*



Macrophage intracellular staining of TNF and IL-10.

Representative images of macrophage ($CD45^+CD3^-B220^-Ly6G^-Ly6C^-MHCII^+CD64^+$) intracellular expression of TNF and IL-10 assessed by flow cytometry. Response to LPS stimulation in young chow-fed mice for intracellular staining of (A) TNF and (B) IL-10.

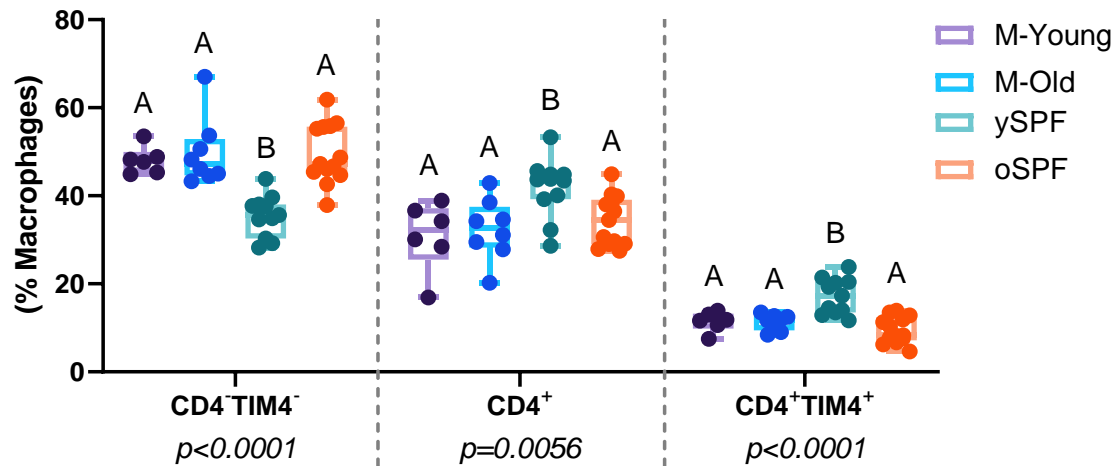
Appendix III.



Comparison of macrophage populations in young naïve germ free mice, colonized mice, and SPF mice.

Intestinal macrophage populations (CD4⁺TIM4⁻, CD4⁺ and CD4⁺TIM4⁺) were assessed by flow cytometry in the colon (A) and ileum (B). (C) colon length. (D) small intestine length. Data in A-B are presented as box and whisker plots, minimum to maximum, where the center line indicates the median. Data in C-D are presented with box height at the mean with error bars indicating \pm standard deviation. Each data point indicates a single mouse. CS-Chow: ex-germ free mice with microbiota from chow-fed SPF mice. CS-HF: ex-germ-free mice with microbiota from 60% high fat-fed SPF mice. Data for CS-HF and CS-Chow are from Figure 6.3.3. Statistical significance was assessed by one-way ANOVA with Tukey's post-hoc for comparisons within each macrophage population. Data in C-D have letters showing statistical similarities and differences. * $p < 0.05$, *** $p < 0.001$.

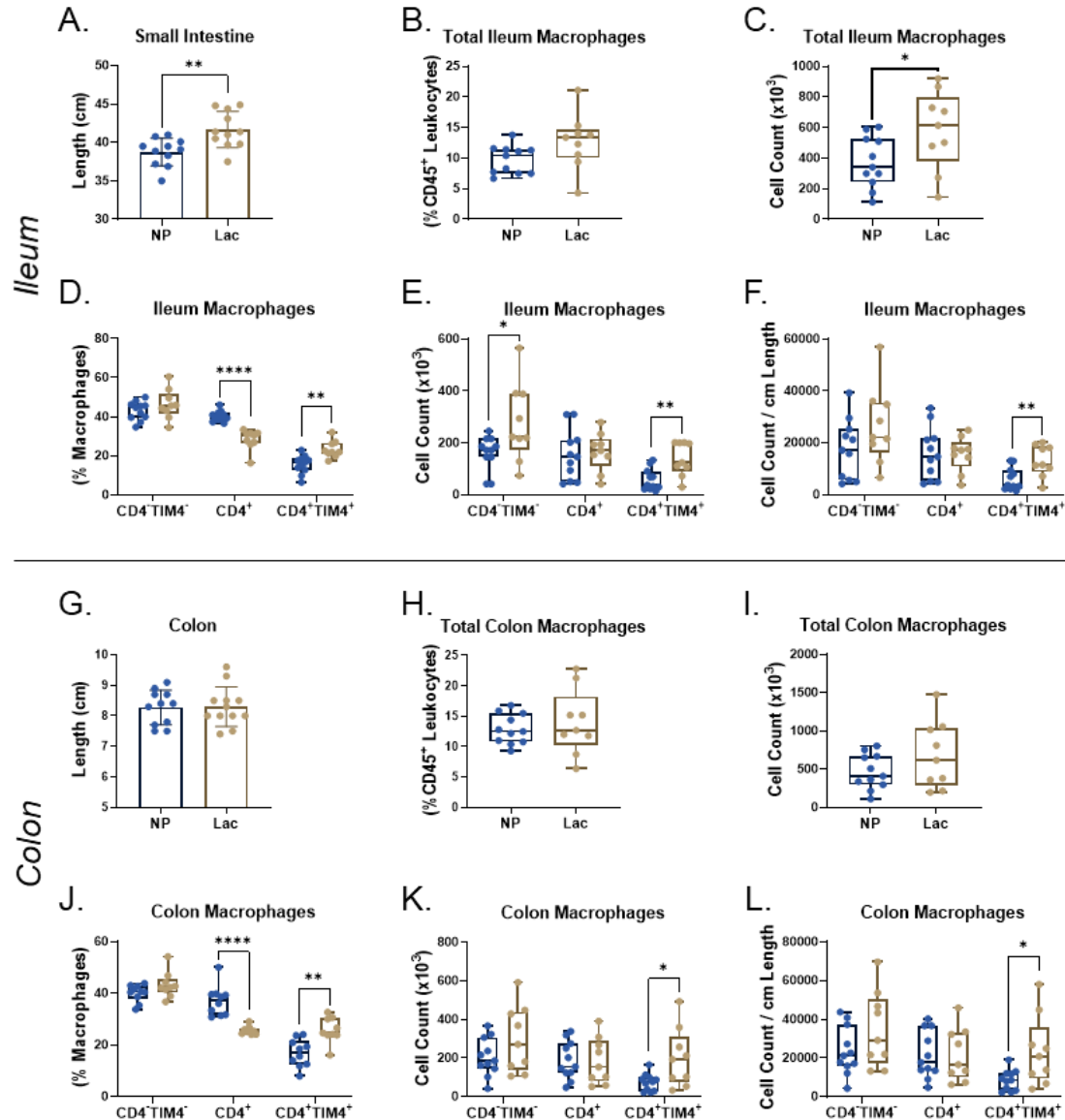
Appendix IV.



Colon macrophage prevalence in GF mice colonized with young or old microbiota and young and old SPF mice.

Prevalence of colon CD4⁻TIM4⁻, CD4⁺, and CD4⁺TIM4⁺ macrophages as a proportion of total macrophages in GF mice colonized with microbiota from young mice (M-Young) or old mice (M-Old) and aged to ~19-22 months, from Figure 6.4.6, and in SPF young (ySPF, 3-5 months) and old mice (oSPF, 18-24 months) from Figure 6.4.1. Data are presented as box and whisker plots, minimum to maximum, where the center line indicates the median. Data are from one independent experiment with M-Young n=6 and M-Old n=8, or combined from multiple independent experiments of n=1-4 mice per group: ySPF n=11, oSPF n=13. Statistical significance was assessed by one-way ANOVA. Letters indicate statistical similarity and differences between mouse groups within each macrophage population.

Appendix V.



Intestine lengths and macrophage populations in chow-fed non-pregnant non-lactating female mice and in dams at P21.

Intestinal measures from age-matched (18-24 weeks) non-pregnant non-lactating female mice (NP) and P21 dams (Lac) on standard chow diet. (A) small intestine length. (B) prevalence of ileum macrophages as a proportion of total leukocytes. (C) absolute cell count of ileum macrophages. CD4⁺TIM4⁺, CD4⁺, and CD4⁺TIM4⁺ ileum macrophages: (D) as a proportion of total macrophages, (E) absolute cell counts, (F) absolute cell counts by tissue length. (G) colon length. (H) prevalence of colon macrophages as a proportion of total leukocytes. (I) absolute cell count of colon macrophages. CD4⁺TIM4⁺, CD4⁺, and CD4⁺TIM4⁺ colon macrophages: (J) as a proportion of total macrophages, (K) absolute cell counts, (L) absolute cell counts by tissue length. Each dot indicates an individual mouse. Data in A and G are presented with box height at the mean and error bars at \pm standard deviation. Data in B-F and H-L are presented as box and whisker plots, minimum to maximum, with the center line at the median. NP n=11, Lac n=9. Statistical significance was assessed by Student's two-tailed t test. * $p < 0.05$, ** $p < 0.01$, *** $p < 0.0001$.

Under conditions of homeostasis (Chapter 3), we observed that biological sex influenced numbers and the relative prevalence of peripheral blood immune cells, with greater variability of immunophenotype in C57BL/6J male mice compared to female mice, and we found that peripheral blood immunophenotype was similar between stages of the female reproductive cycle. We also identified that there are mouse-strain-dependent impacts on peripheral immune cells that vary by biological sex. In male mice (Chapter 4) we identified that diet-induced obesity increased circulating Ly6C^{high} monocytes in a TNF-dependent manner, which correlated with insulin resistance. We observed that female mice (Chapter 5) also had increased circulating Ly6C^{high} monocytes in diet-induced obesity, but this was not mediated by TNF. We found that blood immunophenotype changed across pregnancy and lactation, with an increase in myeloid cells and a decrease in lymphocytes. Pregravid obesity altered immunophenotype at mid-pregnancy, increasing the numbers of monocytes and B cells, and in late pregnancy the absence of TNF did not prevent obesity-associated changes to immunophenotype. We also found that excess gestational weight gain influenced the prevalence of maternal peripheral blood B cells and NK cells, and monocyte phenotype, in lactation. We identified that diet-induced obesity, excess gestational weight gain, lactation, and age had distinct effects on ileum and colon CD4⁻TIM4⁻, CD4⁺, and CD4⁺TIM4⁺ tissue macrophage dynamics (Chapter 6). There were tissue-specific, microbiota-associated, and age-associated factors that contributed to those changes, and the microbiota alone was insufficient to confer peripheral and intestinal immunological characteristics of diet-induced obesity, or modulate intestinal macrophage dynamics in the context of biological aging. This may be due to diet-microbiota or age-microbiota interactions, respectively.

Overall, the studies in this thesis provided novel information on the influence of biological sex on peripheral blood immunophenotype in homeostasis, as well as insights into how peripheral monocytes and intestinal macrophages change in response to chronic inflammation, and the differential roles of TNF and the microbiota in mediating those changes under various biological conditions across the life course. As data were discussed within the individual chapters, the following discussion will briefly integrate and extend interpretation of these data, identify limitations, and outline directions for future research.

Effects of TNF on cellular inflammation in obesity

To gain insight into the effects of chronic inflammation on peripheral cellular changes, intestinal permeability, and intestinal macrophages in obesity, we used WT and TNF^{-/-} mice and models of HF diet-induced obesity. We hypothesized that TNF^{-/-} mice would be protected from effects of cellular inflammation compared to WT mice. Consistent with previous studies^{526, 527, 528}, we showed that whole-body genetic ablation of TNF in male mice reduced adiposity, macrophage accumulation in adipose tissue, and insulin resistance. We also found that TNF^{-/-} male mice fed a HF diet were protected from an obesity-associated increase in circulating Ly6C^{high} monocytes in comparison to HF-fed WT mice. In contrast, HF-fed TNF^{-/-} female mice, compared to HF-fed WT female mice, had similar adiposity as well as prevalence and cell counts of peripheral blood Ly6C^{high} monocytes. To our knowledge this observation of sexual dimorphism is a new discovery about the role of TNF in peripheral monocyte changes in diet-induced obesity. In addition, our data suggested that TNF^{-/-} and WT female mice fed a HF diet had similar intestinal permeability, decreases in small intestine and colon length, and similar changes to numbers of ileum and colon Ly6C^{high} monocytes, total macrophages, and CD4⁺TIM4⁺,

CD4⁺, and CD4⁺TIM4⁺ macrophages. It is unclear whether these data on intestinal immune cells and permeability reflect the pleiotropic effects of TNF that, as we previously mentioned, have been reported in acute and chronic models of intestinal inflammation^{699, 700, 701, 702, 703}, or if different results would be observed in male mice, so this should be investigated in future experiments. Consistent with our data in non-pregnant female mice, our data in pregnancy suggest that TNF is not a primary mediator of HF diet-induced immune changes in late pregnancy, as ablation of TNF (i.e. using TNF^{-/-} mice) had similar effects on circulating immune cells as in WT mice. Together, these data indicate that the absence of TNF in the context of diet-induced obesity in female mice does not prevent changes to monocytes in the periphery, or ileum or colon tissue macrophages.

We proposed that the difference in the action of TNF on peripheral cellular inflammation between female and male mice is due to effects of TNF on insulin resistance, and/or the “resilience” of female mice to the metabolic consequences of diet-induced obesity. These sex-dependent effects on regulation of TNF imply that clinical anti-TNF treatments may be more efficacious in obese men, or in men for treatment of other TNF-mediated chronic inflammatory disorders. While few clinical studies have addressed if biological sex contributes to variable outcomes of immunotherapies, there is evidence that anti-TNF treatments for rheumatoid arthritis, a chronic inflammatory disease that leads to the destruction of joints, show sex-specific differences in efficacy⁸¹⁹. Male patients have higher remission rates and less adverse outcomes compared to female patients^{820, 821, 822}. The underlying biological basis for why anti-TNF therapies for rheumatoid arthritis have less efficacy in females is unknown, however it may be due to

differences in circulating monocytes and synovial macrophages. In rheumatoid arthritis, monocytes are recruited to the synovium (the soft connective tissue that lines joints and surrounds the fluid-filled joint cavity) and differentiate into pro-inflammatory macrophages which activate surrounding immune cells⁸²³. The success of anti-TNF therapy in rheumatoid arthritis has been linked to changes to peripheral blood monocyte numbers and activation phenotype⁸²⁴, and a reduction in macrophage accumulation in the synovium^{825, 826, 827}. Treatment response of anti-TNF therapy in individuals with active rheumatoid arthritis has been reported to decrease with increasing patient BMI^{828, 829, 830}, though it is unclear if there are sex differences. Therefore, future studies into the mechanisms underlying sex differences in response to TNF in obesity-associated chronic inflammation, and changes to monocyte and macrophage populations, may also provide insights into other chronic inflammatory disorders, especially if obesity is also present.

Immunological implications of pregravid obesity and excess gestational weight gain

We investigated the effects of pregravid obesity on maternal immunophenotype at mid-gestation (E14.5), the effects of pregravid obesity in TNF^{-/-} and WT mice in late pregnancy (E18.5), and effects of excess gestational weight gain during lactation (P21). Although we used syngeneic pregnancies, we were able to identify trends consistently reported in semiallogeneic human pregnancies, suggesting that there are likely common peripheral immunological adaptations in pregnancy across mammalian species. Albeit observational, these experiments showed that assessment of individual immune cell population phenotype and prevalence, and overall peripheral immunophenotype, is a feasible approach to assess immunological effects of interventions for pregravid obesity, or excess gestational weight gain, in mouse models of pregnancy and lactation.

We collected original data showing that pregravid diet-induced obesity changes peripheral immunophenotype adaptations at mid-gestation and late pregnancy. As discussed, these pregnancy data have implications for maternal susceptibility to infection, vaccination responses, placental development, and fetal-maternal tolerance. Our lactational data have implications for neonatal health. Animal and human studies indicate that maternal blood immune cells and antibodies, and mature maternal leukocytes from the gut mucosa, as well as immunomodulatory cytokines, chemokines, and antimicrobial peptides, can be passed to offspring via milk during normal breastfeeding^{831, 832, 833}. Macrophages and dendritic cells represent >80% of immune cells in breast milk, and monocytes, B cells, T cells, NK cells, and neutrophils also contribute to its immune cell composition^{834, 835}. Maternal immune cells from breast milk have direct roles in infant immune protection as well as development of the immune system^{836, 837}. The composition of breast milk changes according to the health of the mother and infant^{838, 839}, maternal weight⁸⁴⁰, and maternal nutrition and intestinal adaptations that facilitate breast milk production⁸⁴¹. We observed that dams with excess gestational weight gain compared to chow-fed dams had an increased prevalence of peripheral blood B cells, and a reduction of NK cells. We also found that dams with excess gestational weight gain compared to chow-fed dams had reduced small intestine and colon lengths, and altered ileum and colon macrophage numbers and phenotype. These peripheral and intestinal changes could influence the immune cell composition of breast milk, which may impact neonatal susceptibility to infection and development of immune tolerance^{832, 842, 843}.

Both pregravid obesity and excess gestational weight gain are associated with increased risk of later-life maternal obesity and other chronic health conditions^{157, 158}.

Beyond these associations, however, there is little data on the biological mechanisms that lead to long-term detrimental health effects. We observed from our immunophenotype data that in chow-fed dams across pregnancy into lactation there is an increase in circulating myeloid cells, which results in a 2-fold increase in peripheral blood monocyte numbers in lactation compared to a non-pregnant mouse. We found that there were longitudinal increases in Ly6C^{high} monocyte prevalence in non-pregnant female mice fed a HF diet. Ly6C^{high} monocytes were also elevated in dams with pregravid obesity, and there were changes to Ly6C^{high} monocyte prevalence and phenotype in the blood and bone marrow during lactation in dams with excess gestational weight gain.

Trained immunity, or innate immune memory, is a phenomenon in which innate immune cells, after exposure to a stimulus, have augmented responsiveness to subsequent exposure to either related or unrelated stimuli^{844, 845}. While originally studied in the context of acute inflammatory stimuli like PAMPs in infection and vaccination^{845, 846, 847, 848}, it has also been reported that trained innate immunity in myeloid lineage cells can be induced by DAMPs^{846, 849}, stress⁸⁵⁰, high fat high sugar diet⁸⁵¹, and saturated fatty acids⁸⁵². This training involves epigenetic reprogramming of innate immune cell hematopoietic precursors⁸⁴⁷. While speculative, perhaps in conditions of chronic inflammation in pregnancy/lactation, when there is already a predisposition toward increased production of myeloid cells, the changes that occur to monocytes in response to pregravid obesity or excess gestational weight gain could lead to maladaptive epigenetic programming of innate immune cell hematopoietic precursors. This may result in the presence of hyperresponsive monocytes after pregnancy that could contribute to risk of chronic inflammatory disorders including obesity. Therefore, further studies on

monocytes and precursor cells could provide insight into postpartum chronic inflammation and maternal weight retention, as well as later-life obesity.

Intestinal macrophages under conditions of homeostasis and chronic inflammation

We examined intestinal macrophage populations in conditions of homeostasis and chronic inflammation, using a flow cytometry approach that identifies macrophages by their ontogeny. These studies collectively showed that diet-induced obesity, excess gestational weight gain, lactation, and aging, have different affects on intestinal macrophage dynamics (Table 7.1), which are also unique in comparison to other conditions of acute and chronic inflammation.

Table 7.1 Summary of observations of ileum and colon macrophage populations.

Ileum Macrophages								
Experiment	Total		CD4 ⁻ TIM4 ⁻		CD4 ⁺		CD4 ⁺ TIM4 ⁺	
	%	#	%	#	%	#	%	#
Diet-induced obesity (non-pregnant) (60% HF vs chow – section 6.1)	↑	↓	↓	↓	=to↑	↓to=	=to↑	↓to=
Excess gestational weight gain (45% HF vs chow – section 6.5)	=	=	↓	=	↑	↑	↑	=
Lactation vs non-pregnant (section 6.5)	=	↑	=	↑	↓	=	↑	↑
GF pregnancy (E14.5 vs non-pregnant) – section 6.5)	=	na	=	na	=	na	=	na
Colon Macrophages								
Experiment	Total		CD4 ⁻ TIM4 ⁻		CD4 ⁺		CD4 ⁺ TIM4 ⁺	
	%	#	%	#	%	#	%	#
Diet-induced obesity (non-pregnant) (60% HF vs chow – section 6.1)	=to↓	↓to=	=to↓	↓to=	↑	=	↓	↓to=
Excess gestational weight gain (45% HF vs chow – section 6.5)	=	=	↓	=	↑	=	↓	=
Lactation vs non-pregnant (section 6.5)	=	=	=	=	↓	=	↑	↑
GF pregnancy (E14.5 vs non-pregnant) – section 6.5)	=	na	=	na	=	na	=	na
Aging - SPF (old vs young – section 6.4)	↑	=	↑	=	↓	=	↓	↓
Aging - GF (old vs young – section 6.4)	=	=	↑	na	↓	na	=	na

Summary of observations from experiments in female mice in Chapter 6. Macrophage prevalence (%) is reported as a proportion of total macrophages. Numbers (#) are absolute cell counts (not adjusted by tissue length). ‘to’ indicates a change between 6 and 18 weeks HF diet in the non-pregnant female mouse studies.

Consistent with previous studies, under conditions of homeostasis, in SPF mice (fed standard chow diet) we observed that intestinal macrophages can self-renew (via Ki67 staining)⁴⁰⁸, there is a post-birth accumulation of monocyte-derived macrophages in young mice that alters macrophage composition^{214, 233, 235, 409}, and that these changes and intra-macrophage population dynamics were dependent on tissue location (colon or ileum)⁴⁰⁹, and the microbiota^{235, 268, 409, 412}. Also in agreement with previous reports, all intestinal macrophages produced IL-10 as well as TNF^{236, 483}.

Under conditions of homeostasis, macrophage numbers did not increase with biological age in SPF mice, but population dynamics changed, with a decrease in prevalence and numbers of CD4⁺TIM4⁺ macrophages of embryonic origin. We found that intracellular TNF expression was higher in all colon macrophage populations in old mice compared to young mice. In our studies with old and young mice, we also found that GF mice have fewer intestinal macrophages, and altered intra-macrophage population dynamics compared to SPF mice, supporting a role for the microbiota in maintenance of intestinal macrophage populations^{235, 412, 671, 853}. We found that there are age-intrinsic changes to macrophages dynamics in both GF and SPF mice. These data suggest that in addition to macrophage core programming, age-related cell-intrinsic changes, as well as age-associated microbial dysbiosis, and changes to microenvironment tissue structure and secreted cellular signals (e.g. growth factors), alter intestinal macrophage dynamics.

In our studies during lactation, we found that total intestinal macrophage numbers increased, perhaps due to increased requirements for macrophage-mediated activities, or in response to the presence of newly formed tissue niches for macrophages to occupy due to tissue remodelling. We also observed that there were no changes in macrophage

dynamics in non-pregnant GF mice and GF mice at mid-gestation (E14.5). As the intestinal microbiota changes across SPF mouse pregnancy^{178, 179, 180}, the changes in intestinal macrophage composition that we observed between SPF non-pregnant and lactational mice may be in part mediated by microbiota changes that occur in pregnancy/lactation.

In summary, using an ontogeny-based approach for assessment of macrophages, our data confirmed fundamental concepts of tissue macrophage properties and previous observations of intestinal macrophage proliferation, turnover, and intra-macrophage population dynamics, as well as tissue-specific anti-inflammatory programming under conditions of homeostasis, and provided new insights on changes to intestinal macrophages in aging and in pregnancy/lactation. These data improve our understanding of colon and ileum macrophages and can be used to guide future research.

We also studied effects of chronic inflammation on intestinal macrophages. In particular, in diet-induced obesity in non-pregnant young mice, we observed that despite both *in vivo* and *in vitro* evidence of increases in intestinal permeability, monocyte recruitment or accumulation of monocyte-derived CD4⁺TIM4⁺ macrophages was not observed, and macrophages retained or enhanced their production of IL-10 after 6, 12 and 18 weeks of HF diet feeding. In fact, mice with short-term HF diet feeding (6 weeks), compared to chow-fed mice, had reduced monocyte and macrophage numbers in the ileum and colon. From a clinical perspective, these data were not surprising. While human data reports an increased prevalence and risk of obese individuals developing certain gastrointestinal disorders, intestinal inflammation in obesity is not sufficiently severe to cause infiltration of leukocytes and gross pathology unless in combination with

infection or IBD^{854, 855}. A possible explanation for our observations is that the limited extent of barrier disruption (paracellular permeability rather than whole-enterocyte destruction) and lack of pathogenic bacteria (microbial dysbiosis rather than active infection) is insufficient to elicit a local inflammatory response, or the associated leukocyte recruitment response is blocked, preventing recruitment of monocytes and neutrophils. The cytokine production profiles that we observed in CD4⁺TIM4⁺, CD4⁺, and CD4⁺TIM4⁺ macrophages could reflect further attenuation of macrophage responses to any commensal bacteria or bacterial products that enter the lamina propria, as exposure to commensal bacteria can induce macrophage production of IL-10^{412, 671, 730, 853, 856, 857}. Macrophage phagocytosis also has a positive feedback effect on production of IL-10, so clearance of luminal contents from the lamina propria could reinforce macrophage anti-inflammatory tolerogenic properties^{466, 858}. There may be transcriptional activation of chemokines and pro-inflammatory cytokines in intestinal tissues, as has been reported^{643, 644, 645}, but this is insufficient to cause extensive leukocyte infiltration, though it is currently unclear how local macrophages are depleted. Changes to macrophage IL-10 and TNF production, coupled with a decrease in recruitment of monocytes, could therefore collectively be a protective response to increased intestinal permeability and microbial dysbiosis. However, this response may result in a permissive environment for translocation of bacteria, bacterial products, and other antigens, from the lamina propria into blood vessels or mesenteric lymph nodes, which can contribute to the development of systemic chronic inflammation and metabolic dysfunction^{345, 859}.

Colon macrophages across the life course

We observed significant differences in the numbers of peripheral blood monocytes (and other immune cells) of young SPF mice by biological sex under conditions of homeostasis. Sex differences in innate and adaptive immunity affect the microbiota, and *vice versa*^{722, 750, 774, 860, 861}. There are sex differences in expression of genes related to immunological function in colon tissue in young mice⁷⁷⁴ and old mice⁸⁶². It has also been reported that there are sex differences in microbiota composition, maintenance of the intestinal epithelium mucus layer, and expression of immune signalling genes in the ileum and colon between 19 month old male and female mice⁷⁷⁴. These data suggested that there may be differences in intestinal macrophage population dynamics by biological sex, which are dependent on the microbiota in both young and old mice.

We found that biological sex and age had a significant effect on the prevalence of monocyte-derived CD4⁺TIM4⁺ macrophages in both SPF and GF mice. Male mice generally had a higher prevalence of CD4⁺TIM4⁺ macrophages, though this may not be due to increased macrophage turnover, as it has been reported using bone marrow chimeras and genetic fate-mapping techniques that there are no differences in monocyte-derived macrophage turnover in the colon by biological sex, at least in young mice^{214, 232}. We in addition observed that there is an effect of biological sex on CD4⁺ macrophages in SPF mice, but not GF mice, and an effect of biological age, but not biological sex, on CD4⁺TIM4⁺ macrophages in both SPF and GF mice. These observations suggested that there are microbiota-independent and microbiota-dependent effects, and sex-dependent and sex-independent effects, on colon macrophage dynamics in young and old mice.

While there are differences in colon macrophage composition by biological sex, there are similar effects of turnover and gradual replacement of CD4⁺TIM4⁺ macrophages with age. In our experiments comparing young and old female mice, we observed that there is a decrease in the number, relative proportion, and self-renewal of embryonic origin CD4⁺TIM4⁺ colon macrophages in old female SPF mice. We also confirmed that there is a similar reduction of CD4⁺TIM4⁺ colon macrophages with age in SPF male mice. The fact that CD4⁺TIM4⁺ macrophages persist within colon tissues of both SPF and GF mice from their embryonic origins through to old age suggests they have important roles in lifelong maintenance of tissue homeostasis. As mentioned, intestinal embryonic origin macrophages have been implicated in regulation of blood vessel and lymphatic barriers^{771, 772}, enteric neuron signalling⁷⁷⁶, and smooth muscle contraction⁷⁷⁷. Depletion of CD4⁺TIM4⁺ macrophages earlier in life, as observed in the context of diet-induced obesity, could have a detrimental impact on the aging trajectory.

Research in other tissues has identified specific roles for embryonic origin macrophages in health and disease. For example, embryonic cardiac macrophages establish electrical conduction in the heart⁸⁶³, and have been reported to facilitate tissue repair after myocardial infarction⁸⁶⁴. In contrast, it has been reported that embryonic origin macrophages can promote progression of pancreatic cancer²³⁰, lung cancer⁸⁶⁵, and ovarian cancer metastasis⁸⁶⁶. It has been proposed that maternal factors including diet, environmental toxins, stress, infection, and chronic inflammation, may impact fetal hematopoietic stem cell development and epigenetic programming^{867, 868}. Effects of maternal obesity in pregnancy have sexually dimorphic effects on offspring metabolism and immunity⁸⁶⁹. Therefore, there could be differential effects of maternal programming

signals by fetal sex that influence long-lived embryonic origin intestinal macrophage core genetic programming, and their population dynamics and functions in health and disease across the life course.

Limitations and future directions

All of the studies in this thesis were conducted using mouse models. The use of mouse models allowed us to control for effects of genetics and housing environment, to perform experiments at specific time points during pregnancy or lactation, and to specifically manipulate diet and the microbiota⁵⁰⁰. The polycocial nature of mouse pregnancy, and variation in the number of fetuses, can affect maternal adaptations in pregnancy and lactation^{122, 870}. Litter sizes in all of our studies were not significantly different between diet groups, but we tried to limit these effects in the lactation study by reducing litter size to a standard number (of 6 pups) for all dams. For studies on chronic inflammation associated with obesity, we used mouse models of diet-induced obesity. Leptin-deficient homozygous *ob/ob* mice have increased adiposity and intestinal permeability, as well as microbial dysbiosis, in comparison to their wildtype littermate siblings, even when maintained on a standard chow diet^{659, 871}. These mice could be used to examine effects of obesity in the absence of an obesogenic diet, to confirm our data on obesity-associated changes to peripheral immunophenotype and intestinal macrophages, as well as effects of microbial dysbiosis in colonized GF mice, with use of the same diet in all donor and recipient experiment groups. To examine the effects of TNF on adiposity, intestinal permeability, and peripheral and tissue monocyte and macrophage populations, we used a model of whole-body genetic deletion of TNF. To provide further insight into the effects of TNF in diet-induced obesity in male and female mice, future studies should

also use antibody, chemical, and/or RNAi-based methods to suppress TNF in WT mice²⁵. These methods would also allow for dose adjustment to completely ablate TNF, or simply reduce its effects, before or during diet allocation.

We assessed intestinal macrophage populations by whole-tissue digestion with analysis by flow cytometry, in order to examine the CD4⁻TIM4⁻, CD4⁺, and CD4⁺TIM4⁺ subsets recently defined by Shaw and colleagues⁴⁰⁹. While macrophages are present in all layers of the intestines, the highest numbers are found within the lamina propria^{268, 407, 422, 423}. As a result, while our flow cytometry data are representative of global changes to macrophage populations within the intestines, the majority of the cells likely originate from the lamina propria. In addition, we focussed our studies on the ileum and colon, but we also observed that macrophage composition varies along the length of the intestinal tract. Examining macrophage subsets by anatomical location along and within the layers of the intestines will help disentangle their heterogeneity, as well as determine if embryonic and bone marrow origin macrophages maintain different roles, and how they interact within a distinct tissue niche. Future studies should therefore consider combining cell-based flow cytometry and cell sorting and bulk transcriptomic analyses with whole tissue analysis by immunohistochemistry and microscopy⁴⁰⁸, or even *in vivo* live cell imaging²⁶⁸. As the use of specific cell surface markers for identification of macrophages does not allow for a full assessment of their possible diversity or ontogeny, unbiased single-cell RNA sequencing may also provide further insight⁸⁷². This combination of techniques will be extremely important to disentangle macrophage functions and changes in various disease states, and in response to chronic inflammation.

Concluding remarks

The work presented in this thesis identified effects of biological sex on peripheral immunophenotype composition and variability in homeostasis, and examined effects of chronic inflammation in the context of diet-induced obesity, pregnancy, lactation, and biological aging, focussing on peripheral monocytes and intestinal macrophages. We determined that biological sex, but not the female reproductive cycle, affects immunophenotype composition and variability in homeostasis. We demonstrated that in diet-induced obesity, TNF is not a key mediator of changes to peripheral cellular inflammation, intestinal permeability, or intestinal macrophages in female mice, but in male mice TNF is a mediator of monocytois and insulin resistance. We found that effects of microbiota colonization are modified by diet and recipient host age. We showed longitudinal effects of obesity on peripheral and intestinal monocytes and macrophages, reported novel data on maternal immunological adaptations in pregnancy and lactation in mice, and examined effects of pregravid obesity and excess gestational weight gain on those adaptations. We identified that intestinal macrophages change in a biological context-dependent manner across the life course in response to chronic inflammation. Collectively, our data have generated new questions to address in future studies in research areas of immunometabolism, pregnancy, and aging.

References

1. Medzhitov, R. Origin and physiological roles of inflammation. *Nature* **454**, 428-435 (2008).
2. Barton, G.M. A calculated response: control of inflammation by the innate immune system. *The Journal of clinical investigation* **118**, 413-420 (2008).
3. Cramer, T. *et al.* HIF-1alpha is essential for myeloid cell-mediated inflammation. *Cell* **112**, 645-657 (2003).
4. Odegaard, J.I. & Chawla, A. The immune system as a sensor of the metabolic state. *Immunity* **38**, 644-654 (2013).
5. Nathan, C. Points of control in inflammation. *Nature* **420**, 846-852 (2002).
6. Serhan, C.N. Resolution phase of inflammation: novel endogenous anti-inflammatory and proresolving lipid mediators and pathways. *Annual review of immunology* **25**, 101-137 (2007).
7. Serhan, C.N. & Savill, J. Resolution of inflammation: the beginning programs the end. *Nature immunology* **6**, 1191-1197 (2005).
8. Uderhardt, S., Martins, A.J., Tsang, J.S., Lämmermann, T. & Germain, R.N. Resident Macrophages Cloak Tissue Microlesions to Prevent Neutrophil-Driven Inflammatory Damage. *Cell* **177**, 541-555.e517 (2019).
9. Medzhitov, R. & Janeway, C.A., Jr. Innate immunity: the virtues of a nonclonal system of recognition. *Cell* **91**, 295-298 (1997).
10. Feldman, N., Rotter-Maskowitz, A. & Okun, E. DAMPs as mediators of sterile inflammation in aging-related pathologies. *Ageing research reviews* **24**, 29-39 (2015).
11. Mariathasan, S. *et al.* Cryopyrin activates the inflammasome in response to toxins and ATP. *Nature* **440**, 228-232 (2006).
12. Vénéreau, E., Ceriotti, C. & Bianchi, M.E. DAMPs from Cell Death to New Life. *Frontiers in immunology* **6**, 422 (2015).
13. Matzinger, P. Tolerance, danger, and the extended family. *Annual review of immunology* **12**, 991-1045 (1994).
14. Wynn, T.A. Cellular and molecular mechanisms of fibrosis. *J Pathol* **214**, 199-210 (2008).
15. Barth, K., Remick, D.G. & Genco, C.A. Disruption of immune regulation by microbial pathogens and resulting chronic inflammation. *Journal of cellular physiology* **228**, 1413-1422 (2013).
16. Luo, S. *et al.* Chronic Inflammation: A Common Promoter in Tertiary Lymphoid Organ Neogenesis. *Frontiers in immunology* **10**, 2938 (2019).
17. Boettcher, S. & Manz, M.G. Regulation of Inflammation- and Infection-Driven Hematopoiesis. *Trends in immunology* **38**, 345-357 (2017).
18. denDekker, A.D. *et al.* TNF- α regulates diabetic macrophage function through the histone acetyltransferase MOF. *JCI insight* **5** (2020).
19. Baardman, J., Licht, I., de Winther, M.P. & Van den Bossche, J. Metabolic-epigenetic crosstalk in macrophage activation. *Epigenomics* **7**, 1155-1164 (2015).

20. Kittan, N.A. *et al.* Cytokine induced phenotypic and epigenetic signatures are key to establishing specific macrophage phenotypes. *PLoS One* **8**, e78045 (2013).
21. Schafer, M.J., Miller, J.D. & LeBrasseur, N.K. Cellular senescence: Implications for metabolic disease. *Molecular and cellular endocrinology* **455**, 93-102 (2017).
22. Dorhoi, A. & Kaufmann, S.H. Perspectives on host adaptation in response to *Mycobacterium tuberculosis*: modulation of inflammation. *Seminars in immunology* **26**, 533-542 (2014).
23. Zicari, S. *et al.* Immune Activation, Inflammation, and Non-AIDS Co-Morbidities in HIV-Infected Patients under Long-Term ART. *Viruses* **11** (2019).
24. Marzullo, P. *et al.* From obesity through gut microbiota to cardiovascular diseases: a dangerous journey. *International journal of obesity supplements* **10**, 35-49 (2020).
25. Hotamisligil, G.S. Inflammation, metaflammation and immunometabolic disorders. *Nature* **542**, 177-185 (2017).
26. Franceschi, C. *et al.* Inflamm-aging. An evolutionary perspective on immunosenescence. *Annals of the New York Academy of Sciences* **908**, 244-254 (2000).
27. De Martinis, M., Franceschi, C., Monti, D. & Ginaldi, L. Inflamm-ageing and lifelong antigenic load as major determinants of ageing rate and longevity. *FEBS letters* **579**, 2035-2039 (2005).
28. Hauguel-de Mouzon, S. & Guerre-Millo, M. The placenta cytokine network and inflammatory signals. *Placenta* **27**, 794-798 (2006).
29. Howell, K.R. & Powell, T.L. Effects of maternal obesity on placental function and fetal development. *Reproduction (Cambridge, England)* **153**, R97-r108 (2017).
30. World Health Organization. 10 facts on obesity and overweight. 2017.
31. Global BMI Mortality Collaboration *et al.* Body-mass index and all-cause mortality: individual-participant-data meta-analysis of 239 prospective studies in four continents. *Lancet (London, England)* **388**, 776-786 (2016).
32. Hassan, M.K., Joshi, A.V., Madhavan, S.S. & Amonkar, M.M. Obesity and health-related quality of life: a cross-sectional analysis of the US population. *International Journal of Obesity* **27**, 1227-1232 (2003).
33. Wilkins, J., Ghosh, P., Vivar, J., Chakraborty, B. & Ghosh, S. Exploring the associations between systemic inflammation, obesity and healthy days: a health related quality of life (HRQOL) analysis of NHANES 2005-2008. *BMC obesity* **5**, 21 (2018).
34. Dixon, J.B. The effect of obesity on health outcomes. *Molecular and Cellular Endocrinology* **316**, 104-108 (2010).
35. Finkelstein, E.A., Ruhm, C.J. & Kosa, K.M. ECONOMIC CAUSES AND CONSEQUENCES OF OBESITY. *Annual Review of Public Health* **26**, 239-257 (2005).
36. Anis, A.H. *et al.* Obesity and overweight in Canada: an updated cost-of-illness study. *Obesity reviews : an official journal of the International Association for the Study of Obesity* **11**, 31-40 (2010).
37. O'Neill, S. & O'Driscoll, L. Metabolic syndrome: a closer look at the growing epidemic and its associated pathologies. *Obesity reviews : an official journal of the International Association for the Study of Obesity* **16**, 1-12 (2015).

38. Abdullah, A., Peeters, A., de Courten, M. & Stoelwinder, J. The magnitude of association between overweight and obesity and the risk of diabetes: a meta-analysis of prospective cohort studies. *Diabetes research and clinical practice* **89**, 309-319 (2010).
39. Richter-Stretton, G.L., Fenning, A.S. & Vella, R.K. Skeletal muscle - A bystander or influencer of metabolic syndrome? *Diabetes & metabolic syndrome* **14**, 867-875 (2020).
40. Farruggia, M.C. & Small, D.M. Effects of adiposity and metabolic dysfunction on cognition: A review. *Physiology & behavior* **208**, 112578 (2019).
41. O'Brien, P.D., Hinder, L.M., Callaghan, B.C. & Feldman, E.L. Neurological consequences of obesity. *The Lancet Neurology* **16**, 465-477 (2017).
42. Renehan, A.G., Tyson, M., Egger, M., Heller, R.F. & Zwahlen, M. Body-mass index and incidence of cancer: a systematic review and meta-analysis of prospective observational studies. *Lancet (London, England)* **371**, 569-578 (2008).
43. Bhaskaran, K. *et al.* Body-mass index and risk of 22 specific cancers: a population-based cohort study of 5·24 million UK adults. *Lancet (London, England)* **384**, 755-765 (2014).
44. Honce, R. & Schultz-Cherry, S. Impact of Obesity on Influenza A Virus Pathogenesis, Immune Response, and Evolution. *Frontiers in immunology* **10**, 1071 (2019).
45. Sheridan, P.A. *et al.* Obesity is associated with impaired immune response to influenza vaccination in humans. *International journal of obesity (2005)* **36**, 1072-1077 (2012).
46. Hruby, A. & Hu, F.B. The Epidemiology of Obesity: A Big Picture. *Pharmacoeconomics* **33**, 673-689 (2015).
47. Wharton, S. *et al.* Obesity in adults: a clinical practice guideline. *Canadian Medical Association Journal* **192**, E875 (2020).
48. Mechanick, J.I., Hurley, D.L. & Garvey, W.T. ADIPOSITY-BASED CHRONIC DISEASE AS A NEW DIAGNOSTIC TERM: THE AMERICAN ASSOCIATION OF CLINICAL ENDOCRINOLOGISTS AND AMERICAN COLLEGE OF ENDOCRINOLOGY POSITION STATEMENT. *Endocrine practice : official journal of the American College of Endocrinology and the American Association of Clinical Endocrinologists* **23**, 372-378 (2017).
49. Wang, P., Mariman, E., Renes, J. & Keijer, J. The secretory function of adipocytes in the physiology of white adipose tissue. *Journal of cellular physiology* **216**, 3-13 (2008).
50. Weisberg, S.P. *et al.* Obesity is associated with macrophage accumulation in adipose tissue. *The Journal of clinical investigation* **112**, 1796-1808 (2003).
51. Xu, H. *et al.* Chronic inflammation in fat plays a crucial role in the development of obesity-related insulin resistance. *The Journal of clinical investigation* **112**, 1821-1830 (2003).
52. Amano, S.U. *et al.* Local proliferation of macrophages contributes to obesity-associated adipose tissue inflammation. *Cell metabolism* **19**, 162-171 (2014).
53. Luche, E. *et al.* Corrupted adipose tissue endogenous myelopoiesis initiates diet-induced metabolic disease. *eLife* **6** (2017).
54. Ito, A. *et al.* Role of CC chemokine receptor 2 in bone marrow cells in the recruitment of macrophages into obese adipose tissue. *The Journal of biological chemistry* **283**, 35715-35723 (2008).

55. Kamei, N. *et al.* Overexpression of monocyte chemoattractant protein-1 in adipose tissues causes macrophage recruitment and insulin resistance. *The Journal of biological chemistry* **281**, 26602-26614 (2006).
56. Kanda, H. *et al.* MCP-1 contributes to macrophage infiltration into adipose tissue, insulin resistance, and hepatic steatosis in obesity. *The Journal of clinical investigation* **116**, 1494-1505 (2006).
57. Weisberg, S.P. *et al.* CCR2 modulates inflammatory and metabolic effects of high-fat feeding. *The Journal of clinical investigation* **116**, 115-124 (2006).
58. Lumeng, C.N., Bodzin, J.L. & Saltiel, A.R. Obesity induces a phenotypic switch in adipose tissue macrophage polarization. *The Journal of clinical investigation* **117**, 175-184 (2007).
59. Ohmura, K. *et al.* Natural killer T cells are involved in adipose tissues inflammation and glucose intolerance in diet-induced obese mice. *Arteriosclerosis, thrombosis, and vascular biology* **30**, 193-199 (2010).
60. Nishimura, S. *et al.* CD8⁺ effector T cells contribute to macrophage recruitment and adipose tissue inflammation in obesity. *Nature medicine* **15**, 914-920 (2009).
61. Morris, D.L. *et al.* Adipose tissue macrophages function as antigen-presenting cells and regulate adipose tissue CD4⁺ T cells in mice. *Diabetes* **62**, 2762-2772 (2013).
62. Cai, D. *et al.* Local and systemic insulin resistance resulting from hepatic activation of IKK-beta and NF-kappaB. *Nature medicine* **11**, 183-190 (2005).
63. Hirosumi, J. *et al.* A central role for JNK in obesity and insulin resistance. *Nature* **420**, 333-336 (2002).
64. Nakamura, T. *et al.* Double-stranded RNA-dependent protein kinase links pathogen sensing with stress and metabolic homeostasis. *Cell* **140**, 338-348 (2010).
65. Ouchi, N. *et al.* Sfrp5 is an anti-inflammatory adipokine that modulates metabolic dysfunction in obesity. *Science* **329**, 454-457 (2010).
66. Fuster, J.J. *et al.* Noncanonical Wnt signaling promotes obesity-induced adipose tissue inflammation and metabolic dysfunction independent of adipose tissue expansion. *Diabetes* **64**, 1235-1248 (2015).
67. Debnath, M., Agrawal, S., Agrawal, A. & Dubey, G.P. Metaflammatory responses during obesity: Pathomechanism and treatment. *Obesity research & clinical practice* **10**, 103-113 (2016).
68. Alberti, K.G., Zimmet, P. & Shaw, J. The metabolic syndrome--a new worldwide definition. *Lancet (London, England)* **366**, 1059-1062 (2005).
69. Reaven, G.M. Banting lecture 1988. Role of insulin resistance in human disease. *Diabetes* **37**, 1595-1607 (1988).
70. Deng, Y. & Scherer, P.E. Adipokines as novel biomarkers and regulators of the metabolic syndrome. *Annals of the New York Academy of Sciences* **1212**, E1-e19 (2010).
71. Meex, R.C.R. & Watt, M.J. Hepatokines: linking nonalcoholic fatty liver disease and insulin resistance. *Nature reviews. Endocrinology* **13**, 509-520 (2017).
72. Wu, H. & Ballantyne, C.M. Skeletal muscle inflammation and insulin resistance in obesity. *The Journal of clinical investigation* **127**, 43-54 (2017).
73. Thomou, T. *et al.* Adipose-derived circulating miRNAs regulate gene expression in other tissues. *Nature* **542**, 450-455 (2017).

74. Ying, W. *et al.* Adipose Tissue Macrophage-Derived Exosomal miRNAs Can Modulate In Vivo and In Vitro Insulin Sensitivity. *Cell* **171**, 372-384.e312 (2017).
75. Cani, P.D. *et al.* Metabolic endotoxemia initiates obesity and insulin resistance. *Diabetes* **56**, 1761-1772 (2007).
76. Chavez, J.A. & Summers, S.A. A ceramide-centric view of insulin resistance. *Cell metabolism* **15**, 585-594 (2012).
77. Lee, Yun S. *et al.* Increased Adipocyte O₂ Consumption Triggers HIF-1 α , Causing Inflammation and Insulin Resistance in Obesity. *Cell* **157**, 1339-1352 (2014).
78. Lackey, D.E. *et al.* Adipocyte PU.1 knockout promotes insulin sensitivity in HFD-fed obese mice. *Scientific reports* **9**, 14779 (2019).
79. Li, P. *et al.* Adipocyte NCoR Knockout Decreases PPAR γ Phosphorylation and Enhances PPAR γ Activity and Insulin Sensitivity. *Cell* **147**, 815-826 (2011).
80. Mayoral, R. *et al.* Adipocyte SIRT1 knockout promotes PPAR γ activity, adipogenesis and insulin sensitivity in chronic-HFD and obesity. *Molecular metabolism* **4**, 378-391 (2015).
81. Qi, L. *et al.* Adipocyte CREB Promotes Insulin Resistance in Obesity. *Cell metabolism* **9**, 277-286 (2009).
82. Amar, J. *et al.* Involvement of tissue bacteria in the onset of diabetes in humans: evidence for a concept. *Diabetologia* **54**, 3055-3061 (2011).
83. Cani, P.D., Delzenne, N.M., Amar, J. & Burcelin, R. Role of gut microflora in the development of obesity and insulin resistance following high-fat diet feeding. *Pathologie-biologie* **56**, 305-309 (2008).
84. Cani, P.D. *et al.* Changes in gut microbiota control inflammation in obese mice through a mechanism involving GLP-2-driven improvement of gut permeability. *Gut* **58**, 1091-1103 (2009).
85. Lefere, S. & Tacke, F. Macrophages in obesity and non-alcoholic fatty liver disease: Crosstalk with metabolism. *JHEP Reports* **1**, 30-43 (2019).
86. Fink, L.N. *et al.* Pro-inflammatory macrophages increase in skeletal muscle of high fat-fed mice and correlate with metabolic risk markers in humans. *Obesity (Silver Spring, Md.)* **22**, 747-757 (2014).
87. Ying, W., Fu, W., Lee, Y.S. & Olefsky, J.M. The role of macrophages in obesity-associated islet inflammation and β -cell abnormalities. *Nature Reviews Endocrinology* **16**, 81-90 (2020).
88. Boura-Halfon, S., Pecht, T., Jung, S. & Rudich, A. Obesity and dysregulated central and peripheral macrophage–neuron cross-talk. *European journal of immunology* **49**, 19-29 (2019).
89. Kawano, Y. *et al.* Colonic Pro-inflammatory Macrophages Cause Insulin Resistance in an Intestinal Ccl2/Ccr2-Dependent Manner. *Cell metabolism* **24**, 295-310 (2016).
90. Statistics Canada. Table 13-10-0389-01 Life expectancy, at birth and at age 65, by sex, three-year average, Canada, provinces, territories, health regions and peer groups. (2017).
91. Statistics Canada. Canada Year Book 11-402-X. *Minister of Industry* (2011).
92. Salomon, J.A. *et al.* Healthy life expectancy for 187 countries, 1990-2010: a systematic analysis for the Global Burden Disease Study 2010. *Lancet (London, England)* **380**, 2144-2162 (2012).
93. López-Otín, C., Blasco, M.A., Partridge, L., Serrano, M. & Kroemer, G. The hallmarks of aging. *Cell* **153**, 1194-1217 (2013).

94. Aunan, J.R., Watson, M.M., Hagland, H.R. & Søreide, K. Molecular and biological hallmarks of ageing. *The British journal of surgery* **103**, e29-46 (2016).
95. Thomas, R., Wang, W. & Su, D.M. Contributions of Age-Related Thymic Involution to Immunosenescence and Inflammaging. *Immunity & ageing : I & A* **17**, 2 (2020).
96. Steinmann, G.G. Changes in the human thymus during aging. *Current topics in pathology. Ergebnisse der Pathologie* **75**, 43-88 (1986).
97. Cancro, M.P. *et al.* B cells and aging: molecules and mechanisms. *Trends in immunology* **30**, 313-318 (2009).
98. Frasca, D. & Blomberg, B.B. Effects of aging on B cell function. *Current opinion in immunology* **21**, 425-430 (2009).
99. Chinn, I.K., Blackburn, C.C., Manley, N.R. & Sempowski, G.D. Changes in primary lymphoid organs with aging. *Seminars in immunology* **24**, 309-320 (2012).
100. Linton, P.J. *et al.* Intrinsic versus environmental influences on T-cell responses in aging. *Immunological reviews* **205**, 207-219 (2005).
101. Loukov, D., Naidoo, A., Puchta, A., Marin, J.L. & Bowdish, D.M. Tumor necrosis factor drives increased splenic monopoiesis in old mice. *Journal of leukocyte biology* **100**, 121-129 (2016).
102. Pang, W.W. *et al.* Human bone marrow hematopoietic stem cells are increased in frequency and myeloid-biased with age. *Proceedings of the National Academy of Sciences* **108**, 20012 (2011).
103. Nikolich-Zugich, J. The twilight of immunity: emerging concepts in aging of the immune system. *Nature immunology* **19**, 10-19 (2018).
104. Goldberg, E.L., Shaw, A.C. & Montgomery, R.R. How Inflammation Blunts Innate Immunity in Aging. *Interdisciplinary topics in gerontology and geriatrics* **43**, 1-17 (2020).
105. Trzonkowski, P., Myśliwska, J., Pawelec, G. & Myśliwski, A. From bench to bedside and back: the SENIEUR Protocol and the efficacy of influenza vaccination in the elderly. *Biogerontology* **10**, 83-94 (2009).
106. McElhaney, J.E. & Effros, R.B. Immunosenescence: what does it mean to health outcomes in older adults? *Current opinion in immunology* **21**, 418-424 (2009).
107. Kline, K.A. & Bowdish, D.M. Infection in an aging population. *Current opinion in microbiology* **29**, 63-67 (2016).
108. Sendama, W. The effect of ageing on the resolution of inflammation. *Ageing research reviews* **57**, 101000 (2020).
109. Ventura, M.T., Casciaro, M., Gangemi, S. & Buquicchio, R. Immunosenescence in aging: between immune cells depletion and cytokines up-regulation. *Clinical and molecular allergy : CMA* **15**, 21 (2017).
110. Goronzy, J.J. & Weyand, C.M. Immune aging and autoimmunity. *Cellular and molecular life sciences : CMLS* **69**, 1615-1623 (2012).
111. Pawelec, G. & Derhovanessian, E. Role of CMV in immune senescence. *Virus research* **157**, 175-179 (2011).
112. Fulop, T. *et al.* Immunosenescence and Inflamm-Aging As Two Sides of the Same Coin: Friends or Foes? *Frontiers in immunology* **8**, 1960 (2017).

113. Giovannini, S. *et al.* Interleukin-6, C-reactive protein, and tumor necrosis factor-alpha as predictors of mortality in frail, community-living elderly individuals. *Journal of the American Geriatrics Society* **59**, 1679-1685 (2011).
114. Brüünsgaard, H. & Pedersen, B.K. Age-related inflammatory cytokines and disease. *Immunology and allergy clinics of North America* **23**, 15-39 (2003).
115. Evrin, P.E., Nilsson, S.E., Oberg, T. & Malmberg, B. Serum C-reactive protein in elderly men and women: association with mortality, morbidity and various biochemical values. *Scandinavian journal of clinical and laboratory investigation* **65**, 23-31 (2005).
116. Krabbe, K.S., Pedersen, M. & Bruunsgaard, H. Inflammatory mediators in the elderly. *Experimental gerontology* **39**, 687-699 (2004).
117. Varadhan, R. *et al.* Simple biologically informed inflammatory index of two serum cytokines predicts 10 year all-cause mortality in older adults. *The journals of gerontology. Series A, Biological sciences and medical sciences* **69**, 165-173 (2014).
118. Tan, E.K. & Tan, E.L. Alterations in physiology and anatomy during pregnancy. *Best practice & research. Clinical obstetrics & gynaecology* **27**, 791-802 (2013).
119. Torgersen, K.L. & Curran, C.A. A systematic approach to the physiologic adaptations of pregnancy. *Critical care nursing quarterly* **29**, 2-19 (2006).
120. Aghaepour, N. *et al.* An immune clock of human pregnancy. *Science immunology* **2**, ean2946 (2017).
121. Nuriel-Ohayon, M., Neuman, H. & Koren, O. Microbial Changes during Pregnancy, Birth, and Infancy. *Frontiers in microbiology* **7**, 1031 (2016).
122. Hammond, K.A. Adaptation of the maternal intestine during lactation. *Journal of mammary gland biology and neoplasia* **2**, 243-252 (1997).
123. Ireland, M.L. & Ott, S.M. The effects of pregnancy on the musculoskeletal system. *Clinical orthopaedics and related research*, 169-179 (2000).
124. Napso, T., Yong, H.E.J., Lopez-Tello, J. & Sferruzzi-Perri, A.N. The Role of Placental Hormones in Mediating Maternal Adaptations to Support Pregnancy and Lactation. *Front Physiol* **9**, 1091 (2018).
125. Newbern, D. & Freemark, M. Placental hormones and the control of maternal metabolism and fetal growth. *Current opinion in endocrinology, diabetes, and obesity* **18**, 409-416 (2011).
126. Freemark, M. Regulation of maternal metabolism by pituitary and placental hormones: roles in fetal development and metabolic programming. *Hormone research* **65 Suppl 3**, 41-49 (2006).
127. Hunt, J.S., Langat, D.K., McIntire, R.H. & Morales, P.J. The role of HLA-G in human pregnancy. *Reproductive biology and endocrinology : RB&E* **4 Suppl 1**, S10 (2006).
128. Billingham, R.E., Brent, L. & Medawar, P.B. Actively acquired tolerance of foreign cells. *Nature* **172**, 603-606 (1953).
129. Aghaepour, N. *et al.* A proteomic clock of human pregnancy. *American journal of obstetrics and gynecology* **218**, 347.e341-347.e314 (2018).
130. Ghaemi, M.S. *et al.* Multiomics modeling of the immunome, transcriptome, microbiome, proteome and metabolome adaptations during human pregnancy. *Bioinformatics (Oxford, England)* **35**, 95-103 (2019).

131. McMaster, M.T., Newton, R.C., Dey, S.K. & Andrews, G.K. Activation and distribution of inflammatory cells in the mouse uterus during the preimplantation period. *Journal of immunology (Baltimore, Md. : 1950)* **148**, 1699-1705 (1992).
132. Du, M.-R., Wang, S.-C. & Li, D.-J. The integrative roles of chemokines at the maternal-fetal interface in early pregnancy. *Cellular & molecular immunology* **11**, 438-448 (2014).
133. Segerer, S., Kammerer, U., Kapp, M., Dietl, J. & Rieger, L. Upregulation of chemokine and cytokine production during pregnancy. *Gynecologic and obstetric investigation* **67**, 145-150 (2009).
134. Mori, M., Bogdan, A., Balassa, T., Csabai, T. & Szekeres-Bartho, J. The decidua-the maternal bed embracing the embryo-maintains the pregnancy. *Semin Immunopathol* **38**, 635-649 (2016).
135. Liu, S. *et al.* The role of decidual immune cells on human pregnancy. *Journal of reproductive immunology* **124**, 44-53 (2017).
136. Arck, P., Solano, M.E., Maciej, K. & Robertson, S. Reproductive immunology: piece by piece. *Journal of reproductive immunology* **97**, 1 (2013).
137. Arck, P.C. & Hecher, K. Fetomaternal immune cross-talk and its consequences for maternal and offspring's health. *Nature medicine* **19**, 548-556 (2013).
138. Shynlova, O., Lee, Y.H., Srihajan, K. & Lye, S.J. Physiologic uterine inflammation and labor onset: integration of endocrine and mechanical signals. *Reproductive sciences (Thousand Oaks, Calif.)* **20**, 154-167 (2013).
139. Apps, R. *et al.* Multimodal immune phenotyping of maternal peripheral blood in normal human pregnancy. *JCI insight* **5** (2020).
140. Gomez-Lopez, N. *et al.* The Cellular Transcriptome in the Maternal Circulation During Normal Pregnancy: A Longitudinal Study. *Frontiers in immunology* **10**, 2863 (2019).
141. Romero, R. *et al.* The maternal plasma proteome changes as a function of gestational age in normal pregnancy: a longitudinal study. *American journal of obstetrics and gynecology* **217**, 67.e61-67.e21 (2017).
142. Sacks, G.P., Studena, K., Sargent, K. & Redman, C.W. Normal pregnancy and preeclampsia both produce inflammatory changes in peripheral blood leukocytes akin to those of sepsis. *American journal of obstetrics and gynecology* **179**, 80-86 (1998).
143. Sacks, G.P., Clover, L.M., Bainbridge, D.R., Redman, C.W. & Sargent, I.L. Flow cytometric measurement of intracellular Th1 and Th2 cytokine production by human villous and extravillous cytotrophoblast. *Placenta* **22**, 550-559 (2001).
144. Luppi, P. *et al.* Monocytes are progressively activated in the circulation of pregnant women. *Journal of leukocyte biology* **72**, 874-884 (2002).
145. Bianchi, D.W., Zickwolf, G.K., Weil, G.J., Sylvester, S. & DeMaria, M.A. Male fetal progenitor cells persist in maternal blood for as long as 27 years postpartum. *Proceedings of the National Academy of Sciences of the United States of America* **93**, 705-708 (1996).
146. Stelzer, I.A., Thiele, K. & Solano, M.E. Maternal microchimerism: lessons learned from murine models. *Journal of reproductive immunology* **108**, 12-25 (2015).
147. Göhner, C., Plösch, T. & Faas, M.M. Immune-modulatory effects of syncytiotrophoblast extracellular vesicles in pregnancy and preeclampsia. *Placenta* **60 Suppl 1**, S41-s51 (2017).

148. Nair, S. & Salomon, C. Extracellular vesicles and their immunomodulatory functions in pregnancy. *Semin Immunopathol* **40**, 425-437 (2018).
149. Abbassi-Ghanavati, M., Greer, L.G. & Cunningham, F.G. Pregnancy and laboratory studies: a reference table for clinicians. *Obstetrics and gynecology* **114**, 1326-1331 (2009).
150. Christian, L.M. & Porter, K. Longitudinal changes in serum proinflammatory markers across pregnancy and postpartum: effects of maternal body mass index. *Cytokine* **70**, 134-140 (2014).
151. Siegel, I. & Gleicher, N. Changes in peripheral mononuclear cells in pregnancy. *American journal of reproductive immunology (New York, N.Y. : 1989)* **1**, 154-155 (1981).
152. Zhang, J. *et al.* Immunophenotyping and activation status of maternal peripheral blood leukocytes during pregnancy and labour, both term and preterm. *Journal of cellular and molecular medicine* **21**, 2386-2402 (2017).
153. Lampe, R. *et al.* Phagocytic index of neutrophil granulocytes and monocytes in healthy and preeclamptic pregnancy. *Journal of reproductive immunology* **107**, 26-30 (2015).
154. Groen, B. *et al.* Immunological Adaptations to Pregnancy in Women with Type 1 Diabetes. *Scientific reports* **5**, 13618 (2015).
155. Melgert, B.N. *et al.* Pregnancy and preeclampsia affect monocyte subsets in humans and rats. *PLoS One* **7**, e45229 (2012).
156. Pantham, P., Aye, I.L. & Powell, T.L. Inflammation in maternal obesity and gestational diabetes mellitus. *Placenta* **36**, 709-715 (2015).
157. Dudenhausen, J.W., Grünebaum, A. & Kirschner, W. Prepregnancy body weight and gestational weight gain: recommendations and reality in the USA and in Germany. *American Journal of Obstetrics & Gynecology* **213**, 591-592 (2014).
158. McKinley, M.C., Allen-Walker, V., McGirr, C., Rooney, C. & Woodside, J.V. Weight loss after pregnancy: challenges and opportunities. *Nutrition research reviews* **31**, 225-238 (2018).
159. Park, C.K. *et al.* Binge Eating Predicts Excess Gestational Weight Gain: A Pilot Prospective Cohort Study. *Journal of obstetrics and gynaecology Canada : JOGC = Journal d'obstetrique et gynecologie du Canada : JOGC* **37**, 494-507 (2015).
160. Korkmaz, L., Baştuğ, O. & Kurtoğlu, S. Maternal Obesity and its Short- and Long-Term Maternal and Infantile Effects. *Journal of clinical research in pediatric endocrinology* **8**, 114-124 (2016).
161. Norman, J.E. & Reynolds, R.M. The consequences of obesity and excess weight gain in pregnancy. *The Proceedings of the Nutrition Society* **70**, 450-456 (2011).
162. Poston, L. *et al.* Preconceptional and maternal obesity: epidemiology and health consequences. *The lancet. Diabetes & endocrinology* **4**, 1025-1036 (2016).
163. Heslehurst, N. *et al.* The impact of maternal BMI status on pregnancy outcomes with immediate short-term obstetric resource implications: a meta-analysis. *Obesity reviews : an official journal of the International Association for the Study of Obesity* **9**, 635-683 (2008).
164. Birgisdottir, B.E., Gunnarsdottir, I., Thorsdottir, I., Gudnason, V. & Benediktsson, R. Size at birth and glucose intolerance in a relatively genetically homogeneous, high-birth weight population. *The American journal of clinical nutrition* **76**, 399-403 (2002).

165. Thorsdottir, I., Torfadottir, J.E., Birgisdottir, B.E. & Geirsson, R.T. Weight gain in women of normal weight before pregnancy: complications in pregnancy or delivery and birth outcome. *Obstetrics and gynecology* **99**, 799-806 (2002).
166. Frias, A.E. & Grove, K.L. Obesity: a transgenerational problem linked to nutrition during pregnancy. *Seminars in reproductive medicine* **30**, 472-478 (2012).
167. Khambadkone, S.G., Cordner, Z.A. & Tamashiro, K.L.K. Maternal stressors and the developmental origins of neuropsychiatric risk. *Frontiers in neuroendocrinology* **57**, 100834 (2020).
168. Sullivan, E.A. *et al.* Maternal super-obesity and perinatal outcomes in Australia: a national population-based cohort study. *BMC pregnancy and childbirth* **15**, 322 (2015).
169. Hadden, D.R. & McLaughlin, C. Normal and abnormal maternal metabolism during pregnancy. *Seminars in fetal & neonatal medicine* **14**, 66-71 (2009).
170. Catalano, P.M., Tyzbir, E.D., Roman, N.M., Amini, S.B. & Sims, E.A. Longitudinal changes in insulin release and insulin resistance in nonobese pregnant women. *American journal of obstetrics and gynecology* **165**, 1667-1672 (1991).
171. Catalano, P.M. *et al.* Longitudinal changes in basal hepatic glucose production and suppression during insulin infusion in normal pregnant women. *American journal of obstetrics and gynecology* **167**, 913-919 (1992).
172. McIlvride, S. *et al.* A progesterone-brown fat axis is involved in regulating fetal growth. *Scientific reports* **7**, 10671 (2017).
173. Bustamante, J.J., Copple, B.L., Soares, M.J. & Dai, G. Gene profiling of maternal hepatic adaptations to pregnancy. *Liver international : official journal of the International Association for the Study of the Liver* **30**, 406-415 (2010).
174. Douglas, A.J., Johnstone, L.E. & Leng, G. Neuroendocrine mechanisms of change in food intake during pregnancy: a potential role for brain oxytocin. *Physiology & behavior* **91**, 352-365 (2007).
175. Aye, I.L. *et al.* Increasing maternal body mass index is associated with systemic inflammation in the mother and the activation of distinct placental inflammatory pathways. *Biology of reproduction* **90**, 129 (2014).
176. Schmatz, M., Madan, J., Marino, T. & Davis, J. Maternal obesity: the interplay between inflammation, mother and fetus. *Journal of perinatology : official journal of the California Perinatal Association* **30**, 441-446 (2010).
177. Ramsay, J.E. *et al.* Maternal obesity is associated with dysregulation of metabolic, vascular, and inflammatory pathways. *The Journal of clinical endocrinology and metabolism* **87**, 4231-4237 (2002).
178. Wallace, J.G. *et al.* Obesity during pregnancy results in maternal intestinal inflammation, placental hypoxia, and alters fetal glucose metabolism at mid-gestation. *Scientific reports* **9**, 17621 (2019).
179. Gohir, W. *et al.* High-fat diet intake modulates maternal intestinal adaptations to pregnancy and results in placental hypoxia, as well as altered fetal gut barrier proteins and immune markers. *The Journal of physiology* **597**, 3029-3051 (2019).
180. Gohir, W. *et al.* Pregnancy-related changes in the maternal gut microbiota are dependent upon the mother's periconceptual diet. *Gut microbes* **6**, 310-320 (2015).

181. Aye, I.L., Rosario, F.J., Powell, T.L. & Jansson, T. Adiponectin supplementation in pregnant mice prevents the adverse effects of maternal obesity on placental function and fetal growth. *Proceedings of the National Academy of Sciences of the United States of America* **112**, 12858-12863 (2015).
182. Rosario, F.J., Kanai, Y., Powell, T.L. & Jansson, T. Increased placental nutrient transport in a novel mouse model of maternal obesity with fetal overgrowth. *Obesity (Silver Spring, Md.)* **23**, 1663-1670 (2015).
183. Tinius, R.A. *et al.* Metabolic flexibility is impaired in women who are pregnant and overweight/obese and related to insulin resistance and inflammation. *Metabolism: clinical and experimental* **104**, 154142 (2020).
184. Pendeloski, K.P.T., Ono, E., Torloni, M.R., Mattar, R. & Daher, S. Maternal obesity and inflammatory mediators: A controversial association. *American journal of reproductive immunology (New York, N.Y. : 1989)* **77** (2017).
185. Madan, J.C. *et al.* Maternal obesity and markers of inflammation in pregnancy. *Cytokine* **47**, 61-64 (2009).
186. Sureshchandra, S. *et al.* Inflammatory Determinants of Pregravid Obesity in Placenta and Peripheral Blood. *Front Physiol* **9**, 1089 (2018).
187. Roberts, K.A. *et al.* Placental structure and inflammation in pregnancies associated with obesity. *Placenta* **32**, 247-254 (2011).
188. Challier, J.C. *et al.* Obesity in pregnancy stimulates macrophage accumulation and inflammation in the placenta. *Placenta* **29**, 274-281 (2008).
189. Stewart, F.M. *et al.* Longitudinal assessment of maternal endothelial function and markers of inflammation and placental function throughout pregnancy in lean and obese mothers. *The Journal of clinical endocrinology and metabolism* **92**, 969-975 (2007).
190. Metchnikoff, E. Untersuchungen über die mesodermalen Phagocyten einiger Wirbeltiere. *Biologisches centralblatt* **3**, 560-565 (1883).
191. Metchnikoff, E. Über den Kampf der Zellen gegen Erysipelkokken. Ein Beitrag zur Phagocytenlehre. (1887).
192. Metchnikoff, E. *Leçons sur la pathologie comparée de l'inflammation: faites à l'Institut Pasteur en avril et mai 1891*. G. Masson, 1892.
193. Metchnikoff, E. Ueber eine sprosspilzkrankheit der daphnien. Beitrag Zur Lehre Über Den Kampf Der Phagozyten Gegen Krankheitserreger. (1884).
194. Cavaillon, J.M. The historical milestones in the understanding of leukocyte biology initiated by Elie Metchnikoff. *Journal of leukocyte biology* **90**, 413-424 (2011).
195. Epelman, S., Lavine, K.J. & Randolph, G.J. Origin and functions of tissue macrophages. *Immunity* **41**, 21-35 (2014).
196. Gordon, S. & Plüddemann, A. The Mononuclear Phagocytic System. Generation of Diversity. *Frontiers in immunology* **10**, 1893 (2019).
197. Dai, X.M. *et al.* Targeted disruption of the mouse colony-stimulating factor 1 receptor gene results in osteopetrosis, mononuclear phagocyte deficiency, increased primitive progenitor cell frequencies, and reproductive defects. *Blood* **99**, 111-120 (2002).

198. Cecchini, M.G. *et al.* Role of colony stimulating factor-1 in the establishment and regulation of tissue macrophages during postnatal development of the mouse. *Development (Cambridge, England)* **120**, 1357-1372 (1994).
199. Chitu, V. & Stanley, E.R. Regulation of Embryonic and Postnatal Development by the CSF-1 Receptor. *Current topics in developmental biology* **123**, 229-275 (2017).
200. Gouon-Evans, V., Rothenberg, M.E. & Pollard, J.W. Postnatal mammary gland development requires macrophages and eosinophils. *Development (Cambridge, England)* **127**, 2269-2282 (2000).
201. Jones, C.V. & Ricardo, S.D. Macrophages and CSF-1: implications for development and beyond. *Organogenesis* **9**, 249-260 (2013).
202. Aschoff, L. Das reticulo-endotheliale System. *Ergebnisse der inneren Medizin und Kinderheilkunde*. Springer, 1924, pp 1-118.
203. Ebert, R. & Florey, H. The extravascular development of the monocyte observed in vivo. *British journal of experimental pathology* **20**, 342 (1939).
204. Yona, S. & Gordon, S. From the Reticuloendothelial to Mononuclear Phagocyte System - The Unaccounted Years. *Frontiers in immunology* **6**, 328-328 (2015).
205. van Furth, R. *et al.* The mononuclear phagocyte system: a new classification of macrophages, monocytes, and their precursor cells. *Bulletin of the World Health Organization* **46**, 845 (1972).
206. van Furth, R. & Cohn, Z.A. The origin and kinetics of mononuclear phagocytes. *The Journal of experimental medicine* **128**, 415-435 (1968).
207. Virolainen, M. Hematopoietic origin of macrophages as studied by chromosome markers in mice. *The Journal of experimental medicine* **127**, 943-952 (1968).
208. Varol, C., Yona, S. & Jung, S. Origins and tissue-context-dependent fates of blood monocytes. *Immunology & Cell Biology* **87**, 30-38 (2009).
209. Parwaresch, M. & Wacker, H.H. Origin and kinetics of resident tissue macrophages: parabiosis studies with radiolabelled leucocytes. *Cell Proliferation* **17**, 25-39 (1984).
210. Takahashi, K., Yamamura, F. & Naito, M. Differentiation, maturation, and proliferation of macrophages in the mouse yolk sac: a light-microscopic, enzyme-cytochemical, immunohistochemical, and ultrastructural study. *Journal of leukocyte biology* **45**, 87-96 (1989).
211. Guillems, M., Thierry, G.R., Bonnardel, J. & Bajenoff, M. Establishment and Maintenance of the Macrophage Niche. *Immunity* **52**, 434-451 (2020).
212. van de Laar, L. *et al.* Yolk sac macrophages, fetal liver, and adult monocytes can colonize an empty niche and develop into functional tissue-resident macrophages. *Immunity* **44**, 755-768 (2016).
213. Hoeffel, G. *et al.* C-Myb⁺ erythro-myeloid progenitor-derived fetal monocytes give rise to adult tissue-resident macrophages. *Immunity* **42**, 665-678 (2015).
214. Liu, Z. *et al.* Fate mapping via Ms4a3-expression history traces monocyte-derived cells. *Cell* **178**, 1509-1525. e1519 (2019).
215. Ginhoux, F. *et al.* Fate mapping analysis reveals that adult microglia derive from primitive macrophages. *Science (New York, N.Y.)* **330**, 841-845 (2010).

216. Ajami, B., Bennett, J.L., Krieger, C., Tetzlaff, W. & Rossi, F.M. Local self-renewal can sustain CNS microglia maintenance and function throughout adult life. *Nature neuroscience* **10**, 1538-1543 (2007).
217. Sheng, J., Ruedl, C. & Karjalainen, K. Most Tissue-Resident Macrophages Except Microglia Are Derived from Fetal Hematopoietic Stem Cells. *Immunity* **43**, 382-393 (2015).
218. Scott, C.L., Henri, S. & Guillemins, M. Mononuclear phagocytes of the intestine, the skin, and the lung. *Immunological reviews* **262**, 9-24 (2014).
219. Guillemins, M. *et al.* Alveolar macrophages develop from fetal monocytes that differentiate into long-lived cells in the first week of life via GM-CSF. *Journal of Experimental Medicine* **210**, 1977-1992 (2013).
220. Hashimoto, D. *et al.* Tissue-resident macrophages self-maintain locally throughout adult life with minimal contribution from circulating monocytes. *Immunity* **38**, 792-804 (2013).
221. Hoeffel, G. *et al.* Adult Langerhans cells derive predominantly from embryonic fetal liver monocytes with a minor contribution of yolk sac-derived macrophages. *The Journal of experimental medicine* **209**, 1167-1181 (2012).
222. Merad, M. *et al.* Langerhans cells renew in the skin throughout life under steady-state conditions. *Nature immunology* **3**, 1135-1141 (2002).
223. Tamoutounour, S. *et al.* CD64 distinguishes macrophages from dendritic cells in the gut and reveals the Th1-inducing role of mesenteric lymph node macrophages during colitis. *European journal of immunology* **42**, 3150-3166 (2012).
224. Epelman, S. *et al.* Embryonic and adult-derived resident cardiac macrophages are maintained through distinct mechanisms at steady state and during inflammation. *Immunity* **40**, 91-104 (2014).
225. Lavine, K.J. *et al.* Distinct macrophage lineages contribute to disparate patterns of cardiac recovery and remodeling in the neonatal and adult heart. *Proceedings of the National Academy of Sciences of the United States of America* **111**, 16029-16034 (2014).
226. Molawi, K. *et al.* Progressive replacement of embryo-derived cardiac macrophages with age. *Journal of Experimental Medicine* **211**, 2151-2158 (2014).
227. Yona, S. *et al.* Fate mapping reveals origins and dynamics of monocytes and tissue macrophages under homeostasis. *Immunity* **38**, 79-91 (2013).
228. Sawai, C.M. *et al.* Hematopoietic stem cells are the major source of multilineage hematopoiesis in adult animals. *Immunity* **45**, 597-609 (2016).
229. Schulz, C. *et al.* A lineage of myeloid cells independent of Myb and hematopoietic stem cells. *Science* **336**, 86-90 (2012).
230. Zhu, Y. *et al.* Tissue-Resident Macrophages in Pancreatic Ductal Adenocarcinoma Originate from Embryonic Hematopoiesis and Promote Tumor Progression. *Immunity* **47**, 323-338.e326 (2017).
231. Munro, D.A. & Hughes, J. The origins and functions of tissue-resident macrophages in kidney development. *Frontiers in physiology* **8**, 837 (2017).
232. Bain, C.C. *et al.* Long-lived self-renewing bone marrow-derived macrophages displace embryo-derived cells to inhabit adult serous cavities. *Nature communications* **7**, 1-14 (2016).
233. Tamoutounour, S. *et al.* Origins and functional specialization of macrophages and of conventional and monocyte-derived dendritic cells in mouse skin. *Immunity* **39**, 925-938 (2013).

234. Malissen, B., Tamoutounour, S. & Henri, S. The origins and functions of dendritic cells and macrophages in the skin. *Nature Reviews Immunology* **14**, 417-428 (2014).
235. Bain, C.C. *et al.* Constant replenishment from circulating monocytes maintains the macrophage pool in adult intestine. *Nature immunology* **15**, 929-937 (2014).
236. Bain, C.C. *et al.* Resident and pro-inflammatory macrophages in the colon represent alternative context-dependent fates of the same Ly6Chi monocyte precursors. *Mucosal immunology* **6**, 498-510 (2013).
237. Gautier, E.L. *et al.* Systemic analysis of PPAR γ in mouse macrophage populations reveals marked diversity in expression with critical roles in resolution of inflammation and airway immunity. *Journal of immunology (Baltimore, Md. : 1950)* **189**, 2614-2624 (2012).
238. Ginhoux, F. & Guilliams, M. Tissue-resident macrophage ontogeny and homeostasis. *Immunity* **44**, 439-449 (2016).
239. Amit, I., Winter, D.R. & Jung, S. The role of the local environment and epigenetics in shaping macrophage identity and their effect on tissue homeostasis. *Nature immunology* **17**, 18 (2016).
240. Lavin, Y. *et al.* Tissue-resident macrophage enhancer landscapes are shaped by the local microenvironment. *Cell* **159**, 1312-1326 (2014).
241. Aguilar, S.V. *et al.* ImmGen at 15. *Nature immunology* **21**, 700-703 (2020).
242. Schridde, A. *et al.* Tissue-specific differentiation of colonic macrophages requires TGF β receptor-mediated signaling. *Mucosal immunology* **10**, 1387-1399 (2017).
243. Okabe, Y. & Medzhitov, R. Tissue-specific signals control reversible program of localization and functional polarization of macrophages. *Cell* **157**, 832-844 (2014).
244. Gosselin, D. & Glass, C.K. Epigenomics of macrophages. *Immunological reviews* **262**, 96-112 (2014).
245. Gosselin, D. *et al.* Environment drives selection and function of enhancers controlling tissue-specific macrophage identities. *Cell* **159**, 1327-1340 (2014).
246. Li, C. *et al.* Macrophage polarization and meta-inflammation. *Translational research : the journal of laboratory and clinical medicine* (2017).
247. Soucie, E.L. *et al.* Lineage-specific enhancers activate self-renewal genes in macrophages and embryonic stem cells. *Science* **351** (2016).
248. Bajpai, G. *et al.* The human heart contains distinct macrophage subsets with divergent origins and functions. *Nature medicine* **24**, 1234-1245 (2018).
249. Bittmann, I. *et al.* The role of graft-resident Kupffer cells and lymphocytes of donor type during the time course after liver transplantation—a clinico-pathological study. *Virchows Archiv* **443**, 541-548 (2003).
250. Byrne, A.J. *et al.* Dynamics of human monocytes and airway macrophages during healthy aging and after transplant. *Journal of Experimental Medicine* **217** (2020).
251. Mosser, D.M. & Edwards, J.P. Exploring the full spectrum of macrophage activation. *Nat Rev Immunol* **8**, 958-969 (2008).
252. Hume, D.A., Irvine, K.M. & Pridans, C. The Mononuclear Phagocyte System: The Relationship between Monocytes and Macrophages. *Trends in immunology* **40**, 98-112 (2019).

253. Liu, S.X., Gustafson, H.H., Jackson, D.L., Pun, S.H. & Trapnell, C. Trajectory analysis quantifies transcriptional plasticity during macrophage polarization. *Scientific reports* **10**, 12273 (2020).
254. Happle, C. *et al.* Pulmonary transplantation of macrophage progenitors as effective and long-lasting therapy for hereditary pulmonary alveolar proteinosis. *Science translational medicine* **6**, 250ra113 (2014).
255. Suzuki, T. *et al.* Pulmonary macrophage transplantation therapy. *Nature* **514**, 450-454 (2014).
256. Hume, D.A., Perry, V.H. & Gordon, S. The mononuclear phagocyte system of the mouse defined by immunohistochemical localisation of antigen F4/80: macrophages associated with epithelia. *The Anatomical record* **210**, 503-512 (1984).
257. Nathan, C.F., Murray, H.W., Wiebe, M.E. & Rubin, B.Y. Identification of interferon-gamma as the lymphokine that activates human macrophage oxidative metabolism and antimicrobial activity. *The Journal of experimental medicine* **158**, 670-689 (1983).
258. Stein, M., Keshav, S., Harris, N. & Gordon, S. Interleukin 4 potently enhances murine macrophage mannose receptor activity: a marker of alternative immunologic macrophage activation. *The Journal of experimental medicine* **176**, 287-292 (1992).
259. Gordon, S. Alternative activation of macrophages. *Nature reviews immunology* **3**, 23-35 (2003).
260. Mills, C.D., Kincaid, K., Alt, J.M., Heilman, M.J. & Hill, A.M. M-1/M-2 macrophages and the Th1/Th2 paradigm. *Journal of immunology (Baltimore, Md. : 1950)* **164**, 6166-6173 (2000).
261. Martinez, F.O. & Gordon, S. The M1 and M2 paradigm of macrophage activation: time for reassessment. *F1000Prime Rep* **6**, 13-13 (2014).
262. Van den Bossche, J., O'Neill, L.A. & Menon, D. Macrophage immunometabolism: where are we (going)? *Trends in immunology* **38**, 395-406 (2017).
263. Orecchioni, M., Ghosheh, Y., Pramod, A.B. & Ley, K. Macrophage polarization: different gene signatures in M1 (LPS+) vs. classically and M2 (LPS-) vs. alternatively activated macrophages. *Frontiers in immunology* **10**, 1084 (2019).
264. Sica, A. & Mantovani, A. Macrophage plasticity and polarization: in vivo veritas. *The Journal of clinical investigation* **122**, 787-795 (2012).
265. Davies, L.C. & Taylor, P.R. Tissue-resident macrophages: then and now. *Immunology* **144**, 541-548 (2015).
266. Rua, R. & McGavern, D.B. Elucidation of monocyte/macrophage dynamics and function by intravital imaging. *Journal of leukocyte biology* **98**, 319-332 (2015).
267. Gabanyi, I. *et al.* Neuro-immune interactions drive tissue programming in intestinal macrophages. *Cell* **164**, 378-391 (2016).
268. Honda, M. *et al.* Perivascular localization of macrophages in the intestinal mucosa is regulated by Nr4a1 and the microbiome. *Nature communications* **11**, 1-17 (2020).
269. Pappenheim, A. & Ferrata, A. *Über die verschiedenen lymphoiden Zellformen des normalen und pathologischen Blutes*, vol. 10. Klinkhardt, 1911.
270. Yona, S. *et al.* Fate mapping reveals origins and dynamics of monocytes and tissue macrophages under homeostasis. *Immunity* **38**, 79-91 (2013).

271. Clausen, B., Burkhardt, C., Reith, W., Renkawitz, R. & Förster, I. Conditional gene targeting in macrophages and granulocytes using LysMcre mice. *Transgenic research* **8**, 265-277 (1999).
272. Guillemins, M. *et al.* Dendritic cells, monocytes and macrophages: a unified nomenclature based on ontogeny. *Nature Reviews Immunology* **14**, 571-578 (2014).
273. Sathe, P. *et al.* Lymphoid tissue and plasmacytoid dendritic cells and macrophages do not share a common macrophage-dendritic cell-restricted progenitor. *Immunity* **41**, 104-115 (2014).
274. Yáñez, A. *et al.* Granulocyte-monocyte progenitors and monocyte-dendritic cell progenitors independently produce functionally distinct monocytes. *Immunity* **47**, 890-902. e894 (2017).
275. Leuschner, F. *et al.* Rapid monocyte kinetics in acute myocardial infarction are sustained by extramedullary monocytopoiesis. *Journal of Experimental Medicine* **209**, 123-137 (2012).
276. Schultze, J.L., Mass, E. & Schlitzer, A. Emerging principles in myelopoiesis at homeostasis and during infection and inflammation. *Immunity* **50**, 288-301 (2019).
277. Kim, C.H. Homeostatic and pathogenic extramedullary hematopoiesis. *Journal of blood medicine* **1**, 13 (2010).
278. Takizawa, H. *et al.* Pathogen-induced TLR4-TRIF innate immune signaling in hematopoietic stem cells promotes proliferation but reduces competitive fitness. *Cell Stem Cell* **21**, 225-240. e225 (2017).
279. Boettcher, S. & Manz, M.G. Sensing and translation of pathogen signals into demand-adapted myelopoiesis. *Current Opinion in Hematology* **23**, 5-10 (2016).
280. Satoh, T. *et al.* Identification of an atypical monocyte and committed progenitor involved in fibrosis. *Nature* **541**, 96-101 (2017).
281. Askenase, M.H. *et al.* Bone-marrow-resident NK cells prime monocytes for regulatory function during infection. *Immunity* **42**, 1130-1142 (2015).
282. Hume, D.A. *et al.* Phenotypic impacts of CSF1R deficiencies in humans and model organisms. *Journal of leukocyte biology* **107**, 205-219 (2020).
283. Kurotaki, D., Sasaki, H. & Tamura, T. Transcriptional control of monocyte and macrophage development. *International Immunology* **29**, 97-107 (2017).
284. Ziegler-Heitbrock, L. *et al.* Nomenclature of monocytes and dendritic cells in blood. *Blood* **116**, e74-80 (2010).
285. Gordon, S. & Taylor, P.R. Monocyte and macrophage heterogeneity. *Nat Rev Immunol* **5**, 953-964 (2005).
286. Mildner, A. *et al.* Genomic characterization of murine monocytes reveals C/EBP β transcription factor dependence of Ly6C⁺ cells. *Immunity* **46**, 849-862. e847 (2017).
287. Geissmann, F., Jung, S. & Littman, D.R. Blood monocytes consist of two principal subsets with distinct migratory properties. *Immunity* **19**, 71-82 (2003).
288. Zhu, Y.P., Thomas, G.D. & Hedrick, C.C. 2014 Jeffrey M. Hoeg award lecture: transcriptional control of monocyte development. *Arteriosclerosis, thrombosis, and vascular biology* **36**, 1722-1733 (2016).
289. Patel, A.A. *et al.* The fate and lifespan of human monocyte subsets in steady state and systemic inflammation. *Journal of Experimental Medicine* **214**, 1913-1923 (2017).

290. Ingersoll, M.A. *et al.* Comparison of gene expression profiles between human and mouse monocyte subsets. *Blood* **115**, e10-19 (2010).
291. Krow-Lucal, E.R., Kim, C.C., Burt, T.D. & McCune, J.M. Distinct functional programming of human fetal and adult monocytes. *Blood* **123**, 1897-1904 (2014).
292. Lissner, M.M. *et al.* Age-Related Gene Expression Differences in Monocytes from Human Neonates, Young Adults, and Older Adults. *PLoS One* **10**, e0132061 (2015).
293. Hettinger, J. *et al.* Origin of monocytes and macrophages in a committed progenitor. *Nature immunology* **14**, 821-830 (2013).
294. Jakubzick, C. *et al.* Minimal differentiation of classical monocytes as they survey steady-state tissues and transport antigen to lymph nodes. *Immunity* **39**, 599-610 (2013).
295. Tamura, A. *et al.* C/EBP β is required for survival of Ly6C(-) monocytes. *Blood* **130**, 1809-1818 (2017).
296. Kurotaki, D. *et al.* Essential role of the IRF8-KLF4 transcription factor cascade in murine monocyte differentiation. *Blood* **121**, 1839-1849 (2013).
297. Gamrekelashvili, J. *et al.* Regulation of monocyte cell fate by blood vessels mediated by Notch signalling. *Nature communications* **7**, 12597 (2016).
298. Thomas, G.D. *et al.* Deleting an Nr4a1 Super-Enhancer Subdomain Ablates Ly6C(low) Monocytes while Preserving Macrophage Gene Function. *Immunity* **45**, 975-987 (2016).
299. Hanna, R.N. *et al.* The transcription factor NR4A1 (Nur77) controls bone marrow differentiation and the survival of Ly6C- monocytes. *Nature immunology* **12**, 778-785 (2011).
300. Gravina, H.D., Goes, A.M., Murta, S.M. & Ropert, C. MyD88 Adapter-like (Mal)/TIRAP Is Required for Cytokine Production by Splenic Ly6CloTLR2hi but Not by Ly6ChiTLR2hi Monocytes during Trypanosoma cruzi Infection. *The Journal of biological chemistry* **291**, 23832-23841 (2016).
301. Jung, H., Mithal, D.S., Park, J.E. & Miller, R.J. Localized CCR2 Activation in the Bone Marrow Niche Mobilizes Monocytes by Desensitizing CXCR4. *PLoS One* **10**, e0128387 (2015).
302. Liu, Q. *et al.* CXCR4 antagonist AMD3100 redistributes leukocytes from primary immune organs to secondary immune organs, lung, and blood in mice. *European journal of immunology* **45**, 1855-1867 (2015).
303. Jacquelin, S. *et al.* CX3CR1 reduces Ly6Chigh-monocyte motility within and release from the bone marrow after chemotherapy in mice. *Blood* **122**, 674-683 (2013).
304. Chong, S.Z. *et al.* CXCR4 identifies transitional bone marrow premonocytes that replenish the mature monocyte pool for peripheral responses. *The Journal of experimental medicine* **213**, 2293-2314 (2016).
305. Tsou, C.L. *et al.* Critical roles for CCR2 and MCP-3 in monocyte mobilization from bone marrow and recruitment to inflammatory sites. *The Journal of clinical investigation* **117**, 902-909 (2007).
306. Serbina, N.V. & Pamer, E.G. Monocyte emigration from bone marrow during bacterial infection requires signals mediated by chemokine receptor CCR2. *Nature immunology* **7**, 311-317 (2006).
307. Shi, C. *et al.* Bone marrow mesenchymal stem and progenitor cells induce monocyte emigration in response to circulating toll-like receptor ligands. *Immunity* **34**, 590-601 (2011).

308. Kuziel, W.A. *et al.* Severe reduction in leukocyte adhesion and monocyte extravasation in mice deficient in CC chemokine receptor 2. *Proceedings of the National Academy of Sciences of the United States of America* **94**, 12053-12058 (1997).
309. Nourshargh, S. & Alon, R. Leukocyte migration into inflamed tissues. *Immunity* **41**, 694-707 (2014).
310. Gerhardt, T. & Ley, K. Monocyte trafficking across the vessel wall. *Cardiovascular research* **107**, 321-330 (2015).
311. Ley, K., Laudanna, C., Cybulsky, M.I. & Nourshargh, S. Getting to the site of inflammation: the leukocyte adhesion cascade updated. *Nat Rev Immunol* **7**, 678-689 (2007).
312. Debien, E. *et al.* S1PR5 is pivotal for the homeostasis of patrolling monocytes. *European journal of immunology* **43**, 1667-1675 (2013).
313. Carlin, L.M. *et al.* Nr4a1-dependent Ly6C(low) monocytes monitor endothelial cells and orchestrate their disposal. *Cell* **153**, 362-375 (2013).
314. Auffray, C. *et al.* Monitoring of Blood Vessels and Tissues by a Population of Monocytes with Patrolling Behavior. *Science* **317**, 666 (2007).
315. Kuebler, W.M. & Goetz, A.E. The marginated pool. *European surgical research. Europäische chirurgische Forschung. Recherches chirurgicales europeennes* **34**, 92-100 (2002).
316. Rodero, M.P. *et al.* Immune surveillance of the lung by migrating tissue monocytes. *eLife* **4**, e07847 (2015).
317. Devi, S. *et al.* Multiphoton imaging reveals a new leukocyte recruitment paradigm in the glomerulus. *Nature medicine* **19**, 107-112 (2013).
318. Biburger, M. *et al.* Monocyte subsets responsible for immunoglobulin G-dependent effector functions in vivo. *Immunity* **35**, 932-944 (2011).
319. Ingersoll, M.A., Platt, A.M., Potteaux, S. & Randolph, G.J. Monocyte trafficking in acute and chronic inflammation. *Trends in immunology* **32**, 470-477 (2011).
320. Olingy, C.E. *et al.* Non-classical monocytes are biased progenitors of wound healing macrophages during soft tissue injury. *Scientific reports* **7**, 447 (2017).
321. Auffray, C. *et al.* CX3CR1+ CD115+ CD135+ common macrophage/DC precursors and the role of CX3CR1 in their response to inflammation. *Journal of Experimental Medicine* **206**, 595-606 (2009).
322. Shi, C. & Pamer, E.G. Monocyte recruitment during infection and inflammation. *Nature reviews. Immunology* **11**, 762-774 (2011).
323. Weisheit, C. *et al.* Ly6Clow and Not Ly6Chigh Macrophages Accumulate First in the Heart in a Model of Murine Pressure-Overload. *PLOS ONE* **9**, e112710 (2014).
324. Stramer, B.M., Mori, R. & Martin, P. The inflammation–fibrosis link? A Jekyll and Hyde role for blood cells during wound repair. *Journal of Investigative Dermatology* **127**, 1009-1017 (2007).
325. Rodero, M.P. *et al.* In vivo imaging reveals a pioneer wave of monocyte recruitment into mouse skin wounds. *PLoS One* **9**, e108212 (2014).
326. Swirski, F.K., Weissleder, R. & Pittet, M.J. Heterogeneous in vivo behavior of monocyte subsets in atherosclerosis. *Arteriosclerosis, thrombosis, and vascular biology* **29**, 1424-1432 (2009).

327. Bronte, V. & Pittet, M.J. The spleen in local and systemic regulation of immunity. *Immunity* **39**, 806-818 (2013).
328. Mellak, S. *et al.* Angiotensin II mobilizes spleen monocytes to promote the development of abdominal aortic aneurysm in Apoe^{-/-} mice. *Arteriosclerosis, thrombosis, and vascular biology* **35**, 378-388 (2015).
329. Wang, N.-P. *et al.* Recruitment of macrophages from the spleen contributes to myocardial fibrosis and hypertension induced by angiotensin II. *Journal of the Renin-Angiotensin-Aldosterone System* **18**, 1470320317706653 (2017).
330. Sbrana, S., Parri, M.S., De Filippis, R., Gianetti, J. & Clerico, A. Monitoring of monocyte functional state after extracorporeal circulation: a flow cytometry study. *Cytometry Part B: Clinical Cytometry* **58**, 17-24 (2004).
331. Bosschaerts, T. *et al.* Tip-DC development during parasitic infection is regulated by IL-10 and requires CCL2/CCR2, IFN-gamma and MyD88 signaling. *PLoS pathogens* **6**, e1001045 (2010).
332. Yáñez, A., Goodridge, H.S., Gozalbo, D. & Gil, M.L. TLRs control hematopoiesis during infection. *European journal of immunology* **43**, 2526-2533 (2013).
333. Bystrom, J. *et al.* Resolution-phase macrophages possess a unique inflammatory phenotype that is controlled by cAMP. *Blood* **112**, 4117-4127 (2008).
334. Heidt, T. *et al.* Differential contribution of monocytes to heart macrophages in steady-state and after myocardial infarction. *Circulation research* **115**, 284-295 (2014).
335. Movita, D. *et al.* Inflammatory monocytes recruited to the liver within 24 hours after virus-induced inflammation resemble Kupffer cells but are functionally distinct. *Journal of virology* **89**, 4809-4817 (2015).
336. Puchta, A. *et al.* TNF Drives Monocyte Dysfunction with Age and Results in Impaired Anti-pneumococcal Immunity. *PLoS pathogens* **12**, e1005368 (2016).
337. Thevaranjan, N. *et al.* Age-Associated Microbial Dysbiosis Promotes Intestinal Permeability, Systemic Inflammation, and Macrophage Dysfunction. *Cell Host & Microbe* **21**, 455-466.e454 (2017).
338. Ma, W.-T., Gao, F., Gu, K. & Chen, D.-K. The Role of Monocytes and Macrophages in Autoimmune Diseases: A Comprehensive Review. *Frontiers in immunology* **10** (2019).
339. Nielsen, S.R. & Schmid, M.C. Macrophages as Key Drivers of Cancer Progression and Metastasis. *Mediators of inflammation* **2017**, 9624760 (2017).
340. Abumrad, N.A. & Davidson, N.O. Role of the gut in lipid homeostasis. *Physiol Rev* **92**, 1061-1085 (2012).
341. Hegyi, P., Maléth, J., Walters, J.R., Hofmann, A.F. & Keely, S.J. Guts and Gall: Bile Acids in Regulation of Intestinal Epithelial Function in Health and Disease. *Physiol Rev* **98**, 1983-2023 (2018).
342. Ferraris, R.P. & Diamond, J. Regulation of intestinal sugar transport. *Physiol Rev* **77**, 257-302 (1997).
343. Bröer, S. Amino acid transport across mammalian intestinal and renal epithelia. *Physiol Rev* **88**, 249-286 (2008).

344. Kunzelmann, K. & Mall, M. Electrolyte transport in the mammalian colon: mechanisms and implications for disease. *Physiol Rev* **82**, 245-289 (2002).
345. Greenwood-Van Meerveld, B., Johnson, A.C. & Grundy, D. Gastrointestinal Physiology and Function. *Handbook of experimental pharmacology* **239**, 1-16 (2017).
346. Sato, T. *et al.* Paneth cells constitute the niche for Lgr5 stem cells in intestinal crypts. *Nature* **469**, 415-418 (2011).
347. Funk, M.C., Zhou, J. & Boutros, M. Ageing, metabolism and the intestine. *EMBO Rep* **21**, e50047 (2020).
348. Cheng, H. & Leblond, C.P. Origin, differentiation and renewal of the four main epithelial cell types in the mouse small intestine. V. Unitarian Theory of the origin of the four epithelial cell types. *The American journal of anatomy* **141**, 537-561 (1974).
349. Meran, L., Baulies, A. & Li, V.S.W. Intestinal Stem Cell Niche: The Extracellular Matrix and Cellular Components. *Stem cells international* **2017**, 7970385 (2017).
350. Rodríguez-Piñeiro, A.M. *et al.* Studies of mucus in mouse stomach, small intestine, and colon. II. Gastrointestinal mucus proteome reveals Muc2 and Muc5ac accompanied by a set of core proteins. *American journal of physiology. Gastrointestinal and liver physiology* **305**, G348-356 (2013).
351. Gassler, N. Paneth cells in intestinal physiology and pathophysiology. *World J Gastrointest Pathophysiol* **8**, 150-160 (2017).
352. Vaishnava, S. *et al.* The antibacterial lectin RegIIIgamma promotes the spatial segregation of microbiota and host in the intestine. *Science* **334**, 255-258 (2011).
353. Bevins, C.L. & Salzman, N.H. Paneth cells, antimicrobial peptides and maintenance of intestinal homeostasis. *Nature reviews. Microbiology* **9**, 356-368 (2011).
354. Ermund, A., Schütte, A., Johansson, M.E., Gustafsson, J.K. & Hansson, G.C. Studies of mucus in mouse stomach, small intestine, and colon. I. Gastrointestinal mucus layers have different properties depending on location as well as over the Peyer's patches. *American journal of physiology. Gastrointestinal and liver physiology* **305**, G341-347 (2013).
355. Johansson, M.E. *et al.* The inner of the two Muc2 mucin-dependent mucus layers in colon is devoid of bacteria. *Proceedings of the National Academy of Sciences of the United States of America* **105**, 15064-15069 (2008).
356. Koh, A., De Vadder, F., Kovatcheva-Datchary, P. & Bäckhed, F. From dietary fiber to host physiology: short-chain fatty acids as key bacterial metabolites. *Cell* **165**, 1332-1345 (2016).
357. Propheter, D.C., Chara, A.L., Harris, T.A., Ruhn, K.A. & Hooper, L.V. Resistin-like molecule β is a bactericidal protein that promotes spatial segregation of the microbiota and the colonic epithelium. *Proceedings of the National Academy of Sciences of the United States of America* **114**, 11027-11033 (2017).
358. Rogier, E.W., Frantz, A.L., Bruno, M.E. & Kaetzel, C.S. Secretory IgA is concentrated in the outer layer of colonic mucus along with gut bacteria. *Pathogens* **3**, 390-403 (2014).
359. Moor, K. *et al.* High-avidity IgA protects the intestine by enchainning growing bacteria. *Nature* **544**, 498-502 (2017).
360. Lallès, J.-P. Intestinal alkaline phosphatase: novel functions and protective effects. *Nutrition reviews* **72**, 82-94 (2014).

361. Malo, M.S. *et al.* Intestinal alkaline phosphatase promotes gut bacterial growth by reducing the concentration of luminal nucleotide triphosphates. *American Journal of Physiology-Gastrointestinal and Liver Physiology* **306**, G826-G838 (2014).
362. Peterson, L.W. & Artis, D. Intestinal epithelial cells: regulators of barrier function and immune homeostasis. *Nat Rev Immunol* **14**, 141-153 (2014).
363. Tsukita, S., Furuse, M. & Itoh, M. Multifunctional strands in tight junctions. *Nature reviews Molecular cell biology* **2**, 285-293 (2001).
364. Suzuki, T. Regulation of intestinal epithelial permeability by tight junctions. *Cellular and molecular life sciences : CMLS* **70**, 631-659 (2013).
365. Mabbott, N.A., Donaldson, D.S., Ohno, H., Williams, I.R. & Mahajan, A. Microfold (M) cells: important immunosurveillance posts in the intestinal epithelium. *Mucosal immunology* **6**, 666-677 (2013).
366. McDole, J.R. *et al.* Goblet cells deliver luminal antigen to CD103+ dendritic cells in the small intestine. *Nature* **483**, 345-349 (2012).
367. Hase, K. *et al.* Uptake through glycoprotein 2 of FimH+ bacteria by M cells initiates mucosal immune response. *Nature* **462**, 226-230 (2009).
368. Ohno, H. Intestinal M cells. *Journal of biochemistry* **159**, 151-160 (2016).
369. Pasteur, L. *Etudes sur la maladie des vers a soie*, vol. 2. Gauthier-Villars, 1870.
370. Koch, R. Aetiologie der Tuberkulose. *Berliner Klinische Wochenschrift* **19**, 221-230 (1882).
371. Metchnikoff, E. Études sur la flore intestinale. *Ann Inst Pasteur Paris* **22**, 929-955 (1908).
372. Belkaid, Y. & Hand, T.W. Role of the microbiota in immunity and inflammation. *Cell* **157**, 121-141 (2014).
373. Thorburn, Alison N., Macia, L. & Mackay, Charles R. Diet, Metabolites, and “Western-Lifestyle” Inflammatory Diseases. *Immunity* **40**, 833-842 (2014).
374. Kayama, H. & Takeda, K. Manipulation of epithelial integrity and mucosal immunity by host and microbiota-derived metabolites. *European journal of immunology* **50**, 921-931 (2020).
375. Mouries, J. *et al.* Microbiota-driven gut vascular barrier disruption is a prerequisite for non-alcoholic steatohepatitis development. *Journal of Hepatology* **71**, 1216-1228 (2019).
376. De Vadder, F. *et al.* Gut microbiota regulates maturation of the adult enteric nervous system via enteric serotonin networks. *Proceedings of the National Academy of Sciences* **115**, 6458 (2018).
377. Obata, Y. *et al.* Neuronal programming by microbiota regulates intestinal physiology. *Nature* **578**, 284-289 (2020).
378. O'Hara, A.M. & Shanahan, F. The gut flora as a forgotten organ. *EMBO Rep* **7**, 688-693 (2006).
379. Lopez, C.A., Kingsbury, D.D., Velazquez, E.M. & Bäumlér, A.J. Collateral damage: microbiota-derived metabolites and immune function in the antibiotic era. *Cell host & microbe* **16**, 156-163 (2014).
380. Davenport, E.R. *et al.* The human microbiome in evolution. *BMC biology* **15**, 1-12 (2017).

- 381. Atarashi, K. *et al.* T reg induction by a rationally selected mixture of Clostridia strains from the human microbiota. *Nature* **500**, 232-236 (2013).
- 382. Atarashi, K. *et al.* Induction of colonic regulatory T cells by indigenous Clostridium species. *Science* **331**, 337-341 (2011).
- 383. Ivanov, I.I. *et al.* Induction of intestinal Th17 cells by segmented filamentous bacteria. *Cell* **139**, 485-498 (2009).
- 384. Wu, H.-J. *et al.* Gut-residing segmented filamentous bacteria drive autoimmune arthritis via T helper 17 cells. *Immunity* **32**, 815-827 (2010).
- 385. Shaw, M.H., Kamada, N., Kim, Y.-G. & Núñez, G. Microbiota-induced IL-1 β , but not IL-6, is critical for the development of steady-state TH17 cells in the intestine. *Journal of Experimental Medicine* **209**, 251-258 (2012).
- 386. Schroeder, B.O. & Bäckhed, F. Signals from the gut microbiota to distant organs in physiology and disease. *Nature medicine* **22**, 1079-1089 (2016).
- 387. Erny, D. *et al.* Host microbiota constantly control maturation and function of microglia in the CNS. *Nature neuroscience* **18**, 965-977 (2015).
- 388. Wang, Y. *et al.* The Gut-Microglia Connection: Implications for Central Nervous System Diseases. *Frontiers in immunology* **9**, 2325-2325 (2018).
- 389. Amar, J. *et al.* Intestinal mucosal adherence and translocation of commensal bacteria at the early onset of type 2 diabetes: molecular mechanisms and probiotic treatment. *EMBO molecular medicine* **3**, 559-572 (2011).
- 390. Ding, S. *et al.* High-fat diet: bacteria interactions promote intestinal inflammation which precedes and correlates with obesity and insulin resistance in mouse. *PLoS One* **5**, e12191 (2010).
- 391. Henao-Mejia, J. *et al.* Inflammasome-mediated dysbiosis regulates progression of NAFLD and obesity. *Nature* **482**, 179-185 (2012).
- 392. Vijay-Kumar, M. *et al.* Metabolic syndrome and altered gut microbiota in mice lacking Toll-like receptor 5. *Science* **328**, 228-231 (2010).
- 393. Davis, J.E., Braucher, D.R., Walker-Daniels, J. & Spurlock, M.E. Absence of Tlr2 protects against high-fat diet-induced inflammation and results in greater insulin-stimulated glucose transport in cultured adipocytes. *The Journal of nutritional biochemistry* **22**, 136-141 (2011).
- 394. Denou, E. *et al.* Defective NOD 2 peptidoglycan sensing promotes diet-induced inflammation, dysbiosis, and insulin resistance. *EMBO molecular medicine* **7**, 259-274 (2015).
- 395. Duggan, B.M., Cavallari, J.F., Foley, K.P., Barra, N.G. & Schertzer, J.D. RIPK2 Dictates Insulin Responses to Tyrosine Kinase Inhibitors in Obese Male Mice. *Endocrinology* **161** (2020).
- 396. Shi, H. *et al.* TLR4 links innate immunity and fatty acid-induced insulin resistance. *The Journal of clinical investigation* **116**, 3015-3025 (2006).
- 397. Everard, A. *et al.* Intestinal epithelial MyD88 is a sensor switching host metabolism towards obesity according to nutritional status. *Nature communications* **5**, 5648 (2014).
- 398. Tran, H.Q. *et al.* "Western Diet"-Induced Adipose Inflammation Requires a Complex Gut Microbiota. *Cellular and molecular gastroenterology and hepatology* **9**, 313-333 (2020).

399. Bäckhed, F., Manchester, J.K., Semenkovich, C.F. & Gordon, J.I. Mechanisms underlying the resistance to diet-induced obesity in germ-free mice. *Proceedings of the National Academy of Sciences of the United States of America* **104**, 979-984 (2007).
400. Eckburg, P.B. *et al.* Diversity of the human intestinal microbial flora. *Science* **308**, 1635-1638 (2005).
401. Ley, R.E. *et al.* Obesity alters gut microbial ecology. *Proceedings of the national academy of sciences* **102**, 11070-11075 (2005).
402. Ley, R.E., Turnbaugh, P.J., Klein, S. & Gordon, J.I. Human gut microbes associated with obesity. *nature* **444**, 1022-1023 (2006).
403. Zheng, D., Liwinski, T. & Elinav, E. Interaction between microbiota and immunity in health and disease. *Cell Research* **30**, 492-506 (2020).
404. Cummings, R.J. *et al.* Different tissue phagocytes sample apoptotic cells to direct distinct homeostasis programs. *Nature* **539**, 565-569 (2016).
405. Grainger, J.R., Konkel, J.E., Zangerle-Murray, T. & Shaw, T.N. Macrophages in gastrointestinal homeostasis and inflammation. *Pflugers Archiv : European journal of physiology* **469**, 527-539 (2017).
406. Bain, C.C. & Schridde, A. Origin, Differentiation, and Function of Intestinal Macrophages. *Frontiers in immunology* **9**, 2733-2733 (2018).
407. Viola, M.F. & Boeckxstaens, G. Intestinal resident macrophages: Multitaskers of the gut. *Neurogastroenterology and motility : the official journal of the European Gastrointestinal Motility Society* **32**, e13843 (2020).
408. De Schepper, S. *et al.* Self-Maintaining Gut Macrophages Are Essential for Intestinal Homeostasis. *Cell* **175**, 400-415.e413 (2018).
409. Shaw, T.N. *et al.* Tissue-resident macrophages in the intestine are long lived and defined by Tim-4 and CD4 expression. *The Journal of experimental medicine* **215**, 1507-1518 (2018).
410. Bujko, A. *et al.* Transcriptional and functional profiling defines human small intestinal macrophage subsets. *The Journal of experimental medicine* **215**, 441-458 (2018).
411. Bernardo, D. *et al.* Human intestinal pro-inflammatory CD11c(high)CCR2(+)CX3CR1(+) macrophages, but not their tolerogenic CD11c(-)CCR2(-)CX3CR1(-) counterparts, are expanded in inflammatory bowel disease. *Mucosal immunology* **11**, 1114-1126 (2018).
412. Kang, B. *et al.* Commensal microbiota drive the functional diversification of colon macrophages. *Mucosal immunology* **13**, 216-229 (2020).
413. Desalegn, G. & Pabst, O. Inflammation triggers immediate rather than progressive changes in monocyte differentiation in the small intestine. *Nature communications* **10**, 3229 (2019).
414. Takada, Y. *et al.* Monocyte chemoattractant protein-1 contributes to gut homeostasis and intestinal inflammation by composition of IL-10-producing regulatory macrophage subset. *Journal of immunology (Baltimore, Md. : 1950)* **184**, 2671-2676 (2010).
415. Zigmond, E. *et al.* Ly6C hi monocytes in the inflamed colon give rise to proinflammatory effector cells and migratory antigen-presenting cells. *Immunity* **37**, 1076-1090 (2012).
416. Wuggenig, P. *et al.* Loss of the branched-chain amino acid transporter CD98hc alters the development of colonic macrophages in mice. *Communications biology* **3**, 130 (2020).

417. Weber, B., Saurer, L., Schenk, M., Dickgreber, N. & Mueller, C. CX3CR1 defines functionally distinct intestinal mononuclear phagocyte subsets which maintain their respective functions during homeostatic and inflammatory conditions. *European journal of immunology* **41**, 773-779 (2011).
418. Gross-Vered, M. *et al.* Defining murine monocyte differentiation into colonic and ileal macrophages. *eLife* **9** (2020).
419. Jaensson, E. *et al.* Small intestinal CD103+ dendritic cells display unique functional properties that are conserved between mice and humans. *The Journal of experimental medicine* **205**, 2139-2149 (2008).
420. Lee, S.H., Starkey, P.M. & Gordon, S. Quantitative analysis of total macrophage content in adult mouse tissues. Immunochemical studies with monoclonal antibody F4/80. *The Journal of experimental medicine* **161**, 475-489 (1985).
421. Vitetta, L., Vitetta, G. & Hall, S. Immunological Tolerance and Function: Associations Between Intestinal Bacteria, Probiotics, Prebiotics, and Phages. *Frontiers in immunology* **9**, 2240-2240 (2018).
422. Mikkelsen, H., Mirsky, R., Jessen, K. & Thuneberg, L. Macrophage-like cells in muscularis externa of mouse small intestine: immunohistochemical localization of F4/80, M1/70, and Ia-antigen. *Cell and tissue research* **252**, 301-306 (1988).
423. Mikkelsen, H., Thuneberg, L., Rumessen, J. & Thorball, N. Macrophage-like cells in the muscularis externa of mouse small intestine. *The Anatomical record* **213**, 77-86 (1985).
424. Mikkelsen, H.B. Interstitial cells of Cajal, macrophages and mast cells in the gut musculature: morphology, distribution, spatial and possible functional interactions. *Journal of cellular and molecular medicine* **14**, 818-832 (2010).
425. Mikkelsen, H.B., Larsen, J.O., Froh, P. & Nguyen, T.H. Quantitative Assessment of Macrophages in the Muscularis Externa of Mouse Intestines. *The Anatomical record* **294**, 1557-1565 (2011).
426. Created with BioRender.com; 2020.
427. Palay, S.L. & Karlin, L.J. An electron microscopic study of the intestinal villus. I. The fasting animal. *The Journal of biophysical and biochemical cytology* **5**, 363-372 (1959).
428. Bonnardel, J. *et al.* Innate and adaptive immune functions of peyer's patch monocyte-derived cells. *Cell reports* **11**, 770-784 (2015).
429. Sehgal, A. *et al.* The role of CSF1R-dependent macrophages in control of the intestinal stem-cell niche. *Nature communications* **9**, 1272 (2018).
430. Farache, J., Zigmond, E., Shakhar, G. & Jung, S. Contributions of dendritic cells and macrophages to intestinal homeostasis and immune defense. *Immunology and cell biology* **91**, 232-239 (2013).
431. Mazzini, E., Massimiliano, L., Penna, G. & Rescigno, M. Oral tolerance can be established via gap junction transfer of fed antigens from CX3CR1⁺ macrophages to CD103⁺ dendritic cells. *Immunity* **40**, 248-261 (2014).
432. A-Gonzalez, N. *et al.* Phagocytosis imprints heterogeneity in tissue-resident macrophages. *The Journal of experimental medicine* **214**, 1281-1296 (2017).
433. Grainger, J.R. *et al.* Inflammatory monocytes regulate pathologic responses to commensals during acute gastrointestinal infection. *Nature medicine* **19**, 713-721 (2013).

434. Smythies, L.E. *et al.* Human intestinal macrophages display profound inflammatory anergy despite avid phagocytic and bacteriocidal activity. *The Journal of clinical investigation* **115**, 66-75 (2005).
435. Zigmond, E. *et al.* Macrophage-restricted interleukin-10 receptor deficiency, but not IL-10 deficiency, causes severe spontaneous colitis. *Immunity* **40**, 720-733 (2014).
436. Huynh, D. *et al.* CSF-1 receptor-dependent colon development, homeostasis and inflammatory stress response. *PLoS One* **8**, e56951 (2013).
437. Ortiz-Masia, D. *et al.* Hypoxic macrophages impair autophagy in epithelial cells through Wnt1: relevance in IBD. *Mucosal immunology* **7**, 929-938 (2014).
438. Cosin-Roger, J. *et al.* The activation of Wnt signaling by a STAT6-dependent macrophage phenotype promotes mucosal repair in murine IBD. *Mucosal immunology* **9**, 986-998 (2016).
439. D'Angelo, F. *et al.* Macrophages promote epithelial repair through hepatocyte growth factor secretion. *Clinical & Experimental Immunology* **174**, 60-72 (2013).
440. Pull, S.L., Doherty, J.M., Mills, J.C., Gordon, J.I. & Stappenbeck, T.S. Activated macrophages are an adaptive element of the colonic epithelial progenitor niche necessary for regenerative responses to injury. *Proceedings of the National Academy of Sciences* **102**, 99-104 (2005).
441. Seno, H. *et al.* Efficient colonic mucosal wound repair requires Trem2 signaling. *Proceedings of the National Academy of Sciences* **106**, 256-261 (2009).
442. Brauer, R. *et al.* MMP-19 deficiency causes aggravation of colitis due to defects in innate immune cell function. *Mucosal immunology* **9**, 974-985 (2016).
443. Niess, J.H. *et al.* CX3CR1-mediated dendritic cell access to the intestinal lumen and bacterial clearance. *Science* **307**, 254-258 (2005).
444. Chieppa, M., Rescigno, M., Huang, A.Y. & Germain, R.N. Dynamic imaging of dendritic cell extension into the small bowel lumen in response to epithelial cell TLR engagement. *The Journal of experimental medicine* **203**, 2841-2852 (2006).
445. Schulz, O. *et al.* Intestinal CD103+, but not CX3CR1+, antigen sampling cells migrate in lymph and serve classical dendritic cell functions. *The Journal of experimental medicine* **206**, 3101-3114 (2009).
446. Hadis, U. *et al.* Intestinal tolerance requires gut homing and expansion of FoxP3+ regulatory T cells in the lamina propria. *Immunity* **34**, 237-246 (2011).
447. Murai, M. *et al.* Interleukin 10 acts on regulatory T cells to maintain expression of the transcription factor Foxp3 and suppressive function in mice with colitis. *Nature immunology* **10**, 1178-1184 (2009).
448. Ip, W.K.E., Hoshi, N., Shouval, D.S., Snapper, S. & Medzhitov, R. Anti-inflammatory effect of IL-10 mediated by metabolic reprogramming of macrophages. *Science* **356**, 513 (2017).
449. Bauché, D. *et al.* LAG3(+) Regulatory T Cells Restrain Interleukin-23-Producing CX3CR1(+) Gut-Resident Macrophages during Group 3 Innate Lymphoid Cell-Driven Colitis. *Immunity* **49**, 342-352.e345 (2018).
450. Panea, C. *et al.* Intestinal monocyte-derived macrophages control commensal-specific Th17 responses. *Cell reports* **12**, 1314-1324 (2015).
451. Mortha, A. *et al.* Microbiota-dependent crosstalk between macrophages and ILC3 promotes intestinal homeostasis. *Science* **343** (2014).

452. Denning, T.L., Wang, Y.C., Patel, S.R., Williams, I.R. & Pulendran, B. Lamina propria macrophages and dendritic cells differentially induce regulatory and interleukin 17-producing T cell responses. *Nature immunology* **8**, 1086-1094 (2007).
453. Asano, K. *et al.* Intestinal CD169+ macrophages initiate mucosal inflammation by secreting CCL8 that recruits inflammatory monocytes. *Nature communications* **6**, 1-14 (2015).
454. Hiemstra, I.H. *et al.* The identification and developmental requirements of colonic CD 169+ macrophages. *Immunology* **142**, 269-278 (2014).
455. Kim, M. *et al.* Critical role for the microbiota in CX3CR1+ intestinal mononuclear phagocyte regulation of intestinal T cell responses. *Immunity* **49**, 151-163. e155 (2018).
456. Muller, P.A. *et al.* Crosstalk between Muscularis Macrophages and Enteric Neurons Regulates Gastrointestinal Motility. *Cell* **158**, 1210 (2014).
457. Cipriani, G. *et al.* Muscularis Propria Macrophages Alter the Proportion of Nitrergic but Not Cholinergic Gastric Myenteric Neurons. *Cellular and molecular gastroenterology and hepatology* **7**, 689-691.e684 (2019).
458. Monteleone, I., Platt, A.M., Jaensson, E., Agace, W.W. & Mowat, A.M. IL-10-dependent partial refractoriness to Toll-like receptor stimulation modulates gut mucosal dendritic cell function. *European journal of immunology* **38**, 1533-1547 (2008).
459. Smythies, L.E. *et al.* Inflammation anergy in human intestinal macrophages is due to Smad-induced IkappaB α expression and NF-kappaB inactivation. *The Journal of biological chemistry* **285**, 19593-19604 (2010).
460. Hirotani, T. *et al.* The nuclear IkappaB protein IkappaBNS selectively inhibits lipopolysaccharide-induced IL-6 production in macrophages of the colonic lamina propria. *Journal of immunology (Baltimore, Md. : 1950)* **174**, 3650-3657 (2005).
461. Shouval, D.S. *et al.* Interleukin-10 receptor signaling in innate immune cells regulates mucosal immune tolerance and anti-inflammatory macrophage function. *Immunity* **40**, 706-719 (2014).
462. Glocker, E.-O. *et al.* Inflammatory bowel disease and mutations affecting the interleukin-10 receptor. *New England Journal of Medicine* **361**, 2033-2045 (2009).
463. Biswas, A. *et al.* WASP-mediated regulation of anti-inflammatory macrophages is IL-10 dependent and is critical for intestinal homeostasis. *Nature communications* **9**, 1779 (2018).
464. Kelly, A. *et al.* Human monocytes and macrophages regulate immune tolerance via integrin $\alpha\beta 8$ -mediated TGF β activation. *Journal of Experimental Medicine* **215**, 2725-2736 (2018).
465. Rani, R., Smulian, A.G., Greaves, D.R., Hogan, S.P. & Herbert, D.B.R. TGF- β limits IL-33 production and promotes the resolution of colitis through regulation of macrophage function. *European journal of immunology* **41**, 2000-2009 (2011).
466. Fadok, V.A. *et al.* Macrophages that have ingested apoptotic cells in vitro inhibit proinflammatory cytokine production through autocrine/paracrine mechanisms involving TGF-beta, PGE2, and PAF. *The Journal of clinical investigation* **101**, 890-898 (1998).
467. Rimoldi, M. *et al.* Monocyte-derived dendritic cells activated by bacteria or by bacteria-stimulated epithelial cells are functionally different. *Blood* **106**, 2818-2826 (2005).
468. Zeuthen, L.H., Fink, L.N. & Frokiaer, H. Epithelial cells prime the immune response to an array of gut-derived commensals towards a tolerogenic phenotype through distinct actions of thymic stromal lymphopoietin and transforming growth factor-beta. *Immunology* **123**, 197-208 (2008).

469. Taylor, B.C. *et al.* TSLP regulates intestinal immunity and inflammation in mouse models of helminth infection and colitis. *The Journal of experimental medicine* **206**, 655-667 (2009).
470. Cox, M.A. *et al.* Short-chain fatty acids act as antiinflammatory mediators by regulating prostaglandin E(2) and cytokines. *World J Gastroenterol* **15**, 5549-5557 (2009).
471. Schulthess, J. *et al.* The Short Chain Fatty Acid Butyrate Imprints an Antimicrobial Program in Macrophages. *Immunity* **50**, 432-445.e437 (2019).
472. Marelli, G., Belgiovine, C., Mantovani, A., Erreni, M. & Allavena, P. Non-redundant role of the chemokine receptor CX3CR1 in the anti-inflammatory function of gut macrophages. *Immunobiology* **222**, 463-472 (2017).
473. Fernández-Prieto, M. *et al.* CX3CL1-CX3CR1 Axis: A New Player in Coeliac Disease Pathogenesis. *Nutrients* **11** (2019).
474. Kim, Y.G. *et al.* The Nod2 sensor promotes intestinal pathogen eradication via the chemokine CCL2-dependent recruitment of inflammatory monocytes. *Immunity* **34**, 769-780 (2011).
475. Müller, A.J. *et al.* Salmonella gut invasion involves TTSS-2-dependent epithelial traversal, basolateral exit, and uptake by epithelium-sampling lamina propria phagocytes. *Cell Host Microbe* **11**, 19-32 (2012).
476. Dunay, I.R. *et al.* Gr1(+) inflammatory monocytes are required for mucosal resistance to the pathogen *Toxoplasma gondii*. *Immunity* **29**, 306-317 (2008).
477. Schulthess, J. *et al.* Interleukin-15-dependent NKp46+ innate lymphoid cells control intestinal inflammation by recruiting inflammatory monocytes. *Immunity* **37**, 108-121 (2012).
478. Anthony, R.M. *et al.* Memory T(H)2 cells induce alternatively activated macrophages to mediate protection against nematode parasites. *Nature medicine* **12**, 955-960 (2006).
479. Waddell, A. *et al.* Colonic eosinophilic inflammation in experimental colitis is mediated by Ly6C(high) CCR2(+) inflammatory monocyte/macrophage-derived CCL11. *Journal of immunology (Baltimore, Md. : 1950)* **186**, 5993-6003 (2011).
480. Platt, A.M., Bain, C.C., Bordon, Y., Sester, D.P. & Mowat, A.M. An independent subset of TLR expressing CCR2-dependent macrophages promotes colonic inflammation. *Journal of immunology (Baltimore, Md. : 1950)* **184**, 6843-6854 (2010).
481. Hamers, A.A. *et al.* Deficiency of Nuclear Receptor Nur77 Aggravates Mouse Experimental Colitis by Increased NFκB Activity in Macrophages. *PLoS One* **10**, e0133598 (2015).
482. He, J. *et al.* Fbxw7 increases CCL2/7 in CX3CR1hi macrophages to promote intestinal inflammation. *The Journal of clinical investigation* **129**, 3877-3893 (2019).
483. Rivollier, A., He, J., Kole, A., Valatas, V. & Kelsall, B.L. Inflammation switches the differentiation program of Ly6Chi monocytes from antiinflammatory macrophages to inflammatory dendritic cells in the colon. *The Journal of experimental medicine* **209**, 139-155 (2012).
484. Arnold, I.C. *et al.* CD11c(+) monocyte/macrophages promote chronic *Helicobacter hepaticus*-induced intestinal inflammation through the production of IL-23. *Mucosal immunology* **9**, 352-363 (2016).
485. Bain, C.C., Oliphant, C.J., Thomson, C.A., Kullberg, M.C. & Mowat, A.M. Proinflammatory Role of Monocyte-Derived CX3CR1(int) Macrophages in *Helicobacter hepaticus*-Induced Colitis. *Infection and immunity* **86** (2018).

486. Varol, C. *et al.* Intestinal lamina propria dendritic cell subsets have different origin and functions. *Immunity* **31**, 502-512 (2009).
487. Nakanishi, Y., Sato, T., Takahashi, K. & Ohteki, T. IFN- γ -dependent epigenetic regulation instructs colitogenic monocyte/macrophage lineage differentiation in vivo. *Mucosal immunology* **11**, 871-880 (2018).
488. Thiesen, S. *et al.* CD14(hi)HLA-DR(dim) macrophages, with a resemblance to classical blood monocytes, dominate inflamed mucosa in Crohn's disease. *Journal of leukocyte biology* **95**, 531-541 (2014).
489. Lissner, D. *et al.* Monocyte and M1 Macrophage-induced Barrier Defect Contributes to Chronic Intestinal Inflammation in IBD. *Inflamm Bowel Dis* **21**, 1297-1305 (2015).
490. Chapuy, L. *et al.* Two distinct colonic CD14(+) subsets characterized by single-cell RNA profiling in Crohn's disease. *Mucosal immunology* **12**, 703-719 (2019).
491. Satsu, H. *et al.* Induction by activated macrophage-like THP-1 cells of apoptotic and necrotic cell death in intestinal epithelial Caco-2 monolayers via tumor necrosis factor- α . *Experimental cell research* **312**, 3909-3919 (2006).
492. Al-Sadi, R., Boivin, M. & Ma, T. Mechanism of cytokine modulation of epithelial tight junction barrier. *Frontiers in bioscience: a journal and virtual library* **14**, 2765 (2009).
493. Friedrich, M., Pohin, M. & Powrie, F. Cytokine networks in the pathophysiology of inflammatory bowel disease. *Immunity* **50**, 992-1006 (2019).
494. Man, A.L. *et al.* CX3CR1+ Cell-Mediated Salmonella Exclusion Protects the Intestinal Mucosa during the Initial Stage of Infection. *Journal of immunology (Baltimore, Md. : 1950)* **198**, 335-343 (2017).
495. Qualls, J.E., Kaplan, A.M., van Rooijen, N. & Cohen, D.A. Suppression of experimental colitis by intestinal mononuclear phagocytes. *Journal of leukocyte biology* **80**, 802-815 (2006).
496. Girard-Madoux, M.J.H. *et al.* IL-10 control of CD11c+ myeloid cells is essential to maintain immune homeostasis in the small and large intestine. *Oncotarget* **7**, 32015-32030 (2016).
497. Malvin, N.P., Seno, H. & Stappenbeck, T.S. Colonic epithelial response to injury requires Myd88 signaling in myeloid cells. *Mucosal immunology* **5**, 194-206 (2012).
498. GBD 2017 Causes of Death Collaborators. Global, regional, and national age-sex-specific mortality for 282 causes of death in 195 countries and territories, 1980-2017: a systematic analysis for the Global Burden of Disease Study 2017. *Lancet (London, England)* **392**, 1736-1788 (2018).
499. Furman, D. *et al.* Chronic inflammation in the etiology of disease across the life span. *Nature medicine* **25**, 1822-1832 (2019).
500. Robertson, S.J. *et al.* Comparison of Co-housing and Littermate Methods for Microbiota Standardization in Mouse Models. *Cell reports* **27**, 1910-1919.e1912 (2019).
501. Howie, G.J., Sloboda, D.M., Kamal, T. & Vickers, M.H. Maternal nutritional history predicts obesity in adult offspring independent of postnatal diet. *The Journal of physiology* **587**, 905-915 (2009).
502. Sloboda, D.M., Howie, G.J., Pleasants, A., Gluckman, P.D. & Vickers, M.H. Pre- and postnatal nutritional histories influence reproductive maturation and ovarian function in the rat. *PLoS One* **4**, e6744 (2009).

503. Tsoulis, M.W. *et al.* Maternal High-Fat Diet-Induced Loss of Fetal Oocytes Is Associated with Compromised Follicle Growth in Adult Rat Offspring. *Biology of reproduction* **94**, 94-94 (2016).
504. Schertzer, J.D. *et al.* A transgenic mouse model to study glucose transporter 4myc regulation in skeletal muscle. *Endocrinology* **150**, 1935-1940 (2009).
505. Schertzer, J.D. *et al.* NOD1 activators link innate immunity to insulin resistance. *Diabetes* **60**, 2206-2215 (2011).
506. Pinier, M. *et al.* The copolymer P(HEMA-co-SS) binds gluten and reduces immune response in gluten-sensitized mice and human tissues. *Gastroenterology* **142**, 316-325.e311-312 (2012).
507. Silva, M.A. *et al.* Increased bacterial translocation in gluten-sensitive mice is independent of small intestinal paracellular permeability defect. *Digestive diseases and sciences* **57**, 38-47 (2012).
508. Schneider, C.A., Rasband, W.S. & Eliceiri, K.W. NIH Image to ImageJ: 25 years of image analysis. *Nature Methods* **9**, 671 (2012).
509. Pick, R., He, W., Chen, C.-S. & Scheiermann, C. Time-of-Day-Dependent Trafficking and Function of Leukocyte Subsets. *Trends in immunology* **40**, 524-537 (2019).
510. Sun, C.M. *et al.* Small intestine lamina propria dendritic cells promote de novo generation of Foxp3 T reg cells via retinoic acid. *The Journal of experimental medicine* **204**, 1775-1785 (2007).
511. Thevaranjan, N. The interplay between microbial dysbiosis and immune dysfunction with age. MSc thesis, McMaster University, 2016.
512. Oh, D.Y., Morinaga, H., Talukdar, S., Bae, E.J. & Olefsky, J.M. Increased macrophage migration into adipose tissue in obese mice. *Diabetes* **61**, 346-354 (2012).
513. Gutierrez, D.A. *et al.* Aberrant accumulation of undifferentiated myeloid cells in the adipose tissue of CCR2-deficient mice delays improvements in insulin sensitivity. *Diabetes* **60**, 2820-2829 (2011).
514. Mulder, P., van den Hoek, A.M. & Kleemann, R. The CCR2 Inhibitor Propagermanium Attenuates Diet-Induced Insulin Resistance, Adipose Tissue Inflammation and Non-Alcoholic Steatohepatitis. *PLoS One* **12**, e0169740 (2017).
515. Finucane, O.M. *et al.* Macrophage migration inhibitory factor deficiency ameliorates high-fat diet induced insulin resistance in mice with reduced adipose inflammation and hepatic steatosis. *PLoS One* **9**, e113369 (2014).
516. Kim, B.S. *et al.* Differential regulation of macrophage activation by the MIF cytokine superfamily members MIF and MIF-2 in adipose tissue during endotoxemia. *FASEB journal : official publication of the Federation of American Societies for Experimental Biology* **34**, 4219-4233 (2020).
517. Kullo, I.J., Hensrud, D.D. & Allison, T.G. Comparison of numbers of circulating blood monocytes in men grouped by body mass index (<25, 25 to <30, > or =30). *The American journal of cardiology* **89**, 1441-1443 (2002).
518. Devèvre, E.F. *et al.* Profiling of the three circulating monocyte subpopulations in human obesity. *Journal of immunology (Baltimore, Md. : 1950)* **194**, 3917-3923 (2015).
519. Poitou, C. *et al.* CD14^{dim}CD16⁺ and CD14⁺CD16⁺ monocytes in obesity and during weight loss: relationships with fat mass and subclinical atherosclerosis. *Arteriosclerosis, thrombosis, and vascular biology* **31**, 2322-2330 (2011).

520. Krinninger, P. *et al.* Peripheral monocytes of obese women display increased chemokine receptor expression and migration capacity. *The Journal of clinical endocrinology and metabolism* **99**, 2500-2509 (2014).
521. Figueroa-Vega, N. *et al.* Analysis of the percentages of monocyte subsets and ILC2s, their relationships with metabolic variables and response to hypocaloric restriction in obesity. *PLOS ONE* **15**, e0228637 (2020).
522. Friedrich, K. *et al.* Perturbation of the Monocyte Compartment in Human Obesity. *Frontiers in immunology* **10**, 1874 (2019).
523. Singer, K. *et al.* Differences in Hematopoietic Stem Cells Contribute to Sexually Dimorphic Inflammatory Responses to High Fat Diet-induced Obesity. *The Journal of biological chemistry* **290**, 13250-13262 (2015).
524. Singer, K. *et al.* Diet-induced obesity promotes myelopoiesis in hematopoietic stem cells. *Molecular metabolism* **3**, 664-675 (2014).
525. Nagareddy, P.R. *et al.* Adipose tissue macrophages promote myelopoiesis and monocytosis in obesity. *Cell metabolism* **19**, 821-835 (2014).
526. Uysal, K.T., Wiesbrock, S.M., Marino, M.W. & Hotamisligil, G.S. Protection from obesity-induced insulin resistance in mice lacking TNF- α function. *Nature* **389**, 610-614 (1997).
527. Ventre, J. *et al.* Targeted Disruption of the Tumor Necrosis Factor- α Gene: Metabolic Consequences in Obese and Nonobese Mice. *Diabetes* **46**, 1526 (1997).
528. Bouter, B., Geary, N., Langhans, W. & Asarian, L. Diet-genotype interactions in the early development of obesity and insulin resistance in mice with a genetic deficiency in tumor necrosis factor- α . *Metabolism: clinical and experimental* **59**, 1065-1073 (2010).
529. Araújo, E.P. *et al.* Infliximab restores glucose homeostasis in an animal model of diet-induced obesity and diabetes. *Endocrinology* **148**, 5991-5997 (2007).
530. Ishikawa, K. *et al.* Subcutaneous fat modulates insulin sensitivity in mice by regulating TNF- α expression in visceral fat. *Horm Metab Res* **38**, 631-638 (2006).
531. Borst, S.E. & Bagby, G.J. Neutralization of tumor necrosis factor reverses age-induced impairment of insulin responsiveness in skeletal muscle of Sprague-Dawley rats. *Metabolism: clinical and experimental* **51**, 1061-1064 (2002).
532. Borst, S.E., Lee, Y., Conover, C.F., Shek, E.W. & Bagby, G.J. Neutralization of tumor necrosis factor- α reverses insulin resistance in skeletal muscle but not adipose tissue. *American journal of physiology. Endocrinology and metabolism* **287**, E934-938 (2004).
533. Aouadi, M. *et al.* Gene silencing in adipose tissue macrophages regulates whole-body metabolism in obese mice. *Proceedings of the National Academy of Sciences of the United States of America* **110**, 8278-8283 (2013).
534. Feingold, K.R. *et al.* Effect of tumor necrosis factor (TNF) on lipid metabolism in the diabetic rat. Evidence that inhibition of adipose tissue lipoprotein lipase activity is not required for TNF-induced hyperlipidemia. *The Journal of clinical investigation* **83**, 1116-1121 (1989).
535. Ling, P.R., Bistrian, B.R., Mendez, B. & Istfan, N.W. Effects of systemic infusions of endotoxin, tumor necrosis factor, and interleukin-1 on glucose metabolism in the rat: relationship to endogenous glucose production and peripheral tissue glucose uptake. *Metabolism: clinical and experimental* **43**, 279-284 (1994).

536. Miles, P.D. *et al.* TNF- α -induced insulin resistance in vivo and its prevention by troglitazone. *Diabetes* **46**, 1678-1683 (1997).
537. Uysal, K.T., Wiesbrock, S.M. & Hotamisligil, G.S. Functional analysis of tumor necrosis factor (TNF) receptors in TNF- α -mediated insulin resistance in genetic obesity. *Endocrinology* **139**, 4832-4838 (1998).
538. Steinberg, G.R. *et al.* Tumor necrosis factor α -induced skeletal muscle insulin resistance involves suppression of AMP-kinase signaling. *Cell metabolism* **4**, 465-474 (2006).
539. Liang, H. *et al.* Blockade of tumor necrosis factor (TNF) receptor type 1-mediated TNF- α signaling protected Wistar rats from diet-induced obesity and insulin resistance. *Endocrinology* **149**, 2943-2951 (2008).
540. Gal-Oz, S.T. *et al.* ImmGen report: sexual dimorphism in the immune system transcriptome. *Nature communications* **10**, 4295 (2019).
541. Mamrut, S. *et al.* Integrative analysis of methylome and transcriptome in human blood identifies extensive sex- and immune cell-specific differentially methylated regions. *Epigenetics* **10**, 943-957 (2015).
542. Márquez, E.J. *et al.* Sexual-dimorphism in human immune system aging. *Nature communications* **11**, 751 (2020).
543. Lovejoy, J.C. & Sainsbury, A. Sex differences in obesity and the regulation of energy homeostasis. *Obesity reviews : an official journal of the International Association for the Study of Obesity* **10**, 154-167 (2009).
544. Bloor, I.D. & Symonds, M.E. Sexual dimorphism in white and brown adipose tissue with obesity and inflammation. *Hormones and behavior* **66**, 95-103 (2014).
545. Wang, C. & Xu, Y. Mechanisms for Sex Differences in Energy Homeostasis. *Journal of molecular endocrinology* **62**, R129-r143 (2019).
546. Collins, S., Martin, T.L., Surwit, R.S. & Robidoux, J. Genetic vulnerability to diet-induced obesity in the C57BL/6J mouse: physiological and molecular characteristics. *Physiology & behavior* **81**, 243-248 (2004).
547. Avtanski, D., Pavlov, V.A., Tracey, K.J. & Poretsky, L. Characterization of inflammation and insulin resistance in high-fat diet-induced male C57BL/6J mouse model of obesity. *Animal models and experimental medicine* **2**, 252-258 (2019).
548. Clegg, D. *et al.* Sex Hormones and Cardiometabolic Health: Role of Estrogen and Estrogen Receptors. *Endocrinology* **158**, 1095-1105 (2017).
549. Salinero, A.E., Anderson, B.M. & Zuloaga, K.L. Sex differences in the metabolic effects of diet-induced obesity vary by age of onset. *International journal of obesity (2005)* **42**, 1088-1091 (2018).
550. Xu, E. *et al.* Temporal and tissue-specific requirements for T-lymphocyte IL-6 signalling in obesity-associated inflammation and insulin resistance. *Nature communications* **8**, 14803 (2017).
551. Rizwan, M.Z., Mehltz, S., Grattan, D.R. & Tups, A. Temporal and regional onset of leptin resistance in diet-induced obese mice. *Journal of neuroendocrinology* **29** (2017).
552. Hoffler, U. *et al.* Diet-induced obesity is associated with hyperleptinemia, hyperinsulinemia, hepatic steatosis, and glomerulopathy in C57Bl/6J mice. *Endocrine* **36**, 311-325 (2009).

553. Kim, A.K., Hamadani, C., Zeidel, M.L. & Hill, W.G. Urological complications of obesity and diabetes in males and females of three mouse models: temporal manifestations. *American journal of physiology. Renal physiology* **318**, F160-f174 (2020).
554. Burchfield, J.G. *et al.* High dietary fat and sucrose results in an extensive and time-dependent deterioration in health of multiple physiological systems in mice. *The Journal of biological chemistry* **293**, 5731-5745 (2018).
555. Pasparakis, M., Alexopoulou, L., Episkopou, V. & Kollias, G. Immune and inflammatory responses in TNF alpha-deficient mice: a critical requirement for TNF alpha in the formation of primary B cell follicles, follicular dendritic cell networks and germinal centers, and in the maturation of the humoral immune response. *The Journal of experimental medicine* **184**, 1397-1411 (1996).
556. Eugster, H.P. *et al.* Multiple immune abnormalities in tumor necrosis factor and lymphotoxin-alpha double-deficient mice. *Int Immunol* **8**, 23-36 (1996).
557. Endres, R. *et al.* Mature follicular dendritic cell networks depend on expression of lymphotoxin beta receptor by radioresistant stromal cells and of lymphotoxin beta and tumor necrosis factor by B cells. *The Journal of experimental medicine* **189**, 159-168 (1999).
558. Kuprash, D.V. *et al.* Novel tumor necrosis factor-knockout mice that lack Peyer's patches. *European journal of immunology* **35**, 1592-1600 (2005).
559. Liu, Y., Lu, X., Li, X., Du, P. & Qin, G. High-fat diet triggers obesity-related early infiltration of macrophages into adipose tissue and transient reduction of blood monocyte count. *Molecular immunology* **117**, 139-146 (2020).
560. Nagareddy, P.R. *et al.* Hyperglycemia promotes myelopoiesis and impairs the resolution of atherosclerosis. *Cell metabolism* **17**, 695-708 (2013).
561. Pettersson, U.S., Waldén, T.B., Carlsson, P.-O., Jansson, L. & Phillipson, M. Female mice are protected against high-fat diet induced metabolic syndrome and increase the regulatory T cell population in adipose tissue. *PloS one* **7**, e46057-e46057 (2012).
562. Ludgero-Correia Jr, A., Aguila, M.B., Mandarin-de-Lacerda, C.A. & Faria, T.S. Effects of high-fat diet on plasma lipids, adiposity, and inflammatory markers in ovariectomized C57BL/6 mice. *Nutrition* **28**, 316-323 (2012).
563. Arcones, A.C., Cruces-Sande, M., Ramos, P., Mayor, F., Jr. & Murga, C. Sex Differences in High Fat Diet-Induced Metabolic Alterations Correlate with Changes in the Modulation of GRK2 Levels. *Cells* **8** (2019).
564. Medrikova, D. *et al.* Sex differences during the course of diet-induced obesity in mice: adipose tissue expandability and glycemic control. *International journal of obesity (2005)* **36**, 262-272 (2012).
565. Matsumiya, T. *et al.* Characterization of synergistic induction of CX3CL1/fractalkine by TNF-alpha and IFN-gamma in vascular endothelial cells: an essential role for TNF-alpha in post-transcriptional regulation of CX3CL1. *Journal of immunology (Baltimore, Md. : 1950)* **184**, 4205-4214 (2010).
566. Rennert, K. *et al.* Recruitment of CD16(+) monocytes to endothelial cells in response to LPS-treatment and concomitant TNF release is regulated by CX3CR1 and interfered by soluble fractalkine. *Cytokine* **83**, 41-52 (2016).
567. Sung, M.J. *et al.* Genistein suppression of TNF-alpha-induced fractalkine expression in endothelial cells. *Cellular physiology and biochemistry : international journal of experimental cellular physiology, biochemistry, and pharmacology* **26**, 431-440 (2010).

568. Foley, K.P. *et al.* Long term but not short term exposure to obesity related microbiota promotes host insulin resistance. *Nature communications* **9**, 4681 (2018).
569. Lang, P., Hasselwander, S., Li, H. & Xia, N. Effects of different diets used in diet-induced obesity models on insulin resistance and vascular dysfunction in C57BL/6 mice. *Scientific reports* **9**, 19556 (2019).
570. Racicot, K., Kwon, J.Y., Aldo, P., Silasi, M. & Mor, G. Understanding the complexity of the immune system during pregnancy. *American journal of reproductive immunology (New York, N.Y. : 1989)* **72**, 107-116 (2014).
571. Mor, G. & Cardenas, I. The immune system in pregnancy: a unique complexity. *American journal of reproductive immunology (New York, N.Y. : 1989)* **63**, 425-433 (2010).
572. Faas, M.M. *et al.* Microbiota Induced Changes in the Immune Response in Pregnant Mice. *Frontiers in immunology* **10**, 2976 (2019).
573. Naccasha, N. *et al.* Phenotypic and metabolic characteristics of monocytes and granulocytes in normal pregnancy and maternal infection. *American journal of obstetrics and gynecology* **185**, 1118-1123 (2001).
574. Gervasi, M.T. *et al.* Phenotypic and metabolic characteristics of monocytes and granulocytes in preeclampsia. *American journal of obstetrics and gynecology* **185**, 792-797 (2001).
575. Faas, M.M., Spaans, F. & De Vos, P. Monocytes and macrophages in pregnancy and pre-eclampsia. *Frontiers in immunology* **5**, 298 (2014).
576. Faas, M. *et al.* The immune response during the luteal phase of the ovarian cycle: a Th2-type response? *Fertility and sterility* **74**, 1008-1013 (2000).
577. Le Gars, M. *et al.* Increased Proinflammatory Responses of Monocytes and Plasmacytoid Dendritic Cells to Influenza A Virus Infection During Pregnancy. *The Journal of infectious diseases* **214**, 1666-1671 (2016).
578. Kitzmiller, J.L., Stoneburner, L., Yelenosky, P.F. & Lucas, W.E. Serum complement in normal pregnancy and pre-eclampsia. *American journal of obstetrics and gynecology* **117**, 312-315 (1973).
579. Richani, K. *et al.* Normal pregnancy is characterized by systemic activation of the complement system. *The journal of maternal-fetal & neonatal medicine : the official journal of the European Association of Perinatal Medicine, the Federation of Asia and Oceania Perinatal Societies, the International Society of Perinatal Obstet* **17**, 239-245 (2005).
580. Baines, M.G., Millar, K.G. & Mills, P. Studies of complement levels in normal human pregnancy. *Obstetrics and gynecology* **43**, 806-810 (1974).
581. Comeglio, P. *et al.* Blood clotting activation during normal pregnancy. *Thrombosis research* **84**, 199-202 (1996).
582. Veenstra van Nieuwenhoven, A.L. *et al.* Cytokine production in natural killer cells and lymphocytes in pregnant women compared with women in the follicular phase of the ovarian cycle. *Fertility and sterility* **77**, 1032-1037 (2002).
583. Le Gars, M. *et al.* Pregnancy-Induced Alterations in NK Cell Phenotype and Function. *Frontiers in immunology* **10**, 2469 (2019).
584. Heng, Y.J. *et al.* Maternal Whole Blood Gene Expression at 18 and 28 Weeks of Gestation Associated with Spontaneous Preterm Birth in Asymptomatic Women. *PLoS One* **11**, e0155191 (2016).

585. Al-Garawi, A. *et al.* The Role of Vitamin D in the Transcriptional Program of Human Pregnancy. *PLoS One* **11**, e0163832 (2016).
586. Sen, S. *et al.* Obesity impairs cell-mediated immunity during the second trimester of pregnancy. *American journal of obstetrics and gynecology* **208**, 139.e131-138 (2013).
587. Somerset, D.A., Zheng, Y., Kilby, M.D., Sansom, D.M. & Drayson, M.T. Normal human pregnancy is associated with an elevation in the immune suppressive CD25+ CD4+ regulatory T-cell subset. *Immunology* **112**, 38-43 (2004).
588. Saito, S., Nakashima, A., Shima, T. & Ito, M. Th1/Th2/Th17 and regulatory T-cell paradigm in pregnancy. *American journal of reproductive immunology* **63**, 601-610 (2010).
589. Figueiredo, A.S. & Schumacher, A. The T helper type 17/regulatory T cell paradigm in pregnancy. *Immunology* **148**, 13-21 (2016).
590. Elderman, M. *et al.* Changes in intestinal gene expression and microbiota composition during late pregnancy are mouse strain dependent. *Scientific reports* **8**, 1-12 (2018).
591. Norton, M.T., Fortner, K.A., Bizargity, P. & Bonney, E.A. Pregnancy alters the proliferation and apoptosis of mouse splenic erythroid lineage cells and leukocytes. *Biology of reproduction* **81**, 457-464 (2009).
592. Maroni, E. & de Sousa, M.A. The lymphoid organs during pregnancy in the mouse. A comparison between a syngeneic and an allogeneic mating. *Clinical and experimental immunology* **13**, 107 (1973).
593. Barden, A. *et al.* Neutrophil CD11B expression and neutrophil activation in pre-eclampsia. *Clinical Science* **92**, 37-44 (1997).
594. Al-ofi, E., Coffelt, S.B. & Anumba, D.O. Monocyte subpopulations from pre-eclamptic patients are abnormally skewed and exhibit exaggerated responses to Toll-like receptor ligands. *PLoS One* **7**, e42217 (2012).
595. McClure, C.K., Catov, J.M., Ness, R. & Bodnar, L.M. Associations between gestational weight gain and BMI, abdominal adiposity, and traditional measures of cardiometabolic risk in mothers 8 y postpartum. *The American journal of clinical nutrition* **98**, 1218-1225 (2013).
596. Mamun, A.A. *et al.* Associations of excess weight gain during pregnancy with long-term maternal overweight and obesity: evidence from 21 y postpartum follow-up. *The American journal of clinical nutrition* **91**, 1336-1341 (2010).
597. Amorim, A.R., Rössner, S., Neovius, M., Lourenço, P.M. & Linné, Y. Does excess pregnancy weight gain constitute a major risk for increasing long-term BMI? *Obesity* **15**, 1278-1286 (2007).
598. Gunderson, E.P., Abrams, B. & Selvin, S. The relative importance of gestational gain and maternal characteristics associated with the risk of becoming overweight after pregnancy. *International journal of obesity* **24**, 1660-1668 (2000).
599. Olson, C., Strawderman, M., Hinton, P. & Pearson, T. Gestational weight gain and postpartum behaviors associated with weight change from early pregnancy to 1 y postpartum. *International journal of obesity* **27**, 117-127 (2003).
600. Alijotas-Reig, J., Esteve-Valverde, E., Ferrer-Oliveras, R., Llurba, E. & Gris, J.M. Tumor Necrosis Factor-Alpha and Pregnancy: Focus on Biologics. An Updated and Comprehensive Review. *Clinical reviews in allergy & immunology* **53**, 40-53 (2017).

601. Kirwan, J.P. *et al.* TNF-alpha is a predictor of insulin resistance in human pregnancy. *Diabetes* **51**, 2207-2213 (2002).
602. Cackovic, M. *et al.* Fractional excretion of tumor necrosis factor-alpha in women with severe preeclampsia. *Obstetrics and gynecology* **112**, 93-100 (2008).
603. Hung, T.H., Charnock-Jones, D.S., Skepper, J.N. & Burton, G.J. Secretion of tumor necrosis factor-alpha from human placental tissues induced by hypoxia-reoxygenation causes endothelial cell activation in vitro: a potential mediator of the inflammatory response in preeclampsia. *The American journal of pathology* **164**, 1049-1061 (2004).
604. Azizieh, F.Y. & Raghupathy, R.G. Tumor necrosis factor- α and pregnancy complications: a prospective study. *Medical principles and practice : international journal of the Kuwait University, Health Science Centre* **24**, 165-170 (2015).
605. Jones, H.N. *et al.* High-fat diet before and during pregnancy causes marked up-regulation of placental nutrient transport and fetal overgrowth in C57/BL6 mice. *FASEB journal : official publication of the Federation of American Societies for Experimental Biology* **23**, 271-278 (2009).
606. Samuelsson, A.-M. *et al.* Diet-Induced Obesity in Female Mice Leads to Offspring Hyperphagia, Adiposity, Hypertension, and Insulin Resistance. *Hypertension (Dallas, Tex. : 1979)* **51**, 383-392 (2008).
607. Valdimarsson, H., Mulholland, C., Fridriksdottir, V. & Coleman, D.V. A longitudinal study of leucocyte blood counts and lymphocyte responses in pregnancy: a marked early increase of monocyte-lymphocyte ratio. *Clinical and experimental immunology* **53**, 437-443 (1983).
608. Lurie, S., Rahamim, E., Piper, I., Golan, A. & Sadan, O. Total and differential leukocyte counts percentiles in normal pregnancy. *European journal of obstetrics, gynecology, and reproductive biology* **136**, 16-19 (2008).
609. Bhat, N.M., Mithal, A., Bieber, M.M., Herzenberg, L.A. & Teng, N.N. Human CD5+ B lymphocytes (B-1 cells) decrease in peripheral blood during pregnancy. *Journal of reproductive immunology* **28**, 53-60 (1995).
610. Iwatani, Y. *et al.* Changes of lymphocyte subsets in normal pregnant and postpartum women: postpartum increase in NK/K (Leu 7) cells. *American journal of reproductive immunology and microbiology : AJRIM* **18**, 52-55 (1988).
611. Watanabe, M. *et al.* Changes in T, B, and NK lymphocyte subsets during and after normal pregnancy. *American journal of reproductive immunology (New York, N.Y. : 1989)* **37**, 368-377 (1997).
612. Medina, K.L., Smithson, G. & Kincade, P.W. Suppression of B lymphopoiesis during normal pregnancy. *The Journal of experimental medicine* **178**, 1507-1515 (1993).
613. Park, Y., Fox, L., Hamilton, M. & Davis, W. Bovine mononuclear leukocyte subpopulations in peripheral blood and mammary gland secretions during lactation. *Journal of dairy science* **75**, 998-1006 (1992).
614. Frasca, D. & Blomberg, B.B. The Impact of Obesity and Metabolic Syndrome on Vaccination Success. *Interdisciplinary topics in gerontology and geriatrics* **43**, 86-97 (2020).
615. Neidich, S.D. *et al.* Increased risk of influenza among vaccinated adults who are obese. *International journal of obesity* **41**, 1324-1330 (2017).

616. Frasca, D. *et al.* Obesity decreases B cell responses in young and elderly individuals. *Obesity (Silver Spring, Md.)* **24**, 615-625 (2016).
617. Aguilar, E.G. & Murphy, W.J. Obesity induced T cell dysfunction and implications for cancer immunotherapy. *Current opinion in immunology* **51**, 181-186 (2018).
618. Tagliani, E. *et al.* Coordinate regulation of tissue macrophage and dendritic cell population dynamics by CSF-1. *The Journal of experimental medicine* **208**, 1901-1916 (2011).
619. Gustafsson, C. *et al.* Gene expression profiling of human decidual macrophages: evidence for immunosuppressive phenotype. *PLoS One* **3**, e2078 (2008).
620. Kämmerer, U. *et al.* Unique appearance of proliferating antigen-presenting cells expressing DC-SIGN (CD209) in the decidua of early human pregnancy. *The American journal of pathology* **162**, 887-896 (2003).
621. Care, A.S. *et al.* Macrophages regulate corpus luteum development during embryo implantation in mice. *The Journal of clinical investigation* **123**, 3472-3487 (2013).
622. Buckley, R.J., Whitley, G.S., Dumitriu, I.E. & Cartwright, J.E. Macrophage polarisation affects their regulation of trophoblast behaviour. *Placenta* **47**, 73-80 (2016).
623. Jetten, N. *et al.* Anti-inflammatory M2, but not pro-inflammatory M1 macrophages promote angiogenesis in vivo. *Angiogenesis* **17**, 109-118 (2014).
624. Reister, F. *et al.* Macrophage-induced apoptosis limits endovascular trophoblast invasion in the uterine wall of preeclamptic women. *Laboratory investigation; a journal of technical methods and pathology* **81**, 1143-1152 (2001).
625. Erlebacher, A. Immunology of the maternal-fetal interface. *Annual review of immunology* **31**, 387-411 (2013).
626. Co, E.C. *et al.* Maternal decidual macrophages inhibit NK cell killing of invasive cytotrophoblasts during human pregnancy. *Biology of reproduction* **88**, 155 (2013).
627. Vacca, P. *et al.* Crosstalk between decidual NK and CD14+ myelomonocytic cells results in induction of Tregs and immunosuppression. *Proceedings of the National Academy of Sciences of the United States of America* **107**, 11918-11923 (2010).
628. Quillay, H. *et al.* NK cells control HIV-1 infection of macrophages through soluble factors and cellular contacts in the human decidua. *Retrovirology* **13**, 39 (2016).
629. Renaud, S.J. & Graham, C.H. The role of macrophages in utero-placental interactions during normal and pathological pregnancy. *Immunological investigations* **37**, 535-564 (2008).
630. Houser, B.L., Tilburgs, T., Hill, J., Nicotra, M.L. & Strominger, J.L. Two unique human decidual macrophage populations. *Journal of immunology (Baltimore, Md. : 1950)* **186**, 2633-2642 (2011).
631. Ingvorsen, C. *et al.* Effects of pregnancy on obesity-induced inflammation in a mouse model of fetal programming. *International journal of obesity* **38**, 1282-1289 (2014).
632. Friis, C.M. *et al.* Adiposity-related inflammation: effects of pregnancy. *Obesity (Silver Spring, Md.)* **21**, E124-130 (2013).
633. Pedroni, S.M. *et al.* Pregnancy in obese mice protects selectively against visceral adiposity and is associated with increased adipocyte estrogen signalling. *PLoS One* **9**, e94680 (2014).

634. Forbes, S. *et al.* Convergence in insulin resistance between very severely obese and lean women at the end of pregnancy. *Diabetologia* **58**, 2615-2626 (2015).
635. Bozkurt, L. *et al.* The impact of preconceptional obesity on trajectories of maternal lipids during gestation. *Scientific reports* **6**, 29971 (2016).
636. Roland, M.C.P., Lekva, T., Godang, K., Bollerslev, J. & Henriksen, T. Changes in maternal blood glucose and lipid concentrations during pregnancy differ by maternal body mass index and are related to birthweight: A prospective, longitudinal study of healthy pregnancies. *PLOS ONE* **15**, e0232749 (2020).
637. Jenkins, S.J. *et al.* Local macrophage proliferation, rather than recruitment from the blood, is a signature of TH2 inflammation. *Science* **332**, 1284-1288 (2011).
638. Zheng, C. *et al.* CD11b regulates obesity-induced insulin resistance via limiting alternative activation and proliferation of adipose tissue macrophages. *Proceedings of the National Academy of Sciences* **112**, E7239-E7248 (2015).
639. Li, H. *et al.* Intestinal, adipose, and liver inflammation in diet-induced obese mice. *Metabolism: clinical and experimental* **57**, 1704-1710 (2008).
640. Luck, H. *et al.* Gut-associated IgA(+) immune cells regulate obesity-related insulin resistance. *Nature communications* **10**, 3650 (2019).
641. Luck, H. *et al.* Regulation of obesity-related insulin resistance with gut anti-inflammatory agents. *Cell metabolism* **21**, 527-542 (2015).
642. Gulhane, M. *et al.* High Fat Diets Induce Colonic Epithelial Cell Stress and Inflammation that is Reversed by IL-22. *Scientific reports* **6**, 28990-28990 (2016).
643. Liu, Z. *et al.* Diet-induced obesity elevates colonic TNF-alpha in mice and is accompanied by an activation of Wnt signaling: a mechanism for obesity-associated colorectal cancer. *The Journal of nutritional biochemistry* **23**, 1207-1213 (2012).
644. Teixeira, L.G. *et al.* The combination of high-fat diet-induced obesity and chronic ulcerative colitis reciprocally exacerbates adipose tissue and colon inflammation. *Lipids in health and disease* **10**, 204 (2011).
645. Lam, Y.Y. *et al.* Increased gut permeability and microbiota change associate with mesenteric fat inflammation and metabolic dysfunction in diet-induced obese mice. *PLoS One* **7**, e34233 (2012).
646. Gruber, L. *et al.* High fat diet accelerates pathogenesis of murine Crohn's disease-like ileitis independently of obesity. *PLoS One* **8**, e71661 (2013).
647. Paik, J., Fierce, Y., Treuting, P.M., Brabb, T. & Maggio-Price, L. High-fat diet-induced obesity exacerbates inflammatory bowel disease in genetically susceptible Mdr1a-/- male mice. *The Journal of nutrition* **143**, 1240-1247 (2013).
648. Kim, I.-W. *et al.* Western-style diets induce macrophage infiltration and contribute to colitis-associated carcinogenesis. *Journal of Gastroenterology and Hepatology* **25**, 1785-1794 (2010).
649. Laroui, H. *et al.* Dextran sodium sulfate (DSS) induces colitis in mice by forming nano-lipocomplexes with medium-chain-length fatty acids in the colon. *PloS one* **7**, e32084-e32084 (2012).
650. Mushref, M.A. & Srinivasan, S. Effect of high fat-diet and obesity on gastrointestinal motility. *Annals of translational medicine* **1**, 14 (2013).

651. Stenkamp-Strahm, C., Patterson, S., Boren, J., Gericke, M. & Balemba, O. High-fat diet and age-dependent effects on enteric glial cell populations of mouse small intestine. *Autonomic neuroscience : basic & clinical* **177**, 199-210 (2013).
652. Mah, A.T., Van Landeghem, L., Gavin, H.E., Magness, S.T. & Lund, P.K. Impact of diet-induced obesity on intestinal stem cells: hyperproliferation but impaired intrinsic function that requires insulin/IGF1. *Endocrinology* **155**, 3302-3314 (2014).
653. Zhou, W., Davis, E.A. & Dailey, M.J. Obesity, independent of diet, drives lasting effects on intestinal epithelial stem cell proliferation in mice. *Experimental biology and medicine (Maywood, N.J.)* **243**, 826-835 (2018).
654. Kataru, R.P. *et al.* Regulation of Lymphatic Function in Obesity. *Front Physiol* **11**, 459 (2020).
655. Shan, K. *et al.* Distinct Gut Microbiota Induced by Different Fat-to-Sugar-Ratio High-Energy Diets Share Similar Pro-obesity Genetic and Metabolite Profiles in Prediabetic Mice. *MSystems* **4**, e00219-00219 (2019).
656. Al-Sadi, R., Guo, S., Ye, D. & Ma, T.Y. TNF- α modulation of intestinal epithelial tight junction barrier is regulated by ERK1/2 activation of Elk-1. *The American journal of pathology* **183**, 1871-1884 (2013).
657. Wang, F. *et al.* Interferon-gamma and tumor necrosis factor-alpha synergize to induce intestinal epithelial barrier dysfunction by up-regulating myosin light chain kinase expression. *The American journal of pathology* **166**, 409-419 (2005).
658. Rohm, T.V., Alasfoor, S., Bosch, A.J. & Cavelti-Weder, C. Targeting Intestinal Macrophages as a Potential Therapeutic Option in Obesity. *Diabetes* **67**, 283-OR (2018).
659. Johnson, A.M. *et al.* High fat diet causes depletion of intestinal eosinophils associated with intestinal permeability. *PLoS One* **10**, e0122195 (2015).
660. Garidou, L. *et al.* The Gut Microbiota Regulates Intestinal CD4 T Cells Expressing ROR γ t and Controls Metabolic Disease. *Cell metabolism* **22**, 100-112 (2015).
661. Hong, C.P. *et al.* Gut-Specific Delivery of T-Helper 17 Cells Reduces Obesity and Insulin Resistance in Mice. *Gastroenterology* **152**, 1998-2010 (2017).
662. de Wit, N.J. *et al.* The role of the small intestine in the development of dietary fat-induced obesity and insulin resistance in C57BL/6J mice. *BMC medical genomics* **1**, 14 (2008).
663. Navarrete, J., Vásquez, B. & Del Sol, M. Morphoquantitative analysis of the Ileum of C57BL/6 mice (*Mus musculus*) fed with a high-fat diet. *International journal of clinical and experimental pathology* **8**, 14649-14657 (2015).
664. Nilaweera, K.N. & Speakman, J.R. Regulation of intestinal growth in response to variations in energy supply and demand. *Obesity reviews : an official journal of the International Association for the Study of Obesity* **19 Suppl 1**, 61-72 (2018).
665. Yan, Y. *et al.* Temporal and spatial analysis of clinical and molecular parameters in dextran sodium sulfate induced colitis. *PloS one* **4**, e6073 (2009).
666. Kaliannan, K. *et al.* Estrogen-mediated gut microbiome alterations influence sexual dimorphism in metabolic syndrome in mice. *Microbiome* **6**, 205 (2018).
667. Collins, F.L. *et al.* Temporal and regional intestinal changes in permeability, tight junction, and cytokine gene expression following ovariectomy-induced estrogen deficiency. *Physiological reports* **5** (2017).

668. Bábíčková, J. *et al.* Sex Differences in Experimentally Induced Colitis in Mice: a Role for Estrogens. *Inflammation* **38**, 1996-2006 (2015).
669. Clarke, L.L. A guide to Ussing chamber studies of mouse intestine. *American journal of physiology. Gastrointestinal and liver physiology* **296**, G1151-1166 (2009).
670. Thomson, A. *et al.* The Ussing chamber system for measuring intestinal permeability in health and disease. *BMC gastroenterology* **19**, 98 (2019).
671. Ueda, Y. *et al.* Commensal microbiota induce LPS hyporesponsiveness in colonic macrophages via the production of IL-10. *Int Immunol* **22**, 953-962 (2010).
672. Ma, T.Y. *et al.* TNF- α -induced increase in intestinal epithelial tight junction permeability requires NF- κ B activation. *American Journal of Physiology-Gastrointestinal and Liver Physiology* **286**, G367-G376 (2004).
673. Delgado, M.E. & Brunner, T. The many faces of tumor necrosis factor signaling in the intestinal epithelium. *Genes and immunity* **20**, 609-626 (2019).
674. Kobayashi, N. *et al.* TIM-1 and TIM-4 glycoproteins bind phosphatidylserine and mediate uptake of apoptotic cells. *Immunity* **27**, 927-940 (2007).
675. Yanagihashi, Y., Segawa, K., Maeda, R., Nabeshima, Y.I. & Nagata, S. Mouse macrophages show different requirements for phosphatidylserine receptor Tim4 in efferocytosis. *Proceedings of the National Academy of Sciences of the United States of America* **114**, 8800-8805 (2017).
676. Edberg, J.C. *et al.* The CY domain of the Fc γ RI α alpha-chain (CD64) alters gamma-chain tyrosine-based signaling and phagocytosis. *The Journal of biological chemistry* **277**, 41287-41293 (2002).
677. Swisher, J.F. & Feldman, G.M. The many faces of Fc γ RI: implications for therapeutic antibody function. *Immunological reviews* **268**, 160-174 (2015).
678. Mendoza-Coronel, E. & Ortega, E. Macrophage Polarization Modulates Fc γ R- and CD13-Mediated Phagocytosis and Reactive Oxygen Species Production, Independently of Receptor Membrane Expression. *Frontiers in immunology* **8**, 303 (2017).
679. Cho, K.W. *et al.* An MHC II-dependent activation loop between adipose tissue macrophages and CD4⁺ T cells controls obesity-induced inflammation. *Cell reports* **9**, 605-617 (2014).
680. Buxadé, M. *et al.* Macrophage-specific MHCII expression is regulated by a remote Ciita enhancer controlled by NFAT5. *Journal of Experimental Medicine* **215**, 2901-2918 (2018).
681. Rennick, D.M. & Fort, M.M. Lessons from genetically engineered animal models. XII. IL-10-deficient (IL-10^{-/-}) mice and intestinal inflammation. *American journal of physiology. Gastrointestinal and liver physiology* **278**, G829-833 (2000).
682. Kowalski, G.M. *et al.* Deficiency of haematopoietic-cell-derived IL-10 does not exacerbate high-fat-diet-induced inflammation or insulin resistance in mice. *Diabetologia* **54**, 888-899 (2011).
683. Keshav, S. *et al.* Tumor necrosis factor mRNA localized to Paneth cells of normal murine intestinal epithelium by in situ hybridization. *The Journal of experimental medicine* **171**, 327-332 (1990).
684. Roulis, M., Armaka, M., Manoloukos, M., Apostolaki, M. & Kollias, G. Intestinal epithelial cells as producers but not targets of chronic TNF suffice to cause murine Crohn-like pathology. *Proceedings of the National Academy of Sciences of the United States of America* **108**, 5396-5401 (2011).

685. Bradford, E.M. *et al.* Epithelial TNF receptor signaling promotes mucosal repair in inflammatory bowel disease. *The Journal of Immunology* **199**, 1886-1897 (2017).
686. Leppkes, M., Roulis, M., Neurath, M.F., Kollias, G. & Becker, C. Pleiotropic functions of TNF- α in the regulation of the intestinal epithelial response to inflammation. *International immunology* **26**, 509-515 (2014).
687. Graham, W.V. *et al.* Intracellular MLCK1 diversion reverses barrier loss to restore mucosal homeostasis. *Nature medicine* **25**, 690-700 (2019).
688. Koelink, P.J. *et al.* Anti-TNF therapy in IBD exerts its therapeutic effect through macrophage IL-10 signalling. *Gut* **69**, 1053-1063 (2020).
689. MacDonald, T., Hutchings, P., Choy, M.Y., Murch, S. & Cooke, A. Tumour necrosis factor- α and interferon- γ production measured at the single cell level in normal and inflamed human intestine. *Clinical & Experimental Immunology* **81**, 301-305 (1990).
690. Arrieta, M.-C., Madsen, K., Doyle, J. & Meddings, J. Reducing small intestinal permeability attenuates colitis in the IL10 gene-deficient mouse. *Gut* **58**, 41-48 (2009).
691. Berg, D.J. *et al.* Enterocolitis and colon cancer in interleukin-10-deficient mice are associated with aberrant cytokine production and CD4 (+) TH1-like responses. *The Journal of clinical investigation* **98**, 1010-1020 (1996).
692. Neurath, M.F. & Pettersson, S. Predominant role of NF- κ B p65 in the pathogenesis of chronic intestinal inflammation. *Immunobiology* **198**, 91-98 (1997).
693. Delgado, M.E., Grabinger, T. & Brunner, T. Cell death at the intestinal epithelial front line. *The FEBS journal* **283**, 2701-2719 (2016).
694. McElroy, S.J. *et al.* Tumor necrosis factor receptor 1-dependent depletion of mucus in immature small intestine: a potential role in neonatal necrotizing enterocolitis. *American Journal of Physiology-Gastrointestinal and Liver Physiology* **301**, G656-G666 (2011).
695. Van Hauwermeiren, F. *et al.* TNFR1-induced lethal inflammation is mediated by goblet and Paneth cell dysfunction. *Mucosal immunology* **8**, 828-840 (2015).
696. Kontoyiannis, D. *et al.* Interleukin-10 targets p38 MAPK to modulate ARE-dependent TNF mRNA translation and limit intestinal pathology. *The EMBO journal* **20**, 3760-3770 (2001).
697. Kontoyiannis, D., Pasparakis, M., Pizarro, T.T., Cominelli, F. & Kollias, G. Impaired on/off regulation of TNF biosynthesis in mice lacking TNF AU-rich elements: implications for joint and gut-associated immunopathologies. *Immunity* **10**, 387-398 (1999).
698. Baur, P. *et al.* Metabolic phenotyping of the Crohn's disease-like IBD etiopathology in the TNF Δ ARE/WT mouse model. *Journal of proteome research* **10**, 5523-5535 (2011).
699. Noti, M., Corazza, N., Mueller, C., Berger, B. & Brunner, T. TNF suppresses acute intestinal inflammation by inducing local glucocorticoid synthesis. *Journal of experimental medicine* **207**, 1057-1066 (2010).
700. Kojouharoff, G. *et al.* Neutralization of tumour necrosis factor (TNF) but not of IL-1 reduces inflammation in chronic dextran sulphate sodium-induced colitis in mice. *Clinical & Experimental Immunology* **107**, 353-358 (1997).
701. Arnold, J.W. *et al.* Tumor necrosis factor- α mediates the early pathology in Salmonella infection of the gastrointestinal tract. *Microbial pathogenesis* **14**, 217-227 (1993).

702. Goncalves, N. *et al.* Increased susceptibility of TNFRp55 deficient mice to *Citrobacter rodentium* (mouse EPEC) infection. *Gut* **48**, A75-A75 (2001).
703. McDermott, A.J. *et al.* The role of Gr-1+ cells and tumour necrosis factor- α signalling during *Clostridium difficile* colitis in mice. *Immunology* **144**, 704-716 (2015).
704. Fine, S., Papamichael, K. & Cheifetz, A.S. Etiology and Management of Lack or Loss of Response to Anti-Tumor Necrosis Factor Therapy in Patients With Inflammatory Bowel Disease. *Gastroenterol Hepatol (N Y)* **15**, 656-665 (2019).
705. Turnbaugh, P.J. *et al.* An obesity-associated gut microbiome with increased capacity for energy harvest. *Nature* **444**, 1027-1031 (2006).
706. Cotillard, A. *et al.* Dietary intervention impact on gut microbial gene richness. *Nature* **500**, 585-588 (2013).
707. Caesar, R., Tremaroli, V., Kovatcheva-Datchary, P., Cani, P.D. & Bäckhed, F. Crosstalk between gut microbiota and dietary lipids aggravates WAT inflammation through TLR signaling. *Cell metabolism* **22**, 658-668 (2015).
708. Le Chatelier, E. *et al.* Richness of human gut microbiome correlates with metabolic markers. *Nature* **500**, 541-546 (2013).
709. Turnbaugh, P.J. *et al.* The effect of diet on the human gut microbiome: a metagenomic analysis in humanized gnotobiotic mice. *Science translational medicine* **1**, 6ra14 (2009).
710. Daniel, H. *et al.* High-fat diet alters gut microbiota physiology in mice. *The ISME journal* **8**, 295-308 (2014).
711. Walker, A. *et al.* Distinct signatures of host-microbial meta-metabolome and gut microbiome in two C57BL/6 strains under high-fat diet. *The ISME journal* **8**, 2380-2396 (2014).
712. Gu, Y. *et al.* Metabolic and Gut Microbial Characterization of Obesity-Prone Mice under a High-Fat Diet. *Journal of proteome research* **18**, 1703-1714 (2019).
713. Caesar, R. *et al.* Gut-derived lipopolysaccharide augments adipose macrophage accumulation but is not essential for impaired glucose or insulin tolerance in mice. *Gut* **61**, 1701-1707 (2012).
714. Rogala, A.R., Oka, A. & Sartor, R.B. Strategies to Dissect Host-Microbial Immune Interactions That Determine Mucosal Homeostasis vs. Intestinal Inflammation in Gnotobiotic Mice. *Frontiers in immunology* **11**, 214 (2020).
715. Pleasants, J.R. Rearing germfree cesarean-born rats, mice, and rabbits through weaning. *Annals of the New York Academy of Sciences* **78**, 116-126 (1959).
716. Bäckhed, F. *et al.* The gut microbiota as an environmental factor that regulates fat storage. *Proceedings of the National Academy of Sciences of the United States of America* **101**, 15718-15723 (2004).
717. Ridaura, V.K. *et al.* Gut microbiota from twins discordant for obesity modulate metabolism in mice. *Science* **341**, 1241214 (2013).
718. Kovatcheva-Datchary, P. *et al.* Simplified Intestinal Microbiota to Study Microbe-Diet-Host Interactions in a Mouse Model. *Cell reports* **26**, 3772-3783.e3776 (2019).
719. Miyoshi, J. *et al.* Minimizing confounders and increasing data quality in murine models for studies of the gut microbiome. *PeerJ* **6**, e5166 (2018).

720. Laukens, D., Brinkman, B.M., Raes, J., De Vos, M. & Vandenabeele, P. Heterogeneity of the gut microbiome in mice: guidelines for optimizing experimental design. *FEMS microbiology reviews* **40**, 117-132 (2016).
721. Martín, R., Bermúdez-Humarán, L.G. & Langella, P. Gnotobiotic Rodents: An In Vivo Model for the Study of Microbe-Microbe Interactions. *Frontiers in microbiology* **7**, 409 (2016).
722. Vemuri, R. *et al.* The microgenderome revealed: sex differences in bidirectional interactions between the microbiota, hormones, immunity and disease susceptibility. *Semin Immunopathol* **41**, 265-275 (2019).
723. El Aidy, S. *et al.* The gut microbiota elicits a profound metabolic reorientation in the mouse jejunal mucosa during conventionalisation. *Gut* **62**, 1306-1314 (2013).
724. El Aidy, S. *et al.* Temporal and spatial interplay of microbiota and intestinal mucosa drive establishment of immune homeostasis in conventionalized mice. *Mucosal immunology* **5**, 567-579 (2012).
725. Gaboriau-Routhiau, V. *et al.* The key role of segmented filamentous bacteria in the coordinated maturation of gut helper T cell responses. *Immunity* **31**, 677-689 (2009).
726. Johansson, M.E. *et al.* Normalization of Host Intestinal Mucus Layers Requires Long-Term Microbial Colonization. *Cell Host Microbe* **18**, 582-592 (2015).
727. Le Roy, T. *et al.* Comparative Evaluation of Microbiota Engraftment Following Fecal Microbiota Transfer in Mice Models: Age, Kinetic and Microbial Status Matter. *Frontiers in microbiology* **9**, 3289 (2018).
728. Larsson, E. *et al.* Analysis of gut microbial regulation of host gene expression along the length of the gut and regulation of gut microbial ecology through MyD88. *Gut* **61**, 1124-1131 (2012).
729. Maslowski, K.M. *et al.* Regulation of inflammatory responses by gut microbiota and chemoattractant receptor GPR43. *Nature* **461**, 1282-1286 (2009).
730. Grainger, J., Daw, R. & Wemyss, K. Systemic instruction of cell-mediated immunity by the intestinal microbiome. *F1000Research* **7** (2018).
731. Rodriguez, D.M., Benninghoff, A.D., Aardema, N.D.J., Phatak, S. & Hintze, K.J. Basal Diet Determined Long-Term Composition of the Gut Microbiome and Mouse Phenotype to a Greater Extent than Fecal Microbiome Transfer from Lean or Obese Human Donors. *Nutrients* **11**, 1630 (2019).
732. Rabot, S. *et al.* High fat diet drives obesity regardless the composition of gut microbiota in mice. *Scientific reports* **6**, 32484 (2016).
733. Llewellyn, S.R. *et al.* Interactions between diet and the intestinal microbiota alter intestinal permeability and colitis severity in mice. *Gastroenterology* **154**, 1037-1046. e1032 (2018).
734. Kostovcikova, K. *et al.* Diet rich in animal protein promotes pro-inflammatory macrophage response and exacerbates colitis in mice. *Frontiers in immunology* **10**, 919 (2019).
735. Gual-Grau, A., Guirro, M., Mayneris-Perxachs, J., Arola, L. & Boqué, N. Impact of different hypercaloric diets on obesity features in rats: a metagenomics and metabolomics integrative approach. *The Journal of nutritional biochemistry* **71**, 122-131 (2019).
736. Nagpal, R. *et al.* Gut microbiome and aging: Physiological and mechanistic insights. *Nutr Healthy Aging* **4**, 267-285 (2018).

737. Claesson, M.J. *et al.* Gut microbiota composition correlates with diet and health in the elderly. *Nature* **488**, 178-184 (2012).
738. Kavanagh, K. *et al.* Biomarkers of leaky gut are related to inflammation and reduced physical function in older adults with cardiometabolic disease and mobility limitations. *GeroScience* **41**, 923-933 (2019).
739. Clark, R.I. *et al.* Distinct Shifts in Microbiota Composition during *Drosophila* Aging Impair Intestinal Function and Drive Mortality. *Cell reports* **12**, 1656-1667 (2015).
740. Ahmadi, S. *et al.* A human-origin probiotic cocktail ameliorates aging-related leaky gut and inflammation via modulating the microbiota/taurine/tight junction axis. *JCI insight* **5** (2020).
741. Tran, L. & Greenwood-Van Meerveld, B. Age-associated remodeling of the intestinal epithelial barrier. *The journals of gerontology. Series A, Biological sciences and medical sciences* **68**, 1045-1056 (2013).
742. Mitchell, E.L. *et al.* Reduced Intestinal Motility, Mucosal Barrier Function, and Inflammation in Aged Monkeys. *The journal of nutrition, health & aging* **21**, 354-361 (2017).
743. Ma, T.Y., Hollander, D., Dadufalza, V. & Krugliak, P. Effect of aging and caloric restriction on intestinal permeability. *Experimental gerontology* **27**, 321-333 (1992).
744. Ren, W.Y. *et al.* Age-related changes in small intestinal mucosa epithelium architecture and epithelial tight junction in rat models. *Aging clinical and experimental research* **26**, 183-191 (2014).
745. Wen, S.W. *et al.* Advanced age promotes colonic dysfunction and gut-derived lung infection after stroke. *Aging cell* **18**, e12980 (2019).
746. Scott, K.A. *et al.* Revisiting Metchnikoff: Age-related alterations in microbiota-gut-brain axis in the mouse. *Brain, behavior, and immunity* **65**, 20-32 (2017).
747. DeJong, E.N., Surette, M.G. & Bowdish, D.M.E. The Gut Microbiota and Unhealthy Aging: Disentangling Cause from Consequence. *Cell Host Microbe* **28**, 180-189 (2020).
748. Kain, V. *et al.* Obesogenic diet in aging mice disrupts gut microbe composition and alters neutrophil:lymphocyte ratio, leading to inflamed milieu in acute heart failure. *FASEB journal : official publication of the Federation of American Societies for Experimental Biology* **33**, 6456-6469 (2019).
749. Nunes-Souza, V. *et al.* Aging Increases Susceptibility to High Fat Diet-Induced Metabolic Syndrome in C57BL/6 Mice: Improvement in Glycemic and Lipid Profile after Antioxidant Therapy. *Oxidative medicine and cellular longevity* **2016**, 1987960 (2016).
750. Fransen, F. *et al.* Aged Gut Microbiota Contributes to Systemical Inflammaging after Transfer to Germ-Free Mice. *Frontiers in immunology* **8**, 1385 (2017).
751. Kaur, H. *et al.* Probiotics ameliorate intestinal pathophysiology in a mouse model of Alzheimer's disease. *Neurobiology of aging* **92**, 114-134 (2020).
752. Krumbeck, J.A. *et al.* Probiotic Bifidobacterium strains and galactooligosaccharides improve intestinal barrier function in obese adults but show no synergism when used together as synbiotics. *Microbiome* **6**, 121 (2018).
753. Stebegg, M. *et al.* Heterochronic faecal transplantation boosts gut germinal centres in aged mice. *Nature communications* **10**, 2443 (2019).

754. Donaldson, D.S., Pollock, J., Vohra, P., Stevens, M.P. & Mabbott, N.A. Microbial Stimulation Reverses the Age-Related Decline in M Cells in Aged Mice. *iScience* **23**, 101147 (2020).
755. Verschoor, C.P. *et al.* Alterations to the frequency and function of peripheral blood monocytes and associations with chronic disease in the advanced-age, frail elderly. *PLoS One* **9**, e104522 (2014).
756. Hearps, A.C. *et al.* Aging is associated with chronic innate immune activation and dysregulation of monocyte phenotype and function. *Aging cell* **11**, 867-875 (2012).
757. Nyugen, J., Agrawal, S., Gollapudi, S. & Gupta, S. Impaired functions of peripheral blood monocyte subpopulations in aged humans. *Journal of clinical immunology* **30**, 806-813 (2010).
758. Ong, S.-M. *et al.* The pro-inflammatory phenotype of the human non-classical monocyte subset is attributed to senescence. *Cell death & disease* **9**, 1-12 (2018).
759. Esplin, B.L. *et al.* Chronic exposure to a TLR ligand injures hematopoietic stem cells. *Journal of immunology (Baltimore, Md. : 1950)* **186**, 5367-5375 (2011).
760. Swift, M.E., Burns, A.L., Gray, K.L. & DiPietro, L.A. Age-related alterations in the inflammatory response to dermal injury. *The Journal of investigative dermatology* **117**, 1027-1035 (2001).
761. De La Fuente, M. Changes in the macrophage function with aging. *Comparative biochemistry and physiology. A, Comparative physiology* **81**, 935-938 (1985).
762. Koike, E., Kobayashi, T., Mochitate, K. & Murakami, M. Effect of aging on nitric oxide production by rat alveolar macrophages. *Experimental gerontology* **34**, 889-894 (1999).
763. Kissin, E., Tomasi, M., McCartney-Francis, N., Gibbs, C.L. & Smith, P.D. Age-related decline in murine macrophage production of nitric oxide. *The Journal of infectious diseases* **175**, 1004-1007 (1997).
764. Renshaw, M. *et al.* Cutting edge: impaired Toll-like receptor expression and function in aging. *Journal of immunology (Baltimore, Md. : 1950)* **169**, 4697-4701 (2002).
765. Boehmer, E.D., Meehan, M.J., Cutro, B.T. & Kovacs, E.J. Aging negatively skews macrophage TLR2- and TLR4-mediated pro-inflammatory responses without affecting the IL-2-stimulated pathway. *Mechanisms of ageing and development* **126**, 1305-1313 (2005).
766. Herrero, C., Marqués, L., Lloberas, J. & Celada, A. IFN-gamma-dependent transcription of MHC class II IA is impaired in macrophages from aged mice. *The Journal of clinical investigation* **107**, 485-493 (2001).
767. Herrero, C. *et al.* Immunosenescence of macrophages: reduced MHC class II gene expression. *Experimental gerontology* **37**, 389-394 (2002).
768. Linehan, E. & Fitzgerald, D.C. Ageing and the immune system: focus on macrophages. *Eur J Microbiol Immunol (Bp)* **5**, 14-24 (2015).
769. Bouchlaka, M.N. *et al.* Aging predisposes to acute inflammatory induced pathology after tumor immunotherapy. *The Journal of experimental medicine* **210**, 2223-2237 (2013).
770. Saffrey, M.J. Aging of the mammalian gastrointestinal tract: a complex organ system. *AGE* **36**, 9603 (2013).
771. Bäcker, V., Cheung, F.Y., Siveke, J.T., Fandrey, J. & Winning, S. Knockdown of myeloid cell hypoxia-inducible factor-1 α ameliorates the acute pathology in DSS-induced colitis. *PLoS One* **12**, e0190074 (2017).

772. Kim, Y.E. *et al.* HIF-1 α activation in myeloid cells accelerates dextran sodium sulfate-induced colitis progression in mice. *Disease models & mechanisms* **11** (2018).
773. Kazakevych, J., Stoyanova, E., Liebert, A. & Varga-Weisz, P. Transcriptome analysis identifies a robust gene expression program in the mouse intestinal epithelium on aging. *Scientific reports* **9**, 10410 (2019).
774. Elderman, M. *et al.* The effect of age on the intestinal mucus thickness, microbiota composition and immunity in relation to sex in mice. *PLoS One* **12**, e0184274 (2017).
775. Thompson, G.R. & Trexler, P.C. Gastrointestinal structure and function in germ-free or gnotobiotic animals. *Gut* **12**, 230-235 (1971).
776. Saffrey, M.J. Cellular changes in the enteric nervous system during ageing. *Developmental Biology* **382**, 344-355 (2013).
777. Bitar, K., Greenwood-Van Meerveld, B., Saad, R. & Wiley, J.W. Aging and gastrointestinal neuromuscular function: insights from within and outside the gut. *Neurogastroenterology and motility : the official journal of the European Gastrointestinal Motility Society* **23**, 490-501 (2011).
778. Becker, L. *et al.* Age-dependent shift in macrophage polarisation causes inflammation-mediated degeneration of enteric nervous system. *Gut* **67**, 827-836 (2018).
779. den Besten, G. *et al.* The role of short-chain fatty acids in the interplay between diet, gut microbiota, and host energy metabolism. *J Lipid Res* **54**, 2325-2340 (2013).
780. Naidoo, A. TNF Alters Monocyte and Macrophage Phenotype and Function in Models of Chronic Inflammatory Disease. MSc thesis, McMaster University, 2016.
781. Becker, L., Spear, E.T., Sinha, S.R., Haileselassie, Y. & Habtezion, A. Age-Related Changes in Gut Microbiota Alter Phenotype of Muscularis Macrophages and Disrupt Gastrointestinal Motility. *Cellular and molecular gastroenterology and hepatology* **7**, 243-245.e242 (2019).
782. Harmatz, P.R., Carrington, P.W., Giovino-Barry, V., Hatz, R.A. & Bloch, K.J. Intestinal adaptation during lactation in the mouse. II. Altered intestinal processing of a dietary protein. *The American journal of physiology* **264**, G1126-1132 (1993).
783. Caton, J.S. *et al.* Effects of maternal nutrition and stage of gestation on body weight, visceral organ mass, and indices of jejunal cellularity, proliferation, and vascularity in pregnant ewe lambs. *Journal of animal science* **87**, 222-235 (2009).
784. Prieto, R.M., Ferrer, M., Fe, J.M., Rayó, J.M. & Tur, J.A. Morphological adaptive changes of small intestinal tract regions due to pregnancy and lactation in rats. *Annals of nutrition & metabolism* **38**, 295-300 (1994).
785. Casirola, D.M. & Ferraris, R.P. Role of the small intestine in postpartum weight retention in mice. *The American journal of clinical nutrition* **78**, 1178-1187 (2003).
786. Cripps, A.W. & Williams, V.J. The effect of pregnancy and lactation on food intake, gastrointestinal anatomy and the absorptive capacity of the small intestine in the albino rat. *The British journal of nutrition* **33**, 17-32 (1975).
787. Craft, I.L. The influence of pregnancy and lactation on the morphology and absorptive capacity of the rat small intestine. *Clin Sci* **38**, 287-295 (1970).
788. Klinger, S. *et al.* Gastrointestinal transport of calcium and glucose in lactating ewes. *Physiological reports* **4** (2016).

789. Okine, E.K., Glimm, D.R., Thompson, J.R. & Kennelly, J.J. Influence of stage of lactation on glucose and glutamine metabolism in isolated enterocytes from dairy cattle. *Metabolism: clinical and experimental* **44**, 325-331 (1995).
790. Vonnahme, K.A., Lemley, C.O., Caton, J.S. & Meyer, A.M. Impacts of Maternal Nutrition on Vascularity of Nutrient Transferring Tissues during Gestation and Lactation. *Nutrients* **7**, 3497-3523 (2015).
791. Scheaffer, A.N., Caton, J.S., Redmer, D.A., Arnold, D.R. & Reynolds, L.P. Effect of dietary restriction, pregnancy, and fetal type on intestinal cellularity and vascularity in Columbia and Romanov ewes. *Journal of animal science* **82**, 3024-3033 (2004).
792. Reyes, H. *et al.* Is a leaky gut involved in the pathogenesis of intrahepatic cholestasis of pregnancy? *Hepatology (Baltimore, Md.)* **43**, 715-722 (2006).
793. Collado, M.C., Isolauri, E., Laitinen, K. & Salminen, S. Distinct composition of gut microbiota during pregnancy in overweight and normal-weight women. *The American journal of clinical nutrition* **88**, 894-899 (2008).
794. Santacruz, A. *et al.* Gut microbiota composition is associated with body weight, weight gain and biochemical parameters in pregnant women. *The British journal of nutrition* **104**, 83-92 (2010).
795. Vernon, R.G., Denis, R.G., Sorensen, A. & Williams, G. Leptin and the adaptations of lactation in rodents and ruminants. *Horm Metab Res* **34**, 678-685 (2002).
796. Yao, Z. *et al.* 16S rRNA Gene-Based Analysis Reveals the Effects of Gestational Diabetes on the Gut Microbiota of Mice During Pregnancy. *Indian journal of microbiology* **60**, 239-245 (2020).
797. Loughner, C.L. *et al.* Organization, evolution and functions of the human and mouse Ly6/uPAR family genes. *Human genomics* **10**, 10 (2016).
798. Sunderkötter, C. *et al.* Subpopulations of mouse blood monocytes differ in maturation stage and inflammatory response. *Journal of immunology (Baltimore, Md. : 1950)* **172**, 4410-4417 (2004).
799. van der Poel, C.E., Spaapen, R.M., van de Winkel, J.G. & Leusen, J.H. Functional characteristics of the high affinity IgG receptor, FcγRI. *Journal of immunology (Baltimore, Md. : 1950)* **186**, 2699-2704 (2011).
800. Ambarus, C.A. *et al.* Soluble immune complexes shift the TLR-induced cytokine production of distinct polarized human macrophage subsets towards IL-10. *PLoS One* **7**, e35994 (2012).
801. Deshmane, S.L., Kremlev, S., Amini, S. & Sawaya, B.E. Monocyte chemoattractant protein-1 (MCP-1): an overview. *Journal of interferon & cytokine research : the official journal of the International Society for Interferon and Cytokine Research* **29**, 313-326 (2009).
802. Marchalonis, J.J., Jensen, I. & Schluter, S.F. Structural, antigenic and evolutionary analyses of immunoglobulins and T cell receptors. *Journal of molecular recognition : JMR* **15**, 260-271 (2002).
803. Alkhatib, G. The biology of CCR5 and CXCR4. *Current opinion in HIV and AIDS* **4**, 96-103 (2009).
804. Wilen, C.B., Tilton, J.C. & Doms, R.W. HIV: cell binding and entry. *Cold Spring Harbor perspectives in medicine* **2** (2012).
805. Freeman, G.J., Casasnovas, J.M., Umetsu, D.T. & DeKruyff, R.H. TIM genes: a family of cell surface phosphatidylserine receptors that regulate innate and adaptive immunity. *Immunological reviews* **235**, 172-189 (2010).

806. Sims, B. *et al.* Role of TIM-4 in exosome-dependent entry of HIV-1 into human immune cells. *International journal of nanomedicine* **12**, 4823-4833 (2017).
807. Albacker, L.A. *et al.* TIM-4, a receptor for phosphatidylserine, controls adaptive immunity by regulating the removal of antigen-specific T cells. *Journal of immunology (Baltimore, Md. : 1950)* **185**, 6839-6849 (2010).
808. Thornley, T.B. *et al.* Fragile TIM-4-expressing tissue resident macrophages are migratory and immunoregulatory. *The Journal of clinical investigation* **124**, 3443-3454 (2014).
809. Miyanishi, M., Segawa, K. & Nagata, S. Synergistic effect of Tim4 and MFG-E8 null mutations on the development of autoimmunity. *Int Immunol* **24**, 551-559 (2012).
810. Abe, Y. *et al.* TIM-4 has dual function in the induction and effector phases of murine arthritis. *Journal of immunology (Baltimore, Md. : 1950)* **191**, 4562-4572 (2013).
811. Liu, W. *et al.* Tim-4 in Health and Disease: Friend or Foe? *Frontiers in immunology* **11** (2020).
812. Foks, A.C. *et al.* Blockade of Tim-1 and Tim-4 Enhances Atherosclerosis in Low-Density Lipoprotein Receptor-Deficient Mice. *Arteriosclerosis, thrombosis, and vascular biology* **36**, 456-465 (2016).
813. Liu, W. *et al.* Tim-4 Inhibits NLRP3 Inflammasome via the LKB1/AMPK α Pathway in Macrophages. *Journal of immunology (Baltimore, Md. : 1950)* **203**, 990-1000 (2019).
814. Lin, H.H. *et al.* The macrophage F4/80 receptor is required for the induction of antigen-specific efferent regulatory T cells in peripheral tolerance. *The Journal of experimental medicine* **201**, 1615-1625 (2005).
815. Ezekowitz, R.A. & Gordon, S. Down-regulation of mannosyl receptor-mediated endocytosis and antigen F4/80 in bacillus Calmette-Guérin-activated mouse macrophages. Role of T lymphocytes and lymphokines. *The Journal of experimental medicine* **155**, 1623-1637 (1982).
816. Ezekowitz, R.A., Austyn, J., Stahl, P.D. & Gordon, S. Surface properties of bacillus Calmette-Guérin-activated mouse macrophages. Reduced expression of mannose-specific endocytosis, Fc receptors, and antigen F4/80 accompanies induction of Ia. *The Journal of experimental medicine* **154**, 60-76 (1981).
817. Podolnikova, N.P., Podolnikov, A.V., Haas, T.A., Lishko, V.K. & Ugarova, T.P. Ligand recognition specificity of leukocyte integrin α M β 2 (Mac-1, CD11b/CD18) and its functional consequences. *Biochemistry* **54**, 1408-1420 (2015).
818. Han, C. *et al.* Integrin CD11b negatively regulates TLR-triggered inflammatory responses by activating Syk and promoting degradation of MyD88 and TRIF via Cbl-b. *Nature immunology* **11**, 734-742 (2010).
819. Klein, S.L. & Morgan, R. The impact of sex and gender on immunotherapy outcomes. *Biology of sex differences* **11**, 24 (2020).
820. Jawaheer, D., Olsen, J. & Hetland, M.L. Sex differences in response to anti-tumor necrosis factor therapy in early and established rheumatoid arthritis—results from the DANBIO registry. *The Journal of rheumatology* **39**, 46-53 (2012).
821. Hyrich, K., Watson, K., Silman, A. & Symmons, D. Predictors of response to anti-TNF- α therapy among patients with rheumatoid arthritis: results from the British Society for Rheumatology Biologics Register. *Rheumatology* **45**, 1558-1565 (2006).

822. Jayakumar, K. *et al.* Sustained clinical remission in rheumatoid arthritis: prevalence and prognostic factors in an inception cohort of patients treated with conventional DMARDS. *Rheumatology* **51**, 169-175 (2012).
823. McInnes, I.B. & Schett, G. The pathogenesis of rheumatoid arthritis. *The New England journal of medicine* **365**, 2205-2219 (2011).
824. Chara, L. *et al.* The number of circulating monocytes as biomarkers of the clinical response to methotrexate in untreated patients with rheumatoid arthritis. *Journal of Translational Medicine* **13**, 2 (2015).
825. Haringman, J.J. *et al.* Synovial tissue macrophages: a sensitive biomarker for response to treatment in patients with rheumatoid arthritis. *Annals of the rheumatic diseases* **64**, 834-838 (2005).
826. Wijbrandts, C.A. *et al.* Absence of changes in the number of synovial sublining macrophages after ineffective treatment for rheumatoid arthritis: Implications for use of synovial sublining macrophages as a biomarker. *Arthritis and rheumatism* **56**, 3869-3871 (2007).
827. Wikaningrum, R. *et al.* Pathogenic mechanisms in the rheumatoid nodule: comparison of proinflammatory cytokine production and cell adhesion molecule expression in rheumatoid nodules and synovial membranes from the same patient. *Arthritis and rheumatism* **41**, 1783-1797 (1998).
828. Klaasen, R., Wijbrandts, C.A., Gerlag, D.M. & Tak, P.P. Body mass index and clinical response to infliximab in rheumatoid arthritis. *Arthritis & Rheumatism* **63**, 359-364 (2011).
829. Schäfer, M. *et al.* Obesity reduces the real-world effectiveness of cytokine-targeted but not cell-targeted disease-modifying agents in rheumatoid arthritis. *Rheumatology (Oxford, England)* **59**, 1916-1926 (2020).
830. Moroni, L., Farina, N. & Dagna, L. Obesity and its role in the management of rheumatoid and psoriatic arthritis. *Clinical Rheumatology* **39**, 1039-1047 (2020).
831. Cacho, N.T. & Lawrence, R.M. Innate Immunity and Breast Milk. *Frontiers in immunology* **8**, 584 (2017).
832. Cabinian, A. *et al.* Transfer of Maternal Immune Cells by Breastfeeding: Maternal Cytotoxic T Lymphocytes Present in Breast Milk Localize in the Peyer's Patches of the Nursed Infant. *PLoS One* **11**, e0156762 (2016).
833. Molès, J.P. *et al.* Breastmilk cell trafficking induces microchimerism-mediated immune system maturation in the infant. *Pediatric allergy and immunology : official publication of the European Society of Pediatric Allergy and Immunology* **29**, 133-143 (2018).
834. Hassiotou, F. & Geddes, D.T. Immune cell-mediated protection of the mammary gland and the infant during breastfeeding. *Advances in nutrition (Bethesda, Md.)* **6**, 267-275 (2015).
835. Hassiotou, F., Geddes, D.T. & Hartmann, P.E. Cells in human milk: state of the science. *Journal of human lactation : official journal of International Lactation Consultant Association* **29**, 171-182 (2013).
836. Laouar, A. Maternal Leukocytes and Infant Immune Programming during Breastfeeding. *Trends in immunology* **41**, 225-239 (2020).
837. Sakaguchi, K. *et al.* Breast-feeding regulates immune system development via transforming growth factor- β in mice pups. *Pediatrics international : official journal of the Japan Pediatric Society* **60**, 224-231 (2018).

838. Riskin, A. *et al.* Changes in immunomodulatory constituents of human milk in response to active infection in the nursing infant. *Pediatric research* **71**, 220-225 (2012).
839. Valea, D. *et al.* CD4+ T cells spontaneously producing human immunodeficiency virus type I in breast milk from women with or without antiretroviral drugs. *Retrovirology* **8**, 34 (2011).
840. Cabrera-Rubio, R. *et al.* The human milk microbiome changes over lactation and is shaped by maternal weight and mode of delivery. *The American journal of clinical nutrition* **96**, 544-551 (2012).
841. Meyer, A.M. & Caton, J.S. Role of the Small Intestine in Developmental Programming: Impact of Maternal Nutrition on the Dam and Offspring. *Advances in nutrition (Bethesda, Md.)* **7**, 169-178 (2016).
842. Hanson, L.A. *et al.* Immune system modulation by human milk. *Advances in experimental medicine and biology* **503**, 99-106 (2002).
843. Lepage, P. & Van de Perre, P. The immune system of breast milk: antimicrobial and anti-inflammatory properties. *Advances in experimental medicine and biology* **743**, 121-137 (2012).
844. Netea, M.G., Latz, E., Mills, K.H. & O'Neill, L.A. Innate immune memory: a paradigm shift in understanding host defense. *Nature immunology* **16**, 675-679 (2015).
845. Netea, M.G., Quintin, J. & Van Der Meer, J.W. Trained immunity: a memory for innate host defense. *Cell host & microbe* **9**, 355-361 (2011).
846. Arts, R.J.W. *et al.* BCG Vaccination Protects against Experimental Viral Infection in Humans through the Induction of Cytokines Associated with Trained Immunity. *Cell Host & Microbe* **23**, 89-100.e105 (2018).
847. Mitroulis, I. *et al.* Modulation of Myelopoiesis Progenitors Is an Integral Component of Trained Immunity. *Cell* **172**, 147-161.e112 (2018).
848. Kleinnijenhuis, J. *et al.* Long-lasting effects of BCG vaccination on both heterologous Th1/Th17 responses and innate trained immunity. *Journal of innate immunity* **6**, 152-158 (2014).
849. Di Gioia, M. *et al.* Endogenous oxidized phospholipids reprogram cellular metabolism and boost hyperinflammation. *Nature immunology* **21**, 42-53 (2020).
850. Ramirez, K., Shea, D.T., McKim, D.B., Reader, B.F. & Sheridan, J.F. Imipramine attenuates neuroinflammatory signaling and reverses stress-induced social avoidance. *Brain, behavior, and immunity* **46**, 212-220 (2015).
851. Christ, A. *et al.* Western Diet Triggers NLRP3-Dependent Innate Immune Reprogramming. *Cell* **172**, 162-175.e114 (2018).
852. Gianfrancesco, M.A. *et al.* Saturated fatty acids induce NLRP3 activation in human macrophages through K⁺ efflux resulting from phospholipid saturation and Na⁺, K⁺-ATPase disruption. *Biochimica et Biophysica Acta (BBA) - Molecular and Cell Biology of Lipids* **1864**, 1017-1030 (2019).
853. Hayes, C.L. *et al.* Commensal microbiota induces colonic barrier structure and functions that contribute to homeostasis. *Scientific reports* **8**, 14184 (2018).
854. Acosta, A. & Camilleri, M. Gastrointestinal morbidity in obesity. *Annals of the New York Academy of Sciences* **1311**, 42-56 (2014).
855. Camilleri, M., Malhi, H. & Acosta, A. Gastrointestinal Complications of Obesity. *Gastroenterology* **152**, 1656-1670 (2017).

856. Mirpuri, J. *et al.* Lactobacillus rhamnosus (LGG) regulates IL-10 signaling in the developing murine colon through upregulation of the IL-10R2 receptor subunit. *PLoS One* **7**, e51955 (2012).
857. Chelakkot, C., Ghim, J. & Ryu, S.H. Mechanisms regulating intestinal barrier integrity and its pathological implications. *Experimental & Molecular Medicine* **50**, 103 (2018).
858. Xu, W. *et al.* IL-10-producing macrophages preferentially clear early apoptotic cells. *Blood* **107**, 4930-4937 (2006).
859. Medina-Contreras, O. *et al.* CX3CR1 regulates intestinal macrophage homeostasis, bacterial translocation, and colitogenic Th17 responses in mice. *The Journal of clinical investigation* **121**, 4787-4795 (2011).
860. Kosiewicz, M.M., Dryden, G.W., Chhabra, A. & Alard, P. Relationship between gut microbiota and development of T cell associated disease. *FEBS letters* **588**, 4195-4206 (2014).
861. Org, E. *et al.* Sex differences and hormonal effects on gut microbiota composition in mice. *Gut microbes* **7**, 313-322 (2016).
862. Steegenga, W.T. *et al.* Structural, functional and molecular analysis of the effects of aging in the small intestine and colon of C57BL/6J mice. *BMC medical genomics* **5**, 38 (2012).
863. Hulsmans, M. *et al.* Macrophages facilitate electrical conduction in the heart. *Cell* **169**, 510-522. e520 (2017).
864. Dick, S.A. *et al.* Self-renewing resident cardiac macrophages limit adverse remodeling following myocardial infarction. *Nature immunology* **20**, 29-39 (2019).
865. Loyher, P.L. *et al.* Macrophages of distinct origins contribute to tumor development in the lung. *The Journal of experimental medicine* **215**, 2536-2553 (2018).
866. Etzerodt, A. *et al.* Tissue-resident macrophages in omentum promote metastatic spread of ovarian cancer. *The Journal of experimental medicine* **217** (2020).
867. Levy, O. & Wynn, J.L. A prime time for trained immunity: innate immune memory in newborns and infants. *Neonatology* **105**, 136-141 (2014).
868. Apostol, A.C., Jensen, K.D.C. & Beaudin, A.E. Training the Fetal Immune System Through Maternal Inflammation-A Layered Hygiene Hypothesis. *Frontiers in immunology* **11**, 123-123 (2020).
869. Talbot, C.P.J. & Dolinsky, V.W. Sex differences in the developmental origins of cardiometabolic disease following exposure to maternal obesity and gestational diabetes (1). *Applied physiology, nutrition, and metabolism = Physiologie appliquee, nutrition et metabolisme* **44**, 687-695 (2019).
870. Armitage, J.A., Khan, I.Y., Taylor, P.D., Nathanielsz, P.W. & Poston, L. Developmental programming of the metabolic syndrome by maternal nutritional imbalance: how strong is the evidence from experimental models in mammals? *The Journal of physiology* **561**, 355-377 (2004).
871. Brun, P. *et al.* Increased intestinal permeability in obese mice: new evidence in the pathogenesis of nonalcoholic steatohepatitis. *American Journal of Physiology-Gastrointestinal and Liver Physiology* **292**, G518-G525 (2007).
872. Hwang, B., Lee, J.H. & Bang, D. Single-cell RNA sequencing technologies and bioinformatics pipelines. *Experimental & Molecular Medicine* **50**, 96 (2018).